



XXXIII SIMGBM CONGRESS 2019 - ANTIMICROBIALS AND HOST- PATHOGEN INTERACTIONS

EDITED BY: Paolo Visca, Pietro Alifano, Paolo Landini and Flavia Marinelli
PUBLISHED IN: *Frontiers in Microbiology*



frontiers

Frontiers eBook Copyright Statement

The copyright in the text of individual articles in this eBook is the property of their respective authors or their respective institutions or funders. The copyright in graphics and images within each article may be subject to copyright of other parties. In both cases this is subject to a license granted to Frontiers.

The compilation of articles constituting this eBook is the property of Frontiers.

Each article within this eBook, and the eBook itself, are published under the most recent version of the Creative Commons CC-BY licence.

The version current at the date of publication of this eBook is CC-BY 4.0. If the CC-BY licence is updated, the licence granted by Frontiers is automatically updated to the new version.

When exercising any right under the CC-BY licence, Frontiers must be attributed as the original publisher of the article or eBook, as applicable.

Authors have the responsibility of ensuring that any graphics or other materials which are the property of others may be included in the CC-BY licence, but this should be checked before relying on the CC-BY licence to reproduce those materials. Any copyright notices relating to those materials must be complied with.

Copyright and source acknowledgement notices may not be removed and must be displayed in any copy, derivative work or partial copy which includes the elements in question.

All copyright, and all rights therein, are protected by national and international copyright laws. The above represents a summary only. For further information please read Frontiers' Conditions for Website Use and Copyright Statement, and the applicable CC-BY licence.

ISSN 1664-8714

ISBN 978-2-88966-788-8

DOI 10.3389/978-2-88966-788-8

About Frontiers

Frontiers is more than just an open-access publisher of scholarly articles: it is a pioneering approach to the world of academia, radically improving the way scholarly research is managed. The grand vision of Frontiers is a world where all people have an equal opportunity to seek, share and generate knowledge. Frontiers provides immediate and permanent online open access to all its publications, but this alone is not enough to realize our grand goals.

Frontiers Journal Series

The Frontiers Journal Series is a multi-tier and interdisciplinary set of open-access, online journals, promising a paradigm shift from the current review, selection and dissemination processes in academic publishing. All Frontiers journals are driven by researchers for researchers; therefore, they constitute a service to the scholarly community. At the same time, the Frontiers Journal Series operates on a revolutionary invention, the tiered publishing system, initially addressing specific communities of scholars, and gradually climbing up to broader public understanding, thus serving the interests of the lay society, too.

Dedication to Quality

Each Frontiers article is a landmark of the highest quality, thanks to genuinely collaborative interactions between authors and review editors, who include some of the world's best academicians. Research must be certified by peers before entering a stream of knowledge that may eventually reach the public - and shape society; therefore, Frontiers only applies the most rigorous and unbiased reviews.

Frontiers revolutionizes research publishing by freely delivering the most outstanding research, evaluated with no bias from both the academic and social point of view. By applying the most advanced information technologies, Frontiers is catapulting scholarly publishing into a new generation.

What are Frontiers Research Topics?

Frontiers Research Topics are very popular trademarks of the Frontiers Journals Series: they are collections of at least ten articles, all centered on a particular subject. With their unique mix of varied contributions from Original Research to Review Articles, Frontiers Research Topics unify the most influential researchers, the latest key findings and historical advances in a hot research area! Find out more on how to host your own Frontiers Research Topic or contribute to one as an author by contacting the Frontiers Editorial Office: frontiersin.org/about/contact

XXXIII SIMGBM CONGRESS 2019 - ANTIMICROBIALS AND HOST- PATHOGEN INTERACTIONS

Topic Editors:

Paolo Visca, Roma Tre University, Italy

Pietro Alifano, University of Salento, Italy

Paolo Landini, University of Milan, Italy

Flavia Marinelli, University of Insubria, Italy

Citation: Visca, P., Alifano, P., Landini, P., Marinelli, F., eds. (2021). XXXIII SIMGBM Congress 2019 - Antimicrobials And Host-Pathogen Interactions. Lausanne: Frontiers Media SA. doi: 10.3389/978-2-88966-788-8

Table of Contents

- 05 Editorial: XXXIII SIMGBM Congress 2019 - Antimicrobials and Host-Pathogen Interactions**
Flavia Marinelli, Pietro Alifano, Paolo Landini and Paolo Visca
- 10 In silico Selection and Experimental Validation of FDA-Approved Drugs as Anti-quorum Sensing Agents**
Marta Mellini, Elena Di Muzio, Francesca D'Angelo, Valerio Baldelli, Serena Ferrillo, Paolo Visca, Livia Leoni, Fabio Polticelli and Giordano Rampioni
- 24 Genomic Stability of Composite SCCmec ACME and COMER-Like Genetic Elements in Staphylococcus epidermidis Correlates With Rate of Excision**
Nada Almehairik, Roxana Zamudio, Corinne Ironside, Chaitanya Joshi, Joseph D. Ralph, Adam P. Roberts, Ian M. Gould, Julie A. Morrissey, Karolin Hijazi and Marco R. Oggioni
- 36 Rv0579 Is Involved in the Resistance to the TP053 Antitubercular Prodrug**
Giorgia Mori, Beatrice Silvia Orena, Laurent R. Chiarelli, Giulia Degiacomi, Olga Riabova, José Camilla Sammartino, Vadim Makarov, Giovanna Riccardi and Maria Rosalia Pasca
- 43 Escaping the Phagocytic Oxidative Burst: The Role of SODB in the Survival of Pseudomonas aeruginosa Within Macrophages**
Luca Cavinato, Elena Genise, Francesco R. Luly, Enea G. Di Domenico, Paola Del Porto and Fiorentina Ascenzioni
- 55 Chemical, Metabolic, and Cellular Characterization of a FtsZ Inhibitor Effective Against Burkholderia cenocepacia**
Laurent R. Chiarelli, Viola Camilla Scoffone, Gabriele Trespidi, Giulia Barbieri, Olga Riabova, Natalia Monakhova, Alessio Porta, Giulia Manina, Giovanna Riccardi, Vadim Makarov and Silvia Buroni
- 70 The Cultivable Bacterial Microbiota Associated to the Medicinal Plant Origanum vulgare L.: From Antibiotic Resistance to Growth-Inhibitory Properties**
Lara Mitia Castronovo, Carmela Calonico, Roberta Ascrizzi, Sara Del Duca, Vania Delfino, Sofia Chioccioli, Alberto Vassallo, Iolanda Strozza, Marinella De Leo, Sauro Biffi, Giovanni Bacci, Patrizia Bogani, Valentina Maggini, Alessio Mengoni, Luisa Pistelli, Antonella Lo Nostro, Fabio Firenzuoli and Renato Fani
- 87 Thanatin Impairs Lipopolysaccharide Transport Complex Assembly by Targeting LptC–LptA Interaction and Decreasing LptA Stability**
Elisabete C. C. M. Moura, Tiago Baeta, Alessandra Romanelli, Cedric Laguri, Alessandra M. Martorana, Emanuela Erba, Jean-Pierre Simorre, Paola Sperandeo and Alessandra Polissi
- 102 An in vitro Reconstructed Human Skin Equivalent Model to Study the Role of Skin Integration Around Percutaneous Devices Against Bacterial Infection**
Eleonore C. L. Bolle, Anthony D. Verderosa, Rabeb Dhouib, Tony J. Parker, John F. Fraser, Tim R. Dargaville and Makrina Totsika

- 115 Glycopeptide Antibiotic Resistance Genes: Distribution and Function in the Producer Actinomycetes**
Oleksandr Yushchuk, Elisa Binda and Flavia Marinelli
- 124 Identification and Characterization of Planktonic Biofilm-Like Aggregates in Infected Synovial Fluids From Joint Infections**
Alessandro Bidossi, Marta Bottagisio, Paolo Savadori and Elena De Vecchi
- 137 The Obligate Symbiont “*Candidatus Megaira polyxenophila*” Has Variable Effects on the Growth of Different Host Species**
Chiara Pasqualetti, Franziska Szokoli, Luca Rindi, Giulio Petroni and Martina Schrällhammer
- 147 Defining the *Helicobacter pylori* Disease-Specific Antigenic Repertoire**
Maria Felicia Soluri, Simone Puccio, Giada Caredda, Paolo Edomi, Mario Milco D’Elios, Fabio Cianchi, Arianna Troilo, Claudio Santoro, Daniele Sblattero and Clelia Peano
- 161 Genomic and Long-Term Transcriptomic Imprints Related to the Daptomycin Mechanism of Action Occurring in Daptomycin- and Methicillin-Resistant *Staphylococcus aureus* Under Daptomycin Exposure**
Viviana Cafiso, Stefano Stracquadanio, Flavia Lo Verde, Irene De Guidi, Alessandra Zega, Giuseppe Pigola and Stefania Stefani
- 178 Expression Profile of Multidrug Resistance Efflux Pumps During Intracellular Life of Adherent-Invasive *Escherichia coli* Strain LF82**
Giulia Fanelli, Martina Pasqua, Bianca Colonna, Gianni Prosseda and Milena Grossi
- 188 Antibiotic Resistance: Moving From Individual Health Norms to Social Norms in One Health and Global Health**
Sara Hernando-Amado, Teresa M. Coque, Fernando Baquero and José L. Martínez
- 208 Inhibitory Effects of Lipopeptides and Glycolipids on *C. albicans*–*Staphylococcus spp.* Dual-Species Biofilms**
Chiara Ceresa, Maurizio Rinaldi, Francesco Tessarolo, Devid Maniglio, Emanuele Fedeli, Erica Tambone, Patrizio Caciagli, Ibrahim M. Banat, Mayri Alessandra Diaz De Rienzo and Letizia Fracchia



Editorial: XXXIII SIMGBM Congress 2019 - Antimicrobials and Host-Pathogen Interactions

Flavia Marinelli¹, Pietro Alifano², Paolo Landini³ and Paolo Visca^{4*}

¹ Dipartimento di Biotecnologie e Scienze della Vita, Università degli Studi dell'Insubria, Varese, Italy, ² Dipartimento di Scienze e Tecnologie Biologiche ed Ambientali, Università del Salento, Lecce, Italy, ³ Dipartimento di Bioscienze, Università degli Studi di Milano Statale, Milano, Italy, ⁴ Dipartimento di Scienze, Università degli Studi Roma Tre, Roma, Italy

Keywords: antibiotics, bacteria, fungi, bacterial communication, host-pathogen interactions, pathogenesis, antimicrobial resistance, cell-to-cell signaling

Editorial on the Research Topic

XXXIII SIMGBM Congress 2019 - Antimicrobials and Host-Pathogen Interactions

This Research Topic (RT) is intended to provide a collection of selected contributions in the broad area “Antimicrobials and Host-Pathogen Interactions” from the participants of “Microbiology 2019” congress organized by the Italian Society for General Microbiology and Microbial Biotechnology (SIMGBM, www.simgbm.it), which was held in Florence, Italy, on June 19–22, 2019. The congress was attended by 224 scientists from all over the world, and contributions relevant to this RT were collected from presentations in the following congress sessions: (i) Antibiotic resistance: where do antibiotic resistance genes come from? (ii) New antimicrobial strategies in the post-antibiotic era; (iii) Intercellular communication in host-pathogen interactions; (iv) New approaches to unravel fungal-host interactions; (v) Bacterial cell surface and signaling. The unifying concept of this RT originates from the increasing awareness that antimicrobial resistance (AMR) is a complex problem which should be addressed by a multifocal approach. Fundamental microbiological investigations in this direction involve understanding of the flow of AMR genes from the environment to human and animal pathogens, the development of new drugs to tackle AMR, and the discovery of new druggable targets to impair microbial growth and/or pathogenicity.

OPEN ACCESS

Edited by:

Rustam Aminov,
University of Aberdeen,
United Kingdom

Reviewed by:

Miklos Fuzi,
Semmelweis University, Hungary

*Correspondence:

Paolo Visca
paolo.visca@uniroma3.it

Specialty section:

This article was submitted to
Antimicrobials, Resistance and
Chemotherapy,
a section of the journal
Frontiers in Microbiology

Received: 25 February 2021

Accepted: 15 March 2021

Published: 07 April 2021

Citation:

Marinelli F, Alifano P, Landini P and
Visca P (2021) Editorial: XXXIII
SIMGBM Congress 2019 -
Antimicrobials and Host-Pathogen
Interactions.
Front. Microbiol. 12:672517.
doi: 10.3389/fmicb.2021.672517

ANTIMICROBIAL RESISTANCE

AMR has initially been observed and studied in hospitals, since the massive use of antimicrobials in clinical settings was considered as its major driving force. However, the origin of AMR is currently considered to be a natural phenomenon that predates the antimicrobial use by humans (D'Costa et al., 2011). AMR genes constitute the so-called resistome, which is defined as the environmental pool of genes conferring either intrinsic or acquired AMR (Surette and Wright, 2017). In their review, Hernando-Amado et al. highlighted that the dissemination of AMR genes is not limited only to the environments characterized by the exposure to high antimicrobial concentrations. Sub-inhibitory antimicrobial levels and the presence of heavy metals promote horizontal gene transfer (HGT), thus increasing further environmental dissemination of AMR genes. In environmental bacteria, AMR genes are often co-localized with mobile genetic elements (MGEs) (e.g., transposons, plasmids, and integrons) that facilitate their intra and inter species transfer. In the case of transmissible infections, a socioecological global approach is needed to preserve the health of the environment, since an increasing crowding of human and food animal populations, the consequent environmental pollution and misuse of drugs favors pathogen transmission both at the local and global levels.

A possible environmental source of AMR genes can be identified among the soil-dwelling bacteria, which produce antibiotics and need protection from them (Binda et al., 2014). Recently, a massive sequencing effort of antibiotic-producer genomes revealed that AMR genes are often clustered together with antibiotic biosynthesis genes and respond to the same regulatory circuits controlling both the production and resistance. In the minireview by Yushchuk et al., this association was confirmed for the environmental actinobacteria, which produce glycopeptide antibiotics and belong to the *Amycolatopsis*, *Actinoplanes*, *Nonomuraea*, and *Streptomyces* genera. Glycopeptide antibiotics such as vancomycin, teicoplanin, and dalbavancin are clinically important drugs for treating severe hospital-acquired infections caused by multiresistant Gram-positive bacteria (Marcone et al., 2018). A recent pioneering work on the phylogenetic reconstruction of glycopeptide biosynthetic gene clusters has paved the way to track the simultaneous evolution of glycopeptide synthesis and resistance genes, and the recruitment and combination of the latter in pathogens (Waglechner et al., 2019).

One of the most common and difficult-to-treat healthcare-associated infections is due to methicillin-resistant *Staphylococcus aureus* (MRSA). Worryingly, an increasing number of MRSA is becoming resistant to other antibiotics, such as β -lactams, carbapenems, glycopeptides, and to the drug of last resort, daptomycin (Shariati et al., 2020). Daptomycin is a lipopeptide, which is naturally produced by the soil saprotroph *Streptomyces roseosporus* (Miao et al., 2005). Both the mode of action and mechanism of resistance toward daptomycin have not completely elucidated yet (Miller et al., 2016). In the paper of Cafiso et al., the authors interrogated the multifactorial nature of MRSA resistance to daptomycin by comparing a clinical daptomycin-resistant isolate vs. its isogenic daptomycin-sensitive strain and by using comparative genomics and late-growth phase transcriptomics. Both strains were isolated from the same patient undergoing daptomycin therapy in hospital during a period of several months. The daptomycin-resistant strain acquired a diverse set of genomic changes under antibiotic selection, which included mutations in genes encoding cell membrane proteins and transcriptional regulators. Transcriptomic changes were found in cell wall and cell membrane organization genes, in the autolytic system, and in primary metabolism genes switching it toward fermentation.

The paper by Almebairik et al. described the role of MGEs in the evolution of *Staphylococcus epidermidis* from a commensal to a nosocomial diseases-causing agent. *S. epidermidis* and other coagulase negative staphylococci represent a leading cause of both bloodstream and skin and soft tissue infections in nosocomial settings (Otto, 2009). Whole genome sequencing of 58 *S. epidermidis* bacteremic isolates revealed the prevalence and evolution of arginine catabolic mobile element (ACME) and copper and mercury resistance (COMER)-like mobile elements, frequently associated with staphylococcal cassette chromosome *mec* (SCCmec) forming composite genetic elements. Considerable variations of ACME occurred even between isolates belonging to the same ACME and sequence types (ST). Similarly, the authors could detect previously

undescribed COMER-like elements showing high stability in 11 *S. epidermidis* isolates belonging to ST2, i.e., one of the two major hospital-adapted drug-resistant lineages. The difference in stability at the genomic level correlated well with the higher excision frequency found for the SCCmec elements in ACME-containing isolates compared to COMER-like element-containing isolates, suggesting that the presence of COMER-like elements represents the most prominent accessory genome feature determining the epidemiological success of ST2 *S. epidermidis* lineage.

NOVEL TARGETS AND MOLECULES

Notwithstanding the AMR crisis, the number of novel antibiotic classes being introduced into the clinical practice since 2000 has been very limited, and daptomycin is one of the few antimicrobial drugs launched since the 2000s (Payne et al., 2007). This situation is even more worrisome for Gram-negative pathogens, where treatment options are extremely limited (Van Camp et al., 2020). Consequently, new druggable targets and active molecules are urgently needed to treat infections caused by Gram-negative bacteria.

Mellini et al. exploited the possibility of targeting the PqsR quorum sensing (QS) regulatory protein to suppress *Pseudomonas aeruginosa* virulence. QS is involved in an intercellular communication process, and it is a global regulator of expression of key virulence traits. Therefore, PqsR inhibitors could be potential anti-virulence agents (Ellermann and Sperandio, 2020). Starting from the virtual screening of a large library of FDA-approved drugs, five compounds were selected based on *in silico* prediction of their binding affinity to PqsR. One of these compounds reduced the expression of *P. aeruginosa* virulence traits *in vitro*, highlighting the potential of virtual screening and drug repositioning in the selection of new FDA-approved anti-virulence drugs (Konreddy et al., 2019). Structural knowledge of bacterial proteins implicated in vital functions or host interactions, combined with computational predictions of their potential ligands, made the strategy described by Mellini et al. a promising approach to the rapid identification of potential inhibitors.

A target-based approach was also used by Chiarelli et al. to identify small molecules inhibiting the function of the FtsZ protein in *Burkholderia cenocepacia*. Since FtsZ is an essential and extremely conserved component of the bacterial divisome, it represents an attractive target for antimicrobials (Haranahalli et al., 2016). The growing clinical importance of *B. cenocepacia*, especially among cystic fibrosis patients, and its intrinsic antibiotic resistance pose an urgent need to discover new effective drugs against this pathogen (Scoffone et al., 2017). More than 50 derivatives of the benzothiadiazole compound C109 were tested *in vitro* using purified *B. cenocepacia* FtsZ as a target, with the IC₅₀ range between 3 and 100 μ M. The growth inhibiting activity was further investigated by conventional susceptibility tests with *B. cenocepacia*, *P. aeruginosa* and *S. aureus*. Although C109 showed some limitations for *B. cenocepacia* growth inhibition, being the substrate for efflux pumps and modification enzymes, it

was endowed with a potent antibacterial activity against *S. aureus* and displayed relatively low cytotoxicity. The study highlighted a rationale for choosing a broadly conserved target, such as FtsZ, in the successful screening campaign of bacterial growth inhibitors.

The paper by Moura et al. pointed to the bacterial outer membrane as a promising target for the development of novel antibiotics against Gram-negative bacteria. Thanatin, a 21-residue inducible cationic defense peptide isolated from the hemipteran insect *Podisus maculiventris*, has a unique mode of action targeting the lipopolysaccharide (LPS) transport (Lpt) system by binding to the N-terminal β -strand of LptA and causing defects in membrane assembly (Vetterli et al., 2018). The authors implemented the Bacterial Adenylate Cyclase Two-Hybrid (BACTH) system to probe *in vivo* the Lpt interactome in the periplasm, and found that thanatin targets both LptC–LptA and LptA–LptA interactions, with a greater inhibitory effect on the former. The disruption of LptC–LptA interaction was confirmed *in vitro* by nuclear magnetic resonance and surface plasmon resonance experiments, while LPS analysis in crude extracts demonstrated that in cells treated with thanatin, LPS accumulates at the periplasmic side of the inner membrane, where it is decorated with colanic acid, in a dead-end reaction diagnostic of defects in the Lpt system (Sperandeo et al., 2011).

Tuberculosis (TB) is the leading cause of morbidity and mortality due to a single infectious agent. About one-quarter of the world population has the latent form of TB, thus representing a large and persistent reservoir for active infection. Due to this, the emergence of multidrug resistant *Mycobacterium tuberculosis* strains represents a major public health threat worldwide (Koch et al., 2018). The thienopyrimidine TP053 is a promising new antitubercular lead, with a potent activity against both replicating and non-replicating *M. tuberculosis* cells (Albesa-Jové et al., 2014). Its mode of action involves the metabolic activation to a nitric oxide (NO)-releasing intermediate by mycobacterial mycothiol-dependent reductase Mrx2. To gain further insights into the mechanism of action of TP053, Mori et al. isolated *M. tuberculosis* TP053-resistant mutants, which carried a L240V substitution in Rv0579, which is still an uncharacterized protein. Protein co-purification experiments demonstrated that activated TP053 binds not only to Mrx2, but also to Rv0579, suggesting that a direct interaction between the activated prodrug and Rv0579 is implicated in resistance. Intriguingly, TP053 treatment caused the up-regulation of Rv0582, which encodes the VapC26 toxin in wild-type *M. tuberculosis*, but not in the Rv0579 resistant mutant, suggesting that Rv0579 could be involved in the regulation of VapC26 expression. While the actual role of Rv0579 in *M. tuberculosis* physiology remains still elusive, the data reported in this paper point to an involvement of Rv0579 in RNA metabolism and expression of the mycobacterial toxin anti-toxin system.

MICROBIAL BIOFILMS

Many bacterial pathogens are able to form biofilms during infection, which render them less susceptible to antimicrobials and to the action of the host immune system, thus contributing

to antibiotic therapy failure. Microbial biofilms are notoriously more tolerant to antibiotics than planktonic cells (Wolfmeier et al., 2018). However, results from *ex vivo* analysis of pathological samples indicate that there is a continuum between the biofilm and planktonic lifestyles, since suspended bacterial aggregates are a major form of bacterial communities in chronic infection sites (Cai, 2020).

Bidossi et al. collected synovial fluids from joint infections and confirmed the presence of fibrin-embedded *S. aureus* and *Staphylococcus lugdunensis* planktonic aggregates in their samples. Clumps were also generated *in vitro*, when bacteria were grown in synovial fluid, and this resulted in an up to 32-fold increase of recalcitrance to antibiotic treatments. Moreover, exposure to synovial fluid caused morphological alterations of staphylococcal biofilm structures on a titanium surface and increased the overall biofilm volume. This *ex vivo* evidence uncovers the mechanism of staphylococcal adaptation to the growth in synovial fluids implemented in the aggregated form. This finding highlights the importance of antibiotic susceptibility testing under conditions which should be closer to *in vivo* situations, in order to configure a successful therapy of joint infection.

The introduction of a foreign body (e.g., an implantable device) is known to trigger bacterial adhesion and biofilm formation as some bacteria have a preferred tropism for abiotic surfaces (Arciola et al., 2018). Several bacterial infections are linked to the utilization of medical percutaneous devices, such as catheters or electrical drivelines. By perforating the skin to reach internal organs, these devices often serve as entry points for opportunistic pathogens found on our skin, such as *S. aureus*. Bolle et al. developed a model of skin broken by a mock electrical driveline and performed experimental infection experiments with *S. aureus* to evaluate the efficacy of human skin equivalent. They showed that *S. aureus* migration into the wound, biofilm formation and tissue damage could be mitigated by human skin equivalent, particularly when seeded with fibroblasts.

Although most tissue and medical device-associated infections are caused by a single pathogen, an increasing number of polymicrobial infections have recently been reported (Rodrigues et al., 2019). The microorganisms involved are thought to coexist in synergistic relations within the biofilm environment, thus resulting in enhanced pathogenicity, virulence, and resistance to antimicrobials. Ceresa et al. investigated the effect of bacterial-sourced biosurfactants as inhibitors of clinically relevant fungal/bacterial dual-species biofilms, which are formed on polystyrene plates and on medical-grade silicones. They tested a rhamnolipid produced by *P. aeruginosa*, a lipopeptide from *Bacillus subtilis* and a sophorolipid from *Candida albicans* by measuring their effect on biofilm-forming *C. albicans* and *Staphylococcus* spp. The rhamnolipid was the most effective, reducing the metabolic activity and biomass of biofilms by >90% within 72 h. It was active when used adsorbed on silicone, and it was not-cytotoxic, supporting its potential in controlling device-associated infections.

Endophytic bacteria leaving in association with different plant tissues can be exploited as a source of new antimicrobials.

With this aim, Castronovo et al., investigated the microbiota of the essential oil-producing *Origanum vulgare*, by culture dependent and independent approaches, and next-generation sequence analysis. Bacterial isolates from different anatomic parts of the plant were tested for antibiotic resistance, antagonistic interactions, and antimicrobial activity against multidrug resistant pathogens. Nearly 50% of them were found to release compounds active against at least one bacterial pathogen, with a marked selectivity against Gram-positive rather than Gram-negative bacteria, substantiating the idea that novel molecules can be discovered by mining microbe-plant interactions.

HOST-PATHOGEN AND SYMBIOTIC INTERACTIONS

There is constant communication between hosts and bacteria that can lead to two alternative scenarios: either tolerance and/or resistance of the bacterial species within the host that leads to quiescent host habitation, or disease characterized by host tissue damage and rapid replication of the bacteria (Casadevall and Pirofski, 2000). Opportunistic pathogens, often in the context of multifactorial diseases, such as *P. aeruginosa*, *Helicobacter pylori*, and adherent-invasive *Escherichia coli*, play a role in exacerbation of cystic fibrosis, stomach cancer, and Crohn's disease, respectively.

Cavinato et al. addressed the role of superoxide dismutases (SOD) in *P. aeruginosa* survival in macrophages. In intracellular pathogens, SODs can counteract the bactericidal effect of ROS generated in macrophages by the NOX2 NADPH oxidase (Lam et al., 2010). The authors showed, counterintuitively, that knocking out *sodB*, which is one of the two genes encoding periplasmic SODs in *P. aeruginosa*, leads to the enhanced bacterial survival in macrophages, apparently due to the reduced turnover of O_2^- into the even more reactive oxygen species H_2O_2 . However, the *sodB* mutant showed reduced long-term intracellular survival, due to its inability to inhibit autophagy in the macrophage. This work highlights the specialized roles of SOD isoenzymes in response to the macrophage oxidative burst, thus providing survival mechanisms for different stages of bacterial infection.

Soluri et al. probed the yet unclear connection between *H. pylori* and oncogenesis, and pursued the hypothesis that some *H. pylori* antigens may trigger an overly inflammatory reaction, leading to gastric ulcers, which, in turn, can progress to cancer. Using a phage display technology, the authors constructed a phage library encompassing the whole *H. pylori* genome, and searched for proteins that would strongly react with the sera of patients affected by *H. pylori*-related oncological pathologies. This approach led to the identification of the CagY/Cag7 protein, an already known *H. pylori* virulence factor (Rohde et al., 2003), as a specific antigen in cancer patients. These results point to a possible role of this protein (or for antibodies against it) as a potential marker for early detection of stomach cancer.

Adherent-invasive *E. coli* (AIEC) are overrepresented in the microbiota of Crohn's disease patients, where they play a pivotal role in triggering chronic inflammation typical of the

disease, especially due to their ability to survive intracellularly. Fanelli et al. investigated the role of genes encoding efflux pumps involved in multidrug resistance, monitoring their expression during bacterial invasion of either intestinal epithelial cells or macrophages. The authors showed that several efflux pump genes are induced during intracellular infection and that one efflux pump in particular (MdtE) contributed to AIEC survival in human macrophages. In addition to improving our understanding of AIEC pathogenesis mechanisms, these results suggest that efflux pumps might be targets for drugs alleviating AIEC-induced inflammation in Crohn's disease.

Obligate intracellular bacteria represent a useful model to investigate bacterial interactions with host cells, and *Rickettsiaceae* provide a paradigmatic example of bacterial endosymbiosis with a number of eukaryotic organisms (protists, green algae, and metazoan) (Salje, 2021). Pasqualetti et al. investigated the newly described "*Candidatus Megaira polyxenophila*," an endosymbiont of eukaryotes living in marine, brackish, or freshwater habitats. By analyzing two phylogenetically close species of the freshwater ciliate *Paramecium* that are naturally infected by "*Ca. M. polyxenophila*," the authors found that both *Paramecium* species have growth advantages in the presence of *Ca. M. polyxenophila*. This advantage is reproduced at every tested salinity condition, although the fitness effects of the endosymbiosis vary between the two *Paramecium* species and environmental conditions. They observed the loss of the endosymbiont after prolonged exposure to higher salinity levels, and this explains why "*Ca. M. polyxenophila*" is more abundant in freshwater than in marine habitats. Infection experiments with these bacteria had so far been unsuccessful under laboratory conditions, so this work provides the very first insights into possible effects of *Ca. M. polyxenophila* on its host.

CONCLUDING REMARKS

As reflected in articles of this RT, antimicrobial resistance, new antibacterial drugs and the mechanisms of host-pathogen interactions remain hot topics, which attracted many contributions and provided a rather faithful snapshot of the quality and the variety of subjects presented at the XXXIII SIMGBM Congress 2019. Progress in these fields is rapidly advancing, and we hope that we will be able to discuss them at the next SIMGBM meeting. Our meeting, planned for 2020, has been put on hold due to the Covid-19 pandemic. We hope to host a meeting "in the flesh" on 15th–18th September 2021, to be held in Cagliari, on the beautiful island of Sardinia, if the public health emergency allows it. We wish to encourage our readers to stay tuned to the news on this conference, and we consider it as a new "kick-off" in attending a meeting after a long time of unavoidable restrictions imposed on social and scientific events.

AUTHOR CONTRIBUTIONS

FM, PA, PL, and PV gave the same contribution to the drafting of the article and have made a substantial, direct, intellectual contribution to the work. All authors contributed to the article and approved the submitted version.

ACKNOWLEDGMENTS

Special thanks to the Section Editor, Prof. Rustam Aminov, all the Associate and Review Editors, all reviewers and Frontiers in Microbiology Editorial Staff for their support and advice. This is a

short text to acknowledge the contributions of specific colleagues, institutions, or agencies that aided the efforts of the authors, and of the Federation of European Microbiological Societies (FEMS) and commercial sponsors for their financial support to the XXXIII SIMGBM Congress 2019.

REFERENCES

- Albesa-Jové, D., Chiarelli, L. R., Makarov, V., Pasca, M. R., Urresti, S., Mori, G., et al. (2014). Rv2466c mediates the activation of TP053 to kill replicating and non-replicating *Mycobacterium tuberculosis*. *ACS Chem. Biol.* 9, 1567–1575. doi: 10.1021/cb500149m
- Arciola, C. R., Campoccia, D., and Montanaro, L. (2018). Implant infections: adhesion, biofilm formation and immune evasion. *Nat. Rev. Microbiol.* 16, 397–409. doi: 10.1038/s41579-018-0019-y
- Binda, E., Marinelli, F., and Marcone, G. L. (2014). Old and new glycopeptide antibiotics: action and resistance. *Antibiotics* 3, 572–594. doi: 10.3390/antibiotics3040572
- Cai, Y. M. (2020). Non-surface attached bacterial aggregates: a ubiquitous third lifestyle. *Front. Microbiol.* 11:557035. doi: 10.3389/fmicb.2020.557035
- Casadevall, A., and Pirofski, L. A. (2000). Host-pathogen interactions: basic concepts of microbial commensalism, colonization, infection, and disease. *Infect. Immun.* 68, 6511–6518. doi: 10.1128/IAI.68.12.6511-6518.2000
- D'Costa, V. M., King, C. E., Kalan, L., Morar, M., Sung, W. W., Schwarz, C., et al. (2011). Antibiotic resistance is ancient. *Nature* 477, 457–461. doi: 10.1038/nature10388
- Ellermann, M., and Sperandio, V. (2020). Bacterial signalling as an antimicrobial target. *Curr. Opin. Microbiol.* 57, 78–86. doi: 10.1016/j.mib.2020.08.001
- Haranahalli, K., Tong, S., and Ojima, I. (2016). Recent advances in the discovery and development of antibacterial agents targeting the cell-division protein FtsZ. *Bioorg. Med. Chem.* 24, 6354–6369. doi: 10.1016/j.bmc.2016.05.003
- Koch, A., Cox, H., and Mizrahi, V. (2018). Drug-resistant tuberculosis: challenges and opportunities for diagnosis and treatment. *Curr. Opin. Pharmacol.* 42, 7–15. doi: 10.1016/j.coph.2018.05.013
- Konreddy, A. K., Rani, G. U., Lee, K., and Choi, Y. (2019). Recent drug-repurposing-driven advances in the discovery of novel antibiotics. *Curr. Med. Chem.* 26, 5363–5388. doi: 10.2174/0929867325666180706101404
- Lam, G. Y., Huang, J., and Brummell, J. H. (2010). The many roles of NOX2 NADPH oxidase-derived ROS in immunity. *Semin. Immunopathol.* 32, 415–430. doi: 10.1007/s00281-010-0221-0
- Marcone, G. L., Binda, E., Berini, F., and Marinelli, F. (2018). Old and new glycopeptide antibiotics: from product to gene and back in the post-genomic era. *Biotechnol. Adv.* 36, 534–554. doi: 10.1016/j.biotechadv.2018.02.009
- Miao, V., Coëffet-LeGal, M. F., Brian, P., Brost, R., Penn, J., Whiting, A., et al. (2005). Daptomycin biosynthesis in *Streptomyces roseosporus*: cloning and analysis of the gene cluster and revision of peptide stereochemistry. *Microbiology* 151, 1507–1523. doi: 10.1099/mic.0.27757-0
- Miller, W. R., Munita, J. M., and Arias, C. A. (2016). Mechanism of action and resistance to daptomycin in *Staphylococcus aureus* and enterococci. *Cold Spring Harb. Perspect. Med.* 6:a026997. doi: 10.1101/cshperspect.a026997
- Otto, M. (2009). *Staphylococcus epidermidis* — the “accidental” pathogen. *Nat. Rev. Microbiol.* 7, 555–567. doi: 10.1038/nrmicro2182
- Payne, D. J., Gwynn, M. N., Holmes, D. J., and Pompliano, D. L. (2007). Drugs for bad bugs: confronting the challenges of antibacterial discovery. *Nat. Rev. Drug Discov.* 6, 29–40. doi: 10.1038/nrd2201
- Rodrigues, M. E., Gomes, F., and Rodrigues, C. F. (2019). *Candida* spp./bacteria mixed biofilms. *J. Fungi* 6:5. doi: 10.3390/jof6010005
- Rohde, M., Püls, J., Buhrdorf, R., Fischer, W., and Haas, R. (2003). A novel sheathed surface organelle of the *Helicobacter pylori* cag type IV secretion system. *Mol. Microbiol.* 49, 219–234. doi: 10.1046/j.1365-2958.2003.03549.x
- Salje, J. (2021). Cells within cells: *Rickettsiales* and the obligate intracellular bacterial lifestyle. *Nat. Rev. Microbiol.* doi: 10.1038/s41579-020-00507-2. [Epub ahead of print].
- Scoffone, V. C., Chiarelli, L. R., Trespidi, G., Mentasti, M., Riccardi, G., and Buroni, S. (2017). *Burkholderia cenocepacia* infections in cystic fibrosis patients: drug resistance and therapeutic approaches. *Front. Microbiol.* 8:1592. doi: 10.3389/fmicb.2017.01592
- Shariati, A., Dadashi, M., Chegini, Z., van Belkum, A., Mirzaii, M., Khoramrooz, S. S., et al. (2020). The global prevalence of Daptomycin, Tigecycline, Quinupristin/Dalfopristin, and Linezolid-resistant *Staphylococcus aureus* and coagulase-negative staphylococci strains: a systematic review and meta-analysis. *Antimicrob. Resist. Infect. Control* 9:56. doi: 10.1186/s13756-020-00714-9
- Sperandio, P., Villa, R., Martorana, A. M., Samalikova, M., Grandori, R., Deho, G., et al. (2011). New insights into the Lpt machinery for lipopolysaccharide transport to the cell surface: LptA-LptC interaction and LptA stability as sensors of a properly assembled transenvelope complex. *J. Bacteriol.* 193, 1042–1053. doi: 10.1128/JB.01037-10
- Surette, M. D., and Wright, G. D. (2017). Lessons from the environmental antibiotic resistome. *Annu. Rev. Microbiol.* 71, 309–329. doi: 10.1146/annurev-micro-090816-093420
- Van Camp, P. J., Haslam, D. B., and Porollo, A. (2020). Prediction of antimicrobial resistance in Gram-negative bacteria from whole-genome sequencing data. *Front. Microbiol.* 11:1013. doi: 10.3389/fmicb.2020.01013
- Vetterli, S. U., Zerbe, K., Müller, M., Urfer, M., Mondal, M., Wang, S., et al. (2018). Thanatin targets the intermembrane protein complex required for lipopolysaccharide transport in *Escherichia coli*. *Sci. Adv.* 4:2634. doi: 10.1126/sciadv.aau2634
- Waglechner, N., McArthur, A. G., and Wright, G. D. (2019). Phylogenetic reconciliation reveals the natural history of glycopeptide antibiotic biosynthesis and resistance. *Nat. Microbiol.* 4, 1862–1871. doi: 10.1038/s41564-019-0531-5
- Wolfmeier, H., Pletzer, D., Mansour, S. C., and Hancock, R. E. W. (2018). New perspectives in biofilm eradication. *ACS Infect. Dis.* 4, 93–106. doi: 10.1021/acsinfectdis.7b00170

Conflict of Interest: The authors declare that the research was conducted in the absence of any commercial or financial relationships that could be construed as a potential conflict of interest.

Copyright © 2021 Marinelli, Alifano, Landini and Visca. This is an open-access article distributed under the terms of the Creative Commons Attribution License (CC BY). The use, distribution or reproduction in other forums is permitted, provided the original author(s) and the copyright owner(s) are credited and that the original publication in this journal is cited, in accordance with accepted academic practice. No use, distribution or reproduction is permitted which does not comply with these terms.



In silico Selection and Experimental Validation of FDA-Approved Drugs as Anti-quorum Sensing Agents

Marta Mellini¹, Elena Di Muzio¹, Francesca D'Angelo^{1†}, Valerio Baldelli¹, Serena Ferrillo¹, Paolo Visca¹, Livia Leoni¹, Fabio Polticelli^{1,2*} and Giordano Rampioni^{1*}

OPEN ACCESS

Edited by:

Rustam Aminov,
University of Aberdeen,
United Kingdom

Reviewed by:

Natalia V. Kirienko,
Rice University, United States
Fadi Soukariéh,
University of Nottingham,
United Kingdom

*Correspondence:

Fabio Polticelli
fabio.polticelli@uniroma3.it
Giordano Rampioni
giordano.rampioni@uniroma3.it

†Present address:

Francesca D'Angelo,
Institut Pasteur, Paris, France

Specialty section:

This article was submitted to
Antimicrobials, Resistance
and Chemotherapy,
a section of the journal
Frontiers in Microbiology

Received: 01 August 2019

Accepted: 27 September 2019

Published: 10 October 2019

Citation:

Mellini M, Di Muzio E, D'Angelo F,
Baldelli V, Ferrillo S, Visca P, Leoni L,
Polticelli F and Rampioni G (2019)
In silico Selection and Experimental
Validation of FDA-Approved Drugs as
Anti-quorum Sensing Agents.
Front. Microbiol. 10:2355.
doi: 10.3389/fmicb.2019.02355

¹ Department of Science, University Roma Tre, Rome, Italy, ² National Institute of Nuclear Physics, Roma Tre Section, Rome, Italy

The emergence of antibiotic resistant bacterial pathogens is increasing at an unprecedented pace, calling for the development of new therapeutic options. Small molecules interfering with virulence processes rather than growth hold promise as an alternative to conventional antibiotics. Anti-virulence agents are expected to decrease bacterial virulence and to pose reduced selective pressure for the emergence of resistance. In the opportunistic pathogen *Pseudomonas aeruginosa* the expression of key virulence traits is controlled by quorum sensing (QS), an intercellular communication process that coordinates gene expression at the population level. Hence, QS inhibitors represent promising anti-virulence agents against *P. aeruginosa*. Virtual screenings allow fast and cost-effective selection of target ligands among vast libraries of molecules, thus accelerating the time and limiting the cost of conventional drug-discovery processes, while the drug-repurposing approach is based on the identification of off-target activity of FDA-approved drugs, likely endowed with low cytotoxicity and favorable pharmacological properties. This study aims at combining the advantages of virtual screening and drug-repurposing approaches to identify new QS inhibitors targeting the *pqs* QS system of *P. aeruginosa*. An *in silico* library of 1,467 FDA-approved drugs has been screened by molecular docking, and 5 hits showing the highest predicted binding affinity for the *pqs* QS receptor PqsR (also known as MvfR) have been selected. *In vitro* experiments have been performed by engineering *ad hoc* biosensor strains, which were used to verify the ability of hit compounds to decrease PqsR activity in *P. aeruginosa*. Phenotypic analyses confirmed the impact of the most promising hit, the antipsychotic drug pimozide, on the expression of *P. aeruginosa* PqsR-controlled virulence traits. Overall, this study highlights the potential of virtual screening campaigns of FDA-approved drugs to rapidly select new inhibitors of important bacterial functions.

Keywords: *Pseudomonas aeruginosa*, anti-virulence strategy, quorum sensing inhibition, pimozide, *in silico* screening, molecular docking, new therapeutics, PqsR

INTRODUCTION

The long-term use of antibiotics has dramatically accelerated the emergence of multi-drug and even pan-drug resistant bacterial pathogens worldwide, leading to an alarming increase of difficult-to-treat infections. This worrying scenario especially concerns the ESKAPE pathogens (*Enterococcus faecium*, *Staphylococcus aureus*, *Klebsiella pneumoniae*, *Acinetobacter baumannii*, *Pseudomonas aeruginosa*, and *Enterobacter* species), a group of bacteria that “escape” the action of almost all available antibiotics (Rice, 2008; Boucher et al., 2009). The trend toward antibiotic resistance is even more alarming if considering that only a handful of new antibiotics have been approved by the U.S. Food and Drug Administration (FDA) in the last decade, with many companies considering the R&D for new antibiotics a less attractive asset compared to more rewarding therapeutic areas. Indeed, *de novo* antibiotic development requires large investments that might not grant an economic reward due to the short commercial lifespan of antibiotics, caused by the rapid emergence of resistance (Ventola, 2015; Mohr, 2016; Luepke et al., 2017).

The awareness about the risk of antibiotic resistance for human health has increased in parallel with our comprehension of bacterial pathobiology, so that virulence mechanisms are now recognized as molecular targets for the development of novel anti-virulence drugs targeting the infection process rather than bacterial growth (Rasko and Sperandio, 2010). Although resistance mechanisms to anti-virulence drugs have been described (Zhu et al., 1998; Hung et al., 2005; Maeda et al., 2012; Imperi et al., 2019), targeting virulence rather than growth is expected to pose a reduced selective pressure for the emergence of resistance (Allen et al., 2014). In particular, *in vitro* evolution experiments indicate that drug resistant clones are counterselected if “public goods” that are shared among members of a bacterial population are targeted (e.g., toxins, exo-proteases, and siderophores) (Mellbye and Schuster, 2011; Vale et al., 2016). Since drug-resistant strains are likely to emerge only if they gain a “private” advantage over the susceptible population, quorum sensing (QS) is recognized as an ideal target for the development of anti-virulence agents. Indeed, QS is an intercellular communication system based on the production, secretion and reception of signal molecules that coordinate the expression of secreted virulence factors in different bacterial pathogens (Rampioni et al., 2014; Kalia et al., 2019).

The ESKAPE pathogen *P. aeruginosa* is a model organism for the development of anti-virulence drugs targeting QS (Soukarieh et al., 2018b). This Gram-negative bacterium, that is one of the most dreaded nosocomial pathogens and the main cause of death in cystic fibrosis (CF) patients, has recently been included by the World Health Organization in the list of pathogens for which new therapeutic options are urgently needed (Priority 1: Critical)¹. The ability of *P. aeruginosa* to cause both acute and chronic infections in different districts of the human body mainly relies on its capacity to adapt to the host by fine-tuning

the expression of a wide array of virulence factors, many of which are QS-controlled. As a consequence, numerous anti-virulence drugs targeting the *P. aeruginosa* QS circuitry have been identified in recent years, and their ability to reduce *P. aeruginosa* pathogenicity has been confirmed both *in vitro* and *in vivo* (Rampioni et al., 2014; Soukarieh et al., 2018b). Unfortunately, the majority of the QS inhibitors identified to date are not suitable as lead-like compounds for further drug development, mainly due to their cytotoxicity and unfavorable pharmacological properties (Maura et al., 2016; Soukarieh et al., 2018b).

With the aim to identify bioavailable and safe QS inhibitors that can faster move into clinical trials or serve as leads for drug optimization programs, our group recently undertook whole-cell biosensor-based screening campaigns of libraries of FDA-approved drugs. This drug-repurposing approach led to the identification of niclosamide, an anthelmintic drug, and clofocetol, an antibiotic active against Gram-positive bacteria, as potent and safe QS inhibitors targeting the acyl-homoserine lactones (AHL)-based and the 2-alkyl-4(1H)quinolone (AQ)-based QS systems of *P. aeruginosa*, respectively (Imperi et al., 2013; D’Angelo et al., 2018). These FDA-approved drugs effectively reduced *P. aeruginosa* pathogenic potential in animal models of infection, hence representing promising candidates for preclinical studies.

In the last decades *in silico* approaches have been proved as valid aids to conventional drug-discovery programs. In particular, virtual screens carried out through molecular docking simulations allow to preselect promising drug candidates in vast libraries of molecules, so that only a reduced number of predicted hits have to be validated by means of *in vitro* experiments. In this way, time and costs associated to conventional screening campaigns are reduced. In addition, docking simulations allow to predict the likely binding mode of candidate hits onto the selected target, providing a molecular basis for their optimization in terms of binding affinity (Reuter et al., 2015).

On this basis, the present study aims at combining the advantages of drug-repurposing and virtual screening approaches to identify FDA-approved drugs targeting the *pqs* QS system of *P. aeruginosa* via *in silico* molecular docking.

In *P. aeruginosa* the *pqs* QS system is based on the AQs 2-heptyl-4-hydroxyquinoline (HHQ) and 2-heptyl-3-hydroxy-4(1H)-quinolone (PQS) as signal molecules. HHQ is synthesized by the enzymes coded by the *pqsABCDE-phnAB* operon, and is converted to PQS by the monooxygenase PqsH. Both HHQ and PQS can bind to and activate the transcriptional regulator PqsR (also known as MvfR), that in the active form binds to the *PpqsA* promoter region and promotes *pqsABCDE-phnAB* transcription. Hence, HHQ and PQS act as autoinducers to accelerate their own synthesis (Bredenbruch et al., 2005; Heeb et al., 2011; Dulcey et al., 2013; Drees and Fetzner, 2015). While the main role of HHQ is to trigger this PqsR-dependent positive feedback loop, the signal molecule PQS and the protein PqsE (the latter coded by the fifth gene of the *pqsABCDE-phnAB* operon) are the main effectors of the *pqs* QS system. Besides activating PqsR, PQS acts as an iron chelator, is required for the biogenesis of outer membrane vesicles, and promotes the expression of virulence genes via a PqsR-independent pathway (Bredenbruch et al., 2005; Mashburn and Whiteley, 2005; Diggle et al., 2007; Rampioni et al.,

¹ <http://www.who.int/en/news-room/detail/27-02-2017-who-publishes-list-of-bacteria-for-which-new-antibiotics-are-urgently-needed>

2016; Lin et al., 2017). PqsE is a multifunctional protein that participates in the synthesis of HHQ and positively controls the expression of multiple virulence factors independently of AQs, likely by activating the transcriptional regulator RhlR *via* the production of an uncharacterized signal molecule that links the *pqs* and *rhl* QS systems (Drees and Fetzner, 2015; Hazan et al., 2010; Rampioni et al., 2010; Rampioni et al., 2016; Mukherjee et al., 2018). Overall, the production of PQS and the expression of PqsE require activated PqsR, and consequently PqsR-inhibitors have been shown to attenuate *P. aeruginosa* virulence both *in vitro* and in animal models of infection (Klein et al., 2012; Ilangovan et al., 2013; Zender et al., 2013; Lu et al., 2014; Starkey et al., 2014; Maura and Rahme, 2017; Maura et al., 2017; D'Angelo et al., 2018; Soukarieh et al., 2018a). Since the three-dimensional structure of the PqsR domain that interacts with HHQ and PQS (co-inducer binding domain; CBD) has recently been solved (Ilangovan et al., 2013; Kitao et al., 2018), this QS transcriptional regulator now constitutes an ideal target for the identification of new *P. aeruginosa* anti-virulence drugs *via* molecular docking simulations.

In this study, a virtual screening approach has been used to predict PqsR ligands in a library of 1,467 FDA-approved drugs. The ability of the best 5 hits to decrease *PpqsA* activity and AQs level has been tested in wild type *P. aeruginosa* and in *ad hoc* engineered strains. This process led to the identification of the antipsychotic drug pimozide as a specific PqsR inhibitor. Phenotypic assays showed that pimozide hampers the expression of PqsR-controlled virulence traits, such as the production of the virulence factor pyocyanin, swarming motility and biofilm formation, and docking simulations suggest a possible competition with native AQs for PqsR binding. These results provide a proof-of-concept that the drug-repurposing and virtual screening approaches can be combined to accelerate the selection of anti-QS molecules among FDA-approved drugs.

MATERIALS AND METHODS

Bacterial Strains, Media and Chemicals

Bacterial strains used in this study are reported in Table 1. Bacterial strains were routinely grown at 37°C in Luria-Bertani (LB) broth in shaking conditions, or in LB supplemented with 15 g/L agar.

When required, tetracycline (Tc; 200 µg/mL), isopropyl β-D-1-thiogalactopyranoside (IPTG), dimethyl sulfoxide (DMSO), or synthetic PQS were added to the medium. IPTG, DMSO and synthetic PQS were used at the concentrations indicated in the text. Synthetic PQS stock solution was prepared in MeOH at 20 mM concentration (synthetic PQS was kindly provided by Paul Williams and Miguel Cámara – University of Nottingham, United Kingdom). Ergotamine and pimozide were available in our laboratory as drugs of the PHARMAKON library (10 mM stock solutions in DMSO). Dutasteride, eltrombopag and conivaptan were purchased from Sigma-Aldrich, Carbosynth Ltd., and MCE Medchem Express, respectively, and dissolved in DMSO at 10 mM concentration. Pimozide was also purchased

TABLE 1 | Bacterial strains used in this study.

<i>P. aeruginosa</i> strains	Characteristics	References
PAO1	Nottingham collection wild type strain.	
PAO1 pMRP9-1	PAO1 wild type strain carrying a pMRP9 derivative for constitutive expression of GFP; Ap ^R /Cb ^R .	D'Angelo et al., 2018
Δ <i>pqsR</i>	PAO1 mutant strain with in frame clear deletion of the <i>pqsR</i> gene.	Rampioni et al., 2010
Δ <i>pqsR</i> pMRP9-1	PAO1 mutant strain with in frame clear deletion of the <i>pqsR</i> gene carrying a pMRP9 derivative for constitutive expression of GFP; Ap ^R /Cb ^R .	D'Angelo et al., 2018
PAO1 <i>PpqsA::lux</i>	PAO1 wild type strain carrying chromosomal insertion of the <i>PpqsA::lux</i> transcriptional fusion; Tc ^R .	Fletcher et al., 2007
Δ <i>pqsA</i> <i>PpqsA::lux</i>	PAO1 mutant strain deleted in <i>pqsA</i> gene carrying chromosomal insertion of the <i>PpqsA::lux</i> transcriptional fusion; Tc ^R (named AQ-Rep).	Diggle et al., 2007
Δ <i>pqsA</i> mini-CTX:: <i>lux</i>	PAO1 mutant strain deleted in <i>pqsA</i> gene carrying chromosomal insertion of the mini-CTX:: <i>lux</i> empty vector; Tc ^R (named C-Rep).	D'Angelo et al., 2018
Δ <i>pqsR</i> (pFD- <i>pqsABCD</i>)	PAO1 mutant strain with in frame clear deletion of the <i>pqsR</i> gene, carrying the pFD- <i>pqsABCD</i> plasmid for PqsR-independent production of AQs; Km ^R .	D'Angelo et al., 2018
Δ <i>pqsAHR</i> <i>PpqsA::lux</i> (pPqsR-6H)	PAO1 triple mutant strain deleted in <i>pqsA</i> , <i>pqsH</i> and <i>pqsR</i> genes carrying chromosomal insertion of the <i>PpqsA::lux</i> transcriptional fusion and the pPqsR-6H plasmid for IPTG-inducible expression of PqsR; Tc ^R .	Ilangovan et al., 2013

from Sigma-Aldrich for further analyses, and dissolved in DMSO at 40 mM concentration.

Virtual Screening *via* Molecular Docking

Molecular docking simulations were carried out using DockingApp (Di Muzio et al., 2017), a user friendly interface to the molecular docking program AutoDock Vina (Trott and Olson, 2010), on 1,467 FDA-approved molecules extracted from the DrugBank Database and provided in ready-to-dock format as part of the DockingApp package. DockingApp is a freely available platform-independent application to perform docking simulations and virtual screening using AutoDock Vina. An intuitive graphical user interface facilitates the input phase while an embedded Jmol applet allows to visualize and analyse the results. The application comes with the DrugBank set of ready-to-dock FDA-approved drugs for virtual screening and drug-repurposing purposes. In all simulations, the search space (docking grid) included the whole PqsR co-inducer binding domain (CBD) structure, in order to carry out “blind” predictions of the “hit” compounds binding sites. Simulations were first carried out on the apo form of the protein (PDB ID: 4JVC) (Ilangovan et al., 2013), by keeping all protein

residues rigid. The ten best-ranking compounds, according to the AutoDock Vina scoring function, were then selected for a refinement round in which molecular docking simulations were carried out allowing flexibility of the residues building up the PqsR binding pocket (*i.e.*, Ile149, Ala168, Val170, Ile186, Leu189, Leu207, Leu208, Phe221, Ile236, Tyr258, Asp264, and Thr265) (Ilangoan et al., 2013). The results of docking simulations were analyzed using the molecular graphics program UCSF-Chimera, version 1.12 (Pettersen et al., 2004).

Bioluminescence Assay

Analyses of PqsR activity in the presence of potential inhibitors has been performed by using *ad hoc* engineered reporter systems in which bioluminescence emission is proportional to PqsR activity.

The primary screening for potential PqsR inhibitors was performed as previously described (D'Angelo et al., 2018). Briefly, the screening was based on the co-culture of *P. aeruginosa* PAO1 wild type (PAO1) and the reporter strain PAO1 $\Delta pqsA$ *PpqsA::lux* (AQ-Rep). PAO1 and AQ-Rep were grown for 16 h at 37°C with shaking (200 rpm) in LB broth or in LB broth supplemented with 200 μ g/L Tc, respectively. After growth, PAO1 and AQ-Rep were washed with sterile saline and mixed into LB broth to a final OD₆₀₀ of 0.03 and 0.1, respectively (wild type/reporter ratio \approx 1/3). Two-hundred μ L aliquots of the diluted co-cultures were dispensed into 96-wells black clear-bottom microtiter plates. All compounds used in the primary screening were dissolved in DMSO to 10 mM concentration. The compounds were added to the microtiter plates containing the co-cultures at the final concentrations of 20 and 200 μ M. As untreated controls, the same amount of DMSO alone as in the treated samples was added to the microtiter wells containing the co-culture.

For further analysis with pimozide from Sigma-Aldrich, 100 μ L LB-grown aliquots of the PAO1/AQ-Rep co-culture (OD₆₀₀ = 0.06 and 0.2, respectively) or of other reporter systems indicated in the text (OD₆₀₀ = 0.02) were dispensed into 96-wells black clear-bottom microtiter plates, and 100 μ L of pimozide diluted in LB at concentrations ranging from 50 to 400 μ M were added to each well. Also in this case, DMSO alone was used as a control.

For all light emission assays, plates were incubated at 37°C with shaking (120 rpm) for 5 h, and then light emission (RLU) and cell density (OD₆₀₀) of the reporter system were recorded by using an automated Spark 10 M luminometer-spectrophotometer (Tecan). Reporter activity was evaluated as Relative Light Units (RLU) normalized to cell density (OD₆₀₀). Alteration in promoter activity induced by the tested compounds was determined by comparing the promoter activity of the specific biosensor system in untreated and treated samples.

Quantification of AQs

AQ signal molecules in *P. aeruginosa* PAO1 culture supernatants were quantified as previously described (Fletcher et al., 2007). PAO1 wild type cultures were grown at 37°C in 96-well microtiter plates with shaking (120 rpm) in LB broth supplemented with the tested compounds or solvent vehicle (*i.e.*, DMSO) as a control. After 7 h of incubation, cell-free supernatants of PAO1 wild type

cultures were collected and 5 μ L were added to 195 μ L of the AQ-Rep biosensor (OD₆₀₀ = 0.1) dispensed into 96-wells black clear-bottom microtiter plates. Plates were incubated for 5 h at 37°C with shaking (120 rpm), and light emission (RLU) and cell density (OD₆₀₀) of the cultures were recorded by using an automated Spark 10 M luminometer-spectrophotometer (Tecan). A calibration curve was generated by growing the AQ-Rep biosensor strain with synthetic PQS at concentrations ranging from \sim 45 nM to 300 μ M. The resulting dose-response curve was used as a landmark to determine the concentration of the AQs in each culture supernatant.

Pyocyanin Production, Swarming Motility and Biofilm Formation Assays

The assay for pyocyanin extraction and quantification has been performed as previously described (Essar et al., 1990) on PAO1 wild type and PAO1 $\Delta pqsR$ strains. Bacterial strains were grown for 16 h at 37°C with shaking (200 rpm) in LB broth in the presence of 100 μ M pimozide or 0.25% (v/v) DMSO (solvent vehicle control).

Swarming motility assays were performed on PAO1 wild type and PAO1 $\Delta pqsR$ by using swarming plates [0.8% (w/v) nutrient broth N.2, 0.5% (w/v) glucose, 0.5% (w/v) bacteriological agar] (Rampioni et al., 2009). Plates were supplemented with 100 μ M pimozide or 0.25% (v/v) DMSO (solvent vehicle control). Swarming motility was directly observed at the air-agar interface after 16 h of incubation at 37°C.

The biofilm formation assay was performed in eight-well chamber slides as previously described (Jurcisek et al., 2011; D'Angelo et al., 2018), with minor modifications. Briefly, PAO1 wild type and PAO1 $\Delta pqsR$ constitutively expressing GFP *via* the pMRP9-1 plasmid (Davies et al., 1998) were inoculated in an eight-well chamber slide at an OD₆₀₀ of 0.02 in 700 μ L of M9 minimal medium supplemented with 20 mM glucose as carbon source, in the presence of 0.25% (v/v) DMSO (solvent vehicle control) or 100 μ M pimozide. Bacterial cultures were incubated at 30°C for 24 h. Planktonic cells were gently removed and the wells of the chamber slide were rinsed with sterile saline before confocal microscope (Leica TCS SP5) imaging of the bacterial cells adhered to the glass surface.

Statistical Analysis

For statistical analysis the software GraphPad Prism 5 was used; one-way analysis of variance (ANOVA) followed by Tukey-Kramer multiple comparison tests were performed. Differences having a *p* value < 0.05 were considered statistically significant.

RESULTS

Virtual Screening for the Identification of FDA-Approved PqsR Ligands

We performed a virtual screening to select possible PqsR ligands in a library of 1,467 FDA-approved compounds extracted from the DrugBank database² and already provided in ready-to-dock

²<https://www.drugbank.ca/>

format as part of the DockingApp software package (see section “Materials and Methods,” for details).

PqsR is a multi-domain transcriptional regulator composed by a *N*-terminal helix-turn-helix DNA-binding domain and a *C*-terminal co-inducer binding domain (CBD). Since the three-dimensional structure of full-length PqsR is unavailable, molecular docking simulations were performed based on the crystal structure of PqsR-CBD. The CBD of PqsR has been crystallized in the apo form (PDB ID: 4JVC) or as a complex with the native AQ ligand 2-nonyl-4-hydroxy-quinoline (NHQ) (PDB ID: 4JVD) or with the quinazolinone (QZN) inhibitor 3-NH₂-7Cl-C9-QZN (PDB ID: 4JVI) (Ilangovan et al., 2013). It has been shown that both the native ligand and the inhibitor bind to the CBD of PqsR in a site consisting of two adjacent pockets: the quinolone ring is accommodated in pocket B, while the aliphatic chain makes hydrophobic interactions with pocket A (Ilangovan et al., 2013). More recently, the benzamide-benzimidazole inhibitor M64 was shown to bind to PqsR-CBD in a similar way as NHQ and 3-NH₂-7Cl-C9-QZN, with its benzimidazole group bound in pocket B and the phenoxy group occupying pocket A (PDB ID: 6B8A; Kitao et al., 2018). To avoid selection bias, molecular docking simulations were performed on the apo form of PqsR-CBD. In addition, to increase the reliability of the simulations, the docking search space was not restricted to the A and B binding pockets, but extended to the entire PqsR-CBD, *i.e.*, a “blind” docking procedure was carried out. To speed up the process, the initial screening of the 1,467 FDA-approved compounds was carried out by keeping all amino acid residues rigid.

Possible PqsR ligands were ranked based on the predicted binding affinity calculated with the AutoDock Vina scoring function. In the case of multiple ligands with the same binding affinity, these were prioritized based on the size-independent ligand efficiency (SILE) coefficient. SILE is a normalized parameter derived from the ligand efficiency (LE), a predictive measure of the *per*-atom binding affinity of a ligand to its binding partner (Kuntz et al., 1999).

Following the above procedure, the ten best-ranking putative PqsR ligands (predicted binding affinity ranging from -11.2 to -10.0 kcal/mol) were selected for a second round of molecular docking simulations in which residues previously reported to be involved in the binding of the natural ligand NHQ to the PqsR-CBD (Ilangovan et al., 2013) were considered flexible (see section “Materials and Methods,” for details). The five molecules predicted to display the highest affinity to PqsR-CBD with fixed residues ranked in the first five positions also in the analysis with flexible residues, and are listed in **Table 2**. Conivaptan is a non-peptide inhibitor of the vasopressin receptor subtypes V1a and V2, commonly used to treat euvolemic and hypervolemic hyponatremia (Ferguson-Myrthil, 2010); ergotamine is an alkaloid acting as a serotonin agonist with vasoconstrictor and analgesic properties (Saxena and De Deyn, 1992); eltrombopag, an agonist of the thrombopoietin physiological target, is used for the treatment of thrombocytopenia (McCormack, 2015); pimozide is an antipsychotic drug used to treat schizophrenia, chronic psychosis, Tourette’s syndrome, and resistant tics (Tueth

and Cheong, 1993); dutasteride is a 5 α -reductase inhibitor used to treat benign prostatic hyperplasia (Azzouni and Mohler, 2012).

Superimposition of the five PqsR-ligand molecular complexes obtained by docking simulations with the crystal structure of the PqsR-NHQ complex (PDB ID: 4JVD) (Ilangovan et al., 2013) predicts that all the five ligands bind in the NHQ binding site, interacting with residues building up the A and B pockets of PqsR-CBD, as observed for the natural ligand NHQ (**Figure 1**).

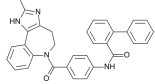
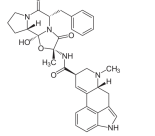
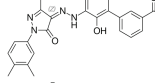
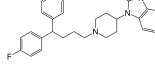
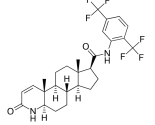
Anti-QS Activity of the Predicted PqsR Ligands

To validate the ability of the predicted PqsR ligands to inhibit PqsR activity in *P. aeruginosa*, the best 5 hits were tested for their ability to reduce bioluminescence in a co-culture system based on wild type *P. aeruginosa* PAO1 (Nottingham collection; herein referred to as PAO1) and isogenic *P. aeruginosa* PAO1 $\Delta pqsA$ *PpqsA::lux* (named AQ-Rep) (Fletcher et al., 2007; D’Angelo et al., 2018). The AQ-Rep biosensor strain is unable to synthesize HHQ and PQS signal molecules as a consequence of *pqsA* mutation, and it carries single-copy chromosomal insertion of a transcriptional fusion between the PqsR-activated promoter *PpqsA* and the *luxCDABE* operon for light emission. Therefore, in the PAO1/AQ-Rep co-culture the Aqs produced by PAO1 activate PqsR in AQ-Rep, and consequently promote bioluminescence; hence, a PqsR inhibitor is expected to reduce light emission in this reporter system. The use of the PAO1/AQ-Rep co-culture recently allowed the identification of new PqsR inhibitors (D’Angelo et al., 2018), thus proving its efficacy for the selection of anti-virulence drugs targeting the *pqs* QS system. A co-culture of PAO1 and of a $\Delta pqsA$ derivative strain carrying the mini-CTX::*lux* empty vector for constitutive light emission (named C-Rep) was used to discriminate between molecules targeting PqsR and molecules affecting light emission in a PqsR-independent way.

The PAO1/AQ-Rep co-culture was incubated with the predicted PqsR-ligands identified *via* the preliminary virtual screening: conivaptan, ergotamine, eltrombopag, pimozide, and dutasteride. Molecules were tested at 20 μ M and 200 μ M concentrations. Since these drugs were dissolved in DMSO, solvent vehicle control samples in which 0.2% or 2% DMSO alone was added were also analyzed. To ensure specificity, the predicted ligands of PqsR were also analyzed by using the PAO1/C-Rep control co-culture. For each predicted ligand, the residual reporter activity (RLU/OD₆₀₀) was calculated by comparing the reporter activity of the culture grown in the presence of the tested molecule to the reporter activity of the same culture grown in the presence of solvent vehicle, considered as 100%.

As reported in **Table 3**, 200 μ M ergotamine, eltrombopag and pimozide were able to reduce light emission in the PAO1/AQ-Rep co-culture system by 27.9, 30.4, and 46.3%, respectively, while conivaptan and dutasteride did not affect reporter activity. However, 200 μ M eltrombopag reduced light emission also in the PAO1/C-Rep control co-culture system (38.5% reduction), suggesting PqsR-independent light inhibition, while ergotamine and pimozide did not significantly alter light emission in the control samples. Notably, ergotamine and

TABLE 2 | Putative FDA-approved ligands of PqsR-CBD identified via molecular docking.

Drug name and property	Structure	ΔDG^a
Conivaptan: vasopressin receptors V1a and V2 inhibitor, used for the treatment of euvolemic and hypervolemic hyponatremia		-14.3 (-10.7)
Ergotamine: Alkaloid vasoconstrictor used as analgesic		-12.3 (-10.7)
Eltrombopag: Agonist of the Tpo receptor for the treatment of chronic thrombocytopenia		-12.1 (-10.6)
Pimozide: Blocker of dopaminergic receptors used as antipsychotic drug		-12.0 (-10.9)
Dutasteride: Oxo-steroid 5- α -reductase inhibitor for the treatment of benign prostatic hyperplasia		-11.3 (-11.2)

^a ΔG values (kcal/mol) for drugs binding to the PqsR-CBD apo form (PDB ID: 4JVC; Ilangovan et al., 2013) with flexible residues, predicted by the AutoDock Vina scoring function; the ΔG values (kcal/mol) in parenthesis refer to the affinity of the same molecules for the PqsR-CBD obtained in docking simulations with fixed residues.

pimozide reduced reporter activity at 20 μ M concentration (10.1 and 12.3% reduction, respectively), and none of the tested drugs significantly altered *P. aeruginosa* cell density (data not shown). Since ergotamine and pimozide were effective in specifically reducing light emission in the PAO1/AQ-Rep co-culture, without altering bacterial growth, these molecules were selected for further investigations.

A secondary screening was performed investigating the ability of ergotamine and pimozide to affect the production of the signal molecules AQs. To this end, PAO1 was grown in LB supplemented with ergotamine or pimozide (20 μ M and 200 μ M) or with DMSO, as a control. The amount of AQs in the corresponding cell-free supernatants was evaluated by using the AQ-Rep biosensor strain, in which light emission is proportional to the amount of AQs present in the medium. As shown in Table 3, ergotamine slightly decreased the level of AQs at both 20 μ M and 200 μ M (4.7 and 6.2% reduction, respectively), while pimozide reduced the production of these QS signal molecules of 15.1% and 49.5% at 20 μ M and 200 μ M, respectively.

Pimozide Inhibits the *pqs* QS System and PqsR-Controlled Virulence Traits

According to the primary and secondary screenings (Table 3) pimozide from the PHARMAKON library reduced *PpqsA* activity in the co-culture system PAO1/AQ-Rep and AQs production in PAO1, without altering bacterial growth. To confirm these data, experiments were replicated with pimozide purchased from a different vendor (Sigma-Aldrich).

Growth curves reported in Figure 2A show that up to 400 μ M pimozide does not alter the growth profile of PAO1. Data

reported in Figure 2B confirmed that pimozide significantly reduces light emission in the PAO1/AQ-Rep co-culture in a dose-dependent manner. In detail, 100 μ M, 200 μ M and 400 μ M pimozide significantly reduced PAO1/AQ-Rep activity of 30.1, 45.2, and 64.7%, respectively (Figure 2B, white bars). Hence, the decrease in light emission from the co-culture system was comparable to what previously observed for 200 μ M pimozide in the primary screening (reduction of PAO1/AQ-Rep activity = 46.3%; Table 3). Conversely, pimozide did not affect bioluminescence in the PAO1/C-Rep control system up to 400 μ M (Figure 2B, gray bars).

Pimozide was effective in reducing the activity of the PqsR-controlled *PpqsA* promoter in a dose-dependent manner also in PAO1 wild type, with reductions in bioluminescence emission of 17.6%, 33.1 and 45.5% for pimozide concentrations of 100 μ M, 200 μ M, and 400 μ M, respectively (Figure 2C, white bars).

To validate the results of the secondary screening, PAO1 was grown in the absence or in the presence of pimozide at different concentrations, and AQ levels were measured in cell-free supernatants by means of the AQ-Rep biosensor strain. In these conditions, pimozide significantly decreased AQ production in a dose-dependent manner only at 200 μ M (22.9% reduction) and 400 μ M (33.8% reduction) (Figure 2C, gray bars).

Due to its ability to hamper the *pqs* QS signaling system, pimozide is expected to reduce the expression of *pqs*-controlled virulence traits, such as pyocyanin production, swarming motility and biofilm formation. As shown in Figure 3A, 100 μ M pimozide reduced pyocyanin production in PAO1 (24.8% reduction of pyocyanin level in pimozide-treated cultures relative to the control sample supplemented with the solvent vehicle DMSO). Moreover, exposure to 100 μ M pimozide significantly altered the

swarming motility phenotype by abolishing dendrites formation (**Figure 3B**) and reduced biofilm formation in a PAO1 strain constitutively expressing GFP (**Figure 3C**). Despite exerting a milder effect, the inhibition exerted by pimozide on the tested phenotypes in wild type PAO1 mimicked *pqsR* deletion ($\Delta pqsR$

isogenic strain; **Figure 3**), thus supporting the hypothesis that PqsR is the likely target of pimozide.

Validation of the Molecular Mechanism of Action of Pimozide

The inhibitory activity exerted by pimozide on *PpqsA* activity, combined with the reduction of AQs level and attenuation of *pqs*-dependent virulence traits, does not allow to rule out the possibility that pimozide affects AQs biosynthesis instead of, or in addition to, AQs reception by PqsR. To tackle this issue, the effect of pimozide on *PpqsA* promoter activity has been tested in the AQ-Rep biosensor strain grown in the presence of 5 μ M synthetic PQS. As shown in **Figure 4A**, pimozide reduced *PpqsA* activity also in this experimental setting, in which the AQ molecule PQS required to activate PqsR is not endogenously produced by PAO1. Secondly, AQs production was measured in a PAO1 $\Delta pqsR$ mutant strain carrying the pFD-*pqsABCD* plasmid for constitutive expression of the AQs biosynthetic enzymes. In this genetic background, in which AQ synthesis is PqsR-independent, pimozide did not reduce AQ levels (**Figure 4B**), indicating that this drug does not affect the activity of the AQs biosynthetic enzymes. Taken together, these experiments indicate that pimozide targets the PqsR-dependent AQs response rather than AQs biosynthesis.

To further support target specificity, the effect of pimozide on *PpqsA* activity was evaluated in a *P. aeruginosa* recombinant strain with tunable levels of PqsR, named PAO1 $\Delta pqsAHR$ *PpqsA::lux* (pPqsR-6H). This strain carries the *PpqsA::lux* transcriptional fusion and deletion of the *pqsA*, *pqsH* and *pqsR* genes, therefore it does not synthesize AQs and does not produce the native PqsR regulator, which can be expressed upon IPTG induction *via* the pPqsR-6H plasmid. Therefore, in the absence of IPTG and in the presence of synthetic PQS, the PAO1 $\Delta pqsAHR$ *PpqsA::lux* (pPqsR-6H) strain should express basal level of active PqsR, and the effect of a PqsR inhibitor on *PpqsA* activity should be maximal due to target paucity. Conversely, increasing concentrations of IPTG in the presence of synthetic PQS should result in increased levels of active PqsR, thus reducing the effect of PqsR inhibitors due to increased target abundance. As shown in **Figure 4C**, in this recombinant strain the repressive effect exerted

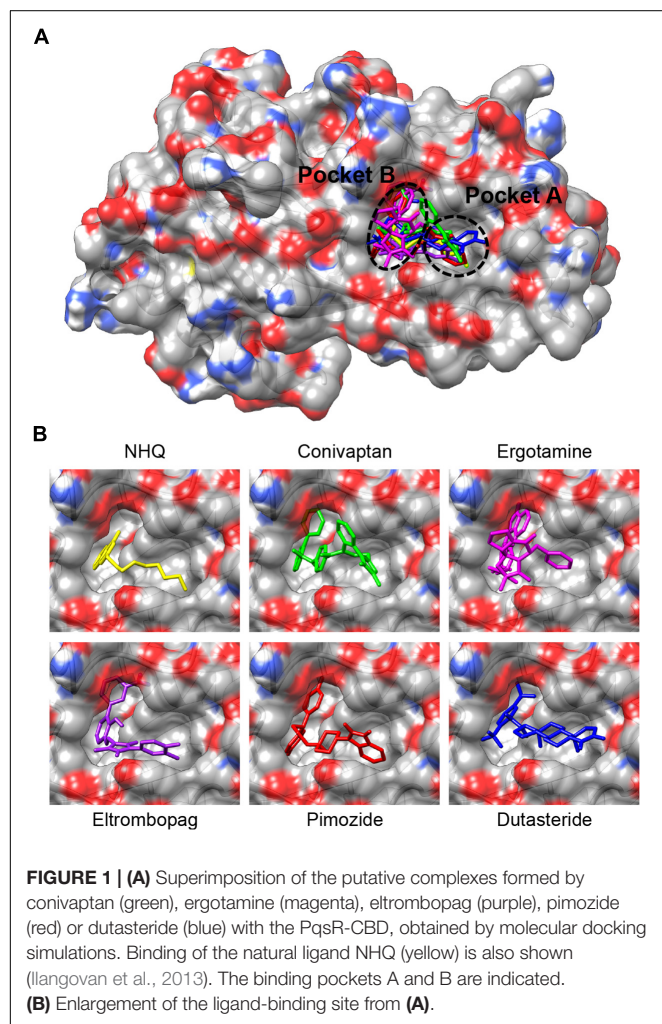
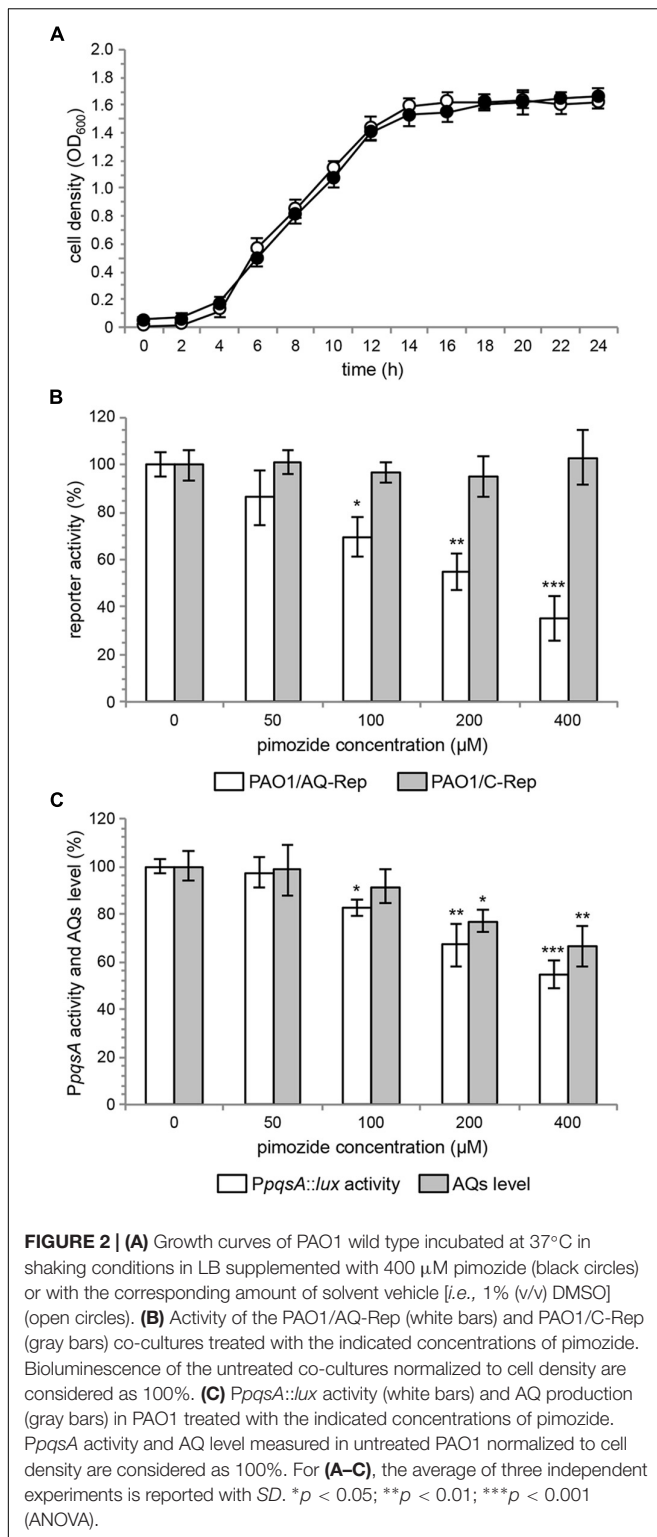


TABLE 3 | Primary and secondary screenings.

Drug name	Residual reporter activity (%) ^a		Residual AQ production (%) ^b	
	20 μ M	200 μ M	20 μ M	200 μ M
Conivaptan	103.7 (103.1)	100.5 (95.6)	n.d.	n.d.
Ergotamine	89.9 (99.8)	72.1 (98.3)	95.3	93.8
Eltrombopag	99.4 (109.7)	69.6 (61.5)	n.d.	n.d.
Pimozide	87.7 (109.9)	53.7 (99.4)	84.9	50.5
Dutasteride	105.9 (102.4)	111.2 (98.7)	n.d.	n.d.

^aThe first value refers to the residual reporter activity of the PAO1/AQ-Rep reporter system treated with 20 μ M or 200 μ M of the indicated drug relative to the untreated sample (in this case the same amount of DMSO was used as control). The second value, in brackets, refers to the residual reporter activity of the PAO1/C-Rep control coculture in the same conditions. Activity of the reporter systems in untreated samples are considered as 100%. The average of three independent experiments is reported.

^bResidual production of AQ molecules in *P. aeruginosa* PAO1 cultures treated with 20 μ M or 200 μ M of the indicated drug relative to the untreated sample (also in this case DMSO was used as control). AQ levels measured in untreated samples are considered as 100%. The average of three independent experiments is reported. n.d., not determined.



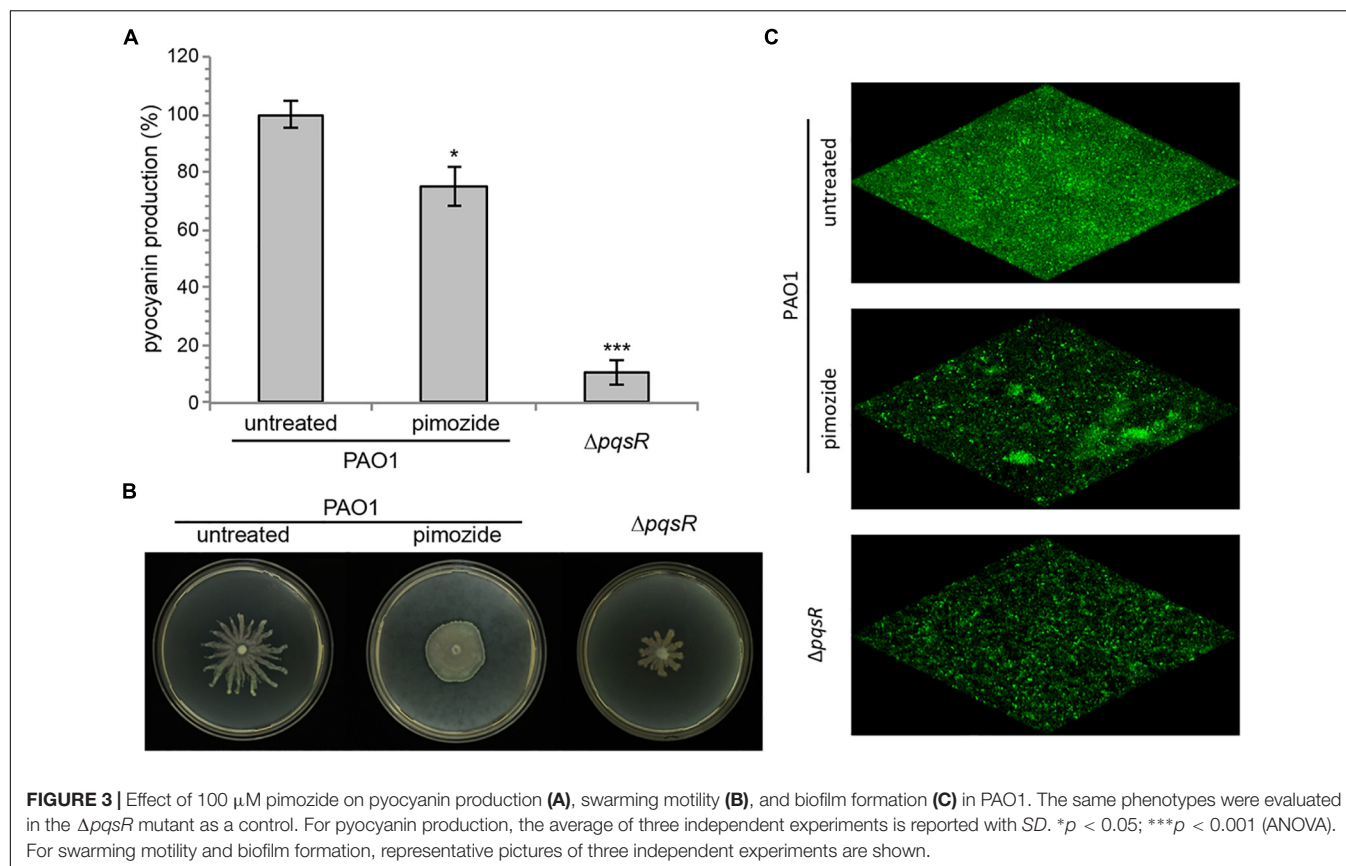
by 100 μ M pimozide on *PpqsA* activity was apparent only for IPTG concentrations ≤ 10 μ M, while pimozide had no significant effect on the *PpqsA* promoter for IPTG concentrations ≥ 20 μ M. These observations support the hypothesis that pimozide is a ligand and an inhibitor of PqsR.

As shown in **Figure 5**, pimozide is predicted to bind to the PqsR CBD establishing mainly hydrophobic interactions that closely match those of the natural ligand NHQ (Ilangovan et al., 2013), at least as far as pocket A is concerned. Slightly different interactions are instead observed in pocket B, likely due to a rearrangement of the pocket residues needed to accommodate the bulkier bis(fluorophenyl) moiety of pimozide. Interestingly, pimozide binding to pocket A is predicted to be stabilized also by a π -stacking interaction between the drug benzimidazole group and the Tyr258 aromatic ring (**Figure 5**, bottom panel), an interaction that mimics the π -stacking interaction experimentally observed between the phenoxy group of the PqsR competitive inhibitor M64 and Tyr258 (Kitao et al., 2018).

DISCUSSION

Anti-virulence drugs that do not affect bacterial growth hold promise as new therapeutic agents since they are expected to decrease bacterial adaptability to the host environment and to pose a reduced selective pressure for the emergence of resistance with respect to antibiotics. Moreover, virulence mechanisms are often pathogen-specific, thus anti-virulence drugs could avoid dysbiosis usually associated to antibiotic treatments (Rampioni et al., 2014, 2017; Monserrat-Martinez et al., 2019).

The *pqs* QS system controls the expression of multiple virulence factors and biofilm formation, so that *P. aeruginosa* mutants defective in the *pqs* QS system display attenuated pathogenicity in different plant and animal models of infection (Cao et al., 2001; Déziel et al., 2005; Xiao et al., 2006; Lesic et al., 2007; Rampioni et al., 2010; Dubern et al., 2015). Notably, the *pqs* QS system is active during the infection (Collier et al., 2002; Barr et al., 2015), and while *P. aeruginosa* mutants impaired in the *las* QS system are frequently isolated from CF patients (Hoffman et al., 2009; Feltner et al., 2016), the highest proportion of *P. aeruginosa* strains isolated from CF lung are proficient for AQs production (Guina et al., 2003; Jiricny et al., 2014). Moreover, AQ-based QS systems have not been described in the human microbiota so far, suggesting that drugs targeting PqsR should exert a limited effect on the host microbiota. Intriguingly, recent reports indicate that the *pqs* QS system might contribute to the RhlR-dependent activation of virulence genes in the absence of functional LasR (Chen et al., 2019; Kostylev et al., 2019), and that this compensatory role might involve a yet uncharacterized signal molecule produced by PqsE and perceived by RhlR in addition to C4-HSL (Mukherjee et al., 2018). Therefore, by hampering PqsE expression, PqsR inhibitors would impact on virulence factors controlled by both the *pqs* and the *rhl* QS systems, and could be particularly active against *las*-deficient strains emerging during chronic infection in CF patients. On this basis, many inhibitors of the *pqs* QS system have been described in the last decade, proving the ability of anti-*pqs* drugs to reduce the expression of *P. aeruginosa* virulence traits both *in vitro* and in animal models of infection (Calfee et al., 2001; Lesic et al., 2007; Klein et al., 2012; Storz et al., 2012; Ilangovan et al., 2013; Sahner et al., 2013; Weidel et al., 2013; Zender et al., 2013; Lu et al., 2014; Starkey et al., 2014; Sahner et al., 2015; Ji et al., 2016; Thomann et al.,



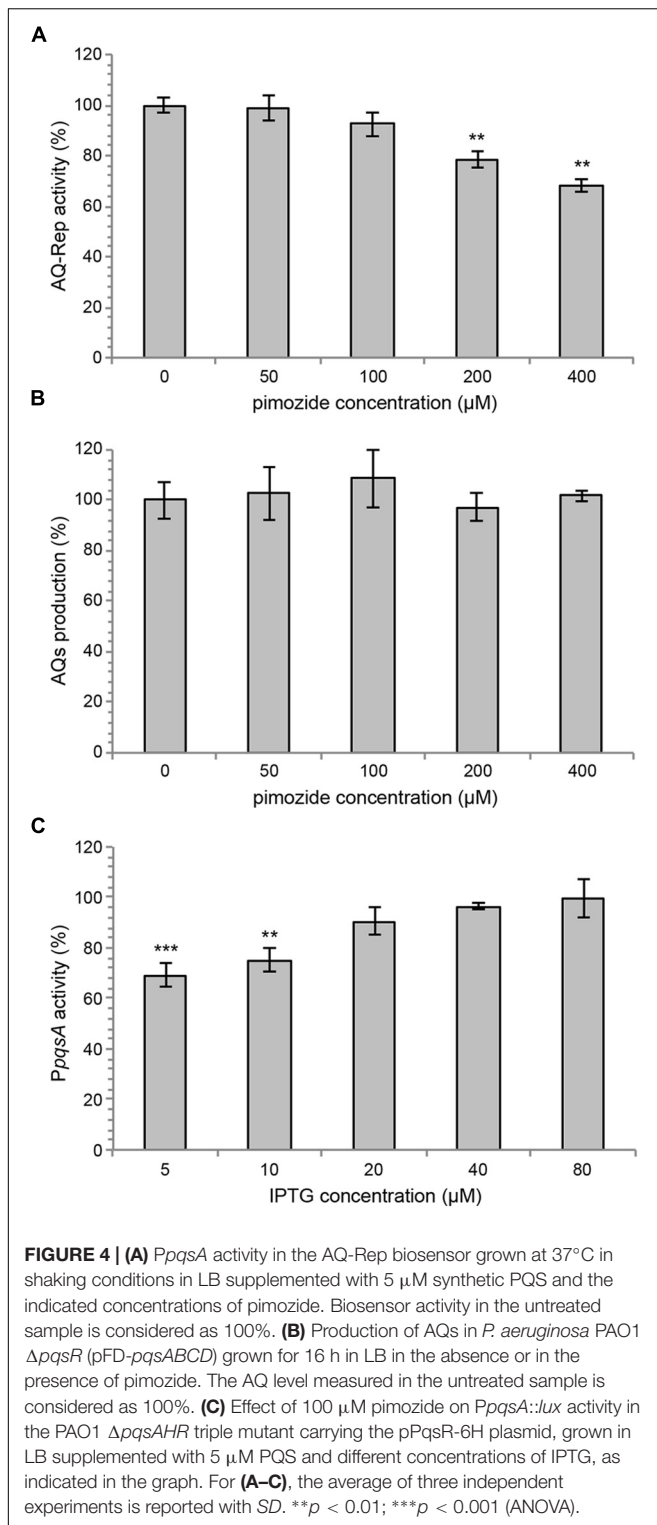
2016; Maura and Rahme, 2017; Maura et al., 2017; D'Angelo et al., 2018; Soukarieh et al., 2018a).

Despite the promise of anti-*pqs* agents for the treatment of *P. aeruginosa* infection, none of these molecules has entered clinical trials so far, likely due to poor pharmacological properties and to the lack of ADME-TOX studies required for their evaluation in humans (Maura et al., 2016; Soukarieh et al., 2018b). To overcome this limitation, we recently exploited a drug-repurposing strategy for the identification of anti-*pqs* drugs via whole-cell biosensor-based screening. This strategy succeeded in identifying the FDA-approved drugs clofexol, miconazole and clotrimazole as new inhibitors of PqsR (D'Angelo et al., 2018).

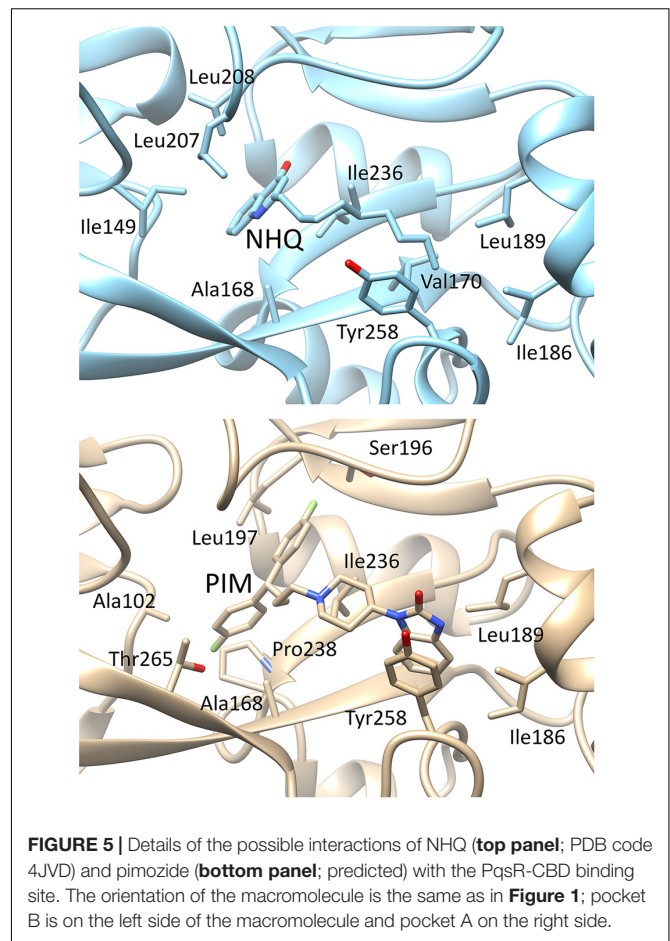
Most *pqs*-inhibitors have been identified via costly and time-consuming biosensor-based screenings or via the rational design and experimental validation of AQ analogs or precursors based on the structure of PqsR and of AQ biosynthetic enzymes. Virtual screenings could reduce the time and costs associated to conventional drug discovery programs, hence *in silico* techniques have been extensively applied for the identification of molecules hampering the *las* QS system of *P. aeruginosa* (Yang et al., 2009; Skovstrup et al., 2013; Tan et al., 2013; Soheili et al., 2015; Gökalsın et al., 2017; Kalia et al., 2017; Xu et al., 2017) or QS systems in other bacteria (Zhu et al., 2012; Ali et al., 2018; Ding et al., 2018, 2019; Medarametla et al., 2018). To the best of our knowledge, only synthetic quinoline-based molecules have so far been identified as PqsR antagonists by means of *in silico* docking analyses (Soukarieh et al., 2018a).

In this study we combined the advantages of drug-repurposing and *in silico* screening approaches by exploiting recent knowledge of PqsR-CBD structure and availability of advanced molecular docking tools to identify new FDA-approved drugs with anti-*pqs* activity. The virtual screening led to selection of five hits for which high binding affinity for PqsR was predicted, and *in vitro* experiments demonstrated the anti-*pqs* activity of two of them, namely pimozide and ergotamine. Since pimozide showed the highest inhibitory activity, this drug was experimentally characterized. Phenotypic assays showed that exposure of *P. aeruginosa* PAO1 to pimozide decreased key PqsR-controlled virulence determinants, such as AQ signal molecules, pyocyanin, swarming motility and biofilm formation, without altering bacterial growth, as one would expect for an anti-virulence drug. Additional experiments performed with *ad hoc* engineered *P. aeruginosa* strains and refined *in silico* docking simulations suggest that pimozide competes with the natural ligands HHQ and PQS for PqsR binding, hence hampering the activity of the *PpqsA* promoter. Indeed, analysis of the highest ranking pimozide-PqsR docking complex indicated that the drug interacts with the binding pocket occupying the same position of the natural ligand NHQ (Figure 5), and establishes interactions experimentally demonstrated for both the natural ligand and the competitive inhibitor M64 (Ilango et al., 2013; Kitao et al., 2018).

The inability of the predicted PqsR ligands conivaptan and dutasteride to hamper the *pqs* QS system in *P. aeruginosa* and



to decrease bioluminescence in the control biosensor system may be related to drawbacks typically associated to virtual screening approaches, including cell impermeability to the selected compound or its modification/inactivation by cellular metabolism. This is in line with the notion that hits emerging



from *in vitro* screens, as well as from screens employing heterologous organisms, may lack activity or even function as agonists when tested on the target pathogen (Galloway et al., 2011). As an example, the HHQ analog 2-heptyl-6-nitroquinolin-4(1H)-one acted as an antagonist in an *Escherichia coli*-based AQ-reporter strain, but as an agonist in *P. aeruginosa* as a consequence of metabolic modification (Lu et al., 2012). However, a subsequent synthetic modification of this molecule resulted in a strong PqsR antagonist also in *P. aeruginosa*, showing that agonists may still prove useful in the search for antagonists (Lu et al., 2014). More often, the inability of selected hits identified *in silico* or *in vitro* to inhibit target functionality in bacterial cell relates to a lack of internalization or to active efflux. This does not seem to be the case for eltrombopag, since the inhibitory effect exerted by this drug on both the specific and control reporter systems indicates its ability to penetrate *P. aeruginosa* cells, suggesting a QS-independent effect on bioluminescence. In a commentary on the use of whole-cell reporter systems for screens of QS inhibitors, the need for adequate control experiments to assess off-target effects of the tested compounds on reporter activity was emphasized (Defoirdt et al., 2013). For example, pyrogallol was reported to act as a potent inhibitor of AI-2 dependent QS in *V. harveyi*, but subsequent experiments revealed that the apparent inhibitory

activity of pyrogallol was a side effect of its peroxide-generating activity on the reporter system, rather than on QS itself (Defoirdt et al., 2013). In our case, unspecific effects of eltrombopag on the reporter system may mask its impact on PqsR functionality. Obviously, the possibility that the virtual screening approach could select false positive hits cannot be ruled out. When molecular assays for *in vitro* evaluation of PqsR activity will be available, it will be possible to verify the ability of the five hits identified in this study to hamper PqsR functionality in a cell-free system.

Searching for side activities in FDA-approved drugs represents a shortcut to develop new therapeutic agents, with considerable potential for shortening the time-consuming and expensive hit-to-lead and lead-optimization phases of drug-discovery programs (Rangel-Vega et al., 2015). In the last years an increasing number of studies identified some antibacterial activity in several drugs approved for different purposes, including anticancer, antifungal, cardiovascular and antipsychotic therapies (Miró-Canturri et al., 2019). However, a possible drawback of drug-repurposing approaches relies on the primary activity of the repurposed drug. As an example, the antipsychotic activity of the dopamine antagonist pimozide, clinically used for the treatment of Tourette's syndrome and schizophrenia (Tueth and Cheong, 1993), could limit its therapeutic use as anti-virulence drug against *P. aeruginosa*. In fact, it has to be considered that, although rarely, pimozide has been associated to potentially serious adverse effects, including arrhythmia, cardiac arrest, seizures, and neutropenia (Singer, 2010). Neutropenia, in particular, is a worrisome adverse effect for patients suffering a bacterial infection. In addition, the peak serum concentration of pimozide in conventional treatment as an antipsychotic drug is in the nanomolar range (Yan et al., 2010), far below the concentration required to inhibit the *pqs* QS system in *P. aeruginosa*. In spite of these limitations, the pimozide molecular scaffold could serve as the basis for chemical modifications aimed at lowering its dopamine antagonistic activity, while improving membrane permeability and affinity for the PqsR active site, in line with the selective optimization of side activity (SOSA) approach (Wermuth, 2006). However, such a hit-to-lead optimization process would partly compromise the advantage of drug repurposing, since chemical modification of pimozide would invalidate the FDA-approval, with additional pharmacological testing being required by regulatory agencies. It must be recognized that repurposing of old drugs for new therapies can result in seamless adoption into the clinical practice only if their off-target effect overcomes their primary activity.

That said, pimozide has already been repurposed to inhibit *Listeria monocytogenes* virulence by decreasing cell invasion, vacuole escape and cell-to-cell spread in phagocytic host cells

(Lieberman and Higgins, 2009), to inhibit the growth of the protozoan parasite *Toxoplasma gondii* (Dittmar et al., 2016) and for the treatment of breast cancer (Dakir et al., 2018; Elmaci and Altinoz, 2018). Notably, pimozide also inhibited Chikungunya virus (CHIKV) replication in a mouse model of Chikungunya infection when administered in combination with the fatty acid synthesis inhibitor 5-tetradecyloxy-2-furoic acid, with low toxicity *in vivo* (Karlas et al., 2016).

In conclusion, despite low potency of pimozide as a *pqs* inhibitor and predictable side-effects due to its primary antipsychotic activity, this study demonstrates for the first time the potential of virtual screening campaigns to rapidly select new FDA-approved QS inhibitors.

DATA AVAILABILITY STATEMENT

All datasets generated for this study are included in the manuscript/supplementary files.

AUTHOR CONTRIBUTIONS

FP and GR conceived the study. FP, GR, LL, and PV designed the experiments and contributed reagents, materials, and analysis tools. MM, ED, FD, VB, and SF performed the experiments. FP, GR, LL, MM, FD, ED, and VB analyzed the data. GR, FP, and MM wrote the manuscript. All authors corrected, amended the draft of the manuscript, and approved the submitted version.

FUNDING

This work was supported by the Italian Ministry for Education, University and Research (Futuro in Ricerca n. RBFR10LHD1_002 to GR, PRIN 2017 grant protocol 2017483NH8 to FP, and PRIN 2017 grant protocol 20177J5Y3P to PV), Italian Cystic Fibrosis Research Foundation (FFC 17/2018 to LL). The Grant of Excellence Departments, MIUR-Italy (ARTICOLO 1, COMMI 314 – 337 LEGGE 232/2016) is gratefully acknowledged.

ACKNOWLEDGMENTS

We thank Prof. Paul Williams and Miguel Càmara (Centre for Biomolecular Sciences, University of Nottingham, United Kingdom) for kindly providing the synthetic AQs HHQ and PQS. We are grateful to the Reviewers for constructive criticisms to the manuscript.

REFERENCES

- Ali, F., Yao, Z., Li, W., Sun, L., Lin, W., and Lin, X. (2018). *In silico* prediction and modeling of the quorum sensing LuxS protein and inhibition of AI-2 biosynthesis in *Aeromonas hydrophila*. *Molecules* 23:E2627. doi: 10.3390/molecules23102627
- Allen, R. C., Popat, R., Diggle, S. P., and Brown, S. P. (2014). Targeting virulence: can we make evolution-proof drugs? *Nat. Rev. Microbiol.* 12, 300–308. doi: 10.1038/nrmicro3232
- Azzouni, F., and Mohler, J. (2012). Role of 5 α -reductase inhibitors in prostate cancer prevention and treatment. *Urology* 79, 1197–1205. doi: 10.1016/j.urolgy.2012.01.024

- Barr, H. L., Halliday, N., Cámara, M., Barrett, D. A., Williams, P., Forrester, D. L., et al. (2015). *Pseudomonas aeruginosa* quorum sensing molecules correlate with clinical status in cystic fibrosis. *Eur. Respir. J.* 46, 1046–1054. doi: 10.1183/09031936.00225214
- Boucher, H. W., Talbot, G. H., Bradley, J. S., Edwards, J. E., Gilbert, D., Rice, L. B., et al. (2009). Bad bugs, no drugs: no ESKAPE! An update from the infectious diseases society of America. *Clin. Infect. Dis.* 48, 1–12. doi: 10.1086/595011
- Bredenbruch, F., Nimtz, M., Wray, V., Morr, M., Müller, R., and Häussler, S. (2005). Biosynthetic pathway of *Pseudomonas aeruginosa* 4-hydroxy-2-alkylquinolines. *J. Bacteriol.* 187, 3630–3635. doi: 10.1128/jb.187.11.3630-3635.2005
- Calfee, M. W., Coleman, J. P., and Pesci, E. C. (2001). Interference with *Pseudomonas* quinolone signal synthesis inhibits virulence factor expression by *Pseudomonas aeruginosa*. *Proc. Natl. Acad. Sci. U.S.A.* 98, 11633–11637. doi: 10.1073/pnas.201328498
- Cao, H., Krishnan, G., Goumnerov, B., Tsongalis, J., Tompkins, R., and Rahme, L. G. (2001). A quorum sensing-associated virulence gene of *Pseudomonas aeruginosa* encodes a LysR-like transcription regulator with a unique self-regulatory mechanism. *Proc. Natl. Acad. Sci. U.S.A.* 98, 14613–14618. doi: 10.1073/pnas.251465298
- Chen, R., Déziel, E., Groleau, M. C., Schaefer, A. L., and Greenberg, E. P. (2019). Social cheating in a *Pseudomonas aeruginosa* quorum-sensing variant. *Proc. Natl. Acad. Sci. U.S.A.* 116, 7021–7026. doi: 10.1073/pnas.1819801116
- Collier, D. N., Anderson, L., McKnight, S. L., Noah, T. L., Knowles, M., Boucher, R., et al. (2002). A bacterial cell to cell signal in the lungs of cystic fibrosis patients. *FEMS Microbiol. Lett.* 215, 41–46. doi: 10.1016/s0378-1097(02)00937-0
- Dakir, E. H., Pickard, A., Srivastava, K., McCrudden, C. M., Gross, S. R., Lloyd, S., et al. (2018). The anti-psychotic drug pimozide is a novel chemotherapeutic for breast cancer. *Oncotarget* 9, 34889–34910. doi: 10.18632/oncotarget.26175
- D'Angelo, F., Baldelli, V., Halliday, N., Pantalone, P., Polticelli, F., Fiscarelli, E., et al. (2018). Identification of FDA-approved drugs as antivirulence agents targeting the *pqs* quorum-sensing system of *Pseudomonas aeruginosa*. *Antimicrob. Agents Chemother.* 62:e1296-18. doi: 10.1128/AAC.01296-18
- Davies, D. G., Parsek, M. R., Pearson, J. P., Iglewski, B. H., Costerton, J. W., and Greenberg, E. P. (1998). The involvement of cell-to-cell signals in the development of a bacterial biofilm. *Science* 280, 295–298. doi: 10.1126/science.280.5361.295
- Deiford, T., Brackman, G., and Coenye, T. (2013). Quorum sensing inhibitors: how strong is the evidence? *Trends Microbiol.* 21, 619–624. doi: 10.1016/j.tim.2013.09.006
- Déziel, E., Gopalan, S., Tampakaki, A. P., Lépine, F., Padfield, K. E., Saucier, M., et al. (2005). The contribution of MvfR to *Pseudomonas aeruginosa* pathogenesis and quorum sensing circuitry regulation: multiple quorum sensing-regulated genes are modulated without affecting *lasRI*, *rhlRI* or the production of *N*-acyl-L-homoserine lactones. *Mol. Microbiol.* 55, 998–1014. doi: 10.1111/j.1365-2958.2004.04448.x
- Di Muzio, E., Toti, D., and Polticelli, F. (2017). DockingApp: a user friendly interface for facilitated docking simulations with AutoDock Vina. *J. Comput. Aided Mol. Des.* 31, 213–218. doi: 10.1007/s10822-016-0006-1
- Diggle, S. P., Matthijs, S., Wright, V. J., Fletcher, M. P., Chhabra, S. R., Lamont, I. L., et al. (2007). The *Pseudomonas aeruginosa* 4-quinolone signal molecules HHQ and PQS play multifunctional roles in quorum sensing and iron entrapment. *Chem. Biol.* 14, 87–96. doi: 10.1016/j.chembiol.2006.11.014
- Ding, T., Li, T., and Li, J. (2018). Identification of natural product compounds as quorum sensing inhibitors in *Pseudomonas fluorescens* P07 through virtual screening. *Bioorg. Med. Chem.* 26, 4088–4099. doi: 10.1016/j.bmc.2018.06.039
- Ding, T., Li, T., and Li, J. (2019). Virtual screening for quorum-sensing inhibitors of *Pseudomonas fluorescens* P07 from a food-derived compound database. *J. Appl. Microbiol.* 127, 763–777. doi: 10.1111/jam.14333
- Dittmar, A. J., Drozda, A. A., and Blader, I. J. (2016). Drug repurposing screening identifies novel compounds that effectively inhibit *Toxoplasma gondii* growth. *mSphere* 1:e042-15. doi: 10.1128/mSphere.00042-15
- Drees, S. L., and Fetzner, S. (2015). PqsE of *Pseudomonas aeruginosa* acts as pathway-specific thioesterase in the biosynthesis of alkylquinolone signaling molecules. *Chem. Biol.* 22, 611–618. doi: 10.1016/j.chembiol.2015.04.012
- Dubern, J. F., Cigana, C., De Simone, M., Lazenby, J., Juhas, M., Schwager, S., et al. (2015). Integrated whole-genome screening for *Pseudomonas aeruginosa* virulence genes using multiple disease models reveals that pathogenicity is host specific. *Environ. Microbiol.* 17, 4379–4393. doi: 10.1111/1462-2920.12863
- Dulcey, C. E., Dekimpe, V., Fauvel, D. A., Milot, S., Groleau, M. C., Doucet, N., et al. (2013). The end of an old hypothesis: the *Pseudomonas* signaling molecules 4-hydroxy-2-alkylquinolines derive from fatty acids, not 3-ketofatty acids. *Chem. Biol.* 20, 1481–1491. doi: 10.1016/j.chembiol.2013.09.021
- Elmaci, I., and Altinoz, M. A. (2018). Targeting the cellular schizophrénia. Likely employment of the antipsychotic agent pimozide in treatment of refractory cancers and glioblastoma. *Crit. Rev. Oncol. Hematol.* 128, 96–109. doi: 10.1016/j.critrevonc.2018.06.004
- Essar, D. W., Eberly, L., Hadero, A., and Crawford, I. P. (1990). Identification and characterization of genes for a second anthranilate synthase in *Pseudomonas aeruginosa*: interchangeability of the two anthranilate synthases and evolutionary implications. *J. Bacteriol.* 172, 884–900. doi: 10.1128/jb.172.2.884-900.1990
- Feltner, J. B., Wolter, D. J., Pope, C. E., Groleau, M. C., Smalley, N. E., Greenberg, E. P., et al. (2016). LasR variant cystic fibrosis isolates reveal an adaptable quorum-sensing hierarchy in *Pseudomonas aeruginosa*. *mBio* 7:e1513. doi: 10.1128/mBio.01513-16
- Ferguson-Myrthil, N. (2010). Novel agents for the treatment of hyponatremia: a review of conivaptan and tolvaptan. *Cardiol. Rev.* 18, 313–321. doi: 10.1097/CRD.0b013e3181f5b3b7
- Fletcher, M. P., Diggle, S. P., Crusz, S. A., Chhabra, S. R., Cámara, M., and Williams, P. (2007). A dual biosensor for 2-alkyl-4-quinolone quorum-sensing signal molecules. *Environ. Microbiol.* 9, 2683–2693. doi: 10.1111/j.1462-2920.2007.01380.x
- Galloway, W. R., Hodgkinson, J. T., Bowden, S. D., Welch, M., and Spring, D. R. (2011). Quorum sensing in Gram-negative bacteria: small-molecule modulation of AHL and AI-2 quorum sensing pathways. *Chem. Rev.* 111, 28–67.
- Gökalsın, B., Aksoydan, B., Erman, B., and Sesal, N. C. (2017). Reducing virulence and biofilm of *Pseudomonas aeruginosa* by potential quorum sensing inhibitor Carotenoid: Zeaxanthin. *Microb. Ecol.* 74, 466–473. doi: 10.1007/s00248-017-0949-3
- Guina, T., Purvine, S. O., Yi, E. C., Eng, J., Goodlett, D. R., Aebersold, R., et al. (2003). Quantitative proteomic analysis indicates increased synthesis of a quinolone by *Pseudomonas aeruginosa* isolates from cystic fibrosis airways. *Proc. Natl. Acad. Sci. U.S.A.* 100, 2771–2776. doi: 10.1073/pnas.0435846100
- Hazan, R., He, J., Xiao, G., Dekimpe, V., Apidianakim, Y., Lesic, B., et al. (2010). Homeostatic interplay between bacterial cell-cell signaling and iron in virulence. *PLoS Pathog.* 6:e1000810. doi: 10.1371/journal.ppat.1000810
- Heeb, S., Fletcher, M. P., Chhabra, S. R., Diggle, S. R., Williams, P., and Cámara, M. (2011). Quinolones: from antibiotics to autoinducers. *FEMS Microbiol. Rev.* 35, 247–274. doi: 10.1111/j.1574-6976.2010.00247.x
- Hoffman, L. R., Kulasekara, H. D., Emerson, J., Houston, L. S., Burns, J. L., Ramsey, B. W., et al. (2009). *Pseudomonas aeruginosa* lasR mutants are associated with cystic fibrosis lung disease progression. *J. Cyst. Fibros.* 8, 66–70. doi: 10.1016/j.jcf.2008.09.006
- Hung, D. T., Shakhnovich, E. A., Pierson, E., and Mekalanos, J. J. (2005). Small-molecule inhibitor of *Vibrio cholerae* virulence and intestinal colonization. *Science* 310, 670–674. doi: 10.1126/science.1116739
- Ilangovan, A., Fletcher, M., Rampioni, G., Pustelny, C., Rumbaugh, K., Heeb, S., et al. (2013). Structural basis for native agonist and synthetic inhibitor recognition by the *Pseudomonas aeruginosa* quorum sensing regulator PqsR (MvfR). *PLoS Pathog.* 9:e1003508. doi: 10.1371/journal.ppat.1003508
- Imperi, F., Fiscarelli, E. V., Visaggio, D., Leoni, L., and Visca, P. (2019). Activity and impact on resistance development of two antivirulence fluoropyrimidine drugs in *Pseudomonas aeruginosa*. *Front. Cell. Infect. Microbiol.* 9:49. doi: 10.3389/fcimb.2019.00049
- Imperi, F., Massai, F., Ramachandran Pillai, C., Longo, F., Zennaro, E., Rampioni, G., et al. (2013). New life for an old drug: the anthelmintic drug niclosamide inhibits *Pseudomonas aeruginosa* quorum sensing. *Antimicrob. Agents Chemother.* 57, 996–1005. doi: 10.1128/AAC.01952-12
- Ji, C., Sharma, I., Pratihari, D., Hudson, L. L., Maura, D., Guney, T., et al. (2016). Designed small-molecule inhibitors of the anthranil-CoA synthetase PqsA block quinolone biosynthesis in *Pseudomonas aeruginosa*. *ACS Chem. Biol.* 11, 3061–3067. doi: 10.1021/acschembio.6b00575
- Jiricny, N., Molin, S., Foster, K., Diggle, S. P., Scanlan, P. D., Ghoul, M., et al. (2014). Loss of social behaviours in populations of *Pseudomonas aeruginosa* infecting

- lungs of patients with cystic fibrosis. *PLoS One* 9:e83124. doi: 10.1371/journal.pone.0083124
- Jurcisek, J. A., Dickson, A. C., Bruggeman, M. E., and Bakaletz, L. O. (2011). *In vitro* biofilm formation in an 8-well chamber slide. *J. Vis. Exp.* 47:e2481. doi: 10.3791/2481
- Kalia, M., Singh, P. K., Yadav, V. K., Yadav, B. S., Sharma, D., Narvi, S. S., et al. (2017). Structure based virtual screening for identification of potential quorum sensing inhibitors against LasR master regulator in *Pseudomonas aeruginosa*. *Microb. Pathog.* 107, 136–143. doi: 10.1016/j.micpath.2017.03.026
- Kalia, V. C., Patel, S. K. S., Kang, Y. C., and Lee, J. K. (2019). Quorum sensing inhibitors as antipathogens: biotechnological applications. *Biotechnol. Adv.* 37, 68–90. doi: 10.1016/j.biotechadv.2018.11.006
- Karlas, A., Berre, S., Couderc, T., Varjak, M., Braun, P., Meyer, M., et al. (2016). A human genome-wide loss-of-function screen identifies effective chikungunya antiviral drugs. *Nat. Commun.* 7:11320. doi: 10.1038/ncomms11320
- Kitao, T., Lepine, F., Babloui, S., Walte, F., Steinbacher, S., Maskos, K., et al. (2018). Molecular insights into function and competitive inhibition of *Pseudomonas aeruginosa* multiple virulence factor regulator. *mBio* 9:e02158-17. doi: 10.1128/mBio.02158-17
- Klein, T., Henn, C., de Jong, J. C., Zimmer, C., Kirsch, B., Maurer, C. K., et al. (2012). Identification of small-molecule antagonists of the *Pseudomonas aeruginosa* transcriptional regulator PqsR: biophysically guided hit discovery and optimization. *ACS Chem. Biol.* 7, 1496–1501. doi: 10.1021/cb300208g
- Kostylev, M., Kim, D. Y., Smalley, N. E., Salukhe, I., Greenberg, E. P., and Dandekar, A. A. (2019). Evolution of the *Pseudomonas aeruginosa* quorum-sensing hierarchy. *Proc. Natl. Acad. Sci. U.S.A.* 116, 7027–7032.
- Kuntz, I. D., Chen, K., Sharp, K. A., and Kollman, P. A. (1999). The maximal affinity of ligands. *Proc. Natl. Acad. Sci. U.S.A.* 96, 9997–10002. doi: 10.1073/pnas.96.18.9997
- Lesic, B., Lépine, F., Déziel, E., Zhang, J., Zhang, Q., Padfield, K., et al. (2007). Inhibitors of pathogen intercellular signals as selective anti-infective compounds. *PLoS Pathog.* 3, 1229–1239.
- Lieberman, L. A., and Higgins, D. E. (2009). A small-molecule screen identifies the antipsychotic drug pimozide as an inhibitor of *Listeria monocytogenes* infection. *Antimicrob. Agents Chemother.* 53, 756–764. doi: 10.1128/AAC.00607-08
- Lin, J., Zhang, W., Cheng, J., Yang, X., Zhu, K., Wang, Y., et al. (2017). A *Pseudomonas* T6SS effector recruits PQS-containing outer membrane vesicles for iron acquisition. *Nat. Commun.* 8:14888. doi: 10.1038/ncomms14888
- Lu, C., Kirsch, B., Zimmer, C., de Jong, J. C., Henn, C., Maurer, C. K., et al. (2012). Discovery of antagonists of PqsR, a key player in 2-alkyl-4-quinolone-dependent quorum sensing in *Pseudomonas aeruginosa*. *Chem. Biol.* 19, 381–390. doi: 10.1016/j.chembiol.2012.01.015
- Lu, C., Maurer, C. K., Kirsch, B., Steinbach, A., and Hartmann, R. W. (2014). Overcoming the unexpected functional inversion of a PqsR antagonist in *Pseudomonas aeruginosa*: an *in vivo* potent antivirulence agent targeting pqs quorum sensing. *Angew. Chem. Int. Ed. Engl.* 53, 1109–1112. doi: 10.1002/anie.201307547
- Luepke, K. H., Suda, K. J., Boucher, H., Russo, R. L., Bonney, M. W., Hunt, T. D., et al. (2017). Past, present, and future of antibacterial economics: increasing bacterial resistance, limited antibiotic pipeline, and societal implications. *Pharmacotherapy* 37, 71–84. doi: 10.1002/phar.1868
- Maeda, T., García-Contreras, R., Pu, M., Sheng, L., García, L. R., Tomás, M., et al. (2012). Quorum quenching quinary: resistance to antivirulence compounds. *ISME J.* 6, 493–501. doi: 10.1038/ismej.2011.122
- Mashburn, L. M., and Whiteley, M. (2005). Membrane vesicles traffic signals and facilitate group activities in a prokaryote. *Nature* 437, 422–425. doi: 10.1038/nature03925
- Maura, D., Ballok, A. E., and Rahme, L. G. (2016). Considerations and caveats in anti-virulence drug development. *Curr. Opin. Microbiol.* 33, 41–46. doi: 10.1016/j.mib.2016.06.001
- Maura, D., Drees, S. L., Bandyopadhyaya, A., Kitao, T., Negri, M., Starkey, M., et al. (2017). Polypharmacology approaches against the *Pseudomonas aeruginosa* MvfR regulon and their application in blocking virulence and antibiotic tolerance. *ACS Chem. Biol.* 12, 1435–1443. doi: 10.1021/acscchembio.6b01139
- Maura, D., and Rahme, L. G. (2017). Pharmacological inhibition of the *Pseudomonas aeruginosa* MvfR quorum sensing system interferes with biofilm formation and potentiates antibiotic-mediated biofilm disruption. *Antimicrob. Agents Chemother.* 61:e01362-17. doi: 10.1128/AAC.01362-17
- McCormack, P. L. (2015). Eltrombopag: a review of its use in patients with severe aplastic anaemia. *Drugs* 75, 525–531. doi: 10.1007/s40265-015-0363-4
- Medarametla, P., Gatta, V., Kajander, T., Laitinen, T., Tammela, P., and Poso, A. (2018). Structure-based virtual screening of LsrK kinase inhibitors to target quorum sensing. *ChemMedChem* 13, 2400–2407. doi: 10.1002/cmdc.201800548
- Mellbye, B., and Schuster, M. (2011). The sociomicrobiology of antivirulence drug resistance: a proof of concept. *mBio* 2:e0131-11. doi: 10.1128/mBio.00131-11
- Miró-Canturri, A., Ayerbe-Algaba, R., and Smani, Y. (2019). Drug repurposing for the treatment of bacterial and fungal infections. *Front. Microbiol.* 10:41. doi: 10.3389/fmicb.2019.00041
- Mohr, K. I. (2016). History of antibiotics research. *Curr. Top. Microbiol. Immunol.* 398, 237–272. doi: 10.1007/82_2016_499
- Monserat-Martinez, A., Gambin, Y., and Sierceki, E. (2019). Thinking outside the bug: molecular targets and strategies to overcome antibiotic resistance. *Int. J. Mol. Sci.* 20:E1255. doi: 10.3390/ijms20061255
- Mukherjee, S., Moustafa, D. A., Stergioula, V., Smith, C. D., Goldberg, J. B., and Bassler, B. L. (2018). The PqsE and RhlR proteins are an autoinducer synthase-receptor pair that control virulence and biofilm development in *Pseudomonas aeruginosa*. *Proc. Natl. Acad. Sci. U.S.A.* 115, E9411–E9418. doi: 10.1073/pnas.1814023115
- Pettersen, E. F., Goddard, T. D., Huang, C. C., Couch, G. S., Greenblatt, D. M., Meng, E. C., et al. (2004). UCSF Chimera - a visualization system for exploratory research and analysis. *J. Comput. Chem.* 25, 1605–1612. doi: 10.1002/jcc.20084
- Rampioni, G., Falcone, M., Heeb, S., Frangipani, E., Fletcher, M. P., Dubern, J. F., et al. (2016). Unravelling the genome-wide contributions of specific 2-alkyl-4-quinolones and PqsE to quorum sensing in *Pseudomonas aeruginosa*. *PLoS Pathog.* 12:e1006029. doi: 10.1371/journal.ppat.1006029
- Rampioni, G., Leoni, L., and Williams, P. (2014). The art of antibacterial warfare: deception through interference with quorum sensing-mediated communication. *Bioorg. Chem.* 55, 60–68. doi: 10.1016/j.bioorg.2014.04.005
- Rampioni, G., Pustelny, C., Fletcher, M. P., Wright, V. J., Bruce, M., Rumbaugh, K. P., et al. (2010). Transcriptomic analysis reveals a global alkyl-quinolone-independent regulatory role for PqsE in facilitating the environmental adaptation of *Pseudomonas aeruginosa* to plant and animal hosts. *Environ. Microbiol.* 12, 1659–1673. doi: 10.1111/j.1462-2920.2010.02214.x
- Rampioni, G., Schuster, M., Greenberg, E. P., Zennaro, E., and Leoni, L. (2009). Contribution of the RsaL global regulator to *Pseudomonas aeruginosa* virulence and biofilm formation. *FEMS Microbiol. Lett.* 301, 210–217. doi: 10.1111/j.1574-6968.2009.01817.x
- Rampioni, G., Visca, P., Leoni, L., and Imperi, F. (2017). Drug repurposing for antivirulence therapy against opportunistic bacterial pathogens. *Emerg. Top. Life Sci.* 1, 13–22. doi: 10.1042/etls20160018
- Rangel-Vega, A., Bernstein, L. R., Mandujano-Tinoco, E. A., García-Contreras, S. J., and García-Contreras, R. (2015). Drug repurposing as an alternative for the treatment of recalcitrant bacterial infections. *Front. Microbiol.* 6:282. doi: 10.3389/fmicb.2015.00282
- Rasko, D. A., and Sperandio, V. (2010). Anti-virulence strategies to combat bacteria-mediated disease. *Nat. Rev. Drug Discov.* 9, 117–128. doi: 10.1038/nrd3013
- Reuter, K., Steinbach, A., and Helms, V. (2015). Interfering with bacterial quorum sensing. *Perspect. Med. Chem.* 8, 1–15.
- Rice, L. B. (2008). Federal funding for the study of antimicrobial resistance in nosocomial pathogens: no ESKAPE. *J. Infect. Dis.* 197, 1079–1081. doi: 10.1086/533452
- Sahner, J. H., Brengel, C., Storz, M. P., Groh, M., Plaza, A., Müller, R., et al. (2013). Combining *in silico* and biophysical methods for the development of *Pseudomonas aeruginosa* quorum sensing inhibitors: an alternative approach for structure-based drug design. *J. Med. Chem.* 56, 8656–8664. doi: 10.1021/jm401102e
- Sahner, J. H., Empting, M., Kamal, A., Weidel, E., Groh, M., Börger, C., et al. (2015). Exploring the chemical space of ureidothiophene-2-carboxylic acids as inhibitors of the quorum sensing enzyme PqsD from *Pseudomonas aeruginosa*. *Eur. J. Med. Chem.* 96, 14–21. doi: 10.1016/j.ejmech.2015.04.007
- Saxena, V. K., and De Deyn, P. P. (1992). Ergotamine: its use in the treatment of migraine and its complications. *Acta Neurol.* 14, 140–146.
- Singer, H. S. (2010). Treatment of tics and tourette syndrome. *Curr. Treat. Options Neurol.* 12, 539–561. doi: 10.1007/s11940-010-0095-4

- Skovstrup, S., Le Quement, S. T., Hansen, T., Jakobsen, T. H., Harmsen, M., Tolker-Nielsen, T., et al. (2013). Identification of LasR ligands through a virtual screening approach. *ChemMedChem* 8, 157–163. doi: 10.1002/cmdc.201200434
- Soheili, V., Bazzaz, B. S., Abdollahpour, N., and Hadizadeh, F. (2015). Investigation of *Pseudomonas aeruginosa* quorum-sensing signaling system for identifying multiple inhibitors using molecular docking and structural analysis methodology. *Microb. Pathog.* 89, 73–78. doi: 10.1016/j.micpath.2015.08.017
- Soukarié, F., Vico Oton, E., Dubern, J. F., Gomes, J., Halliday, N., de Pilar Crespo, M., et al. (2018a). In silico and *in vitro*-guided identification of inhibitors of alkylquinolone-dependent quorum sensing in *Pseudomonas aeruginosa*. *Molecules* 23:E257. doi: 10.3390/molecules23020257
- Soukarié, F., Williams, P., Stocks, M. J., and Cámara, M. (2018b). *Pseudomonas aeruginosa* quorum sensing systems as drug discovery targets: current position and future perspectives. *J. Med. Chem.* 61, 10385–10402. doi: 10.1021/acs.jmedchem.8b00540
- Starkey, M., Lepine, F., Maura, D., Bandyopadhyaya, A., Lesic, B., He, J., et al. (2014). Identification of anti-virulence compounds that disrupt quorum-sensing regulated acute and persistent pathogenicity. *PLoS Pathog.* 10:e1004321. doi: 10.1371/journal.ppat.1004321
- Storz, M. P., Maurer, C. K., Zimmer, C., Wagner, N., Brengel, C., de Jong, J. C., et al. (2012). Validation of PqsD as an anti-biofilm target in *Pseudomonas aeruginosa* by development of small-molecule inhibitors. *J. Am. Chem. Soc.* 134, 16143–16146. doi: 10.1021/ja3072397
- Tan, S. Y., Chua, S. L., Chen, Y., Rice, S. A., Kjelleberg, S., Nielsen, T. R., et al. (2013). Identification of five structurally unrelated quorum-sensing inhibitors of *Pseudomonas aeruginosa* from a natural-derivative database. *Antimicrob. Agents Chemother.* 57, 5629–5641. doi: 10.1128/AAC.00955-13
- Thomann, A., de Mello Martins, A. G., Brengel, C., Empting, M., and Hartmann, R. W. (2016). Application of dual inhibition concept within looped autoregulatory systems toward antivirulence agents against *Pseudomonas aeruginosa* infections. *ACS Chem. Biol.* 11, 1279–1286. doi: 10.1021/acschembio.6b00117
- Trott, O., and Olson, A. J. (2010). AutoDock Vina: improving the speed and accuracy of docking with a new scoring function, efficient optimization, and multithreading. *J. Comp. Chem.* 31, 455–461. doi: 10.1002/jcc.21334
- Tueth, M., and Cheong, J. (1993). Clinical uses of pimozide. *South. Med. J.* 86, 344–349. doi: 10.1097/00007611-199303000-00019
- Vale, P. F., McNally, L., Doeschl-Wilson, A., King, K. C., Popat, R., Domingo-Sananes, M. R., et al. (2016). Beyond killing: can we find new ways to manage infection? *Evol. Med. Public Health* 2016, 148–157. doi: 10.1093/emph/eow012
- Ventola, C. L. (2015). The antibiotic resistance crisis: part 1: causes and threats. *P T* 40, 277–283.
- Weidel, E., de Jong, J. C., Brengel, C., Storz, M. P., Braunshausen, A., Negri, M., et al. (2013). Structure optimization of 2-benzamidobenzoic acids as PqsD inhibitors for *Pseudomonas aeruginosa* infections and elucidation of binding mode by SPR, STD NMR, and molecular docking. *J. Med. Chem.* 56, 6146–6155. doi: 10.1021/jm4006302
- Wermuth, C. G. (2006). Selective optimization of side activities: the SOSA approach. *Drug Discov. Today* 11, 160–164. doi: 10.1016/s1359-6446(05)03686-x
- Xiao, G., He, J., and Rahme, L. G. (2006). Mutation analysis of the *Pseudomonas aeruginosa* *mvfR* and *pqsABCDE* gene promoters demonstrates complex quorum-sensing circuitry. *Microbiology* 152, 1679–1686. doi: 10.1099/mic.0.28605-0
- Xu, Y., Tong, X., Sun, P., Bi, L., and Lin, K. (2017). Virtual screening and biological evaluation of biofilm inhibitors on dual targets in quorum sensing system. *Future Med. Chem.* 9, 1983–1994. doi: 10.4155/fmc-2017-0127
- Yan, M., Li, H. D., Chen, B. M., Liu, X. L., Xu, P., and Zhu, Y. G. (2010). Quantitative determination of pimozide in human plasma by liquid chromatography-mass spectrometry and its application in a bioequivalence study. *J. Pharm. Biomed. Anal.* 51, 1161–1164. doi: 10.1016/j.jpba.2009.11.015
- Yang, L., Rybtke, M. T., Jakobsen, T. H., Hentzer, M., Bjarnsholt, T., Givskov, M., et al. (2009). Computer-aided identification of recognized drugs as *Pseudomonas aeruginosa* quorum-sensing inhibitors. *Antimicrob. Agents Chemother.* 53, 2432–2443. doi: 10.1128/AAC.01283-08
- Zender, M., Klein, T., Henn, C., Kirsch, B., Maurer, C. K., Kail, D., et al. (2013). Discovery and biophysical characterization of 2-amino-oxadiazoles as novel antagonists of PqsR, an important regulator of *Pseudomonas aeruginosa* virulence. *J. Med. Chem.* 56, 6761–6774. doi: 10.1021/jm400830r
- Zhu, J., Beaber, J. W., Moré, M. I., Fuqua, C., Eberhard, A., and Winans, S. C. (1998). Analogs of the autoinducer 3-oxooctanoyl-homoserine lactone strongly inhibit activity of the TraR protein of *Agrobacterium tumefaciens*. *J. Bacteriol.* 180, 5398–5405.
- Zhu, P., Peng, H., Ni, N., Wang, B., and Li, M. (2012). Novel AI-2 quorum sensing inhibitors in *Vibrio harveyi* identified through structure-based virtual screening. *Bioorg. Med. Chem. Lett.* 22, 6413–6417. doi: 10.1016/j.bmcl.2012.08.062

Conflict of Interest: The authors declare that the research was conducted in the absence of any commercial or financial relationships that could be construed as a potential conflict of interest.

Copyright © 2019 Mellini, Di Muzio, D'Angelo, Baldelli, Ferrillo, Visca, Leoni, Politicelli and Rampioni. This is an open-access article distributed under the terms of the Creative Commons Attribution License (CC BY). The use, distribution or reproduction in other forums is permitted, provided the original author(s) and the copyright owner(s) are credited and that the original publication in this journal is cited, in accordance with accepted academic practice. No use, distribution or reproduction is permitted which does not comply with these terms.



Genomic Stability of Composite SCCmec ACME and COMER-Like Genetic Elements in *Staphylococcus epidermidis* Correlates With Rate of Excision

OPEN ACCESS

Edited by:

Paolo Visca,
Roma Tre University, Italy

Reviewed by:

Marat R. Sadykov,
University of Nebraska Medical
Center, United States
Timothy J. Foster,
Trinity College Dublin, Ireland

*Correspondence:

Marco R. Oggioni
mro5@leicester.ac.uk;
mro5@leicester.ac.uk

† Present address:

Roxana Zamudio,
The Quadram Institute Bioscience,
Norwich, United Kingdom

Specialty section:

This article was submitted to
Antimicrobials, Resistance
and Chemotherapy,
a section of the journal
Frontiers in Microbiology

Received: 13 December 2019

Accepted: 23 January 2020

Published: 12 February 2020

Citation:

Almebairik N, Zamudio R,
Ironsides C, Joshi C, Ralph JD,
Roberts AP, Gould IM, Morrissey JA,
Hijazi K and Oggioni MR (2020)
Genomic Stability of Composite
SCCmec ACME and COMER-Like
Genetic Elements in *Staphylococcus
epidermidis* Correlates With Rate
of Excision. *Front. Microbiol.* 11:166.
doi: 10.3389/fmicb.2020.00166

Nada Almebairik¹, Roxana Zamudio^{1†}, Corinne Ironside², Chaitanya Joshi²,
Joseph D. Ralph¹, Adam P. Roberts³, Ian M. Gould², Julie A. Morrissey¹, Karolin Hijazi²
and Marco R. Oggioni^{1*}

¹ Department of Genetics and Genome Biology, University of Leicester, Leicester, United Kingdom, ² School of Medicine, Medical Sciences and Nutrition, University of Aberdeen, Aberdeen, United Kingdom, ³ Department of Tropical Disease Biology, Liverpool School of Tropical Medicine, Liverpool, United Kingdom

The epidemiological success of methicillin-resistant *Staphylococcus aureus* USA300 has been associated with the presence of two mobile elements, the arginine catabolic mobile element (ACME) and the copper and mercury resistance (COMER) element. These two mobile elements are associated with resistance to copper, which has been related to host fitness and survival within macrophages. Several studies found that ACME is more prevalent, and exhibits greater diversity, in *Staphylococcus epidermidis* while COMER has not been identified in *S. epidermidis* or any other staphylococcal species. We aimed in this study to evaluate the presence and diversity of ACME and COMER-like elements in our *S. epidermidis* clinical isolates. The genomes of 58 *S. epidermidis* clinical isolates, collected between 2009 and 2018 in a Scottish hospital, were sequenced. A core-genome phylogenetic tree and genome based MLST typing showed that more than half of the isolates belong to the clinically predominant sequence type2 (ST2) and these isolates have been found to split into two lineages within the phylogenetic tree. Analysis showed the presence of SCCmec in the majority of isolates. Comparative analysis identified a cluster of ACME-positive isolates with most of them belonging to ST48. ACME showed high variation even between isolates of the same ACME type and ST. COMER-like elements have been identified in one of the two major hospital adapted drug resistant ST2 lineages; and showed high stability. This difference in stability at the genomic level correlates well with the up to one hundred times higher excision frequency found for the SCCmec elements in ACME-containing isolates compared to COMER-like element containing isolates. ACME/COMER-like element positive isolates did not show a significant phenotype of decreased copper susceptibility, while resistance to mercury was over-represented in COMER-like element

positive isolates. To the best of our knowledge, this is the first molecular characterization of COMER-like elements in *S. epidermidis* isolates. The presence of the COMER-like elements is the most prominent accessory genome feature of these successful lineages suggesting that this chromosomal island contributes to the success and wide clinical distribution of ST2 *S. epidermidis*.

Keywords: *Staphylococcus epidermidis*, mobile genetic element, ACME, COMER, SCCmec

INTRODUCTION

Staphylococcus epidermidis and other coagulase negative staphylococci are a leading cause of nosocomial bloodstream and skin and soft tissue infections world-wide (Otto, 2009). Phylogenetic analyses have identified within the species *S. epidermidis* three major phylogenetic groups of hospital adapted isolates, two of ST2 and one of ST23 (Lee et al., 2018; Méric et al., 2018; Espadinha et al., 2019). The evolutionary pressure of the main nosocomial lineages is thought to be related to the hospital environment, but other evidence suggests that initial core genome changes in sequence type 2 (ST2) isolates result in increased acquisition of resistance traits (Lee et al., 2018). The important role of horizontal gene transfer in the evolution of *S. epidermidis* (Méric et al., 2018) and the well-established role of *Staphylococcus aureus* chromosomal cassette elements in bacterial fitness (Purves et al., 2018; Zapotoczna et al., 2018; Rosario-Cruz et al., 2019), suggest that the stepwise evolution of the cassette chromosomal elements and *mecA* gene is critical to spread of staphylococcal resistance, thus leading to the MRSA and MRSE epidemic (Rolo et al., 2017). The fine balance between acquisition and maintenance of accessory chromosomal elements shapes the evolutionary fitness of *S. epidermidis* (Zamudio et al., 2019).

The arginine catabolic mobile element (ACME) is a genomic island that first described in *Staphylococcus aureus* (MRSA) clone USA300 North American epidemic (USA300-NAE) and in *S. epidermidis* ATCC12228 (Diep et al., 2006; Planet et al., 2015). ACME is thought to increase the fitness of staphylococcus species by enhancing their ability to colonize skin and mucous membranes (Diep et al., 2008). ACME shows similar characteristics to the staphylococcal cassette chromosome *mec* (SCCmec) element in that it integrates into the staphylococcal chromosome at the attachment site *attB*, which is flanked by direct repeat sequences and is mobilized by the SCCmec encoded *ccrAB* genes. Moreover, ACME is known to commonly form a composite island with the SCCmec or SCC-associated genes (Diep et al., 2006; Planet et al., 2013; Lindgren et al., 2014; O'Connor et al., 2018a). To date, five distinct ACME types have been described in *S. epidermidis*; type I harbors the *arc* and *opp3* operons, type II harbors the *arc* operon only, type III harbors the *opp3* operon only, type IV harbors the *arc* and the *kdp* operons, and type V harbors all three *arc*, *opp3*, and *kdp* operons. The three characteristic gene clusters; *arc*, *opp3*, and *kdp* encode an arginine deaminase pathway, an oligopeptide permease ABC transporter and potassium ABC transporter respectively. Type IV and V ACME have been identified in oral *S. epidermidis* only (Diep et al., 2006; O'Connor et al., 2018a,b).

The copper and mercury resistance (COMER) mobile element was described for the first time in *S. aureus* (MRSA) strain USA300 South American epidemic (USA300-SAE) (Planet et al., 2015). This mobile element located in the USA300-SAE chromosome appears to replace ACME in USA300-NAE adjacent to the SCCmec type IV and it is thought to play a role in COMER which increases fitness as a result of increased survival to copper-mediated killing in macrophages (Planet et al., 2015; Purves et al., 2018; Zapotoczna et al., 2018). The COMER mobile element is associated with an abortive phage infection system and two main gene clusters, the *mer* operon composed of the *merR/A/B* genes and the *cop* operon composed of the *copB/L/mco* genes (Planet et al., 2015; Purves et al., 2018). To date, the COMER mobile element has not been detected in *S. epidermidis* strains.

This study investigated the prevalence and evolution of ACME and COMER mobile elements in 58 *S. epidermidis* clinical isolates retrieved from blood samples. ACME and COMER were detected and characterized using whole genome sequencing (WGS) analysis. This analysis revealed the presence of several variations of ACME as well as detection of previously undescribed COMER-like element in 11 *S. epidermidis* isolates. The excision and circularization of the ACME and COMER-like elements was investigated.

MATERIALS AND METHODS

Bacterial Isolates

A collection of 58 *S. epidermidis* clinical isolates collected between 2009 and 2018 from blood cultures of patients admitted to the ICU of Aberdeen Royal Infirmary (Aberdeen, United Kingdom) were investigated in this study (Table 1). Twenty-five of these isolates were analyzed previously for their biocide resistance gene content (Hijazi et al., 2016). The *S. epidermidis* strains were stored at -80°C in tryptic soy broth (TSB, BD, France) with 50% glycerol (Thermo Fisher Scientific, United Kingdom). The strains were streaked on tryptic soy agar (TSA) plates (prepared by adding 1.5% agarose to TSB) and incubated at 37°C for 16–24 h. Single colonies were then sub-cultured in TSB and incubated overnight at $37^{\circ}\text{C}/200$ rpm in a shaking incubator (Innova 4000, New Brunswick Scientific, United Kingdom).

Whole Genome Sequencing

Genomic DNA extraction was performed using NucleoSpin Tissue Kit (Macherey-Nagel, Germany) following the manufacturer's instructions. Genomic DNA was eluted in 30 μl pure water, and the concentration and purity measured

TABLE 1 | *S. epidermidis* isolates.

	Isolate	Accession	Date	MLST	COMER-like	ACME	SCCmec type
NB22338Q	STAPH 48	SAMN12840226	July 2009	ST559			SCCmec-IV
NB23267V	STAPH 49	SAMN12840227	July 2009	ST2	COMER		SCCmec-III
NB41003Z	STAPH 51	SAMN12840228	May 2010	ST83			SCCmec-IV
NB14428Z	STAPH 53	SAMN12840229	May 2010	ST5		ACME-V	SCCmec-IV
NB21991B	STAPH 54	SAMN12840230	July 2010	ST5			SCCmec-IV
NB24551C	STAPH 56	SAMN12840231	August 2010	ST2			SCCmec-IV
NB06465P	STAPH 58	SAMN12840232	March 2011	ST2			SCCmec-IV
NB12208Q	STAPH 59	SAMN12840233	April 2011	ST83			SCCmec-IV
NB24506S	STAPH 60	SAMN12840234	August 2011	ST2	COMER		SCCmec-III
NB25777X	STAPH 61	SAMN12840235	September 2011	ST2	COMER		SCCmec-III
NB26250A	STAPH 62	SAMN12840236	September 2011	ST2	COMER		SCCmec-III
NB26865Y	STAPH 63	SAMN12840237	September 2011	ST2	COMER		SCCmec-III
NB28476A	STAPH 64	SAMN12840238	October 2011	ST2	COMER		SCCmec-III
NB13883R	STAPH 66	SAMN12840239	April 2012	ST19			
NB25117Z	STAPH 67	SAMN12840240	July 2012	ST210			
NB25100R	STAPH 68	SAMN12840241	July 2012	ST54		ACME-I	
NB29474S	STAPH 69	SAMN12840242	September 2012	ST2			SCCmec-IV
NB41238E	STAPH 70	SAMN12840243	December 2012	ST2			SCCmec-IV
NB01101D	STAPH 73	SAMN12840244	January 2013	ST204			
NB02243Y	STAPH 74	SAMN12840245	January 2013	ST470		ACME-IV	
NB03947K	STAPH 75	SAMN12840246	January 2013	ST2	COMER		SCCmec-III
NB22235H	STAPH 77	SAMN12840247	January 2013	ST59			SCCmec-IV
NB26073F	STAPH 78	SAMN12840248	July 2013	ST2	COMER		SCCmec-III
NB33101Z	STAPH 79	SAMN12840249	September 2013	ST48		ACME-I	SCCmec-IV
NB671022	STAPH 83	SAMN12840250	February 2014	ST2			SCCmec-IV
NB03169X	STAPH 1	SAMN12840193	January 2016	ST2	COMER		SCCmec-III
NB03186T	STAPH 2	SAMN12840194	January 2016	ST35		ACME-I	SCCmec-IV
NB09909V	STAPH 3	SAMN12840195	March 2016	ST48		ACME-I	SCCmec-IV
NB10503A_1	STAPH 4	SAMN12840196	March 2016	ST59			SCCmec-IV
NB10503A_2	STAPH 5	SAMN12840197	March 2016	ST5			SCCmec-IV
NB11089T	STAPH 6	SAMN12840198	March 2016	ST5			SCCmec-IV
NB11582T	STAPH 7	SAMN12840199	April 2016	ST2			SCCmec-IV
NB12943Y	STAPH 8	SAMN12840200	April 2016	ST2	COMER		SCCmec-III
NB13468Z	STAPH 9	SAMN12840201	April 2016	ST23			SCCmec-IX
NB13483J	STAPH 10	SAMN12840202	April 2016	ST2	COMER		SCCmec-III
NB17762B	STAPH 12	SAMN12840203	May 2016	ST528		ACME-I	
NB18619Q	STAPH 13	SAMN12840204	June 2016	ST2			SCCmec-IV
NB20483A	STAPH 14	SAMN12840205	June 2016	ST2			SCCmec-IV
NB21362A	STAPH 15	SAMN12840206	June 2016	ST2			SCCmec-IV
NB24986M	STAPH 16	SAMN12840207	July 2017	ST54		ACME-I	SCCmec-IV
NB24987J	STAPH 17	SAMN12840208	July 2017	ST210		ACME-IV	SCCmec-IV
NB31156H	STAPH 18	SAMN12840209	September 2017	ST65			
NB31437E	STAPH 19	SAMN12840210	September 2017	ST73		ACME-II	
NB34495N	STAPH 20	SAMN12840211	October 2017	ST2			SCCmec-IV
NB36056Y	STAPH 21	SAMN12840212	October 2017	ST2			SCCmec-IV
NB36246W	STAPH 22	SAMN12840213	October 2017	ST210		ACME-IV	SCCmec-V
NB37325D	STAPH 23	SAMN12840214	October 2017	ST2			SCCmec-IV
NB37754V_1	STAPH 24	SAMN12840215	October 2017	ST2			SCCmec-IV
NB37754V_2	STAPH 25	SAMN12840216	October 2017	ST591			SCCmec-IV
NB38801E	STAPH 27	SAMN12840217	November 2017	ST2			SCCmec-IV
NB40693L	STAPH 28	SAMN12840218	November 2017	ST2			SCCmec-IV
NB41771A	STAPH 29	SAMN12840219	November 2017	ST2			SCCmec-IV

(Continued)

TABLE 1 | Continued

	Isolate	Accession	Date	MLST	COMER-like	ACME	SCCmec type
NB42838N	STAPH 30	SAMN12840220	December 2017	ST2			SCCmec-V
NB43408J	STAPH 31	SAMN12840221	December 2017	ST2			SCCmec-V
NB03117S	STAPH 32	SAMN12840222	January 2018	ST2			SCCmec-IV
NB03149G	STAPH 33	SAMN12840223	January 2018	ST2			SCCmec-IV
NB05012Y	STAPH 34	SAMN12840224	January 2018	ST48		ACME-I	SCCmec-IV
NB05684Z	STAPH 35	SAMN12840225	February 2018	ST48		ACME-I	SCCmec-IV

by the NanoDrop 2000c spectrophotometer (Thermo Fisher Scientific, United Kingdom). Genomic DNA was sequenced on a HiSeq 4000 sequencer (Illumina, The Wellcome Trust Centre for Human Genetics at the University of Oxford) with 150 bp paired-end reads. Genome sequences were trimmed using Trimmomatic (Bolger et al., 2014), then assembled using SPAdes software version v3.9.0 (Nurk et al., 2013) and quality-assessed with QUAST (Gurevich et al., 2013). The draft genomes in contig level for all 58 isolates were submitted to the GenBank under the project number PRJNA574294, the GenBank accession number for the isolates is shown in Table 1.

Multilocus Sequence Typing (MLST) and Core-Genome Phylogeny Tree

The sequence type (ST) of each isolate was specified by submitting the whole genome sequence (WGS) to the *S. epidermidis* MLST 2.0 online database (Larsen et al., 2012). The core-genome alignment was generated using Roary software version 3.11.2 (Page et al., 2015). Then a maximum likelihood tree for 58 Aberdeen isolates and the BPH0662 reference genome was build using RAXML software version 8.2.X (Stamatakis, 2014). Rstudio v 1.1.453¹ and the R package ggtree v 1.13.5 (Yu et al., 2017) was used for visualization and annotation of the phylogeny tree.

Maximum likelihood tree for the 58 Aberdeen isolates and 225 isolates from Lee's collection (NCBI BioProject numbers: PRJEB12090, PRJNA470534, and PRJNA470752) (Lee et al., 2018) and the BPH0662 reference genome (doi: 10.1099/mgen.0.000077) was generated through the iqtree tool (doi: 10.1093/molbev/msu300) by using the Hasegawa–Kishino–Yano model and gamma distribution (Yang, 1994) (doi: 10.1007/bf00160154).

Identification of SCCmec, ACME, and COMER-Like Elements

For each isolate, the presence and the type of the SCCmec mobile element was determined by submitting the genome sequence to the SCCmecFinder 1.2 online database (Kaya et al., 2018). Contigs were aligned to the ACME and COMER elements previously characterized in *S. aureus* USA300 strain FPR3757 (GenBank accession number CP000255) and strain CA12 (GenBank accession number CP007672) respectively using the BLAST software (Altschul et al., 1990) in order to detect the presence of ACME and COMER elements in the study isolates. In

some isolates the ACME and COMER element-associated genes were identified on three and five separate contigs – in this case ACME-I and COMER elements were assembled by PCR. These contigs were organized, reoriented and assembled using BLAST software, Reverse complement tool² and ISfinder online database (Siguier, 2006). For further investigations, contigs were annotated using the RAST server (Aziz et al., 2008), Artemis sequence viewer (Berriman, 2003) and SnapGene viewer (GSL Biotech)³. This is followed by multiple alignment of the ACME and COMER mobile elements using Mauve software to detect the variation in these elements among the isolates (Darling, 2004).

Metal Susceptibility

The susceptibility of these isolates to several metals including copper sulfate (CuSO₄), nickel sulfate (NiSO₄), iron chloride (FeCl₃), manganese sulfate (MnSO₄), zinc sulfate (ZnSO₄), cobalt bromide (CoBr₂), cadmium chloride (CdCl₂), mercuric chloride (HgCl₂), and sodium arsenate (AsNa₂) (all Sigma) was determined using disc diffusion testing. Several colonies from overnight TSA cultures were collected with a sterile loop and re-suspended into Mueller Hinton broth (Oxoid, United Kingdom) to OD₆₀₀ = 0.5. A Mueller Hinton agar (MHA) plate was seeded with the culture using a sterile swab in three different directions to obtain uniform growth. Ten microliter of 1M solutions of each metal were loaded into a sterile filter discs, obtained from filter papers (Munktell, United Kingdom), and allowed to dry for 15 min. Filter discs were then firmly applied to the surface of the MHA plate and incubated overnight at 37°C. The metal susceptibility was determined using the epidemiological cut-off values (ECOFF) (Morrissey et al., 2014) followed by Fisher's Exact test to find the susceptibility association among the isolates⁴. A linear regression model was applied to predict the disk diffusion values based on the presence or absence of the composite element by using the lm function from stats's R package.

Site-Specific Excision of SCCmec, ACME, and COMER-Like Elements

A qPCR-based method was used to quantify the rate of excision and circularization of the composite SCCmec and ACME/COMER-like elements. Specific primers were designed using SnapGene viewer software (Table 2) and used to amplify

¹www.rstudio.com/

²www.bioinformatics.org/sms/rev_comp.html

³Snapgene.com

⁴https://www.socscistatistics.com

TABLE 2 | Primers and probes used in the study.

Primers	Sequence	Annealing temperature (°C)
SCCmec-IV AND ACME PRIMERS		
qAttR1 fw	TACGCTCTATCATTGAGCACTATGA	55
qAttR1 rev	ATGATAAGCTTCTTAAAAACATAACAGC	55
Probe R1	CACCAAATGATGCGCGTCATATTGATAGA	61
qAttR2 fw	AAACCAAAGTCGATATCATTTTTG	55
qAttR2 rev	CAGCATTATCGTAAGTTAACTACATT	55
Probe R2	CGACTTTAATTATAAAAAACGCACTCTTAACCG	61
qAttL fw	GAAGTGATTTTACGATATCACCTTCT	55
qAttL rev	CATTTAAGATGGAATCAAATTTTATTTACTTTC	54
Probe L	TATATTCAGTAGGCCACCGACGTATACAGAATCA	61
SCCmec-III AND COMER-LIKE PRIMERS		
qAttR1 fw	CTCTCTTAAATTTTGTGTTGATTAGATTAGACC	56
qAttR1 rev	ACTTGAAATGAAAGACTGCGG	56
Probe R1	ACGCATTCAATATGTCTACACGTGAATTTAGTCT	62
qAttR2 fw	ACACCAAGCTTTCTATGTAGGTAA	55
qAttR2 rev	ATTTTATTGGAGATACTATATACTTAACCAATTTTC	54
Probe R2	GCGAAGAAAGCCATTATTATGAGGTGATTGTAG	61
qAttL fw	GAGCGACAATTCGAATGAATAGTA	55
qAttL rev	ACCAACAATGAATATATAATACATTTAAGATG	54
Probe L	GTCGCTCTTTCGTTTCAGTTAAGGAAAATG	61

the element attachment sites, the circularized SCCmec and SCCmec plus the ACME/COMER-like element and the excision products (chromosome junction after the element excision). Excision of the SCCmec and ACME/COMER-like element was induced in selected isolates using 0.5 µg/ml Mitomycin C (Sigma-Aldrich). qPCR reactions were performed using the TaqMan Fast Advanced Master Mix (Thermo Fisher Scientific) with the following run protocol: initial denaturation step at 95°C for 20 s then 45 cycles of 95°C for 3 s and 60°C for 30 s. The reactions were carried out in MiroAmp Fast 96-Well Reaction Plate (Applied biosystems) using a 7500 real-time PCR machine (Applied Biosystems). The rate of excision was measured using qPCR by comparing the excised circularized element and the reconstituted chromosomal attachment site to the integrated element using this formula: $2^{-\Delta CT}$ (Livak and Schmittgen, 2001).

RESULTS

The evolution of *S. epidermidis* isolates recovered from bloodstream infections between 2009 and 2018 at Aberdeen Royal Infirmary was studied by core-genome phylogenetic analysis (Figure 1). Genome-based MLST revealed that more than 50% of the isolates (31 of 58) belong to the major hospital acquired multidrug resistant ST2 lineage which in turn was found to separate into two sub-lineages as previously described (Lee et al., 2018). The other 16 STs were distributed among different lineages in the phylogenetic tree. Four ST5 isolates, four ST48 isolates and three ST210 isolates. Of the 58 *S. epidermidis* isolates, 86% (50/58) were methicillin resistant *S. epidermidis* (MRSE) as

they harbored the *mecA* gene. The vast majority of these MRSE contained SCCmec types III and IV (Table 1). The other eight isolates (14%) considered methicillin sensitive *S. epidermidis* (MSSE) lacked the *mecA* gene. All the isolates harbored the penicillin resistance *blaZ* gene except isolate STAPH74.

Eleven of the 31 isolates belonging to the clinically predominant ST2 (35%) were found to be positive for a COMER-like element (Figure 1). These eleven isolates were clustered in one of the two ST2 sub-lineages, also containing the reference isolate BPH0662 (doi: 10.1099/mgen.0.000077) (Lee et al., 2018). We have named this element COMER-like element as it harbored the *mer* and *cop* operons as well as *abi* gene that exhibited very high nucleotide sequence identity with the *mer/cop* operons (99.98% identity over 11,028 bp) and *abi* gene cluster (100% identity over 1,197 bp) located on the COMER element of MRSA USA300 strain CA12 (GenBank accession number CP007672) (Figure 2). However, additional genes not present in COMER USA300, including *ars* operon and a type I restriction modification system, were identified in the *S. epidermidis* COMER-like elements. The COMER-like element was found to be a composite island of 99.2 kb in size. The structural organization of this composite island was identical in all eleven isolates with the COMER-like element located immediately downstream of SCCmec-III and encoding the *mecA* gene and the *cad/mer* operons with > 99.8% nucleotide sequence identity with the corresponding genes in SCCmec-III of strain 85/2082 (GenBank accession number AB037671). Additionally, this composite island contained a module harboring the *speG* and *ccrAB4* genes and the gene of a putative further metal transporter (locus_tag = "F9B38_12675) (Figure 2). In contrast to our composite *S. epidermidis* element, the COMER element in USA300 is located downstream of SCCmec-IV (Figure 2). This is the first description of a COMER-like element in *S. epidermidis* strains.

The arginine catabolic mobile element (ACME) was detected in 9/50 (18%) of the MRSE isolates and 4/8 of the MSSE isolates (Figure 1). These ACMEs encoded the *arc* and/or *opp3* and/or *kdp* operons as previously described for ACME in *S. epidermidis* (Miragaia et al., 2009; Barbier et al., 2011; Onishi et al., 2013; Soroush et al., 2016; McManus et al., 2017; O'Connor et al., 2018a). The ACME-I element was the predominant ACME type and all ACME-I containing isolates, except isolate STAPH12 (ST528), found to cluster in one lineage in the phylogenetic tree containing ST48, ST54 and ST35. The ACME-I element in these isolates was assembled and found to harbor the *arc*, *opp3* operons, and the *speG* gene, all flanked by 15 bp direct repeats (DR_B and DR_C). Additionally, one or more modules were found to colocalize with the ACME-I forming a composite island (Figure 3). Comparative analysis tools showed high variability of ACME-I composite island. In 3 out of 7 isolates [ST48 ($n = 2$) and ST54 ($n = 1$)], the ACME-I was located downstream of the SCCmec-IV, separated by a module composed of *ars* and *cop* genes. This module and the SCCmec-IV were flanked by DR_A and B respectively at the 5' end in *orfX* (Figure 3A). In 2 out of 7 ST48 isolates the ACME-I element colocalized with SCCmec-IV but lacked the *ars/cop* gene modules (Figure 3B). In one ST35 isolate an additional module harboring the *ccrAB4* genes flanked

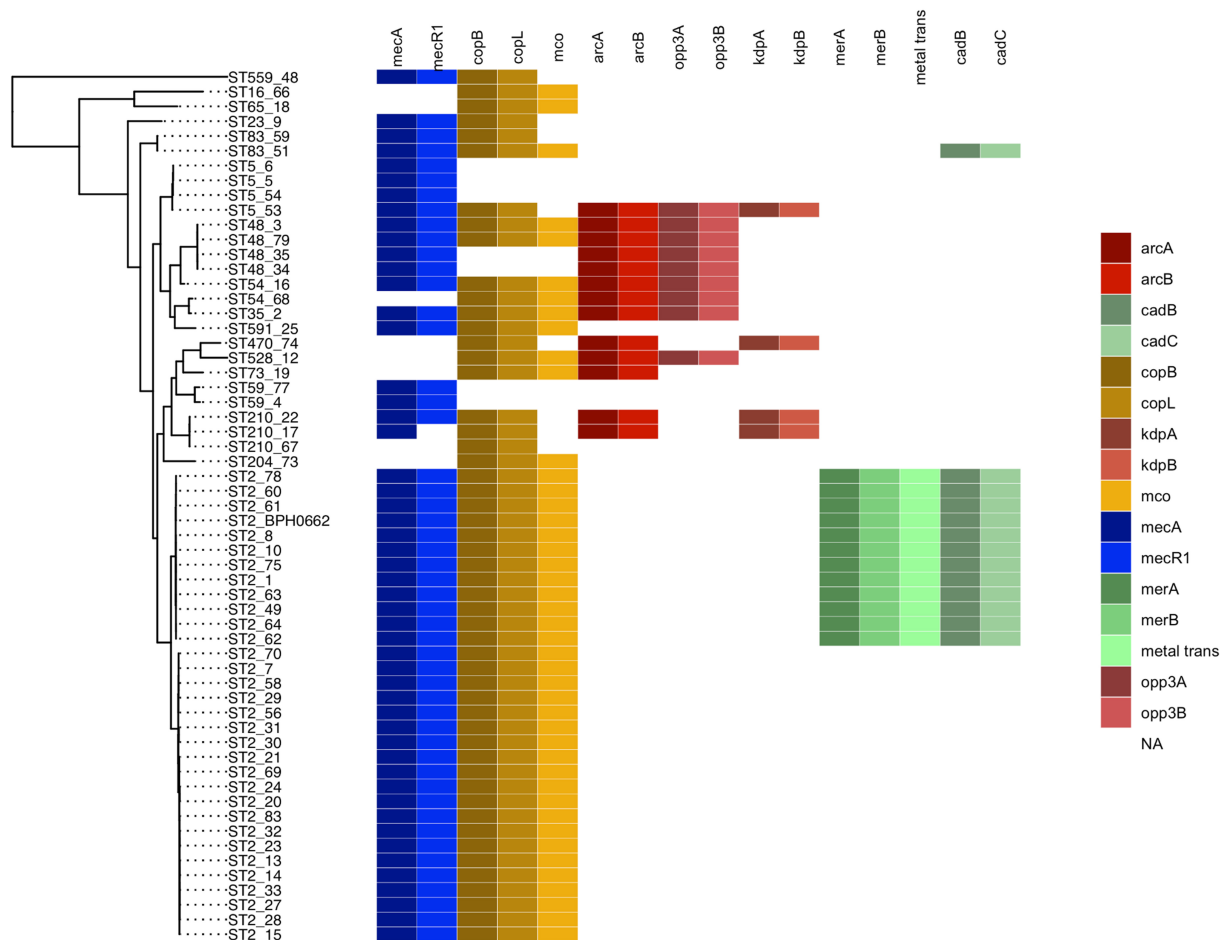


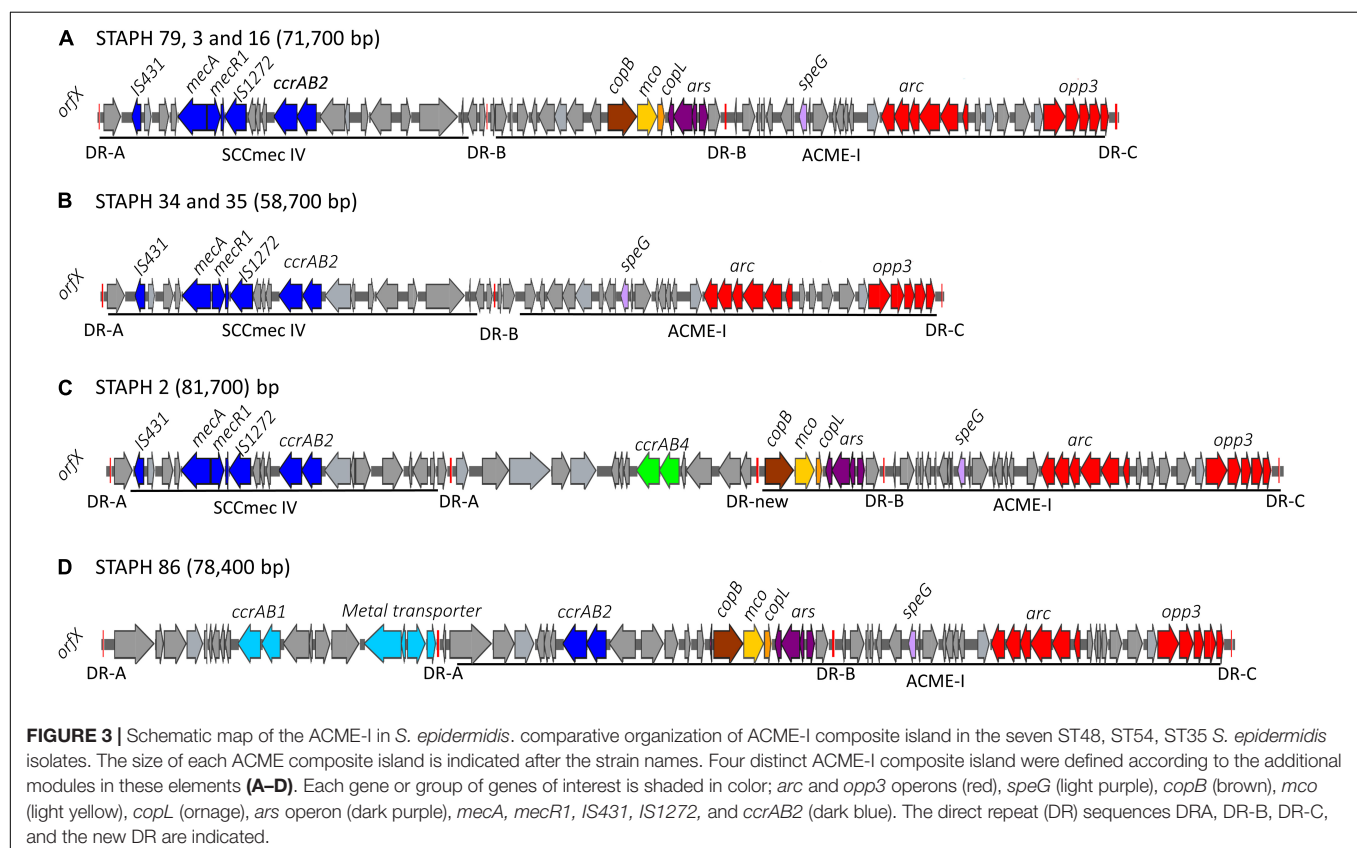
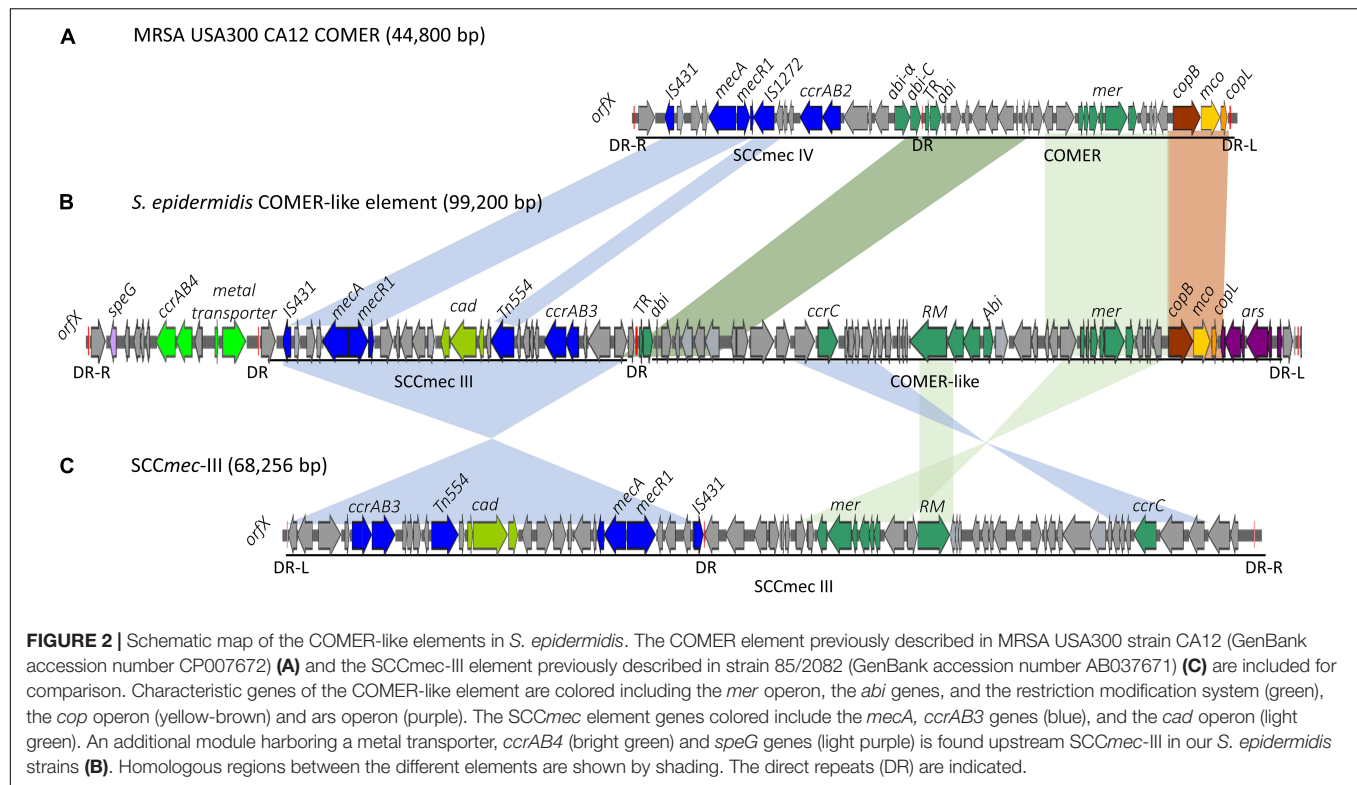
FIGURE 1 | Maximum likelihood phylogenetic tree constructed using core genome alignment from the 58 *S. epidermidis* clinical isolates. The phylogenetic tree is annotated with the isolate's sequence type ST. Colored boxes to the right of each strain name illustrated the distribution of the SCCmec (blue), cop operon (yellow), ACME (red), and COMER-like element (green) characteristic genes among the *S. epidermidis* isolates. *S. epidermidis* BPH0662 used as reference strain in this phylogenetic tree.

by DR_A and DR_Q was inserted between the *ars/cop* gene modules and the SCCmec-IV (**Figure 3C**). The ACME composite island in one ST54 isolate lacked the *mecA* gene and included only two modules located upstream the *ars/cop* genes module and the ACME-I. These two modules were flanked by DR_A, _A, and _B respectively at the 5' end in *orfX* (**Figure 3D**).

To validate the distribution of the composite SCC elements on a larger dataset and at global level, we generated a core genome phylogenetic tree that included a collection of 225 worldwide *S. epidermidis* genomes (Lee et al., 2018; **Figure 4**). The phylogenetic tree was built using the alignment of 1,898 core genes which represent 61.1% (1,706,669 bp) of the reference genome BHP662. This phylogenetic tree combining both datasets showed large clustering of ST2 isolates and their sub-lineages as found in the Scottish collection. Mapping of the key genes of our composite SCC elements, showed again exceptional stability of the COMER-like element. In the larger dataset this element mapped in all 82 isolates belonging ST2 BPH0662 sub-lineage and also partially (38/82)

to a second ST2 sub-lineage of ST2 isolates (**Figure 4**). The mapping in addition confirmed a high variability of ACME elements and their presence in multiple ST and sub-lineages. Copper resistance genes were present in most isolates, even in absence of the COMER-like and ACME elements (**Figure 4**). As expected nearly all isolates carried SCCmec elements.

A phenotypic analysis of metal susceptibility of these isolates was performed by disc diffusion susceptibility testing on our Scottish isolates (**Figure 5**). As no breakpoints for metal resistance exist, we determined the ECOFF (Morrissey et al., 2014). The ECOFF breakpoints, based on the normal distribution of the susceptibility, was defined using the Shapiro–Wilk test. All susceptibility data, except for copper, were not normally distributed. Still we did not define an ECOFF for iron and arsenic as the reduced inhibition zone appears to indicate intrinsic resistance of the all isolates. Isolates belonging to the ST2- BPH0662 lineage carrying the COMER-like element were found to be significantly associated with reduced susceptibility



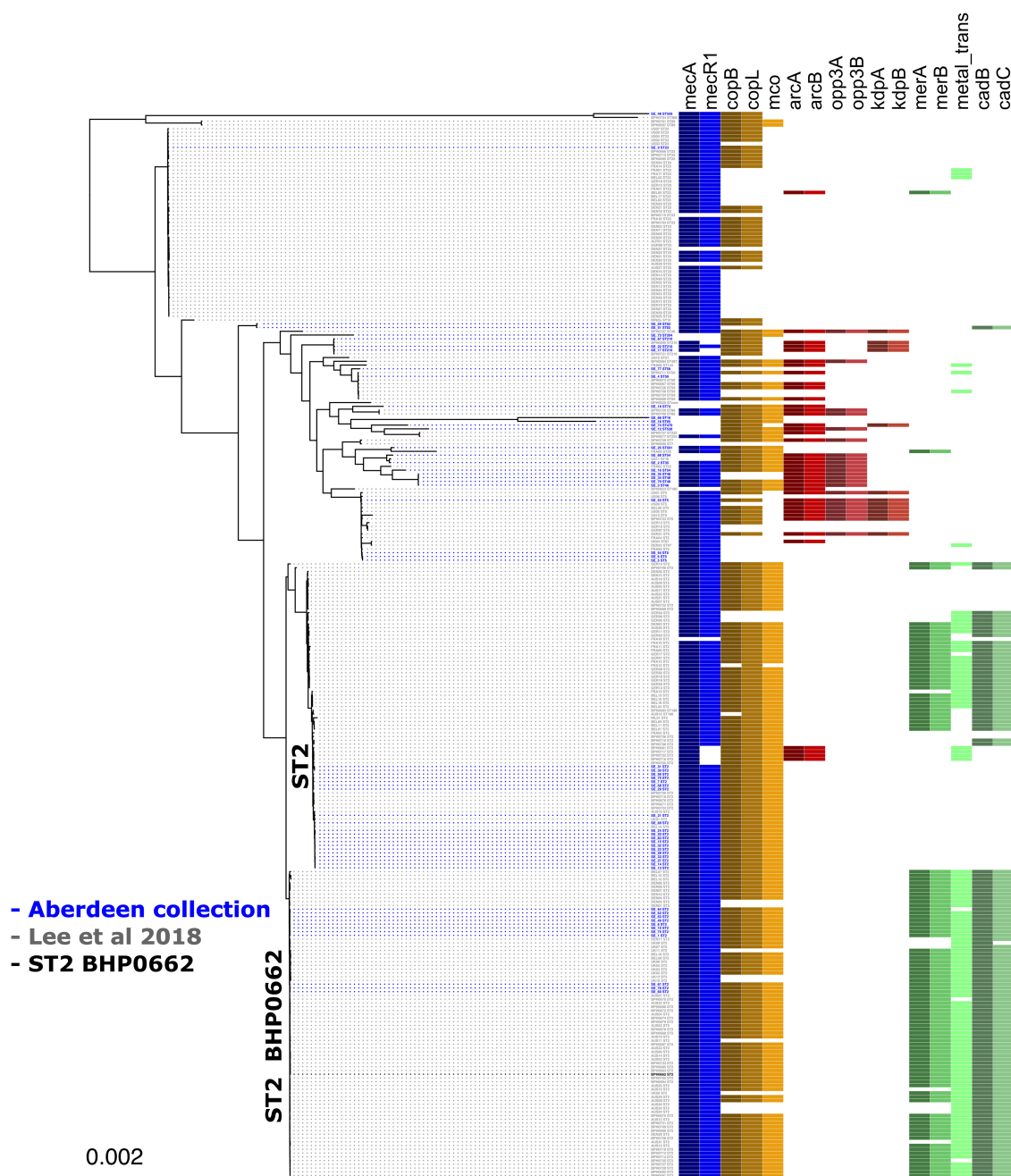
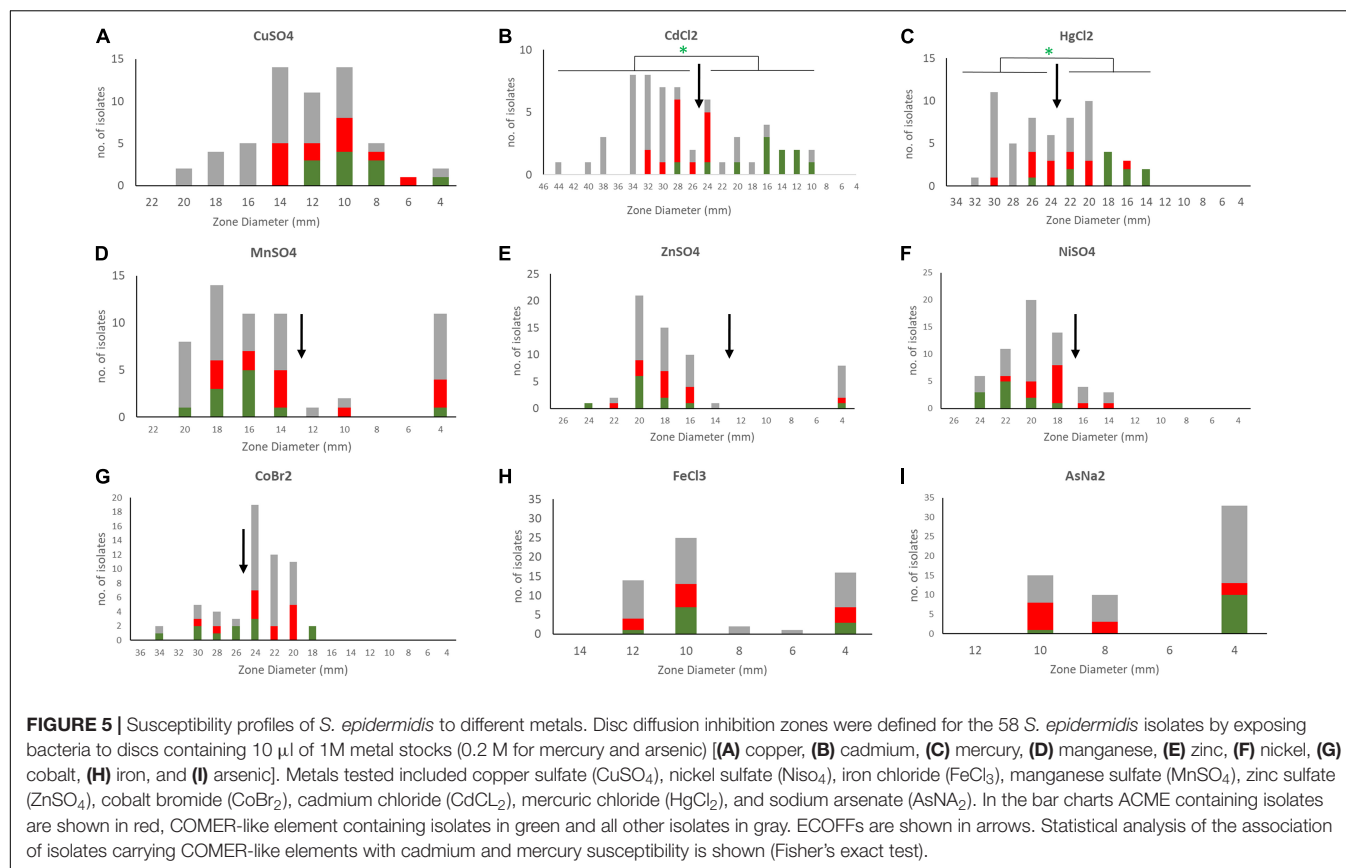


FIGURE 4 | Core genome phylogenetic tree of a world-wide collection of *S. epidermidis* genomes. Maximum likelihood tree of the 58 Scottish isolates (Table 1) (isolates in blue) and the dataset from a world-wide collection of 225 isolates (isolates in gray) (NCBI BioProject numbers: PRJEB12090, PRJNA470534, and PRJNA470752) (Lee et al., 2018). As in Figure 1, the tree is annotated with the isolate's sequence type (ST) and displays the colored boxes of the heatmap illustrating the distribution of the characteristic genes of the SCCmec (blue), cop operon (brown/yellow), ACME (red) and COMER-like element (green) among the *S. epidermidis* isolates. Isolate BHP0662 (isolate in black) is used as reference strain in this phylogenetic tree.

to mercury and cadmium ($p < 0.05$) using Fisher's Exact test (Figures 5B,C). The phenotypes match to the presence of the cadmium and mercury transporter in these strains. The linear regression model was applied to predict the disk diffusion value of the cadmium and mercury based on the presence or absence of the COMER-like element in ST2 isolates, the coefficient of

correlation for mercury was $R^2 = 0.57$ and for cadmium was $R^2 = 0.75$. No association was found for ACME-carrying isolates.

The rate of excision of the composite SCCmec ACME and COMER-like elements was measured by quantitative real time PCR amplification of the reconstituted chromosomal attachment/target site and the circularized elements. Results

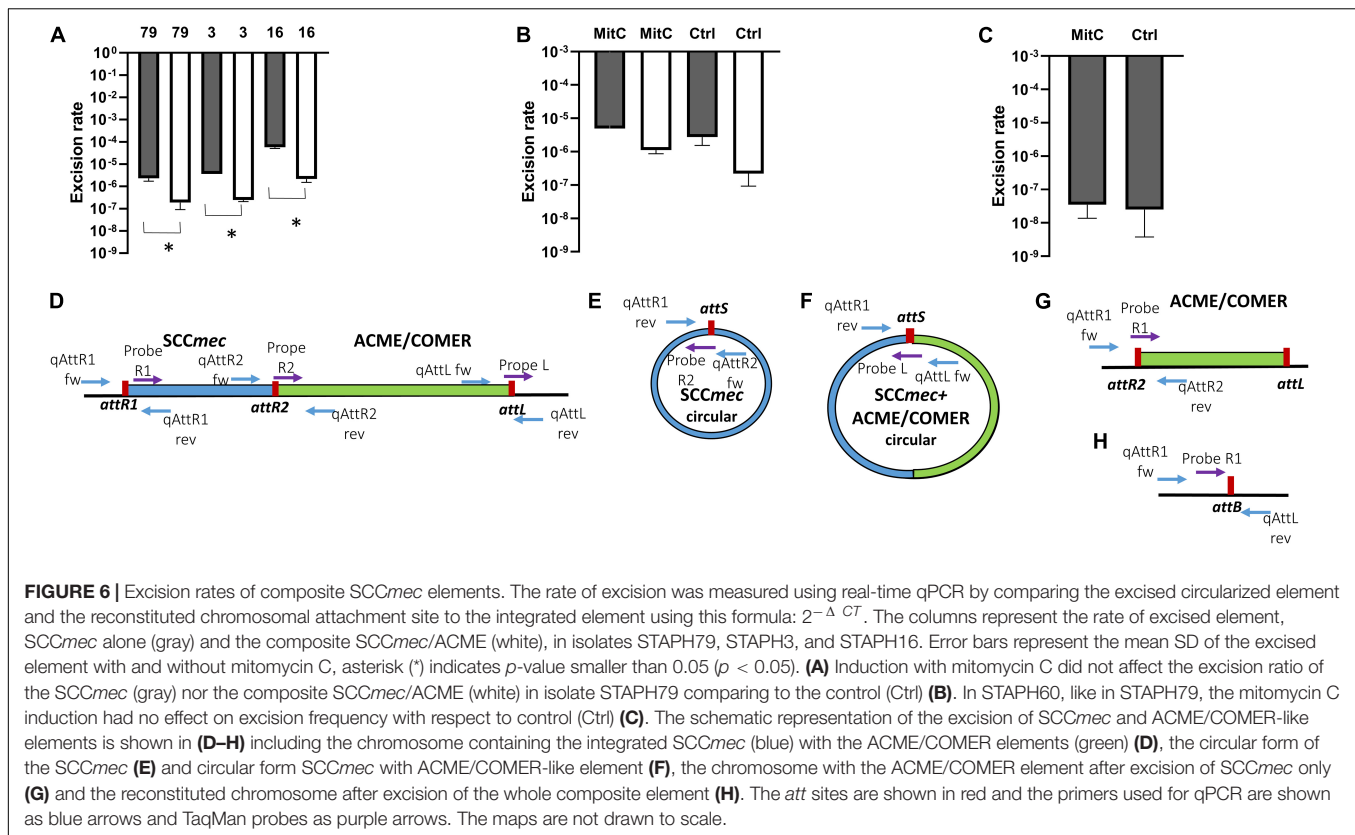


were compared to the quantification of the integrated elements (considered equivalent to the total quantification of chromosomes). Results for the ACME-I isolates STAPH16, STAPH3, and STAPH79 showed that the SCCmec-IV element alone did excise at a frequency ranging from 5.3×10^{-5} (isolate 16) to 2.7×10^{-6} (isolate 79) (Figure 6A). The excision of the whole composite SCCmec-IV/ACME-I element was significantly lower ($1.7 \times 10^{-6} - 1.2 \times 10^{-7}$) ($p < 0.05$) using *t*-test (Figure 6A). The ratio of excision did not significantly change ($p > 0.05$) in the presence of mitomycin C for any of the isolates, as shown for isolate STAPH79 (Figure 6B). Results for the COMER-like element in isolate STAPH60 showed that the SCCmec-III excised alone at a frequency equal to 2.3×10^{-8} and as with ACME the ratio of excision did not change with mitomycin C induction (Figure 6C). The whole composite SCCmec-III/COMER-like element excision was under the detection limit of our assay. The excision of the SCCmec-III is significantly lower than the SCCmec-IV excision by 100 times ($p < 0.05$) using *t*-test.

DISCUSSION

In recent decades, *S. epidermidis* has emerged as a nosocomial pathogen. Genomics showed that the two *S. epidermidis* hospital-adapted lineages within ST2 are nearly pan-drug resistance (Lee et al., 2018). The evolution of *S. epidermidis* from

commensal to disease-causing bacteria is poorly investigated, although several studies suggested that *S. epidermidis* acts as a reservoir of resistance genes for *S. aureus* (Otto, 2009). Comparative genomic analysis of *S. epidermidis* clinical isolates in this study revealed a high prevalence of methicillin resistance and the MLST showed that more than half the isolates belonged to clinically predominant ST2 confirming the dissemination of this multidrug resistance lineage in our study isolates. The increased capacity of ST2 to acquire drug resistance phenotypes has been attributed to a single polymorphism in the core genome RNA polymerase gene *rpoB* (Lee et al., 2018). While this original SNP may well be at the origin of the success of ST2, the dominant presence of a large composite COMER-like element in the ST-2 BPH662 lineage is likely very significant to the success of the lineage. The COMER-like element was exceptionally stable when compared to other SCC composite structures, for example ACME (Miragaia et al., 2009; O'Connor et al., 2018b). In *S. aureus* USA300 the copper resistance phenotype conferred by the COMER element was found to be associated with increased macrophage resistance and fitness (Purves et al., 2018; Zapotoczna et al., 2018). In this study we observed only a mercury and cadmium resistance phenotype only in isolates bearing the COMER-like element, but this may be related to the wide distribution of the copper gene cluster among most *S. epidermidis* isolates. The role of the additional genes within the COMER-like element, and absent in USA300, in the success of the BPH662 lineage, cannot be inferred at this stage.



This investigation analysing the diversity of composite SCC elements identified, in addition to the well-known ACME elements characterized in *S. epidermidis*, a highly conserved COMER-like element in one of the main ST2 clusters, the BPH0662-lineage (Zamudio et al., 2019). Different types of ACME identified in this study, including ACME type IV and V, harbored the *kdp* operon linked previously to oronasal *S. epidermidis* isolates only (O'Connor et al., 2018b). The findings from oronasal *S. epidermidis* isolates harboring ACME suggested that each ACME type emerged from the respective identical or closely related ST rather than the site from which the isolates harboring ACME were recovered (O'Connor et al., 2018b). For example, isolates harboring ACME type II and V investigated in this study belonged to ST73 and ST5 respectively, the same STs harboring ACME types II and V in oronasal *S. epidermidis*. Isolates harboring ACME type I belonged to ST48 as well as ST54 and ST35 (a double locus variant of ST48) and isolates harboring ACME type IV belonged to ST210. However, one isolates with ACME type I and one isolate with ACME type IV belonged to ST528 and a new ST which is closely related to ST470 respectively, suggesting emergence from a different lineage. The variations in the ACME-composite island investigated in this study suggest the rapid evolution of ACME in *S. epidermidis*. Previous studies of ACME prevalence amongst *S. epidermidis* populations reported a higher prevalence of ACME in MSSE than MRSE (Miragaia et al., 2009; Barbier et al., 2011; Onishi et al., 2013). Our data are supportive of this finding as ACME was identified in 9/50 (18%) of the MRSE and in 4/8 (50%) of the MSSE.

In addition to confirm excision of the SCCmec elements as previously reported (Stojanov et al., 2015), we report circularization of the ACME element and the *S. epidermidis* COMER-like element. The excision frequency of the SCCmec-IV in ACME-I containing isolates 16, 3 and 79 ranged from 5.3×10^{-5} to 2.7×10^{-6} while the excision of the composite SCCmec-IV/ACME-I element was approximately 5 times lower. This finding correlates with previous studies on *S. aureus* in which the rate of excision was estimated to be lower than 10^{-4} (Ito et al., 1999; Stojanov et al., 2015). Interestingly, the net production of excision products in the presence of mitomycin C did not change for any of the isolates different to what observed previously by others (Liu et al., 2017). The SCCmec-III excision in COMER-like element containing isolate was up to 100 times lower than the SCCmec-IV excision. This shows a strong correlation of excision frequency and genomic variability. We hypothesize that this difference in excision of both the SCCmec and of the composite elements may explain the high genomic stability of the COMER-like elements compared to the high variability of the ACME elements.

CONCLUSION

In conclusion this work identifies a large composite SCCmec COMER-like element in the main clinical ST-BPH662 lineage of *S. epidermidis*. The exceptional stability of this large element

supports the contribution of this element to the success of this important lineage of clinical *S. epidermidis* isolates.

DATA AVAILABILITY STATEMENT

The datasets generated for this study can be found in the GenBank (accession numbers SAMN12840193–SAMN12840250).

AUTHOR CONTRIBUTIONS

NA performed the bulk of the laboratory and genomic work, and wrote the manuscript. RZ provided genomic training, contributed high throughput genomic data, and participated in the writing of the manuscript. CJ and CI were involved in phenotypic of clinical isolates and DNA extraction for genome sequencing. JR was involved in genome annotation and DNA extraction. AR was co-supervisor of NA and was involved in data analysis and manuscript preparation. IG supervised the

clinical isolate collection and susceptibility testing. JM was co-supervisor of NA and was involved in data analysis and manuscript preparation. KH was involved in planning of the work, data analysis, and manuscript writing. MO conceived and supervised the work and contributed to the writing of the manuscript.

FUNDING

NA was supported by a fellowship of the King Saud University (Riyadh, Saudi Arabia). JR was supported by the BBSRC grant BB/P504737/1.

ACKNOWLEDGMENTS

The authors thank the work of the management team of the ALICE High Performance Computing Facility at the University of Leicester.

REFERENCES

- Altschul, S. F., Gish, W., Miller, W., Myers, E. W., and Lipman, D. J. (1990). Basic local alignment search tool. *J. Microbiol.* 215, 403–410. doi: 10.1016/S0022-2836(05)80360-2
- Aziz, R. K., Bartels, D., Best, A. A., DeJongh, M., Disz, T., Edwards, R. A., et al. (2008). The RAST server: rapid annotations using subsystems technology. *BMC Genomics* 9:75. doi: 10.1186/1471-2164-9-75
- Barbier, F., Lebeaux, D., Hernandez, D., Delannoy, A.-S., Caro, V., François, P., et al. (2011). High prevalence of the arginine catabolic mobile element in carriage isolates of methicillin-resistant *Staphylococcus epidermidis*. *J. Antimicrob. Chemother.* 66, 29–36. doi: 10.1093/jac/dkq410
- Berriman, M. (2003). Viewing and annotating sequence data with Artemis. *Brief. Bioinform.* 4, 124–132. doi: 10.1093/bib/4.2.124
- Bolger, A. M., Lohse, M., and Usadel, B. (2014). Trimmomatic: a flexible trimmer for Illumina sequence data. *Bioinformatics* 30, 2114–2120. doi: 10.1093/bioinformatics/btu170
- Darling, A. C. E. (2004). Mauve: multiple alignment of conserved genomic sequence with rearrangements. *Genome Res.* 14, 1394–1403. doi: 10.1101/gr.2289704
- Diep, B. A., Gill, S. R., Chang, R. F., Phan, T. H., Chen, J. H., Davidson, M. G., et al. (2006). Complete genome sequence of USA300, an epidemic clone of community-acquired methicillin-resistant *Staphylococcus aureus*. *Lancet* 367:9.
- Diep, B. A., Stone, G. G., Basuino, L., Graber, C. J., Miller, A., Etages, S., et al. (2008). The arginine catabolic mobile element and staphylococcal chromosomal cassette mec linkage: convergence of virulence and resistance in the USA300 clone of methicillin-resistant *Staphylococcus aureus*. *J. Infect. Dis.* 197, 1523–1530. doi: 10.1086/587907
- Espadinha, D., Sobral, R. G., Mendes, C. I., Méric, G., Sheppard, S. K., Carriço, J. A., et al. (2019). Distinct phenotypic and genomic signatures underlie contrasting pathogenic potential of *Staphylococcus epidermidis* clonal lineages. *Front. Microbiol.* 10:1971. doi: 10.3389/fmicb.2019.01971
- Gurevich, A., Saveliev, V., Vyahhi, N., and Tesler, G. (2013). QUASt: quality assessment tool for genome assemblies. *Bioinformatics* 29, 1072–1075. doi: 10.1093/bioinformatics/btt086
- Hijazi, K., Mukhopadhyay, I., An-Bott, F., Milne, K., Al-Jabri, Z. J., Oggioni, M. R., et al. (2016). Susceptibility to chlorhexidine amongst multidrug-resistant clinical isolates of *Staphylococcus epidermidis* from bloodstream infections. *Int. J. Antimicrob. Agents* 48, 86–90. doi: 10.1016/j.ijantimicag.2016.04.015
- Ito, T., Katayama, Y., and Hiramatsu, K. (1999). Cloning and nucleotide sequence determination of the entire mec DNA of pre-methicillin-resistant *Staphylococcus aureus* N315. *Antimicrob. Agents Chemother.* 43, 1449–1458. doi: 10.1128/AAC.43.6.1449
- Kaya, H., Hasman, H., Larsen, J., Stegger, M., Johannesen, T. B., Allesøe, R. L., et al. (2018). SCC mec finder, a web-based tool for typing of staphylococcal cassette chromosome mec in *Staphylococcus aureus* using whole-genome sequence data. *mSphere* 3:e00612-17. doi: 10.1128/mSphere.00612-17
- Larsen, M. V., Cosentino, S., Rasmussen, S., Friis, C., Hasman, H., Marvig, R. L., et al. (2012). Multilocus sequence typing of total-genome-sequenced bacteria. *J. Clin. Microbiol.* 50, 1355–1361. doi: 10.1128/JCM.06094-11
- Lee, J. Y. H., Monk, I. R., Gonçalves da Silva, A., Seemann, T., Chua, K. Y. L., Kearns, A., et al. (2018). Global spread of three multidrug-resistant lineages of *Staphylococcus epidermidis*. *Nat. Microbiol.* 3, 1175–1185. doi: 10.1038/s41564-018-0230-7
- Lindgren, J. K., Thomas, V. C., Olson, M. E., Chaudhari, S. S., Nuxoll, A. S., Schaeffer, C. R., et al. (2014). Arginine deiminase in *Staphylococcus epidermidis* functions to augment biofilm maturation through pH homeostasis. *J. Bacteriol.* 196, 2277–2289. doi: 10.1128/JB.00051-14
- Liu, P., Wu, Z., Xue, H., and Zhao, X. (2017). Antibiotics trigger initiation of SCCmec transfer by inducing SOS responses. *Nucleic Acids Res.* 45, 3944–3952. doi: 10.1093/nar/gkx153
- Livak, K. J., and Schmittgen, T. D. (2001). Analysis of relative gene expression data using real-time quantitative PCR and the 2[−]ΔΔCT method. *Methods* 25, 402–408. doi: 10.1006/meth.2001.1262
- McManus, B. A., O'Connor, A. M., Kinnevey, P. M., O'Sullivan, M., Polyzois, I., and Coleman, D. C. (2017). First detailed genetic characterization of the structural organization of type III arginine catabolic mobile elements harbored by *Staphylococcus epidermidis* by using whole-genome sequencing. *Antimicrob. Agents Chemother.* 61:e01216-17. doi: 10.1128/AAC.01216-17
- Méric, G., Mageiros, L., Pensar, J., Laabei, M., Yahara, K., Pascoe, B., et al. (2018). Disease-associated genotypes of the commensal skin bacterium *Staphylococcus epidermidis*. *Nat. Commun.* 9:5034. doi: 10.1038/s41467-018-07368-7
- Miragaia, M., de Lencastre, H., Perdreau-Remington, F., Chambers, H. F., Higashi, J., Sullam, P. M., et al. (2009). Genetic diversity of arginine catabolic mobile element in *Staphylococcus epidermidis*. *PLoS One* 4:e7722. doi: 10.1371/journal.pone.0007722
- Morrissey, I., Oggioni, M. R., Knight, D., Curiao, T., Coque, T., Kalkanci, A., et al. (2014). Evaluation of epidemiological cut-off values indicates that biocide resistant subpopulations are uncommon in natural isolates of clinically-relevant microorganisms. *PLoS One* 9:e86669. doi: 10.1371/journal.pone.0086669
- Nurk, S., Bankevich, A., Antipov, D., Gurevich, A. A., Korobeynikov, A., Lapidus, A., et al. (2013). Assembling single-cell genomes and mini-metagenomes from

- chimeric MDA products. *J. Comput. Biol.* 20, 714–737. doi: 10.1089/cmb.2013.0084
- O'Connor, A. M., McManus, B. A., and Coleman, D. C. (2018a). First description of novel arginine catabolic mobile elements (ACMEs) types IV and V harboring a kdp operon in *Staphylococcus epidermidis* characterized by whole genome sequencing. *Infect. Genet. Evol.* 61, 60–66. doi: 10.1016/j.meegid.2018.03.012
- O'Connor, A. M., McManus, B. A., Kinnevey, P. M., Brennan, G. I., Fleming, T. E., Cashin, P. J., et al. (2018b). Significant enrichment and diversity of the staphylococcal arginine catabolic mobile element ACME in *Staphylococcus epidermidis* isolates from subgingival peri-implantitis sites and periodontal pockets. *Front. Microbiol.* 9:1558. doi: 10.3389/fmicb.2018.01558
- Onishi, M., Urushibara, N., Kawaguchiya, M., Ghosh, S., Shinagawa, M., Watanabe, N., et al. (2013). Prevalence and genetic diversity of arginine catabolic mobile element (ACME) in clinical isolates of coagulase-negative staphylococci: identification of ACME type I variants in *Staphylococcus epidermidis*. *Infect. Genet. Evol.* 20, 381–388. doi: 10.1016/j.meegid.2013.09.018
- Otto, M. (2009). *Staphylococcus epidermidis* — the “accidental” pathogen. *Nat. Rev. Microbiol.* 7, 555–567. doi: 10.1038/nrmicro2182
- Page, A. J., Cummins, C. A., Hunt, M., Wong, V. K., Reuter, S., Holden, M. T. G., et al. (2015). Roary: rapid large-scale prokaryote pan genome analysis. *Bioinformatics* 31, 3691–3693. doi: 10.1093/bioinformatics/btv421
- Planet, P. J., Diaz, L., Kolokotronis, S.-O., Narechania, A., Reyes, J., Xing, G., et al. (2015). Parallel epidemics of community-associated methicillin-resistant *Staphylococcus aureus* USA300 infection in North and South America. *J. Infect. Dis.* 212, 1874–1882. doi: 10.1093/infdis/jiv320
- Planet, P. J., LaRussa, S. J., Dana, A., Smith, H., Xu, A., Ryan, C., et al. (2013). Emergence of the epidemic methicillin-resistant *Staphylococcus aureus* strain USA300 coincides with horizontal transfer of the arginine catabolic mobile element and speG-mediated adaptations for survival on skin. *mBio* 4:e00889-13. doi: 10.1128/mBio.00889-13
- Purves, J., Thomas, J., Riboldi, G. P., Zapotoczna, M., Tarrant, E., Andrew, P. W., et al. (2018). A horizontally gene transferred copper resistance locus confers hyper-resistance to antibacterial copper toxicity and enables survival of community acquired methicillin resistant *Staphylococcus aureus* USA300 in macrophages: *Staphylococcus aureus* copper resistance and innate immunity. *Environ. Microbiol.* 20, 1576–1589. doi: 10.1111/1462-2920.14088
- Rolo, J., Worning, P., Boye Nielsen, J., Sobral, R., Bowden, R., Bouchami, O., et al. (2017). Evidence for the evolutionary steps leading to mecA-mediated β -lactam resistance in staphylococci. *PLoS Genet.* 13:e1006674. doi: 10.1371/journal.pgen.1006674
- Rosario-Cruz, Z., Eletsky, A., Daigham, N. S., Al-Tameemi, H., Swapna, G. V. T., Kahn, P. C., et al. (2019). The *copBL* operon protects *Staphylococcus aureus* from copper toxicity: CopL is an extracellular membrane-associated copper-binding protein. *J. Biol. Chem.* 294, 4027–4044. doi: 10.1074/jbc.RA118.004723
- Siguier, P. (2006). ISfinder: the reference centre for bacterial insertion sequences. *Nucleic Acids Res.* 34, D32–D36. doi: 10.1093/nar/gkj014
- Sorosh, S., Jabalameli, F., Taherikalani, M., Amirmozafari, N., Imani Fooladi, A. A., Asadolahi, K., et al. (2016). Investigation of biofilm formation ability, antimicrobial resistance and the staphylococcal cassette chromosome mec patterns of methicillin resistant *Staphylococcus epidermidis* with different sequence types isolated from children. *Microb. Pathog.* 93, 126–130. doi: 10.1016/j.micpath.2016.01.018
- Stamatakis, A. (2014). RAXML version 8: a tool for phylogenetic analysis and post-analysis of large phylogenies. *Bioinformatics* 30, 1312–1313. doi: 10.1093/bioinformatics/btu033
- Stojanov, M., Moreillon, P., and Sakwinska, O. (2015). Excision of staphylococcal cassette chromosome mec in methicillin-resistant *Staphylococcus aureus* assessed by quantitative PCR. *BMC Res Notes* 8:828. doi: 10.1186/s13104-015-1815-3
- Yang, Z. (1994). Maximum likelihood phylogenetic estimation from DNA sequences with variable rates over sites: approximate methods. *J. Mol. Evol.* 39, 306–314. doi: 10.1007/BF00160154
- Yu, G., Smith, D. K., Zhu, H., Guan, Y., and Lam, T. T.-Y. (2017). ggtree: an R package for visualization and annotation of phylogenetic trees with their covariates and other associated data. *Methods Ecol. Evol.* 8, 28–36. doi: 10.1111/2041-210X.12628
- Zamudio, R., Oggioni, M. R., Gould, I. M., and Hijazi, K. (2019). Time for biocide stewardship? *Nat. Microbiol.* 4, 732–733. doi: 10.1038/s41564-019-0360-6
- Zapotoczna, M., Riboldi, G. P., Moustafa, A. M., Dickson, E., Narechania, A., Morrissey, J. A., et al. (2018). Mobile-genetic-element-encoded hypertolerance to copper protects *Staphylococcus aureus* from killing by host phagocytes. *mBio* 9:e00550-18. doi: 10.1128/mBio.00550-18

Conflict of Interest: The authors declare that the research was conducted in the absence of any commercial or financial relationships that could be construed as a potential conflict of interest.

Copyright © 2020 Almebairik, Zamudio, Ironside, Joshi, Ralph, Roberts, Gould, Morrissey, Hijazi and Oggioni. This is an open-access article distributed under the terms of the Creative Commons Attribution License (CC BY). The use, distribution or reproduction in other forums is permitted, provided the original author(s) and the copyright owner(s) are credited and that the original publication in this journal is cited, in accordance with accepted academic practice. No use, distribution or reproduction is permitted which does not comply with these terms.



Rv0579 Is Involved in the Resistance to the TP053 Antitubercular Prodrug

Giorgia Mori^{††}, Beatrice Silvia Orena^{††}, Laurent R. Chiarelli¹, Giulia Degiacomi¹, Olga Riabova², José Camilla Sammartino¹, Vadim Makarov², Giovanna Riccardi¹ and Maria Rosalia Pasca^{1*}

¹ Department of Biology and Biotechnology "Lazzaro Spallanzani," University of Pavia, Pavia, Italy, ² Bach Institute of Biochemistry, Federal Research Centre "Fundamentals of Biotechnology" of the Russian Academy of Sciences, Moscow, Russia

OPEN ACCESS

Edited by:

Paolo Visca,
Roma Tre University, Italy

Reviewed by:

Giovanni Delogu,
Catholic University of the Sacred
Heart, Italy
Brosch Roland,
Université Louis-Pasteur, France

*Correspondence:

Maria Rosalia Pasca
maria.rosalia.pasca@unipv.it

^{††} These authors have contributed
equally to this work

Specialty section:

This article was submitted to
Antimicrobials, Resistance
and Chemotherapy,
a section of the journal
Frontiers in Microbiology

Received: 12 December 2019

Accepted: 10 February 2020

Published: 25 February 2020

Citation:

Mori G, Orena BS, Chiarelli LR,
Degiacomi G, Riabova O,
Sammartino JC, Makarov V,
Riccardi G and Pasca MR (2020)
Rv0579 Is Involved in the Resistance
to the TP053 Antitubercular Prodrug.
Front. Microbiol. 11:292.
doi: 10.3389/fmicb.2020.00292

Tuberculosis remains one of the leading causes of death from a single pathogen globally. It is estimated that 1/4 of the world's population harbors latent tuberculosis, but only a 5–10% of patients will develop active disease. During latent infection, *Mycobacterium tuberculosis* can persist unaffected by drugs for years in a non-replicating state with low metabolic activity. The rate of the successful tuberculosis treatment is curbed by the presence of these non-replicating bacilli that can resuscitate after decades and also by the spread of *M. tuberculosis* drug-resistant strains. International agencies, including the World Health Organization, urge the international community to combat this global health emergency. The thienopyrimidine TP053 is a promising new antitubercular lead compound highly active against both replicating and non-replicating *M. tuberculosis* cells, with an *in vitro* MIC of 0.125 µg/ml. TP053 is a prodrug activated by the reduced form of the mycothiol-dependent reductase Mrx2, encoded by *Rv2466c* gene. After its activation, TP053 releases nitric oxide and a highly reactive metabolite, explaining its activity also against *M. tuberculosis* non-replicating cells. In this work, a new mechanism of TP053 resistance was discovered. *M. tuberculosis* spontaneous mutants resistant to TP053 were isolated harboring the mutation L240V in *Rv0579*, a protein with unknown function, but without mutation in *Rv2466c* gene. Recombineering method demonstrated that this mutation is linked to TP053 resistance. To better characterize *Rv0579*, the protein was recombinantly produced in *Escherichia coli* and a direct interaction between the Mrx2 activated TP053 and *Rv0579* was shown by an innovative target-fishing experiment based on click chemistry. Thanks to achieved results, a possible contribution of *Rv0579* in *M. tuberculosis* RNA metabolism was hypothesized, linked to toxin anti-toxin system. Overall, these data confirm the role of *Rv0579* in TP053 resistance and consequently in the metabolism of this prodrug.

Keywords: Rv0579, drug resistance, prodrug, tuberculosis, antitubercular drug

INTRODUCTION

Tuberculosis (TB), an old disease considered tied to the past, started again capturing the attention for different reasons, such as the spread of *Mycobacterium tuberculosis* drug-resistant strains (Koch et al., 2018). In the world, in 2018 about 500,000 people were infected by *M. tuberculosis* strains resistant to the most effective first-line drug rifampicin (RR-TB), and 78% of these isolates were

multidrug-resistant (MDR-TB). Three countries accounted for almost half of the world's cases of MDR-TB: India, China and the Russian Federation (World Health Organization [WHO], 2019). In order to fight drug-resistant TB, the treatment options have become limited, thus stressing the need for new therapies.

Another important threat is latent TB (LTB); according to WHO, LTB corresponds to a persistent immune response to stimulation by *M. tuberculosis* antigens without evidence of active TB (World Health Organization [WHO], 2018). The possible progression of LTB to active disease is a complex condition determined by bacterial, host, and environmental factors (Getahun et al., 2015).

About one-quarter of the world population develops LTB and it is considered as a persistent reservoir of active infection. Active TB will develop in 5–15% of individuals with LTB during their lifetimes. Several comorbidities could be related with increased risk of developing active TB, such as the HIV co-infection (Furin et al., 2019; Huaman and Sterling, 2019). Consequently, an effective treatment for LTB should be mandatory.

Current recommended LTB treatments include one of the following options: once-weekly isoniazid plus rifapentine for 3 months, daily rifampin for 4 months, daily isoniazid plus rifampin for 3–4 months, and daily isoniazid for 6–9 months (Huaman and Sterling, 2019). Treatments based on rifamycins seem to cause less adverse events and, consequently, to improve the therapy completion (Villa et al., 2019).

New and more effective drugs against LTB with fewer adverse events are needed in order to prevent active TB and to shorten treatment duration.

In this context, the thienopyrimidine (TP) TP053 is a new promising prodrug killing both replicating (MIC = 0.125 µg/ml) and non-replicating (MIC = 0.8 µg/ml) *M. tuberculosis* cells (Albesa-Jové et al., 2014). By microbiological, genetic, biochemical and crystallographic studies, its mechanism of activation was elucidated; TP053 is a prodrug activated by the reduced form of the DsbA-like mycoredoxin Mrx2 (encoded by *Rv2466c* gene), a mycothiol-dependent reductase with an unusual active-site motif CXXC (Albesa-Jové et al., 2014; Rosado et al., 2017). Mrx2 utilizes a chaperone-like mechanism of conformational changes, mainly in the CXXC active site motif, to recognize TP053 and promoting compound reduction (Albesa-Jové et al., 2015).

Recently, it has been demonstrated that Mrx2 works as a nitroreductase causing a release of nitric oxide (NO) from TP053 (Chiarelli et al., 2020). Thus, conceivably TP053 globally affects *M. tuberculosis* cell growth by NO release, which could be the cause of its activity against non-replicating bacilli, in a similar way to the NO releasing drug pretomanid, upon Ddn activation (Singh et al., 2008).

The study of the *M. tuberculosis* metabolic pathways affected by TP053 exposure, through transcriptional analysis, revealed features consistent with NO release, confirming the characteristic mechanism of action of TP053 against non-replicating bacilli (Chiarelli et al., 2020). Furthermore, it was identified a highly reactive metabolite, 2-(4-mercapto-6-(methylamino)-2-phenylpyrimidin-5-yl)ethan-1-ol, produced upon Mrx2 transformation of TP053, which could be co-responsible for

the antimycobacterial effects on replicating and non-replicating *M. tuberculosis* cells (Chiarelli et al., 2020). However, no potential target of this active metabolite has been identified so far.

In this work, we demonstrated that the Rv0579 protein has a role in the mechanism of resistance of TP053, even if its physiological role in *M. tuberculosis* still remains unclear.

MATERIALS AND METHODS

Bacterial Strains and Growth Conditions

Cloning steps were performed in *Escherichia coli* XL1-Blue, following standard methods (Sambrook and Russell, 2001) and using the oligonucleotides described in **Supplementary Table S1**. Protein expression was achieved in *E. coli* BL21(DE3).

Mycobacterium tuberculosis H37Rv and mutant strains were grown aerobically at 37°C either in Middlebrook 7H9 broth (Difco) or on Middlebrook 7H11 agar (Difco), both supplemented with 10% OADC Middlebrook Enrichment. When necessary, antibiotics were added at the following concentrations: ampicillin 100 µg/ml, hygromycin 200 µg/ml (20 µg/ml for *M. tuberculosis*), and kanamycin 50 µg/ml (20 µg/ml for *M. tuberculosis*).

All the experiments with *M. tuberculosis* were performed in Biosafety level 3 laboratory by authorized and trained researchers.

MIC Determination

MICs for the compounds were determined by means of the micro-broth dilution method. Dilutions of *M. tuberculosis* wild-type and mutant cultures (about 10⁵–10⁶ CFU/ml) were streaked onto 7H11 solid medium containing a range of drug concentrations. Plates were incubated at 37°C for about 21 days and the growth was visually evaluated. The lowest drug dilution at which visible growth failed to occur was taken as the MIC value. Results were expressed as the average of at least three independent replicates.

Isolation and Characterization of *M. tuberculosis* Mutants Resistant to TP053

The isolation of *M. tuberculosis* mutants was performed by plating ~10¹⁰ cells from an exponential growth phase culture of *M. tuberculosis* H37Rv onto 7H11 medium containing different concentrations of TP053, ranging from 5- to 40-fold the MIC of the wild-type strain. Genomic DNA of *M. tuberculosis* resistant mutants was isolated and sequenced by using Illumina HiSeq2000 technology at IGA Technology Services S.R.L. (Udine, Italy). For the bioinformatic analysis of Illumina data, repetitive PE and PPE gene families were discarded as well as SNPs and Indels with less than 50% probability. The mutations identified were confirmed by Sanger sequencing (Eurofins Genomics), after PCR amplification using the primers described in **Supplementary Table S1**. PCR products were purified using the Wizard® SV Gel and PCR Clean-Up system (Promega).

Recombineering Method

Recombineering method utilizing mycobacteriophage-encoded functions was used in order to confirm the role of *Rv0579* mutation in TP053 resistance, as previously described (van Kessel and Hatfull, 2008). Briefly, a *M. tuberculosis* strain that carries the recombineering plasmid pJV62 was induced by acetamide in mid-logarithmic growth and electrocompetent cells were prepared. Electroporation was performed with different concentrations (100 and 500 ng) of *Rv0579*rec oligonucleotide (**Supplementary Table S1**), which anneals to the template for discontinuous DNA synthesis (lagging strand), thus increasing recombination frequency. The introduced point mutation was co-selected by plating the transformations onto a 7H11 plate containing TP053 (1.25 and 5 $\mu\text{g/ml}$ corresponding to 10 \times and 40 \times MIC, respectively) and kanamycin (20 $\mu\text{g/ml}$).

Expression and Purification of *M. tuberculosis* Rv0579

Mycobacterium tuberculosis H37Rv *Rv0579* gene from genomic DNA was amplified by standard PCR, using the primers reported in **Supplementary Table S1**, and PCR fragments were cloned in the pET-SUMO vector (Invitrogen), to give pET-SUMO/*Rv0579* recombinant plasmid. *Rv0579* enzyme was produced in *E. coli* BL21(DE3), by overnight induction with 0.5 mM isopropyl- β -thiogalactopyranoside (IPTG) at 25°C. Thereafter, cells were harvested, re-suspended in 150 ml of buffer A (50 mM Tris-HCl pH 7.5, 300 mM NaCl, 0.5 mM dithiothreitol (DTT), 5% glycerol, 2 mM MgCl_2) containing 1 mM PMSF, disrupted by sonication and centrifuged for 30 min at 50,000 $\times g$. The supernatant was loaded on HisTrap Crude column (1 ml, GE Healthcare), washed with 50 ml of buffer A containing 50 mM of imidazole, then *Rv0579* elution was performed with 250 mM of imidazole in buffer A. The eluted protein was dialyzed using a HiPreP Desalting 26/10 column equilibrated in 50 mM Tris-HCl pH 7.5, 50 mM imidazole, 100 mM NaCl, 0.5 mM DTT, 2 MgCl_2 , 5% glycerol, incubated at 4°C in the presence of 15 μl SUMO-protease and then re-purified on HisTrap Crude column. The purified protein was checked by SDS-PAGE, concentrated to 5 mg/ml, and stored at -80°C . The protein concentration was determined by absorbance at 280 nm (ϵ : 21,680 $\text{M}^{-1}\text{cm}^{-1}$).

Target Fishing

To demonstrate a direct interaction between *Rv0579* protein and TP053, a TP053-azide-PEG3-biotin conjugate complex was used.

The 11526119 derivative of TP053, prepared as described in **Supplementary Material**, was firstly characterized to verify that it showed the same features as TP053. For this reason, Mrx2 enzymatic activity using 11526119 as substrate was assayed as previously described (Albesa-Jové et al., 2014), to confirm that this compound is activated like TP053.

Then, 11526119 was used to perform azide-alkyne cycloaddition reaction with Azide-PEG3-biotin conjugate, to form an adduct which can be immobilized on a streptavidin agarose resin (**Supplementary Figure S1**). To this purpose, in a final volume of 500 μl , 11526119 (200 μM) was incubated with 2-fold excess of Azide-PEG3-biotin conjugate, in the presence

of 250 μM of CuSO_4 and 5 mM Na-ascorbate, overnight at room temperature. The reaction was checked by thin layer chromatography, then incubated 1 h with Streptavidine Agarose resin, and washed with phosphate saline buffer (PBS) to remove any unbound material.

The complex was incubated with *Rv0579* (0.5 mg/ml) in a final volume of 200 μl , in the presence of Mrx2 (2 mg/ml, prepared according to Albesa-Jové et al., 2014), DTT (1 mM) and *Mycobacterium smegmatis* methanolic extract (2%) at 37°C for 30 min, then incubated 1 h with Streptavidine Agarose resin. After the incubation, the resin was washed five times with PBS to remove unbound proteins and then analyzed in SDS-PAGE. As negative control, the same incubation was performed with the only streptavidine-agarose resin, or in absence of *M. smegmatis* methanolic extract, to avoid Mrx2 activation.

Quantitative Real-Time PCR

Quantitative Real-Time PCR was performed on RNA extracted from *M. tuberculosis* H37Rv and *Rv0579* mutant strains, both treated with TP053 (0.06 $\mu\text{g/ml}$; 0.5 \times MIC) or untreated using the Direct-zolTM RNA MiniPrep Kit (Zymo Research). The cDNA was obtained from about 1 μg of total RNA by the Quantitect reverse transcription kit (Qiagen). The RT-PCR experiments were performed using the QuantiTect SYBR Green PCR Master Mix kit (Qiagen) and the “Rotor Gene 6000” thermocycler (Corbett Life Science).

The reaction was carried out in a final volume of 15 μl and contained: 7.5 μl of 2 \times SYBR Green Buffer (supplied by the kit), cDNA, primers (7.5 pmol) and RNase-free water. All reactions were repeated in triplicate and the mean value was considered. The primers used to assess the transcriptional analysis of *sigA* and *Rv0579* genes are present in **Supplementary Table S1**.

RESULTS

The Mutation in *Rv0579* Gene Is Responsible for TP053 Resistance

To identify the TP053 cellular target(s), two *M. tuberculosis* mutants resistant to TP053 (MIC = 2.5 $\mu\text{g/ml}$, 20 \times MIC of wild type strain) have been isolated using a *M. tuberculosis* culture overexpressing *mrx2* gene, coding for the activator (*M. tuberculosis*/pSODIT-*mrx2*) (Albesa-Jové et al., 2014). In this way, the selection of mutation(s) in *mrx2* could be avoided. After the confirmation of the TP053 resistance, to find the mutation(s) responsible for TP053 resistance, whole genome sequencing (WGS) of the new isolated resistant mutants was performed using Illumina method (**Table 1**). Interestingly, *M. tuberculosis* 2466.3 and 2466.4 mutants revealed the same mutation in *Rv0579* gene (C718G \rightarrow L240V), coding for a conserved hypothetical protein (**Table 1**). The presence of the mutation in the *Rv0579* gene was confirmed by Sanger sequencing. No mutation was detected in *mrx2* gene on either the chromosome or the plasmid.

The specific contribution of the mutation in *Rv0579* to TP053 resistance was confirmed by recombineering method (van Kessel and Hatfull, 2008) using different TP053 concentrations (10 \times and 40 \times MIC of the wild type strain), thus allowing the

TABLE 1 | Characteristics of the *M. tuberculosis* spontaneous TP053 resistant mutants.

<i>M. tuberculosis</i> strains	Concentration of isolation of TP053 resistant colonies ($\mu\text{g/ml}$)	Mutation in <i>mrx2</i>		Mutation in <i>Rv0579</i> (aa change)	MIC to TP53 ($\mu\text{g/ml}$)
		On genome	On plasmid		
<i>M. tuberculosis</i> /pSODIT/ <i>mrx2</i>	–	–	–	–	0.125
2466.3 mutant	0.5 ($4\times$ MIC)	No	No	C718G (L240V)	2.5 ($20\times$ MIC)
2466.4 mutant	1 ($8\times$ MIC)	No	No	C718G (L240V)	2.5 ($20\times$ MIC)

generation of the C718G substitution in chromosomal *Rv0579* of wild-type H37Rv (**Supplementary Table S2**). The generated TP053 resistant colonies were screened for the introduction of the *Rv0579* C718G substitution by Sanger sequencing and their TP053 resistance profile confirmed by MIC determination. None of the recombineering-generated mutants harboured mutations in *mrx2*. In every tested mutant, the only presence of *Rv0579* mutation (C718G) conferred TP053 resistance (MIC = $2.5\ \mu\text{g/ml}$, $20\times$ MIC of wild type strain). These results confirmed the role of *Rv0579* in the mechanism of resistance to TP053.

Thus, the possibility that the resistance to TP053 might be due to the overexpression of *Rv0579* gene was excluded by quantitative PCR of *Rv0579* transcripts from both *M. tuberculosis* wild-type and TP053 resistant (Rec5 mutant obtained by recombineering) strains, in presence/absence of prodrug; in fact, no significant difference in the expression of *Rv0579* was observed (**Supplementary Table S3**).

Rv0579 Protein Is Able to Directly Interact With the Activated TP053

In order to further investigate the role of *Rv0579* in the TP053 resistance, the *Rv0579* protein was recombinantly produced in *E. coli* and purified to homogeneity (**Supplementary Figure S2**). The produced protein was found to be bound to nucleic acids. Subsequent DNase and RNase digestion revealed RNA to be the main contaminant (**Supplementary Figure S3**). However, an efficient digestion of RNA was achieved only after partial denaturation of the protein, indicating a strong interaction. For this reason, DNase and RNase were added in the lysis buffer ($100\ \mu\text{l}$, $2\ \text{mg/ml}$) for additional purification steps. Despite several attempts using different chromatographical approaches, the nucleic acids were not completely removed in any case (data not shown).

The achieved recombinant protein was then exploited to demonstrate a possible direct interaction between *Rv0579* and the activated TP053 through a target-fishing experiment based on click chemistry (**Figure 1**). For this experiment, a TP053 derivative (11526119; MIC = $0.5\ \mu\text{g/ml}$) (**Supplementary Material**) was used, which was shown to retain TP053 ability to be activated by *Mrx2* by an *in vitro* enzymatic assay (**Figures 1A,B**). Consequently, the *Rv0579* protein was incubated with a TP053azide-PEG3-biotin conjugate complex in presence of the activator *Mrx2*, then bound on Streptavidin Agarose resin. After several washing steps, the resin was analyzed by SDS-PAGE (**Figure 1C**). As control, the same reaction was performed also in the absence of mycothiols, to avoid *Mrx2* activation, or using the only azide-PEG3-biotin.

The obtained data demonstrated that the activated prodrug binds not only to *Mrx2*, as expected, but also to *Rv0579* (**Figure 1C**), indicating a direct interaction between the activated TP053 and *Rv0579*.

These results confirm the role of *Rv0579* in the mechanism of TP053 resistance.

Understanding the Role of *Rv0579* in TP053 Resistance

Previous RNA-seq experiments demonstrated that the exposure to TP053 ($6\ \mu\text{g/ml}$; $\sim 50\times$ MIC) of *M. tuberculosis* cells caused an over-expression of some toxin-antitoxin (TA) systems (e.g.: HlgAB, VapBC16) (Chiarelli et al., 2020).

Interestingly, on *M. tuberculosis* genome, *Rv0579* is located near to *Rv0581* (coding for the antitoxin VapB26) and *Rv0582* (coding for the toxin VapC26) (Kang et al., 2017). Taking advantage of the availability of our *Rv0579* mutant (Rec5 mutant obtained by recombineering), we performed Real-Time PCR using both *M. tuberculosis* wild type and *Rv0579* mutant cultures treated with TP053 ($0.06\ \mu\text{g/ml}$; $0.5\times$ MIC) (**Supplementary Table S3**) to investigate possible changes in the expression levels of the genes encoding VapBC26 TA system. Untreated cultures were used as control.

Surprisingly, only in *M. tuberculosis* wild type strain an up-regulation of the gene encoding the VapC26 toxin was found; in the *Rv0579* mutant the *Rv0582* over-expression was not detected (**Supplementary Table S3**). These results suggest a possible link between *Rv0579* and VapBC26 system.

Since *Rv0579* protein possesses the two domains Ub-Mut7C and Mut7-C, usually related to RNase activity (Marchler-Bauer et al., 2017), we hypothesized that the link with VapBC26 could involve this possible activity. Unfortunately, we were not able to determine it, because of the nucleic acid contamination of the purified protein (data not shown). Further experiments to support this hypothesis currently were limited until this issue is solved.

DISCUSSION

TP053 is a very promising compound active against replicating and non-replicating *M. tuberculosis* cells with a peculiar mechanism of action (Albesa-Jové et al., 2014; Chiarelli et al., 2020). In fact, this prodrug is activated by *Mrx2* producing an active metabolite by NO release. Furthermore, TP053 inhibits *M. tuberculosis* cell growth by influencing several metabolic pathways such as RNA metabolism (Chiarelli et al., 2020).

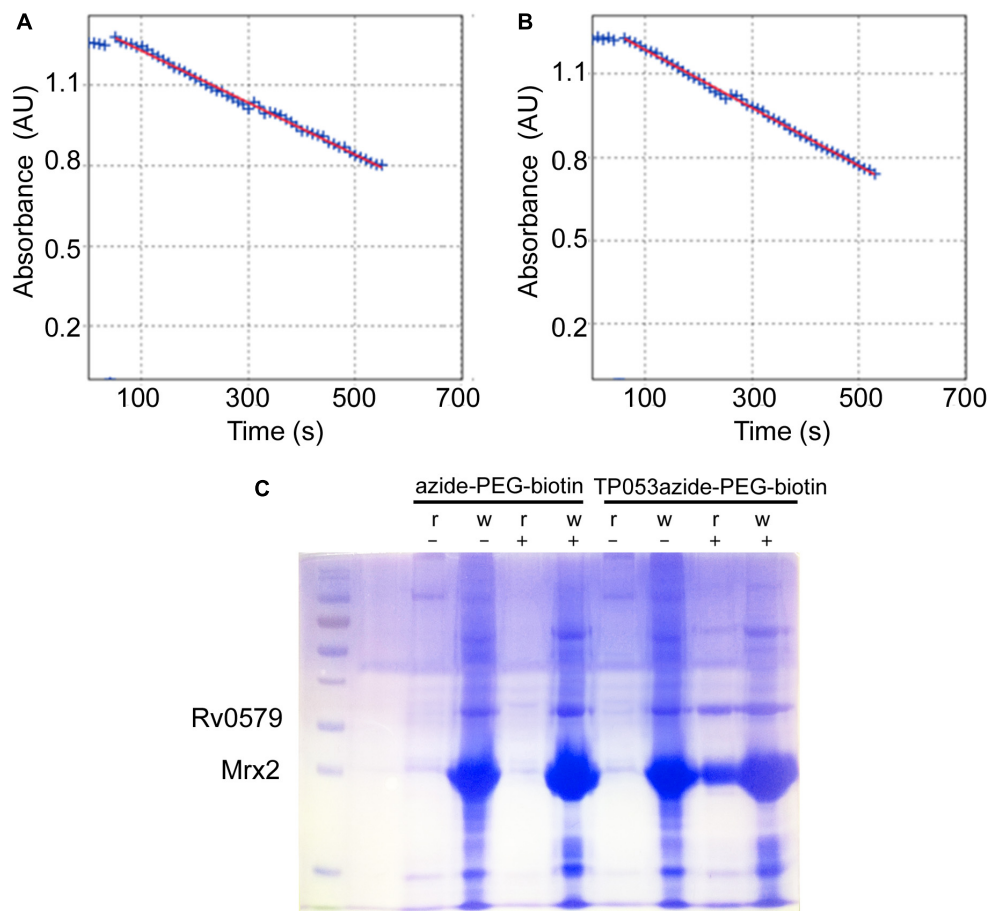


FIGURE 1 | Target fishing experiments. **(A,B)** The enzymatic activity assay of Mrx2 using 11526119 as a substrate **(A)**, was compared with the assay using TP053 **(B)** demonstrating that the compound retaining the same capability to be metabolized by the enzyme. Then, it was suitable for target fishing experiments. **(C)** SDS-PAGE analysis of the target fishing experiments. The streptavidine-agarose resin was incubated 1 h with the TP53-azide-PEG-biotin, or with azide-PEG-biotin complex, reacted with Rv0579. After the incubation the samples were washed with buffer, and both resin and wash fractions analyzed by SDS-PAGE. r, resin; w, wash; +, incubation with Rv0579 in the presence of mycothiols, to allow Mrx2 activation; −, incubation with Rv0579 without mycothiols as blank control. Rv0579 did not show any reactivity with the streptavidine-agarose resin alone, since the protein was found only in wash fractions (lanes 5 and 6). By contrast, Rv0579 was found bound the resin-TP053 complex, but only after Mrx2 activation (lane 9). This experiment demonstrates a direct interaction between the protein and the activated compound, which confirms a role of Rv0579 in resistance to TP053.

In this work, a new mechanism of resistance to TP053 was discovered. *M. tuberculosis* spontaneous mutants resistant to TP053 were isolated harboring a mutation in *Rv0579* gene. The contribution of this mutation to TP053 resistance was confirmed by recombineering method. Moreover, target fishing experiment demonstrated that Rv0579 is able to bind TP053, but only upon Mrx2 activation of the compound.

Rv0579 is a non-essential gene (Griffin et al., 2011), encoding a conserved hypothetical protein with unknown function. The sequence of *Rv0579* protein shows two important domains, usually linked to RNase activity: Ub-Mut7C and Mut7-C (Marchler-Bauer et al., 2017) (**Supplementary Table S4**).

Mut7-C is a RNase domain of the PIN fold with an inserted zinc ribbon located at the C terminus of the protein (Anantharaman et al., 2002); this domain is typical of VapC toxin (toxin-antitoxin system). The mutation found in TP053

resistant *M. tuberculosis* mutants is located at the end of this domain. Ub-Mut7C domain is occasionally present at the N-terminus of the protein with the Mut7-C domain, suggesting an RNA-binding role (Iyer et al., 2006) (**Supplementary Table S4**). In our case, this hypothesis is also corroborated by the finding that the recombinant protein tightly binds RNA (**Supplementary Figure S3**).

Iyer et al. (2006) identified a group of proteins containing the two domains, Ub-Mut7C and Mut7-C, fused; *Rv0579* belongs to this group containing several proteins with unknown function belonging to different bacterial species (**Supplementary Figure S4** and **Supplementary Table S4**). Interestingly, the alignment of these proteins shows that the mutation in *Rv0579* responsible for TP053 resistance is present at the end of Mut7-C domain and it corresponds to a change of an amino acid conserved in some bacterial species (L240; *Streptomyces*

coelicolor, *Nostoc punctiforme*, *Nocardia farcinica*, *Thermobifida fusca*) (**Supplementary Figure S4**). In other tested species, this amino acid changes in Met.

It is noteworthy that TP053 releases NO, consequently affecting RNA metabolism and causing inhibition of respiration, oxidative stress, and DNA damage (Chiarelli et al., 2020). This again suggests that Rv0579 has a role in RNA metabolism, one of the pathways mainly affected by NO release (Darwin et al., 2003; Voskuil et al., 2003; Manjunatha et al., 2009).

From the achieved results, and thanks to a deep analysis of the Rv0579 sequence, a role of Rv0579 in RNA metabolism could be hypothesized, linked to toxin anti-toxin systems (e.g. VapBC26). Indeed, TP053 treatment in wild-type *M. tuberculosis* caused an up-regulation of the Rv0582 gene encoding the VapC26 toxin, while no effect has been seen in *M. tuberculosis* resistant mutant carrying mutation in Rv0579. These evidences thus suggest a role of this protein in the regulation of this toxin-antitoxin system.

Even if the physiological role of Rv0579 is still under investigation, this work unveils some important aspects of the protein, paving the way for further evidences that will allow to clearly elucidate its role in *M. tuberculosis* metabolism and in TP053 resistance.

DATA AVAILABILITY STATEMENT

All datasets generated for this study are included in the article/**Supplementary Material**.

REFERENCES

- Albesa-Jové, D., Chiarelli, L. R., Makarov, V., Pasca, M. R., Urresti, S., Mori, G., et al. (2014). Rv2466c mediates the activation of TP053 to kill replicating and non-replicating *Mycobacterium tuberculosis*. *ACS Chem. Biol.* 9, 1567–1575. doi: 10.1021/cb500149m
- Albesa-Jové, D., Comino, N., Tera, M., Mohorko, E., Urresti, S., Dainese, E., et al. (2015). The redox state regulates the conformation of Rv2466c to activate the antitubercular prodrug TP053. *J. Biol. Chem.* 290, 31077–31089. doi: 10.1074/jbc.M115.677039
- Anantharaman, V., Koonin, E. V., and Aravind, L. (2002). Comparative genomics and evolution of proteins involved in RNA metabolism. *Nucleic Acids Res.* 30, 1427–1464. doi: 10.1093/nar/30.7.1427
- Chiarelli, L. R., Salina, E. G., Mori, G., Azhikina, T., Riabova, O., Lepioshkin, A., et al. (2020). New insights into the mechanism of action of the thienopyrimidine antitubercular prodrug TP053. *ACS Infect. Dis.* 6, 313–323. doi: 10.1021/acinfecdis.9b00388
- Darwin, K. H., Ehrt, S., Gutierrez-Ramos, J. C., Weich, N., and Nathan, C. F. (2003). The proteasome of *Mycobacterium tuberculosis* is required for resistance to nitric oxide. *Science* 302, 1963–1966. doi: 10.1126/science.1091176
- Furin, J., Cox, H., and Pai, M. (2019). Tuberculosis. *Lancet* 393, 1642–1656. doi: 10.1016/S0140-6736(19)30308-30303
- Getahun, H., Chaisson, R. E., and Ravignone, M. (2015). Latent mycobacterium tuberculosis infection. *N. Engl. J. Med.* 373, 1179–1180. doi: 10.1056/NEJMc1508223
- Griffin, J. E., Gawronski, J. D., Dejesus, M. A., Ioerger, T. R., Akerley, B. J., and Sassetti, C. M. (2011). High-resolution phenotypic profiling defines genes essential for mycobacterial growth and cholesterol catabolism. *PLoS Pathog.* 7:e1002251. doi: 10.1371/journal.ppat.1002251

AUTHOR CONTRIBUTIONS

GM, BO, LC, and MP designed the study. LC, VM, GR, and MP wrote the manuscript and interpreted the data. GM, BO, LC, GD, OR, and JS performed the experiments. All authors approved the final version of the manuscript.

FUNDING

This work was supported by the European Community's Seventh Framework Program (Grant 260872) and the University of Pavia, Italy ("Universitiamo-Tubercolosi: un killer riemergente"). This work was also supported by the Italian Ministry of Education, University and Research (MIUR): Dipartimenti di Eccellenza Program (2018–2022) – Department of Biology and Biotechnology "L. Spallanzani," University of Pavia.

ACKNOWLEDGMENTS

We thank Prof. G. F. Hatfull for kindly giving us pJV62 plasmid to perform recombineering method.

SUPPLEMENTARY MATERIAL

The Supplementary Material for this article can be found online at: <https://www.frontiersin.org/articles/10.3389/fmicb.2020.00292/full#supplementary-material>

- Huaman, M. A., and Sterling, T. R. (2019). Treatment of latent tuberculosis infection—an update. *Clin. Chest. Med.* 40, 839–848. doi: 10.1016/j.ccm.2019.07.008
- Iyer, L. M., Burroughs, A. M., and Aravind, L. (2006). The prokaryotic antecedents of the ubiquitin-signaling system and the early evolution of ubiquitin-like beta-grasp domains. *Genome Biol.* 7:R60.
- Kang, S. M., Kim, D. H., Lee, K. Y., Park, S. J., Yoon, H. J., Lee, S. J., et al. (2017). Functional details of the *Mycobacterium tuberculosis* VapBC26 toxin-antitoxin system based on a structural study: insights into unique binding and antibiotic peptides. *Nucleic Acids Res.* 45, 8564–8580. doi: 10.1093/nar/gkx489
- Koch, A., Cox, H., and Mizrahi, V. (2018). Drug-resistant tuberculosis: challenges and opportunities for diagnosis and treatment. *Curr. Opin. Pharmacol.* 42, 7–15. doi: 10.1016/j.coph.2018.05.013
- Manjunatha, U., Boshoff, H. I., and Barry, C. E. III (2009). The mechanism of action of PA-824: novel insights from transcriptional profiling. *Commun. Integr. Biol.* 2, 215–218. doi: 10.4161/cib.2.3.7926
- Marchler-Bauer, A., Bo, Y., Han, L., He, J., Lanczycki, C. J., Lu, S., et al. (2017). CDD/SPARCLE: functional classification of proteins via subfamily domain architectures. *Nucleic Acids Res.* 45, D200–D203. doi: 10.1093/nar/gkw1129
- Rosado, L. A., Wahn, K., Degiacomi, G., Pedre, B., Young, D., and de la Rubia, A. G. (2017). The antibacterial prodrug activator Rv2466c is a mycothiol-dependent reductase in the oxidative stress response of *Mycobacterium tuberculosis*. *J. Biol. Chem.* 292, 13097–13110. doi: 10.1074/jbc.M117.797837
- Sambrook, J., and Russell, D. W. (2001). *Molecular Cloning: A Laboratory Manual*, 3rd Edn, Cold Spring Harbor, NY: Cold Spring Harbor Laboratory Press.
- Singh, R., Manjunatha, U., Boshoff, H. I., Ha, Y. H., Niyomrattanakit, P., Ledwidge, R., et al. (2008). PA-824 kills nonreplicating *Mycobacterium tuberculosis* by intracellular NO release. *Science* 322, 1392–1395. doi: 10.1126/science.1164571

- van Kessel, J. C., and Hatfull, G. F. (2008). Mycobacterial recombineering. *Methods Mol. Biol.* 435, 203–215. doi: 10.1007/978-1-59745-232-8_15
- Villa, S., Ferrarese, M., Sotgiu, G., Castellotti, P. F., Saderi, L., Grecchi, C., et al. (2019). Latent tuberculosis infection treatment completion while shifting prescription from isoniazid-only to rifampicin-containing regimens: a two-decade experience in Milan, Italy. *J Clin Med.* 9:E101. doi: 10.3390/jcm9010101
- Voskuil, M. I., Schnappinger, D., Visconti, K. C., Harrell, M. I., Dolganov, G. M., Sherman, D. R., et al. (2003). Inhibition of respiration by nitric oxide induces a *Mycobacterium tuberculosis* dormancy program. *J. Exp. Med.* 198, 705–713. doi: 10.1084/jem.20030205
- World Health Organization [WHO] (2018). *Latent TB Infection: Updated and Consolidated Guidelines for Programmatic Management*. Geneva: World Health Organization.
- World Health Organization [WHO] (2019). *Global Tuberculosis Report 2018*. Geneva: World Health Organization.
- Conflict of Interest:** The authors declare that the research was conducted in the absence of any commercial or financial relationships that could be construed as a potential conflict of interest.
- Copyright © 2020 Mori, Orena, Chiarelli, Degiacomi, Riabova, Sammartino, Makarov, Riccardi and Pasca. This is an open-access article distributed under the terms of the Creative Commons Attribution License (CC BY). The use, distribution or reproduction in other forums is permitted, provided the original author(s) and the copyright owner(s) are credited and that the original publication in this journal is cited, in accordance with accepted academic practice. No use, distribution or reproduction is permitted which does not comply with these terms.



Escaping the Phagocytic Oxidative Burst: The Role of SODB in the Survival of *Pseudomonas aeruginosa* Within Macrophages

Luca Cavinato¹, Elena Genise¹, Francesco R. Luly¹, Enea G. Di Domenico², Paola Del Porto¹ and Fiorentina Ascenzioni^{1*}

¹ Department of Biology and Biotechnology "Charles Darwin", Sapienza University of Rome, Rome, Italy, ² Microbiology and Virology, San Gallicano Dermatologic Institute, IRCCS, Rome, Italy

OPEN ACCESS

Edited by:

Pietro Alifano,
University of Salento, Italy

Reviewed by:

Jamel El-Benna,
INSERM U1149 Centre de Recherche
sur l'Inflammation, France
Vincenzo Scarlato,
University of Bologna, Italy

*Correspondence:

Fiorentina Ascenzioni
fiorentina.ascenzioni@uniroma1.it

Specialty section:

This article was submitted to
Antimicrobials, Resistance
and Chemotherapy,
a section of the journal
Frontiers in Microbiology

Received: 22 October 2019

Accepted: 14 February 2020

Published: 10 March 2020

Citation:

Cavinato L, Genise E, Luly FR,
Di Domenico EG, Del Porto P and
Ascenzioni F (2020) Escaping
the Phagocytic Oxidative Burst:
The Role of SODB in the Survival
of *Pseudomonas aeruginosa* Within
Macrophages.
Front. Microbiol. 11:326.
doi: 10.3389/fmicb.2020.00326

Reactive oxygen species (ROS) are small oxygen-derived molecules that are used to control infections by phagocytic cells. In macrophages, the oxidative burst produced by the NOX2 NADPH-oxidase is essential to eradicate engulfed pathogens by both oxidative and non-oxidative killing. Indeed, while the superoxide anion (O_2^-) produced by NOX2, and the other ROS derived from its transformation, can directly target pathogens, ROS also contribute to activation of non-oxidative microbicidal effectors. The response of pathogens to the phagocytic oxidative burst includes the expression of different enzymes that target ROS to reduce their toxicity. Superoxide dismutases (SODs) are the primary scavengers of O_2^- , which is transformed into H_2O_2 . In the Gram-negative *Salmonella typhimurium*, periplasmic SODCI has a major role in bacterial resistance to NOX-mediated oxidative stress. In *Pseudomonas aeruginosa*, the two periplasmic SODs, SODB, and SODM, appear to contribute to bacterial virulence in small-animal models. Furthermore, NOX2 oxidative stress is essential to restrict *P. aeruginosa* survival in macrophages early after infection. Here, we focused on the role of *P. aeruginosa* SODs in the counteracting of the lethal effects of the macrophage oxidative burst. Through this study of the survival of *sod* mutants in macrophages and the measurement of ROS in infected macrophages, we have identified a dual, antagonistic, role for SODB in *P. aeruginosa* survival. Indeed, the survival of the *sodB* mutants, but not of the *sodM* mutants, was greater than that of the wild-type (WT) bacteria early after infection, and *sodB*-infected macrophages showed higher levels of O_2^- and lower levels of H_2O_2 . This suggests that SODB contributes to the production of lethal doses of H_2O_2 within the phagosome. However, later on following infection, the *sodB* mutants survived less than the WT bacteria, which highlights the pro-survival role of SODB. We have explained this defensive role through an investigation of the activation of autophagy, which was greater in the *sodB*-infected macrophages.

Keywords: *P. aeruginosa*, SODs, ROS, macrophages, autophagy, oxidative burst

INTRODUCTION

Macrophages are professional phagocytes, and their major role in the control of infectious diseases is the engulfment of microorganisms within phagosomes, which in a complex maturation process acquire disparate microbicidal effectors (Flannagan et al., 2009, 2012). One of the stronger and earlier microbicidal mechanisms is undoubtedly the production of reactive oxygen species (ROS), which are generated by the NOX2 NADPH oxidase (Lam et al., 2010; Panday et al., 2015). Following the engulfment of pathogens by macrophages, the NOX2 multisubunit complex is assembled and activated at the phagosome membrane, where it liberates superoxide anions, O_2^- , into the phagosomal lumen (Lam et al., 2010). In the phagosome, O_2^- can be spontaneously or enzymatically dismutated to H_2O_2 , which might, in turn, be converted to hydroxyl radicals (HO^\bullet) via the Fenton reaction. Importantly, the overall levels of H_2O_2 in phagosomes also depends on H_2O_2 leakage, which is favored by its high stability and neutral charge.

Phagocytic ROS might directly kill the engulfed pathogens or be transformed into other antimicrobial effectors. For example, myeloperoxidase targets H_2O_2 to produce hypochlorous acid, which has potent microbicidal activity (Fang, 2011). However, myeloperoxidase is mainly active in neutrophils, and it does not appear to be essential for host defense (Lanza, 1998; Klebanoff, 2005; Klebanoff et al., 2013). ROS cytotoxicity might also be enhanced by their interactions with other cellular mediators, such as NO (Fang, 2011). Pathogens enclosed within phagosomes are exposed to high levels of ROS, which are produced in their close proximity, and which can directly kill the engulfed bacteria by targeting different microbial macromolecules, such as their DNA and proteins, and in particular, iron-sulfur-clustered protein (Fang, 2011). The oxidative burst response follows specific temporal dynamics that impose high oxidative stress on the engulfed pathogens soon after infection, followed by extended periods of little, if any, ROS production. Therefore, the survival of pathogens in this environment is critically dependent on their detoxification of ROS in the early stages of an infection.

The microbial defenses against ROS include catalases, peroxidases, and superoxide dismutases (SODs) (Mishra and Imlay, 2012). Catalases and peroxidases target H_2O_2 , which produces H_2O and O_2 , while SODs promote dismutation of O_2^- into H_2O_2 (Mishra and Imlay, 2012). Therefore, only the combined actions of these enzymes can directly detoxify the superoxide anions produced by the phagocytic NOX2. Additionally, by reducing the overall levels of superoxide radicals (1 mol O_2^- per 0.5 mol H_2O_2), the SOD activity limits the possible toxicity of O_2^- in this compartment (Craig and Schlauch, 2009) and in the production of other cytotoxic mediators (Fang, 2011). In Gram-negative bacteria, ROS scavenger enzymes can occupy different subcellular compartments, with SODs localized to the periplasm, while catalase and peroxidase are mainly confined to the cytoplasm. This compartmentalization is functional for the targeting of O_2^- , the leakage of which is highly restricted by the negative charge in the periplasm and H_2O_2 in the cytoplasm (Aussel et al., 2011; Fang, 2011). The complexity of the anti-ROS defenses is further increased by the presence of

more than one gene for each class of ROS-scavenger enzyme that encodes enzymes that differ in cofactor requirements, regulation, and sub-cellular localization (Fang, 2011; Imlay, 2019; Johnson and Hug, 2019).

Gram-negative bacteria entrapped within phagosomes can be exposed to rapid increases in the levels of superoxide radicals, which can be targeted by the periplasmic SOD. A major role of this periplasmic SOD to ensure bacterial survival in such environments was demonstrated in *Salmonella*. Indeed, the periplasmic SOD of *Salmonella*, SODCI, was predicted to be the only enzyme that critically impacts upon *Salmonella* survival in the phagosome (De Groote et al., 1997; Craig and Schlauch, 2009), whereby in its absence, the O_2^- levels can increase to lethal doses (Burton et al., 2014; Fenlon and Schlauch, 2014). Additionally, in murine *in vivo* models, it was shown that *Salmonella* infection is controlled by NADPH-dependent oxidative killing, although this only refers to neutrophils, as in macrophages the oxidative burst appears to be sublethal for bacterial cells (Burton et al., 2014).

Pseudomonas aeruginosa is a Gram-negative facultative aerobic opportunistic pathogen that causes infections in humans, and particularly in immunocompromised patients and patients with cystic fibrosis (CF) (Ciofu et al., 2015; Klockgether and Tümmler, 2017). In CF, *P. aeruginosa* intermittently infects the airways of children and young patients, although as the age of the patient increases, *P. aeruginosa* can stably colonize the CF lungs, and represents the major cause of pulmonary disease while contributing to the morbidity and mortality of patients with CF (Elborn, 2016; Malhotra et al., 2019). The CF lungs are dominated by high levels of ROS, which result from chronic bacterial infections, large inflammatory responses, and defective antioxidant production, such as glutathione (Galli et al., 2012; de Bari et al., 2018; Malhotra et al., 2019). This scenario clearly suggests that the ROS defense of *P. aeruginosa* must be decisively important for colonization of the CF lungs. This colonization has been assigned in part to the impaired activity of innate immune cells, which do not appear to eradicate infections (Bruscia and Bonfield, 2016). Accordingly, we and others have demonstrated that the microbicidal activity against *P. aeruginosa* of CF macrophages is impaired (Del Porto et al., 2011; Simonin-Le Jeune et al., 2013). However, we have shown that the oxidative burst of human CF macrophages is similar to that of non-CF cells, and is functional to kill *P. aeruginosa* early after infection (Cifani et al., 2013).

Thus, to better understand how *P. aeruginosa* tackles this oxidative killing by the macrophages, we investigated the role of the bacterial SODs, which are the first enzymatic activities involved in superoxide radical detoxification. *P. aeruginosa* SODs have been shown previously to contribute to bacterial virulence in the small-animal model of the silkworm *Bombyx mori*, the mortality of which was reduced by infection with *P. aeruginosa* *sod* mutants, with respect to wild-type (WT) strains (Iiyama et al., 2007). Furthermore, analysis of *sodB* and *sodM* mutants has showed that for *P. aeruginosa* virulence, SODB is more critical than SODM. SODB is an iron-cofactored SOD (Fe-SOD), while SODM requires manganese (Mn-SOD), and both localize to the periplasm (Winsor et al., 2016). The expression of these SODs is regulated by the availability of the iron and manganese cofactors

and specific environmental conditions, although SODB is highly expressed under all growth conditions, while SODM is restricted to low-Fe requirements (Hassett et al., 1993, 1995).

Here, by analyzing the survival of the *P. aeruginosa* WT and *sod* mutant strains in murine and human macrophages, we demonstrate a dual antagonistic role of *P. aeruginosa* SODB, which modulates the microbicidal activity of macrophages by acting first as a pro-microbicidal and then as a pro-survival.

MATERIALS AND METHODS

Macrophages, Media, and Supplements

RAW246.7 murine macrophages (ATCC, TIB71) were cultivated in Dulbecco's modified Eagle's medium (DMEM; Corning, United States) supplemented with 10% fetal bovine serum, 1 mM glutamine, 100 U/μL penicillin and 100 μg/mL streptomycin (all from EuroClone, Italy). The cells were grown in tissue culture flasks or multiwell plates, at 37°C and 5% CO₂. Human monocyte-derived macrophages (HMDMs) were differentiated *in vitro* from monocytes isolated from the buffy coats of healthy donors, as previously described (Del Porto et al., 2011). Briefly, peripheral blood mononuclear cells were isolated by density gradient centrifugation (Lympholyte; Cedarlane, Hornby, CA, United States), and were selected with an anti-CD14 monoclonal antibody coupled to magnetic beads (Miltenyi Biotec, Bergisch Gladbach, Germany). The CD14⁺ cells were differentiated for 7 days in Roswell Park Memorial Institute (RPMI) 1640 (Gibco-BRL, Invitrogen Corporation, Carlsbad, CA, United States) supplemented with 20% fetal bovine serum and 100 ng/mL recombinant macrophage colony stimulating factor (PeproTech Inc, Rocky Hill, NY, United States).

Bacterial Strains and Growth Conditions

The bacterial strains and plasmid used in this study are listed in **Table 1**. The *P. aeruginosa* mutant strains were recovered from frozen stocks and analyzed for the gene deletions. Genomic DNA extraction and gene amplification were performed as previously reported (Di Domenico et al., 2015), using primers listed in **Supplementary Table S1**. As expected, *sodB* and *sodM* amplification bands were detected in the *P. aeruginosa* WT (PAO1). In contrast, *sodB* and *sodM* amplification bands were absent in the *sodB* and *sodM* mutants, respectively

(**Supplementary Figure S1**). All of these strains were grown from single colonies in Luria-Bertani (LB) medium (Sigma, United States) at 30°C, with liquid cultures grown with shaking at 180 rpm. The *sodB* and *sodM* mutant strains were routinely grown in LB medium containing 50 μg/mL tetracycline and gentamycin, respectively. As expected from previous studies (Hassett et al., 1995; Iiyama et al., 2007), the *sodB* mutant grew more slowly than the parental PAO1 strain (**Supplementary Figure S2**). The *P. aeruginosa* strains that expressed green fluorescent protein (GFP) were obtained by electroporation of pUC30T-*gfpmut3* (Barbier and Damron, 2016) and selection in 15 μg/mL gentamycin on LB agar plates.

P. aeruginosa Killing by Macrophages

The day before infection, the macrophages were seeded into 48-well plates (10⁵ cells/well) in culture medium without antibiotics, and incubated at 37°C in 5% CO₂. When applied, the macrophages were pretreated (i.e., before infection) with the NADPH oxidase inhibitor, diphenyleneiodonium (DPI; Sigma, United States), at 10 μM for 30 min. Exponentially growing *P. aeruginosa* cells were prepared by refreshing the overnight cultures in LB broth at 30°C (**Supplementary Material**). After two washes in phosphate-buffered saline (PBS), the *P. aeruginosa* were resuspended in antibiotic-free cell-culture medium and added to the macrophages at a multiplicity of infection (MOI) of 10. The infection was synchronized by centrifugation of the multiwell plates (550 × *g* for 5 min), which were then incubated at 37°C in 5% CO₂ for 30 min to 60 min. At the end of the infection, the cells were washed with PBS and incubated in DMEM containing 1 mg/mL amikacin and 1 mg/mL ceftazidime for 15 min. Afterward, the macrophages in selected wells (defined as *t*₀) were lysed in 1% Triton X-100 for 10 min at room temperature, and finally diluted to 1 mL PBS. The cell viability was determined according to the colony-forming unit (CFU) assay. In the remaining wells, the medium was replaced with culture medium supplemented with a sub-inhibitory concentration of the antibiotics (0.1 mg/mL amikacin; 0.1 mg/mL ceftazidime) and incubated for a further 60 min (*t*₆₀) or 180 min (*t*₁₈₀). At the end of the incubations, the live *P. aeruginosa* were recovered as described above. The bacteria survival was calculated according to Eq. 1:

$$100 - \left\{ \left[\left(\text{CFU}_{t_0} - \text{CFU}_{t_{180}} \right) / \text{CFU}_{t_0} \right] \times 100 \right\} \quad (1)$$

Phagocytosis Assays

The macrophages (i.e., RAW 264.7 cells, HMDMs) were seeded in 24-well plates (2 × 10⁵ cells/well) in antibiotics-free medium the day before infection, and then infected with GFP-expressing PAO1 and PAO1 *sodB* *P. aeruginosa* strains, at a MOI of 25. Phagocytosis was carried out by incubation of the infected macrophages for 30 min or 60 min at 37°C in 5% CO₂. Afterward, the cells were gently washed two or three times with PBS, enzymatically detached, and analyzed by flow cytometry (BD FACSCalibur, France). Phagocytosis was evaluated as the fraction of GFP⁺ cells in the bulk population. The data were analyzed using the CellQuest software, and the images were processed with FlowJo.

TABLE 1 | Bacterial strains and plasmid used in this study.

Name	Description ^a	References
PAO1	Wild-type strain	Iiyama et al., 2007
PAO1 <i>sodB</i>	PAO1 <i>sodB</i> mutant; <i>sodB</i> :ΩTc, Tc ^r	Iiyama et al., 2007
PAO1 <i>sodM</i>	PAO1 <i>sodM</i> mutant; <i>sodM</i> :Ωaac, Gm ^r	Iiyama et al., 2007
pUC30T- <i>gfpmut3</i>	Plasmid encoding GFP, Gm ^r	Barbier and Damron, 2016

^aTc^r, tetracycline resistance; Gm^r, gentamicin resistance; GFP, green fluorescence protein.

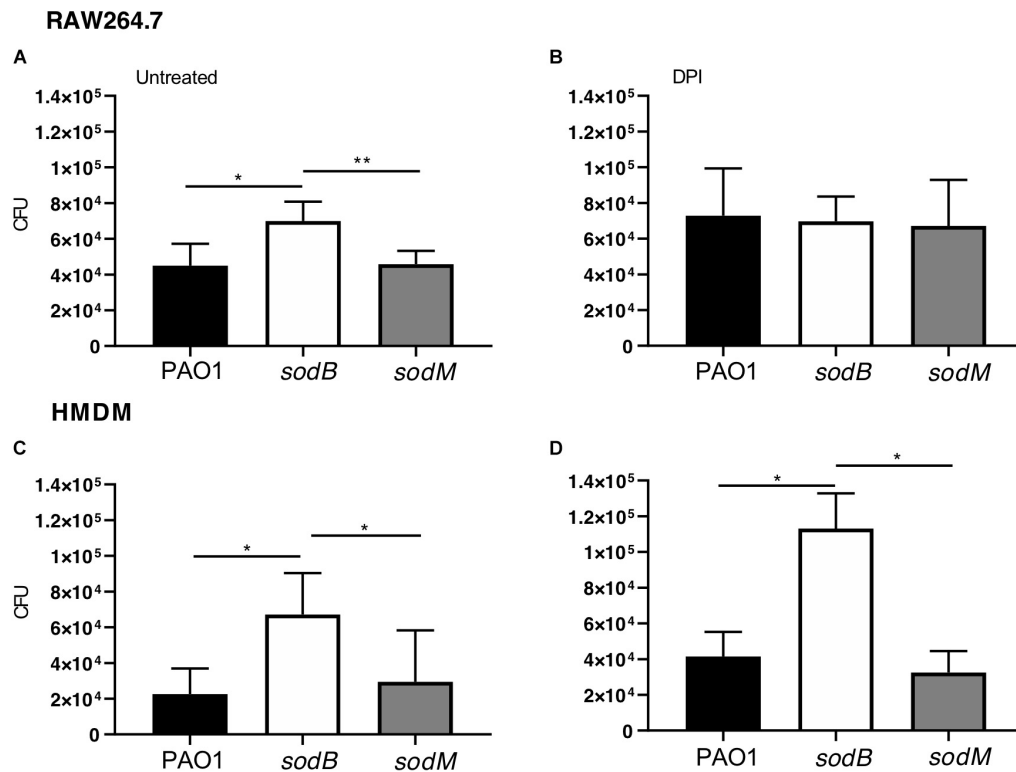


FIGURE 1 | Short-term survival of *Pseudomonas aeruginosa* *sod* mutants in macrophages. Intracellular survival of *P. aeruginosa* in macrophages infected with PAO1 WT, *sodB*, and *sodM* mutant strains. RAW264.7 macrophages (**A,B**) and HMDMs (**C,D**) were infected with the indicated strains, treated with antibiotics, and lysed with 1% Triton X-100. The total live bacteria recovered on LB medium is reported (CFU). (**B,D**) The cells were pretreated with the NADPH oxidase inhibitor diphenyleneiodonium (DPI; 10 μ M for 30 min). Data are means \pm standard deviation of six (**A,B**) and three (**C,D**) independent experiments. * $P < 0.05$; ** $P < 0.01$ (Student's *t*-tests).

ROS Measurements

Intracellular O_2^- levels were measured using luminol (Sigma, United States). Briefly, the macrophages were resuspended in Hank's balanced salt solution (HBSS) without phenol red (Sigma, United States), supplemented with 25 μ g/mL luminol, and seeded in white 96-well plates (Sarstedt, Germany). The RAW264.7 macrophages were seeded at 3×10^5 cells/well, with the HMDMs at 10^5 cells/well. The macrophages were challenged with the *P. aeruginosa* strains at a MOI of 10, and the chemiluminescence was measured at given time using a multilabel counter (Wallac 1420 Victor2). The data were corrected based on the controls without macrophages. Quantitative analysis was performed by determination of the areas under the curve (AUC) using the GraphPad Prism software. Furthermore, O_2^- levels were measured by the nitroblue tetrazolium (NBT, Sigma) reduction assay, which was carried out according to Choi et al. (2006), with minor modifications. Briefly, the macrophages seeded in 24-well plates were supplemented with 1 mg/mL NBT, and infected with the *P. aeruginosa* strains (MOI = 10). After 60 min of infection, intracellular NBT was solubilized and the optical densities were determined spectrophotometrically (**Supplementary Material**).

The extracellular H_2O_2 released from the infected macrophages was measured by the production of Resofurin,

using Amplex Red assays (Invitrogen). Briefly, HMDMs were seeded in 96-well plates (10^5 cells/well) in antibiotic-free culture medium the day before infection, and then washed with PBS and incubated with 50 μ M Amplex Red and 0.1 U/mL horse-radish peroxidase in KRPG buffer (145 mM NaCl, 5.7 mM sodium phosphate, 4.86 mM KCl, 0.54 mM $CaCl_2$, 1.22 mM $MgSO_4$, 5.5 mM glucose, pH 7.35). Macrophages were challenged with *P. aeruginosa* strains at a MOI of 10 and fluorescence was measured at 30 min intervals with a fluorescence scanner (Amersham Typhoon 9600). Values were corrected for controls without macrophages in KRPG supplemented with 50 μ M Amplex Red and 0.1 U/mL horse-radish peroxidase. The concentration of H_2O_2 in the samples was calculated using standard curves obtained with defined H_2O_2 concentrations (0–20 μ M).

Immunoblotting

10^6 RAW264.7 macrophages were infected with *P. aeruginosa* strains for 1 h, as described above. After infection, macrophages were gently washed and lysed in Hepes 50 mM pH 7.4, NaCl 150 mM, EDTA 20 mM, NaF 100 mM, Na_3VO_4 10 mM, 1% Triton X-100, protease inhibitor cocktail. 25–30 μ g protein samples were separated by SDS-PAGE and transferred to nitrocellulose blotting membrane (GE Healthcare, Italy).

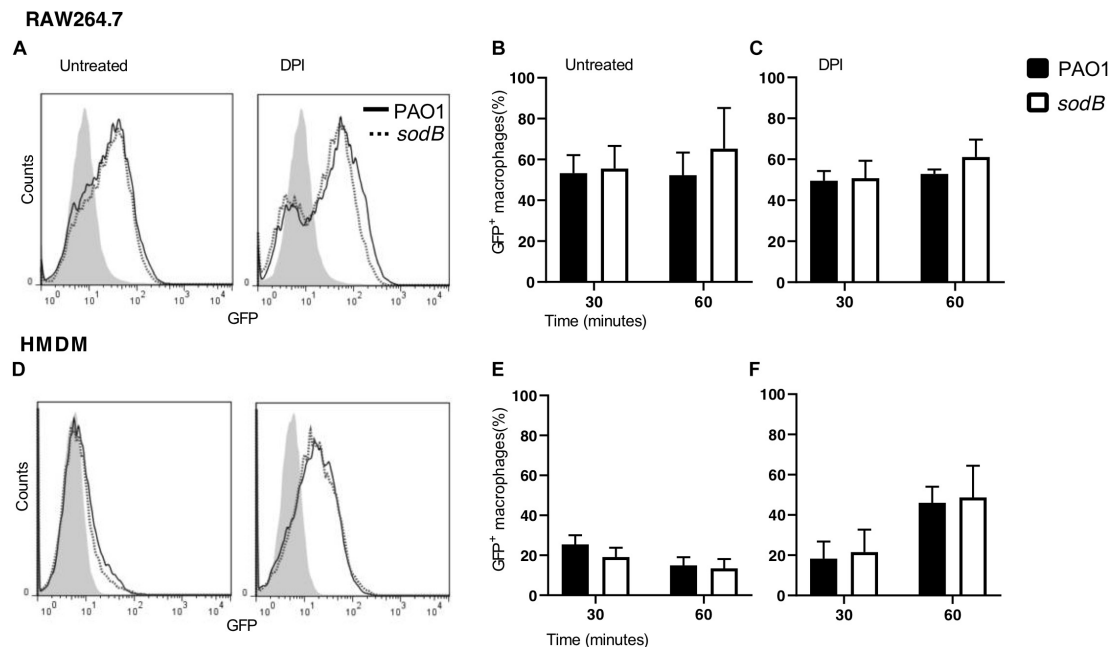


FIGURE 2 | *Pseudomonas aeruginosa* phagocytosis is not affected by SODB. Representative plots of RAW264.7 macrophages (**A**) and HMDMs (**D**), untreated (left) or treated with the NADPH oxidase inhibitor diphenyleneiodonium (DPI; right) and infected with GFP-expressing PAO1 WT and the *sodB* mutant, as indicated. The proportions of GFP⁺ macrophages at the indicated time of infection was evaluated by flow cytometry (**B,C,E,F**). Data are means \pm standard deviation of three independent experiments. No significant differences were found between PAO1- and *sodB*-infected macrophages (two-way ANOVA; Student's *t*-tests).

After blocking in PBS, Tween 0.1%, skim milk 5% (SIGMA, United States), membranes were incubated with the primary antibody for 16–18 h at 4°C. Next day, membranes were washed, incubated at room temperature with the horse-radish-peroxidase-conjugated secondary antibody (GE Healthcare, Italy) and visualized with a Chemi Doc XRS system (Bio-Rad Laboratories Ltd., Hemel Hempstead, United Kingdom). Quantitative Western blotting was performed using the ImageJ software. The primary antibodies used were: LC3 (Cell Signaling, Italy; #2775), diluted at 1:1000; and GAPDH (Santa Cruz, Italy; sc-47724), diluted at 1:400.

Statistical Analysis

All of the data are reported as a means \pm standard deviation. The Figures and statistical analyses were constructed using the GraphPad Prism software (GraphPad Software Inc.). The statistical tests used are indicated in the corresponding Figures. Differences were significant for a *P*-value cut-off of 0.05.

RESULTS

SODB Contributes to Short-Term Intracellular *P. aeruginosa* Killing by Macrophages

The periplasmic *P. aeruginosa* SOD might contribute directly to the scavenging of the superoxide anion (O_2^-) produced by the macrophage NOX2, with a possible impact on the bacterial

survival. To test this hypothesis, we analyzed the survival of the *P. aeruginosa* *sod* mutants in the macrophages. For this, RAW264.7 macrophages were infected with WT PAO1 or the *sod* mutants, as either PAO1 *sodB* or *sodM*, and the live intracellular bacteria were determined using the CFU assay. These data showed greater intracellular survival of the PAO1 *sodB* mutant, with respect to the PAO1 WT and PAO1 *sodM*, with these last two showing similar survivals (**Figure 1A**). As expected, inhibition of NADPH oxidase by the DPI pretreatment resulted in significant increases in the live *P. aeruginosa* recovered from the macrophages infected with PAO1 WT or PAO1 *sodM*, which confirmed the oxidative burst as the primary killing mechanism in the macrophages early after infection (**Figure 1B**). However, no differences were detected in the PAO1 *sodB* survival in DPI-treated macrophages, with respect to the untreated cells (**Figures 1A,B**). These data suggested that SODB contributes to the NADPH-dependent killing of *P. aeruginosa* by the macrophages. Similarly, HMDMs showed significant increases in the intracellular survival of PAO1 *sodB*, but not PAO1 *sodM*, with respect to PAO1, in both the untreated and DPI-treated cells (**Figures 1C,D**). This thus extended the role of *P. aeruginosa* SODB to primary human macrophages.

To further support these data, we analyzed phagocytosis by determining the fraction of macrophages that engulfed the PAO1 or PAO1 *sodB* strains. RAW264.7 macrophages and HMDMs were infected with GFP-expressing strains for 30 and 60 min. Subsequently, the non-internalized *P. aeruginosa* were removed by several washes, and the sub-population of infected macrophages (GFP⁺) was evaluated by flow

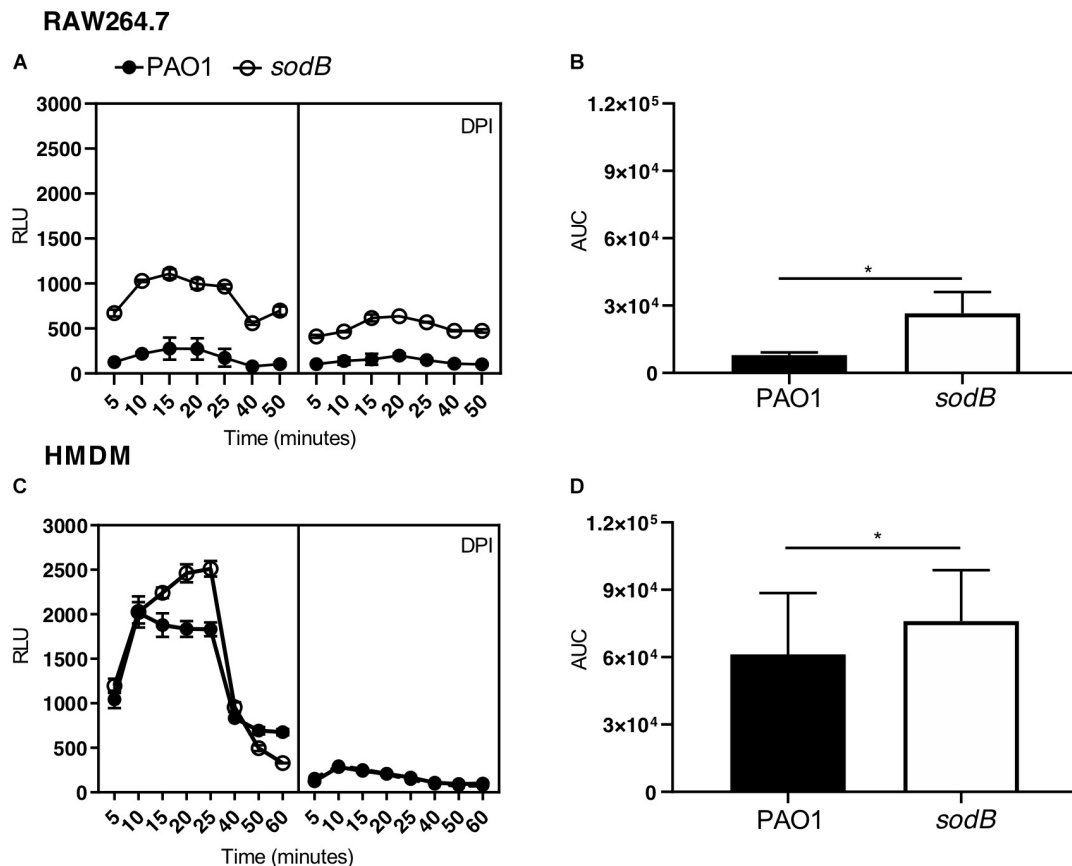


FIGURE 3 | *Pseudomonas aeruginosa* SODB targets the phagocytic O_2^- . Measurements of superoxide anions using luminol in RAW264.7 macrophages (A,B) and HMDMs (C,D). Representative time courses of luminol chemiluminescence in the untreated cells (A,C, left panel) and cells pretreated with the NADPH oxidase inhibitor diphenyleneiodonium (A,C, right panel) (DPI; 10 μ M), and infected with the indicated *P. aeruginosa* strains at a multiplicity of infection of 10. Data are means \pm standard deviation of three technical replicates. (B,D) Quantification of O_2^- , as determined by the area under the curve (AUC) from three independent experiments, each carried out in triplicate. RLU, relative luminescent units; * $P < 0.05$ (Student's *t*-tests).

cytometry. Figures 2A,D show no differences in the GFP⁺ sub-population between the cells infected with PAO1 WT and the PAO1 *sodB* mutant, in both the untreated and DPI-treated macrophages. Furthermore, quantitative analysis confirmed that the GFP⁺ sub-populations were similar, irrespective of whether the *P. aeruginosa* infecting strain was PAO1 WT or the PAO1 *sodB* mutant, and whether macrophages were untreated (Figures 2B,E) or DPI-treated (Figures 2C,F). Collectively, these data strongly suggest that the phagocytosis of PAO1 and PAO1 *sodB* was substantially similar at 30 and 60 min after infection.

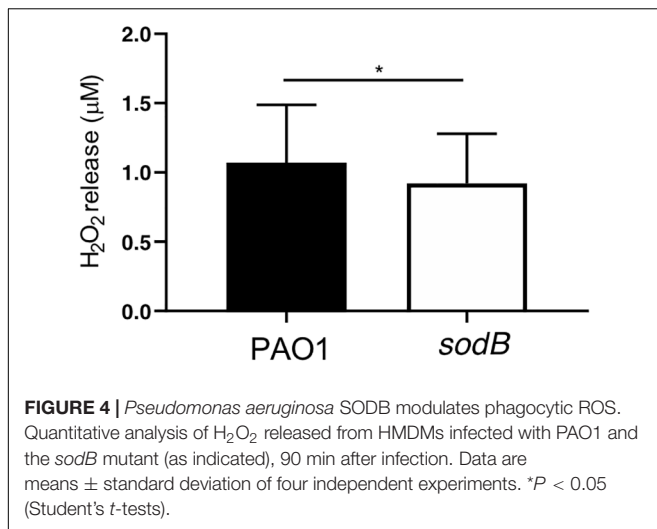
Having observed greater survival of PAO1 *sodB* with respect to PAO1 WT and no differences in bacterial phagocytosis, we hypothesized that the bacterial SOD, and in particular SODB, contributes to the killing of the intracellular *P. aeruginosa* through the modulation of NADPH-dependent ROS production.

High O_2^- and Low H_2O_2 Differentiate Macrophages Infected With PAO1 *sodB*

Taking into consideration the enzymatic activities of NADPH oxidase and SOD, the most likely hypothesis to explain these data

was that the superoxide radicals produced by the macrophage NOX2 were promptly converted into H_2O_2 by the bacterial SOD, which in turn contributes to the killing of the intracellular *P. aeruginosa*. If this is the case, the macrophages infected with the *sod* mutants should be characterized by higher O_2^- and lower H_2O_2 levels than those infected with PAO1 WT. Therefore, we analyzed the O_2^- and H_2O_2 levels in macrophages infected with PAO1 WT and the *sodB* mutant. To differentiate between O_2^- and H_2O_2 , we took advantage of their different mobilities through the membrane. Indeed, while the mobility of O_2^- is highly restricted by its negative charge, as H_2O_2 is neutral and long-lived, it can leak from the cells (Fang, 2011). Thus, O_2^- was measured intracellularly by luminol oxidation (Bedouhène et al., 2017), and H_2O_2 extracellularly using Amplex Red assays (Schürmann et al., 2017).

Macrophages challenged with PAO1 WT and PAO1 *sodB* were loaded with luminol, and ROS production was determined by chemiluminescence measurements. Kinetics analysis revealed a rapid increase in luminol chemiluminescence, which is a readout of O_2^- production, with peaks at 15 to 25 min (Figure 3). Additionally, the macrophages infected with PAO1 *sodB* showed



higher chemiluminescence signals than those infected with PAO1 WT, both for the RAW264.7 cells (Figure 3A) and the HMDMs (Figure 3C). As expected, inhibition of NADPH oxidase with DPI greatly reduced the luminol oxidation (Figures 3A,C). Quantitative analysis of the luminol chemiluminescence AUC confirmed the significantly higher O₂⁻ production in the cells infected with PAO1 *sodB*, with respect to PAO1 WT (Figures 3B,D). Similar data were obtained with nitroblue tetrazolium reduction assays, which detected higher levels of the superoxide anion in macrophages infected with the *sodB* mutant, with respect to PAO1 WT (Supplementary Figure S3). Collectively, these data suggest that *P. aeruginosa* SODB contributes to O₂⁻ dismutation, and that the extent of its contribution depends on the total amount of O₂⁻ produced by the host cells, which, in our experimental models is higher in human than murine macrophages.

According to our hypothesis, the absence of bacterial SODB activity increases O₂⁻ levels and decreases H₂O₂ production in macrophages infected with the *sodB* mutant. To confirm this, we evaluated extracellular H₂O₂ leakage using the Amplex Red assay. As expected, infection of HMDMs with the *P. aeruginosa* *sodB* mutant was associated with lower H₂O₂ release, with respect to cells infected with PAO1 WT (Figure 4). No signal above the background (i.e., uninfected macrophages) was detected for the RAW264.7 macrophages, possibly due to the low levels of ROS produced upon infection (data not shown).

Overall, the macrophages infected with the PAO1 *sodB* mutants were characterized by higher O₂⁻ levels and lower H₂O₂ levels, with respect to the cells infected with the WT bacteria. This supported the concept that *P. aeruginosa* SODB converts the phagocytic O₂⁻ to H₂O₂.

SODB Promotes Long-Term *P. aeruginosa* Survival in Macrophages

It has been well established that macrophages can kill engulfed bacteria using different mechanisms that can be activated

sequentially, starting with the oxidative burst, which in turn activates other mechanisms, including autophagy (Huang et al., 2009; Lam et al., 2010). Thus, to evaluate the possible role of the bacterial SODB in microbicidal mechanisms other than the oxidative burst, we analyzed *P. aeruginosa* survival at later time points after infection. After infection and treatment with antibiotics, the RAW264.7 macrophages were incubated in bacteria-free medium for 1 h and 3 h, and the live intracellular bacteria were counted using the CFU assay (Figures 5A–C). As previously observed, at the end of the infection (*t*₀), more viable PAO1 *sodB* were recovered from the infected macrophages than the PAO1 WT (Figures 5A,B, time 0). However, the CFU recovered from the infected macrophages at 1 h and 3 h from the infection were similar, independent of the bacterial strains (Figures 5A,B). Similar data were obtained in the HMDMs (Figures 5D,E). Consequently, the long-term survival of PAO1 WT appeared to be greater than that of PAO1 *sodB* in both of these macrophage models (Figures 5C,F). This was also described by the slopes of the killing curves, which represent the rates of bacterial killing, and which were higher for PAO1 *sodB*, with respect to PAO1 WT (Supplementary Table S2).

Collectively, these data demonstrate that the long-term survival of the PAO1 *sodB* mutant in both murine and human macrophages is less than for PAO1 WT, which suggests that SODB ultimately promotes bacteria survival.

SODB Contributes to Decreased Autophagy Activation in Macrophages

It has been shown that autophagy activation by Toll-like receptor signaling or receptor-mediated phagocytosis depends on NOX2 activity and ROS production, with the latter required to recruit LC3 to phagosomes and to target intracellular *Salmonella typhimurium* to (auto)phagosomes (Huang et al., 2009). Additionally, autophagy activation by *P. aeruginosa* has been demonstrated in different cell types, including macrophages, where it contributes to restrict intracellular survival (Yuan et al., 2012; Junkins et al., 2013; Jabir et al., 2014). Having observed that *P. aeruginosa* SODB contributed to the long-term survival of *P. aeruginosa* within macrophages, we speculated that it might inhibit autophagy through reduction of the levels of intracellular O₂⁻. To test this hypothesis, RAW264.7 cells and HMDM macrophages were infected with PAO1 WT and PAO1 *sodB*, and autophagy activation was monitored by analysis of changes in the levels of lipidated LC3 (LC3-II) with Western blotting (Kabeya et al., 2000). In whole-cell lysates from these non-infected macrophages, LC3-I and LC3-II were detected at similar levels in the RAW264.7 cells, while in HMDMs the intensity of the LC3-II band was slightly higher than that of LC3-I. In contrast, 1 h after infection, LC3-II increased specifically in the infected macrophages (Figures 6A,C). Accordingly, quantitative Western blotting showed higher levels of LC3-II in cells infected with the PAO1 *sodB* mutant, with respect to those infected with PAO1 WT (Figures 6B,D). This suggests that the SODB activity of the intracellular *P. aeruginosa* reduces autophagy activation, which thus provides a link between the oxidative and

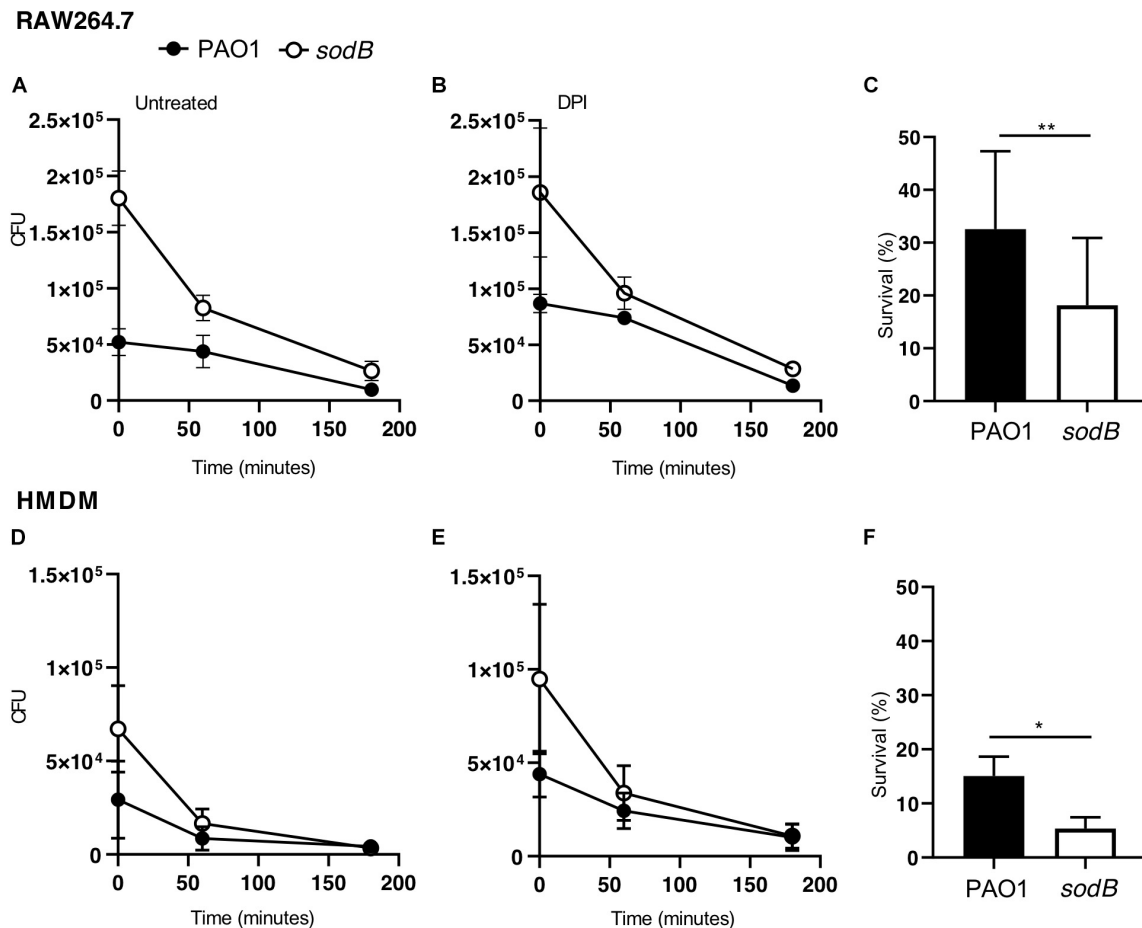


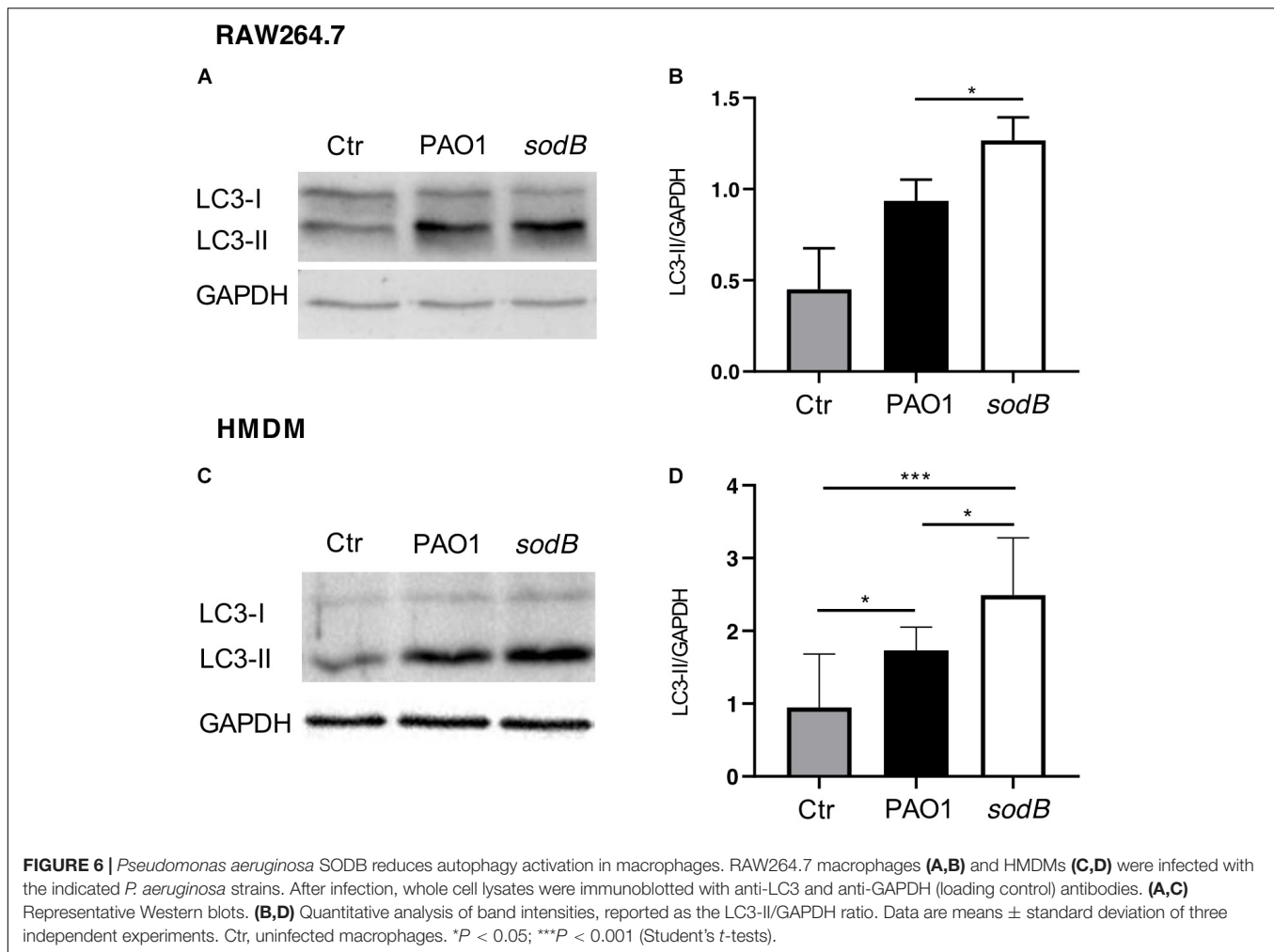
FIGURE 5 | Bacterial SODB enhances long-term intracellular survival within macrophages. Survival curves of *Pseudomonas aeruginosa* in RAW264.7 macrophages (**A,B**) and HMDMs (**D,E**). The cells were infected with the indicated *P. aeruginosa* strains, and untreated and pretreated with the NADPH oxidase inhibitor diphenyleneiodonium (DPI; 10 μ M for 30 min), as indicated. At the end of the infection macrophages (time 0) and after 60 and 180 min, samples were collected and the CFU determined. (**C,F**) Bacterial survival in untreated RAW264.7 (**C**) and HMDMs (**F**) at 180 min from the end of infection. Data are means \pm standard deviation of three independent experiments. * $P < 0.05$; ** $P < 0.01$ (Student's *t*-tests).

non-oxidative roles of SODB in modulation of *P. aeruginosa* survival in macrophages.

DISCUSSION

Macrophages are key players in the innate immune system, due to their engulfing of pathogens and activation of an arsenal of antimicrobial weapons. However, whether macrophages successfully accomplish this task is also dependent on microbial responses to the microbicidal mechanisms. NADPH oxidase activation is an early response to infection by macrophages, and this contributes to killing of intracellular bacteria and activation of other microbicidal mechanisms, such as autophagy. Consequently, ROS scavengers should be a determinant for the engulfed bacteria to survive the hostile intracellular environment, both in the immediate phase and in the later phases of infection. *P. aeruginosa* has two SOD genes, *sodB* and *sodM*, which encode the iron- and manganese-cofactored SODs, respectively, both

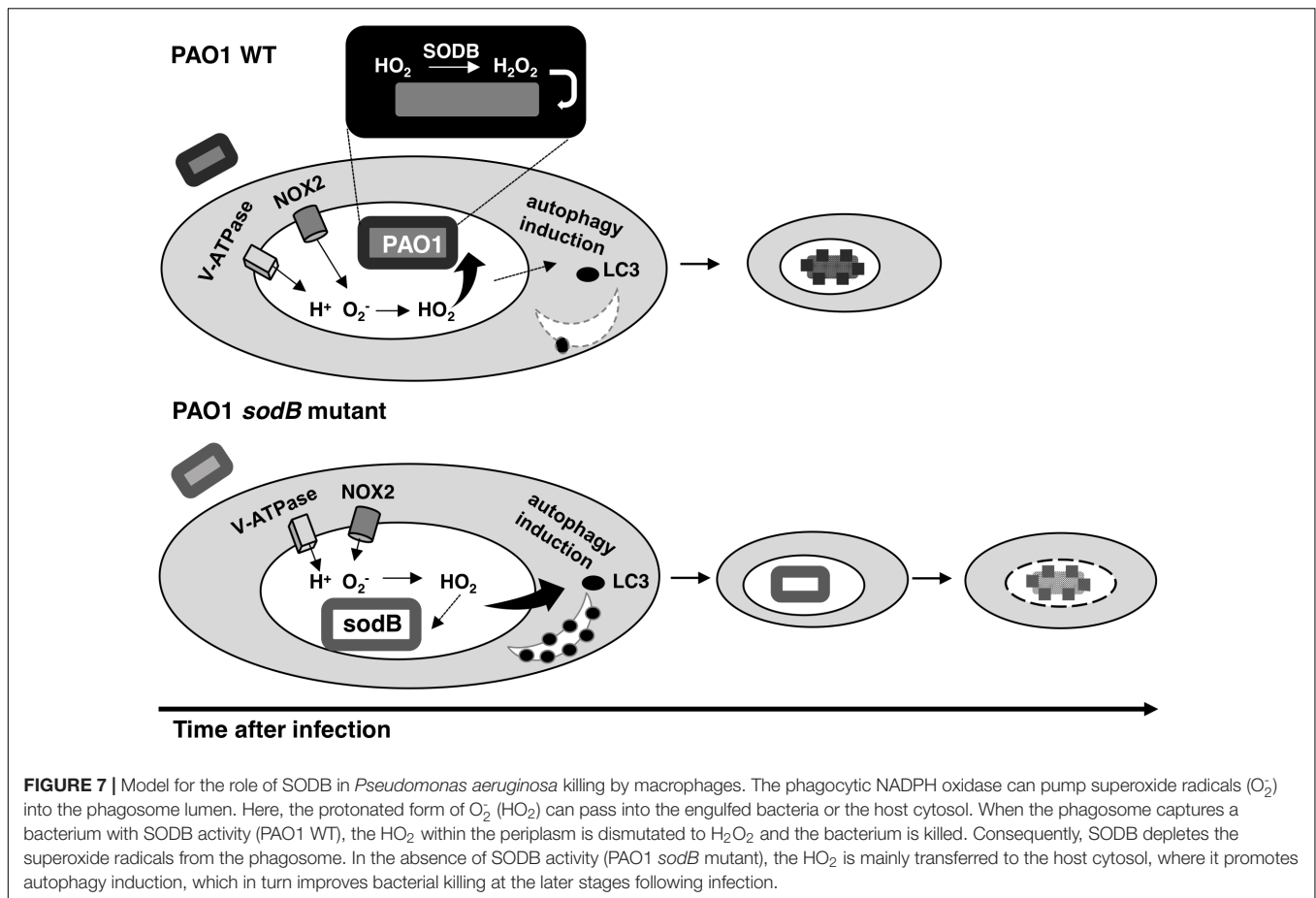
of which have been identified as periplasmic enzymes (Yu et al., 2010). These SODs are part of the bacterial defenses that target the different forms of ROS and transform them into less toxic compounds. The periplasmic localization of the SODs is strategic, as this allows targeting of the superoxide radicals (O_2^-), which might enter this compartment from the environment. For bacteria enclosed in phagosomes, the superoxide radicals produced by NADPH-oxidase are likely to be rapidly transferred into the periplasm, both facilitated by their protonation to HO_2 , and aided by the V-ATPase that pumps H^+ within the phagosomal lumen (Burton et al., 2014). In the bacterial periplasm, the HO_2 can be targeted by SODs and dismutated to H_2O_2 . The resulting H_2O_2 can be further processed by other bacterial scavenger enzymes, catalases, and peroxidases, although it might also contribute to bacterial killing, depending on the balance between the oxidative stress imposed by the host cell and the scavenger activities of the engulfed bacteria. Here, we have shown that macrophages infected with PAO1 *sodB* are differentiated by increased levels of O_2^- and lower



levels of H_2O_2 , with respect to those infected with PAO1 WT. This turns out to have a negative impact on bacterial survival within the macrophages, as we found that the short-term survival of the PAO1 *sodB* mutant was greater than that of PAO1 WT. Taken together, these data allow us to speculate that for the bacterial cells, periplasmic O_2^- is less toxic than H_2O_2 , possibly because few, if any, O_2^- targets are present in this compartment, and/or because of the high mobility of H_2O_2 , which allows its entry into the cytoplasm, which contains the most vulnerable ROS targets. Furthermore, as SOD restricts *P. aeruginosa* survival within macrophages, we identified this activity as pro-microbicidal for the bacterial cells, rather than pro-survival. From another point of view, it can be speculated that macrophages improve their microbicidal activity using the bacterial SOD activity. Of the two *P. aeruginosa* SODs, we show here that only SODB has a role in intracellular survival, which suggests that the iron-cofactor is not limiting in this environment, and that SODB is the major enzyme that acts within phagocytes. This finding is in agreement with previous studies that were also based on the analysis of SOD activities in clinical isolates, which indicates that SODB is more important than SODM in the protection of *P. aeruginosa* from oxidative

stress (Hassett et al., 1995; Britigan et al., 2001). Interestingly, a lung *P. aeruginosa* isolate that lacks SODM activity has been reported (Polack et al., 1996).

The SODB pro-microbicidal activity appears to be difficult to reconcile with the role of this gene in mediating *P. aeruginosa* virulence (Hassett et al., 1995; Britigan et al., 2001; Iiyama et al., 2007). Furthermore, considering that we have analyzed the survival of intracellular *P. aeruginosa* and that macrophages show different microbicidal mechanisms, it is reasonable to surmise that SODB activity might ultimately be pro-survival. Indeed, as macrophages trigger the different microbicidal mechanisms in a time-dependent manner, and as some of these are activated by ROS, we have reasoned that *P. aeruginosa* modulation of phagocytic ROS might have an impact on the activation of non-oxidative microbicidal mechanisms. Our data here show that 3 h after infection, the survival of PAO1 *sodB* was reduced, with respect to PAO1 WT, which suggests that SODB activity indirectly promotes long-term bacterial survival. As microbicidal mechanisms are activated stepwise after phagocytosis, with the oxidative burst being rapidly exhausted (Figures 3A,C), we reasoned that non-oxidative, but ROS dependent, microbicidal mechanisms might be modulated by the bacterial SODB.



Accordingly, we observed that macrophages infected with the PAO1 *sodB* mutant showed stronger activation of autophagy, as assessed by LC3 lipidation, which suggests that SODB inhibits autophagy activation. This is possible, as SODB changes the levels of the different ROS formed within the *P. aeruginosa*-infected phagosomes in favor of H₂O₂, which might be further detoxified or be removed from the host cells. By doing so, the engulfed bacteria consume NOX2-dependent superoxide radicals, and concomitantly, reduce the signal for autophagy activation, and hence for further bacterial killing. In brief, while SODB initially imposes higher oxidative stress on the bacteria within the phagosome, by reducing the O₂⁻ levels later on, it contributes to the dampening of the autophagy activation. This might directly target bacteria enclosed in the LC3 Associated Phagosome (LAP) or bacteria that escape the phagosome and are intercepted in the cytosol by the autophagic flux. In favor of the latter mechanism, it was recently reported that *P. aeruginosa* first resides in the phagosome, and then following phagosome rupture, it can be detected in the cytosol (Garai et al., 2019).

Overall, our data are summarized in the model depicted in **Figure 7**, which considers the pro-microbicidal and pro-survival activities of *P. aeruginosa* SODB within macrophages. Importantly, our model is supported by these data obtained with both murine and human macrophages, although these

two cellular models differ in the O₂⁻ levels produced by these macrophages in response to bacterial infections.

DATA AVAILABILITY STATEMENT

All datasets generated for this study are included in the article/**Supplementary Material**.

ETHICS STATEMENT

The studies involving human participants were reviewed and approved by local ethics committee (Comitato Etico, Azienda Policlinico Umberto I, Rome, Italy; 1233/2016). The patients/participants provided their written informed consent to participate in this study.

AUTHOR CONTRIBUTIONS

FA and PD conceptualized and defined the experimental design. LC, EG, and FL performed the experiments. PD and ED contributed materials and analysis tools. LC and FA carried out the data analysis and Figure preparation, and wrote the manuscript.

FUNDING

This work was supported by Sapienza, University of Rome, Italy, grant nos. C26A14HF84, C26A1543KX, and RM11916B88E57B66 to FA.

ACKNOWLEDGMENTS

We thank Dr. Kazuhiro Iiyama (Kyushu University, Japan) for providing the *P. aeruginosa* *sod* mutant strains, and

Mariette Barbier (West Virginia University School of Medicine, Morgantown, WV, United States) for the bacterial fluorescence labeling vectors. We also thank Federica Lucantoni for FACS analysis.

SUPPLEMENTARY MATERIAL

The Supplementary Material for this article can be found online at: <https://www.frontiersin.org/articles/10.3389/fmicb.2020.00326/full#supplementary-material>

REFERENCES

- Aussel, L., Zhao, W., Hébrard, M., Guilhon, A.-A., Viala, J. P. M., Henri, S., et al. (2011). *Salmonella* detoxifying enzymes are sufficient to cope with the host oxidative burst. *Mol. Microbiol.* 80, 628–640. doi: 10.1111/j.1365-2958.2011.07611.x
- Barbier, M., and Damron, F. H. (2016). Rainbow vectors for broad-range bacterial fluorescence labeling. *PLoS One* 11:e0146827. doi: 10.1371/journal.pone.0146827
- Bedouhène, S., Mouti-Mati, F., Hurtado-Nedelec, M., Dang, P. M.-C., and El-Benna, J. (2017). Luminol-amplified chemiluminescence detects mainly superoxide anion produced by human neutrophils. *Am. J. Blood Res.* 7, 41–48.
- Britigan, B. E., Miller, R. A., Hassett, D. J., Pfaller, M. A., McCormick, M. L., and Rasmussen, G. T. (2001). Antioxidant enzyme expression in clinical isolates of *Pseudomonas aeruginosa*: identification of an atypical form of manganese superoxide dismutase. *Infect. Immun.* 69, 7396–7401. doi: 10.1128/IAI.69.12.7396-7401.2001
- Bruscia, E. M., and Bonfield, T. L. (2016). Cystic fibrosis lung immunity: the role of the macrophage. *J. Innate Immun.* 8, 550–563. doi: 10.1159/000446825
- Burton, N. A., Schürmann, N., Casse, O., Steeb, A. K., Claudi, B., Zankl, J., et al. (2014). Disparate impact of oxidative host defenses determines the fate of *Salmonella* during systemic infection in mice. *Cell Host Microbe* 15, 72–83. doi: 10.1016/j.chom.2013.12.006
- Choi, H. S., Kim, J. W., Cha, Y.-N., and Kim, C. (2006). A quantitative nitroblue tetrazolium assay for determining intracellular superoxide anion production in phagocytic cells. *J. Immunoassay Immunochem.* 27, 31–44. doi: 10.1080/15321810500403722
- Cifani, N., Pompili, B., Anile, M., Patella, M., Diso, D., Venuta, F., et al. (2013). Reactive-oxygen-species-mediated *P. aeruginosa* killing is functional in human cystic fibrosis macrophages. *PLoS One* 8:e071717. doi: 10.1371/journal.pone.0071717
- Ciofu, O., Tolker-Nielsen, T., Jensen, P. Ø., Wang, H., and Hoiby, N. (2015). Antimicrobial resistance, respiratory tract infections and role of biofilms in lung infections in cystic fibrosis patients. *Adv. Drug. Deliv. Rev.* 85, 7–23. doi: 10.1016/j.addr.2014.11.017
- Craig, M., and Schlauch, J. M. (2009). Phagocytic superoxide specifically damages an extracytoplasmic target to inhibit or kill *Salmonella*. *PLoS One* 4:e04975. doi: 10.1371/journal.pone.0004975
- de Bari, L., Favia, M., Bobba, A., Lassandro, R., Guerra, L., and Atlante, A. (2018). Aberrant GSH reductase and NOX activities concur with defective CFTR to pro-oxidative imbalance in cystic fibrosis airways. *J. Bioenerg. Biomembr.* 50, 117–129. doi: 10.1007/s10863-018-9748-x
- De Groote, M. A., Ochsner, U. A., Shiloh, M. U., Nathan, C., McCord, J. M., Dinuer, M. C., et al. (1997). Periplasmic superoxide dismutase protects *Salmonella* from products of phagocyte NADPH-oxidase and nitric oxide synthase. *Proc. Natl. Acad. Sci. U.S.A.* 94, 13997–14001. doi: 10.1073/pnas.94.25.13997
- Del Porto, P., Cifani, N., Guarnieri, S., Di Domenico, E. G., Mariggiò, M. A., Spadaro, F., et al. (2011). Dysfunctional CFTR alters the bactericidal activity of human macrophages against *Pseudomonas aeruginosa*. *PLoS One* 6:e19970. doi: 10.1371/journal.pone.0019970
- Di Domenico, E. G., Petroni, G., Mancini, D., Geri, A., Di Palma, L., and Ascenzioni, F. (2015). Development of electroactive and anaerobic ammonium-oxidizing (Anammox) biofilms from digestate in microbial fuel cells. *Biomed. Res. Int.* 2015:351014. doi: 10.1155/2015/351014
- Elborn, J. S. (2016). Cystic fibrosis. *Lancet* 388, 2519–2531. doi: 10.1016/S0140-6736(16)00576-6
- Fang, F. C. (2011). Antimicrobial actions of reactive oxygen species. *MBio* 2:e0141-11. doi: 10.1128/mBio.00141-11
- Fenlon, L. A., and Schlauch, J. M. (2014). Phagocyte roulette in *Salmonella* killing. *Cell Host Microbe* 15, 7–8. doi: 10.1016/j.chom.2014.01.001
- Flannagan, R. S., Cosío, G., and Grinstein, S. (2009). Antimicrobial mechanisms of phagocytes and bacterial evasion strategies. *Nat. Rev. Microbiol.* 7, 355–366. doi: 10.1038/nrmicro2128
- Flannagan, R. S., Jaumouillé, V., and Grinstein, S. (2012). The cell biology of phagocytosis. *Annu. Rev. Pathol.* 7, 61–98. doi: 10.1146/annurev-pathol-011811-132445
- Galli, F., Battistoni, A., Gambari, R., Pompella, A., Bragonzi, A., Pilolli, F., et al. (2012). Oxidative stress and antioxidant therapy in cystic fibrosis. *Biochim. Biophys. Acta* 1822, 690–713. doi: 10.1016/j.bbdis.2011.12.012
- Garai, P., Berry, L., Moussouni, M., Bleves, S., and Blanc-Potard, A.-B. (2019). Killing from the inside: intracellular role of T3SS in the fate of *Pseudomonas aeruginosa* within macrophages revealed by *mgfC* and *oprF* mutants. *PLoS Pathog.* 15:e1007812. doi: 10.1371/journal.ppat.1007812
- Hassett, D. J., Schweizer, H. P., and Ohman, D. E. (1995). *Pseudomonas aeruginosa* *sodA* and *sodB* mutants defective in manganese- and iron-cofactored superoxide dismutase activity demonstrate the importance of the iron-cofactored form in aerobic metabolism. *J. Bacteriol.* 177, 6330–6337. doi: 10.1128/jb.177.22.6330-6337.1995
- Hassett, D. J., Woodruff, W. A., Wozniak, D. J., Vasil, M. L., Cohen, M. S., and Ohman, D. E. (1993). Cloning and characterization of the *Pseudomonas aeruginosa* *sodA* and *sodB* genes encoding manganese- and iron-cofactored superoxide dismutase: demonstration of increased manganese superoxide dismutase activity in alginate-producing bacteria. *J. Bacteriol.* 175, 7658–7665. doi: 10.1128/jb.175.23.7658-7665.1993
- Huang, J., Canadian, V., Lam, G. Y., Steinberg, B. E., Dinuer, M. C., Magalhaes, M. A. O., et al. (2009). Activation of antibacterial autophagy by NADPH oxidases. *Proc. Natl. Acad. Sci. U.S.A.* 106, 6226–6231. doi: 10.1073/pnas.0811045106
- Iiyama, K., Chieda, Y., Lee, J. M., Kusakabe, T., Yasunaga-Aoki, C., and Shimizu, S. (2007). Effect of superoxide dismutase gene inactivation on virulence of *Pseudomonas aeruginosa* PAO1 toward the silkworm. *Bombyx mori*. *Appl. Environ. Microbiol.* 73, 1569–1575. doi: 10.1128/AEM.00981-0627
- Imlay, J. A. (2019). Where in the world do bacteria experience oxidative stress? *Environ. Microbiol.* 21, 521–530. doi: 10.1111/1462-2920.14445
- Jabir, M. S., Ritchie, N. D., Li, D., Bayes, H. K., Tourlomousis, P., Puleston, D., et al. (2014). Caspase-1 cleavage of the TLR adaptor TRIF inhibits autophagy and β -interferon production during *Pseudomonas aeruginosa* infection. *Cell Host Microbe* 15, 214–227. doi: 10.1016/j.chom.2014.01.010
- Johnson, L. A., and Hug, L. A. (2019). Distribution of reactive oxygen species defense mechanisms across domain bacteria. *Free Radic. Biol. Med.* 140, 93–102. doi: 10.1016/j.freeradbiomed.2019.03.032

- Junkins, R. D., Shen, A., Rosen, K., McCormick, C., and Lin, T.-J. (2013). Autophagy enhances bacterial clearance during *P. aeruginosa* lung infection. *PLoS One* 8:e72263. doi: 10.1371/journal.pone.0072263
- Kabeya, Y., Mizushima, N., Ueno, T., Yamamoto, A., Kirisako, T., Noda, T., et al. (2000). LC3, a mammalian homologue of yeast Apg8p is localized in autophagosome membranes after processing. *EMBO J.* 19, 5720–5728. doi: 10.1093/emboj/19.21.5720
- Klebanoff, S. J. (2005). Myeloperoxidase: friend and foe. *J. Leukoc Biol.* 77, 598–625. doi: 10.1189/jlb.1204697
- Klebanoff, S. J., Kettle, A. J., Rosen, H., Winterbourn, C. C., and Nauseef, W. M. (2013). Myeloperoxidase: a front-line defender against phagocytosed microorganisms. *J. Leukoc Biol.* 93, 185–198. doi: 10.1189/jlb.0712349
- Klockgether, J., and Tümmler, B. (2017). Recent advances in understanding *Pseudomonas aeruginosa* as a pathogen. *F1000Res.* 6:1261. doi: 10.12688/f1000research.10506.1
- Lam, G. Y., Huang, J., and Brumell, J. H. (2010). The many roles of NOX2 NADPH oxidase-derived ROS in immunity. *Semin. Immunopathol.* 32, 415–430. doi: 10.1007/s00281-010-0221-0
- Lanza, F. (1998). Clinical manifestation of myeloperoxidase deficiency. *J. Mol. Med.* 76, 676–681. doi: 10.1007/s001090050267
- Malhotra, S., Hayes, D., and Wozniak, D. J. (2019). Cystic fibrosis and *Pseudomonas aeruginosa*: the host-microbe interface. *Clin. Microbiol. Rev.* 32:e0138-18. doi: 10.1128/CMR.00138-18
- Mishra, S., and Imlay, J. (2012). Why do bacteria use so many enzymes to scavenge hydrogen peroxide? *Arch. Biochem. Biophys.* 525, 145–160. doi: 10.1016/j.abb.2012.04.014
- Panday, A., Sahoo, M. K., Osorio, D., and Batra, S. (2015). NADPH oxidases: an overview from structure to innate immunity-associated pathologies. *Cell Mol. Immunol.* 12, 5–23. doi: 10.1038/cmi.2014.89
- Polack, B., Dacheux, D., Delic-Attree, I., Toussaint, B., and Vignais, P. M. (1996). The *Pseudomonas aeruginosa* *fumC* and *soda* genes belong to an iron-responsive operon. *Biochem. Biophys. Res. Commun.* 226, 555–560. doi: 10.1006/bbrc.1996.1393
- Schürmann, N., Forrer, P., Casse, O., Li, J., Felmy, B., Burgener, A.-V., et al. (2017). Myeloperoxidase targets oxidative host attacks to *Salmonella* and prevents collateral tissue damage. *Nat. Microbiol.* 2:16268. doi: 10.1038/nmicrobiol.2016.268
- Simonin-Le Jeune, K., Le Jeune, A., Jouneau, S., Belleguic, C., Roux, P. F., Jaguin, M., et al. (2013). Impaired functions of macrophage from cystic fibrosis patients: CD11b, TLR-5 decrease and sCD14, inflammatory cytokines increase. *PLoS One* 8:e75667. doi: 10.1371/journal.pone.0075667
- Winsor, G. L., Griffiths, E. J., Lo, R., Dhillon, B. K., Shay, J. A., and Brinkman, F. S. L. (2016). Enhanced annotations and features for comparing thousands of *Pseudomonas* genomes in the *Pseudomonas* genome database. *Nucleic Acids Res.* 44, D646–D653. doi: 10.1093/nar/gkv1227
- Yu, N. Y., Wagner, J. R., Laird, M. R., Melli, G., Rey, S., Lo, R., et al. (2010). PSORTb 3.0: improved protein subcellular localization prediction with refined localization subcategories and predictive capabilities for all prokaryotes. *Bioinformatics* 26, 1608–1615. doi: 10.1093/bioinformatics/btq249
- Yuan, K., Huang, C., Fox, J., Laturnus, D., Carlson, E., Zhang, B., et al. (2012). Autophagy plays an essential role in the clearance of *Pseudomonas aeruginosa* by alveolar macrophages. *J. Cell Sci.* 125, 507–515. doi: 10.1242/jcs.094573

Conflict of Interest: The authors declare that the research was conducted in the absence of any commercial or financial relationships that could be construed as a potential conflict of interest.

Copyright © 2020 Cavinato, Genise, Luly, Di Domenico, Del Porto and Ascenzioni. This is an open-access article distributed under the terms of the Creative Commons Attribution License (CC BY). The use, distribution or reproduction in other forums is permitted, provided the original author(s) and the copyright owner(s) are credited and that the original publication in this journal is cited, in accordance with accepted academic practice. No use, distribution or reproduction is permitted which does not comply with these terms.



Chemical, Metabolic, and Cellular Characterization of a FtsZ Inhibitor Effective Against *Burkholderia cenocepacia*

Laurent R. Chiarelli^{1†}, Viola Camilla Scoffone^{1†}, Gabriele Trespidi¹, Giulia Barbieri¹, Olga Riabova², Natalia Monakhova², Alessio Porta³, Giulia Manina⁴, Giovanna Riccardi¹, Vadim Makarov² and Silvia Buroni^{1*}

¹ Laboratory of Molecular Microbiology, Department of Biology and Biotechnology "L. Spallanzani", University of Pavia, Pavia, Italy, ² Federal Research Centre "Fundamentals of Biotechnology" of the Russian Academy of Sciences, Moscow, Russia, ³ Organic Chemistry Section, Department of Chemistry, University of Pavia, Pavia, Italy, ⁴ Microbial Individuality and Infection Group, Cell Biology and Infection Department, Institut Pasteur, Paris, France

OPEN ACCESS

Edited by:

Paolo Visca,
Roma Tre University, Italy

Reviewed by:

Orietta Massidda,
University of Cagliari, Italy
Eshwar Mahenthiralingam,
Cardiff University, United Kingdom

*Correspondence:

Silvia Buroni
silvia.buroni@unipv.it

[†]These authors have contributed
equally to this work

Specialty section:

This article was submitted to
Antimicrobials, Resistance and
Chemotherapy,
a section of the journal
Frontiers in Microbiology

Received: 31 January 2020

Accepted: 16 March 2020

Published: 07 April 2020

Citation:

Chiarelli LR, Scoffone VC, Trespidi G, Barbieri G, Riabova O, Monakhova N, Porta A, Manina G, Riccardi G, Makarov V and Buroni S (2020) Chemical, Metabolic, and Cellular Characterization of a FtsZ Inhibitor Effective Against *Burkholderia cenocepacia*.
Front. Microbiol. 11:562.
doi: 10.3389/fmicb.2020.00562

There is an urgent need for new antimicrobials to treat the opportunistic Gram-negative *Burkholderia cenocepacia*, which represents a problematic challenge for cystic fibrosis patients. Recently, a benzothiadiazole derivative, C109, was shown to be effective against the infections caused by *B. cenocepacia* and other Gram-negative and-positive bacteria. C109 has a promising cellular target, the cell division protein FtsZ, and a recently developed PEGylated formulation make it an attractive molecule to counteract *Burkholderia* infections. However, the ability of efflux pumps to extrude it out of the cell represents a limitation for its use. Here, more than 50 derivatives of C109 were synthesized and tested against Gram-negative species and the Gram-positive *Staphylococcus aureus*. In addition, their activity was evaluated on the purified FtsZ protein. The chemical, metabolic and cellular stability of C109 has been assayed using different biological systems, including quantitative single-cell imaging. However, no further improvement on C109 was achieved, and the role of efflux in resistance was further confirmed. Also, a novel nitroreductase that can inactivate the compound was characterized, but it does not appear to play a role in natural resistance. All these data allowed a deep characterization of the compound, which will contribute to a further improvement of its properties.

Keywords: *Burkholderia cenocepacia*, new antimicrobials, drug resistance, cell division, cystic fibrosis

INTRODUCTION

Cystic fibrosis (CF) patients are continuously subjected to antibiotic therapies due to lung colonization both by Gram-positive and -negative bacteria. Among the latter, *Burkholderia cenocepacia* represents a main concern being responsible for the so-called "cepacia syndrome," a necrotizing pneumonia which can lead to patient's death (Salsgiver et al., 2016). Indeed, this opportunistic pathogen is among the bacterial species CF patients should be worried about (Jones, 2019). Moreover, infections caused by *B. cenocepacia* are still a major contraindication to lung transplantation, although certain centers do admit infected patients in the list (Dupont, 2017). An

important characteristic, which renders these bacteria particularly dangerous, is their resistance toward most antibiotics used in clinical practice (Scoffone et al., 2017). This limits the therapeutic options available to treat the infections, and there are no standardized set of antibiotics for treatment. In this context, new antibacterials are highly necessary, although their development may be limited by poor commercial interest in *Burkholderia* infections because they are rare, with approximately 2.6% of CF patients infected with these bacteria (<https://www.cff.org/Research/Researcher-Resources/Patient-Registry/>).

During the last few years, we focused our attention on this topic, proposing new targets, such as the glutamate racemase (Israyilova et al., 2016), new strategies, such as the inhibition of quorum sensing (Scoffone et al., 2016; Buroni et al., 2018) and new drugs (Scoffone et al., 2014), to fight *B. cenocepacia* infections. We found that the benzothiadiazole derivative C109 is highly effective against *B. cenocepacia* (Scoffone et al., 2015) and other Gram-negative and -positive bacteria, including *Mycobacterium abscessus* (Hogan et al., 2018). We were also able to identify the cellular target of C109 as the highly conserved cell division protein FtsZ (Hogan et al., 2018). This protein has recently emerged as a new promising target for the development of pharmacological agents against CF pathogens (Buroni et al., 2020). This not only justifies the broad-spectrum activity of C109, but also validates it as a robust molecule that hits an essential pathway, which is evolutionarily distant from its eukaryotic counterpart.

Due to the poor solubility of C109, we recently described the development of PEGylated nanocrystals in which the compound was stabilized with D- α -tocopheryl polyethylene glycol 1000 succinate embedded in hydroxypropyl- β -cyclodextrin (Costabile et al., 2020). This powder formulation allows its re-dispersion in water for *in vitro* aerosolization. The ability of these C109 nanocrystals to diffuse through artificial mucus and possess low toxicity toward human bronchial epithelial cells was also demonstrated (Costabile et al., 2020). The great potentiality of this formulation has been shown also by its activity against both planktonic and sessile *B. cenocepacia* strains, and by its efficacy in combination with piperacillin (Costabile et al., 2020).

Despite its promising activity and low toxicity, we previously showed that C109 can be extruded out of the cell by an RND efflux pump (Scoffone et al., 2015). For this reason, in the present work we synthesized and characterized more than 50 C109 derivatives, by performing a deep structure-activity relationship (SAR) analysis to screen for compounds less prone to efflux. The Minimal Inhibitory Concentration (MIC) of all the compounds and their activity against the purified FtsZ protein were assessed. The C109 resistance mechanism, chemical, metabolic and cellular stability were also studied at the single-cell level.

MATERIALS AND METHODS

Chemical Synthesis of C109 Derivatives

The chemical synthesis of C109 derivatives is described in **Supplementary Data**.

Bacterial Strains and Growth Conditions

Burkholderia cenocepacia strains, *Escherichia coli* ATCC 25922, *Pseudomonas aeruginosa* PAO1, and *Staphylococcus aureus* ATCC 25923 were grown in Luria-Bertani (LB) medium (Difco), if not differently specified, with shaking at 200 rpm, or on LB agar, at 37°C.

MIC Determination and Checkerboard Assays

The effectiveness of C109 compound and of its derivatives against *B. cenocepacia* J2315, FCF19, and FCF22, *E. coli* ATCC 25922, *P. aeruginosa* PAO1, and *S. aureus* ATCC 25923 was assessed determining MICs in LB medium by the 2-fold microdilution method in U-bottom 96-well microtiter plates, and inoculating about 10^5 CFU. The microtiter plates were incubated at 37°C for 48 (for *B. cenocepacia*) or 24 h (for all the other strains) and growth was determined by the resazurin method (Martin et al., 2006). A solution of resazurin sodium salt (Sigma Aldrich) was prepared at 0.01% in distilled water and filter-sterilized. Thirty microliter of resazurin solution were added to each well after 1 or 2 days of incubation at 37°C, and the microtiters were re-incubated at the same temperature for 4 h. The MIC was defined as the lowest concentration of the drug that prevented a change in color from blue to pink, which indicates bacterial growth.

Checkerboard assays of C109 or its derivatives with concentrations ranging from 0 to 128 μ g/ml in combination with the efflux pump inhibitor Pa β N MC-207.110 (0–128 μ g/ml) were set up, as previously described (Saiman et al., 1996) and the results determined using the resazurin MIC method.

Three independent biological replicates were used for each MIC determination.

Quantitative Reverse Transcription PCR (qRT-PCR) of RND-9 Efflux Pump and Nitroreductase Genes

Total RNA was extracted from *B. cenocepacia* J2315, FCF19, and FCF22 clinical isolates (1×10^9 CFU) using the RiboPure Bacteria Kit (Ambion), following the manufacturer's instructions. A 30 min incubation of each sample with DNaseI (Ambion) was performed, following the manufacturer's protocol. One-microgram of total RNA was used for cDNA generation using the QuantiTect reverse Transcription kit (Qiagen) according to the manufacturer's instructions, but diluting the cDNA 1:2 before qRT-PCR.

qRT-PCRs were performed on *BCAM1946* gene using the primers BCAM1946Rtfor (5'-TGCTCGTCGTGATCCTGTTT-3') and BCAM1946Rtrev (5'-CGAACAGCGTGAGCGTATTG-3') and on *BCAL0539* using primers NitroIntFor (5'-GTGTCGCCGTATATCGA-3') and NitroIntRev (5'-TTCTCGTCGCGGCCGAT-3'). All reactions were performed on a Rotor-Gene-6000 cyler (Corbett), using the Quanti-Tect SYBR Green PCR Kit (Qiagen), according to manufacturer's instructions. Cycling conditions were: 95°C for 15 min (1 cycle), 94°C for 15 s followed by 54°C for 30 s (for *BCAM1946*) or 40°C for 30 s (for *BCAL0539*) and 72°C for 30 s (40 cycles). A melting curve analysis was included at the end of each run.

Each sample was spotted in triplicate and control samples without cDNA were included in each experiment. *BCAM0918* (*rpoD*) gene was used as reference gene with the primers 0918F (5'-GCCAACCTGCGTCTCGT-3') and 0918R (5'-AACTGTCCACCGCCTT-3'), using an annealing temperature of 50°C. The fold difference in gene expression between the FCF19 and FCF22 and J2315 strains was assessed using the comparative Ct-method (Livak and Schmittgen, 2001). The results are the average of three independent replicates. Mann-Whitney test was used to determine if differences in expression were significant ($P < 0.05$).

FtsZ Proteins Expression and Purification and Enzymatic Assay

The gene *ftsZ* (*BCAL3457*) was amplified from *B. cenocepacia* FCF19 using the primers pet28presFtsZfor (5'-ATGGGTGCGGATCCCTGGAAGTTCTGTTCCAGGGGCCCATGGAA TTCGAAATGCTGGA-3') and pet28ftsZrev (5'-TGCGGC CGCAAGCTTTCAGTCAGCCTGCTTGCGCA-3'). The gene *ftsZ* of *P. aeruginosa* was amplified from the genomic DNA using the primers ftsZPAOfor28a (5'-ATGGGTGCGCGGA TCCCTGGAAGTTCTGTTCCAGGGGCCCTTTGAAC TGTCGATAACAT 3') and ftsZPAOrev28a (5'-TGCGGCCGC AAGCTTTCACAGGCCGGTGGCGACTAC-3'). The PCR products were cloned into the pET-28a vector (Novagen) using the In-Fusion HD Cloning kit (TaKaRa), according to the manufacturer's instructions.

All the recombinant FtsZ proteins were expressed at 20°C overnight in *E. coli* BL21(DE3) cells, upon induction with 0.5 mM IPTG, and purified using the same protocol assessed for the wild-type *B. cenocepacia* FtsZ (Hogan et al., 2018).

GTPase enzyme activity was determined using a pyruvate kinase/L-lactic dehydrogenase (PK/LDH) spectrophotometric coupled assay (Ingelman and Nunnari, 2005). The assays were performed at 30°C, in a reaction mixture containing 50 μM Hepes pH 7.5, 5 mM MgCl₂, 5 mM KCl, 10 U PK/LDH, 0.25 mM NADH, 0.25 mM PEP, and 5–10 μM FtsZ, and initiated by the addition of 0.5 mM GTP. Alternatively, GTPase activity was determined by measuring the release of phosphate using the malachite green assay (Baykov et al., 1988).

Steady-state kinetic analysis was performed by assaying the activity at different GTP concentrations and parameters determined by fitting the data to the Michaelis-Menten equation using Origin 8 software. All experiments were performed in triplicate.

Initial Inhibition assays were performed at 100 μM of each compound (stock solution 20 mM in DMSO) and, for compounds significantly active, the inhibitory concentration (IC₅₀) was determined. To this purpose, GTPase activity of FtsZ was evaluated in the presence of different concentrations of compounds, ranging from 0.5 μM to 100 μM, and IC₅₀ value was determined by the Equation 1 using Origin 8 software:

$$A_{[I]} = A_{[0]} \times \left(1 - \frac{[I]}{[I] + IC_{50}}\right) \quad (1)$$

where $A_{[I]}$ is the enzyme activity at inhibitor concentration $[I]$ and $A_{[0]}$ is the enzyme activity without inhibitor.

Metabolic Transformation of C109 in *B. cenocepacia* Cultures

To identify the products of C109 transformation in the cellular environment, 200 ml *B. cenocepacia* J2315 culture were grown overnight at 37°C in LB medium, then 20 mg C109 were added. After 1.5 h, a chloroform extraction (100 ml × 3) was performed. Organic phase obtained from the extraction was evaporated, residues were resuspended in hexane/ethyl acetate 9:1 and subjected to flash column chromatography (Merck SiO₂ 60, 230–400 mesh). Visualization of metabolites was achieved under UV light at a wavelength of 254 nm.

The isolated metabolites were analyzed in UPLC/MS. The chromatographic analysis was performed with a JASCO X-LC (Lecco, Italy) system, coupled with a Thermo Fisher Scientific (Milan, Italy) LTQ XL HESI-MS/MS system. Chromatography was performed on a Waters Acquity column, 3 μm particle size, 0.3 ml/min, gradient 10 min from 90:10 H₂O/MeCN to 100% MeCN, then 4 min in 100% MeCN. The analyses were performed in full-scan from 150 and 2,000 u.m.a. in positive mode, and base peaks were analyzed with dependent scan method with @CID = 32 eV. Run were also monitored by recording the absorbance at 220 nm.

Nitroreductase BCAL0539 Expression, Purification, and Characterization

In order to obtain the *B. cenocepacia* putative nitroreductase (BcNR), the *BCAL0539* gene was amplified using the primers pet28BC0539for (5'-ATGGGTGCGCGATCCCTGGAAGT TCTGTTCCAGGGGCCCATGTCCGTCCCCACTGCTT-3') and pet28BC0539rev (5'-TGCGGCCGCAAGCTTTC AAGC GAAAAAGCGCGCG-3'), and PCR products cloned into the pET-28a vector by the "In-Fusion[®] HD Cloning." To facilitate the purification process, the forward primer was designed to insert the sequence encoding the cleavage site of the PreScission Protease (GE Healthcare) downstream the N-terminal His-tag sequence (italicized in the primer sequence). Best protein expression was achieved in *E. coli* BL21(DE3) cells, by induction with 0.5 mM IPTG overnight at 25°C. Cells were frozen at −20°C until use.

Frozen cells were resuspended in 50 mM potassium phosphate pH 8.0, 500 mM KCl (buffer A) containing 1 mM phenylmethylsulfonylfluoride, lysed by sonication, and clarified by centrifugation at 50,000 × *g* for 1 h. Cell free extract was then applied on a HisTrapFF Crude (1 ml, GE Healthcare) column, washed with 50 mM imidazole in buffer A, then BcNR was eluted with 250 mM imidazole in the same buffer. Proteins were dialyzed against 50 mM potassium phosphate pH 8.0, 150 mM KCl (buffer B), containing 1 mM DTT, treated with PreScission Protease to remove the N-terminal histidine tag, then further purified by size exclusion chromatography on a HiLoad 16/60 Superdex-75 column (GE Healthcare) equilibrated in buffer B. Protein was concentrated to 10 mg/ml and stored at −80°C until use. As BcNR was produced as a flavoprotein, we explored

whether the prosthetic group is covalently bound to the enzyme. To this purpose, 0.5 μ l of the protein (2 mg/ml) were incubated at 100°C for 10 min, and centrifuged for 20 min at 12,000 \times g. The denaturated protein was resuspended in the same initial volume of 2% SDS, and the spectra of both supernatant and resuspended pellet were recorded.

Enzyme activity assay was determined at 37°C using 4-nitrobenzoic acid or C109 as a substrate and NADPH as cofactor, by measuring the decrease in absorbance at 340 nm of NADPH ($\epsilon = 6,220 \text{ M}^{-1} \text{ cm}^{-1}$). The reaction mixture typically contained 50 mM potassium phosphate pH 8.0, 50 mM KCl, 5–10 μ M BcNR, and reactions were started by adding the substrate. Steady-state kinetics parameters were determined by assaying the enzyme at variable concentrations of substrate (10–500 μ M). The experiments were performed in triplicate, and the kinetic constants K_m and k_{cat} determined by fitting the data to the Michaelis-Menten equation using Origin 8 software.

To determine the BcNR metabolite of C109, 5 mg of compound were incubated with 10 mg of BcNR in 50 mM potassium phosphate pH 8.0, 200 μ M NADPH, at 37°C, in a final volume of 35 ml for 1 h under agitation. The reaction mixture was then partitioned between water and dichloromethane (DCM), the aqueous layer was extracted with DCM, and combined organic layer washed with brine and dried over Na_2SO_4 . Solvent was removed under reduced pressure and residue purified by flash column chromatography with hexane-ethyl acetate 8:2 as eluent. The isolated metabolites were analyzed in UPLC/MS, as described above. Analysis were performed in full-scan from 90 and 1,000 u.m.a. and base peaks were analyzed with dependent scan method with @CID = 28 eV.

Time-Lapse Microscopy

B. cenocepacia J2315 was cultured over-night in Middlebrook 7H9 broth, supplemented with 10% (v/v) DS enrichment (20 g dextrose, 8.5 g sodium chloride in 1 L water) and 5% (v/v) of a casamino acids solution (10 g casamino acids in 100 ml water). Cells were diluted 10-fold in the same fresh 7H9 medium, and 5 μ l of the diluted cell suspension were inoculated into a custom-made microfluidic *hexa*-device, as previously described (Manina et al., 2019). Silicone tubing (0.76 mm ID) was connected to each inlet and outlet ports of the *hexa*-device to enable medium circulation. Two 50 ml syringes were connected to the inlet tubing, and prewarmed 7H9 medium was pumped through the microfluidic device at 15 μ l/min. The outlet tubing were inserted into a waste receptacle containing bleach. The syringes were switched to 7H9 medium containing C109 (100 μ g/ml) when appropriate. Bacteria were imaged in phase contrast, using a UPLFLN100XO2/PH3/1.30 objective (Olympus) and a high-speed sCMOS camera, with the help of an automated epifluorescence inverted microscope (DeltaVision Elite, GE Healthcare). The microscope was equipped with an environmental chamber maintained at 37°C. Images were recorded at 20-min intervals and up to 46 h. Exposure conditions were as follows: phase 50% T, 150 ms. In each experiment,

190 XY fields were imaged. The same experimental set-up was carried out twice.

Single-Cell Image Analysis

Manual segmentation of individual cells and analysis of image stacks were performed using the ImageJ 1.52a software. The Selection Brush Tools was used to draw polygons corresponding to the shape of individual cells and to extract the cell planar area (μm^2). Measurements of the cell area were repeated throughout the generation time of individual cells, to calculate the growth rate by fitting an exponential curve. Division and lysis events were scored from the total number of cells constituting a microcolony before and during both the first and second exposure to C109, and used to calculate both division and lysis rates, as previously described (Manina et al., 2015).

RESULTS

Chemistry and Structure-Activity Relationship of C109 Derivatives

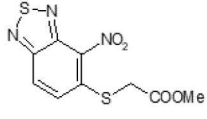
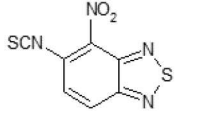
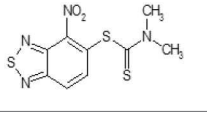
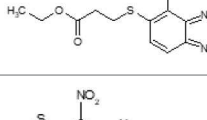
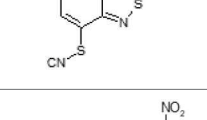
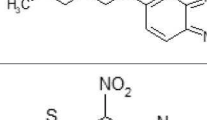
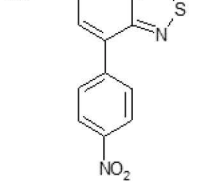
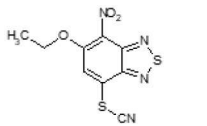
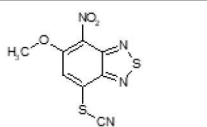
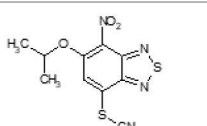
During our research in the field of the discovery of new anti-tuberculosis and anti-leprosy agents, we synthesized broad spectrum ortho-nitrodithiocarbomoyl heterocycles and analogs (Makarov et al., 2006). As a continuation of this research, we investigated the activity of some of these compounds on *B. cenocepacia* and surprisingly only compound C109 showed significant activity in whole cell screening (Scoffone et al., 2015). So, the primary aim of our current study was to improve the chemical properties of C109 in order to find new derivatives with lower MIC values toward *B. cenocepacia* and/or other bacteria, lower toxicity and, possibly, not extruded out of the cell by efflux mechanisms. To study structure activity and to design new active derivatives of C109, we used known medicinal chemistry methods to synthesize a broad spectrum of compounds and to probe their activity.

After screening 51 C109 derivatives (Supplementary Table 1), 23 compounds that showed inhibitory activity were examined to understand structure activity relationship.

The primary compound, C109, is a methyl [(4-nitro-2,1,3-benzothiadiazol-5-yl)thio]acetate (Scoffone et al., 2015). As a first step, we investigated the activity of several heterocyclic compounds having methylthioacetate moiety in ortho position to nitro group and observed that 2,1,3-benzothiadiazol scaffold is essential to preserve antibacterial activity. Also, our efforts to change methylthioacetate moiety to other sulfur containing nucleophilic substituents, such as dithiocarbamates, rhodano, imidothiocarbamate did not lead to any compounds with significant activity. Therefore, all other modifications have been limited with efforts to modify the nitro group and methylthioacetate side chain. The nitro group was explored to understand the essentiality of this reactive moiety. All the compounds lacking this group failed to be active both against the FtsZ activity and all the bacteria tested, confirming its essentiality.

Another way to modify the C109 compound was achieved through the synthesis of derivatives close to the original molecule, by modifying the size or hydrophobicity of the side chain, and introducing different moieties or atoms. This part of the molecule

TABLE 1 | Chemical structure, MICs and IC₅₀ of C109 and of selected derivatives.

Molecule	Chemical structure	MIC (μg/ml)				Inhibition of Bc FtsZ*	
		<i>B. cenocepacia</i> J2315	<i>E. coli</i> 25922	<i>S. aureus</i> 25923	<i>P. aeruginosa</i> PAO1	At 100 μM	IC ₅₀ (μM)
C109		8	8	4	128	Yes	8
10026149		32	16	2	16	Yes	20
10126130		>128	512	32	>128	Yes	10
10226047		>512	>512	>512	>128	No	-
10626056		>64	>512	8	>128	Yes	52
10726015		>64	>512	512	>128	No	-
11026176		>512	>512	4	>128	Yes	17
11026177		>512	>512	4	64	Yes	19
11126009		>128	>512	8	>128	Yes	4
11126010		>128	>512	4	>128	Yes	15

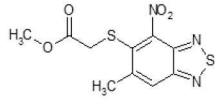
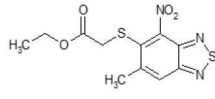
(Continued)

TABLE 1 | Continued

Molecule	Chemical structure	MIC ($\mu\text{g/ml}$)				Inhibition of Bc FtsZ*	
		<i>B. cenocepacia</i> J2315	<i>E. coli</i> 25922	<i>S. aureus</i> 25923	<i>P. aeruginosa</i> PAO1	At 100 μM	IC ₅₀ (μM)
11126015		>128	>512	32	>128	Yes	36
11426142		32	8	4	32	Yes	21
11426177		>128	>512	256	ND	No	–
11626109		512	>512	>512	ND	No	–
11726041		>256	>512	>256	ND	No	–
11726042		>256	>512	>256	ND	No	–
11726256		128	128	8	>256	No	–
11726257		16	8	8	128	Yes	3
11726258		256	>256	256	>256	Yes	15
11826109		256	128	16	>256	Yes	30
11826110		16	32	32	>256	No	–
11826363		16	16	64	256	Yes	30

(Continued)

TABLE 1 | Continued

Molecule	Chemical structure	MIC (μg/ml)				Inhibition of Bc FtsZ*	
		<i>B. cenocepacia</i> J2315	<i>E. coli</i> 25922	<i>S. aureus</i> 25923	<i>P. aeruginosa</i> PAO1	At 100 μM	IC ₅₀ (μM)
11926141		>256	>256	32	>256	Yes	100
11926142		>256	>256	32	>256	Yes	100

ND, Values Not Detected because of the resistance detected in the other bacteria. * *Burkholderia cenocepacia* purified FtsZ protein.

was explored as it can influence not only the binding of the compound to the molecular target FtsZ, but also the permeability across cell wall, as well as the affinity for efflux systems. For instance, the corresponding ethyl acetate derivative (11426142) partially lost activity against both bacteria and the purified enzyme (Table 1). The same was observed in the case of exchange of one proton inside chain on methyl group (11826110). We also observed completely loss of activity in the case of exchange of sulfur atom to oxygen (11726041), or nitrogen (11726042), or side chain length extension (10226047) (Table 1).

Then, we explored typical metabolic processes such as hydrolysis, oxidation and reduction during which C109 can be transformed into its active metabolites. Hydrolysis followed by free acid formation led to the isolation of compound 11426177 (Table 1). Although this compound can be easily transferred to water soluble salt, unfortunately it is not active against *B. cenocepacia*. During oxidation process, we isolated two compounds with different level of sulfur oxidation. The result of mono oxidation, the sulfinyl derivative 11726257, showed an activity on *B. cenocepacia* similar to C109 (Table 1). A deeper oxidation of sulfur, which resulted in the sulfonyl derivative 11826109 showed loss of activity. We also studied the reduction process of nitro group of xenobiotics: several chemical methods of reduction were explored but, surprisingly, in all cases we isolated only products of the reduction followed by cyclisation of the thiozine ring with formation of the interesting tricyclic compound 7H-[1,2,5]thiadiazolo[3,4-f][1,4]benzothiazin-8(9H)-one 11626109. This considerable modification of C109 structure caused loss of activity (Table 1).

Collectively these data show that the C109 molecule is very sensitive to any change, and that its structure is therefore most likely “terminal” for this class of compounds and for the activity against *B. cenocepacia*.

C109 Derivatives Exhibit a Broad Spectrum Efficacy

Overall, none of the derivatives showed better MIC values against *B. cenocepacia* than C109 (Table 1 and Supplementary Table 1). To check whether the compounds were effective against other Gram-negatives, the MICs against *E. coli* were evaluated, as described in Material and Methods, showing results very similar

to those achieved for *B. cenocepacia* (Table 1). The activity of the identified compounds was assessed also against *P. aeruginosa* and the Gram-positive *S. aureus*. Seven of them (10626056, 11026176, 11026177, 11126009, 11126010, 11126015, and 11726256) showed activity only against *S. aureus*, indicating that probably these molecules cannot enter the Gram-negative cells, due to the different composition of the cell wall and the presence of the outer membrane. However, compounds 10026149 and 11426142 had better MIC values than C109 against *P. aeruginosa* (16 and 32 μg/ml, respectively vs. 128 μg/ml).

To extend the basic antimicrobial inhibitory activity screening, we also determined the ability of all the C109 derivatives, showing activity against at least one of the microorganisms, to inhibit their cellular target, i.e., the cell division protein FtsZ. The IC₅₀ of the selected compounds was assayed on the *B. cenocepacia* FtsZ recombinant protein, as previously described (Hogan et al., 2018). As expected, all the compounds showed inhibitory activity, having an IC₅₀ ranging from 3 μM (11726257) to 100 μM (11926141 and 11926142, Table 1), thus confirming that the resistance identified is probably due to either limited cell penetration or increased efflux.

Being that 11426142 was effective against all the microorganisms tested, including *P. aeruginosa*, and showing an IC₅₀ against FtsZ of 21 μM (Table 1), we also determined its toxicity against a CF bronchial epithelial (CFBE41o-) cell line using the MTT assay, as previously described (Hogan et al., 2018). The toxic concentration at 50% (TC₅₀) of C109 on these cell lines is about 75 μM (Hogan et al., 2018; Costabile et al., 2020), while 11426142 showed a TC₅₀ of 50 μM (data not shown), confirming once more that C109 remains the best compound in our hands.

Analysis of C109 Resistant Strains

As we previously described that a mechanism of resistance to C109 relies on efflux mediated by the RND-9 transporter (Scoffone et al., 2015), we decided to investigate the resistance of *P. aeruginosa*, being the MIC of C109 equal to 128 μg/ml. A checkerboard assay, using increasing concentrations of C109 (from 0 to 128 μg/ml) in combination with the efflux pump inhibitor PaβN MC-207.110, was set up as described in Materials

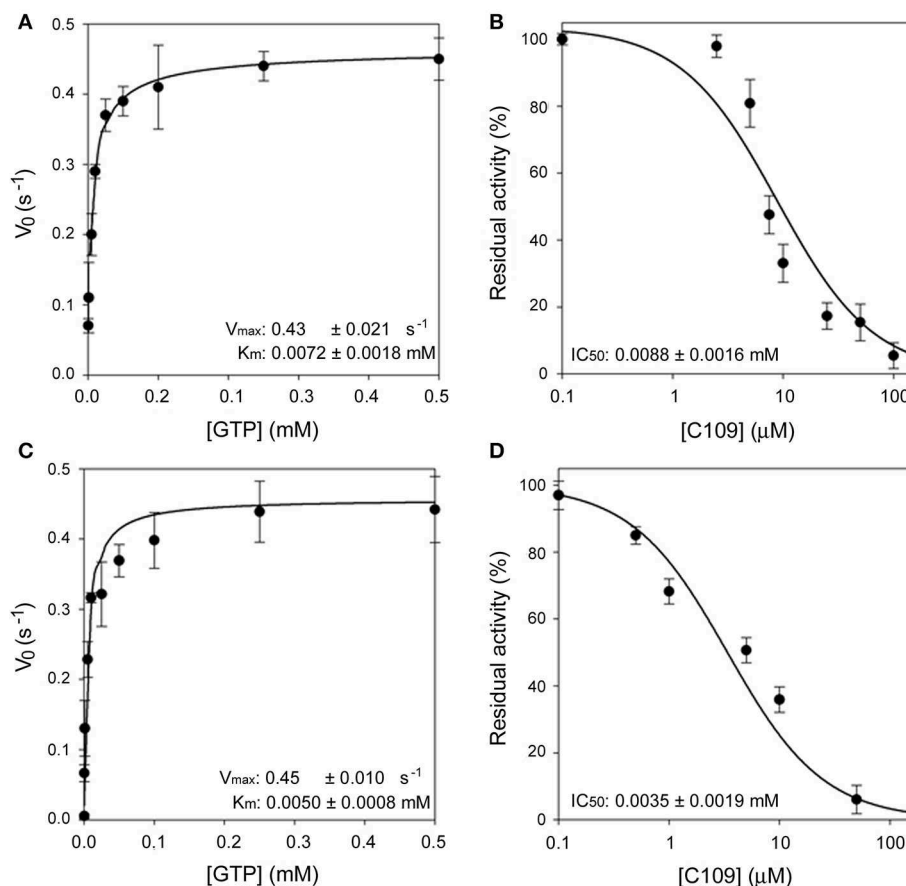


FIGURE 1 | Enzymatic characterization of FCF19-FtsZ and PAO1-FtsZ. **(A)** Steady state kinetic analysis of FCF19-FtsZ mutant as a function of GTP. **(B)** IC₅₀ determination of C109 toward FCF19-FtsZ mutant. **(C)** Steady state kinetic analysis of PAO1-FtsZ mutant as a function of GTP. **(D)** IC₅₀ determination of C109 toward PAO1-FtsZ.

and Methods. The use of the efflux pump inhibitor PaβN MC-207.110 (Pagès et al., 2005) in combination with the C109 molecule showed a synergistic effect. In fact, in the presence of 16–128 μg/ml of MC-207.110, the C109 MIC decreased to 1 μg/ml (data not shown). These data clearly indicate that an efflux mechanism is responsible for the resistance of *P. aeruginosa* to C109.

Moreover, the *ftsZ* gene from *P. aeruginosa* PAO1 was cloned and expressed in *E. coli* using the same protocol followed for FtsZ from *B. cenocepacia* (see Materials and Methods). The purified PAO1-FtsZ showed kinetic parameters comparable to the ones of *B. cenocepacia* enzyme and the protein was sensitive to the effect of C109, being the IC₅₀ even lower than toward *B. cenocepacia* FtsZ ($3.5 \pm 1.9 \mu\text{M}$ vs. $8.2 \pm 1.3 \mu\text{M}$), showing that the compound is able to inhibit the activity of this protein (Figure 1). As the two proteins share a 53% amino acid sequence identity, this result was not unexpected but further confirmed that the conserved FtsZ protein is the cellular target of C109.

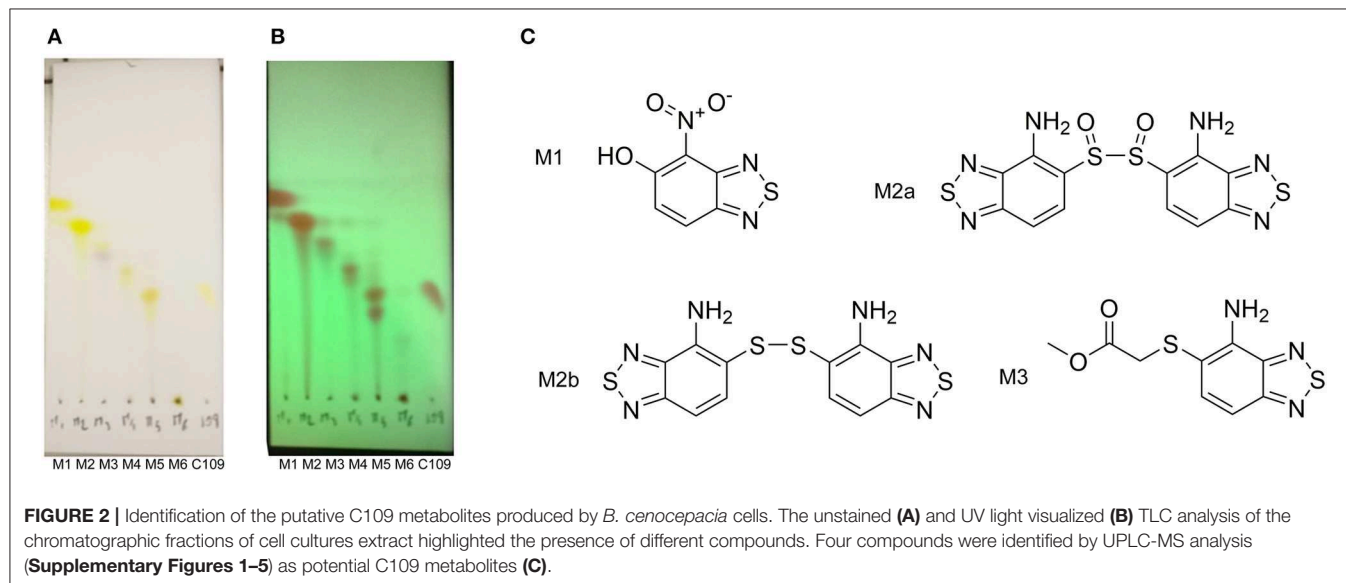
Next, we decided to investigate the origin of resistance to C109 in two clinical isolates of *B. cenocepacia*, namely FCF19 and FCF22 (Papaleo et al., 2010) for which C109 MIC is 128

and 256 μg/ml, respectively. Initially, we checked whether the gene encoding the C109 target, *ftsZ*, was mutated in these clinical isolates. Indeed, three mutations were found in the *ftsZ* gene of FCF19 strain, which lead to the following amino acidic changes: Pro347Gln; Ala348Pro; Gln349His. In contrast, no mutations were found in the *ftsZ* gene of FCF22 strain compared to the sequence of the reference strain J2315. Consequently, FCF19-FtsZ was expressed and purified in the same conditions of the wild-type FtsZ and showed to have kinetic parameters identical to those of the wild-type FtsZ (Figure 1). Moreover, the IC₅₀ of C109 on FCF19-FtsZ resulted to be almost identical to the one for the wild-type protein ($8.8 \pm 1.6 \mu\text{M}$), thus demonstrating that the mutated residues in FCF19-FtsZ are not responsible for the resistance phenotype.

Based on these findings, we sought whether the RND-9 efflux pump was implicated in the resistance phenotype of the two clinical isolates. We performed qRT-PCR analyses to check the level of expression of the RND-9 encoding gene. We found that the *BCAM1946* gene, encoding the RND-9 transporter, was overexpressed in both FCF19 and FCF22 clinical isolates of 12 and 20 times, respectively, compared to the wild-type J2315

TABLE 2 | MICs and RND-9 qRT-PCR results of *B. cenocepacia* FCF19 and FCF22 strains.

Strain	C109 MIC ($\mu\text{g/ml}$)	C109 MIC in the presence of MC-207.110 ($\mu\text{g/ml}$)	10026149 MIC ($\mu\text{g/ml}$)	11426142 MIC ($\mu\text{g/ml}$)	RND-9 overexpression \pm S.D.
FCF19	128	8	64	32	12 \pm 1.2
FCF22	256	16	256	32	20 \pm 3.5



strain (Table 2). As we previously isolated C109 resistant strains that carried mutations in the RND-9 regulator encoding gene (*BCAM1948*) or in the intergenic region, in between the first gene encoding RND-9 (*BCAM1947*) and the regulator (Scoffone et al., 2015), we sequenced the same region also in the two clinical isolates FCF19 and FCF22. However, no mutations were found in either the *BCAM1948* coding sequence or the intergenic region.

In order to determine whether the inhibition of the activity of efflux could affect the MIC of C109 in these strains, a checkerboard assay was set up using the compound C109 and the efflux pump inhibitor PaßN MC-207.110, as described above for *P. aeruginosa*. The MIC value of the C109 molecule in the presence of 128 $\mu\text{g/ml}$ of the efflux inhibitor (Table 2) was reduced in both clinical isolates (from 128 $\mu\text{g/ml}$ to 8 $\mu\text{g/ml}$ for the strain FCF19 and from 256 to 16 $\mu\text{g/ml}$ for FCF22), and comparable to the wild-type strain J2315. These data clearly indicate that an unidentified efflux mechanism is responsible for the resistance of these two clinical isolates.

Finally, the MIC of the C109 derivatives, having a lower MIC against *P. aeruginosa* (namely, 10026149 and 11426142), was determined also against the clinical isolates of *B. cenocepacia*, naturally resistant to C109, aiming to check whether they may be more effective and not subject to efflux. Both FCF19 and FCF22 clinical isolates showed resistance to the compound 10026149, whereas the MIC of the compound 11426142 was lower compared to the MIC of the compound C109 (32 $\mu\text{g/ml}$ for both strains, Table 2). This value, which is identical to the MIC against *B. cenocepacia* J2315, did not change in the presence of different concentrations (0–128 $\mu\text{g/ml}$) of the MC-207.110 efflux inhibitor. In contrast, the MIC of 11426142 decreased from 32 to

2 $\mu\text{g/ml}$ in the presence of MC-207.110 when the checkerboard assay was carried out using *P. aeruginosa*.

Metabolic Transformation of C109 Upon Contact With *B. cenocepacia* Cells

The TLC of the chromatographic fractions of C109 metabolites (Figure 2) showed that at least 6 different compounds could be isolated. All these fractions were subjected to UPLC-MS analysis to characterize the compounds, allowing us to identify four putative C109 metabolites, present in fractions 1 (M1), 2 (M2a and M2b) and 3 (M3) (Figure 2 and Supplementary Figures 1–4). Moreover, fraction M5 partly contained untransformed C109 (Supplementary Figure 5), whereas it was not possible to identify the compounds present in fractions 4 and 6 (data not shown).

The identified metabolites should derive from hydrolysis of C109 between the sulfur atom and the benzothiazole or the methylacetate moieties, and from reductive reactions particularly on the nitro group of the compound. To verify if these conversions lead to the inactivation of the compound, the MIC of these metabolites was determined using the resazurin method. None of the metabolites retained an antimicrobial activity, being all the MIC values >256 $\mu\text{g/ml}$ (data not shown).

B. cenocepacia Nitroreductase BCAL0539 Has the Potential to Inactivate C109

Since in three out of four identified metabolites of C109 the nitro group resulted to be reduced to amino, leading to loss of activity, we investigated whether an enzyme could be responsible for such reaction. Searching in the *Burkholderia* Genome

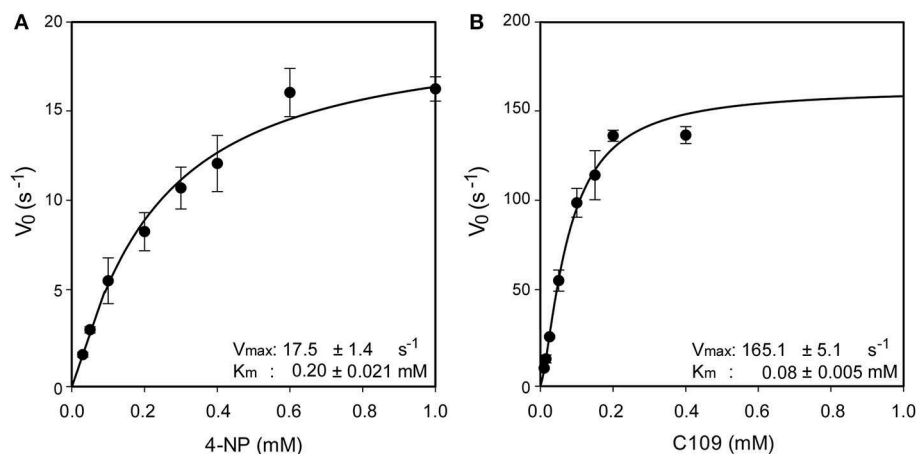


FIGURE 3 | Steady state kinetic analysis of BcNR, using 4-nitrobenzoic acid **(A)** and C109 **(B)** as substrate.

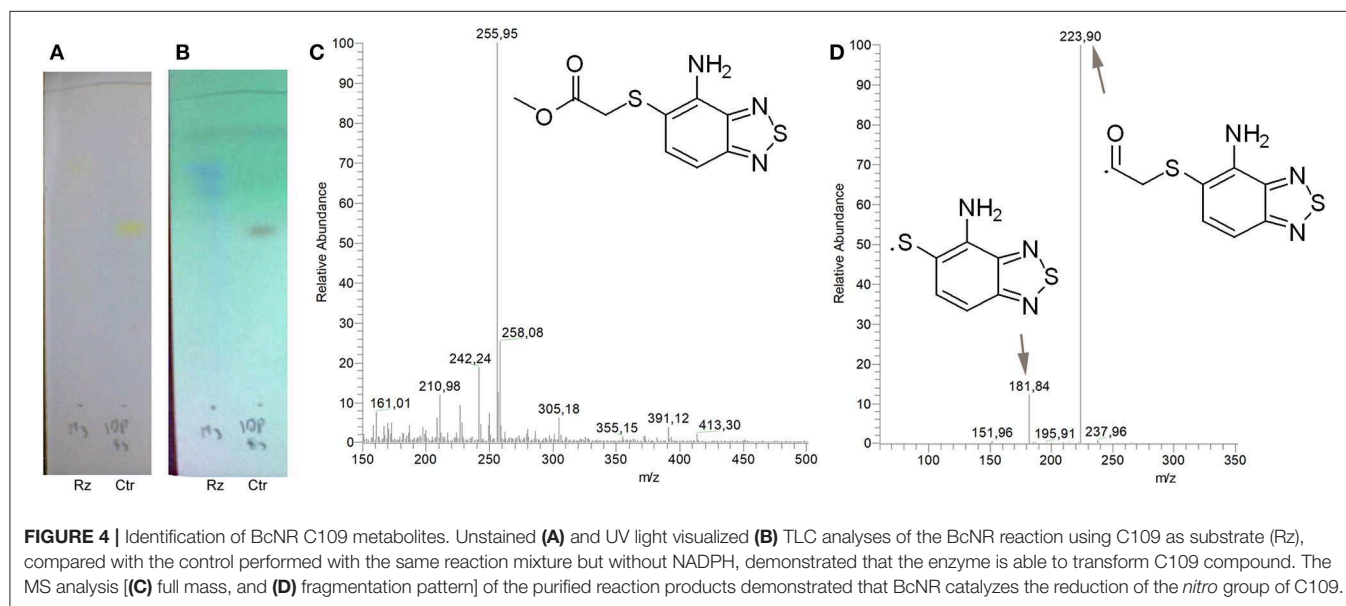


FIGURE 4 | Identification of BcNR C109 metabolites. Unstained **(A)** and UV light visualized **(B)** TLC analyses of the BcNR reaction using C109 as substrate (Rz), compared with the control performed with the same reaction mixture but without NADPH, demonstrated that the enzyme is able to transform C109 compound. The MS analysis **(C)** full mass, and **(D)** fragmentation pattern of the purified reaction products demonstrated that BcNR catalyzes the reduction of the *nitro* group of C109.

Database (www.burkholderia.com) we found the *BCAL0539* gene, which encodes a putative nitroreductase/4-nitrobenzoic reductase, belonging to the FMN—NAD(P)H-dependent nitroreductase family. To probe the role of this enzyme in the metabolism of C109, we produced the recombinant *B. cenocepacia* nitroreductase BCAL0539 (BcNR) protein in *E. coli*, and purified to homogeneity with a good yield (about 2 mg of protein per g of cells). The UV-vis spectrum of BcNR showed two peaks at 370 and 450 nm, demonstrating that the enzyme is expressed as a flavoprotein (**Supplementary Figure 6**). We found that the cofactor was not covalently linked to the enzyme because, after heat denaturation, the resuspended enzyme lost the two typical peaks of the flavin, which were instead present in the spectrum of the supernatant (**Supplementary Figure 7**). Since the enzyme is predicted to be a NAD(P)H dependent nitroreductase that uses 4-nitrobenzoic acid, we carried out a spectrophotometric activity assay, which follows the decrease

in absorbance at 340 nm of the cofactor. Moreover, the enzyme activity was also assayed by using C109 as substrate. As shown in **Supplementary Figure 8**, BcNR is strictly NADPH-dependent, and is able to reduce both 4-nitrobenzoic acid and C109. Furthermore, the kinetic analysis showed that the enzyme is able to use C109 very efficiently, showing a specificity constant of $2063.7 \pm 20.1 \text{ s}^{-1} \text{ mM}^{-1}$, about 20-fold higher than that for 4-nitrobenzoic acid, due to a 10-fold higher V_{max} and about a 2-fold lower K_m values (**Figure 3** and **Supplementary Table 2**).

To identify and characterize the C109 reaction product of BcNR, 5 mg of the compound were incubated for 1 h with the enzyme, in the presence of NADPH. The reaction mixture was then extracted with DCM, products isolated by silica gel chromatography and analyzed by mass spectrometry (**Figure 4**). Only a major metabolite was found, corresponding to the analogous amino metabolite of C109 M3, isolated in cell cultures (**Figure 2**),

demonstrating that BcNR catalyzes the nitroreduction of the C109 compound.

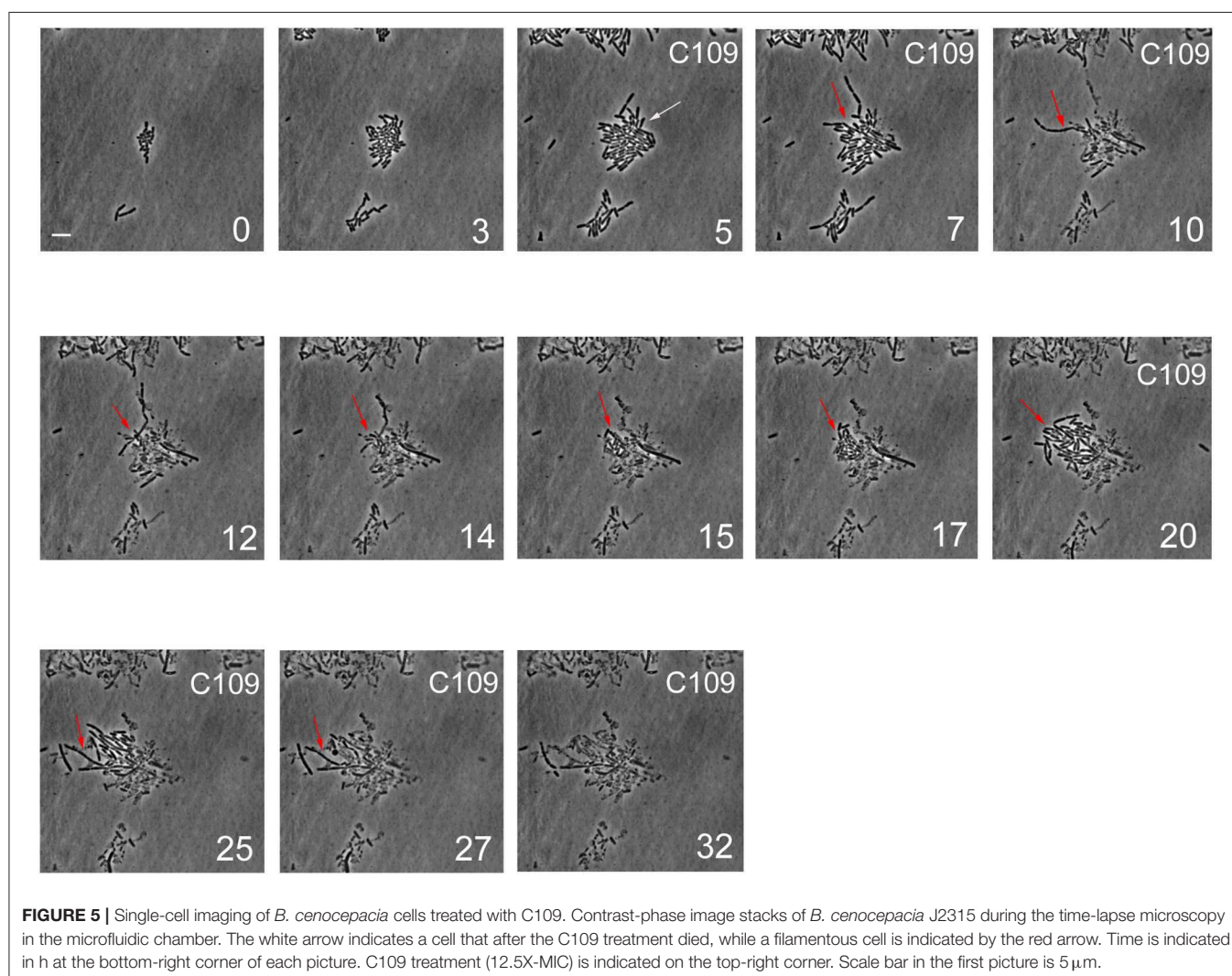
To assess whether the resulting BcNR reduction product could inhibit *B. cenocepacia* growth, we carried out a resazurin-based assay. We set up three reactions: (i) a complete reaction in the presence of 1 mM C109; (ii) a reaction without the cofactor NADPH; (iii) a reaction without C109. All these reactions were assayed along with the C109 nitro derivative 11626109 (Table 1), revealing that the metabolite resulting from the complete reduction is not active against *B. cenocepacia* growth (as 11626109), while in the absence of NADPH the BcNR does not work, C109 is not reduced and, consequently, still active. All these data confirm a role of BcNR in the inactivation of the compound, thus suggesting a possible involvement of the enzyme in the resistance mechanism to C109.

For this reason, the *BCAL0539* gene expression was analyzed in the wild type J2315 and in the clinical isolates FCF19 and FCF22, which are resistant to C109 (see above). However, the *BCAL0539* gene was not expressed, either in the wild type or in

the resistant strains, implying that the BcNR is not implicated in C109 inactivation and resistance mechanism.

Time-Lapse Microscopy of *B. cenocepacia* Treated With C109 Reveals a Fraction of Possible Persistent Cells

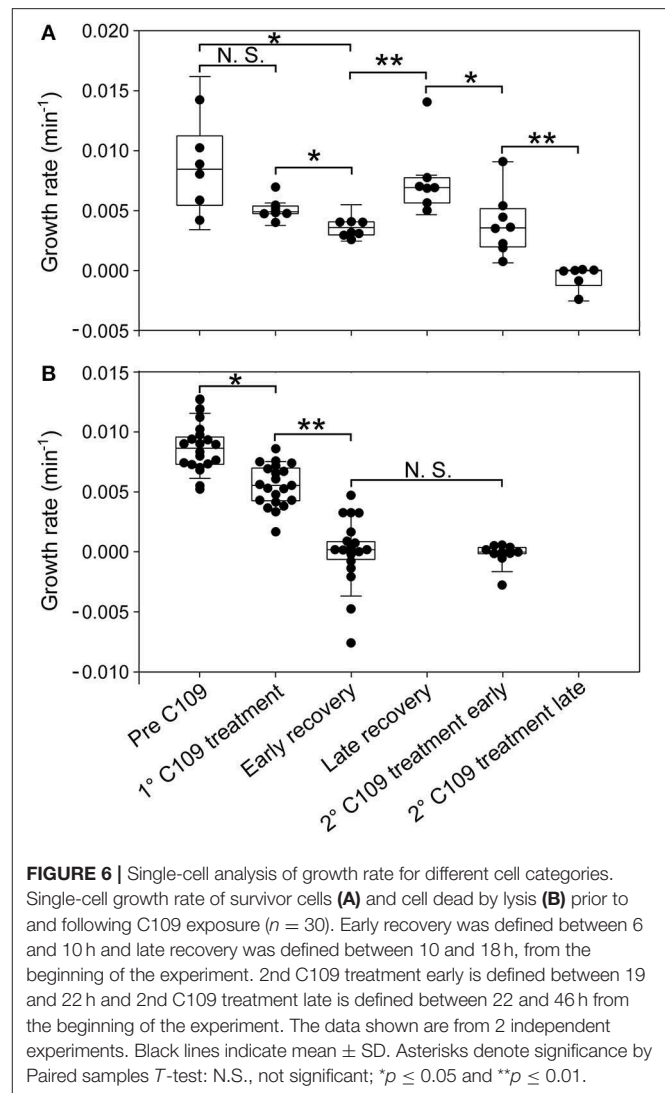
The killing dynamics of *B. cenocepacia* with the compound C109 at the bulk-population level were shown to be concentration dependent and biphasic (Scoffone et al., 2015). Biphasic killing represents the typical pattern of drug persistence, whereby the initial linear mortality of the population is followed by a second phase where a subpopulation of cells is able to endure inhibitory drug concentrations in the absence of genetic mutations (Van den Bergh et al., 2017). In contrast to drug-resistant cells, which continue to replicate in the presence of the drug, drug-persistent cells either derive from pre-existing non-growing cells or slow down their growth during drug exposure, and their progeny is killed with kinetics similar to that of the initial population (Van den Bergh et al., 2017; Balaban et al., 2019). Possible



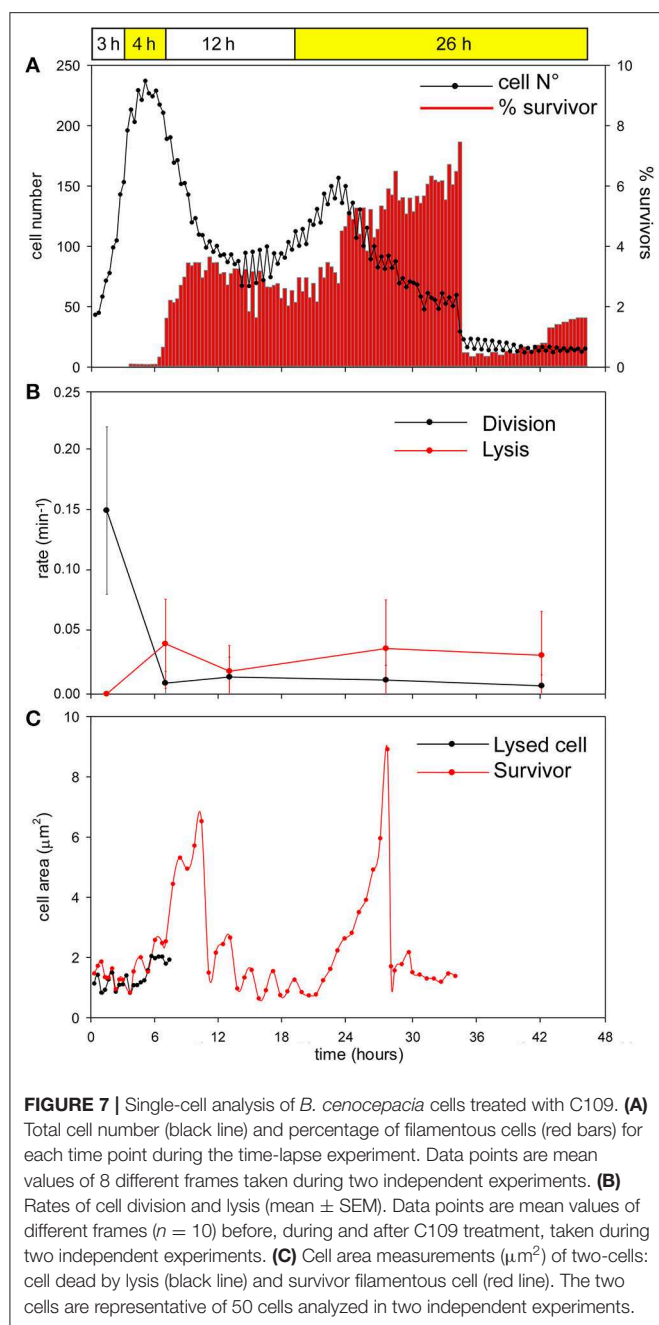
mechanisms that can bring about heterogeneous responses to drugs, such as drug persistence, include uneven expression and partitioning of efflux systems among single bacterial cells (Pu et al., 2016; Bergmiller et al., 2017). Importantly, the mechanism of resistance to the C109 compound is mediated by the RND-9 efflux transporter (Scoffone et al., 2015). To examine the C109 killing dynamics of *B. cenocepacia* at the single-cell level, we carried out a time-lapse microscopy experiment, divided into several steps. Wild type *B. cenocepacia* J2315 cells were first seeded into a microfluidic device (Manina et al., 2019), and perfused with prewarmed 7H9 medium for 3 h, to allow the cells to adapt to the microfluidic environment. After a few events of cell division, the cells were exposed to 100 $\mu\text{g/ml}$ of C109 (12.5X-MIC for the wild-type strain used in this work) for 4 h, equivalent to about 4 replication cycles. Cells were then perfused with C109-free 7H9 medium for 12 h, enabling the recovery and expansion of surviving cells. Finally, to understand whether the survivors had acquired genetic resistance, cells were exposed a second time to C109 (12.5X-MIC) for 24 h, equivalent to about 24 replication cycles. During the time-lapse imaging, cells were monitored every 20 min for a total of 46 h. The total number of cells, the single-cell area, and the number of division and lysis events were measured during each step of the experiment.

During the first 3 h phase, *B. cenocepacia* cells were able to adapt to the microfluidic device and replicate every 60 min (Figures 5, 6). After the first treatment with C109 (12.5X-MIC), 70% of the cells died from lysis (Figures 5, 7A) and the growth rate and the number of cell divisions decreased (Figures 6, 7B), until cells stopped dividing (Figure 7B). During the recovery phase in fresh 7H9 medium, 3.5 % of the remaining intact cells (30%) were able to resume growth and the cell number and the division rate increased again (Figures 5, 7A,B). After, the cells that had survived and resumed growth were treated for the second time with C109 (12.5X-MIC), we found that the compound caused again a decline in cell population by 92%, and finally cells stopped dividing (Figure 7A). Importantly, during the second treatment with C109 the population derived from the subpopulation of survivors showed a lysis rate comparable to the lysis rate of the initial population subject to the first treatment with C109, implying the absence of stable genetic resistance in the survivors, and reminiscent of a phenotype conceivably ascribable to persistent cells (Figure 7B).

From the single-cell point of view, the *B. cenocepacia* cell population exhibited two different phenotypes in the presence of C109 compound. During the first treatment with C109, 70% of the cells slowly decreased their rate of growth and division (Figures 5, 6B, 7B), increasing their area of 2-fold, and then died by lysis (Figures 5, 7C). These results were expected and consistent with previous observations upon inhibition of an essential component of the cell divisome by treatment with C109, and in case of other FtsZ inhibitors (Scoffone et al., 2015; Hogan et al., 2018; Tripathy and Sahu, 2019). The lytic phenotype could be explained because FtsZ is an essential component of the cell divisome and controls the cell wall biosynthesis at the septum site (Yang et al., 2017). Interestingly, 3.5% of cells decreased their growth rates, but were still able to grow and underwent considerable filamentation, increasing the cell area up to 5-fold



(Figures 5, 6A, 7C and Supplementary Movie 1). During C109 washout with the fresh medium, 30% of these filamentous cells started again to divide from both poles, decreasing the cell area to 1.5 μm^2 , which is comparable to the size of healthy wt cells (Figures 5, 6A, 7B,C and Supplementary Movie 1), while the other cells remained frozen to the initial state. To determine whether the cell population that expanded from the cells that survived the first treatment with C109 had become genetically resistant, we treated the cells a second time with the C109 compound for 24 h. The population showed again both phenotypes; namely, 94% of the cells stopped to divide during the treatment (Figures 5, 6A, 7A,B and Supplementary Movie 1), while a smaller population (about the 6% of the total cell number) showed again the elongated phenotype (Figures 5, 7C and Supplementary Movie 1). These cells were unable to divide but increased their area up to 10-fold (8–10 μm^2) the normal size of the cell (Figures 5, 7C and Supplementary Movie 1). Then, these elongated cells stopped to increase their area and died during the exposure to C109 (Figures 5, 7C and Supplementary Movie 1).



These results indicate that *B. cenocepacia* cells exposed to C109 produce a subpopulation with a phenotype ascribable to possible persistent cells. In particular, these survivor cells remain elongated in presence of the compound but restore their normal size and life cycle once the C109 is removed, giving rise to a new non-filamentous population. The latter population, once treated again with C109, shows again both phenotypes, i.e., a fraction of cells (94%) that is again sensitive to C109 and a second fraction of elongated cells (6%) that is still sensitive to C109 extended exposure, and does not show any sign of resistance. Among a representative population of 3,000 elongated cells that formed during the first exposure to C109, 8 cells

(0.27%) resumed normal growth during drug washout and, being sensitive to the second exposure to C109, were ascribable to possible persistent cells.

DISCUSSION

Burkholderia spp infections represent a problematic threat for CF patients. However, due to the low infection rate, the development of novel antimicrobials has been limited and remains an urgent priority for these patients (Regan and Bhatt, 2019). For this reason, in the past few years we identified and characterized the FtsZ inhibitor C109, which showed strong activity against *B. cenocepacia*, including several clinical isolates (Scoffone et al., 2015; Hogan et al., 2018). Moreover, this compound proved to be active against both planktonic and sessile *B. cenocepacia* strains, and against different other Gram-positive and -negative bacteria (Hogan et al., 2018; Costabile et al., 2020).

However, despite its great potential, this compound displays two main drawbacks. First, we showed that C109 is a substrate of the RND-9 efflux pump (Scoffone et al., 2015), and efflux pumps are known to be among the most common mechanisms of resistance to antibiotics in *B. cenocepacia* (Perrin et al., 2010). Second, the compound is characterized by the presence of a nitro group, which is considered a structural alert in a potential drug, due to its possible association with mutagenicity and genotoxicity (Nepali et al., 2019). In addition, this nitro group could be the substrate of modifying nitroreductase enzymes, which can alter the efficacy of the compound (Nepali et al., 2019).

In particular, we explored the effects of the typical metabolic reactions of hydrolysis, oxidation and reduction on the activity of C109. However, none of the synthesized derivatives showed improved potency. Similarly, the modification introduced to synthesize close derivatives, such as acetylation, methylation of the benzothiadiazole group, substitution of the sulfur atom with oxygen or nitrogen atom, or the extension of the side chain, gave no improvement.

It is noteworthy that the majority of the derivatives, showing worsened potency in *B. cenocepacia* and in *E. coli*, maintained a similar or improved activity in *S. aureus*, further confirming that the main drawback of these compounds is the difficulty to access the cell, or to be maintained into Gram-negative cells. Indeed, the main issue of these compounds is that they are good substrate of efflux pumps, as we demonstrated in both *B. cenocepacia* clinical isolates and *P. aeruginosa*.

The other drawback of our benzothiadiazole compound is the presence of an essential nitro group, that could be subjected to different modifications. It is noteworthy that modifications occurring to nitro group could lead to the inactivation of the drug (Nepali et al., 2019), whereas in the case of pro-drugs these modifications can cause their activation (Mori et al., 2017). Thus, to better characterize the behavior of C109, we investigated how it can be metabolized by *B. cenocepacia* cells. As expected, the main transformations taking place are reductive reactions on the nitro moiety, and hydrolytic reactions occurring between the sulfur atom linking the benzothiadiazole with the methylacetate. We were able to isolate and characterize certain C109 metabolites, but

all of them were shown to be inactive, demonstrating that the compound is not subjected to any activation process. However, having found that C109 is intracellularly inactivated through nitroreduction, we looked for possible enzymes responsible for this reaction. We found that *B. cenocepacia* possesses a gene encoding the putative nitroreductase BcNR. However, we exclude that BcNR confers resistance to the compound, being its basal level of expression negligible. At this stage, we cannot exclude that there are other possible endogenous nitroreductases that could be responsible for the inactivation of C109 in *B. cenocepacia*, although none has been reported in the literature so far.

The C109 compound is also particularly susceptible to the action of the RND-9 efflux pump, which is over-expressed in two clinical isolates we tested (Papaleo et al., 2010; Scoffone et al., 2015). Remarkably, stochastic expression of efflux pumps can induce a fraction of the bacterial population to become persistent to drugs (Pu et al., 2016; Bergmiller et al., 2017). Furthermore, it has been recently proposed that recurrent drug-persistent infections, such as those caused by *B. cenocepacia* in CF patients, may promote the onset of genetic drug resistance (Balaban et al., 2019). Here we decided to assess the single-cell behavior of a clonal population of *B. cenocepacia* J2315 when confronted with the compound C109, by using quantitative time-lapse imaging. Although the majority of the bacterial population stopped dividing and died during treatment, consistent with the essentiality of FtsZ and with the mislocalization of FtsZ-GFP in *E. coli* cells treated with C109 (Hogan et al., 2018), a small fraction of *B. cenocepacia* cells was still viable and exhibited a considerable filamentous phenotype, which reflects the ability of a subpopulation to tolerate dysfunctional cytokinesis. During the recovery in C109-free medium, these surviving cells gave rise to a new population with normal cell size that, following a second treatment, was still sensitive to C109 and did not develop stable resistance to the compound. These results imply that these transient filamentous cells could be considered cells with a phenotype ascribable to possible persisters, which will be subjected to further investigations. Interestingly, we found that cells that survived the C109 compound originated from metabolically active cells, which had a growth rate comparable to drug-sensitive cells, as previously described in different bacterial species (Van den Bergh et al., 2017). Although non-growing populations are usually enriched with drug-persistent cells, the phenomenon of persistence is not exclusively linked to the absence of growth ahead of drug exposure, but is multifactorial and can also be associated with the environmental conditions; species-specific factors; pre-existing cell-to-cell phenotypic variation; the drug class and the dynamics of drug exposure (Van den Bergh et al., 2017; Balaban et al., 2019; Goormaghtigh and Van Melderen, 2019; Manina et al., 2019). Here we report that the single-cell growth rate prior to C109 exposure is not predictive of survival toward C109 compound in *B. cenocepacia*. At present, we cannot discriminate whether C109-survivors might result from the exposure to the compound, or might derive from a subpopulation having a distinct phenotype before exposure to the compound. In the future, it will be interesting to explore whether

stochastic over-expression of RND-9 or of another efflux pump may be responsible for the onset of persistence in a subpopulation of *B. cenocepacia*. We think that a better understanding of this phenomenon may help to conceive a drug combination that makes C109 more effective against *B. cenocepacia*.

In conclusion, within this work, we thoroughly characterized the potential of the C109 scaffold for the development of new antimicrobial compounds against microbial species that are life-threatening for CF patients. Despite most of the derivatives being effective against the cellular target FtsZ *in vitro*, none showed improved activity against Gram negative bacteria. However, five of these derivatives (10026149, 11026176, 11026177, 11126010, 11426142) showed promising activity against the CF and nosocomial pathogen *S. aureus*, suggesting another possible application for this class of compounds.

DATA AVAILABILITY STATEMENT

All necessary datasets generated for this study are included in the article.

AUTHOR CONTRIBUTIONS

SB, VM, and GR contributed conception and design of the study. LC expressed and purified the proteins and performed enzymatic and metabolic assays. VS performed cloning, enzymatic assays, and time lapse experiments. GT expressed and purified the proteins and performed qRT-PCR. GB analyzed data. OR and NM synthesized and analyzed all tested compounds. AP performed MS assays and analysis. GM performed time lapse experiments. SB performed microbiological experiments. All authors contributed to manuscript revision, read, and approved the submitted version.

FUNDING

This work was supported by the US Cystic Fibrosis Foundation (grant RICCAR17G0 to GR), by a BlueSky research grant of the University of Pavia to SB, by the Italian Ministry of Education, University and Research (MIUR) (Dipartimenti di Eccellenza, Program 2018-2022) to Department of Biology and Biotechnology, L. Spallanzani, University of Pavia (to GR, SB, LC), by the PRIN 2017 grant prot. 20177J5Y3P (to GR), and by the French Government's Investments for the future, Laboratoire d'Excellence Integrative Biology of Emerging Infectious Diseases (ANR-10-LABX-62-IBEID, to GM).

ACKNOWLEDGMENTS

The authors are grateful to Dr. Alberto Azzalin (Department of Biology and Biotechnology, University of Pavia) for microscopy and MTT assays technical assistance.

SUPPLEMENTARY MATERIAL

The Supplementary Material for this article can be found online at: <https://www.frontiersin.org/articles/10.3389/fmicb.2020.00562/full#supplementary-material>

REFERENCES

- Balaban, N. Q., Helaine, S., Lewis, K., Ackermann, M., Aldridge, B., Andersson, D. I., et al. (2019). Definitions and guidelines for research on antibiotic persistence. *Nat. Rev. Microbiol.* 17, 441–448. doi: 10.1038/s41579-019-0196-3
- Baykov, A. A., Evtushenko, O. A., and Avaeva, S. M. (1988). A malachite green procedure for orthophosphate determination and its use in alkaline phosphatase-based enzyme immunoassay. *Anal. Biochem.* 171, 266–270. doi: 10.1016/0003-2697(88)90484-8
- Bergmiller, T., Andersson, A. M. C., Tomasek, K., Balleza, E., Kiviet, D. J., Hauschild, R., et al. (2017). Biased partitioning of the multidrug efflux pump AcrAB_TolC underlies long lived phenotypic heterogeneity. *Science* 356, 311–315. doi: 10.1126/science.aaf4762
- Buroni, S., Makarov, V., Scoffone, V. C., Trespidi, G., Riccardi, G., and Chiarelli, L. R. (2020). The cell division protein FtsZ as a cellular target to hit cystic fibrosis pathogens. *Eur. J. Med. Chem.* 190:112132. doi: 10.1016/j.ejmech.2020.112132
- Buroni, S., Scoffone, V. C., Fumagalli, M., Makarov, V., Cagnone, M., Trespidi, G., et al. (2018). Investigating the mechanism of action of diketopiperazines inhibitors of the *Burkholderia cenocepacia* quorum sensing synthase CepI: a site-directed mutagenesis study. *Front. Pharmacol.* 9:836. doi: 10.3389/fphar.2018.00836
- Costabile, G., Provenzano, R., Azzalin, A., Scoffone, V. C., Chiarelli, L. R., Rondelli, V., et al. (2020). PEGylated mucus-penetrating nanocrystals for lung delivery of a new FtsZ inhibitor against *Burkholderia cenocepacia* infection. *Nanomedicine* 23:102113. doi: 10.1016/j.nano.2019.102113
- Dupont, L. (2017). Lung transplantation in cystic fibrosis patients with difficult to treat lung infections. *Curr. Opin. Pulm. Med.* 23, 574–579. doi: 10.1097/MCP.0000000000000431
- Goormaghtigh, F., and Van Melderen, L. (2019). Single-cell imaging and characterization of *Escherichia coli* persister cells to ofloxacin in exponential cultures. *Sci. Adv.* 5:eav9462. doi: 10.1126/sciadv.aav9462
- Hogan, A. M., Scoffone, V. C., Makarov, V., Gislason, A. S., Tesfu, H., Stietz, M. S., et al. (2018). Competitive fitness of essential gene knockdowns reveals a broad-spectrum antibacterial inhibitor of the cell division protein FtsZ. *Antimicrob. Agents Chemother.* 62, e01231–18. doi: 10.1128/AAC.01231-18
- Ingerman, E., and Nunnari, J. (2005). A continuous, regenerative coupled GTPase assay for dynamin-related proteins. *Methods Enzymol.* 404, 611–619. doi: 10.1016/S0076-6879(05)04053-X
- Israyilova, A., Buroni, S., Forneris, F., Scoffone, V. C., Shixaliyev, N. Q., Riccardi, G., et al. (2016). Biochemical characterization of glutamate racemase—a new candidate drug target against *Burkholderia cenocepacia* infections. *PLoS ONE* 11:e0167350. doi: 10.1371/journal.pone.0167350
- Jones, A. M. (2019). Which pathogens should we worry about? *Paediatr. Respir. Rev.* 31, 15–17. doi: 10.1016/j.prrv.2019.02.007
- Livak, K. J., and Schmittgen, T. D. (2001). Analysis of relative gene expression data using real-time quantitative PCR and the $2^{-\Delta\Delta C_T}$ method. *Methods* 25, 402–408. doi: 10.1006/meth.2001.1262
- Makarov, V., Riabova, O. B., Yuschenko, A., Urlyapova, N., Daudova, A., Zipfel, P. F., et al. (2006). Synthesis and antileprosy activity of some dialkylthiocarbamates. *J. Antimicrob. Chemother.* 57, 1134–1138. doi: 10.1093/jac/dkl095
- Manina, G., Dhar, N., and McKinney, J. D. (2015). Stress and host immunity amplify *Mycobacterium tuberculosis* phenotypic heterogeneity and induce nongrowing metabolically active forms. *Cell Host Microbe* 17, 32–46. doi: 10.1016/j.chom.2014.11.016
- Manina, G., Griego, A., Singh, L. K., McKinney, J. D., and Dhar, N. (2019). Preexisting variation in DNA damage response predicts the fate of single mycobacteria under stress. *EMBO J.* 38:e101876. doi: 10.15252/embj.2019101876
- Martin, A., Takiff, H., Vandamme, P., Swings, J., Palomino, J. C., and Portaels, F. (2006). A new rapid and simple colorimetric method to detect pyrazinamide resistance in *Mycobacterium tuberculosis* using nicotinamide. *J. Antimicrob. Chemother.* 58, 327–331. doi: 10.1093/jac/dkl231
- Mori, G., Chiarelli, L. R., Riccardi, G., and Pasca, M. R. (2017). New prodrugs against tuberculosis. *Drug Discov. Today* 22, 519–525. doi: 10.1016/j.drudis.2016.09.006
- Nepali, K., Lee, H. Y., and Liou, J. P. (2019). Nitro-group-containing drugs. *J. Med. Chem.* 62, 2851–2893. doi: 10.1021/acs.jmedchem.8b00147
- Pages, J. M., Masi, M., and Barbe, J. (2005). Inhibitors of efflux pumps in gram-negative bacteria. *Trends Mol. Med.* 11, 382–389. doi: 10.1016/j.molmed.2005.06.006
- Papaleo, M. C., Perrin, E., Maida, I., Fondi, M., Fani, R., and Vandamme, P. (2010). Identification of species of the *Burkholderia cepacia* complex by sequence analysis of the *hisA* gene. *J. Med. Microbiol.* 59, 1163–1170. doi: 10.1099/jmm.0.019844-0
- Perrin, E., Fondi, M., Papaleo, M. C., Maida, I., Buroni, S., Pasca, M. R., et al. (2010). Exploring the HME and HAE1 efflux systems in the genus *Burkholderia*. *BMC Evol. Biol.* 10:164. doi: 10.1186/1471-2148-10-164
- Pu, Y., Zhao, Z., Li, Y., Zou, J., Ma, Q., Zhao, Y., et al. (2016). Enhanced efflux activity facilitates drug tolerance in dormant bacterial cells. *Mol. Cell.* 62, 284–294. doi: 10.1016/j.molcel.2016.03.035
- Regan, K. H., and Bhatt, J. (2019). Eradication therapy for *Burkholderia cepacia* complex in people with cystic fibrosis. *Cochrane Database Syst. Rev.* 4:CD009876. doi: 10.1002/14651858.CD009876.pub4
- Saiman, L., Mehar, F., Niu, W. W., Neu, H. C., Shaw, K. J., Miller, G., et al. (1996). Antibiotic susceptibility of multiply resistant *Pseudomonas aeruginosa* isolated from patients with cystic fibrosis, including candidates for transplantation. *Clin. Infect. Dis.* 23, 532–537. doi: 10.1093/clinids/23.3.532
- Salsgiver, E. L., Fink, A. K., Knapp, E. A., LiPuma, J. J., Olivier, K. N., Marshall, B. C., et al. (2016). Changing epidemiology of the respiratory bacteriology of patients with cystic fibrosis. *Chest* 149, 390–400. doi: 10.1378/chest.15-0676
- Scoffone, V. C., Chiarelli, L. R., Makarov, V., Brackman, G., Israyilova, A., Azzalin, A., et al. (2016). Discovery of new diketopiperazines inhibiting *Burkholderia cenocepacia* quorum sensing *in vitro* and *in vivo*. *Sci. Rep.* 6:32487. doi: 10.1038/srep32487
- Scoffone, V. C., Chiarelli, L. R., Trespidi, G., Mentasti, M., Riccardi, G., and Buroni, S. (2017). *Burkholderia cenocepacia* infections in cystic fibrosis patients: drug resistance and therapeutic approaches. *Front. Microbiol.* 8:1592. doi: 10.3389/fmicb.2017.01592
- Scoffone, V. C., Ryabova, O., Makarov, V., Iadarola, P., Fumagalli, M., Fondi, M., et al. (2015). Efflux-mediated resistance to a benzothiadiazole derivative effective against *Burkholderia cenocepacia*. *Front. Microbiol.* 6:815. doi: 10.3389/fmicb.2015.00815
- Scoffone, V. C., Spadaro, F., Udine, C., Makarov, V., Fondi, M., Fani, R., et al. (2014). Mechanism of resistance to an antitubercular 2-thiopyridine derivative that is also active against *Burkholderia cenocepacia*. *Antimicrob. Agents Chemother.* 58, 2415–2417. doi: 10.1128/AAC.02438-13
- Tripathy, S., and Sahu, S. K. (2019). FtsZ inhibitors as a new genera of antibacterial agents. *Bioorg. Chem.* 91:103169. doi: 10.1016/j.bioorg.2019.103169
- Van den Bergh, B., Fauvart, M., and Michiels, J. (2017). Formation, physiology, ecology, evolution and clinical importance of bacterial persisters. *FEMS Microbiol. Rev.* 41, 219–251. doi: 10.1093/femsre/fux001
- Yang, X., Lyu, Z., Miguel, A., McQuillen, R., Huang, K. C., and Xiao, J. (2017). GTPase activity-coupled treadmilling of the bacterial tubulin FtsZ organizes septal cell wall synthesis. *Science* 355, 744–747. doi: 10.1126/science.aa k9995

Conflict of Interest: The authors declare that the research was conducted in the absence of any commercial or financial relationships that could be construed as a potential conflict of interest.

Copyright © 2020 Chiarelli, Scoffone, Trespidi, Barbieri, Riabova, Monakhova, Porta, Manina, Riccardi, Makarov and Buroni. This is an open-access article distributed under the terms of the Creative Commons Attribution License (CC BY). The use, distribution or reproduction in other forums is permitted, provided the original author(s) and the copyright owner(s) are credited and that the original publication in this journal is cited, in accordance with accepted academic practice. No use, distribution or reproduction is permitted which does not comply with these terms.



The Cultivable Bacterial Microbiota Associated to the Medicinal Plant *Origanum vulgare* L.: From Antibiotic Resistance to Growth-Inhibitory Properties

Lara Mitia Castronovo¹, Carmela Calonico², Roberta Ascrizzi³, Sara Del Duca¹, Vania Delfino², Sofia Chioccioli¹, Alberto Vassallo¹, Iolanda Strozza¹, Marinella De Leo³, Sauro Biffi⁴, Giovanni Bacci¹, Patrizia Bogani¹, Valentina Maggini^{1,5}, Alessio Mengoni¹, Luisa Pistelli³, Antonella Lo Nostro², Fabio Firenzuoli⁵ and Renato Fani^{1*}

OPEN ACCESS

Edited by:

Paolo Visca,
Roma Tre University, Italy

Reviewed by:

Christian Milani,
University of Parma, Italy
Daniela Minerdi,
University of Turin, Italy

*Correspondence:

Renato Fani
renato.fani@unifi.it

Specialty section:

This article was submitted to
Antimicrobials, Resistance
and Chemotherapy,
a section of the journal
Frontiers in Microbiology

Received: 17 February 2020

Accepted: 09 April 2020

Published: 08 May 2020

Citation:

Castronovo LM, Calonico C, Ascrizzi R, Del Duca S, Delfino V, Chioccioli S, Vassallo A, Strozza I, De Leo M, Biffi S, Bacci G, Bogani P, Maggini V, Mengoni A, Pistelli L, Lo Nostro A, Firenzuoli F and Fani R (2020) The Cultivable Bacterial Microbiota Associated to the Medicinal Plant *Origanum vulgare* L.: From Antibiotic Resistance to Growth-Inhibitory Properties. *Front. Microbiol.* 11:862. doi: 10.3389/fmicb.2020.00862

¹ Department of Biology, University of Florence, Sesto Fiorentino, Italy, ² Department of Health Sciences, University of Florence, Florence, Italy, ³ Department of Pharmacy, University of Pisa, Pisa, Italy, ⁴ Giardino delle Erbe, Casola Valsenio, Italy, ⁵ Research and Innovation Center in Phytotherapy and Integrated Medicine – CERFIT Careggi University Hospital, Florence, Italy

The insurgence of antibiotic resistance and emergence of multidrug-resistant (MDR) pathogens prioritize research to discover new antimicrobials. In this context, medicinal plants produce bioactive compounds of pharmacological interest: some extracts have antimicrobial properties that can contrast different pathogens. For such a purpose, *Origanum vulgare* L. (Lamiaceae family) is a medicinal aromatic plant, whose essential oil (EO) is recognized for its antiseptic, antimicrobial and antiviral activities. The cultivable bacteria from different compartments (i.e., flower, leaf, stem and soil) were isolated in order to: (i) characterize the bacterial microbiota associated to the plant, determining the forces responsible for the structuring of its composition (by evaluation of cross inhibition); (ii) investigate if bacterial endophytes demonstrate antimicrobial activities against human pathogens. A pool of plants belonging to *O. vulgare* species was collected and the specimen chemotype was defined by hydrodistillation of its essential oil. The isolation of plant associated bacteria was performed from the four compartments. Microbiota was further characterized through a culture-independent approach and next-generation sequencing analysis, as well. Isolates were molecularly typed by Random Amplified Polymorphic DNA (RAPD) profiling and taxonomically assigned by 16S rRNA gene sequencing. Antibiotic resistance profiles of isolates and pairwise cross-inhibition of isolates on agar plates (i.e., antagonistic interactions) were also assessed. High level of diversity of bacterial isolates was detected at both genus and strain level in all different compartments. Most strains were tolerant against common antibiotics; moreover, they produced antagonistic patterns of interactions mainly with strains from different compartments with respect to that of original isolation. Strains that exhibited high inhibitory properties were further tested against human pathogens, revealing a strong capacity to inhibit the growth of strains resistant to several antibiotics. In

conclusion, this study regarded the characterization of *O. vulgare* L. chemotype and of the bacterial communities associated to this medicinal plant, also allowing the evaluation of antibiotic resistance and antagonistic interactions. This study provided the bases for further analyses on the possible involvement of endophytic bacteria in the production of antimicrobial molecules that could have an important role in clinical and therapeutic applications.

Keywords: antimicrobial compounds, medicinal plants, *Origanum vulgare*, endophytic bacteria, antibiotic resistance

INTRODUCTION

Increasing antibiotic resistance, due to an overuse of antibiotics, and emergence of multidrug-resistant (MDR) pathogens prioritize research to discover new antimicrobials. The use of plants or their derivatives for prevention and treatment of various health ailments and infections is in practice from immemorial time (Sahoo et al., 2010): in fact, some plant extracts have antimicrobial properties able to affect different pathogens (Shityakova et al., 2019).

Microorganisms are naturally associated to plants in different ways (Reinhold-Hurek and Hurek, 2011). According to a widely used definition, “endophytic bacteria and fungi internally colonize the host tissues, sometimes in high numbers, without damaging the host or eliciting symptoms of plant disease” (Quispel, 1992). Most of the microorganisms inhabiting plants are important for the host’s development and health, despite, sometimes they could also be neutral (Mendes et al., 2013; Philippot et al., 2013).

Increasing knowledge indicates that microbes and/or their interactions with the host are responsible for the synthesis of natural products (Gunatilaka, 2006): for several medicinal plants, according to Köberl et al. (2013), “it is presumed that the plant-associated microbiome, especially the complex community of the endomicrobiome, is directly or indirectly involved in the production of bioactive phytochemicals”. Indeed, endophytic microorganisms play an important role in searching for natural bioactive compounds, with potential use in the health sector and in drug discovery (Lam, 2007). It is well known that, within plant diversity, a distinctive microbiota is harbored by medicinal plant species due to their structurally divergent and unique secondary metabolites (Qi et al., 2012).

Origanum vulgare L. is a medicinal aromatic plant belonging to the *Lamiaceae* family, which comprises many essential oil (EO) producing species. *O. vulgare* is morphologically considered to be one of the most variable species within the genus *Origanum*. Moreover, its variability is also exhibited in the chemotype, which is highly influenced by the plant growth environment. The most represented compounds in oregano EO are phenolic monoterpenes, such as carvacrol and thymol (Werker et al., 1985; De Mastro et al., 2017), followed by linalool and linalyl acetate (De Mastro et al., 2017). Thymol and carvacrol have been reported to exert a substantial inhibitory activity against microbes (Lambert et al., 2001): in fact, it is known that the antibacterial properties of EO are mainly due to its phenolic compounds (Cosentino et al., 1999). Other published studies

report EO compositions rich in sesquiterpene hydrocarbons, such as germacrene D and β -caryophyllene (Mockute et al., 2001). These two compounds are major components also in other medicinal plants EOs, such as those of *Cedrus libani* A. Rich. and *Artemisia vulgaris* L., and they are known to act as antimicrobial, anesthetic and anti-inflammatory compounds, with cytotoxic activity against several cancer cell lines (Saab et al., 2018; Malik et al., 2019). According to Checcucci et al. (2017), the plant species (medicinal or aromatic ones) that produce EOs could represent a suitable model for “testing the hypothesis of an effect of the endophyte-microbiome dichotomy on the production of EOs and, consequently, of a colonization of plant tissues by bacteria resistant to these oils,” as well as the role of plant-bacteria interaction in the modulation of medicinal plant secondary metabolism (Maggini et al., 2019a,b, 2020).

In this work, the chemotype of *O. vulgare* EO was determined and the cultivable bacteria from different compartments (flower, leaf, stem and soil) were isolated. The main goals were (i) to characterize the bacterial microbiota associated to the plant, determining the forces responsible for the structuring of its composition (by evaluation of cross inhibition); (ii) to investigate if bacterial endophytes demonstrate antimicrobial activities against human pathogens.

MATERIALS AND METHODS

Hydrodistillation of the Essential Oil

A pool of three plants of *O. vulgare* L. cultivated in an open-air common garden at the “Giardino delle Erbe - Augusto Rinaldi Ceroni,” Casola Valsenio (Ravenna, Italy), were collected in July 2018. 1 kg of above ground tissues was distilled. The steam distillation of EO was carried out at the Giardino delle Erbe (Casola Valsenio, RA, Italy), following the method described in Hanci et al. (2003).

Determination of the Essential Oil Composition

The pure EO was diluted at 5% in HPLC-grade *n*-hexane and then injected in the GC/EI-MS apparatus. The GC/EI-MS analyses were performed with a Varian CP-3800 apparatus equipped with a DB-5 capillary column (30 m \times 0.25 mm i. d., film thickness 0.25 μ m) and a Varian Saturn 2000 ion-trap mass detector. The oven temperature was programmed rising from 60 to 240°C at 3°C/min. The set temperatures were as

follows: injector temperature, 220°C; transfer-line temperature, 240°C. The carrier gas was He, at 1 ml/min flow. The injection volume was set at 1 µl. The acquisition was performed with the following parameters: full scan, with a scan range of 35–300 *m/z*; scan time: 1.0 s; threshold: 1 count. The identification of the constituents was based on the comparison of their retention times (*t_R*) with those of pure reference samples and their linear retention indices (LRIs), which were determined relatively to the *t_R* of a series of *n*-alkanes. The detected mass spectra were compared with those listed in the commercial libraries NIST 14 and ADAMS, as well as in a homemade mass-spectral library, built up from pure substances and components of commercial essential oils of known compositions, and in MS literature data (Masada, 1976; Jennings and Shibamoto, 1982; Davies, 1990; Swigar and Silverstein, 1992; Adams, 1995; Adams et al., 1997).

Sampling of *O. vulgare* and Plant-Associated Bacteria Extraction

From the same pool of plants of *O. vulgare* used for hydrodistillation, plant anatomical parts (i.e., flower, leaf, stem) and soil near the plant roots (bulk soil) were separately collected and treated as independent samples. Flowers were grouped and pooled, as well as the stems and leaves. 1 g of fresh tissue from each pool was surface sterilized with 1% v/v HClO in a sterile 50 ml tube at room temperature in order to remove the epiphytic bacteria, as described in Chiellini et al. (2014). After this, samples were washed three times with sterile water, and then they were potted in a sterile mortar with the addition of 2 ml of 0.9% w/v NaCl sterile solution. Water used for the last wash was plated on TSA to verify sterility of sample external surface. Bulk soil was treated separately at room temperature for 1 h with 20 ml of 10 mM Mg₂SO₄ in a 50 ml sterile tube under shaking, to allow the detachment of bacteria from soil particles.

Extraction of Genomic DNA and NGS Sequence Analysis

Genomic DNA was extracted from flower, leaf and stem samples using PowerLyzer® PowerSoil® DNA Isolation Kit (MO BIO laboratories, Inc., Carlsbad, CA, United States) following the manufacturer's instruction. Hypervariable regions of bacterial 16S rRNA gene (V1–V9) (Chakravorty et al., 2007; Petrosino et al., 2009) were used as molecular markers for bacterial identification in HTS analysis (Huse et al., 2008). In this study, the V3–V4 regions were sequenced using the primer 341F and 805R (Herlemann et al., 2011) according to the protocol reported in the 16S Metagenomic Sequencing Library Preparation protocol from Illumina (Kozich et al., 2013). Library preparation and demultiplexing were performed following Illumina's standard pipeline (Caporaso et al., 2012). Libraries were sequenced in a single run using Illumina MiSeq technology with pair-end sequencing strategy with MiSeq Reagent Kit v3. Library construction and sequencing were performed by an external company (BMR Genomics, Padua, Italy). Sequence files have been submitted in the NCBI sequence read archive (SRA) and are available under the accession PRJNA606513.

Amplicon Sequence Variant Inference

Sequences were clustered into ASVs using the DADA2 pipeline reported at <https://benjjneb.github.io/dada2/tutorial.html> (Callahan et al., 2016). PCR primers were removed with cutadapt (Martin, 2011) with default settings. Sequences were discarded if the software did not detect one or both primers (–discard-untrimmed option). To ensure that sequences were paired after the trimming process the ‘-pair-filter = any’ option was used. Sequences were then filtered using the ‘filterAndTrim’ function of DADA2 with a maximum error rate of 2 and a fixed length of 270 and 200bp for forward and reverse reads, respectively. Trimmed sequences were used for error rate estimation (the ‘learnErrors’ function with default parameters). Finally, sequences were denoised and merged, and variants were inferred using the DADA2 algorithm. Taxonomic annotation was performed after chimera removal using DECIPHER package (Murali et al., 2018) (version 2.0) with the Silva training set 132 (Quast et al., 2013). Tables produced by the DADA2 pipeline were imported into phyloseq (through the phyloseq R package version 1.22.3), ASVs assigned to chloroplasts and mitochondria have been excluded, and bacterial communities of the three compartments were analyzed.

Count and Isolation of Cultivable Bacteria

Tissue extracts and soil suspensions were diluted (10⁻¹, 10⁻³, 10⁻⁵, 10⁻⁷) and 100 µl of each dilution were plated on tryptic soy agar (TSA) medium (Bio-Rad) in triplicate. Plates were incubated at 30°C and the CFU (colony forming units) were counted after 48 h. For each compartment about 25 different colonies were randomly chosen; then, they were streaked on TSA medium and grown at 30°C for 48 h.

Bacterial Strains and Growth Conditions

The bacterial collection is represented by a panel of 97 isolates from different compartments of *O. vulgare* L. plants (24 isolates from flower compartment, 24 from leaf, 25 from stem and 24 from bulk soil). Isolates are referred to as OV followed by F, L, S or T for flower, leaf, stem and bulk soil districts, respectively, and numerated. Bacterial isolates were grown on TSA medium for 48 h at 30°C.

Random Amplified Polymorphic DNA Analysis

Cell lysates were prepared by processing a single isolated colony resuspended in 20 µl of sterile dH₂O, by thermal lysis (95°C for 10 min), followed by cooling on ice for 5 min. RAPD profiles of the bacterial isolates were obtained using the primer 1253 (Table 1). The reaction mix was performed in a 25 µl-volume with 1× DreamTaq Buffer, 200 µM dNTPs, 500 ng of primer 1253, 1 U of DreamTaq DNA Polymerase (Thermo Scientific) and 2 µl of thermal lysate used as template. The PCR cycling adopted was set up in a Bio-Rad T100 thermal cycler as follows: 90°C for 1 min, 95°C for 95 s followed by 45 cycles of 95°C for 30 s, 36°C for 1 min, 75°C for 2 min, then 75°C for 10 min and finally 60°C for 10 min. Amplicons were visualized through a 2% w/v

TABLE 1 | Primers used in this work.

Primer	Sequence (5' > 3')	Amplicon	References
P0	GAGAGTTTGATCCTGGCTCAG	16S rDNA	Di Cello and Fani, 1996
P6	CTACGGCTACCTTGTACGA		
1253	GTTTCGGCCC	RAPDs	Mori et al., 1999

agarose gel electrophoresis. The assignment of different isolates to the same haplotype group was determined on the basis of the fingerprint pattern of each RAPD product, comparing them for the presence/absence of bands. For haplotypes represented by more than one isolate derived from the same compartment, a single bacterial isolate was randomly chosen as representative strain for that RAPD haplotype.

16S rRNA Gene Sequences

For each recognized RAPD haplotype, the 16S rRNA coding gene sequence was used for the taxonomic affiliation of the bacterial isolates. Amplification of 16S rDNA gene was obtained in a total volume of 20 µl, containing 1× DreamTaq Buffer, 250 µM dNTPs, 0.6 µM of primers P0 and P6 (Table 1), 2 U of DreamTaq DNA Polymerase (Thermo Scientific), and 1 µl of thermal lysate used as template. Samples were incubated for 3 min in a thermal cycler (Bio-Rad T100) at 95°C, then amplification was achieved with 30 cycles of 30 s at 95°C, 30 s at 50°C, and 1 min at 72°C, with a final extension at 72°C for 10 min. Amplicons were analyzed through a 0.8% w/v agarose gel electrophoresis. Sequencing of the 16S rDNA amplicons was performed by the Microsynth Seqlab (Germany). Each sequence was submitted to Gene Bank and the accession numbers from No MN811044 to No MN811099 (Supplementary Table S1).

Phylogenetic Tree Analysis

Taxonomic affiliation of the strains was determined through the analysis of 16S rRNA gene sequences obtained. They were aligned to those of type strains retrieved from the Ribosomal Database Project (RDP) (Cole et al., 2014) using BioEdit (Hall, 1999). The obtained alignment was then used to build a phylogenetic tree through MEGA X (Kumar et al., 2018) for each genus, applying the Neighbor-Joining algorithm with a 1000-bootstrap resampling.

Antibiotics Resistance Profile of Cultivable Bacteria Associated to *O. vulgare*

Evaluation of antibiotic resistance was performed by streaking each strain on TSA medium containing different concentration of selected antibiotics, according to Mengoni et al. (2014). The chosen antibiotics were chloramphenicol, ciprofloxacin, rifampicin, streptomycin, kanamycin, and tetracycline (Table 2). After growing on TSA medium for 48 h at 30°C, a colony of each strain was suspended in 100 µl saline solution (0.9% w/v NaCl), streaked on TSA medium supplemented with different antibiotics and then incubated at 30°C for 48 h. The following antibiotic

TABLE 2 | Classes and targets of the antibiotics used in this work.

Antibiotic	Class	Target
Chloramphenicol	Phenicol	Ribosome
Ciprofloxacin	Fluoroquinolones	Topoisomerases
Kanamycin	Aminoglycosides	Ribosome
Rifampicin	Ansamycins	RNA polymerase
Streptomycin	Aminoglycosides	Ribosome
Tetracycline	Tetracyclines	Ribosome

concentrations (µg/ml) were tested: chloramphenicol (1-2.5-5-10-25-50); ciprofloxacin, streptomycin and kanamycin (0.5-1-2.5-5-10-50); rifampicin (5-10-25-50-100); tetracycline (0.5-1.25-2.5-5-12.5-25). The different growth levels were indicated as follows: complete growth (+ +), strong (+), weak (+ -), very weak (+ -), and absence of growth (-), and MIC (Minimal Inhibiting Concentration) values were identified.

Analysis of Antagonistic Interactions Through Cross-Streaking

Bacterial strains isolated from each compartment of *O. vulgare* plants were tested for cross antagonism, using representatives of each RAPD haplotype. Antagonistic interactions were assayed between each compartment of *O. vulgare* within-niche and cross-niche. Tester strains were firstly streaked across one half of a TSA plate and grown at 30°C for 48 h in order to allow the possible production of antimicrobial compounds. Target strains were then streaked perpendicularly to the tester strain and plates were incubated at 30°C for further 48 h. Additionally, target strains were grown at 30°C for 48 h in the absence of the tester, as growth control. The antagonistic effect was evaluated as the absence or reduction of the target strains growth compared to their growth in the absence of the tester strain. The different inhibition levels were indicated with numbers from 0 to 3 as follows: complete (3, red), strong (2, orange), weak (1, salmon), and absence (0, white) of inhibition (Maida et al., 2016).

Inhibition of Human Pathogens by *O. vulgare* Associated Bacteria

A panel of selected strains of *O. vulgare* for which high antagonistic interactions were evidenced, was tested against 46 pathogenic strains: 10 for *Staphylococcus aureus*, 10 for Coagulase-negative staphylococci, 10 for *Pseudomonas aeruginosa*, 6 for *Klebsiella pneumoniae* characterized by their resistance to multiple antibiotics (as reported in Table 3), and 10 of a *Burkholderia cepacia* complex (BCC) collection, MDR BCC bacteria able to resist to different antibiotic classes (e.g., polymyxins, most of beta-lactams and aminoglycosides) (Saiman et al., 2003). The bacterial strains were isolated from different sources (hospital devices, foods, patients, healthy subjects, environment), as shown in Table 3. As reported in the BCCM/LMG bacteria collection database, origins of the BCC strains classified as environmental are the following: LMG1222, onion; LMG17588, soil; LMG19182, pea rhizosphere;

TABLE 3 | Pathogenic strains used in the study and related antibiotic resistance profiling.

Pathogens	Strain code	Origin	Antibiotic resistance profiling
<i>S. aureus</i>	ATCC 25923	—	P, NA
	2668	F	AMP, P, DA, TE, E, K, NA
	2749	HS	VA, TEC, DAP
	3709	F	DA, TE, E, K, NA
	3710		DA, TE, E, K, NA
	4070		P, DA, TE, E, CIP, LEV, DAP
	4168		AMP, P, DA, SXT, TE, NA
	4302		P, FOX, SXT, DAP
	4691	P	P, FOX, E, CN, CIP, LEV, DAP
	4708		P, FOX, CN, VA, DAP
<i>S. haemolyticus</i>	5284	HD	P, TE, E, CN, FD
	5285		E, CN, CIP, LEV, FD
	5383		P, FOX, TE, E, CN
	5396	HS	P, FOX, SXT, CN, FD
<i>S. epidermidis</i>	5318	HS	P, E, CN, FD
	5321		P, E, CN, AK, FD
	5323		P, TE, TIG, E, CN
	5377	HD	P, TE, E, TEC
	5403	HS	P, E, TIG, TE
	5419	F	FOX, DA, CIP, LEV, SXT, TIG
<i>P. aeruginosa</i>	ATCC 27853	—	FOX, K
	4177	HD	AK, TOB, CIP, LEV, CAZ, FEP, MEM, IPM, ATM, PRL, TZP
	4189		AK, TOB, CIP, LEV, CAZ, FEP, MEM, IPM, PRL, TZP
	5234		AK, CAZ, ATM, TZP, PRL, FEP, CN, IPM, MEM, LEV, CIP, TOB
	5245		CAZ, ATM, PRL, FEP, CN, LEV, CIP, IPM, MEM, TOB
	5246		CAZ, ATM, TZP, PRL, FEP, CN, IPM, MEM, LEV, CIP, TOB
	5255		AK, ATM, CN, FEP, TOB
	5139		CIP, CN, FEP, LEV, TOB
	5009		ATM, CAZ, CIP, CN, FEP, IPM, LEV, MEM, PRL, TOB, TZP
	5236		AK, ATM, CAZ, CIP, FEP, IPM, LEV, MEM, TOB
	ATCC 700603	—	CAZ, AMP, ATM, PRL, TE
	4409	P	AK, AMX, FEP, CTX, CAZ, CIP, ETP, IPM, MEM, TZP, SXT, FFL, CL, TIG
<i>K. pneumoniae</i>	4412		AMX, FEP, CTX, CAZ, CIP, ETP, IPM, MEM, TZP, SXT, FFL, TIG
	4417		AK, AMX, FEP, CTX, CAZ, CIP, ETP, IPM, MEM, TZP, SXT, FFL, CL, TIG
	4420		AK, AMX, FEP, CTX, CAZ, CIP, IPM, MEM, TZP, SXT, FFL, CL, CN
	4422		AK, AMX, FEP, CTX, CAZ, CIP, ETP, IPM, MEM, TZP, SXT, FFL
<i>B. cepacia</i>	FCF3	CF	
<i>B. cenocepacia</i>	FCF23		
<i>B. multivorans</i>	LMG13010		

(Continued)

TABLE 3 | Continued

Pathogens	Strain code	Origin	Antibiotic resistance profiling
<i>B. ambifaria</i>	LMG_16656		
<i>B. cenocepacia</i>	LMG_21462		
<i>B. cenocepacia</i>	LMG_24506		
<i>B. cepacia</i>	LMG_1222	E	
<i>B. multivorans</i>	LMG_17588		
<i>B. ambifaria</i>	LMG_19182		
<i>B. cenocepacia</i>	LMG_19230		

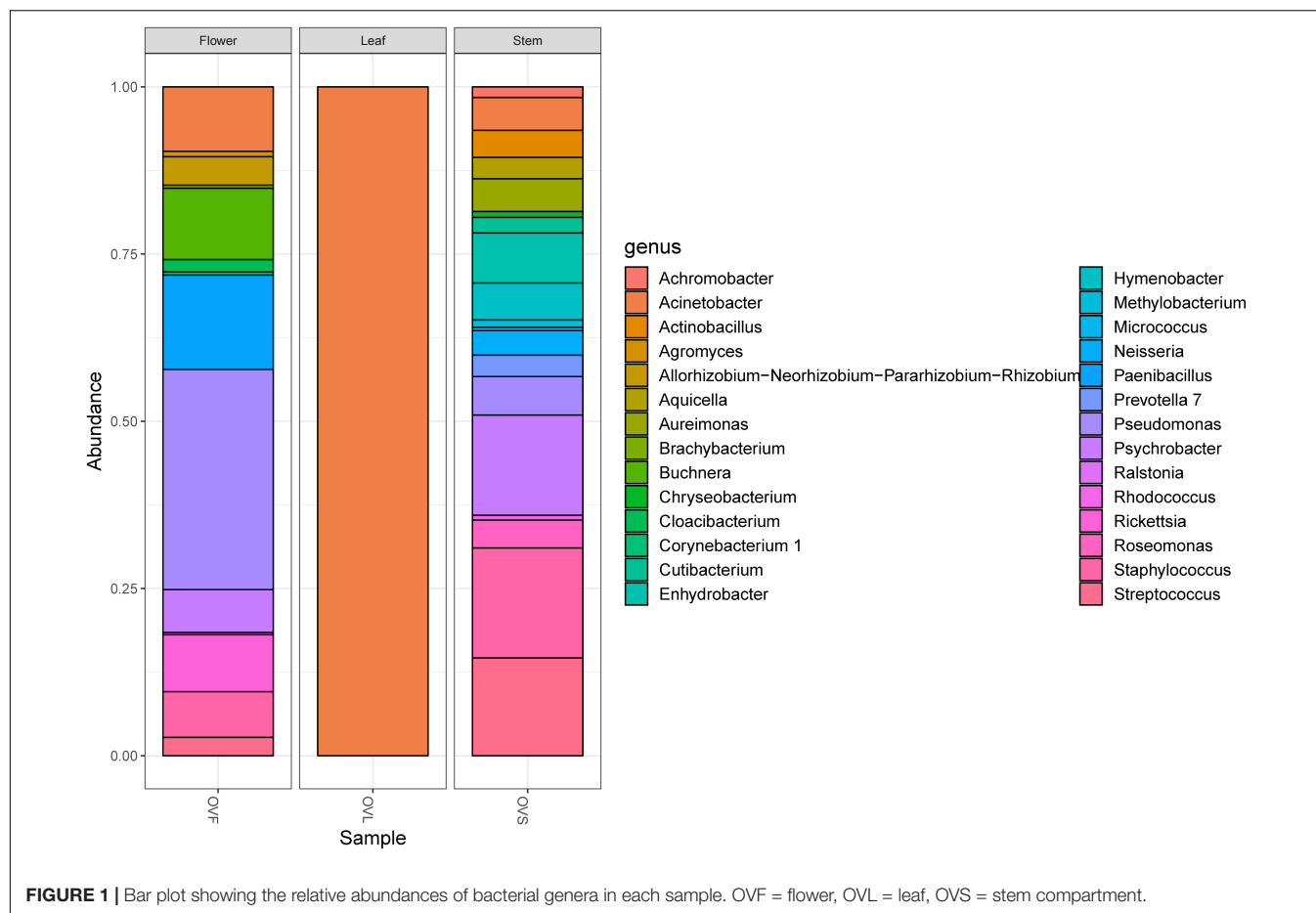
F = food, HD = hospital devices, HS = healthy subjects, P = patients, CF = Cystic Fibrosis, E = environment. Amikacin (AK), Amoxicillin (AMX), Ampicillin (AMP), Aztreonam (ATM), Cefepime (FEP), Cefotaxime (CTX), Cefoxitin (FOX), Ceftazidime (CAZ), Ciprofloxacin (CIP), Clindamycin (DA), Colistin (CL), Daptomycin (DAP), Ertapenem (ETP), Erythromycin (E), Florfenicol (FFL), Fusidic Acid (FD), Gentamicin (CN), Imipenem (IPM), Kanamycin (K), Levofloxacin (LEV), Meropenem (MEM), Nalidixic Acid (NA), Penicillin G (P), Piperacillin (PRL), Piperacillin/Tazobactam (TZP), Sulfamethoxazole/Trimethoprim (SXT), Teicoplanin (TEC), Tetracycline (TE), Tigecycline (TIG), Tobramycin (TOB), Vancomycin (VA).

LMG19230, wheat roots. Each strain was maintained at -80°C under glycerol (25%, v/v) stock, cultured in Brain Heart Infusion Broth (Thermo Scientific) for 24 h at 37°C , then streaked on TSA, and incubated at 37°C for 24 h before the use. The isolated bacterial strains (*S. aureus*, CoNS, *P. aeruginosa*, *K. pneumoniae*) were provided from the Applied Microbiology laboratory (Health Sciences Dept., University of Florence, Italy), while the standard bacteria *Staphylococcus aureus* ATCC 25923, *Pseudomonas aeruginosa* ATCC 27853 and *Klebsiella pneumoniae* ATCC 700603 were obtained from Thermo Fisher Diagnostics S.p.A. The antimicrobial activity was evaluated through the cross-streak method, as previously described, except for the incubation temperature of target strains: 48 h at 37°C for CoNS (Coagulase-negative staphylococci) and 24 h at 37°C for all the other pathogens. The degree of antagonistic effect was evaluated by measuring the inhibition or reduction zone and the results were presented with numbers from 0 to 3 as previously described. The sum of numbers of each bacterial strain represents the total score of inhibition (TSI) ability against human pathogens. TSI was scored as absence of activity (TSI = 0), very low activity (TSI = 1–10), low activity (TSI = 11–20), strong activity (TSI = 21–27), and very strong activity (TSI = 28–30) (Maida et al., 2016).

RESULTS

Chemical Characterization of the *O. vulgare* L. Essential Oil and Chemotype Attribution

The complete composition of the EO hydrodistilled from the analyzed *O. vulgare* specimen is reported in **Supplementary Table S2**. Terpene hydrocarbons dominated the composition, since they were detected in a relative amount accounting for over 90% of the total. Sesquiterpene hydrocarbons, in particular, added up to over 70% of the total: among them, germacrene D and β -caryophyllene were the most abundant, exhibiting relative



abundances of 29.4 and 19.2%, respectively. The plant was, thus, a germacrene D/ β -caryophyllene chemotype. The oxygenated terpenes were far less represented, accounting only for the remaining 8.6%: among them, only 4-terpineol, caryophyllene oxide and spathulenol exhibited relative concentrations higher than 1%.

Characterization of the Plant Microbiota

Bacterial communities of plant samples of the same compartments from which the EO of *O. vulgare* plants was obtained (i.e., flower, leaf, and stem) were examined through NGS. Quality filtering steps obtained a total of 53 ASVs, and representative sequences for each ASV were classified into 28 genera belonging to 4 phyla according to the Silva database, with a different distribution between leaves (with only one genus, *Acinetobacter*, found) and the other two compartments. The majority of the ASVs (62.26%) belong to *Proteobacteria* phylum, followed by *Firmicutes* (15.09%), *Actinobacteria* (11.32%), and *Bacteroidetes* (11.32%). Data obtained are shown in **Figure 1**.

Isolation of Cultivable Bacteria

Bacteria extracted from flower, leaf, stem of *O. vulgare* plants and bulk soil were plated as described in Materials and Methods. Data obtained revealed that the highest bacterial titers were detected in

the soil (5.1×10^5), while the lowest CFU/g value was represented by the leaves (7×10^2); flower and stem compartments had 2.16×10^5 and 8.5×10^3 CFU/g, respectively.

Strain-Level Profiling of Isolates

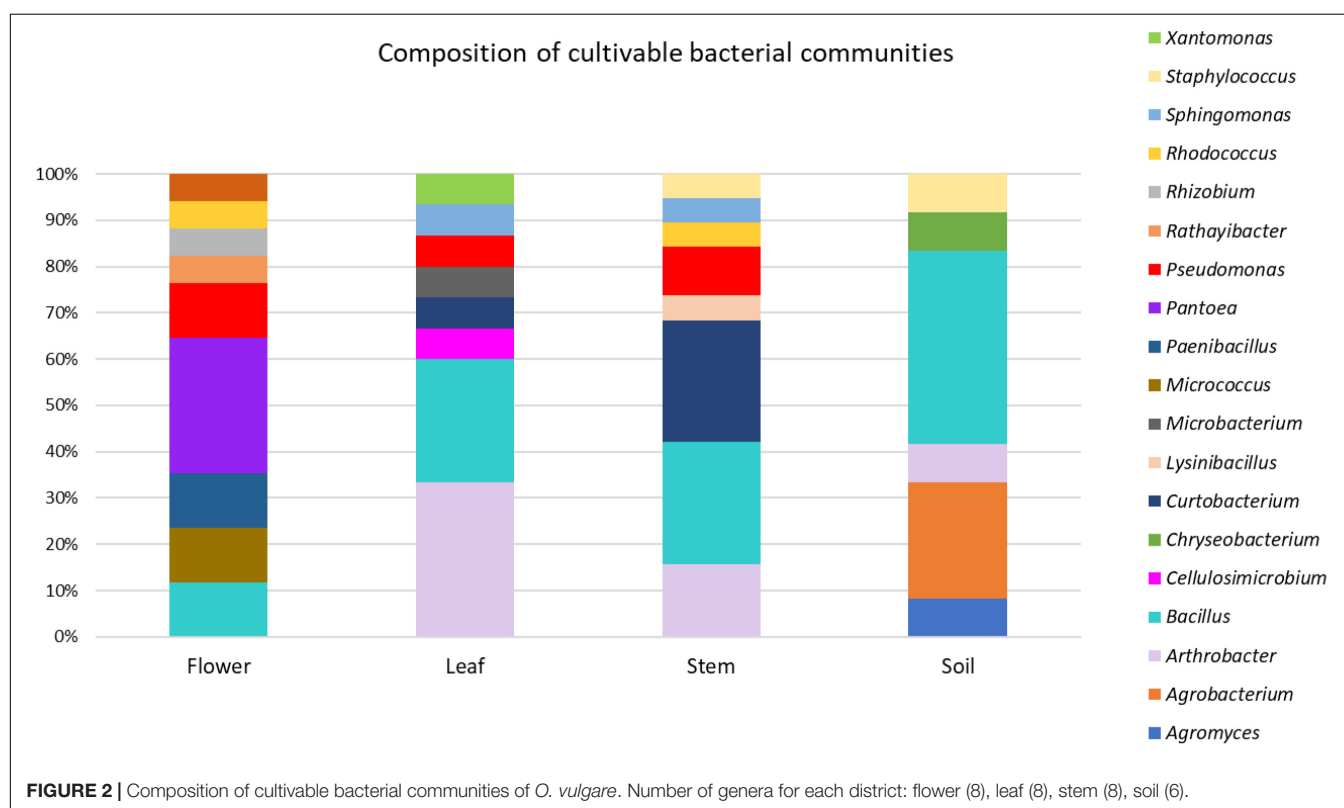
To investigate the structure of the culturable microbiota and to define the haplotypes (i.e., individual genotypes) present, a RAPD analysis was performed assuming that isolates sharing the same RAPD fingerprinting correspond to the same strain (Chiellini et al., 2014 and references therein): a total of 62 different RAPD haplotypes was identified, corresponding to 62 different bacterial strains. The distribution of the RAPD haplotypes within the different compartments is shown in **Supplementary Table S3**. The highest number of haplotypes was detected in the stem compartment (19 haplotypes out of 25 bacterial isolates), while the soil compartment exhibited the lowest number of haplotypes (12 haplotypes out of 24 isolates) as shown in **Table 4**. Notably, a very low number of haplotypes was shared between the different compartments: indeed, only 2 strains were shared by the leaf and stem compartments.

Taxonomic Assignment of Strains

The taxonomic identification of strains from RAPD haplotyping by 16S rRNA gene sequencing is summarized in **Figure 2**.

TABLE 4 | Distribution of bacterial haplotypes, species, and genera detected in the four districts of *O. vulgare* plant.

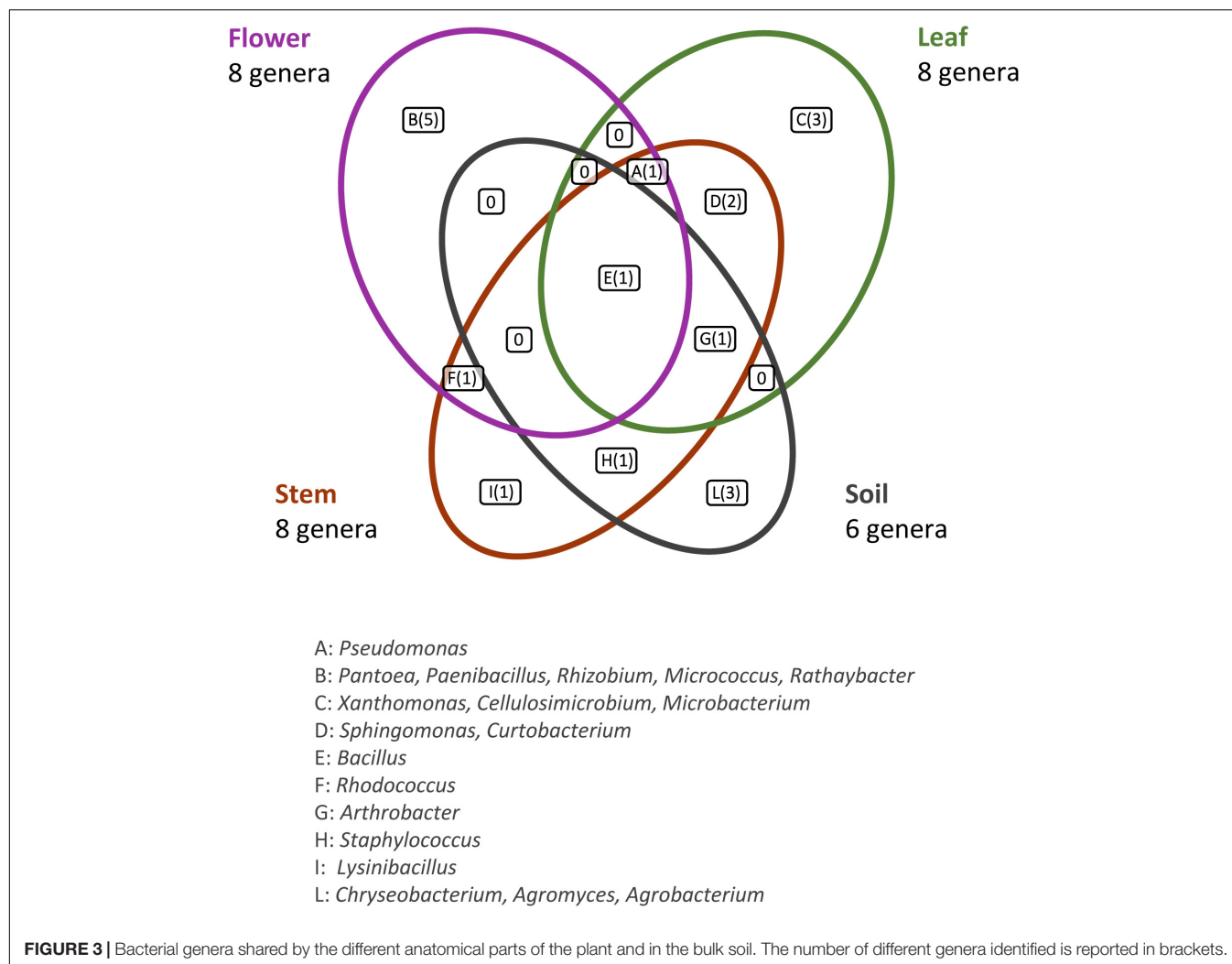
		Flower (OVF)	Leaf (OVL)	Stem (OVS)	Soil (OVT)	Total	%
N. of isolates		24	24	25	24	97	/
N. of haplotypes		16	17	19	12	62	/
N. of species		11	13	13	9	32	/
N. of genera		8	8	8	6	19	/
N. of shared haplotypes	Flower	—	0	0	0	2	3.2
	Leaf	—	—	2	0		
	Stem	—	—	—	0		
	Soil	—	—	—	—		
N. of shared species	Flower	—	1	3	2	9	28
	Leaf	—	—	5	4		
	Stem	—	—	—	5		
	Soil	—	—	—	—		
N. of shared genera	Flower	—	2	3	1	7	37
	Leaf	—	—	5	0		
	Stem	—	—	—	1		
	Soil	—	—	—	—		



This analysis revealed that: (i) strains were affiliated to 19 different bacterial genera (42.1% Gram negative, 57.9% Gram positive); (ii) the majority of the 16S rDNA gene sequences was affiliated to the genus *Bacillus* (28.12%); (iii) *Arthrobacter* was the second most highly represented genus (14.06%); (iv) seven genera (*Pseudomonas*, *Sphingomonas*, *Curtobacterium*, *Arthrobacter*, *Bacillus*, *Staphylococcus*, *Rhodococcus*) were shared among compartments, however just the genus *Bacillus* was shared by all the four districts. Moreover, a total of 12 genera

were represented in only a single district, such as *Pantoea*, *Rhizobium*, *Paenibacillus*, *Micrococcus*, and *Rathayibacter*, which were detected only in the flower compartment (**Figure 3**).

For each genus a 16S rRNA gene phylogenetic tree was constructed as described in Materials and Methods. The analysis of the obtained phylogenetic trees (shown in **Supplementary Material** from **Figures S1** to **Figure S18**) allowed to affiliate the 62 strains to 32 (possible) different species. The 28.1% of species resulted to be shared by the flower, leaf, stem, and



soil compartments. Only one species (i.e., *Bacillus megaterium*) resulted to be shared between all the four districts. The compartments with the highest number of species were leaf and stem districts (for both of them 13 different species were identified).

Antibiotics Resistance Profiles

The antibiotic resistance profiles of bacteria associated to the four *O. vulgare* compartments were investigated, as described in Materials and Methods. The Minimal Inhibitory Concentration (MIC) of each antibiotic was evaluated and the values are reported in **Table 5**. The 45.16% of the *O. vulgare* associated bacteria showed MIC value for the antibiotic streptomycin < 2.5 µg/ml, and the 37.09% showed a very high MIC level (50 µg/ml). Regarding the antibiotic kanamycin the 41.93% revealed MIC value at the maximum concentration used or more. In particular, a very high tolerance to streptomycin and kanamycin, even to the highest concentrations used (MIC values > 50 µg/ml), was revealed by some strains associated to the bulk soil and leaves. MIC value for tetracycline was

evaluated at low concentrations (< 2.5 µg/ml) for the majority of the strains (83.87%). Some strains showed the capacity to grow in presence of low concentrations of chloramphenicol and ciprofloxacin, and only a few strains (12 out of 62) demonstrated to tolerate the lowest concentrations (5 µg/ml) of rifampicin as well. Moreover, the 89.40% of the bacteria associated to the stem were almost totally inhibited by streptomycin, even at the lowest concentration. The different antibiotic resistance profiles seemed to not correlate with the species affiliation and/or the districts from whom bacteria were isolated. Nonetheless, just in case of streptomycin resistance of *Arthrobacter* strains, those isolated from the stem were much more sensitive in comparison to those ones associated to the leaves. Overall, strains associated to the bulk soil resulted tolerant to the great majority of the antibiotics tested, even at the highest concentrations used.

Antagonistic Interaction Between *O. vulgare* Associated Bacteria

Antagonistic interactions, at both inter- and intra-compartment level, were tested through cross-streak test, as described in

TABLE 5 | Antibiotic resistance assay of *O. vulgare* associated bacteria.

Compartment	Strain	Taxonomy	MIC (μg/ml)					
			Str.	Tet.	Cip.	Kan.	Chl.	Rif.
T	OVT1	<i>Agrobacterium</i>	>50	2.5	<0.5	50	25	10
T	OVT8	<i>Agrobacterium</i>	>50	2.5	<0.5	50	25	10
T	OVT17	<i>Agrobacterium</i>	>50	2.5	<0.5	50	25	10
T	OVT2	<i>Agromyces</i>	>50	>25	50	>50	10	<5
S	OVS8	<i>Arthrobacter</i>	<0.5	<0.5	5	50	<1	<5
S	OVS18	<i>Arthrobacter</i>	<0.5	<0.5	5	>50	<1	<5
S	OVS23	<i>Arthrobacter</i>	<0.5	1.25	2.5	50	<1	<5
L	OVL1	<i>Arthrobacter</i>	>50	<0.5	10	>50	<1	<5
L	OVL3	<i>Arthrobacter</i>	50	<0.5	5	>50	<1	<5
L	OVL4	<i>Arthrobacter</i>	50	<0.5	2.5	>50	<1	<5
L	OVL20	<i>Arthrobacter</i>	50	<0.5	5	>50	<1	<5
L	OVL22	<i>Arthrobacter</i>	50	<0.5	5	>50	<1	<5
T	OVT23	<i>Arthrobacter</i>	50	<0.5	5	>50	2.5	<5
L	OVL7	<i>Bacillus</i>	<0.5	<0.5	<0.5	<0.5	2.5	<5
L	OVL8	<i>Bacillus</i>	5.0	<0.5	<0.5	1	5	<5
S	OVS6	<i>Bacillus</i>	<0.5	<0.5	<0.5	<0.5	10	<5
S	OVS10	<i>Bacillus</i>	<0.5	2.5	<0.5	<0.5	2.5	<5
S	OVS21	<i>Bacillus</i>	<0.5	2.5	<0.5	<0.5	2.5	<5
F	OVF22	<i>Bacillus</i>	2.5	2.5	<0.5	<0.5	<1	<5
L	OVL9	<i>Bacillus</i>	2.5	1.25	<0.5	1	<1	<5
S	OVS26	<i>Bacillus</i>	2.5	1.25	<0.5	2.5	2.5	<5
T	OVT16	<i>Bacillus</i>	2.5	2.5	<0.5	<0.5	10	<5
T	OVT24	<i>Bacillus</i>	2.5	1.25	<0.5	<0.5	2.5	<5
L	OVL12	<i>Bacillus</i>	10	5	<0.5	1	<1	<5
T	OVT5	<i>Bacillus</i>	10	<0.5	<0.5	2.5	2.5	<5
F	OVF21	<i>Bacillus</i>	50	2.5	<0.5	10	2.5	<5
S	OVS24	<i>Bacillus</i>	>50	<0.5	<0.5	5	2.5	<5
T	OVT10	<i>Bacillus</i>	50	<0.5	<0.5	5	2.5	<5
T	OVT20	<i>Bacillus</i>	50	5	<0.5	10	2.5	<5
L	OVL16	<i>Cellulosimicrobium</i>	>50	12.5	50	>50	10	<5
T	OVT9	<i>Chryseobacterium</i>	>50	>25	1	>50	>50	<5
S	OVS2	<i>Curtobacterium</i>	<0.5	2.5	2.5	>50	2.5	<5
S	OVS11	<i>Curtobacterium</i>	<0.5	12.5	50	>50	<1	<5
S	OVS12	<i>Curtobacterium</i>	<0.5	12.5	50	>50	<1	<5
S	OVS13	<i>Curtobacterium</i>	<0.5	2.5	50	50	<1	<5
S	OVS15	<i>Curtobacterium</i>	<0.5	12.5	50	>50	<1	<5
L	OVL10	<i>Curtobacterium</i>	2.5	1.25	<0.5	10	<1	<5
S	OVS27	<i>Lysinibacillus</i>	>50	1.25	2.5	1	2.5	10
L	OVL14	<i>Microbacterium</i>	5	12.5	5	>50	<1	<5
F	OVF19	<i>Micrococcus</i>	10	1.25	5	50	<1	<5
F	OVF24	<i>Micrococcus</i>	>50	1.25	5	50	<1	<5
F	OVF3	<i>Paenibacillus</i>	2.5	<0.5	<0.5	<0.5	2.5	10
F	OVF10	<i>Paenibacillus</i>	2.5	2.5	<0.5	<0.5	<1	<5
F	OVF2	<i>Pantoea</i>	10	2.5	<0.5	10	2.5	10
F	OVF14	<i>Pantoea</i>	10	2.5	<0.5	10	2.5	10
F	OVF1	<i>Pantoea</i>	>50	2.5	<0.5	10	2.5	10
F	OVF9	<i>Pantoea</i>	50	2.5	<0.5	10	2.5	10
F	OVF11	<i>Pantoea</i>	50	2.5	<0.5	5	2.5	10
F	OVF4	<i>Pseudomonas</i>	5	2.5	<0.5	2.5	25	<5
L	OVL17	<i>Pseudomonas</i>	5	2.5	<0.5	1	25	<5
S	OVS9	<i>Pseudomonas</i>	<0.5	2.5	<0.5	2.5	25	10

(Continued)

TABLE 5 | Continued

Compartment	Strain	Taxonomy	MIC (μg/ml)					
			Str.	Tet.	Cip.	Kan.	Chl.	Rif.
S	OVS14	<i>Pseudomonas</i>	<0.5	1.25	<0.5	<0.5	25	10
F	OVF7	<i>Pseudomonas</i>	2.5	<0.5	<0.5	<0.5	2.5	<5
F	OVF17	<i>Rathaybacter</i>	2.5	<0.5	2.5	10	<1	<5
F	OVF6	<i>Rhizobium</i>	5	2.5	<0.5	50	2.5	<5
S	OVS20	<i>Rhodococcus</i>	<0.5	2.5	<0.5	10	<1	<5
F	OVF18	<i>Rhodococcus</i>	2.5	2.5	<0.5	5	<1	<5
S	OVS7	<i>Sphingomonas</i>	<0.5	<0.5	1	<0.5	<1	<5
L	OVL6	<i>Sphingomonas</i>	50	< 0.5	<0.5	10	2.5	<5
S	OVS22	<i>Staphylococcus</i>	<0.5	1.25	1	>50	2.5	<5
T	OVT21	<i>Staphylococcus</i>	10	<0.5	<0.5	>50	2.5	<5
L	OVL18	<i>Xanthomonas</i>	50	5	<0.5	10	5	<5

MIC values are reported as μg/ml. Str = Streptomycin, Tet = Tetracycline, Cip = Ciprofloxacin, Kan = Kanamycin, Chl = Chloramphenicol, Rif = Rifampicin. F = flower, L = leaf, S = stem, T = soil compartment.

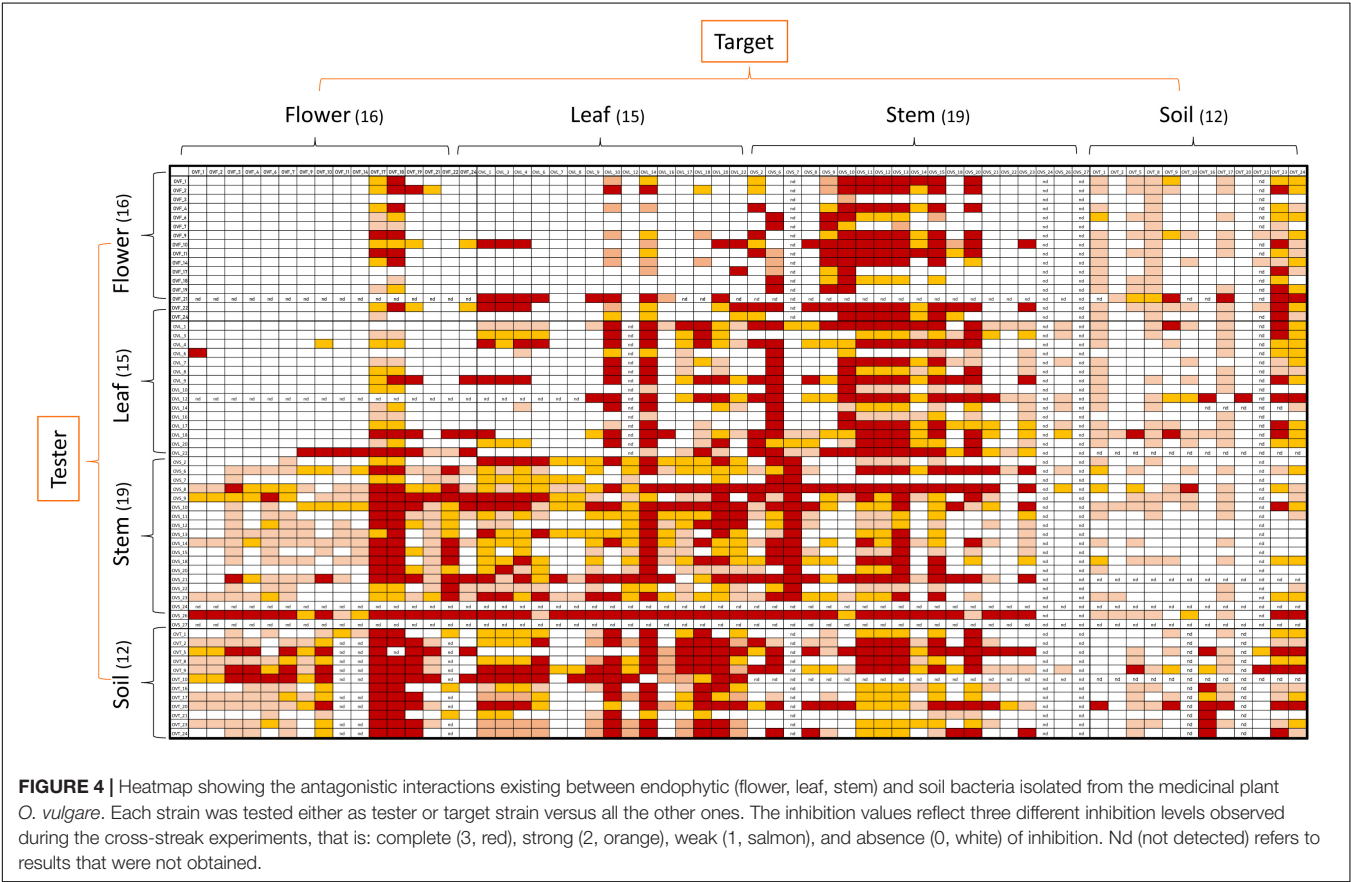


FIGURE 4 | Heatmap showing the antagonistic interactions existing between endophytic (flower, leaf, stem) and soil bacteria isolated from the medicinal plant *O. vulgare*. Each strain was tested either as tester or target strain versus all the other ones. The inhibition values reflect three different inhibition levels observed during the cross-streak experiments, that is: complete (3, red), strong (2, orange), weak (1, salmon), and absence (0, white) of inhibition. Nd (not detected) refers to results that were not obtained.

Materials and Methods. To this purpose, each strain was used either as a tester or target. The antagonistic effect was indicated by the absence or reduction of the target strain growth. Data obtained, schematically shown in **Figure 4**, revealed that: (i) all the tested strains were able to inhibit at least one strain; (ii) soil-associated bacteria revealed a higher capacity to inhibit strains belonging to the other compartments, with those from stem and leaf following; (iii) flowers associated bacteria revealed

the lowest capacity to inhibit other strains; (iv) regarding the inhibition sensitivity, the highest values were obtained from stem compartment, with leaf and flower following; and (v) the lowest inhibition sensitivity was revealed by soil-associated bacteria, as they were less inhibited by strains extracted from the different anatomical part of the plants. **Figure 5** shows a representation of the inhibitory pattern among strains from the same and different compartments. In

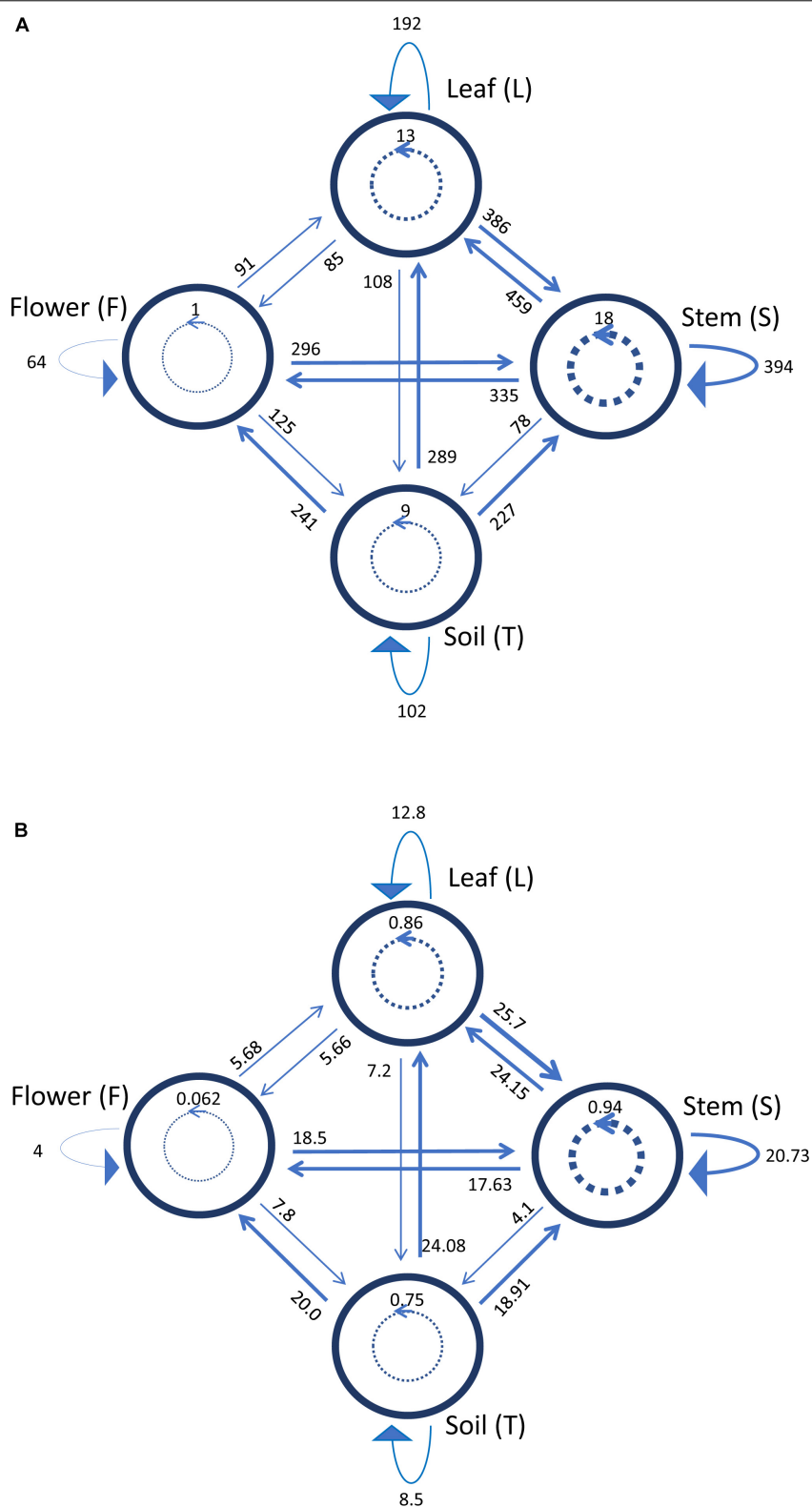


FIGURE 5 | Schematic representation of inhibiting activity of bacterial strains isolated from the medicinal plant *O. vulgare* bulk soil (T), stem (S), leaf (L) and flowers (F). Each node represents a plant compartment whereas numbers represent the sum of the inhibiting scores of the bacteria isolated from those compartments **(A)** and the inhibition potential of the tester strains calculated as the sum of inhibition scores divided by the tester number **(B)**. Directed links represent inhibition patterns. Dashed links indicate the occurrence and the extent of self-inhibition.

TABLE 6 | Inhibitory and sensitivity score of the endophytic bacteria associated to the four compartments of *O. vulgare*.

Compartment	Inhibitory score	Sensitivity score
Soil	63.41	20.25
Stem	47.62	47.99
Leaf	44.21	56.26
Flowers	32.27	46.39

this scheme, each node represents a plant compartment whereas numbers indicate the sum of the inhibiting scores of the bacteria isolated from those compartments and the inhibition potential of tester strains calculated as the sum of inhibition scores divided by the tester number. Inhibition patterns were represented by directed links, while the occurrence and the extent of self-inhibition were reported with dashed links.

The analysis of these results suggested that the bacterial communities from stem and soil were much more able to antagonize the growth of bacteria belonging to the other two compartments (Table 6). The relative degree of inhibitory score and sensitivity score of strains belonging to different compartments are respectively as following: soil > stem \geq leaves > flowers; soil < stem \leq flowers < leaf. Additionally, stem community showed the highest self-inhibition, whereas flower-associated bacteria revealed the lowest one. So, the different antagonistic activity observed could be, apparently, influenced by the ecological niche inhabited by bacteria.

Inhibition of Human Pathogens by *O. vulgare* Associated Bacteria

The endophytic strains (Table 7) exhibiting high antagonistic interactions, have been further tested against human pathogens through cross-streak method, as described in Materials and Methods.

In Figure 6 the antagonistic interactions of *O. vulgare* tester strains against 46 human pathogens are shown.

Interestingly, focusing on the antagonistic activity against BCC, *O. vulgare* strains were much more able to inhibit the growth of BCC members isolated from CF patients than those of environmental origins (Figure 7). All the flower testers exhibited a low total score of inhibition (TSI = 11–20), the 50% of leaves tester a strong TSI (TSI = 21–27), the 44.5% of stem tester a strong or very strong TSI (TSI = 21–27, 28–30), all the soil testers had a strong or very strong total score of inhibition (TSI = 21–27, 28–30).

Focusing on the antagonistic activity against *S. aureus*, CoNS, *P. aeruginosa*, *K. pneumoniae*, among the 23 endophytes strains screened for antimicrobial activity, 11 (47.8%) showed antagonistic activity against at least one human pathogenic strain (Figure 6). This preliminary test demonstrated that 54.5% of the inhibitory strains belong to *Bacillus* genera, 27.3% to *Arthrobacter* and the remaining 18.2% to *Paenibacillus* and *Chryseobacterium* genera. Moreover, the interaction among inhibitory endophytes and pathogens gave better antagonistic results for Gram-positive bacteria (25.9%) than for Gram-negative bacteria (3.98%). The

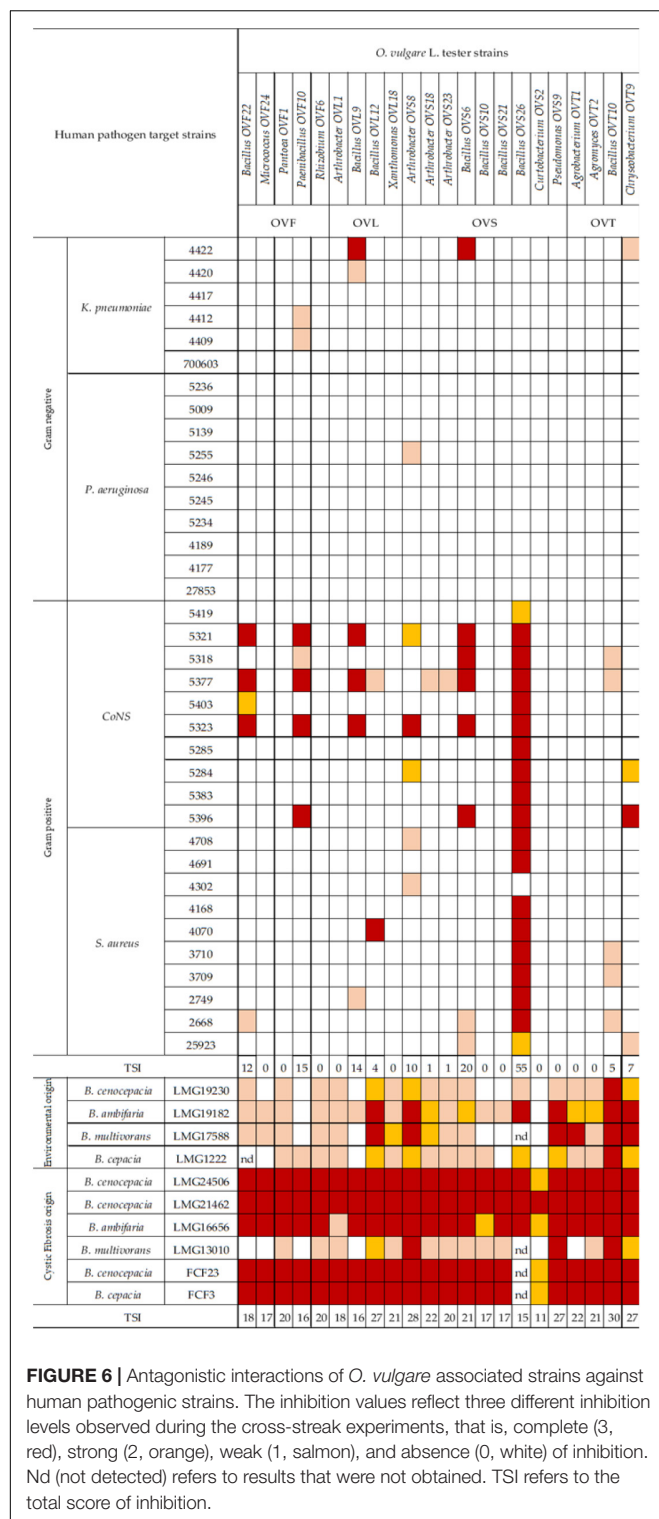
TABLE 7 | *O. vulgare* associated bacteria tested against 46 pathogenic strains.

Compartment	Strain code	Taxonomy
Flower (F)	OVF 10	<i>Paenibacillus</i>
	OVF 22	<i>Bacillus</i>
	OVF11	<i>Pantoea</i>
	OVF 6	<i>Rhizobium</i>
	OVF 1	<i>Pantoea</i>
	OVF 24	<i>Micrococcus</i>
Leaf (L)	OVL 9	<i>Bacillus</i>
	OVL 1	<i>Arthrobacter</i>
	OVL 12	<i>Bacillus</i>
	OVL 18	<i>Xanthomonas</i>
Stem (S)	OVS 6	<i>Bacillus</i>
	OVS 8	<i>Arthrobacter</i>
	OVS26	<i>Bacillus</i>
	OVS 2	<i>Curtobacterium</i>
	OVS10	<i>Bacillus</i>
	OVS 23	<i>Arthrobacter</i>
	OVS 9	<i>Pseudomonas</i>
	OVS 18	<i>Arthrobacter</i>
	OVS 21	<i>Bacillus</i>
Soil (T)	OVT 9	<i>Chryseobacterium</i>
	OVT 1	<i>Agrobacterium</i>
	OVT 2	<i>Agromyces</i>
	OVT 10	<i>Bacillus</i>

obtained data revealed that the major effect was recorded against the CoNS strains; the inhibitory interactions observed against this group of bacteria, indeed, were strong or complete in most cases (83.8%). In particular, the multidrug resistant strains *S. epidermidis* 5323, 5377 and 5321 were strongly inhibited by the endophytic isolates. Finally, stem-associated bacteria revealed the highest ability to inhibit pathogenic strains, while bulk soil associated bacteria revealed the lowest ability of inhibition. Figure 8A shows the percentage of the antagonistic activity exhibited by endophytes isolates against human pathogenic bacteria. OVS 26 showed broad spectrum of antagonistic activity against *S. aureus* and CoNS isolates (90% and 100%, respectively); the endophytes OVF 10, OVL 9, OVS 6 and OVT 9 showed the capacity to be active against four strains of *K. pneumoniae* (from 16.7 to 33.3%), while just OVS 8 was able to inhibit one *P. aeruginosa* strain. In general, all the eleven inhibitory endophytes showed degrees of antagonism against CoNS from 10 to 100%. Figure 8B shows the TSI of the antagonistic activity exhibited by endophytes strains against *S. aureus*, CoNS, *P. aeruginosa*, *K. pneumoniae* human pathogenic bacteria.

DISCUSSION AND CONCLUSION

The potential of endophytes from medicinal plants to produce antibacterial, anticancer, and antifungal compounds is an emerging area in the last years (Miller et al., 2012; Maida et al., 2016; Chiellini et al., 2017; Maggini et al., 2018). *O. vulgare* is an aromatic and medicinal plant, whose EO has been



extensively studied because of its diverse compositions among different specimens and remarkable characteristics (Lukas et al., 2015). Ecological and environmental effects, along with genetic variability, are some of the various reasons why EOs of *Origanum* species show major differences in their chemical composition

(Vokou et al., 1993). The studied specimen, in particular, exhibited a germacrene D/ β -caryophyllene chemotype, showing a predominance of the sesquiterpene hydrocarbon fraction. Other than the volatile compounds, the aerial parts of *O. vulgare* contain a remarkable variety of therapeutic bioactive compounds, including phenolic glycosides, flavonoids, tannins, sterols and high amounts of terpenoids (Pezzani et al., 2017).

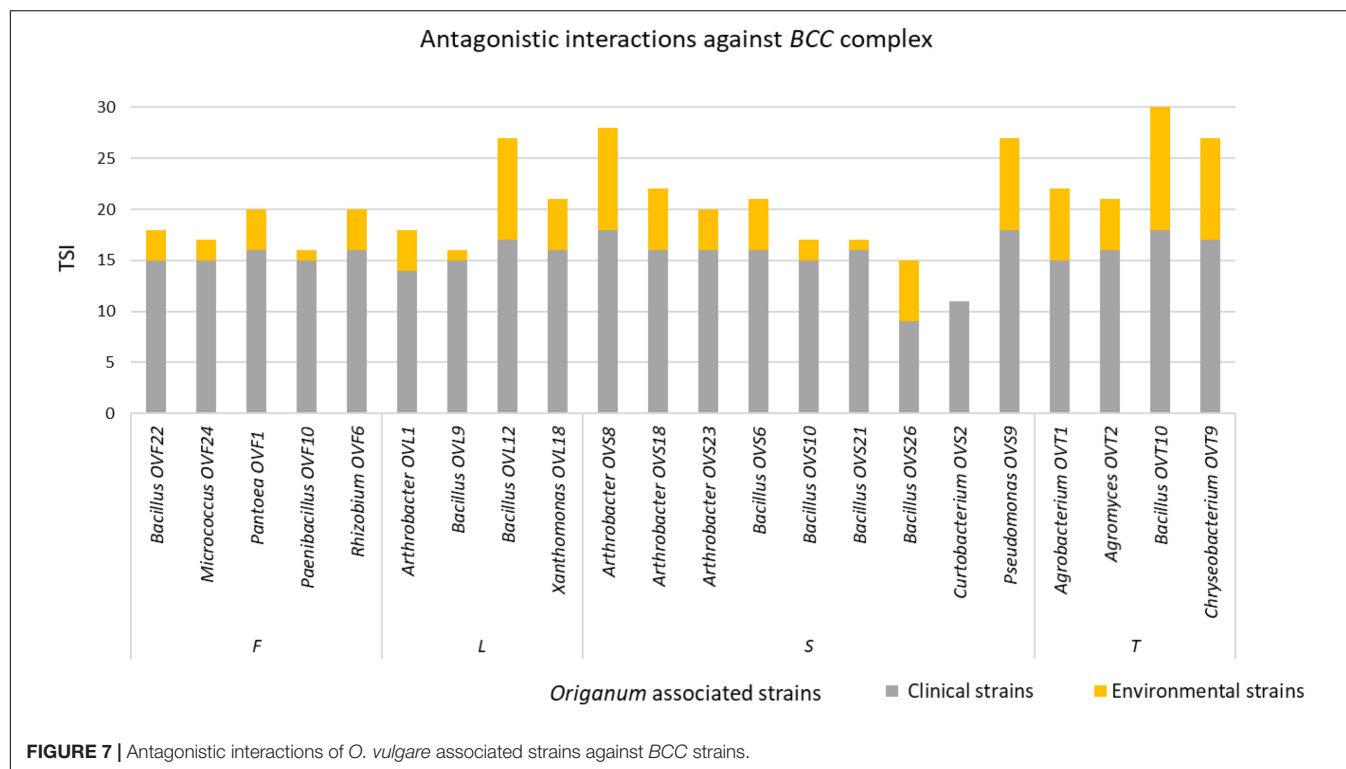
The analysis of the total microbiota, obtained through NGS analysis, revealed that flower and stem compartments host a similar endophytic community, with a high diversity of genera; on the contrary, the leaf compartment appears to be very less diverse, containing only *Acinetobacter* genus.

The cultivable bacterial load in *O. vulgare* different districts ranged from about 10^2 to 10^5 CFU/g of soil, stem, leaf and flowers (fresh weight); these data are in agreement with previous reports on other different medicinal plant species (Emiliani et al., 2014; Checcucci et al., 2017).

The analysis of the structure of bacterial communities revealed that the dataset obtained with RAPD analysis highlights a high level of biodiversity at the strain level, especially regarding the anatomical parts of the plant. On the contrary, fingerprinting of the isolates associated to the bulk soil revealed a more clonal community. Moreover, a very low degree of sharing (3.1%) between the different compartments was revealed (only two haplotypes were shared between the leaf and the stem compartments), in agreement with data reported by Chiellini et al. (2014) about cultivable bacterial communities isolated from *Echinacea purpurea* (L.) Moench and *Echinacea angustifolia* (DC.).

The different genera identified through 16S rDNA gene amplification in *O. vulgare* plant have been detected in other plant species too, such as *E. purpurea* and *E. angustifolia* (Chiellini et al., 2014). In this work, *Bacillus* resulted to be the most represented genus and it was present in all districts analyzed, while other genera were exclusively present in specific ones. Overall, the RAPD and 16S rRNA gene analysis revealed that the selection of bacteria mainly occurs at the strain level, in agreement with previous data obtained with other medicinal plants, such as *Lavandula angustifolia* Mill. (Emiliani et al., 2014), *Echinacea purpurea* and *Echinacea angustifolia* (Chiellini et al., 2014; Maida et al., 2016). Therefore, different endophytic bacterial species are selected not only at the root or stem level, but also within plant tissues, as the different distribution of genera could suggest. Hence, it is possible that plant might “select” specific taxa to access its compartments.

In this work we have analyzed the antibiotic resistance profile of 62 cultivable bacterial strains isolated from different anatomical parts of *O. vulgare* plant and from the bulk soil. The obtained data revealed that: (i) most of the strains showed tolerance to at least the lowest concentrations of the antibiotic streptomycin and kanamycin used, and only a few strains were able to grow in presence of low concentrations of the antibiotic chloramphenicol and ciprofloxacin; a similar trend has already been evidenced in the case of *E. purpurea* (Mengoni et al., 2014); (ii) only a small number of strains (2 out of 19) tolerated the lowest concentrations of rifampicin; (iii) strains associated to the bulk soil resulted resistant against the great majority of the



antibiotics tested, even at the highest concentrations used. The high tolerance to both streptomycin and kanamycin, shown by tested strains, could be due to similar resistance mechanisms. Moreover, the high resistance of strains associated to the bulk soil might be probably due to their exposure to commonly used antibiotics: in this scenario, their greater resistance to antibiotics could be explained.

Antagonistic inter and intra- compartment interactions were also evaluated. These analyses suggested that the bacterial communities from the stem and the soil compartments were particularly able to antagonize the growth of bacteria belonging to the other two compartments. Moreover, stem community revealed the highest self-inhibition levels, whereas flower-associated bacteria revealed the lowest one. Thus, the different antagonistic activity observed could be (apparently) influenced by the ecological niche inhabited by bacteria. Overall, the obtained results suggest that antagonistic interactions between bacterial strains might play a role in driving the diverse composition of the bacterial communities in the anatomical districts of the plants. It is important to stress that the used medium could influence the inhibitory patterns, and also that in different environmental conditions the inhibitory patterns could be different: for example, strains that do not show any inhibition on plates, *in vivo* could be stronger antagonists, and *vice versa*.

Strains that exhibited high inhibitory properties were tested against multidrug resistant human pathogens. Interestingly, regarding the antagonistic activity against BCC, *O. vulgare* strains were much more able to inhibit the growth of BCC members isolated from CF patients than those of environmental origins. On the other hand, 47.8% of *O. vulgare* strains showed

antagonistic activity against at least one human pathogenic strain among *S. aureus*, Coagulase-negative staphylococci (CoNS), *P. aeruginosa* and *K. pneumoniae*, with the most active isolates displaying greater capacity of inhibition mainly against Gram-positive bacteria than Gram-negative ones. It has been proposed that, regarding Gram-negative bacteria, the presence of the outer polysaccharide membrane (made of various lipopolysaccharide constituents) could make them impermeable to lipophilic solutes (Silhavy et al., 2010; Naikpatil and Rathod, 2011).

At the same time, we can speculate that the different antimicrobial activity can depend on the different type of habitats that bacteria occupy: *Staphylococcus aureus* and CoNS are common colonizers of human epithelia, while *P. aeruginosa* and *K. pneumoniae* are opportunistic pathogens widely recovered from the environment. Hence, it is reasonable that bacteria capable of colonizing environmental habitats can exhibit intrinsic or acquired resistance against antimicrobial compounds produced by competing bacteria commonly found in the same ecological niches. Further studies should be performed to better understand this behavior.

In our opinion, data obtained in this work offer a preliminary but very promising example of the biotechnological potential of bacteria isolated from medicinal plants. In fact, the majority of the tested strains revealed a marked inhibitory effect between different compartments, widespread resistance to common antibiotics, and a strong capacity to inhibit the growth of MDR human pathogens. This last point is very important: nowadays research for new molecules active against human pathogens (MDR in particular) is one of the most important goals to achieve, mainly due to the

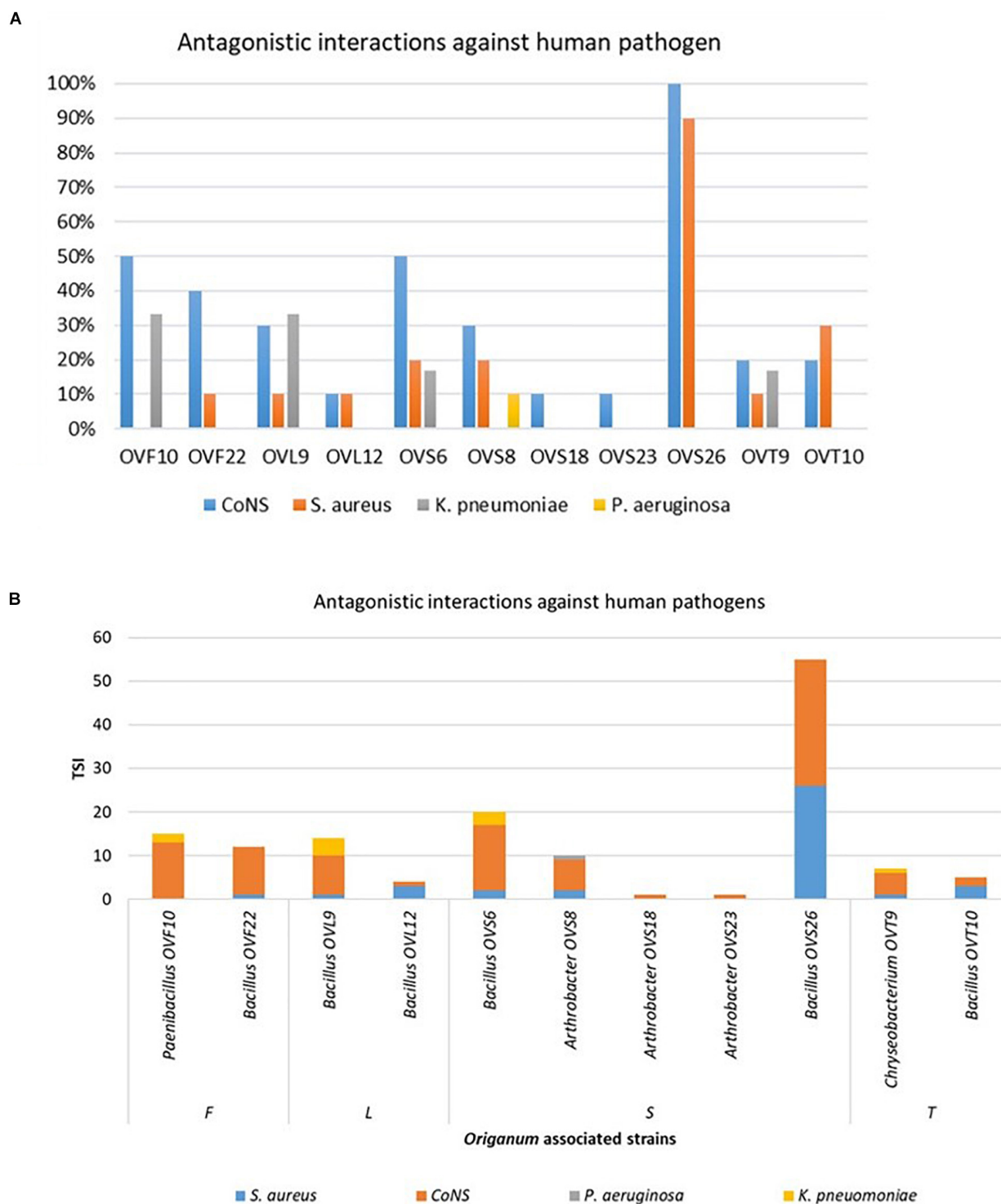


FIGURE 8 | Antagonistic activity exhibited by endophytes strains against human pathogenic bacteria (*S. aureus*, CoNS, *P. aeruginosa*, *K. pneumoniae*) expressed as percentage of the antagonistic activity (A) and TSI (B).

increased resistance to commercially used antibiotics, an inevitable side effect of both the unsuitable use and over prescription of antibiotics in human medicine therapy and

the antibiotics released into the environment (Helal et al., 2019). As known, medicinal plants and their associated microbiome represent a natural *reservoir* for bioactive

compounds of pharmacological interest. Therefore, the bioactive compounds of selected strains could be purified and then tested for their bioactivity (or cytotoxicity) on human cultures and on animal models; it could be interesting to find out if the production of antimicrobial molecules in *O. vulgare* could be dependent on its associated microbiota. Furthermore, this study suggests that antagonistic interactions between bacterial strains might play a role in driving the diverse composition of the bacterial communities in the anatomical districts of the plants.

DATA AVAILABILITY STATEMENT

The datasets generated for this study can be found in the NCBI sequence read archive PRJNA606513, Gene Bank MN811044-MN811099.

AUTHOR CONTRIBUTIONS

RF, LP, AL, PB, and LC conceptualized the study and worked on the methodology. LC, CC, GB, and RA contributed to data curation and formal analysis. LC, SD, SC, AV, CC, IS, VD, RA, GB,

and SB carried out the investigation. RF, LP, AL, and FF helped with project administration. FF was responsible for the resource. LC, SD, SC, AV, AL, CC, IS, VD, LP, RA, and GB validated the study. LC, CC, and RA wrote the original draft. LC, AV, SD, SC, CC, AL, VD, LP, RA, MD, VM, PB, AM, and RF reviewed and edited the manuscript.

FUNDING

This work was supported by Tuscany Region (Italy; Resolution n. 1224/2016 “Medicine Complementari”) and by Fondazione Cassa di Risparmio di Firenze (project #2016.0936, Herbiome: new antibiotic molecules from endophytic bacteria isolated from medicinal plants). The funding sources had no involvement in any part of the study.

SUPPLEMENTARY MATERIAL

The Supplementary Material for this article can be found online at: <https://www.frontiersin.org/articles/10.3389/fmicb.2020.00862/full#supplementary-material>

REFERENCES

- Adams, R. P. (1995). *Identification of Essential Oil Components by Gas Chromatography/Quadrupole Mass Spectroscopy*. Carol Stream, IL: Allured Publishing Corporation.
- Adams, R. P., Zanoni, T. A., Lara, A., Barrero, A. F., and Cool, L. G. (1997). Comparisons among *Cupressus arizonica* Greene, *C. benthamii* Endl., *C. lindleyi* Klotz, ex Endl. and *C. lusitanica* Mill, using leaf essential oils and DNA fingerprinting. *J. Essent. Oil Res.* 9, 303–309. doi: 10.1080/10412905.1997.10554249
- Callahan, B. J., McMurdie, P. J., Rosen, M. J., Han, A. W., Johnson, A. J. A., and Holmes, S. P. (2016). DADA2: high-resolution sample inference from Illumina amplicon data. *Nat. Methods* 13, 581–583. doi: 10.1038/nmeth.3869
- Caporaso, J. G., Lauber, C. L., Walters, W. A., Berg-Lyons, D., Huntley, J., Fierer, N., et al. (2012). Ultra-high-throughput microbial community analysis on the Illumina HiSeq and MiSeq platforms. *ISME J.* 6, 1621–1624. doi: 10.1038/ismej.2012.8
- Chakravorty, S., Helb, D., Burday, M., Connell, N., and Alland, D. (2007). A detailed analysis of 16S ribosomal RNA gene segments for the diagnosis of pathogenic bacteria. *J. Microbiol. Methods* 69, 330–339. doi: 10.1016/j.mimet.2007.02.005
- Checucci, A., Maida, I., Bacci, G., Ninno, C., Bilia, A. R., Biffi, S., et al. (2017). Is the plant-associated microbiota of *Thymus* spp. adapted to plant essential oil? *Res. Microbiol.* 168, 276–282. doi: 10.1016/j.resmic.2016.11.004
- Chiellini, C., Maida, I., Emiliani, G., Mengoni, A., Mocali, S., Fabiani, A., et al. (2014). Endophytic and rhizospheric bacterial communities isolated from the medicinal plants *Echinacea purpurea* and *Echinacea angustifolia*. *Int. Microbiol.* 17, 165–174. doi: 10.2436/20.1501.01.219
- Chiellini, C., Maida, I., Maggini, V., Bosi, E., Mocali, S., Emiliani, G., et al. (2017). Preliminary data on antibacterial activity of *Echinacea purpurea*-associated bacterial communities against *Burkholderia cepacia* complex strains, opportunistic pathogens of Cystic Fibrosis patients. *Microbiol. Res.* 196, 34–43. doi: 10.1016/j.micres.2016.12.001
- Cole, J. R., Wang, Q., Fish, J. A., Chai, B., McGarrell, D. M., Sun, Y., et al. (2014). Ribosomal Database Project: data and tools for high throughput rRNA analysis. *Nucleic Acids Res.* 42, D633–D642. doi: 10.1093/nar/gkt1244
- Cosentino, S., Tuberoso, C. I., Pisano, B., Satta, M., Mascia, V., Arzedi, E., et al. (1999). In-vitro antimicrobial activity and chemical composition of Sardinian
- Thymus* essential oils. *Lett. Appl. Microbiol.* 29, 130–135. doi: 10.1046/j.1472-765x.1999.00605
- Davies, N. W. (1990). Gas chromatographic retention indices of monoterpenes and sesquiterpenes on Methyl Silicon and Carbowax 20M phases. *J. Chromatogr.* 503, 1–24.
- De Mastro, G., Tarraf, W., Verdini, L., Brunetti, G., and Ruta, C. (2017). Essential oil diversity of *Origanum vulgare* L. populations from Southern Italy. *Food Chem.* 235, 1–6. doi: 10.1016/j.foodchem.2017.05.019
- Di Cello, F., and Fani, R. (1996). A molecular strategy for the study of natural bacterial communities by PCR-based techniques. *Minerva Biotechnol.* 8, 126–134.
- Emiliani, G., Mengoni, A., Maida, I., Perrin, E., Chiellini, C., Fondi, M., et al. (2014). Linking bacterial endophytic communities to essential oils: clues from *Lavandula angustifolia* Mill. *Evid. Based Complement. Alternat. Med.* 2014:650905. doi: 10.1155/2014/650905
- Gunatilaka, A. A. (2006). Natural products from plant-associated microorganisms: distribution, structural diversity, bioactivity, and implications of their occurrence. *J. Nat. Prod.* 69, 509–526. doi: 10.1021/np058128n
- Hall, T. A. (1999). BioEdit: a user-friendly biological sequence alignment editor and analysis program for Windows 95/98/NT. *Nucleic Acids Symp.* 41, 95–98.
- Hanci, S., Sahin, S., and Yilmaz, L. (2003). Isolation of volatile oil from thyme (*Thymbra spicata*) by steam distillation. *Nahrung* 47, 252–255. doi: 10.1002/food.200390059
- Helal, I. M., El-Bessoumy, A., Al-Bataineh, E., Joseph, M. R. P., Rajagopalan, P., Chandramoorthy, H. C., et al. (2019). Antimicrobial efficiency of essential oils from traditional medicinal plants of asir region, Saudi Arabia, over drug resistant isolates. *Biomed Res. Int.* 2019:8928306. doi: 10.1155/2019/8928306
- Herlemann, D. P. R., Labrenz, M., Jürgens, K., Bertilsson, S., Waniek, J. J., and Andersson, A. F. (2011). Transitions in bacterial communities along the 2000 km salinity gradient of the Baltic Sea. *ISME J.* 5, 1571–1579. doi: 10.1038/ismej.2011.41
- Huse, S. M., Dethlefsen, L., Huber, J. A., Welch, D. M., Relman, D. A., and Sogin, M. L. (2008). Exploring microbial diversity and taxonomy using SSU rRNA hypervariable tag sequencing. *PLoS Genet.* 4:e1000255. doi: 10.1371/journal.pgen.1000255
- Jennings, W., and Shibamoto, T. (1982). *Qualitative Analysis of Flavor and Fragrance Volatiles by Glass Capillary Gas Chromatography*. New York, NY: Academic Press.

- Köberl, M., Schmidt, R., Ramadan, E. M., Bauer, R., and Berg, G. (2013). The microbiome of medicinal plants: diversity and importance for plant growth, quality, and health. *Front. Microbiol.* 4:400. doi: 10.3389/fmicb.2013.00400
- Kozich, J. J., Westcott, S. L., Baxter, N. T., Highlander, S. K., and Schloss, P. D. (2013). Development of a dual-index sequencing strategy and curation pipeline for analyzing amplicon sequence data on the MiSeq Illumina sequencing platform. *Appl. Environ. Microbiol.* 79, 5112–5120. doi: 10.1128/AEM.01043-13
- Kumar, S., Stecher, G., Li, M., Knyaz, C., and Tamura, K. (2018). MEGA X: molecular evolutionary genetics analysis across computing platforms. *Mol. Biol. Evol.* 35, 1547–1549. doi: 10.1093/molbev/msy096
- Lam, K. S. (2007). New aspects of natural products in drug discovery. *Trends Microbiol.* 15, 279–289. doi: 10.1016/j.tim.2007.04.001
- Lambert, R. J., Skandamis, P. N., Coote, P. J., and Nychas, G. J. (2001). A study of the minimum inhibitory concentration and mode of action of oregano essential oil, thymol and carvacrol. *J. Appl. Microbiol.* 91, 453–462. doi: 10.1046/j.1365-2672.2001.01428.x
- Lukas, B., Schmider, C., and Novak, J. (2015). Essential oil diversity of European *Origanum vulgare* L. (Lamiaceae). *Phytochemistry* 119, 32–40. doi: 10.1016/j.phytochem.2015.09.008
- Maggini, V., Bandeira Reidel, R. V., De Leo, M., Mengoni, A., Gallo, E. R., Miceli, E., et al. (2019a). Volatile profile of *Echinacea purpurea* plants after in vitro endophyte infection. *Nat. Prod. Res.* 25, 1–6. doi: 10.1080/14786419.2019.1579810
- Maggini, V., De Leo, M., Granchi, C., Tuccinardi, T., Mengoni, A., Gallo, E. R., et al. (2019b). The influence of *Echinacea purpurea* leaf microbiota on chicoric acid level. *Sci. Rep.* 9:10897. doi: 10.1038/s41598-019-47329-8
- Maggini, V., Mengoni, A., Bogani, P., Firenzuoli, F., and Fani, R. (2020). Promoting model systems of microbiota-medicinal plant interactions. *Trends Plant Sci.* 25, 223–225. doi: 10.1016/j.tplants.2019.12.013
- Maggini, V., Miceli, E., Fagorzi, C., Maida, I., Fondi, M., Perrin, E., et al. (2018). Antagonism and antibiotic resistance drive a species-specific plant microbiota differentiation in *Echinacea* spp. *FEMS Microbiol. Ecol.* 94:fiy118. doi: 10.1093/femsec/fiy118
- Maida, I., Chiellini, C., Mengoni, A., Bosi, E., Firenzuoli, F., Fondi, M., et al. (2016). Antagonistic interactions between endophytic cultivable bacterial communities isolated from the medicinal plant *Echinacea purpurea*. *Environ. Microbiol.* 18, 2357–2365. doi: 10.1111/1462-2920.12911
- Malik, S., de Mesquita, L. S. S., Silva, C. R., de Mesquita, J. W. C., de Sá Rocha, E., Bose, J., et al. (2019). Chemical profile and biological activities of essential oil from *Artemisia vulgaris* L. cultivated in Brazil. *Pharmaceuticals* 12:E49. doi: 10.3390/ph12020049
- Martin, M. (2011). Cutadapt removes adapter sequences from high-throughput sequencing reads. *EMBnet J.* 17, 10–12. doi: 10.14806/ej.17.1.200
- Masada, Y. (1976). *Analysis of Essential Oils by Gas Chromatography and Mass Spectrometry*. New York, NY: John Wiley & Sons, Inc.
- Mendes, R., Garbeva, P., and Raaijmakers, J. M. (2013). The rhizosphere microbiome: significance of plant beneficial, plant pathogenic, and human pathogenic microorganisms. *FEMS Microbiol. Rev.* 37, 634–663. doi: 10.1111/1574-6976.12028
- Mengoni, A., Maida, I., Chiellini, C., Emiliani, G., Mocali, S., Fabiani, A., et al. (2014). Antibiotic resistance differentiates *Echinacea purpurea* endophytic bacterial communities with respect to plant organs. *Res. Microbiol.* 165, 686–694. doi: 10.1016/j.resmic.2014.09.008
- Miller, K. I., Qing, C., Sze, D. M., Roufogalis, B. D., and Neilan, B. A. (2012). Culturable endophytes of medicinal plants and the genetic basis for their bioactivity. *Microb. Ecol.* 64, 431–449. doi: 10.1007/s00248-012-0044-8
- Mockute, D., Bernotiene, G., and Judzentiene, A. (2001). The essential oil of *Origanum vulgare* L. ssp. *vulgare* growing wild in Vilnius district (Lithuania). *Phytochemistry* 57, 65–69. doi: 10.1016/S0031-9422(00)00474-X
- Mori, E., Liò, P., Daly, S., Damiani, G., Perito, B., and Fani, R. (1999). Molecular nature of RAPD markers from *Haemophilus influenzae* Rd genome. *Res. Microbiol.* 150, 83–93. doi: 10.1016/s0923-2508(99)80026-6
- Murali, A., Bhargava, A., and Wright, E. S. (2018). IDTAXA: a novel approach for accurate taxonomic classification of microbiome sequences. *Microbiome* 6:140. doi: 10.1186/s40168-018-0521-5
- Naikpatil, S. V., and Rathod, J. L. (2011). Selective isolation and antimicrobial activity of rare actinomycetes from mangrove sediment of Karwar. *J. Ecobiotechnol.* 3, 48–53.
- Petrosino, J. F., Highlander, S., Luna, R. A., Gibbs, R. A., and Versalovic, J. (2009). Metagenomic pyrosequencing and microbial identification. *Clin. Chem.* 55, 856–866. doi: 10.1373/clinchem.2008.107565
- Pezzani, R., Vitalini, S., and Iriti, M. (2017). Bioactivities of *Origanum vulgare* L.: an update. *Phytochem. Rev.* 16, 1253–1268. doi: 10.1007/s11101-017-9535-z
- Philippot, L., Raaijmakers, J. M., Lemanceau, P., and van der Putten, W. H. (2013). Going back to the roots: the microbial ecology of the rhizosphere. *Nat. Rev. Microbiol.* 11, 789–799. doi: 10.1038/nrmicro3109
- Qi, X., Wang, E., Xing, M., Zhao, W., and Chen, X. (2012). Rhizosphere and non-rhizosphere bacterial community composition of the wild medicinal plant *Rumex patientia*. *World J. Microbiol. Biotechnol.* 28, 2257–2265. doi: 10.1007/s11274-012-1033-2
- Quast, C., Pruesse, E., Yilmaz, P., Gerken, J., Schweer, T., Yarza, P., et al. (2013). The SILVA ribosomal RNA gene database project: improved data processing and web-based tools. *Nucleic Acids Res.* 41, D590–D596. doi: 10.1093/nar/gks1219
- Quispel, A. (1992). “A search of signals in endophytic microorganisms,” in *Molecular Signals in Plant-Microbe Communications*, ed. D. P. S. Verma (Boca Raton, FL: CRC Press), 471–491.
- Reinhold-Hurek, B., and Hurek, T. (2011). Living inside plants: bacterial endophytes. *Curr. Opin. Plant Biol.* 14, 435–443. doi: 10.1016/j.pbi.2011.04.004
- Saab, A. M., Gambari, R., Sacchetti, G., Guerrini, A., Lampronti, I., Tacchini, M., et al. (2018). Phytochemical and pharmacological properties of essential oils from *Cedrus* species. *Nat. Prod. Res.* 32, 1415–1427. doi: 10.1080/14786419.2017.1346648
- Sahoo, N., Padmavati, M., and Satyahari, D. (2010). Herbal drugs: standards and regulation. *Fitoterapia* 81, 462–471. doi: 10.1016/j.fitote.2010.02.001
- Saiman, L., Siegel, J., and Cystic Fibrosis Foundation Consensus Conference on Infection Control Participants (2003). Infection control recommendations for patients with cystic fibrosis: microbiology important pathogens, and infection control practices to prevent patient-to-patient transmission. *Am. J. Infect. Control* 31(Suppl. 3), S1–S62. doi: 10.1067/mic.2003.78
- Shityakova, S., Bigdelian, E., Hussein, A., Bilal Hussaine, M., Tripathi, T. C., Khan, M. U., et al. (2019). Phytochemical and pharmacological attributes of piperine: a bioactive ingredient of black pepper. *Eur. J. Med. Chem.* 176, 149–161. doi: 10.1016/j.ejmech.2019.04.002
- Silhavy, T. J., Kahne, D., and Walker, S. (2010). The bacterial cell envelope. *Cold Spring Harb. Perspect. Biol.* 2:a000414. doi: 10.1101/cshperspect.a000414
- Swiger, A. A., and Silverstein, R. M. (1992). *Monoterpenes*. Milwaukee, WI: Aldrich Chemical Company.
- Vokou, D., Kokkini, S., and Bessiere, J.-M. (1993). Geographic variation of Greek oregano (*Origanum vulgare* ssp. *hirtum*) essential oils. *Biochem. Syst. Ecol.* 21, 287–295.
- Werker, E., Putievsky, E., and Ravid, U. (1985). The essential oils and glandular hairs in different chemotypes of *Origanum vulgare* L. *Ann. Bot.* 55, 793–801. doi: 10.1093/oxfordjournals.aob.a086958

Conflict of Interest: The authors declare that the research was conducted in the absence of any commercial or financial relationships that could be construed as a potential conflict of interest.

Copyright © 2020 Castronovo, Calonico, Ascrizzi, Del Duca, Delfino, Chioccioli, Vassallo, Strozza, De Leo, Biffi, Bacci, Bogani, Maggini, Mengoni, Pistelli, Lo Nostro, Firenzuoli and Fani. This is an open-access article distributed under the terms of the Creative Commons Attribution License (CC BY). The use, distribution or reproduction in other forums is permitted, provided the original author(s) and the copyright owner(s) are credited and that the original publication in this journal is cited, in accordance with accepted academic practice. No use, distribution or reproduction is permitted which does not comply with these terms.



Thanatin Impairs Lipopolysaccharide Transport Complex Assembly by Targeting LptC–LptA Interaction and Decreasing LptA Stability

Elisabete C. C. M. Moura¹, Tiago Baeta^{2†}, Alessandra Romanelli^{3†}, Cedric Laguri², Alessandra M. Martorana¹, Emanuela Erba³, Jean-Pierre Simorre², Paola Sperandeo^{1*} and Alessandra Polissi^{1*}

OPEN ACCESS

Edited by:

Paolo Visca,
Roma Tre University, Italy

Reviewed by:

Changjiang Dong,
University of East Anglia,
United Kingdom
Candice Klug,
Medical College of Wisconsin,
United States

*Correspondence:

Paola Sperandeo
paola.sperandeo@unimi.it
Alessandra Polissi
alessandra.polissi@unimi.it

[†] These authors have contributed
equally to this work

Specialty section:

This article was submitted to
Antimicrobials, Resistance
and Chemotherapy,
a section of the journal
Frontiers in Microbiology

Received: 04 February 2020

Accepted: 17 April 2020

Published: 13 May 2020

Citation:

Moura ECCM, Baeta T,
Romanelli A, Laguri C, Martorana AM,
Erba E, Simorre J-P, Sperandeo P
and Polissi A (2020) Thanatin Impairs
Lipopolysaccharide Transport
Complex Assembly by Targeting
LptC–LptA Interaction
and Decreasing LptA Stability.
Front. Microbiol. 11:909.
doi: 10.3389/fmicb.2020.00909

¹ Dipartimento di Scienze Farmacologiche e Biomolecolari, Università degli Studi di Milano, Milan, Italy, ² Université Grenoble Alpes, CNRS, CEA, IBS, Grenoble, France, ³ Dipartimento di Scienze Farmaceutiche, Università degli Studi di Milano, Milan, Italy

The outer membrane (OM) of Gram-negative bacteria is a highly selective permeability barrier due to its asymmetric structure with lipopolysaccharide (LPS) in the outer leaflet. In *Escherichia coli*, LPS is transported to the cell surface by the LPS transport (Lpt) system composed of seven essential proteins forming a transenvelope bridge. Transport is powered by the ABC transporter LptB₂FGC, which extracts LPS from the inner membrane (IM) and transfers it, through LptC protein, to the periplasmic protein LptA. Then, LptA delivers LPS to the OM LptDE translocon for final assembly at the cell surface. The Lpt protein machinery operates as a single device, since depletion of any component leads to the accumulation of a modified LPS decorated with repeating units of colanic acid at the IM outer leaflet. Moreover, correct machine assembly is essential for LPS transit and disruption of the Lpt complex results in LptA degradation. Due to its vital role in cell physiology, the Lpt system represents a good target for antimicrobial drugs. Thanatin is a naturally occurring antimicrobial peptide reported to cause defects in membrane assembly and demonstrated *in vitro* to bind to the N-terminal β -strand of LptA. Since this region is involved in both LptA dimerization and interaction with LptC, we wanted to elucidate the mechanism of inhibition of thanatin and discriminate whether its antibacterial effect is exerted by the disruption of the interaction of LptA with itself or with LptC. For this purpose, we here implemented the Bacterial Adenylate Cyclase Two-Hybrid (BACTH) system to probe *in vivo* the Lpt interactome in the periplasm. With this system, we found that thanatin targets both LptC–LptA and LptA–LptA interactions, with a greater inhibitory effect on the former. We confirmed *in vitro* the disruption of LptC–LptA interaction using two different biophysical techniques. Finally, we observed that in cells treated with thanatin, LptA undergoes degradation and LPS decorated with colanic acid accumulates. These data further support inhibition or disruption of Lpt complex assembly as the main killing mechanism of thanatin against Gram-negative bacteria.

Keywords: bacterial cell wall, lipopolysaccharide, Lpt system, thanatin, antimicrobial peptides, BACTH technique, NMR

INTRODUCTION

The emergence and spread of multidrug resistant pathogens pose an alarming threat to human and animal health worldwide. The old classes of antibiotics are becoming ineffective at killing an increasing number of pathogens and the decline in the discovery and development of new drugs, experienced in recent years, is seriously eroding the ability of clinicians to control infectious diseases, making the identification of new antimicrobial compounds with novel mechanisms of action an urgent need (Tacconelli et al., 2018). This situation is even more worrisome for Gram-negative pathogens since they are endowed with an asymmetric outer membrane (OM), surrounding the inner membrane (IM) and delimiting a peptidoglycan-containing periplasmic space, that protects them from harmful hydrophobic compounds such as antibiotics (Nikaido, 2003). The peculiar permeability barrier properties of the OM are conferred by the presence of a layer of tightly packed molecules of lipopolysaccharide (LPS) in its outer leaflet (Raetz and Whitfield, 2002; Silhavy et al., 2010). LPS consists of three covalently linked moieties: lipid A, the conserved hydrophobic anchor of the molecule in the membrane; a core oligosaccharide; and a somewhat variable polysaccharide chain, termed O antigen (Raetz and Whitfield, 2002). The biosynthesis of the lipid A-core domain takes place at the cytoplasmic side of the IM, whereas the assembly of mature LPS occurs at the periplasmic side of the IM, after flipping of the lipid A-core across the IM by the essential transporter MsbA (Polissi and Georgopoulos, 1996; Raetz and Whitfield, 2002; Doerrler et al., 2004).

Translocation of LPS from the IM to the OM, across the periplasm, requires the activity of the LPS transport (Lpt) machinery. This assembly is a conserved multiprotein complex composed, in *Escherichia coli*, of seven essential proteins (LptA-G) that bridges the IM and OM (Wu et al., 2006; Sperandio et al., 2007, 2008; Ruiz et al., 2008; Freinkman et al., 2012) (**Figure 1A**). The Lpt partners are organized in three sub-complexes, located in each cell envelope compartment (IM, periplasm, and OM), that interact with each other to allow the transport of LPS to the OM, shielding the hydrophobic moieties of lipid A in the hydrophilic environment of the periplasm (Sperandio et al., 2008). At the IM, the ABC transporter LptB₂FGC provides the energy for LPS extraction from the IM (Okuda et al., 2012; Li et al., 2019; Owens et al., 2019). The unconventional subunit LptC plays a dual role in the transporter, regulating the ATPase activity and providing the docking site for the periplasmic protein LptA at the membrane (Sperandio et al., 2011; Owens et al., 2019). After extraction, LPS is transferred from LptC to LptA (Tran et al., 2010; Okuda et al., 2012), that then interacts at the OM with the periplasmic domain of LptD forming the bridge that connects the IM and OM (Okuda et al., 2016). LptA has the tendency to oligomerize *in vitro* (Suits et al., 2008; Merten et al., 2012; Santambrogio et al., 2013); however, the number of LptA monomers that constitute the Lpt bridge is still not known. At the OM, the translocon composed of the β -barrel protein LptD and the lipoprotein LptE receives LPS from LptA for its final assembly at the cell surface (Freinkman et al., 2011; Dong et al., 2014; Qiao et al., 2014). The interaction between

the Lpt proteins is crucial in building a functional machinery (Sperandio et al., 2011; Falchi et al., 2018) and is mediated by a conserved domain with a peculiar structural architecture (the β -jellyroll fold) shared by all the periplasmic domains of the Lpt proteins (LptF, LptG, LptC, LptA, and LptD) (Suits et al., 2008; Tran et al., 2010; Qiao et al., 2014). Alignment of the β -jellyroll folds of LptF, LptC, LptA, and LptD in a C-terminal-to-N-terminal arrangement is thought to allow the formation of a hydrophobic groove that spans the periplasm and accommodates the acyl chains of the LPS molecules during transport (Villa et al., 2013; Okuda et al., 2016; Sperandio et al., 2019). Inhibition of bridge formation, as a consequence of Lpt protein depletion in conditional expression mutants or due to mutations that interfere with protein-protein interactions at any level in the system, results in cell growth arrest and blocking of Lpt, with accumulation of newly synthesized LPS in the IM and formation of membranous bodies in the periplasm (Wu et al., 2006; Sperandio et al., 2007, 2008; Ruiz et al., 2008). Accumulated LPS molecules can be decorated at the periplasmic side of the IM by the addition of colanic acid units (Majdalani and Gottesman, 2005; Sperandio et al., 2008, 2011). Overall, the Lpt mechanism mediated by the Lpt machinery has been compared to that of a PEZ candy dispenser, where a spring at the base of the dispenser loads the candy into the tube and pushes them up to the cap, which then opens to release them to the customer (Okuda et al., 2016). Interestingly, when the Lpt bridge is not properly assembled, LptA undergoes degradation, suggesting that the steady-state level of LptA in the cell, together with the appearance of colanic acid-modified LPS, are diagnostic of Lpt defects (Sperandio et al., 2011).

Due to its relevance in Gram-negative bacteria cell physiology, LPS biogenesis can be considered a promising target for the development of novel antibacterial molecules. Potent inhibitors of the lipid A biosynthesis were identified in past studies and are continuously in development (Simpson and Trent, 2019). Moreover, two compounds targeting the MsbA-mediated IM translocation process have been recently reported (Ho et al., 2018; Zhang et al., 2018). However, the only inhibitor of LPS biogenesis to have entered, so far, Phase III trials is Murepavadin, a macrocyclic peptidomimetic selectively directed against *Pseudomonas aeruginosa* LptD (Srinivas et al., 2010; Lehman and Grabowicz, 2019). Unfortunately, the clinical trials have been suspended recently due to nephrotoxicity (Lehman and Grabowicz, 2019). Nevertheless, the identification of Murepavadin highlights the Lpt machinery as a good target for the discovery of molecules endowed with antibacterial activity.

Very recently, a screening strategy based on the yeast two-hybrid (YTH) system has allowed the isolation of a compound, IMB-881, that disrupts LptC-LptA interaction, exerting bactericidal activity against *E. coli* and other Enterobacterial species (Zhang et al., 2019).

Here we show the implementation of the Bacterial Adenylate Cyclase Two-Hybrid (BACTH) system (Karimova et al., 1998), based on the interaction-mediated reconstitution of the adenylate cyclase activity in *E. coli*, to allow the detection of LptC-LptA and LptA-LptA interactions in their native environment, the periplasm. We successfully reconstituted both interactions and

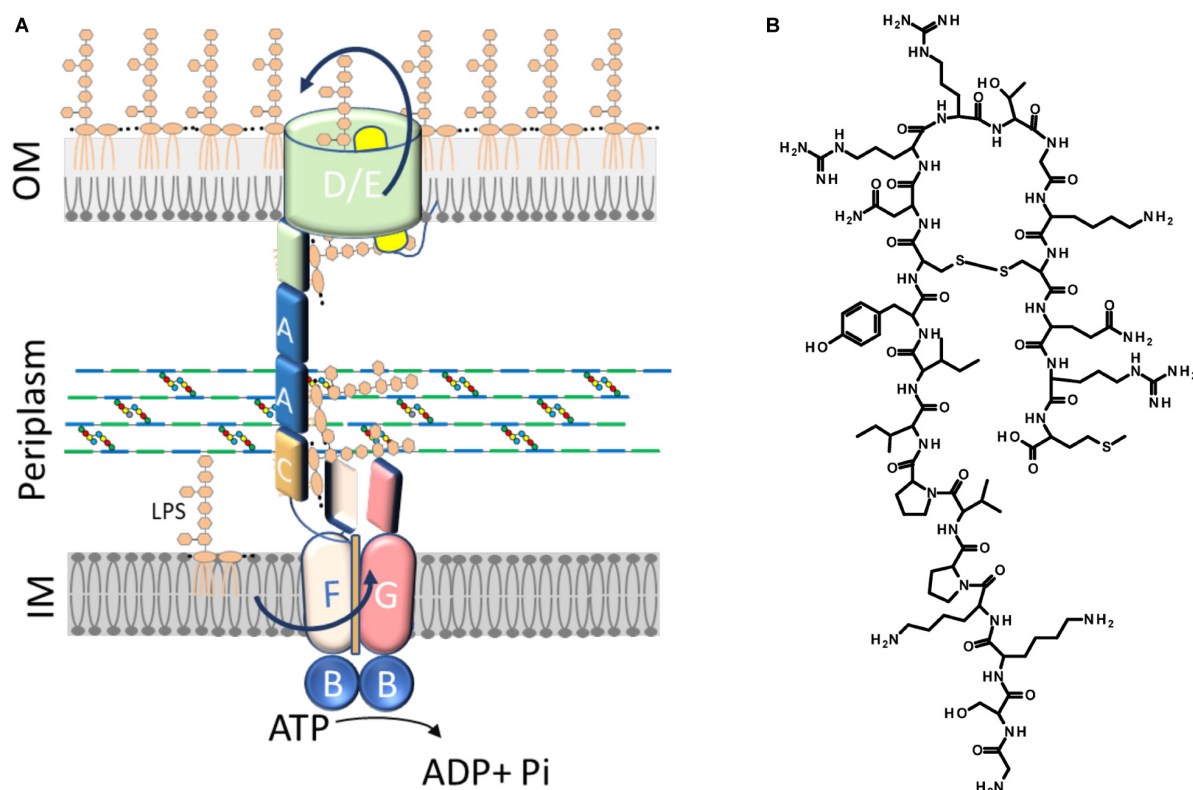


FIGURE 1 | The Lpt machinery and thanatin. **(A)** The lipopolysaccharide transport system in *Escherichia coli* consists of a seven-protein complex organized in an inner membrane (IM) ABC transporter (LptB₂FGC) and an outer membrane (OM) translocon (LptDE) connected by a periplasmic protein, LptA, that bridges the membranes. LptA is anchored to the IM through its interaction with LptC. The number of LptA molecules forming the bridge is not known. For clarity, only two molecules of LptA are depicted. **(B)** Structure of thanatin.

exploited this system to more thoroughly investigate the effect of the antimicrobial peptide thanatin.

Thanatin is a 21-residue inducible cationic defense peptide isolated from the hemipteran insect *Podisus maculiventris*, that contains one disulfide bond and exhibits a broad range of antibacterial and antifungal activity (Fehlbaum et al., 1996) (**Figure 1B**).

Important new insights into thanatin's mode of action against Gram-negative bacteria have been provided by a recent work showing that thanatin binds to *E. coli* LptA and LptD *in vivo* and *in vitro* (Vetterli et al., 2018). Accordingly, spontaneous thanatin-resistant mutants isolated in the same work share a single point mutation in the *lptA* gene, strongly indicating LptA as the major target of thanatin. Analysis of the nuclear magnetic resonance (NMR) structure of the LptA–thanatin complex reveals that the interaction occurs at the N-terminal β -strand of the β -jellyroll of LptA, region involved in LptA interaction with LptC and/or with another monomer of LptA (Suits et al., 2008; Freinkman et al., 2012). It has been thus speculated that thanatin might exert its antibacterial activity by interfering with the interactions established by LptA within the Lpt bridge (Vetterli et al., 2018). However, no evidence supporting this hypothesis has been published yet.

Our investigation provides more insights into thanatin's mode of action against Gram-negative bacteria showing that it interferes with LptC–LptA interaction *in vivo*. Disruption of the Lpt protein bridge is further supported by LptA degradation and appearance of LPS modified by colanic acid in thanatin treated cells. The results of this work strongly validate the assembly of the Lpt machinery as a promising target for the development of a novel class of antibacterial or adjuvant drugs.

MATERIALS AND METHODS

Bacterial Strains and Media

Escherichia coli strains and plasmids used in this study are listed in **Table 1**. AM604 genomic DNA was used as template for PCR and the XL1-Blue strain was used in all cloning steps. The strain MG1655 was used in the study of LptA stability and in the analysis of LPS profiles. BACTH assays were performed with the *E. coli* Δ cya strain BTH101 (Karimova et al., 1998; Ouellette et al., 2017). The strains M15/pREP4 and BL21(DE3) were used in the purification of LptC_{24–191} (Sperandeo et al., 2011) and LptA_m (Laguri et al., 2017), respectively. Bacteria were grown in Luria–Bertani (LB) medium (10 g/L tryptone, 5 g/L yeast extract, 10 g/L NaCl) or LB-agar medium (LB

medium with 10 g/L agar). When required, antibiotics or inducer were added at the following concentrations: ampicillin at 100 µg/mL, spectinomycin at 50 µg/mL, isopropyl-β-D-thiogalactopyranoside (IPTG) at 0.5 mM.

Plasmid Construction

To construct the recombinant plasmids used in the BACTH assay (listed in **Table 1**), the genes encoding the Lpt proteins of interest (or their subdomains) were PCR-amplified using the appropriate primer pairs, as listed in **Table 2**. The PCR products were then digested with the indicated restriction enzymes and subcloned into the corresponding sites of the pSTM25 and pUTM18C vectors. These BACTH vectors, expressing the T25 and T18 fragments of the adenylate cyclase toxin of *Bordetella pertussis* fused at their C-terminal ends with the first transmembrane domain of the *E. coli* OppB protein (TM), were employed in order to study protein interactions in the periplasm (Ouellette et al., 2014). In the recombinant plasmids pSTM25-LptC and pUTM18C-LptC, full-length LptC (comprising its own transmembrane domain) was fused at the C-terminal end of the T25 and T18 fragments, respectively. MalE, LptA, and LptA_m were fused to the C-terminal end of TM to originate the constructs pUTM18C-MalE, pSTM25-LptA, pUTM18C-LptA, pSTM25-LptA_m, and pUTM18C-LptA_m. The recombinant plasmids pSTM25-LptA^{Q62L}, pUTM18C-LptA^{Q62L}, and pUTM18C-LptA_m^{Q62L} were constructed by using a Q5 site-directed mutagenesis kit (New England Biolabs) with the primer pair AP733-AP734. Transformation was performed in XL1-Blue electrocompetent cells and transformants were selected at 30°C on LB plates supplemented with the appropriate antibiotics (ampicillin or spectinomycin), and 0.4% glucose to repress expression. All the cloned DNA regions obtained by PCR were verified by sequencing.

Bacterial Adenylate Cyclase Two-Hybrid (BACTH) Assay

To study protein–protein interactions with the BACTH system, electrocompetent BTH101 cells were co-transformed with each pair of plasmids to be tested (**Figure 2A**), plated onto LB plates containing selective antibiotics (100 µg/mL ampicillin and 50 µg/mL spectinomycin) and incubated at 30°C for 24–48 h. Interaction efficiencies were quantified by determining the β-galactosidase activities in 96-well microtiter plates according to a protocol adapted from Paschos et al. (2011). For this measurement, at least eight clones from each plasmid combination were analyzed for β-galactosidase activity in two independent experiments. Each clone was inoculated in 1 mL of LB medium supplemented with antibiotics and 0.5 mM IPTG for overnight induction. The β-galactosidase activity was measured from 20 µL culture diluted in 80 µL PM2 buffer (70 mM Na₂HPO₄, 12H₂O, 30 mM NaH₂PO₄, H₂O, 1 mM MgSO₄, 0.2 mM MnSO₄, pH 7.0) containing 8 mg/mL *ortho*-nitrophenyl-β-galactoside (ONPG), 0.01% SDS, and 50 mM β-mercaptoethanol. Reaction mixtures were incubated at room temperature for 20–30 min or until a sufficiently yellow color had developed, and the reactions were stopped with 100 µL

1 M Na₂CO₃. The optical densities at 420 and 550 nm were recorded for each sample using a plate reader (EnSpire Multimode Plate Reader, PerkinElmer) and the specific activity was calculated with the formula: Miller units = $[(OD_{420} - (1.75 \times OD_{550})) / (t \times OD_{600} \times (\text{volume in mL}))] \times 1000$, where OD₆₀₀ is the optical density at 600 nm after overnight incubation and *t* is the time in minutes needed for color formation.

Peptide Synthesis

Peptides were synthesized on a 0.1 mmol scale on a Wang resin 0.99 mmol/g. The first amino acid was attached to the resin following a protocol described in the literature (Avitabile et al., 2019). The peptides were then elongated on a Liberty Blue CEM synthesizer using standard protocols. At the end of the synthesis, the peptides were cleaved from the resin and protecting groups were removed by treating the resin with a solution of TFA/thioanisole/H₂O 95/2.5/2.5 v/v/v for 2 h. The peptides were then lyophilized. Wild type (WT) peptide was cyclized as reported by Fehlbaum et al. (1996). Peptides were purified by RP-HPLC on a Jupiter 10µ Proteo 90A° (100 × 21.20 mm) column using a gradient of CH₃CN (0.1% TFA) in H₂O (0.1% TFA) from 10 to 50% in 20 min and analyzed on a Vydac C18 100A 5µ 150 × 4.6 mm column with the same gradient. Peptides were characterized by mass spectrometry on a Thermo Scientific LCQ Fleet ion trap. Pure peptides were then lyophilized three times, the first to eliminate HPLC solvents, the second from a solution 6/4 v/v H₂O /CH₃COOH, and the third in water.

Thanatin WT Cyclic

Sequence: GSKKPVPIIYCNRRGTGKCQRM

Calculated mass (Da): 2433.95; found (Da): 1217.08 [M+2H]²⁺; 812.33 [M+3H]³⁺; 609.29 [M+4H]⁴⁺

Thanatin Scramble (Scr)

Sequence: YVCIRMNKISPQKQRTPGGRCK

Calculated mass (Da): 2435.95; found (Da): 1219.02 [M+2H]²⁺; 813.47 [M+3H]³⁺; 610.50 [M+4H]⁴⁺

Determination of Minimal Inhibitory Concentration (MIC)

The minimal inhibitory concentration (MIC) values of thanatin, thanatin scramble, and vancomycin (as a positive control) were assessed with a protocol adapted from Wiegand et al. (2008) using 96-well microtiter plates. Stationary phase cultures of the *E. coli* WT strain MG1655 (Blattner et al., 1997), the permeabilized mutants AS19 (Sekiguchi and Iida, 1967) and NR698 (Ruiz et al., 2005), and the BACTH strain BTH101 (Karimova et al., 1998; Ouellette et al., 2017) grown at 37°C in LB medium, were diluted in fresh medium adjusting the OD₆₀₀ to a value of 0.05 and incubated in the presence of twofold decreasing concentrations of the compounds ranging from 64 µg/mL to 62.5 ng/mL. After 24 h of incubation at 37°C, the OD₆₀₀ was measured by a plate reader (EnSpire Multimode Plate Reader, PerkinElmer). The MIC value was determined as the lowest concentration of compound leading to no detectable growth.

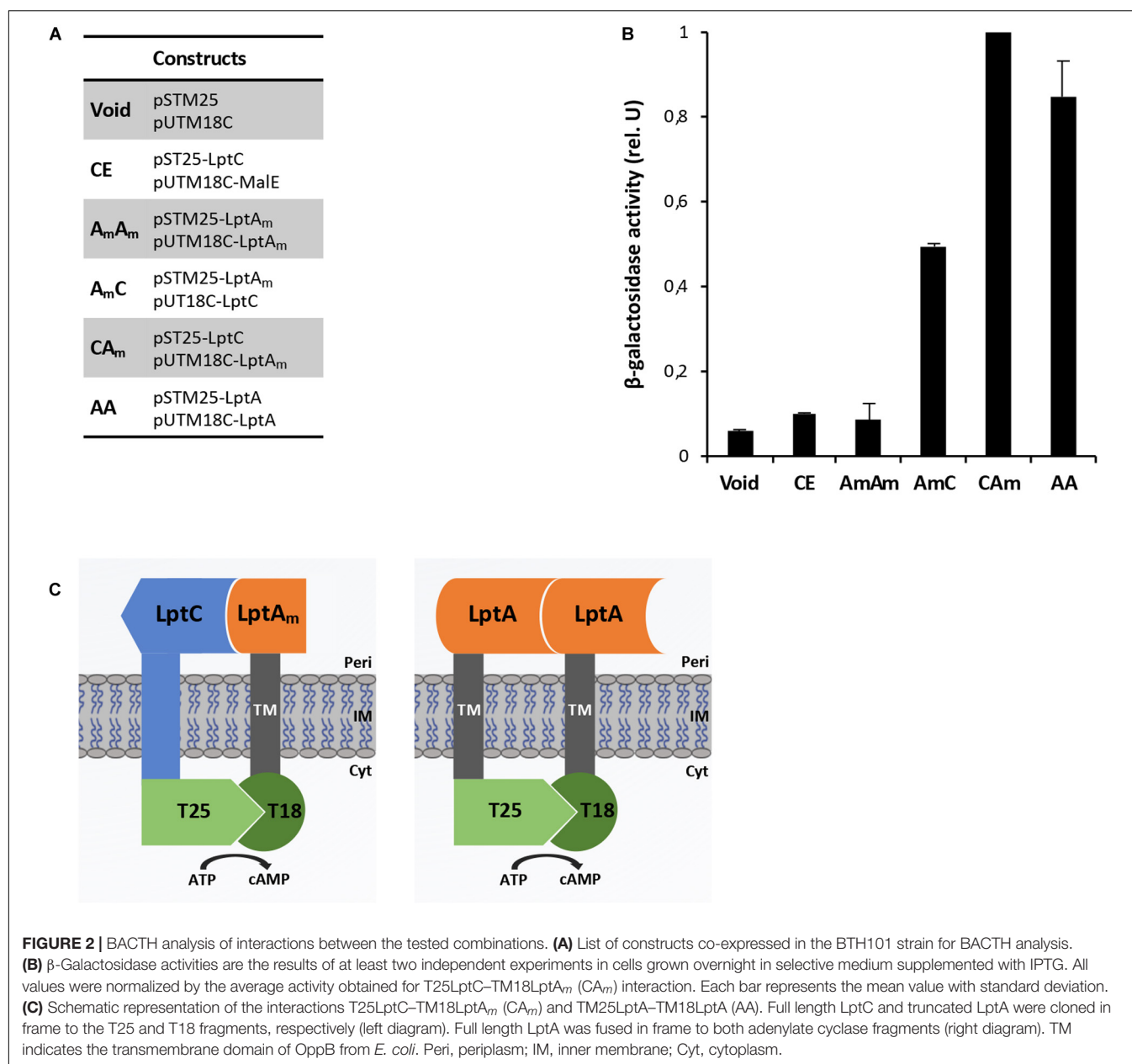
TABLE 1 | *Escherichia coli* strains and plasmids.

Strain or plasmid	Relevant genotype or description	Source or references
Strains		
MG1655	K-12, F ⁻ λ^{-} <i>ilvG⁻ rfb-50 rph-1</i>	Blattner et al., 1997
AM604	MC4100 <i>ara⁺</i>	Wu et al., 2006
AS19	<i>E. coli</i> strain B, hyperpermeable strain	Sekiguchi and Iida, 1967
NR698	<i>imp4213</i>	Ruiz et al., 2005
XL1-Blue	<i>recA1 endA1 gyrA96 (Nal^R) thi-1 hsdR17 supE44 relA1 lac [F' proAB lac^R Z Δ M15 Tn10 (Tet^R)]</i>	NEB
BTH101	F ⁻ <i>cya-99 araD139 galE15 galK16 rpsL1 (Str^R) hsdR2 mcrA1 mcrB1</i>	Karimova et al., 1998; Ouellette et al., 2017
M15/pREP4	F ⁻ <i>lac thi mtl/pREP4</i>	QIAGEN
BL21(DE3)	F ⁻ <i>ompT gal dcm lon hsdS_B(r_B⁻ m_B⁻) (λDE3 [<i>lacI lacUV5-T7 gene 1 ind1 Sam7 nin5</i>])</i>	Studier and Moffatt, 1986
Plasmids		
		ori
pSTM25	<i>aadA P_{lac}::t25-TM</i>	p15A Ouellette et al., 2014
pUTM18C	<i>bla P_{lac}::t18-TM</i>	ColE1 Ouellette et al., 2014
pUTM18C-MalE	<i>malE</i> sequence (residues 27–396) cloned downstream T18-TM	ColE1 This study
pSTM25-LptA _m	<i>lptA</i> sequence (residues 28–159) cloned downstream T25-TM	p15A This study
pUTM18C-LptA _m	<i>lptA</i> sequence (residues 28–159) cloned downstream T18-TM	ColE1 This study
pUTM18C-LptA _m ^{Q62L}	<i>lptA</i> sequence (residues 28–159) bearing a Q-to-L mutation at position 62 cloned downstream T18-TM	ColE1 This study
pSTM25-LptA	<i>lptA</i> sequence (residues 28–185) cloned downstream T25-TM	p15A This study
pSTM25-LptA ^{Q62L}	<i>lptA</i> sequence (residues 28–185) bearing a Q-to-L mutation at position 62 cloned downstream T25-TM	p15A This study
pUTM18C-LptA	<i>lptA</i> sequence (residues 28–185) cloned downstream T18-TM	ColE1 This study
pUTM18C-LptA ^{Q62L}	<i>lptA</i> sequence (residues 28–185) bearing a Q-to-L mutation at position 62 cloned downstream T18-TM	ColE1 This study
pST25-LptC	<i>lptC</i> full-length sequence cloned downstream T25	p15A This study
pUT18C-LptC	<i>lptC</i> full-length sequence cloned downstream T18	ColE1 This study
pQESH- <i>lptC</i>	pQE30 (QIAGEN) derivative, expresses His ₆ -LptC _{24–191} ; <i>bla</i>	Sperandeo et al., 2011
pET-LptA $\Delta_{160-185}$ -H	<i>pT7-lptA$\Delta_{160-185}$ -His₆; bla</i>	Laguri et al., 2017

TABLE 2 | Oligonucleotides.

Name		Sequence (5'–3') ^a	Used to make
AP576	Reverse	attgtggatccTAAAGGCTGAGTTTGTGTTG	<i>lptC</i> cloning in pSTM25 and pUTM18C; BamHI
AP579	Forward	taatgtcgacgAAAATCGAAGAAGGTAACTG	<i>malE</i> cloning in pUTM18C; Sall
AP580	Reverse	aaggatctagaTTACTTGGTGATACGAGTCTGC	<i>malE</i> cloning in pUTM18C; XbaI
AP581	Forward	gagacgagctcgGTAACCGGAGACACTGATCAG	<i>lptA</i> and <i>lptA_m</i> cloning in pUTM18C; SacI
AP582	Reverse	gagaggaattcTTAATTACCCTTCTCTGTGC	<i>lptA</i> cloning in pUTM18C; EcoRI
AP665	Reverse	gagaggaattcTTAGCGCTTGCCCTTTGTGC	<i>lptA_m</i> cloning in pUTM18C; EcoRI
AP666	Forward	aaggatctagagGTAACCGGAGACACTGATCAG	<i>lptA</i> cloning in pSTM25; XbaI
AP667	Reverse	attgtggatccTTAATTACCCTTCTCTGTGC	<i>lptA</i> cloning in pSTM25; BamHI
AP688	Reverse	attgtggatccTTAGCGCTTGCCCTTTGTGC	<i>lptA_m</i> cloning in pSTM25; BamHI
AP689	Forward	gaagatctgcaggATGAGTAAAGCCAGACGTTG	<i>lptC</i> cloning in pSTM25; PstI
AP690	Forward	gaagatctgcaggATGAGTAAAGCCAGACGTTG	<i>lptC</i> cloning in pUTM18C; PstI
AP733	Forward	ATCGTCACCC CTG GGCACCATC	Q62L mutagenesis in <i>lptA</i>
AP734	Reverse	GACATTACCGGTAAGGTAACC	Q62L mutagenesis in <i>lptA</i>

^a*E. coli* genomic sequence in uppercase; restriction sites in underlined lowercase; codon mutated by site-directed mutagenesis in bold.



Analysis of Thanatin's Effect on Lpt Protein Interactions Using the BACTH Assay

To assess thanatin's effect on the periplasmic interactions LptA–LptA and LptC–LptA_m, at least four clones from each combination were cultured in LB medium supplemented with antibiotics at 37°C to an OD₆₀₀ around 1.0. These precultures were used to inoculate 1 mL of LB medium supplemented with antibiotics, 0.5 mM IPTG, and thanatin at different concentrations to an OD₆₀₀ of 0.05; and the cultures were incubated for 18 h (overnight) at 30°C. After overnight induction of the expression of the hybrid proteins, the β-galactosidase activities were determined. For the clones expressing the BACTH

combination T25LptC–TM18LptA_m, thanatin was tested at 0.7, 1.0, and 1.4 μg/mL. For the TM25LptA–TM18LptA pair, a higher concentration of thanatin could be added to the cultures without affecting bacterial growth; thus, values of 0.7, 1.0, 1.4, and 2.8 μg/mL were tested. A scrambled version of thanatin (Scr) was also employed in this assay at the same concentrations as a control for the specificity of interaction inhibition.

Protein Production and Purification

Escherichia coli LptC lacking the first 23 residues of the transmembrane domain was expressed from a plasmid (LptC pQESH, QIAGEN) with an N-terminal His-Tag and purified as described (Laguri et al., 2017). LptC was expressed in ¹⁵N enriched deuterated medium with specific ¹³C-¹H labeling of

Isoleucines $\delta 1$ and Leucine and Valine proR methyl groups according to standard protocols (Kerfah et al., 2015) with NMRbio precursors¹. LptA_m coding for residues 28–159 followed by a SGRVEHHHHHH TAG in a pET21b vector was expressed and purified as described (Laguri et al., 2017). Both proteins were exchanged to 50 mM Na₂HPO₄ pH 8.0, 150 mM NaCl buffer.

NMR Spectroscopy

Nuclear magnetic resonance experiments were recorded at 25°C on Bruker 600 MHz spectrometer equipped with a triple resonance cryoprobe. 2D-[¹H, ¹³C]-methyl-SOFAST experiments were recorded to follow LptC methyl groups on LptC ¹⁵N²H and ¹³C-¹H specifically labeled on I δ 1, L δ 1, and V γ 1 at 20 μ M prepared in 50 mM Na₂HPO₄ pH 8.0, 150 mM NaCl buffer with 10% D₂O. Unlabeled LptA_m at 40 μ M prepared in the exact same buffer was added to LptC to achieve 100% of LptC complexed with LptA_m. Thanatin or Scr at 42 μ M was added to the complex and interaction experiments were followed using 2D-[¹H, ¹³C]-methyl-SOFAST experiments. NMR experiments were processed and analyzed using Topspin 3.2 and CcpNmr 2.4.

Biacore Experiments

Surface plasmon resonance (SPR) experiments were performed on a Biacore T200 with a CM3 chip. HBS-P+ and HBS-N buffers (GE Healthcare) were used for immobilization and interactions, respectively. 66 Resonance units (RUs) of LptA_m were immobilized on a flow cell by the amine (EDC-NHS) coupling method followed by ethanolamine saturation, with a flow cell modified only with EDC-NHS-ethanolamine as reference for subtractions. For interactions, protein and ligands were diluted in HBS-N running buffer and regeneration between injections achieved with a 30 s pulse of 10 mM HCl. Sensorgrams shown were subtracted with the reference flow cell as well as with injection of buffer alone. Determination of LptC–LptA_m K_d was performed by injecting increasing concentrations of LptC (5.6–100 μ M) over immobilized LptA_m. Kinetics analysis of the data was unsuccessful due to very fast association, and the K_d was determined from steady-state binding levels obtained at the end of the association phase with Bioeval software (GE Healthcare).

Determination of LptA, LptD, and LptB Steady-State Levels Upon Thanatin Treatment

LptA, LptD, and LptB (as loading control) steady-state levels were assessed in the MG1655 strain by western blot analysis with polyclonal antibodies raised in rabbit against LptA, LptD, and LptB. Bacterial cultures were grown at 37°C in LB medium. At OD₆₀₀ 0.1, the cells were treated or not with 5.25 μ g/mL of thanatin (1.5 \times MIC). Cell growth was monitored by measuring the OD₆₀₀ value at 30-min intervals and viability was determined by quantifying the colony-forming units (CFU) at 1-h intervals during a time period of 4 h. Whole-cell extracts for protein analysis were collected and harvested by centrifugation (5000 g, 10 min) 20, 30, 40, 60, and 120 min after treatment with thanatin.

¹<http://www.nmr-bio.com/>

The cell pellets were resuspended in a volume (in mL) of SDS Laemmli buffer equal to 1/24 of the total optical density of the sample. The samples were boiled for 5 min and equal volumes (15 μ L) were separated by 12.5% SDS-PAGE. Proteins were transferred onto nitrocellulose membranes (GE Healthcare), and immunodecoration was performed as previously described (Sperandeo et al., 2007). Polyclonal antibodies raised against LptA (GenScript Corporation), LptD (GenScript Corporation), and LptB (kindly provided by D. Kahne and N. Ruiz) were used as primary antibodies at dilutions of 1:1,000, 1:500, and 1:10,000, respectively. As secondary antibody, goat anti-rabbit immunoglobulin (Li-Cor) was used at a dilution of 1:15,000. Bands were visualized by an Odyssey Fc imaging system (Li-Cor GmbH).

LPS Analysis From Whole-Cell Extracts

Whole-cell extract samples for LPS analysis were obtained as described in the previous section. For LPS visualization, equal volumes (20 μ L) of whole-cell extracts were digested with 6 μ g of proteinase K (Sigma–Aldrich) at 60°C for 1 h and then separated by 18% Tricine SDS-PAGE (Lesse et al., 1990). Immunodecoration was performed using anti-LPS core WN1 222-5 monoclonal antibodies (Hycult Biotech) at a dilution of 1:500. As secondary antibody, goat anti-mouse immunoglobulin G-peroxidase (HRP) conjugate (Sigma–Aldrich) was used at a dilution of 1:5000.

RESULTS

Adaptation of the BACTH Assay for the Detection of Lpt Protein Interactions in the Periplasm

The BACTH system was implemented in this work to allow the detection *in vivo* of two crucial protein-protein interactions within the Lpt interactome, namely, LptC–LptA and LptA–LptA. The BACTH assay is based on the interaction-mediated reconstitution of the adenylate cyclase activity of the toxin of *B. pertussis*, whose catalytic domain can be divided in two complementary fragments, T25 and T18 (Karimova et al., 1998; Battesti and Bouveret, 2012). In this work, we used the BACTH vectors expressing these fragments fused in frame with the first transmembrane domain of the *E. coli* OppB protein (TM) (pSTM25 and pUTM18C). These plasmids allow expression of the targeted protein domains fused to TM25 and TM18 into the periplasm (Ouellette et al., 2014) which reflects the physiological environment of the tested interactions. To detect LptA–LptA dimerization, LptA was subcloned into both BACTH vectors at the C-terminal end of the TM, originating the hybrid TM25LptA and TM18LptA proteins. To detect LptC–LptA association, we fused at the C-terminal end of the TM a truncated monomeric version of LptA, referred to as LptA_m, that lacks the last C-terminal β -strand and is not able to self-oligomerize, although still functional *in vivo* (Laguri et al., 2017). We decided to use LptA_m to avoid titration of the fusion protein caused by

interaction of LptA with itself, leading to a decrease in the β -galactosidase signal when testing LptC–LptA interaction with the BACTH technique. Full-length LptC was subcloned into both pSTM25 and pUTM18C vectors, in frame with the C-terminal end of the adenylate cyclase fragments, to obtain the constructs T25LptC and T18LptC.

As negative controls for the assay, we used: (i) the combination between the void plasmids pSTM25 and pUTM18C; (ii) the non-productive LptA_m–LptA_m association; and (iii) the association LptC–MalE, between LptC and the unrelated periplasmic binding subunit of the *E. coli* maltose transporter, MalE (Davidson et al., 1992; Ehrmann et al., 1998). Constructs were transformed into the adenylate cyclase-deficient strain BTH101 and the efficiency of interaction between the various protein fusions was quantified by measuring the β -galactosidase activity. The results for the BACTH complementation assay are presented in **Figures 2A,B**. As expected, LptC–MalE combination did not produce a positive interaction signal, confirming that the BACTH system is suitable to detect specific interactions occurring in the periplasm. Also, truncated LptA was confirmed to be unable to oligomerize. We successfully detected *in vivo* the LptC–LptA_m interaction and the dimerization of LptA (schematic representation in **Figure 2C**). The signal obtained for the pair T25LptC–TM18LptA_m (CA_m) was twofold higher than the one obtained for the complementary combination TM25LptA_m–T18LptC (A_mC). This effect is not surprising since it was previously reported that β -galactosidase measurements may significantly vary according to the T25 and T18 combination chosen for the BACTH assay (Ouellette et al., 2017). Indeed, when testing the LptC–LptA_m interaction, hybrid LptA_m can be titrated away from the reaction by interaction through its N-terminal with native LptA. This effect is likely even more significant in the TM25LptA_m–T18LptC configuration, where LptA_m is expressed from a low-copy number vector (pSTM25), thus further diminishing the number of hybrid LptA_m proteins free to interact with LptC and accounting for the lower β -galactosidase signal observed in A_mC combination. Therefore, we decided to use the pair of constructs T25LptC–TM18LptA_m in further tests. It should be noted that in our assay, the interaction of full-length LptA with itself (LptA–LptA) produced a lower β -galactosidase activity signal compared to LptC–LptA_m. This is consistent with previously published *in vitro* measurements revealing that the affinity between LptA and LptC is stronger than the affinity for LptA oligomerization (Schultz et al., 2013).

Thanatin Inhibits LptC–LptA_m and LptA–LptA Interactions *in vivo*

Interaction between the antibacterial peptide thanatin and LptA was recently demonstrated and NMR experiments clearly showed that the N-terminal strand of the β -hairpin of thanatin docks in parallel orientation onto the first N-terminal β -strand of the β -jellyroll of LptA (Vetterli et al., 2018). It is well known from structural studies that dimerization of LptA monomers with themselves or with LptC involves the N-terminal edge strand of the β -jellyroll of LptA (Suits et al., 2008; Schultz et al., 2013; Laguri et al., 2017). Thanatin's binding site therefore overlaps with the interaction site of LptA with another LptA

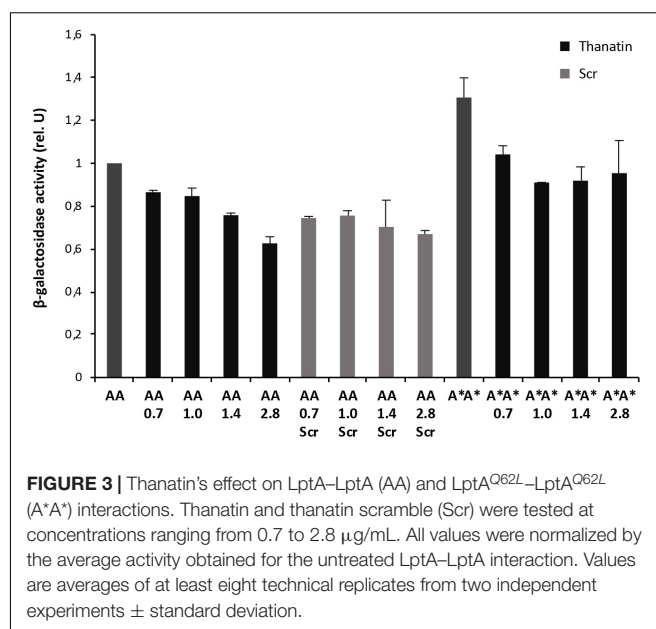


FIGURE 3 | Thanatin's effect on LptA–LptA (AA) and LptA^{Q62L}–LptA^{Q62L} (A*A*) interactions. Thanatin and thanatin scramble (Scr) were tested at concentrations ranging from 0.7 to 2.8 μ g/mL. All values were normalized by the average activity obtained for the untreated LptA–LptA interaction. Values are averages of at least eight technical replicates from two independent experiments \pm standard deviation.

subunit in the homodimer LptA–LptA and with LptC in the heterodimer LptA–LptC, suggesting a possible mechanism for the antibacterial activity. We thus analyzed the effect of thanatin on these interactions with the adapted BACTH assay and used a scrambled version of thanatin, characterized by the same amino acid composition but with a different sequence (thanatin scramble, Scr), as specificity control (**Figures 3, 4**). The MIC of thanatin and thanatin scramble was assessed against WT MG1655, and permeabilized AS19 and NR698 *E. coli* strains. The MIC values were 1.8–3.5 and above 64 μ g/mL for thanatin and thanatin scramble, respectively, when tested against the WT MG1655 strain (**Table 3**). Slightly lower MIC values were obtained for thanatin when tested against the permeabilized *E. coli* mutants (0.1–0.4 μ g/mL). On the contrary, no significant difference relative to the WT strain was observed in the MIC values of thanatin scramble when tested against the permeabilized mutant strains, suggesting that the lower activity of the peptide cannot be attributed to its inability to cross the OM barrier.

To explore whether thanatin's antibacterial activity is due to the inhibition of LptA interaction with itself or with LptC, we evaluated the effect of increasing sub-MIC concentrations of the peptide on the TM25LptA–TM18LptA and T25LptC–TM18LptA_m associations and the results are presented in **Figures 3, 4**, respectively. After overnight induction of the fusion proteins in the presence of thanatin, we could observe inhibition not only of LptA–LptA dimerization but also of LptC–LptA_m interaction, but the inhibitory effect was much greater on the latter. A clear dose-dependent response could only be observed in the inhibition of LptC–LptA_m interaction. The thanatin scramble was not capable of disrupting these periplasmic interactions in a dose-dependent manner, indicating that this is an effect specific to thanatin secondary and tertiary structures rather than to any cationic peptide with the same amino acid composition.

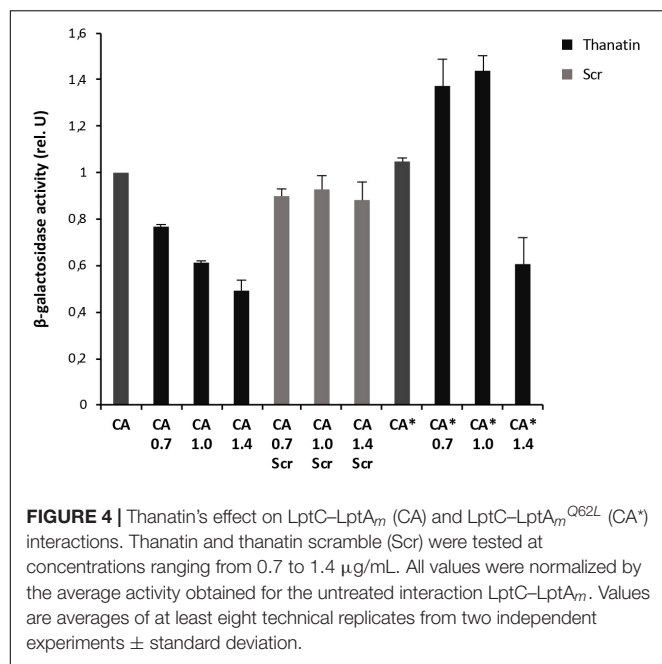


FIGURE 4 | Thanatin's effect on LptC–LptA_m (CA) and LptC–LptA_m^{Q62L} (CA*) interactions. Thanatin and thanatin scramble (Scr) were tested at concentrations ranging from 0.7 to 1.4 μg/mL. All values were normalized by the average activity obtained for the untreated interaction LptC–LptA_m. Values are averages of at least eight technical replicates from two independent experiments ± standard deviation.

TABLE 3 | Minimal inhibitory concentrations (MICs) in μg/mL of thanatin, thanatin scramble, and vancomycin.

Strains	MIC (μg/mL)		
	Thanatin	Thanatin scramble	Vancomycin
MG1655	1.8–3.5	>64	>64
AS19	0.1–0.2	64	4.0–8.0
NR698	0.1–0.4	32–64	0.5–1.0
BTH101	3.5	>64	>64

Compounds were tested against wild-type (MG1655) and permeable (AS19 and NR698) *Escherichia coli* strains. The BTH101 strain used in the BACTH assay was also tested. The data are representative of three biological replicates.

We also tested a previously isolated thanatin-resistant mutant presenting a glutamine to leucine substitution at position 62 in the LptA protein (*lptA*^{Q62L} allele) (Vetterli et al., 2018). The *lptA*-Q62L mutation was introduced into the BACTH constructs and tested as described above (Figures 3, 4). The data obtained suggest that Q62L mutation in LptA specifically impairs the ability of thanatin to disrupt LptC–LptA_m^{Q62L} (CA*) association, since the peptide is not effective against CA* at concentrations at which it is active against the WT CA pair, namely, 0.7 and 1 μg/mL (Figure 4). It should be noted that Q62L mutation exerts an unexpected stabilizing effect on LptA^{Q62L}–LptA^{Q62L} (A*A*) interaction, resulting in a β-galactosidase signal higher than that of the WT LptA–LptA combination. This effect is abolished upon treatment with thanatin, although not in a dose-dependent manner (Figure 3). Residue Q62 is not directly involved in the interaction of LptA with another LptA monomer, LptC, or with thanatin but belongs to a loop of the β-jellyroll of LptA that comes into contact with the short N-terminal α-helix of the WT protein upon thanatin interaction (Vetterli et al., 2018). This effect could be explained assuming that Q62L mutation induces a

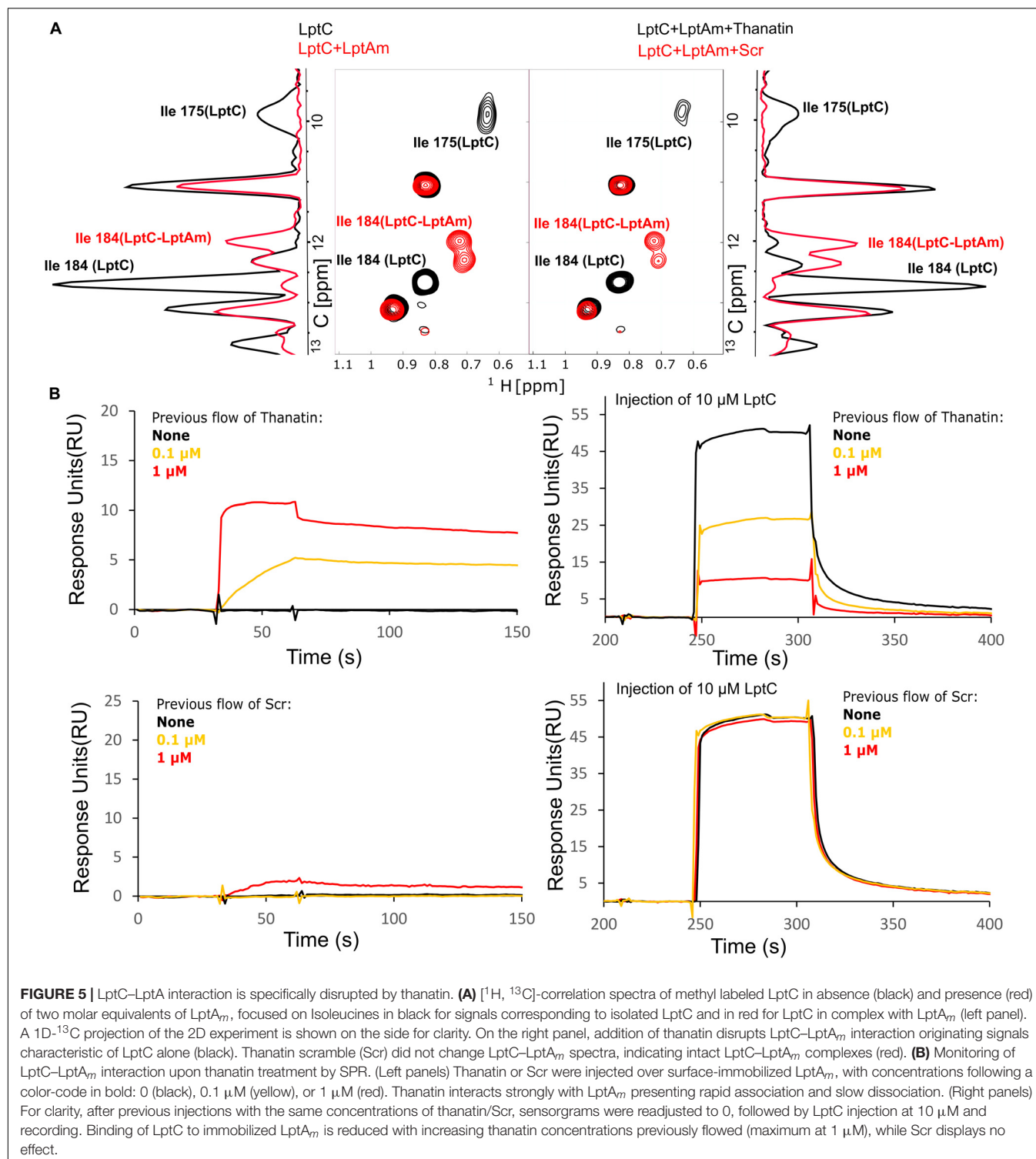
conformational change in the N-terminal region of LptA, which alters the way all these three interactions occur. Since thanatin's binding site overlaps the binding site of LptA with another LptA protein, if the Q62L mutation somehow alters thanatin's binding, then it is possible that it also alters the interaction of LptA^{Q62L} with itself, perhaps by strengthening it.

A similar stabilizing effect is also observed when testing the LptC–LptA_m^{Q62L} combination. However, in this case, the effect is observed only upon treatment with low concentrations of thanatin, since the β-galactosidase signal of non-treated CA* is comparable to that of the WT (Figure 4). This suggests that LptA_m^{Q62L} is still able to bind thanatin and this binding determines a conformational change in the protein that somehow enhances the stability of LptC–LptA_m^{Q62L} complex. At higher thanatin concentrations, however, it seems that the inhibitory effect of the peptide on LptC–LptA_m^{Q62L} prevails over the stabilizing effect. This could be explained by hypothesizing that Q62L mutation in LptA creates a secondary high-affinity binding site for thanatin. According to this hypothesis, when low concentrations of thanatin are added, thanatin binds to the high-affinity site, leaving the binding site for LptC unoccupied (and possibly stabilizing LptC–LptA_m^{Q62L} complex). On the contrary, when higher concentrations of thanatin are used, all the available binding sites are occupied, thus impairing LptC–LptA complex formation.

Thanatin Disrupts LptC–LptA_m Interaction *in vitro*

Thanatin's ability to interfere with LptC–LptA complex formation was assessed by NMR and SPR. For these assays, the monomeric version of LptA (LptA_m) was used to neglect the oligomerization of LptA. ¹H-¹³C NMR of the specifically labeled Isoleucines of LptC efficiently report on the interaction with LptA (Laguri et al., 2017). In particular, Isoleucines 175 (175Ile) and 184 (184Ile) δ1 methyl groups at the C-terminus of LptC and in the vicinity of the binding interface change chemical shifts upon formation of the complex with LptA_m (Figure 5A, left panel). After adding thanatin to the LptC–LptA_m complex, we observed that 175Ile and 184Ile peaks completely shifted to a frequency corresponding to free LptC, indicating a total disruption of LptC–LptA_m dimers (Figure 5A, right panel). The same experiment performed with the thanatin scramble (Scr) showed no disruption of the LptC–LptA_m complex, suggesting specific competition and disruption of the binding interface by the thanatin (Figure 5A, right panel).

Complex disruption was also probed by SPR, in which the surface of a chip was functionalized with LptA_m. First, we confirmed the binding of LptC to the immobilized LptA_m (Supplementary Figure S1A) and we determined the K_d of the interaction (K_d = 80 ± 44 μM). Then, to assess thanatin's effect, we injected thanatin over LptA_m and confirmed stable interaction with LptA_m on the surface, followed by the injection of LptC (Figure 5B, upper panels). We observed that, upon LptC injection, the response values decreased in a dose-dependent manner to the thanatin injected in the system (in concentrations up to 1 μM), indicating fewer surface-free LptA_m epitopes



available to interact with LptC (Figure 5B, upper right panel). The same experiment with the scrambled version showed no or little binding of Scr to immobilized LptA_m and hence no effect on LptC binding (Figure 5B, lower panels), further demonstrating a specific effect of thanatin in preventing the formation of LptC–LptA_m complex.

Thanatin Treatment Results in LptA Degradation and LPS Modification

Depletion of components of the IM and OM Lpt sub-complexes results in LptA degradation, which has been proposed to be a marker of incorrect complex assembly (Sperandeo et al., 2011).

We reasoned that the disruption of LptC–LptA interaction by thanatin treatment could impair Lpt complex assembly. Therefore, we evaluated the LptA steady-state levels in *E. coli* WT cells upon treatment with thanatin. Samples were taken at different time points within 2 h from MG1655 cultures grown in the presence or absence of thanatin at 5.25 $\mu\text{g/mL}$ ($1.5 \times \text{MIC}$) and analyzed by western blotting using anti-LptA antibodies. The abundance of LptD, the OM docking element of LptA, was also assessed and the level of LptB was used as a sample loading control. Culture growth and cell viability were monitored by OD₆₀₀ measurement and determination of CFU, respectively, for a time span of 4 h. In cultures treated with thanatin, we observed a decrease in the OD₆₀₀ with minor effect on cell viability (**Figure 6A**). As shown in **Figure 6B**, substantial LptA degradation occurs within 60 min of incubation with thanatin and, after 120 min, the steady-state level of LptA is very low and almost undetectable with our antibody preparation. The abundance of LptD did not change over time, indicating that the steady-state level of this OM component is not affected by thanatin treatment. The decrease in LptA level suggests that the IM and OM are not properly bridged when cells are treated with thanatin.

Depletion of any Lpt component leads to the accumulation of LPS decorated with colanic acid repeating units at the IM outer leaflet (Ruiz et al., 2008; Sperandeo et al., 2008). This phenotype is diagnostic of defects in Lpt occurring after MsbA-mediated flipping of lipid A-core across the IM. We therefore tested whether treatment with thanatin would induce similar LPS modifications. As shown in **Figure 6C**, LPS decorated with colanic acid, migrating as ladder-like bands in gel electrophoresis, was detected 120 min after adding thanatin to the culture; no LPS modification was observed in untreated cells. These data suggest that thanatin, by disrupting the LptC–LptA interaction, impairs Lpt complex assembly leading to the accumulation of LPS at the periplasmic side of the IM, where it is decorated with colanic acid. The observed LPS profile, together with the LptA degradation kinetic, strongly suggests that the disruption of the Lpt protein bridge could be the major killing mechanism of thanatin against Gram-negative bacteria.

DISCUSSION

The LPS export pathway is a valuable target for novel antibiotic discovery. Murepavadin, a macrocyclic peptidomimetic, has thus far been the most promising antibiotic candidate targeting the Lpt machinery. It was originally identified from a library of structural mimics of class I CAMP (cationic antimicrobial peptide) protegrin and later found to target the β -barrel OM protein LptD (Srinivas et al., 2010; Werneburg et al., 2012; Andolina et al., 2018).

Recent efforts to target the Lpt pathway have led to the identification, through a YTH assay, of IMB-881 as a synthetic molecule inhibiting LptC–LptA interaction (Zhang et al., 2019). The inhibitory activity of IMB-881 further suggests that interfering with the Lpt interactome is a good strategy to prevent Lpt to the cell surface. Nevertheless, in the YTH

system, LptC–LptA interaction occurs in the cytoplasm of a yeast cell, and molecules active in this system may not be able to permeate the bacterial OM. To improve the screening system, we here implemented the BACTH assay (Karimova et al., 1998; Ouellette et al., 2014, 2017) that enables targeting of Lpt protein interactions in their native environment, preserving both protein functionality and folding state. This bacterial two-hybrid technique was used to probe LptC–LptA and LptA–LptA interactions. LptC has an important structural role in the Lpt machinery as it serves as the docking site for LptA binding to the IM LptB₂FGC complex (Sperandeo et al., 2011; Freinkman et al., 2012). Indeed, mutations in LptC compromising interaction with LptA are lethal (Sperandeo et al., 2011; Villa et al., 2013). LptA molecules have a strong tendency to oligomerize in solution (Suits et al., 2008; Merten et al., 2012; Santambrogio et al., 2013) but we still do not know whether LptA self-oligomerization has a physiological relevance, since a monomeric LptA is still able to partially support cell growth (Laguri et al., 2017). In the BACTH assay, LptC–LptA interaction appears stronger than LptA–LptA dimerization, in line with the reported *in vitro* affinities (Schultz et al., 2013); however, we cannot exclude that the observed lower β -galactosidase signal could also be due to the formation of non-productive interactions between LptA molecules fused to the same (T25 or T18) adenylate cyclase fragment. The assay seems robust as no association is detected between unrelated non-interacting proteins: LptC and the maltose periplasmic binding protein MalE (Davidson et al., 1992) or between oligomerization deficient LptA_m proteins (Laguri et al., 2017).

The BACTH system was also employed to explore the mechanism of action of thanatin, an antimicrobial peptide recently shown to bind the first β -strand of LptA (Vetterli et al., 2018). Thanatin inhibits LptC–LptA interaction in a dose-dependent manner, whereas very little and non-dose dependent inhibitory effect is observed against LptA–LptA association. LptA first N-terminal β -strand is a key determinant interacting with the C-terminal region of LptC or the C-terminal region of another LptA in head-to-tail LptA self-oligomerization (Freinkman et al., 2012; Laguri et al., 2017). LptC and LptA share a very similar protein architecture, despite no amino acid sequence similarity (Tran et al., 2010; Villa et al., 2013); indeed, in the LptC–LptA_m complex, LptC precisely occupies the same position as LptA in the LptA oligomer (Laguri et al., 2017). Interestingly, thanatin seems able to discriminate between the two different interactions that LptA is implicated on via its N-terminal region and could, therefore, also serve as a tool to probe the different interactions occurring within the Lpt periplasmic protein bridge. This result is in agreement with earlier data showing that the enantiomeric form of thanatin (D-thanatin) is nearly inactive against Gram-negative strains, suggesting that a stereospecific recognition by a cellular target is required for thanatin to exert its antibacterial effect (Fehlbaum et al., 1996).

A scrambled version of thanatin, that maintains the overall peptide amino acid composition and charge, loses the antibacterial activity, fails to disrupt the LptC–LptA interaction *in vivo* (BACTH assay) and *in vitro* (NMR), and does not bind to LptA_m (SPR analyses). These data further support a specific action of thanatin in binding to LptA and in competing with LptC for the formation of the LptC–LptA complex. Thanatin scramble

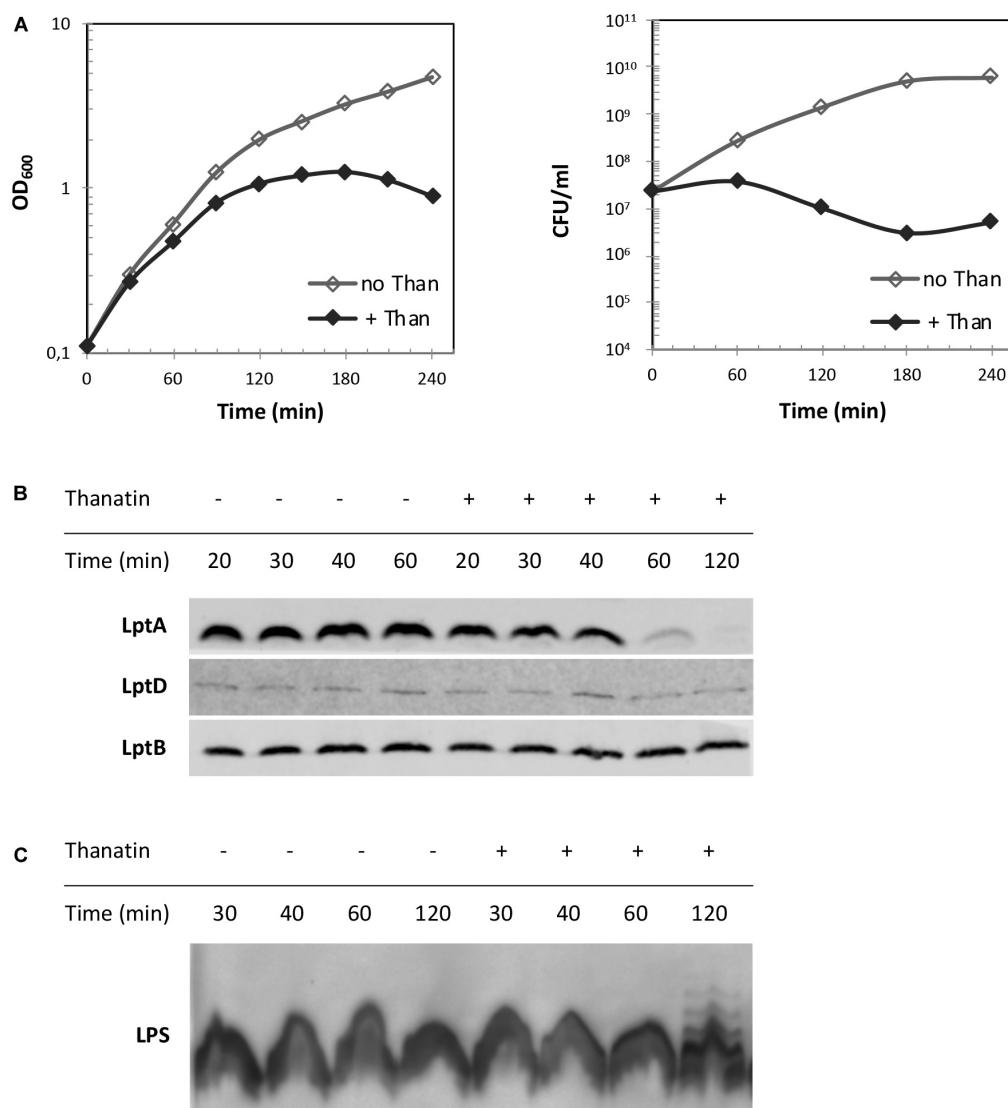


FIGURE 6 | LptA steady-state level and LPS profile upon treatment with thanatin. **(A)** Growth curves of wild type strain MG1655 in the presence (+ Than) and absence (no Than) of thanatin at 5.25 μ g/mL ($1.5 \times$ MIC) concentration. Growth was monitored by measuring the OD₆₀₀ (left panel) and by determining CFU/mL (right panel). **(B)** Western blot analysis to reveal LptA steady-state levels. Samples were collected 20, 30, 40, 60, and 120 min after treatment with thanatin. Whole-cell extracts were prepared and analyzed by western blot with anti-LptA, anti-LptD, anti-LptB (as loading control) antibodies. An equal amount of cells (0.36 OD₆₀₀ units) was loaded into each lane. **(C)** Western blot analysis to reveal LPS profiles. Whole-cell extracts obtained 30, 40, 60, and 120 min after treatment with thanatin were incubated with proteinase K and analyzed by western blot with anti-LPS antibodies. An equal amount of cells (0.48 OD₆₀₀) was loaded into each lane. Results shown are representative of three independent experiments.

does not display antibacterial activity against permeabilized *E. coli* strains, strongly suggesting that the lack of activity of the scrambled peptide is not due to its inability to reach its target in the periplasm.

It has been reported that *E. coli* cells carrying LptA^{Q62L} amino acid substitution become resistant to thanatin (Vetterli et al., 2018). Residue Q62 does not appear to be implicated in thanatin binding and the mechanism underlying resistance is still unknown. LptC–LptA^{Q62L} interaction is not inhibited by thanatin in the BACTH assay and, surprisingly, it appears stronger in the presence of the peptide. In the case of the

interaction between LptA^{Q62L} mutant proteins, the dimerization seems stronger than that observed between WT LptA, even in the absence of thanatin. We can speculate that Q62L mutation somehow alters the stability of both LptC–LptA and LptA–LptA complexes, affecting the binding of thanatin to LptA. However, it is difficult to explain these results since neither the effect of the Q62L substitution on LptA structure nor the mechanism of thanatin resistance are known.

Previous *in vitro* data revealed that besides LptA, thanatin binds to the LptDE complex in the low nanomolar range and, furthermore, its binding site in LptA has been shown by

modeling studies to be highly conserved in the periplasmic domain of LptD (Robinson, 2019). This suggests that thanatin can inhibit multiple protein–protein interactions required for the Lpt complex assembly. It was not possible to test the periplasmic domain of LptD in the BACTH assay, since expression of a folded and functional LptD is strictly dependent on the expression and interaction with LptE (Chng et al., 2010). Nevertheless, the isolation of suppressor mutants exclusively at the N-terminal region of LptA (Vetterli et al., 2018), that is not involved in the LptA–LptD interaction, and the ability of the LptA_m mutant protein, lacking the C-terminal β -strand implicated in both LptA–LptA and LptA–LptD interactions, to partially support the cell growth (Laguri et al., 2017) suggest that LptC–LptA interaction is thanatin's main target.

Thanatin has been related to the group of CAMPs that kill bacteria by cell agglutination. In the host organism, this class of antimicrobial peptides does not permeabilize bacterial cell membranes but rather interacts with LPS or peptidoglycan, favoring cell aggregation and bacterial removal by phagocytosis (Shai, 2002; Jung et al., 2012; Pulido et al., 2012). Thanatin has indeed been shown to bind LPS *in vitro* and promote cell agglutination as a result of cell surface charge neutralization (Sinha et al., 2017). Recently, the comparison of thanatin's affinity to LPS relative to Ca^{2+} and Mg^{2+} revealed that thanatin displaces divalent cations from LPS *in vivo* promoting LPS shedding from bacterial cells at concentrations 10-fold higher than the MIC, increasing OM permeability (Ma et al., 2019). Interestingly, the same study reports that thanatin is able to inhibit the enzymatic activity of New Delhi metallo- β -lactamase-1 (NMD-1), responsible for the resistance to β -lactam antibiotics in several multidrug resistant strains, by binding to the active site of the enzyme with higher affinity than Zn^{2+} , displacing it and reversing carbapenem resistance. This evidences that, alongside a killing effect on Gram-negative pathogens based on OM permeabilization, thanatin may help restoring the activity of β -lactam antibiotics in multidrug resistant pathogens (Ma et al., 2019).

In the reported BACTH assay, inhibition of LptC–LptA interaction is observed at sub-MIC concentrations of thanatin, a condition that does not inhibit the growth of cells expressing LptC and LptA_m protein fusions. Based on our data, we propose that LPS binding is employed by thanatin as a self-promoted mechanism of entry in the periplasm of bacterial cells where the LptA target resides. Supporting this hypothesis is the finding of a mutated version of thanatin, where Arg 13 and Arg 14 residues have been substituted by Ala, that presents reduced LPS binding affinity and loses the antibacterial activity (Sinha et al., 2017).

In *E. coli* cells treated with thanatin, LptA undergoes degradation and LPS is decorated with colanic acid. Notably, these phenotypes are observed in cells where LPS export machinery disassembles and transport of LPS molecules is impaired due to mutations in any of the Lpt complex components (Sperandeo et al., 2008, 2011). These data suggest that the main mechanism of action of thanatin occurring at MIC concentration is the disassembly of the Lpt machinery and consequently the blocking of LPS transport.

Overall, our results highlight OM biogenesis as an excellent target for novel antibiotic discovery. Thanatin joins the

increasing list of molecules that disrupt the assembly of the OM with diverse mechanisms (Hart et al., 2019; Imai et al., 2019; Lehman and Grabowicz, 2019; Psonis et al., 2019). Based on their mechanisms, these compounds could be employed not only to fight multidrug resistant pathogens but also in combination with existing antibiotics not sufficiently effective.

DATA AVAILABILITY STATEMENT

All datasets generated for this study are included in the article/Supplementary Material.

AUTHOR CONTRIBUTIONS

EM performed the BACTH assays and *in vivo* experiments. TB and CL performed NMR and SPR experiments. AR and EE designed and synthesized the peptides. AP, PS, AM, and EM designed the *in vivo* experiments. J-PS, CL, and TB designed the NMR and SPR experiments. EM, AP, PS, CL, TB, and AR wrote the manuscript. All the authors reviewed and approved the manuscript.

FUNDING

AP, J-PS, CL, TB, and EM were supported by the Train2Target project granted from the European Union's Horizon 2020 Research and Innovation Program under the Marie Skłodowska-Curie grant agreement #721484. PS was supported by the Italian Ministry of Education, University and Research, (FABBR)-MIUR 2017, Funding for the financing of basic research activities.

ACKNOWLEDGMENTS

This work used the platforms of the Grenoble Instruct-ERIC center (ISBG; UMS 3518 CNRS-CEA-UGA-EMBL) within the Grenoble Partnership for Structural Biology (PSB), supported by FRISBI (ANR-10-INBS-05-02) and GRAL, financed within the University Grenoble Alpes graduate school (Ecoles Universitaires de Recherche) CBH-EUR-GS (ANR-17-EURE-0003). The authors acknowledge the SPR/BLI platform personal, Jean-Baptiste REISER Ph.D., and Anne Chouquet, for their help and assistance.

SUPPLEMENTARY MATERIAL

The Supplementary Material for this article can be found online at: <https://www.frontiersin.org/articles/10.3389/fmicb.2020.00909/full#supplementary-material>

FIGURE S1 | SPR of LptC–LptA_m interaction and its disruption by thanatin. **(A)** Determination of LptC–LptA_m dissociation constant. Left panel: Sensorgrams of LptC injected at different concentrations over immobilized LptA_m. Right panel: Steady-state analysis of LptC–LptA_m interaction. **(B)** Raw Sensorgrams of the data presented in **Figure 5B**.

REFERENCES

- Andolina, G., Bencze, L. C., Zerbe, K., Muller, M., Steinmann, J., Kocherla, H., et al. (2018). A peptidomimetic antibiotic interacts with the periplasmic domain of LptD from *Pseudomonas aeruginosa*. *ACS Chem Biol.* 13, 666–675. doi: 10.1021/acscchembio.7b00822
- Avitabile, C., Diaferia, C., Roviello, V., Altamura, D., Giannini, C., Vitagliano, L., et al. (2019). Fluorescence and morphology of self-assembled nucleobases and their diphenylalanine hybrid aggregates. *Chemistry* 25, 14850–14857. doi: 10.1002/chem.201902709
- Battesti, A., and Bouveret, E. (2012). The bacterial two-hybrid system based on adenylate cyclase reconstitution in *Escherichia coli*. *Methods* 58, 325–334. doi: 10.1016/j.ymeth.2012.07.018
- Blattner, F. R., Plunkett, G., Bloch, C. A., Perna, N. T., Burland, V., Riley, M., et al. (1997). The complete genome sequence of *Escherichia coli* K-12. *Science* 277, 1453–1462. doi: 10.1126/science.277.5331.1453
- Chng, S. S., Ruiz, N., Chimalakonda, G., Silhavy, T. J., and Kahne, D. (2010). Characterization of the two-protein complex in *Escherichia coli* responsible for lipopolysaccharide assembly at the outer membrane. *Proc. Natl. Acad. Sci. U.S.A.* 107, 5363–5368. doi: 10.1073/pnas.0912872107
- Davidson, A. L., Shuman, H. A., and Nikaido, H. (1992). Mechanism of maltose transport in *Escherichia coli*: transmembrane signaling by periplasmic binding proteins. *Proc. Natl. Acad. Sci. U.S.A.* 89, 2360–2364. doi: 10.1073/pnas.89.6.2360
- Doerfler, W. T., Gibbons, H. S., and Raetz, C. R. (2004). MsbA-dependent translocation of lipids across the inner membrane of *Escherichia coli*. *J. Biol. Chem.* 279, 45102–45109. doi: 10.1074/jbc.M408106200
- Dong, H., Xiang, Q., Gu, Y., Wang, Z., Paterson, N. G., Stansfeld, P. J., et al. (2014). Structural basis for outer membrane lipopolysaccharide insertion. *Nature* 511, 52–56. doi: 10.1038/nature13464
- Ehrmann, M., Ehrle, R., Hofmann, E., Boos, W., and Schlosser, A. (1998). The ABC maltose transporter. *Mol. Microbiol.* 29, 685–694. doi: 10.1046/j.1365-2958.1998.00915.x
- Falchi, F. A., Maccagni, E. A., Puccio, S., Peano, C., De Castro, C., Palmigiano, A., et al. (2018). Mutation and suppressor analysis of the essential lipopolysaccharide transport protein LptA reveals strategies to overcome severe outer membrane permeability defects in *Escherichia coli*. *J. Bacteriol.* 200:e487–17. doi: 10.1128/jb.00487-17
- Fehlbaum, P., Bulet, P., Chernysh, S., Briand, J. P., Roussel, J. P., Letellier, L., et al. (1996). Structure-activity analysis of thanatin, a 21-residue inducible insect defense peptide with sequence homology to frog skin antimicrobial peptides. *Proc. Natl. Acad. Sci. U.S.A.* 93, 1221–1225. doi: 10.1073/pnas.93.3.1221
- Freinkman, E., Chng, S. S., and Kahne, D. (2011). The complex that inserts lipopolysaccharide into the bacterial outer membrane forms a two-protein plug-and-barrel. *Proc. Natl. Acad. Sci. U.S.A.* 108, 2486–2491. doi: 10.1073/pnas.1015617108
- Freinkman, E., Okuda, S., Ruiz, N., and Kahne, D. (2012). Regulated assembly of the transenvelope protein complex required for lipopolysaccharide export. *Biochemistry* 51, 4800–4806. doi: 10.1021/bi300592c
- Hart, E. M., Mitchell, A. M., Konovalova, A., Grabowicz, M., Sheng, J., Han, X., et al. (2019). A small-molecule inhibitor of BamA impervious to efflux and the outer membrane permeability barrier. *Proc. Natl. Acad. Sci. U.S.A.* 116, 21748–21757. doi: 10.1073/pnas.1912345116
- Ho, H., Miu, A., Alexander, M. K., Garcia, N. K., Oh, A., Zilberleyb, I., et al. (2018). Structural basis for dual-mode inhibition of the ABC transporter MsbA. *Nature* 557, 196–201. doi: 10.1038/s41586-018-0083-5
- Imai, Y., Meyer, K. J., Iinishi, A., Favre-Godal, Q., Green, R., Manuse, S., et al. (2019). A new antibiotic selectively kills Gram-negative pathogens. *Nature* 576, 459–464. doi: 10.1038/s41586-019-1791-1
- Jung, S., Sonnichsen, F. D., Hung, C. W., Tholey, A., Boidin-Wichlacz, C., Haeusgen, W., et al. (2012). Macin family of antimicrobial proteins combines antimicrobial and nerve repair activities. *J. Biol. Chem.* 287, 14246–14258. doi: 10.1074/jbc.M111.336495
- Karimova, G., Pidoux, J., Ullmann, A., and Ladant, D. (1998). A bacterial two-hybrid system based on a reconstituted signal transduction pathway. *Proc. Natl. Acad. Sci. U.S.A.* 95, 5752–5756. doi: 10.1073/pnas.95.10.5752
- Kerfah, R., Plevin, M. J., Sounier, R., Gans, P., and Boissbouvier, J. (2015). Methyl-specific isotopic labeling: a molecular tool box for solution NMR studies of large proteins. *Curr. Opin. Struct. Biol.* 32, 113–122. doi: 10.1016/j.sbi.2015.03.009
- Laguri, C., Sperandeo, P., Pounot, K., Ayala, I., Silipo, A., Bougault, C. M., et al. (2017). Interaction of lipopolysaccharides at intermolecular sites of the periplasmic Lpt transport assembly. *Sci. Rep.* 7:9715. doi: 10.1038/s41598-017-10136-0
- Lehman, K. M., and Grabowicz, M. (2019). Countering gram-negative antibiotic resistance: recent progress in disrupting the outer membrane with novel therapeutics. *Antibiotics (Basel.)* 8:E163. doi: 10.3390/antibiotics8040163
- Lesse, A. J., Campagnari, A. A., Bittner, W. E., and Apicella, M. A. (1990). Increased resolution of lipopolysaccharides and lipooligosaccharides utilizing tricine-sodium dodecyl sulfate-polyacrylamide gel electrophoresis. *J. Immunol. Methods* 126, 109–117.
- Li, Y., Orlando, B. J., and Liao, M. (2019). Structural basis of lipopolysaccharide extraction by the LptB2FGC complex. *Nature* 567, 486–490. doi: 10.1038/s41586-019-1025-6
- Ma, B., Fang, C., Lu, L., Wang, M., Xue, X., Zhou, Y., et al. (2019). The antimicrobial peptide thanatin disrupts the bacterial outer membrane and inactivates the NDM-1 metallo-beta-lactamase. *Nat. Commun.* 10:3517. doi: 10.1038/s41467-019-11503-3
- Majdalani, N., and Gottesman, S. (2005). The Rcs phosphorelay: a complex signal transduction system. *Annu. Rev. Microbiol.* 59, 379–405. doi: 10.1146/annurev.micro.59.050405.101230
- Merten, J. A., Schultz, K. M., and Klug, C. S. (2012). Concentration-dependent oligomerization and oligomeric arrangement of LptA. *Protein Sci.* 21, 211–218. doi: 10.1002/pro.2004
- Nikaido, H. (2003). Molecular Basis of Bacterial Outer Membrane Permeability Revisited. *Microbiol. Mol. Biol. Rev.* 67, 593–656. doi: 10.1128/mmbr.67.4.593-656.2003
- Okuda, S., Freinkman, E., and Kahne, D. (2012). Cytoplasmic ATP hydrolysis powers transport of lipopolysaccharide across the periplasm in *E. coli*. *Science* 338, 1214–1217. doi: 10.1126/science.1228984
- Okuda, S., Sherman, D. J., Silhavy, T. J., Ruiz, N., and Kahne, D. (2016). Lipopolysaccharide transport and assembly at the outer membrane: the PEZ model. *Nat. Rev. Microbiol.* 14, 337–345. doi: 10.1038/nrmicro.2016.25
- Ouellette, S. P., Gauliard, E., Antosova, Z., and Ladant, D. (2014). A gateway((R))-compatible bacterial adenylate cyclase-based two-hybrid system. *Environ. Microbiol. Rep.* 6, 259–267. doi: 10.1111/1758-2229.12123
- Ouellette, S. P., Karimova, G., Davi, M., and Ladant, D. (2017). Analysis of membrane protein interactions with a bacterial adenylate cyclase-based two-hybrid (BACTH) technique. *Curr. Protoc. Mol. Biol.* 118, 21–20. doi: 10.1002/cpm.36
- Owens, T. W., Taylor, R. J., Pahil, K. S., Bertani, B. R., Ruiz, N., Kruse, A. C., et al. (2019). Structural basis of unidirectional export of lipopolysaccharide to the cell surface. *Nature* 567, 550–553. doi: 10.1038/s41586-019-1039-0
- Paschos, A., den Hartigh, A., Smith, M. A., Atluri, V. L., Sivanesan, D., Tsois, R. M., et al. (2011). An in vivo high-throughput screening approach targeting the type IV secretion system component VirB8 identified inhibitors of *Brucella abortus* 2308 proliferation. *Infect. Immun.* 79, 1033–1043. doi: 10.1128/iai.00993-10
- Polissi, A., and Georgopoulos, C. (1996). Mutational analysis and properties of the msbA gene of *Escherichia coli*, coding for an essential ABC family transporter. *Mol. Microbiol.* 20, 1221–1233.
- Psonis, J. J., Chahales, P., Henderson, N. S., Rigel, N. W., Hoffman, P. S., and Thanassi, D. G. (2019). The small molecule nitazoxanide selectively disrupts BAM-mediated folding of the outer membrane usher protein. *J. Biol. Chem.* 294, 14357–14369. doi: 10.1074/jbc.RA119.009616
- Pulido, D., Moussaoui, M., Andreu, D., Nogues, M. V., Torrent, M., and Boix, E. (2012). Antimicrobial action and cell agglutination by the eosinophil cationic protein are modulated by the cell wall lipopolysaccharide structure. *Antimicrob. Agents Chemother.* 56, 2378–2385. doi: 10.1128/aac.06107-11
- Qiao, S., Luo, Q., Zhao, Y., Zhang, X. C., and Huang, Y. (2014). Structural basis for lipopolysaccharide insertion in the bacterial outer membrane. *Nature* 511, 108–111. doi: 10.1038/nature13484
- Raetz, C. R., and Whitfield, C. (2002). Lipopolysaccharide endotoxins. *Annu. Rev. Biochem.* 71, 635–700. doi: 10.1146/annurev.biochem.71.110601.135414

- Robinson, J. A. (2019). Folded synthetic peptides and other molecules targeting outer membrane protein complexes in gram-negative bacteria. *Front. Chem.* 7:45. doi: 10.3389/fchem.2019.00045
- Ruiz, N., Falcone, B., Kahne, D., and Silhavy, T. J. (2005). Chemical conditionality: a genetic strategy to probe organelle assembly. *Cell* 121, 307–317. doi: 10.1016/j.cell.2005.02.014
- Ruiz, N., Gronenberg, L. S., Kahne, D., and Silhavy, T. J. (2008). Identification of two inner-membrane proteins required for the transport of lipopolysaccharide to the outer membrane of *Escherichia coli*. *Proc. Natl. Acad. Sci. U.S.A.* 105, 5537–5542. doi: 10.1073/pnas.0801196105
- Santambrogio, C., Sperandio, P., Villa, R., Sobott, F., Polissi, A., and Grandori, R. (2013). LptA assembles into rod-like oligomers involving disorder-to-order transitions. *J. Am. Soc. Mass Spectrom.* 24, 1593–1602. doi: 10.1007/s13361-013-0687-9
- Schultz, K. M., Feix, J. B., and Klug, C. S. (2013). Disruption of LptA oligomerization and affinity of the LptA-LptC interaction. *Protein Sci.* 22, 1639–1645. doi: 10.1002/pro.2369
- Sekiguchi, M., and Iida, S. (1967). Mutants of *Escherichia coli* permeable to actinomycin. *Proc. Natl. Acad. Sci. U.S.A.* 58, 2315–2320. doi: 10.1073/pnas.58.6.2315
- Shai, Y. (2002). Mode of action of membrane active antimicrobial peptides. *Biopolymers* 66, 236–248. doi: 10.1002/bip.10260
- Silhavy, T. J., Kahne, D., and Walker, S. (2010). The bacterial cell envelope. *Cold Spring Harb. Perspect. Biol.* 2:a000414. doi: 10.1101/cshperspect.a000414
- Simpson, B. W., and Trent, M. S. (2019). Pushing the envelope: LPS modifications and their consequences. *Nat. Rev. Microbiol.* 17, 403–416. doi: 10.1038/s41579-019-0201-x
- Sinha, S., Zheng, L., Mu, Y., Ng, W. J., and Bhattacharjya, S. (2017). Structure and interactions of A host defense antimicrobial peptide thanatin in lipopolysaccharide micelles reveal mechanism of bacterial cell agglutination. *Sci. Rep.* 7:17795. doi: 10.1038/s41598-017-18102-6
- Sperandio, P., Cescutti, R., Villa, R., Di Benedetto, C., Candia, D., Deho, G., et al. (2007). Characterization of lptA and lptB, two essential genes implicated in lipopolysaccharide transport to the outer membrane of *Escherichia coli*. *J. Bacteriol.* 189, 244–253. doi: 10.1128/jb.01126-06
- Sperandio, P., Lau, F. K., Carpentieri, A., De Castro, C., Molinaro, A., Deho, G., et al. (2008). Functional analysis of the protein machinery required for transport of lipopolysaccharide to the outer membrane of *Escherichia coli*. *J. Bacteriol.* 190, 4460–4469. doi: 10.1128/jb.00270-08
- Sperandio, P., Martorana, A. M., and Polissi, A. (2019). The Lpt ABC transporter for lipopolysaccharide export to the cell surface. *Res. Microbiol.* 170, 366–373. doi: 10.1016/j.resmic.2019.07.005
- Sperandio, P., Villa, R., Martorana, A. M., Samalikova, M., Grandori, R., Deho, G., et al. (2011). New insights into the Lpt machinery for lipopolysaccharide transport to the cell surface: LptA-LptC interaction and LptA stability as sensors of a properly assembled transenvelope complex. *J. Bacteriol.* 193, 1042–1053. doi: 10.1128/jb.01037-10
- Srinivas, N., Jetter, P., Ueberbacher, B. J., Werneburg, M., Zerbe, K., Steinmann, J., et al. (2010). Peptidomimetic antibiotics target outer-membrane biogenesis in *Pseudomonas aeruginosa*. *Science* 327, 1010–1013. doi: 10.1126/science.1182749
- Studier, F. W., and Moffatt, B. A. (1986). Use of bacteriophage T7 RNA polymerase to direct selective high-level expression of cloned genes. *J. Mol. Biol.* 189, 113–130.
- Suits, M. D. L., Sperandio, P., Dehò, G., Polissi, A., and Jia, Z. (2008). Novel structure of the conserved gram-negative lipopolysaccharide transport protein A and mutagenesis analysis. *J. Mol. Biol.* 380, 476–488. doi: 10.1016/j.jmb.2008.04.045
- Tacconelli, E., Carrara, E., Savoldi, A., Harbarth, S., Mendelson, M., Monnet, D. L., et al. (2018). Discovery, research, and development of new antibiotics: the WHO priority list of antibiotic-resistant bacteria and tuberculosis. *Lancet Infect. Dis.* 18, 318–327. doi: 10.1016/s1473-3099(17)30753-3
- Tran, A. X., Dong, C., and Whitfield, C. (2010). Structure and functional analysis of LptC, a conserved membrane protein involved in the lipopolysaccharide export pathway in *Escherichia coli*. *J. Biol. Chem.* 285, 33529–33539. doi: 10.1074/jbc.M110.144709
- Vetterli, S. U., Zerbe, K., Muller, M., Urfer, M., Mondal, M., Wang, S., et al. (2018). Thanatin targets the intermembrane protein complex required for lipopolysaccharide transport in *Escherichia coli*. *Sci. Adv.* 4:eau2634. doi: 10.1126/sciadv.aau2634
- Villa, R., Martorana, A. M., Okuda, S., Gourlay, L. J., Nardini, M., Sperandio, P., et al. (2013). The *Escherichia coli* Lpt transenvelope protein complex for lipopolysaccharide export is assembled via conserved structurally homologous domains. *J. Bacteriol.* 195, 1100–1108. doi: 10.1128/jb.02057-12
- Werneburg, M., Zerbe, K., Juhas, M., Bigler, L., Stalder, U., Kaech, A., et al. (2012). Inhibition of lipopolysaccharide transport to the outer membrane in *Pseudomonas aeruginosa* by peptidomimetic antibiotics. *Chembiochem* 13, 1767–1775. doi: 10.1002/cbic.201200276
- Wiegand, I., Hilpert, K., and Hancock, R. E. (2008). Agar and broth dilution methods to determine the minimal inhibitory concentration (MIC) of antimicrobial substances. *Nat. Protoc.* 3, 163–175. doi: 10.1038/nprot.2007.521
- Wu, T., McCandlish, A. C., Gronenberg, L. S., Chng, S. S., Silhavy, T. J., and Kahne, D. (2006). Identification of a protein complex that assembles lipopolysaccharide in the outer membrane of *Escherichia coli*. *Proc. Natl. Acad. Sci. U.S.A.* 103, 11754–11759. doi: 10.1073/pnas.0604744103
- Zhang, G., Baidin, V., Pahil, K. S., Moison, E., Tomasek, D., Ramadoss, N. S., et al. (2018). Cell-based screen for discovering lipopolysaccharide biogenesis inhibitors. *Proc. Natl. Acad. Sci. U.S.A.* 115, 6834–6839. doi: 10.1073/pnas.1804670115
- Zhang, X., Li, Y., Wang, W., Zhang, J., Lin, Y., Hong, B., et al. (2019). Identification of an anti-Gram-negative bacteria agent disrupting the interaction between lipopolysaccharide transporters LptA and LptC. *Int. J. Antimicrob. Agents* 53, 442–448. doi: 10.1016/j.ijantimicag.2018.11.016

Conflict of Interest: The authors declare that the research was conducted in the absence of any commercial or financial relationships that could be construed as a potential conflict of interest.

Copyright © 2020 Moura, Baeta, Romanelli, Laguri, Martorana, Erba, Simorre, Sperandio and Polissi. This is an open-access article distributed under the terms of the Creative Commons Attribution License (CC BY). The use, distribution or reproduction in other forums is permitted, provided the original author(s) and the copyright owner(s) are credited and that the original publication in this journal is cited, in accordance with accepted academic practice. No use, distribution or reproduction is permitted which does not comply with these terms.



An *in vitro* Reconstructed Human Skin Equivalent Model to Study the Role of Skin Integration Around Percutaneous Devices Against Bacterial Infection

Eleonore C. L. Bolle^{1,2,3}, Anthony D. Verderosa³, Rabeb Dhouib³, Tony J. Parker¹, John F. Fraser², Tim R. Dargaville¹ and Makrina Totsika^{3*}

OPEN ACCESS

Edited by:

Paolo Landini,
University of Milan, Italy

Reviewed by:

Adam Jorgensen,
Wake Forest Institute for Regenerative
Medicine, United States
Marco Rinaldo Oggioni,
University of Leicester,
United Kingdom

*Correspondence:

Makrina Totsika
makrina.totsika@qut.edu.au;
makrina.totsika@qut.edu.au

Specialty section:

This article was submitted to
Antimicrobials, Resistance
and Chemotherapy,
a section of the journal
Frontiers in Microbiology

Received: 23 December 2019

Accepted: 24 March 2020

Published: 14 May 2020

Citation:

Bolle ECL, Verderosa AD,
Dhouib R, Parker TJ, Fraser JF,
Dargaville TR and Totsika M (2020) An
in vitro Reconstructed Human Skin
Equivalent Model to Study the Role
of Skin Integration Around
Percutaneous Devices Against
Bacterial Infection.
Front. Microbiol. 11:670.
doi: 10.3389/fmicb.2020.00670

¹ Tissue Repair and Translational Physiology Program, Institute of Health and Biomedical Innovation, Queensland University of Technology, Brisbane, QLD, Australia, ² The Innovative Cardiovascular Engineering and Technology Laboratory, Critical Care Research Group, The Prince Charles Hospital, Brisbane, QLD, Australia, ³ Infection and Immunity Research Program, Institute of Health and Biomedical Innovation, School of Biomedical Sciences, Faculty of Health, Queensland University of Technology, Brisbane, QLD, Australia

Percutaneous devices are a key technology in clinical practice, used to connect internal organs to external medical devices. Examples include prosthesis, catheters and electrical drivelines. Percutaneous devices breach the skin's natural barrier and create an entry point for pathogens, making device infections a widespread problem. Modification of the percutaneous implant surface to increase skin integration with the aim to reduce subsequent infection is attracting a great deal of attention. While novel surfaces have been tested in various *in vitro* models used to study skin integration around percutaneous devices, no skin model has been reported, for the study of bacterial infection around percutaneous devices. Here, we report the establishment of an *in vitro* human skin equivalent model for driveline infections caused by *Staphylococcus aureus*, the most common cause of driveline-related infections. Three types of mock drivelines manufactured using melt electrowriting (smooth or porous un-seeded and porous pre-seeded with human fibroblasts) were implanted in human skin constructs and challenged with *S. aureus*. Our results show a high and stable load of *S. aureus* in association with the skin surface and no signs of *S. aureus*-induced tissue damage. Furthermore, our results demonstrate that bacterial migration along the driveline surface occurs in micro-gaps caused by insufficient skin integration between the driveline and the surrounding skin consistent with clinical reports from explanted patient drivelines. Thus, the human skin-driveline infection model presented here provides a clinically-relevant and versatile experimental platform for testing novel device surfaces and infection therapeutics.

Keywords: *Staphylococcus aureus*, 3D skin models, tissue engineered skin, melt electrowriting, percutaneous implant, driveline infections

INTRODUCTION

Percutaneous devices are routinely used in medicine to connect internal organs to external medical devices or their components. Examples include drivelines for the transmission of electrical currents to ventricular assist devices (VADs), urinary peritoneal and vascular catheters for the transfer of fluids, or bone prostheses for the transfer of forces (von Recum, 1984). VADs are a type of mechanical circulatory support used in heart failure therapy. They are attached to the heart and assist the heart in generating sufficient output to ensure adequate end organ perfusion (Koval and Stosor, 2019). VADs are powered and controlled through an external battery pack and controller unit. The connection between the pump and the battery pack and controller unit is maintained via a driveline, which contains insulated wires to carry current and telemetric data (Feldmann et al., 2018). In the United States alone, a minimum of 2,500 patients are added to the patient registry for mechanical circulatory support in any given year (Kirklin et al., 2017). Percutaneous devices, such as drivelines, cross the skin through a surgical incision and disrupt the skin's natural barrier creating an entry point for pathogens (von Recum, 1984). Thus, infections around percutaneous devices are highly prevalent with recent studies reporting catheter infection rates to be in the range of 2–33% over the life of the device, depending on the type of catheter (Salwiczek et al., 2014).

Driveline infections, in particular, account for 83% of ventricular assist device-specific infections, with incidence rates of 1.31 and 1.42 driveline infections per 100 patient months at 3 month pre- and post-device implantation, respectively (INTERMACS, 2015). More importantly, driveline infections are associated with an impaired clinical outcome, with patient survival rates only 76% by 24 month after the first driveline infection (Hannan et al., 2019). Driveline infections are primarily caused by bacteria, with fungal infections also reported less frequently (Hannan et al., 2019; Koval and Stosor, 2019). Gram-positive bacteria from the *Staphylococcus* genus are the most common causative agents, with *Staphylococcus aureus* accounting for 28–44% of all driveline infections (Koval and Stosor, 2019).

The most common drivelines currently in clinical practice are made from a smooth material (silicone or polyurethane, depending on the manufacturer) and surrounded by a porous poly(ethylene terephthalate) sleeve, commercialized as Dacron™. The purpose of the Dacron™ sleeve is to increase tissue integration and prevent pathogen entry. While manufacturer guidelines recommend that the Dacron™ sleeve should be implanted so that it interfaces with the skin at the exit site, recent studies have demonstrated significantly reduced infection rates with the Dacron™ implanted subcutaneously and the smooth section of the driveline crossing the skin instead (Singh et al., 2012; Dean et al., 2015; McCandless et al., 2015; Camboni et al., 2016).

Despite clinical findings demonstrating reduced infection rates when smooth driveline sections cross the skin, there is evidence that smooth surfaces do not allow for sufficient skin integration, thus leading to the formation of a sinus tract around the implant (Winter, 1974; von Recum and Park, 1981;

Isackson et al., 2011). A sinus tract is formed by the epidermal layer migrating downwards parallel to the device, in an attempt to restore epidermal continuity (von Recum, 1984). The epidermal downwards migration can be reduced by increasing skin integration into the implant through the inclusion of pores to the surface of the percutaneous implant (Winter, 1974; Fukano et al., 2010). The prevailing opinion in the field of percutaneous devices is that increased skin and tissue integration will in turn create a tighter biological seal at the device exit site against invading pathogens and thus decrease infection rates (von Recum, 1984; Tagusari et al., 1998; Choi et al., 1999; Fukano et al., 2010; Isackson et al., 2011).

We have previously shown that porous scaffolds manufactured by melt electrowriting (MEW), an additive manufacturing technique, supports fibroblasts growth (Farrugia et al., 2013) and increases skin integration compared to smooth tubes in a 3D reconstructed human skin equivalent (HSE) model. Moreover, pre-seeding the porous scaffolds with human dermal fibroblasts prior to device implantation in HSEs appeared to reduce epidermal downgrowth, compared to un-seeded porous implants (Bolle et al., 2019). Based on these findings, the aim of the present study was to investigate whether increased skin integration around MEW porous implants can create a better biological seal against pathogen entry. Using a reconstructed HSE model, this is the first study to investigate *S. aureus* driveline-specific infections and provides a versatile *in vitro* platform for the detailed investigation of factors contributing to this significant clinical challenge worldwide.

MATERIALS AND METHODS

Keratinocyte and Fibroblast Cell Isolation and Culture

Keratinocytes were isolated from human skin samples obtained from patients undergoing abdominoplasty surgery and breast reduction surgery (Xie et al., 2010) and cultured according to previously published protocols (Rheinwald and Green, 1975; Dawson et al., 2006; Haridas et al., 2016). In brief, following an enzyme digestion overnight in 0.125% trypsin (Invitrogen, Australia) the epidermal layer was separated from the dermal layer. Keratinocytes were isolated from the epidermal layer and cultured on a layer of irradiated 3T3 fibroblasts in keratinocyte growth medium (Invitrogen, Australia). Fibroblasts were isolated from the dermis and cultured in fibroblasts growth medium, as previously described (Haridas et al., 2016).

3D Reconstructed Human Skin Equivalent Preparation and Culture

The de-epidermised dermis (DED) was prepared following protocols described by Chakrabarty et al. (1999) and Dawson et al. (2006). The DEDs were between approximately 15 × 15 mm and 20 × 20 mm in size and were stored at 4°C in antibiotic/antimycotic medium consisting of DMEM supplemented with 1% v/v penicillin/streptomycin

(Invitrogen). Skin constructs, referred to hereafter as HSEs, were generated as described previously (McGovern et al., 2013; Bolle et al., 2019). Briefly, 3.6×10^4 keratinocytes and 1.8×10^4 fibroblasts were seeded onto the DEDs through a stainless-steel ring with an inner diameter of 9 mm and lifted at the air liquid interface 48 h post seeding (**Figure 1**). HSEs were cultured in keratinocyte growth medium with fresh medium replaced every 48 h. DEDs and cells were not patient-matched.

Driveline Manufacture

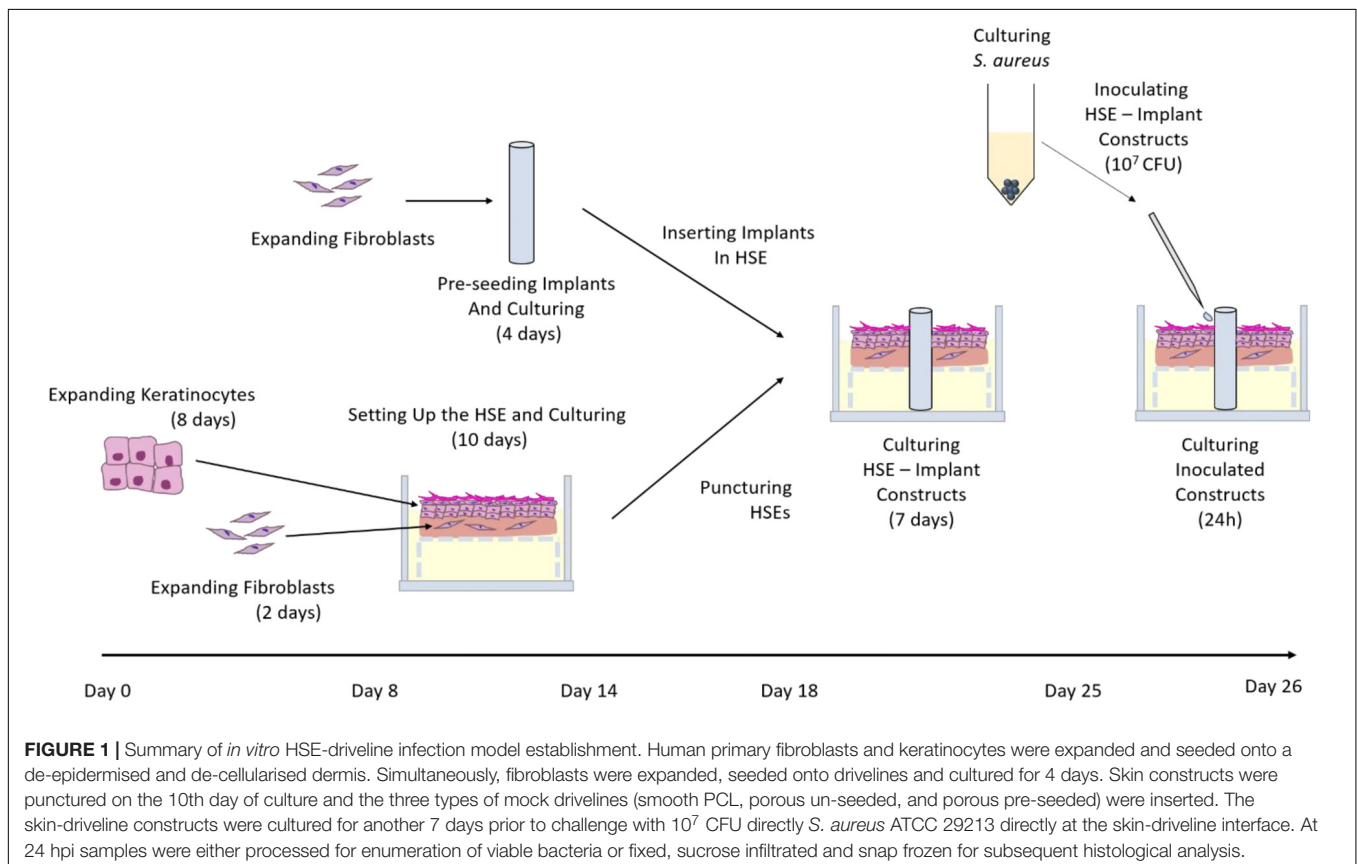
All mock (wireless, i.e., do not carry electrical charge) drivelines utilized in this study were manufactured from medical grade polymer poly(ϵ -caprolactone; PCL, Corbion Purac, Netherlands). PCL scaffolds were manufactured via MEW as previously described (Bolle et al., 2019) using an in-house custom built machine previously described in Wunner et al. (2017). Briefly, the PCL was loaded into a plastic syringe (Nordson EFD, United States), heated (84°C) and extruded by applying air pressure. A voltage of 6.7 kV was applied to the needle and the jet was collected on a grounded and motorized x - y collector plate in a lattice with layers at 90° and 45° to each other. The scaffolds were cut into 10 × 10 mm squares using a scalpel.

To produce mock drivelines with different surfaces, a 4 mm stainless steel mandrel was dip-coated into a 10% w/v solution of PCL in chloroform, as previously described (Bolle et al., 2019).

The mandrel was then immersed in ethanol to aid in the removal of the PCL from the mandrel, resulting in smooth, hollow PCL tubes, from now onward referred to as PCL drivelines. To obtain tubular scaffolds, the scaffolds were wrapped around the heated, PCL coated mandrels to fuse the bottom layers of the scaffolds to the PCL core. The PCL tube-scaffold constructs were removed from the mandrel with the aid of ethanol. This resulted in hollow tubes with a solid core and porous outer surface with an outer diameter of 4.5 mm, referred to as unseeded drivelines from now onward. All drivelines were sterilized by immersion in 80% ethanol for 30 min, dried in a laminar flow hood and exposed to UV light for 20 min on either side. The MEW scaffolds and the PCL tube – scaffold constructs (porous mock drivelines) are shown in **Figure 2**. Scanning electron microscopy (SEM) images were acquired using a Zeiss Sigma Field Emission SEM, equipped with a Zeiss Gemini column at an accelerating voltage of 5 kV. All samples were gold sputter coated prior to imaging using a Leica EM-SCD005. Stereomicroscope images of the samples were acquired on a Nikon SMZ25 stereomicroscope (Nikon, Japan).

Pre-seeding of Porous Mock Drivelines With Human Fibroblasts

The tubular scaffolds were seeded with fibroblasts as previously described (Bolle et al., 2019). Briefly, the scaffolds were placed in 12-well plates following an overnight incubation



in fibroblasts growth medium and seeded with human dermal fibroblasts isolated according to the above described protocol, by applying 30 μL containing 2×10^5 cells onto the scaffold. Following 30 min of incubation to allow for initial cell attachment, the scaffolds were inverted and another 30 μL containing 2×10^5 cells were placed on the scaffolds. Following a further 30 min incubation the samples were submerged in fibroblasts growth medium and cultured for 4 days, with medium changed every 48 h. The pre-seeded scaffolds are hereafter referred to as pre-seeded drivelines.

Implanting Human Skin Equivalents With Mock Drivelines

The mock drivelines were inserted into HSEs 10 day post seeding of fibroblasts and keratinocytes, as previously described (Bolle et al., 2019). Briefly, 4 mm holes were created in the HSEs with a biopsy punch (Stiefel) and the mock drivelines inserted from the dermal side and carefully pulled through using forceps (Figure 1). Skin-driveline constructs were cultured at the air liquid interface with medium replaced every 48 h.

Bacterial Strains and Culture Conditions

Staphylococcus aureus ATCC 29213 was used in this study and routinely cultured in Lysogeny broth (LB) medium with shaking (200 RPM) at 37°C. For HSE inoculations, bacterial cultures were collected at 16 h, centrifuged and resuspended in antibiotic-free keratinocyte growth medium at a cell density of 5×10^8 colony forming units (CFU)/mL. An inoculum volume of 20 μL (1×10^7 CFU) was used in all HSE infection assays.

S. aureus Infection Assay of Human Skin Equivalents Implanted With Mock Drivelines

Human skin equivalent culture medium was replaced with antibiotic-free keratinocyte growth medium 72 h prior to infection. Intact HSEs controls (without a driveline) were inoculated by depositing 1×10^7 CFU *S. aureus* ATCC 29213 in a small 20 μL volume at the centre of the construct surface. HSEs with implants were infected by depositing $4 \times 5 \mu\text{L}$ of *S. aureus* inoculum in a cross-shape around the tubular implant interface. The cross-shaped pattern was chosen to ensure that the inoculum volume was evenly distributed around the entire circumference of the mock drivelines. Inoculated HSEs were incubated in antibiotic-free keratinocyte growth medium at 5% CO_2 and 37°C. At 24 h post inoculation (hpi), HSEs were processed for histology or for viable CFU counts as described in sections below. Time-matched uninfected HSEs served as controls. A schematic overview of the entire experimental timeline is shown in Figure 1.

Enumeration of Viable *S. aureus* From Infected Human Skin Equivalents

Human skin equivalents collected at 24 hpi were dissected (roughly 3×3 mm pieces) under aseptic conditions, weighed and digested in a 1 mg/mL collagenase solution in phosphate buffered saline (PBS; Gibco, Australia) at 37°C for 3 h in a shaking incubator (200 RPM). The samples were then homogenized mechanically in a mini-Beadbeater (Daintree Scientific, Australia) with stainless steel beads (0.5 mm, Daintree Scientific). Samples were homogenized for 15 min in 2 min cycles at 2,500 RPM, with 1 min rest on ice between cycles. HSE homogenates were then serially diluted 10-fold in PBS and viable

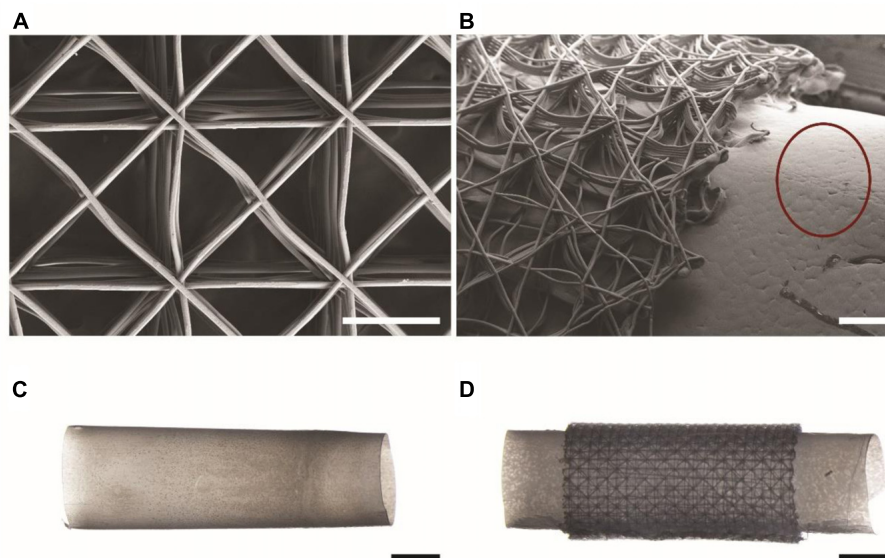


FIGURE 2 | Mock drivelines manufactured by melt electrowriting (MEW). SEM images of (A) a MEW scaffold used for constructing porous mock drivelines and (B) a porous mock driveline showing the MEW scaffold fused to the PCL tube (scale bars: 300 μm). The red circle highlights the surface morphology of the smooth PCL tube. Stereomicroscope images of (C) a smooth PCL tube and (D) a porous driveline (MEW scaffold – PCL tube) construct. Scale bars: 2 mm.

bacteria (CFU) in samples were enumerated by plating triplicate 5 μ L aliquots of each dilution onto LB agar followed by overnight incubation at 37°C.

Histological Examination of *S. aureus* Infected Human Skin Equivalents

Intact HSEs and HSEs with mock drivelines collected at 24 hpi were prepared for histological analysis as described in Bolle et al. (2019). Briefly, the HSEs were rinsed in PBS supplemented with magnesium and calcium and fixed in 4% PFA for a minimum of 30 min. HSEs were then infiltrated in a sucrose–OCT solution (optimal cutting temperature, Tissue Tek, Finland) with increasing ratios of OCT to preserve tissue morphology. HSEs were then snap frozen in a dry ice-ethanol slush and stored at –80°C until required for further processing. Frozen HSE samples were sectioned at 20 μ m thickness on a cryostat (Leica Biosystems) and stained with hematoxylin and eosin (Bolle et al., 2019). Coverslips were applied using prolong gold mounting medium (Life Technologies) and slides were imaged using a Zeiss Axio Imager M2 microscope (Zeiss) or a 3D Histech Scan II Brightfield Slide Scanner (3D Histech, Hungary). For localizing *S. aureus* within the tissue, HSE sections were stained following a published Gram staining protocol, with modifications (Becerra et al., 2016). Briefly, the sections were rinsed, stained with crystal violet for 1 min, incubated with iodine for 2 min, decolorised in acetone and counterstained with safranin for 1 min (ProSciTech, Australia) with a wash performed between each step. Slides were imaged on a Leica DM2500 microscope (Leica, Germany).

Fluorescence Microscopy of Explanted Mock Drivelines and *S. aureus* Staining

Drivelines were carefully removed from HSEs using forceps immediately after collection at 24 hpi and prepared for imaging of *S. aureus* colonization. Live/dead staining of *S. aureus* was performed using the LIVE/DEAD™ BacLight™ Bacterial Viability kit L7007 (Life Technologies, Australia). Explanted drivelines were rinsed in saline (0.9%) for 30 s, then incubated in the dark at 30°C for 25 min, with SYTO9 and Propidium Iodide (PI; 200 μ L). The final applied concentration of SYTO9 and PI was 3.35 μ M and 20 μ M, respectively. Following staining the drivelines were rinsed in saline (0.9%) for 30 s, mounted onto coverslips using ProLong® Diamond Antifade Mountant (Life Technologies, Australia) and immediately imaged on a Zeiss AxioVert A1 FL-LED microscope (Zeiss, Germany) utilizing a 100 \times oil immersion objective. Images were analyzed using the instrument software (Zen 2.3).

Statistical Methods

DEDs from 3 different donors were used for all experiments reported herein. In each experiment, DEDs from the same donor were tested in triplicate for each group (intact, PCL, un-seeded, pre-seeded). A total of 8 samples per group were analyzed by histology and a minimum of 6 for bacterial viability counts. CFU were enumerated by plating on agar plates and presented as CFU per ml of HSE homogenate. CFU from

technical repeats were averaged and the average of each biological repeat is presented in dot plots per group. Group medians were compared for statistical differences by the non-parametric Kruskal Wallis test.

RESULTS

Establishment of an *in vitro* Human Skin Equivalent Driveline Infection Model

Staphylococcus aureus is the leading cause of driveline infections (Koval and Stosor, 2019) and has been previously shown to remain confined to the outermost layer of the epidermis in an HSE wound infection model (Shepherd et al., 2009). This makes it an ideal organism for studying driveline-specific infections in HSEs *in vitro* as it does not invade into deeper tissue, unlike the Gram-negative wound pathogen *Pseudomonas aeruginosa* (Shepherd et al., 2009), ensuring that any bacterial penetration can only occur via the driveline opening. To confirm this in our model, we used reference *S. aureus* ATCC 29213 cultures to inoculate intact HSEs, devoid of a driveline, and HSEs with a PCL driveline mimicking the smooth surface of those currently used in clinical practice. *S. aureus* was recovered at 24 h post inoculation (hpi) in similar numbers from both HSE groups, with an average of 1.2×10^7 CFU/mL recovered from intact HSEs and 1.3×10^7 CFU/mL from HSEs implanted with the PCL driveline (Figure 3A). As the number of bacteria recovered at 24 hpi was similar to the number of inoculated bacteria, this suggests that *S. aureus* ATCC 29213 remained viable in our experimental model over this time-period maintaining a high tissue load.

While bacterial numbers recovered from tissues were similar, the localization of *S. aureus* differed between HSE groups (Figures 3B, 4). Gram staining of cross sections from intact HSEs revealed that *S. aureus* cells were exclusively present in the apical surface of the skin, with bacteria loosely associated with the uppermost layer and no bacteria present in deeper epidermal layers (Figure 3B). Similar analysis of HSEs implanted with PCL drivelines (Figure 4) revealed heavy *S. aureus* colonization at the driveline-skin exit site (inoculation site), with minimal bacterial presence observed further down this interface. Where bacteria were seen to be present deeper into the skin-driveline interface, they appeared to be mostly found in areas where gaps were present between HSE tissue and driveline (Figure 4).

H&E staining confirmed that all HSEs displayed a tissue morphology closely resembling that of native human skin (Figures 3B, 4). The epidermal growth patterns along the smooth PCL drivelines varied, with 5 out of 8 samples exhibiting epidermal downgrowth around the implant and 3 showing epidermal upgrowth. This is in line with our previous findings using smooth PCL drivelines in HSEs (Bolle et al., 2019) and suggests that the presence of *S. aureus* does not affect epidermal growth patterns.

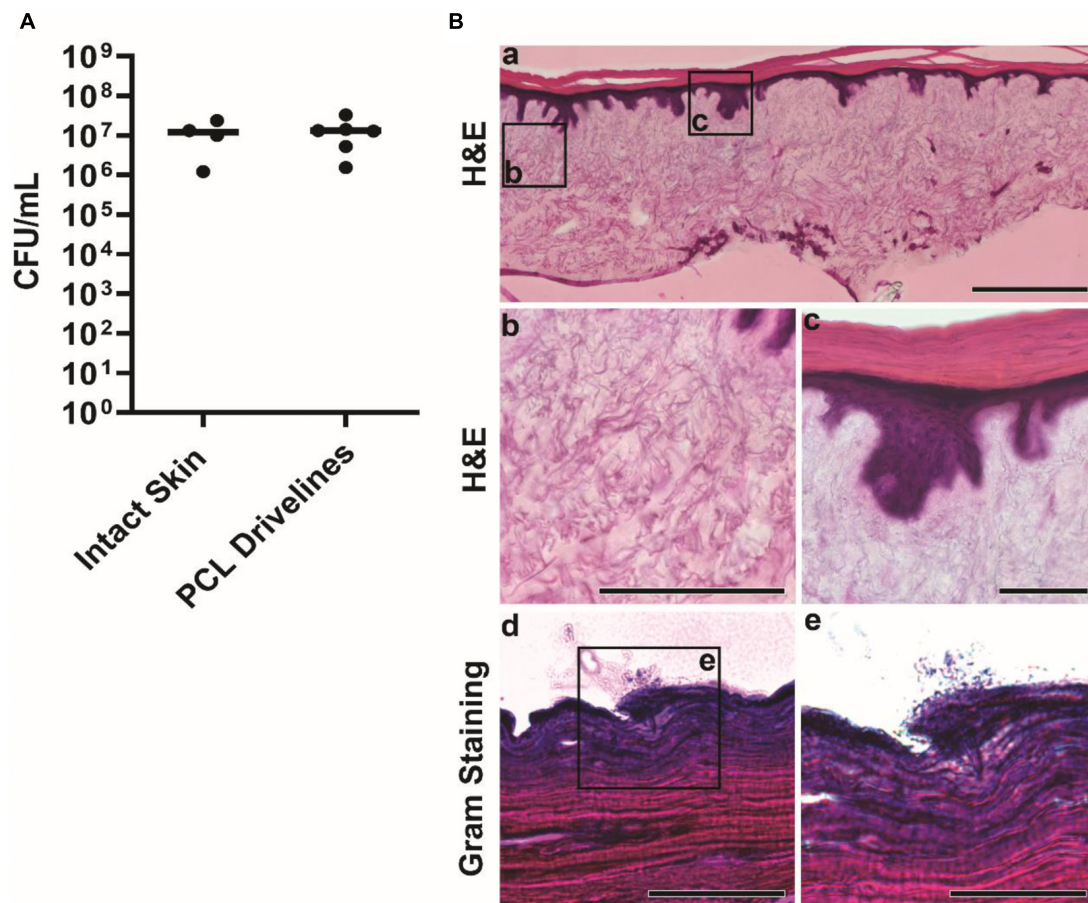


FIGURE 3 | *Staphylococcus aureus* infection of intact HSEs. **(A)** Number of viable *S. aureus* colony forming units (CFU) recovered from intact skin HSEs (no driveline) or HSEs implanted with smooth PCL drivelines at 24 h post inoculation. Bacterial numbers are presented as CFU/mL with group means shown as horizontal lines. Dot plots show data from a minimum of 4 experimental repeats using HSEs derived from 3 skin donors. **(B)** Histological analysis of infected HSEs showing an overview of cross sections of the entire skin construct by H&E staining. Visible features include rete ridges between the epidermis and dermis (panel a, scale bar: 500 μ m), connective dermal tissue (panel b, scale bar: 200 μ m) and the epidermis and stratum corneum (panel c, scale bar: 100 μ m). Gram staining of tissue cross-sections revealed *S. aureus* localizing exclusively on the uppermost layer of the epidermis in loose association with the skin tissue (panels d and e, scale bars: 100 μ m and 50 μ m, respectively).

Collectively, our microbiological and histological analyses suggest that the HSE model is able to sustain a high bacterial load without *S. aureus*-induced tissue damage or invasion of deeper epidermal and dermal layers. Bacterial non-invasiveness was considered a pre-requisite for an HSE-driveline infection model which sought to establish bacterial migration along the opening created by the presence of a driveline. Further, the results with the PCL drivelines suggest that the presence of the driveline does not affect total bacterial counts and that most bacteria are localized at the driveline exit site or associated with the driveline surface as a biofilm. We observed little *S. aureus* migration along the PCL implant interface and only where there were micro-gaps present, similar to recent clinical observations from explanted patient drivelines (Qu et al., 2019a). Thus, we conclude that our established *in vitro* HSE-driveline infection model is a suitable platform for investigating differences in the biological seal created by different driveline surfaces, which we investigated next.

***S. aureus* Forms a Biofilm at the Entry Site of Porous Drivelines and Migrates Along the Driveline-Tissue Interface via Micro-Gaps**

To test whether skin integration around different porous driveline surfaces translates to differences in bacterial migration along the driveline, we inoculated HSEs with *S. aureus* as above, but this time the HSEs were implanted with MEW un-seeded and pre-seeded mock drivelines. The *S. aureus* tissue load recovered at 24 hpi was 3×10^6 CFU/mL and 8×10^6 CFU/mL, for the un-seeded and pre-seeded groups, respectively (Figure 5A). Histological staining revealed infected HSEs with un-seeded and pre-seeded drivelines to have an intact dermis and epidermis, with the lateral side of the pre-seeded drivelines exhibiting an intact thin layer of fibroblasts covering the scaffolds (Figure 5B– top right panel). All HSEs bearing un-seeded implants (8 out of 8) displayed epidermal

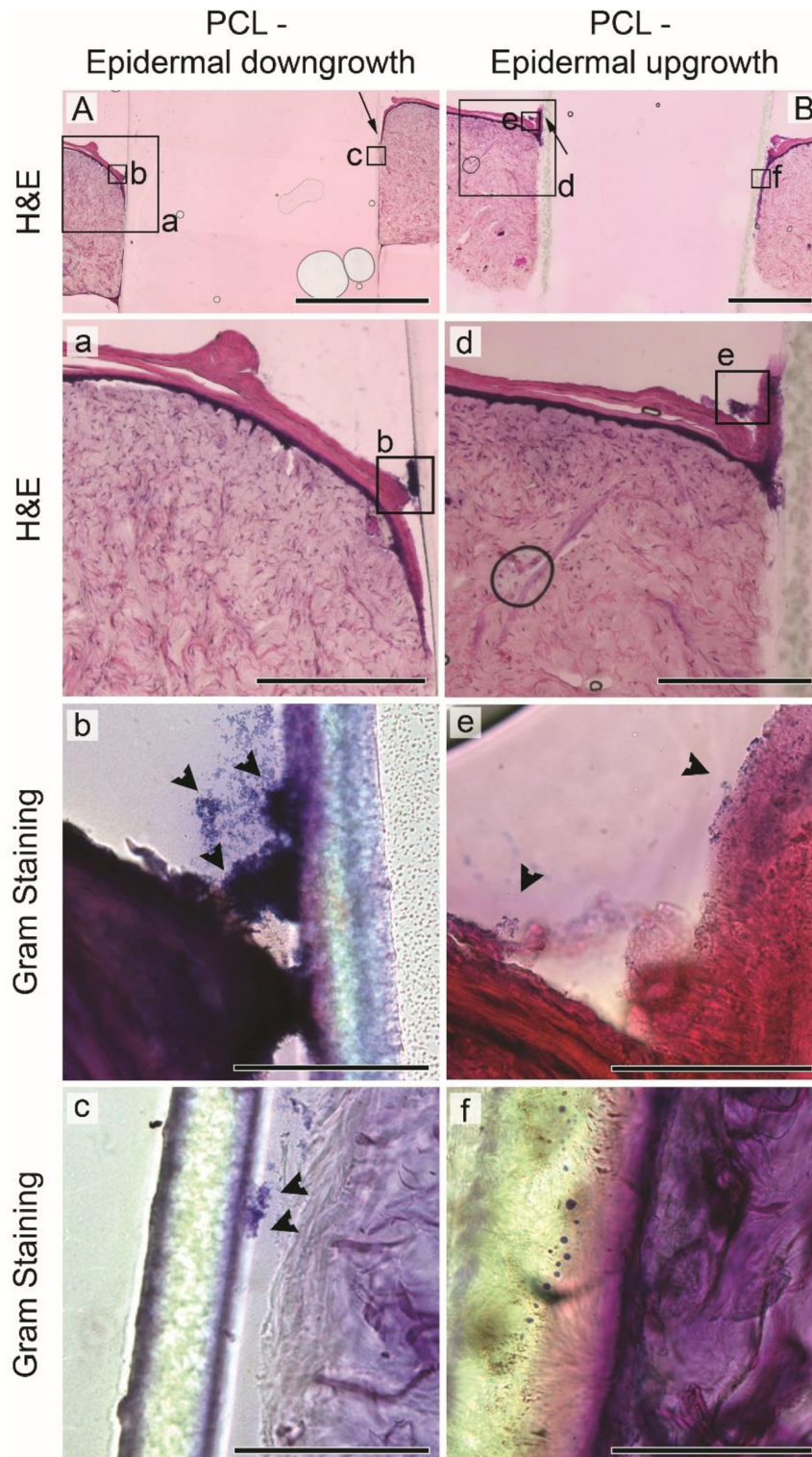


FIGURE 4 | *Staphylococcus aureus* infection of HSEs implanted with smooth drivelines. Histological analysis by H&E staining of cross sections of HSEs implanted with a PCL mock driveline, exhibiting (A) epidermal downgrowth or (B) epidermal upgrowth, as indicated by the black arrows (scale bars: 2 mm). Panels (a) and (d) show digital magnifications of marked regions from H&E images shown in (A,B), scale bars: 500 μ m. Irrespective of epidermal growth pattern, Gram staining revealed bacterial colonization at the driveline entry point [panels (b) and (e)], denoted by black arrowheads, but limited or no presence of bacteria further along the skin – driveline interface [panels (c) and (f), scale bars 100 μ m]. All images are from sections from the same samples with specific regions marked by black boxes in (A,B).



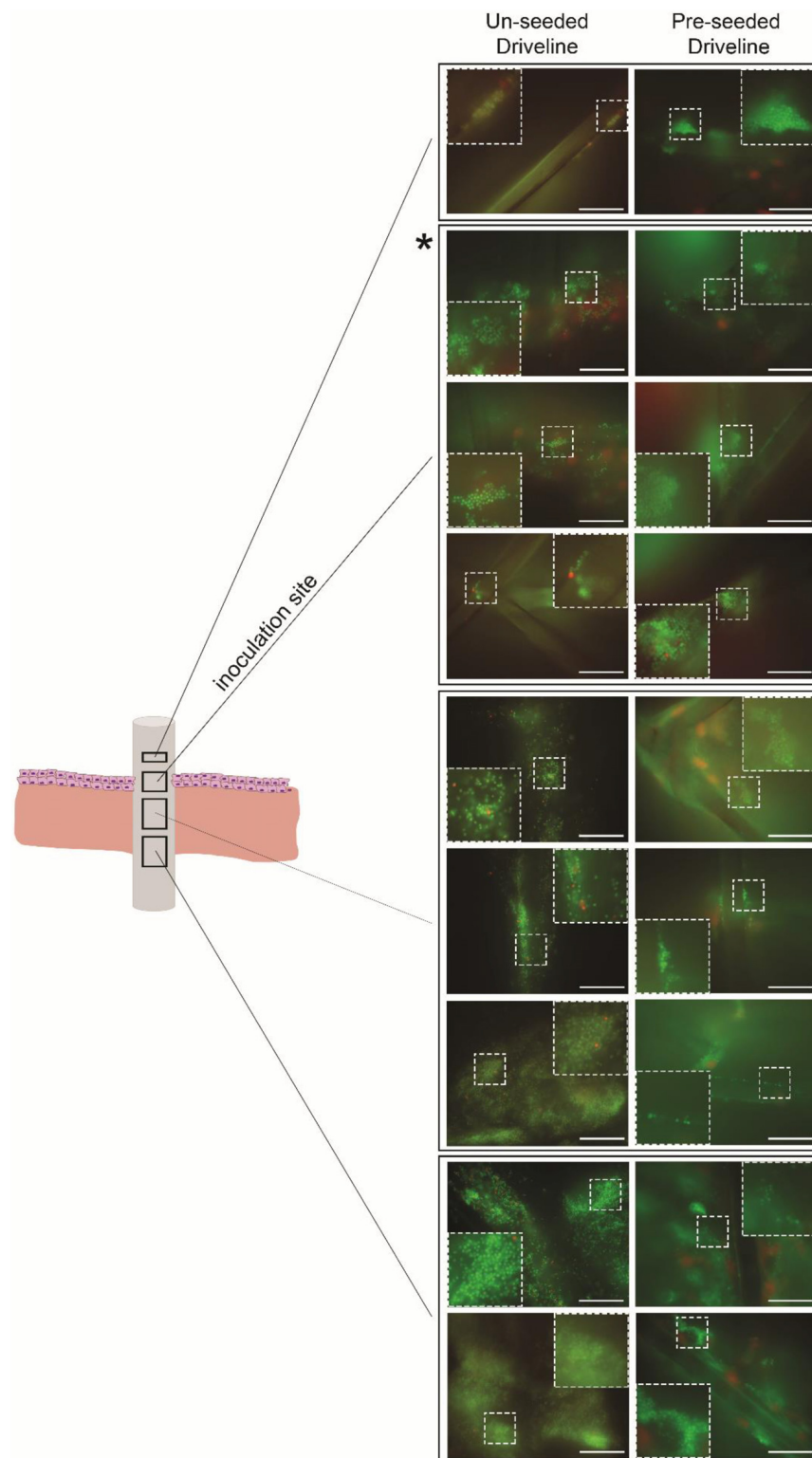


FIGURE 6 | Fluorescence microscopy of infected HSE-explanted drivelines. *S. aureus* cells were stained with bacterial LIVE/DEAD staining (live = green, dead = red). Live *S. aureus* cells (seen as green cocci) were present in the voids and on the fiber struts of the un-seeded and pre-seeded drivelines at the inoculation site (second quadrant from top, denoted by asterisk) and deeper down the driveline surface (left and right panels, respectively; Scale bars: 30 μm). Inserts show a digitally zoomed section (25%) of the region marked by the white dotted line.

DISCUSSION

Infections around percutaneous implants and drivelines are a prevalent clinical problem, since the advent of the earliest VADs, limiting successful outcomes of ventricular assist device therapy (Hannan et al., 2019). It has been hypothesized by us and others that increased skin and tissue integration around the percutaneous device translates to a better biological seal against bacteria, with the potential to reduce bacterial infection rates (von Recum, 1984; Tagusari et al., 1998; Choi et al., 1999; Fukano et al., 2010; Isackson et al., 2011; Bolle et al., 2019). The aim of this study was thus to investigate whether porous scaffolds that were previously shown to increase skin integration and device stability in an HSE model would create a protective biological seal against pathogen entry. This aim necessitated the establishment of the first HSE-driveline infection model for *in vitro* investigations.

In vitro skin models have greatly advanced the field of cutaneous research and are based on excised full thickness skin, or tissue engineered skin with the dermal component based on synthetic matrices or de-cellularised dermis (Abd et al., 2016; Pupovac et al., 2018). The de-cellularised dermis skin model (DED-HSE) is well characterized, closely resembles native human skin and has been shown to re-epithelialise (Topping et al., 2006; Xie et al., 2010; Fernandez et al., 2014). More importantly, it has been used to study bacterial infections of wounds and the efficacy of functionalized biomaterials in reducing the bacterial burden in infected skin (Shepherd et al., 2009, 2011; Zheng et al., 2019).

In vitro skin models, however, have not yet been utilized to study bacterial infections around drivelines. Current knowledge on driveline infections is mainly derived from *in vitro* agar or drip flow bioreactor models, *ex vivo* analysis of explanted drivelines or *in vivo* rodent models (Arrecubieta et al., 2009; Toba et al., 2011; Qu et al., 2019b,a). The *in vitro* agar model was established by Qu et al. (2019b) to mimic microbial biofilm growth on drivelines within the subcutaneous tissue tunnel. The model consists of casting a Hinton or Roswell Park Memorial Institute medium agar mold by placing a piece of smooth driveline into molten agar and removing the driveline upon setting of the agar. Following insertion of an inoculated piece of smooth or porous driveline, the tunnel is covered with a lid from the same agar. To mimic the driveline exit site, the authors use a drip-flow biofilm reactor, whereby they place inoculated pieces of smooth or porous driveline into the incubation chamber while pumping growth medium through the system (Qu et al., 2019b). While these agar models offer suitable *in vitro* models to study biofilm formation and bacterial migration in the subcutaneous tissue, they do not allow examination of epidermal and dermal integration or its association with bacterial migration. *Ex vivo* clinical samples, on the other hand, are highly pertinent to studying various aspects of driveline infections, but observations tend to be subject to biological variation, demanding analyses of large numbers of clinical samples, and as such do not lend themselves as an ideal experimental platform to validate hypotheses. Small animal models have been utilized to study the *in vivo* role of bacterial virulence factors in driveline colonization and infection, such as the SdrF surface protein of *S. aureus* (Arrecubieta et al., 2009) and more generally the role of biofilm formation on driveline

infections by *S. aureus* and *S. epidermidis* (Toba et al., 2011). None of these studies, however, directly investigated the role of skin integration and epidermal growth patterns in protecting from bacterial infection, so the clinical value of rodent driveline infection models to study skin integration remains unknown.

To address the lack of physiologically relevant *in vitro* models to study the correlation between skin integration and bacterial infection around percutaneous drivelines, we established a first-in-field *in vitro* driveline infection model based on the established DED-HSE model. Our model reproduces the clinical features observed in explanted drivelines from infected patients and provides a suitable tool for the investigation of skin-driveline integration properties on infection outcome. To the best of our knowledge, this is the first study to directly test whether increased skin integration around porous drivelines translates to an increased biological seal against pathogen entry.

Our study utilized *S. aureus* as the model pathogen, given *S. aureus* is the most common causative agent of driveline infections (Koval and Stosor, 2019). We deliberately inoculated the driveline exit-site with a relatively high bacterial burden (10^7 CFU of *S. aureus* deposited in a small volume directly at the exit site), to challenge the biological seal created by the different driveline surfaces. Despite the high challenge, histological analysis confirmed that a high bacterial load could be maintained without tissue damage even up to 72 h post inoculation (data not shown). The non-invasiveness of *S. aureus* strains in HSE models, previously reported (Shepherd et al., 2009) and confirmed in this study for reference strain ATCC 29213, was important in ensuring that bacterial entry and migration occurred *via* the driveline and not *via* the tissue.

Our model also reproduced the formation of a sinus tract as a result of epidermal downgrowth around the implanted driveline. Sinus tract formation is a well-known mode of failure of percutaneous devices (von Recum, 1984) and has been hypothesized to create an environment conducive to bacterial proliferation, leading to subsequent device infection (Isackson et al., 2011; Affeld et al., 2012). Our study offers the first *in vitro* validation of this hypothesis, providing evidence of increased bacterial localization in the sinus tract between the driveline and the surrounding tissue. While in our model epidermal upgrowth was also observed, epidermal downgrowth was more frequently associated with implants that did not display tight integration with the surrounding HSE tissue and contained frequent micro-gaps along the length of the interface where bacteria were commonly observed. A recent analysis of infected drivelines explanted from patients undergoing heart transplants revealed insufficient integration between the DacronTM and the surrounding subcutaneous tissue with bacterial presence within similar voids (Qu et al., 2019a). In an *in vitro* study by the same group, challenge of porous DacronTM with the same *S. aureus* strain used in our study, also resulted in biofilm formation within the inter-fiber space of the intricate porous DacronTM structure (Qu et al., 2019b), similar to what we observed with the scaffold voids of mainly un-seeded and some pre-seeded drivelines. These results indicate that a healthy and well-integrated driveline-interface is crucial to reduce bacterial colonization and prevent migration along the implant interface. When the cell viability

of the fibroblast layer forming the tight interface in our pre-seeded driveline-HSEs declined at 72 hpi, we observed increased bacterial migration into the driveline, further supporting this tenet (data not shown).

While there appears to be a consensus from *in vitro* and *ex vivo* studies on bacterial migration along porous drivelines, findings from animal models seem to be conflicting. A study by Isackson et al. (2011) in rabbits investigated four different types of titanium implants, all consisting of a percutaneous post and a subcutaneous anchor, with a smooth, porous or mixed surface (porous percutaneous post and smooth anchor or vice versa). Implants were repeatedly challenged with high-doses of *S. aureus* 4 weeks post implantation until manifestation of Grade II clinical signs of infection (experimental end point). Histological analysis revealed epidermal downgrowth and sinus tract formation in all implants, but implants with smooth components had a 7-fold increased risk of infection compared to implants with a porous surface in one or both components (Isackson et al., 2011). It is noteworthy that while the authors confirmed *S. aureus* to be the only organism isolated from infected implants, bacterial loads from implants or tissues were not determined and localization of bacteria along the implant interface was not examined either. Similarly, older studies in rabbits and pigs reported no signs of infection with porous carbon percutaneous devices (Krouskop et al., 1988; Nowicki et al., 1990). Differences in implant materials could account for these differences in results, as well as the use of different bacterial pathogens, which are known to have distinct biofilm formation properties.

Perhaps the most obvious difference, however, between *in vitro* and *in vivo* studies, is the absence of immune cells from most *in vitro* human skin models. Less than a handful of reconstructed HSE models containing immune cells have been reported to date (Bechetioille et al., 2007; Ouwehand et al., 2011; Linde et al., 2012; Kühbacher et al., 2017), which is testament to the complexity of establishing and maintaining 3D co-culture models (Pupovac et al., 2018). Overcoming those limitations in the near future will greatly enhance the clinical value of *in vitro* HSE-based models, including our HSE-driveline infection model, given the primary role of immune cells in fighting invading pathogens. In addition, the model could be further enhanced by adding movement of the driveline in the HSE through a bioreactor, in order to mimic driveline movement caused by patient breathing and other motion. While in this study we aimed to compare the biological seal created by different porous driveline surfaces (un-seeded and pre-seeded), which were previously shown to promote different skin integration patterns (Bolle et al., 2019), our model lends itself nicely for other types of studies, e.g., comparative efficacy of different driveline materials (Dacron, silicone, etc.) or testing of new and existing antibacterials and disinfectants. Furthermore, the model allows investigation of host-pathogen interactions and could be useful for *in vitro* studies of bacterial factors contributing to skin and/or driveline colonization and translocation. While, in our study we chose to explore bacterial localization in HSE tissues and drivelines by staining and microscopy -analyses which allow bacterial localization but generate image data not optimal for quantitative measurements-, quantification of

viable bacteria in the tissue (as done in our study) could be combined with enumeration of bacteria on the HSE-explanted drivelines (as done in other studies; Qu et al., 2019b,a), to provide total numbers of bacteria colonizing the entire model system. Bacterial migration through the driveline could also be quantified by enumerating viable CFU recovered from media surrounding the HSE in each well (Figure 1), but we would highly recommend using transwells for such investigations to exclude bacteria “spill-over” from the epidermal inoculation site, especially for small-sized HSE constructs (Bolle and Totsika, unpublished observations).

Despite certain limitations, the *in vitro* percutaneous driveline infection model reported herein represents a versatile tool to further our understanding of factors leading to driveline infections and the role of skin integration and driveline surface in reducing bacterial infections. Such models can also provide a valuable early preclinical platform for the testing of new antimicrobial surfaces and therapeutics aimed at reducing the prevalence of device-related infections burdening health systems worldwide.

DATA AVAILABILITY STATEMENT

The datasets generated for this study are available on request to the corresponding author.

ETHICS STATEMENT

The studies involving human participants were reviewed and approved by the Queensland University of Technology Research Ethics Committee (1300000063) and Uniting Healthcare/St Andrew's Hospital Ethics Committee (0346). The patients/participants provided their written informed consent to participate in this study.

AUTHOR CONTRIBUTIONS

EB and MT conceived the study and designed the experiments, analyzed and interpreted the data and wrote the manuscript. EB, AV, and RD conducted the experiments. JE, TP, and TD contributed to the design and implementation of the research. All authors revised the manuscript for content and approved the final version.

FUNDING

The authors would like to recognize the financial assistance provided by The Prince Charles Hospital Foundation (ER2015-14, PRO2014-08, EM2017-03, and TM2017-04), a Clive and Vera Ramaciotti Health Investment Grant (2017HIG0119 to MT), and the National Health and Medical Research Council Centre for Research Excellence (APP1079421) and Project Grant APP1144046. TD is supported by an ARC Future Fellowship (FT150100408) and MT by a QUT Vice-Chancellor's Research Fellowship.

ACKNOWLEDGMENTS

Some of the data reported in this paper were obtained at the Infection and Immunity Ian Potter Foundation Imaging Suite operated by the Institute of Health and Biomedical Innovation

REFERENCES

- Abd, E., Yousef, S. A., Pastore, M. N., Telaprolu, K., Mohammed, Y. H., Namjoshi, S., et al. (2016). Skin models for the testing of transdermal drugs. *Clin. Pharmacol. Adv. Appl.* 8, 163–176. doi: 10.2147/CPAA.S64788
- Affeld, K., Grosshauser, J., Goubergrits, L., and Kertzsch, U. (2012). Percutaneous devices: a review of applications, problems and possible solutions. *Expert Rev. Med. Devices* 9, 389–399. doi: 10.1586/erd.12.25
- Arrecubieta, C., Toba, F. A., Von Bayern, M., Akashi, H., Deng, M. C., Naka, Y., et al. (2009). SdrF, a *Staphylococcus epidermidis* surface protein, contributes to the initiation of ventricular assist device driveline-related infections. *PLoS Pathog.* 5:411. doi: 10.1371/journal.ppat.1000411
- Becerra, S. C., Roy, D. C., Sanchez, C. J., Christy, R. J., and Burmeister, D. M. (2016). An optimized staining technique for the detection of Gram positive and Gram negative bacteria within tissue. *BMC Res. Notes* 9:216. doi: 10.1186/s13104-016-1902-1900
- Bechetille, N., Dezutter-Dambuyant, C., Damour, O., André, V. R., Orly, I., and Perrier, E. (2007). Effects of solar ultraviolet radiation on engineered human skin equivalent containing both langerhans cells and dermal dendritic cells. *Tissue Eng.* 13, 2667–2679. doi: 10.1089/ten.2006.0405
- Bolle, E. C. L., Bartnikowski, N., Haridas, P., Parker, T. J., Fraser, J. F., Gregory, S. D., et al. (2019). Improving skin integration around long-term percutaneous devices using fibrous scaffolds in a reconstructed human skin equivalent model. *J. Biomed. Mater. Res. Part B Appl. Biomater.* 108, 738–749. doi: 10.1002/jbm.b.34428
- Camboni, D., Zerditzki, M., Hirt, S., Tandler, R., Weyand, M., and Schmid, C. (2016). Reduction of INCOR\$driveline infection rate with silicone at the driveline exit site. *Interact. Cardiovasc. Thorac. Surg.* 24, 222–228. doi: 10.1093/icvts/ivw336
- Chakrabarty, K. H., Dawson, R. A., Harris, P., Layton, C., Babu, M., Gould, L., et al. (1999). Development of autologous human dermal-epidermal composites based on sterilized human allografts for clinical use. *Br. J. Dermatol.* 141, 811–823. doi: 10.1046/j.1365-2133.1999.03153.x
- Choi, L., Choudhri, A. F., Pillarisetty, V. G., Sampath, L. A., Carao, L., Brunner, S. R., et al. (1999). Development of an infection-resistant LVAD driveline: a novel approach to the prevention of device-related infections. *J. Heart Lung Transplant.* 18, 1103–1110. doi: 10.1016/S1053-2498(99)00076-5
- Dawson, R. A., Upton, Z., Malda, J., and Harkin, D. G. (2006). Preparation of cultured skin for transplantation using insulin-like growth factor I in conjunction with insulin-like growth factor binding protein 5, epidermal growth factor, and vitronectin. *Transplantation* 81, 1668–1676. doi: 10.1097/01.tp.0000226060.51572.89
- Dean, D., Kallel, F., Ewald, G. A., Tatoes, A., Sheridan, B. C., Brewer, R. J., et al. (2015). Reduction in driveline infection rates: results from the heartmate ii multicenter driveline silicone skin interface (SSI) registry. *J. Heart Lung Transplant.* 34, 781–789. doi: 10.1016/j.healun.2014.11.021
- Farrugia, B. L., Brown, T. D., Upton, Z., Huttmacher, D. W., Dalton, P. D., and Dargaville, T. R. (2013). Dermal fibroblast infiltration of poly(ϵ -caprolactone) scaffolds fabricated by melt electrospinning in a direct writing mode. *Biofabrication* 5:025001. doi: 10.1088/1758-5082/5/2/025001
- Feldmann, C., Chatterjee, A., Haverich, A., and Schmitt, J. D. (2018). “Left ventricular assist devices – a state of the art review,” in *Heart Failure: From Research to Clinical Practice*, Vol. 3, ed. M. S. Islam (Cham: Springer International Publishing), 287–294. doi: 10.1007/978-3-319-4145-1_15
- Fernandez, T. L., Van Lonkhuyzen, D. R., Dawson, R. A., Kimlin, M. G., and Upton, Z. (2014). Characterization of a human skin equivalent model to study the effects of ultraviolet b radiation on keratinocytes. *Tissue Eng. Part C Methods* 20, 588–598. doi: 10.1089/ten.tec.2013.0293
- Fukano, Y., Usui, M. L., Underwood, R. A., Isenhardt, S., Marshall, A. J., Hauch, K. D., et al. (2010). Epidermal and dermal integration into sphere-templated porous poly(2-hydroxyethyl methacrylate) implants in mice. *J. Biomed. Mater. Res. Part A* 94A, 1172–1186. doi: 10.1002/jbm.a.32798
- Hannan, M. M., Xie, R., Cowger, J., Schueler, S., de By, T., Dipchand, A. I., et al. (2019). Epidemiology of infection in mechanical circulatory support: a global analysis from the ISHLT mechanically assisted circulatory support registry. *J. Heart Lung Transplant.* 38, 364–373. doi: 10.1016/j.healun.2019.01.007
- Haridas, P., McGovern, J. A., Kashyap, A. S., McElwain, D. L. S., and Simpson, M. J. (2016). Standard melanoma-associated markers do not identify the MM127 metastatic melanoma cell line. *Sci. Rep.* 6:24569. doi: 10.1038/srep24569
- INTERMACS (2015). Interagency registry for mechanically assisted circulatory support (INTERMACS) quarterly statistical report 2015 Q1. *Statist. Rep.* 126, 1401–1406. doi: 10.1161/circulationaha.112.097816
- Isackson, D., McGill, L. D., and Bachus, K. N. (2011). Percutaneous implants with porous titanium dermal barriers: an in vivo evaluation of infection risk. *Med. Eng. Phys.* 33, 418–426. doi: 10.1016/j.medengphy.2010.11.007
- Kirklin, J. K., Pagani, F. D., Kormos, R. L., Stevenson, L. W., Blume, E. D., Myers, S. L., et al. (2017). Eighth annual INTERMACS report: special focus on framing the impact of adverse events. *J. Heart Lung Transplant.* 36, 1080–1086. doi: 10.1016/j.healun.2017.07.005
- Koval, C. E., and Stosor, V. (2019). Ventricular assist device related infections and solid organ transplantation - guidelines from the american society of transplantation infectious diseases community of practice. *Clin. Transplant.* 33:e13529. doi: 10.1111/ctr.13529
- Krouskop, T., Brown, H., Gray, K., Shively, J., Romovacek, G., Spira, M., et al. (1988). Bacterial challenge study of a porous carbon percutaneous implant. *Biomaterials* 9, 398–404. doi: 10.1016/0142-9612(88)90003-8
- Kühbacher, A., Henkel, H., Stevens, P., Grumaz, C., Finkmeier, D., Burger-Kentischer, A., et al. (2017). Central role for dermal fibroblasts in skin model protection against *Candida albicans*. *J. Infect. Dis.* 215, 1742–1752. doi: 10.1093/infdis/jix153
- Linde, N., Gutschalk, C. M., Hoffmann, C., Yilmaz, D., and Mueller, M. M. (2012). Integrating macrophages into organotypic co-cultures: a 3D in vitro model to study tumor-associated macrophages. *PLoS One* 7:e40058. doi: 10.1371/journal.pone.0040058
- McCandless, S. P., Ledford, I. D., Mason, N. O., Alharethi, R., Rasmussen, B. Y., Budge, D., et al. (2015). Comparing velour versus silicone interfaces at the driveline exit site of HeartMate II devices: infection rates, histopathology, and ultrastructural aspects. *Cardiovasc. Pathol.* 24, 71–75. doi: 10.1016/j.carpath.2014.07.011
- McGovern, J. A., Heinemann, J. R., Burke, L. J., Dawson, R., Parker, T. J., Upton, Z., et al. (2013). Stratum basale keratinocyte expression of the cell-surface glycoprotein CDPC1 during epidermogenesis and its role in keratinocyte migration. *Br. J. Dermatol.* 168, 496–503. doi: 10.1111/bjd.12119
- Nowicki, B., Runyan, R. S., Smith, N., and Krouskop, T. A. (1990). Kinetics of colonization of a porous vitreous carbon percutaneous implant. *Biomaterials* 11, 389–392. doi: 10.1016/0142-9612(90)90092-90095
- Ouweland, K., Spiekstra, S. W., Waaijman, T., Scheper, R. J., de Grijl, T. D., and Gibbs, S. (2011). Technical advance: langerhans cells derived from a human cell line in a full-thickness skin equivalent undergo allergen-induced maturation and migration. *J. Leukoc. Biol.* 90, 1027–1033. doi: 10.1189/jlb.0610374
- Pupovac, A., Senturk, B., Griffoni, C., Maniura-Weber, K., Rottmar, M., and McArthur, S. L. (2018). Toward immunocompetent 3D skin models. *Adv. Healthc. Mater.* 7:1701405. doi: 10.1002/adhm.201701405
- Qu, Y., McGiffin, D., Hayward, C., Robson, D., Kure, C., Thissen, H., et al. (2019a). A study of infected drivelines from ventricular assist device patients: the presence of microbial biofilms and micro-gaps in the driveline tunnel. *J. Heart Lung Transplant.* 38, S102–S103. doi: 10.1016/j.healun.2019.01.240
- Qu, Y., McGiffin, D. C., Kure, C. E., Ozcelik, B., Thissen, H., Fraser, J. F., et al. (2019b). Microbial biofilm formation and migration on ventricular assist device

- drivelines: implications for infection. *J. Thorac. Cardiovasc. Surg.* 37:S134. doi: 10.1016/J.HEALUN.2018.01.323
- Rheinwald, J. G., and Green, H. (1975). Serial cultivation of strains of human epidermal keratinocytes: the formation keratinized colonies from single cell. *Cell* 6, 331–343. doi: 10.1016/s0092-8674(75)80001-8
- Salwiczek, M., Qu, Y., Gardiner, J., Strugnell, R. A., Lithgow, T., McLean, K. M., et al. (2014). Emerging rules for effective antimicrobial coatings. *Trends Biotechnol.* 32, 82–90. doi: 10.1016/j.tibtech.2013.09.008
- Shepherd, J., Douglas, I., Rimmer, S., Swanson, L., and MacNeil, S. (2009). Development of three-dimensional tissue-engineered models of bacterial infected human skin wounds. *Tissue Eng. Part C Methods* 15, 475–484. doi: 10.1089/ten.tec.2008.0614
- Shepherd, J., Sarker, P., Rimmer, S., Swanson, L., MacNeil, S., and Douglas, I. (2011). Hyperbranched poly(NIPAM) polymers modified with antibiotics for the reduction of bacterial burden in infected human tissue engineered skin. *Biomaterials* 32, 258–267. doi: 10.1016/j.biomaterials.2010.08.084
- Singh, A., Russo, M. J., Valeroso, T. B., Johnson, E. M., Anderson, A. S., Fedson, S. E., et al. (2012). Modified HeartMate II driveline externalization technique significantly decreases incidence of infection and improves long-term survival. *J. Hear. Lung Transplant.* 31:S20. doi: 10.1016/j.healun.2012.01.035
- Tagusari, O., Yamazaki, K., Litwak, P., Kojima, A., Klein, E. C., Antaki, J. F., et al. (1998). Fine trabecularized carbon: ideal material and texture for percutaneous device system of permanent left ventricular assist device. *Artif. Organs* 22, 481–487. doi: 10.1046/j.1525-1594.1998.06152.x
- Toba, F. A., Akashi, H., Arrecubieta, C., and Lowy, F. D. (2011). Role of biofilm in *Staphylococcus aureus* and *Staphylococcus epidermis* in ventricular assist device infection. *J. Thorac. Cardiovasc. Surg.* 141, 1259–1264. doi: 10.1016/j.jtcvs.2010.07.016.Role
- Topping, G., Malda, J., Dawson, R., and Upton, Z. (2006). Development and characterisation of human skin equivalents and their potential application as a burn wound model. *J. Wound Manag.* 14, 14–21.
- von Recum, A. F. (1984). Applications and failure modes of percutaneous devices: a review. *J. Biomed. Mater. Res.* 18, 323–336. doi: 10.1002/jbm.820180403
- von Recum, A. F., and Park, J. B. (1981). Permanent percutaneous devices. *Crit. Rev. Bioeng.* 5, 37–77.
- Winter, G. D. (1974). Transcutaneous implants: reactions of the skin? implant interface. *J. Biomed. Mater. Res.* 8, 99–113. doi: 10.1002/jbm.820080311
- Wunner, F. M., Bas, O., Saidy, N. T., Dalton, P. D., Pardo, E. M. D.-J., and Hutmacher, D. W. (2017). Melt electrospinning writing of three-dimensional Poly(ϵ -caprolactone) scaffolds with controllable morphologies for tissue engineering applications. *J. Vis. Exp.* 45:e56289. doi: 10.3791/56289
- Xie, Y., Rizzi, S. C., Dawson, R., Lynam, E., Richards, S., Leavesley, D. I., et al. (2010). Development of a three-dimensional human skin equivalent wound model for investigating novel wound healing therapies. *Tissue Eng. Part C Methods* 16, 1111–1123. doi: 10.1089/ten.TEC.2009.0725
- Zheng, K., Balasubramanian, P., Paterson, T. E., Stein, R., MacNeil, S., Fiorilli, S., et al. (2019). Ag modified mesoporous bioactive glass nanoparticles for enhanced antibacterial activity in 3D infected skin model. *Mater. Sci. Eng. C* 103:109764. doi: 10.1016/j.msec.2019.109764

Conflict of Interest: The authors declare that the research was conducted in the absence of any commercial or financial relationships that could be construed as a potential conflict of interest.

Copyright © 2020 Bolle, Verderosa, Dhoub, Parker, Fraser, Dargaville and Totsika. This is an open-access article distributed under the terms of the Creative Commons Attribution License (CC BY). The use, distribution or reproduction in other forums is permitted, provided the original author(s) and the copyright owner(s) are credited and that the original publication in this journal is cited, in accordance with accepted academic practice. No use, distribution or reproduction is permitted which does not comply with these terms.



Glycopeptide Antibiotic Resistance Genes: Distribution and Function in the Producer Actinomycetes

Oleksandr Yushchuk[†], Elisa Binda[†] and Flavia Marinelli^{*}

Department of Biotechnology and Life Sciences, University of Insubria, Varese, Italy

OPEN ACCESS

Edited by:

Jose L. Martinez,
Consejo Superior de Investigaciones
Científicas (CSIC), Spain

Reviewed by:

Kapil Tahlán,
Memorial University of
Newfoundland, Canada
Sonia Gullón,
Centro Nacional de Biotecnología
(CNB), Spain

*Correspondence:

Flavia Marinelli
flavia.marinelli@uninsubria.it

[†]These authors have contributed
equally to this work

Specialty section:

This article was submitted to
Antimicrobials, Resistance and
Chemotherapy,
a section of the journal
Frontiers in Microbiology

Received: 14 February 2020

Accepted: 07 May 2020

Published: 17 June 2020

Citation:

Yushchuk O, Binda E and Marinelli F
(2020) Glycopeptide Antibiotic
Resistance Genes: Distribution and
Function in the Producer
Actinomycetes.
Front. Microbiol. 11:1173.
doi: 10.3389/fmicb.2020.01173

Glycopeptide antibiotics (GPAs) are considered drugs of “last resort” for the treatment of life-threatening infections caused by relevant Gram-positive pathogens (enterococci, staphylococci, and clostridia). Driven by the issue of the never-stopping evolution of bacterial antibiotic resistance, research on GPA biosynthesis and resistance is developing fast in modern “post-genomic” era. It is today widely accepted that resistance mechanisms emerging in pathogens have been acquired from the soil-dwelling antibiotic-producing actinomycetes, which use them to avoid suicide during production, rather than being orchestrated *de novo* by pathogen bacteria upon continued treatment. Actually, more and more genomes of GPA producers are being unraveled, carrying a broad collection of differently arranged GPA resistance (named *van*) genes. In the producer actinomycetes, *van* genes are generally associated with the antibiotic biosynthetic gene clusters (BGCs) deputized to GPA biosynthesis, being probably transferred/arranged together, favoring a possible co-regulation between antibiotic production and self-resistance. GPA BGC-associated *van* genes have been also found mining public databases of bacterial genomic and metagenomic sequences. Interestingly, some BGCs for antibiotics, seemingly unrelated to GPAs (e.g., feglymycin), carry *van* gene homologues. Herein, we would like to cover the recent advances on the distribution of GPA resistance genes in genomic and metagenomics datasets related to GPA potential/proved producer microorganisms. A thorough understanding of GPA resistance in the producing microorganisms may prove useful in the future surveillance of emerging mechanisms of resistance to this clinically relevant antibiotic class.

Keywords: antimicrobial resistance, glycopeptide antibiotics, *van* genes, glycopeptide producers, biosynthetic gene clusters

GPA MODE OF ACTION AND RESISTANCE GENES IN GRAM-POSITIVE PATHOGENS

According to a recent report (WHO, 2017), drug-resistant infections will kill more people than cancer in just over three decades: by 2050, 10 million people are going to die every year due to antimicrobial resistance (AMR). Consequently, it is mandatory to stimulate discovery and development of novel antibiotics to counteract AMR (O'Neill, 2016). Glycopeptide antibiotics (GPAs) are frequently used to treat life-threatening infections caused by multidrug-resistant Gram-positive pathogens, such as *Staphylococcus aureus*, *Enterococcus* spp., and *Clostridium difficile* (for a review on their discovery and development, see Marcone et al., 2018; on their

antimicrobial activity and clinical use, Zeng et al., 2016). GPAs inhibit bacterial cell wall synthesis in Gram-positive bacteria by binding to D-alanyl-D-alanine (D-Ala-D-Ala) dipeptide terminus of peptidoglycan (PG) precursors, sequestering the substrate from transpeptidation and transglycosylation reactions in the late extracellular stages of PG cross-linking. Thus, GPA action ultimately results in destabilizing cell wall integrity, causing bacterial cell death (Perkins and Nieto, 1974). Gram-negative microorganisms are intrinsically resistant to GPAs, because of their outer membrane, which prevents these molecules entering into the periplasm. In Gram-positive bacteria, the onset of vancomycin resistance was long-delayed in comparison to other antibiotic classes. The first vancomycin-resistant clinical isolate – an *Enterococcus faecium* strain – was reported in 1987, more than 30 years after the clinical introduction of vancomycin (Leclercq et al., 1988; Miller et al., 2016). Unfortunately, today a vast majority of *E. faecium* isolates harbor vancomycin resistance genes (*van*) (Vehreschild et al., 2019). The first vancomycin-resistant *S. aureus* (VRSA) isolate was reported in 2002 as a result of horizontal gene transfer from resistant enterococci (Bartley, 2002; Weigel et al., 2003); nowadays, 52 VRSA strains have been described worldwide (Cong et al., 2020).

The GPA resistance mechanisms in Gram-positive pathogens were intensively studied starting from the pioneering work published in the 1990s (Arthur et al., 1992, 1996). Gram-positive pathogens escape GPA action by reprogramming PG precursor biosynthesis, replacing the terminal D-Ala with D-lactate (D-Ala-D-Lac) or D-serine (D-Ala-D-Ser), thus reducing the affinity for cellular targets (Arthur et al., 1992, 1996; Courvalin, 2006). In enterococci, many different GPA-resistant phenotypes have been described according to their *van* gene operon organization (for a review, see Binda et al., 2014): in *vanA*, *vanB*, *vanD*, and *vanM* the key ligase determines the replacement of the terminus D-Ala with D-Lac, whereas in *vanC*, *vanE*, *vanG*, *vanL*, and *vanN* D-Ala. The D-Ala-D-Lac-type operons are located either on plasmids or on chromosomes, whereas the D-Ala-D-Ser-type ones are exclusively on the bacterial chromosome, except the case of *vanN* found on a plasmid in *E. faecium*. Operon expression could be inducible by GPAs (*vanA*, *vanB*, *vanG*, *vanE*, *vanL*, and *vanM*) or constitutive (*vanC*, *vanD*, and *vanN*) (Reynolds and Courvalin, 2005; Depardieu et al., 2007; Binda et al., 2014). The most clinically relevant manifestation of GPA resistance occurs in VanA enterococci and staphylococci, and in VanB enterococci. The first group is highly resistant to both vancomycin and teicoplanin, whereas the second group only to vancomycin. In both of them, resistance is mediated by the GPA-induced expression of the transposone-located *vanHAX* gene operon under the transcriptional control of the VanR/VanS two-component system (TCS). VanS is a membrane-associated sensor that in VanA bacteria is activated by the presence of either vancomycin or teicoplanin, whereas in VanB it is activated only by vancomycin. Consequently, VanB enterococci are sensitive to teicoplanin (Arthur et al., 1997, 1999; Arthur and Quintilliani, 2001). Activated VanS transfers a phosphoryl group to VanR, which is the response regulator that controls the co-transcription of

the *vanH*, *vanA*, *vanX*, and *vanY* genes (Wright et al., 1993; Arthur et al., 1997, 1999; Arthur and Quintilliani, 2001). VanH is a dehydrogenase that reduces pyruvate to D-lactate; VanA is the key ligase that catalyzes the formation of the D-Ala-D-Lac resistant depsipeptide (Bugg et al., 1991; Arthur et al., 1992); VanX is a D,D-dipeptidase, which removes the intracellular pool of D-Ala-D-Ala produced by the native enterococcal ligase, ensuring that D-Ala-D-Lac is incorporated into PG precursors (Reynolds et al., 1994; Wu et al., 1995); and finally VanY has an ancillary role as a D,D-carboxypeptidase cleaving the last D-Ala from the residual pentapeptide PG precursors terminating in D-Ala-D-Ala (Arthur et al., 1998). Among the D-Ala-D-Ser-type operons, the better investigated was the *vanC*. It encodes for a racemase (VanT) that converts L-Ser to D-Ser, a ligase (VanC) that synthesizes D-Ala-D-Ser, and a bi-functional D,D-dipeptidase/D,D-carboxypeptidase (VanXYc) that cleaves the residual pools of D-Ala-D-Ala (Billot-Klein et al., 1994; Reynolds and Courvalin, 2005). In VanC phenotype, the TCS VanRcSc is located downstream the operon, but the resistance is constitutive due to mutations in the sensor VanSc (Healy et al., 2000; Hong et al., 2008; Koteva et al., 2010). VanC enterococci are intrinsically resistant to low levels of vancomycin, although they remain sensitive to teicoplanin.

Additional variants of these *van* gene operons were found in other Gram-positive pathogens including *Listeria* spp., streptococci, clostridia (Biavasco et al., 1996; Poyart et al., 1997; Peltier et al., 2013), and also in nonpathogenic Gram-positives, including *Bacillus circulans*, *Oerskovia* spp., *Corynebacterium* spp., and *Streptomyces coelicolor* (Power et al., 1995; Fontana et al., 1997; Hong et al., 2004). A novel vancomycin *vanF* operon (*vanY_FZ_FH_FFX_F*) was described in *Paenibacillus popilliae*, an environmental bacteria used as biopesticide to counteract beetle larvae that caused milky disease in Japan (Patel et al., 2000; Ahmed and Baptiste, 2018). The dissemination of GPA resistance more recently reached zoonotic pathogens such as the emergent *Streptococcus suis*, where the low level of vancomycin-resistance is due to the presence of a *vanG*-like operon (Huang et al., 2018). Herein, we focus our attention on *van* genes distribution and function in the GPA-producing actinomycetes, which are considered the putative primary source of the variety of GPA-resistant determinants occurring in environmental bacteria and pathogens (Marshall et al., 1998; Beltrametti et al., 2007; Marcone et al., 2010, 2014; Schäberle et al., 2011).

UPDATING THE GLYCOPEPTIDE RESISTANCE PARADIGM FOR THE GPA-PRODUCING STRAINS: VAN GENES AND THEIR ORGANIZATION IN KNOWN AND PUTATIVE GPA BGCs

Actinomycetes are Gram-positive soil-dwelling bacteria, which produce about two-thirds of the naturally derived antibiotics with clinical use (Bérdy, 2012; Barka et al., 2015), including GPAs (Nicolaou et al., 1999). Clinically relevant GPAs are produced by *Amycolatopsis orientalis* (vancomycin), *Actinoplanes*

teichomyceticus (teicoplanin), and *Nonomuraea gerenzanensis* (dalbavancin precursor – A40926) (Zeng et al., 2016; Marccone et al., 2018). GPA producers require self-resistance mechanisms to avoid suicide during antibiotic production and, like in pathogens, such resistance is due to *van* genes, whose description dates back to the end of the 1990s, one decade later than in pathogens (Marshall et al., 1997, 1998). Sequence and operon structure similarities of *van* genes between pathogens and GPA-producers are significant (Hong et al., 2008; Binda et al., 2014). The intriguing aspect is that in GPA producers, *van* genes are usually located within the GPA biosynthetic gene clusters (BGCs) deputized to the antibiotic biosynthesis (Pootoolal et al., 2002; Beltrametti et al., 2007; Marccone et al., 2010, 2014; Schäberle et al., 2011). In the last two decades, multiple novel GPA BGCs from actinomycetes were sequenced and annotated, and each of them (with few exceptions, see below) contains *van* genes (Figure 1).

Thus far, the majority of GPA BGCs were found in members of the genus *Amycolatopsis* (Adamek et al., 2018), which belongs to the *Pseudonocardiaceae* family. Besides the vancomycin producers, other *Amycolatopsis* spp. produce avoparcin, decaplanin, nogabecin, ristocetin, teicoplanin aglycone-like GPA, norvancomycin, balhimycin, and chloroeremomycin. In their corresponding BGCs, *van* genes were found just upstream the genes coding for the StrR-like pathway-specific regulators (orthologues of *bbr* from balhimycin BGC, Figure 1). We excluded from this comparison the chloroeremomycin BGC from *Amycolatopsis orientalis* PA-42867 (?) (van Wageningen et al., 1998), which apparently was not completely covered with sequencing. Thus, three patterns for the organization of *van* genes are recognizable (Figure 1) in *Pseudonocardiaceae* GPA producers. In the producers of avoparcin, decaplanin, nogabecin, ristocetin, and teicoplanin-like aglycone GPA, the GPA BGCs carry *vanHAX* orthologues, but not *vanY* or *vanRS* orthologues. In vancomycin and norvancomycin producers, *vanY* orthologues are clustered with *vanHAX* ones. Balhimycin producer – *Amycolatopsis balhimycina* – possesses a BGC with *vanRS* (*vanR_{Ab}S_{Ab}*) and *vanY* (*vanY_{Ab}*) orthologues, but *vanHAX* orthologues (*vanH_{Ab}A_{Ab}X_{Ab}*) were actually found 2 kbp away from balhimycin BGC (Schäberle et al., 2011; Fräsch et al., 2015). Indeed, no cluster-situated *van* genes were found sequencing the genome of *Kibdelosporangium aridum* – the producer of kibdelins (Shearer et al., 1986) – which also belongs to *Pseudonocardiaceae* family (Figure 1).

Other known GPA BGCs are from *Actinoplanes* spp. (family *Micromonosporaceae*) and *Nonomuraea* spp. (family *Streptosporangiaceae*). *Act. teichomyceticus* and *Actinoplanes* sp. ATCC 53533 produce teicoplanin (Bardone et al., 1978) and UK-68,597 (Skelton et al., 1990), respectively. Teicoplanin BGC (named *tei*) contains *vanHAX* and *vanRS* orthologues (*tei7-6-5* and *tei2-3*, respectively) organized in two separate operons, but none *vanY* orthologue (Figure 1; Li et al., 2004; Yushchuk et al., 2020b). In contrast, UK-68,597 BGC contains a *vanH*, not contiguous *vanR* and *vanS*, and a *vanY* orthologue (Figure 1; Yim et al., 2014). In the genus *Nonomuraea*, *N. gerenzanensis* ATCC 39727 and *Nonomuraea* sp. ATCC 55076 produce A40926 (Goldstein et al., 1987) and the type V glycopeptide kistamicin

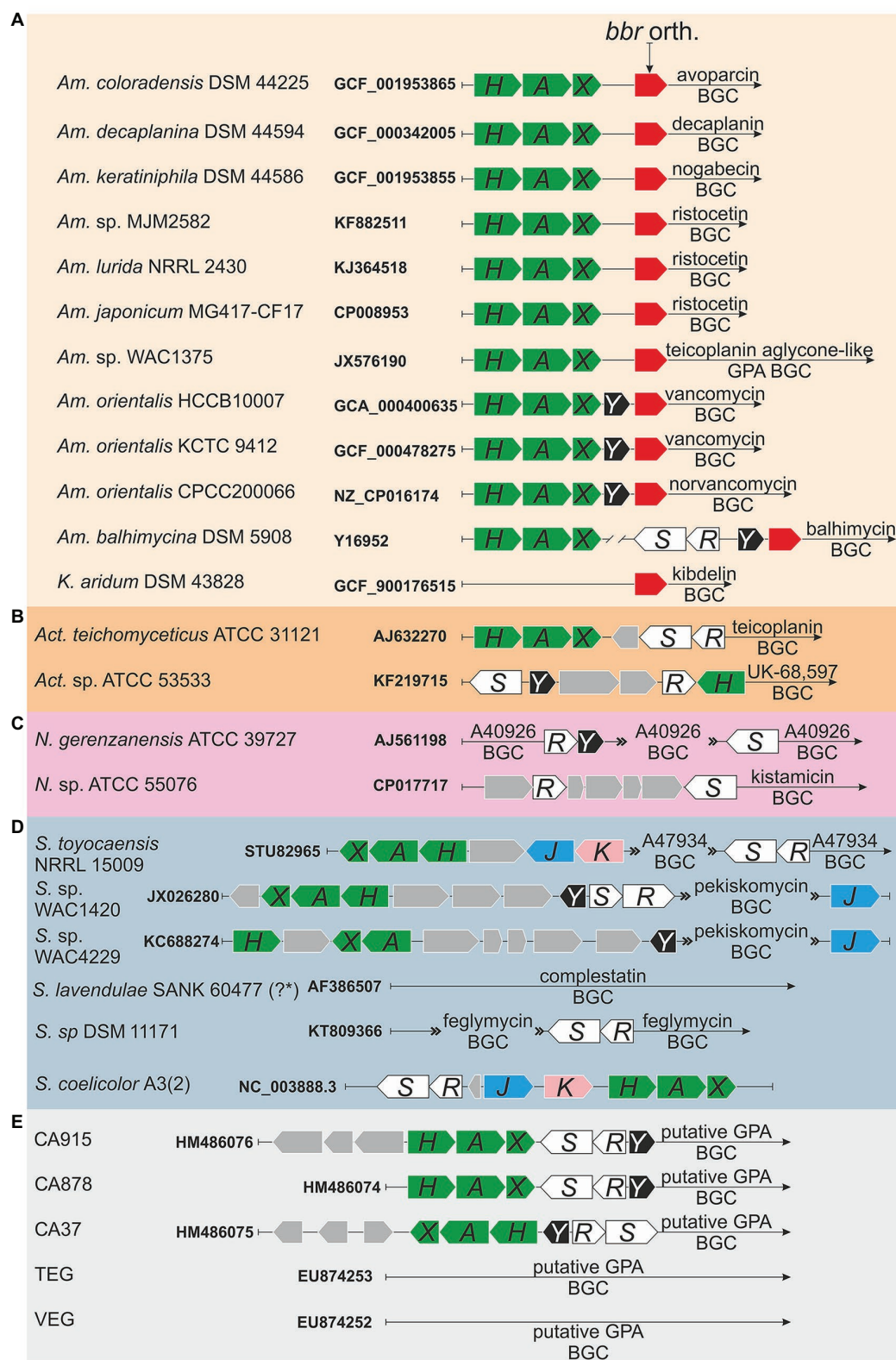
(Naruse et al., 1993), respectively. In A40926 BGC (named *dbv*) (Sosio et al., 2003), *vanR* and *vanS* homologues (*dbv6* and *dbv22*, respectively) are not contiguous and GPA resistance is due to the expression of *vanY* orthologue (*dbv7*, Figure 1; Marccone et al., 2010, 2014; Binda et al., 2012;). No *vanHAXY* genes are present in kistamicin BGC, although kistamicin BGC contains homologues of *vanS* and *vanR* named *kisG* and *kisB* (Nazari et al., 2017).

GPA are also produced by few *Streptomyces* species (Figure 1). Interestingly, functional *van* genes were also found in *S. coelicolor*, which is not a GPA producer (Hong et al., 2004). A47934 BGC from *Streptomyces toyocaensis* NRRL 15009 contains *vanH_{St}A_{St}X_{St}* and *vanR_{St}S_{St}* operons, together with *staO* and *staP* orthologues to *S. coelicolor* *vanJ* and *vanK*, respectively (Pootoolal et al., 2002). Pekiskomycin BGC from *Streptomyces* sp. WAC1420 contains *vanY*, *vanJ* as well as *vanHAX* and *vanRS* homologues, but pekiskomycin BGC from *Streptomyces* sp. WAC4229 lacks *vanRS* homologues (Thaker et al., 2013). No homologues of *van* genes were found in complestatin (type V GPA) BGC from *S. lavendulae* SANK 60477 (?) (Chiu et al., 2001), although this antibiotic possesses a moderate antibacterial activity. However, complestatin was shown to inhibit the fatty acid biosynthesis in Gram-positive bacteria (Kwon et al., 2015), therefore the producer may require no cell wall remodeling for complestatin self-resistance. Finally, feglymycin BGC from *Streptomyces* sp. DSM11171 (Figure 1) encodes for a 13-mer peptide antibiotic acting on bacterial cell wall biosynthesis by inhibiting MurA and MurC. Albeit the structure and the mode of action of feglymycin differs from the ones of GPAs, feglymycin BGC shares a high level of similarity with GPA BGCs (Gonsior et al., 2015; Yushchuk et al., 2020a), including the presence of *vanRS*-like genes – *fegM* and *fegN*.

To conclude, CA915, CA37, and CA878 GPA BGCs (Banik et al., 2010), which were sequenced from metagenomics samples, contain *vanHAX*, *vanY* and *vanRS* homologues, whereas none *van* gene was found in other metagenome-derived GPA BGCs as TEG and VEG (Banik and Brady, 2008; Figure 1).

UPDATING ON WHAT IS KNOWN ABOUT THE *IN VIVO* FUNCTION OF VAN GENES IN GPA-PRODUCING STRAINS

Although *van* genes were found in multiple GPA BGCs, only for few of them the function was experimentally proven. Balhimycin resistance in *Am. balhimycina* is likely the most deeply investigated model among GPA producers (Figure 2A). *vanH_{Ab}A_{Ab}X_{Ab}*, that is located outside the BGC (Figure 1), was shown to be constitutively expressed through all the periods of growth and during balhimycin production (Schäberle et al., 2011). Deletion of *vanH_{Ab}A_{Ab}X_{Ab}* genes makes *Am. balhimycina* significantly more sensitive to its own product, decreasing its MIC from 5 to 0.25 mg/ml, and causing an earlier expression of the BGC-situated *vanY_{Ab}* (Fräsch et al., 2015). However, *vanY_{Ab}* itself does not play a decisive role in GPA-resistance since its deletion did not alter the GPA resistance phenotype



* it is unclear from the literature whether the nucleotide sequence corresponds to this particular strain.

FIGURE 1 | (Continued)

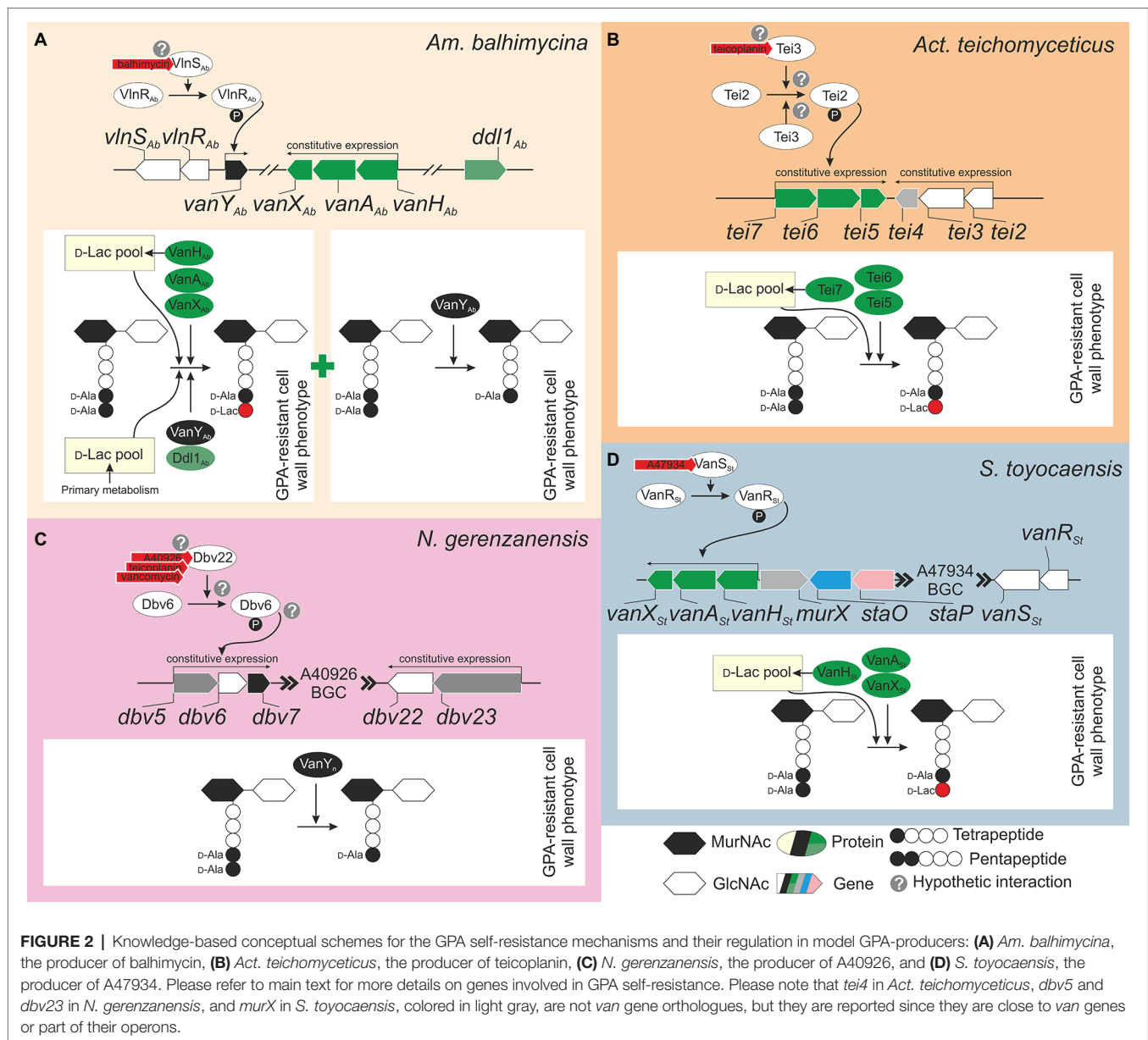
FIGURE 1 | Organization of *van* genes orthologues in glycopeptide antibiotic (GPA) biosynthetic gene clusters (BGCs) of producers and metagenomics sequences: **(A)** family *Pseudonocardiaceae*: *Amycolatopsis coloradensis* DSM 44225 (GCF_001953865) – avoparcin producer (Kunstmann et al., 1968; Labeda, 1995); *Amycolatopsis decaplanina* DSM 44594 (GCF_000342005, Kaur et al., 2013) – decaplanin producer (Sanchez et al., 1992); *Amycolatopsis keratiniphila* subsp. *nogabecina* DSM 44586 (= *Amycolatopsis keratiniphila* subsp. *nogabecina* FH1893, GCF_001953855) – nogabecin producer (Wink et al., 2003); *Amycolatopsis* sp. MJM2582 (KF882511, Truman et al., 2014), *Amycolatopsis lurida* NRRL2430 (KJ364518, Truman et al., 2014), *Amycolatopsis japonicum* MG417-CF17 (CP008953, Spohn et al., 2014) – ristocetin producers; *Amycolatopsis* sp. WAC4169 (JX576190, Thaker et al., 2013) – producer of teicoplanin aglycone-like GPA; *Amycolatopsis orientalis* HCCB10007 (= *Am. keratiniphila*, GCA_000400635, Xu et al., 2014) and *Amycolatopsis orientalis* KCTC 9412 (= *Am. orientalis* DSM 40040, GCF_000478275, Jeong et al., 2013) – vancomycin producers; *Amycolatopsis orientalis* CPCC200066 (= *Am. orientalis* B-37, NZ_CP016174, Lei et al., 2015) – norvancomycin producer; *Amycolatopsis balhimycina* DSM 5908 (Y16952, Shawky et al., 2007) – balhimycin producer (Nadkarni et al., 1994; Wink et al., 2003); *Kibdelosporangium aridum* DSM 43828 (GCF_900176515) – the producer of kibdelins (Shearer et al., 1985), **(B)** genus *Actinoplanes* (please see main text for more details), **(C)** genus *Nonomuraea* (please see main text for more details), **(D)** genus *Streptomyces* (please see main text for more details); although *S. coelicolor* is not a GPA producer, organization of *S. coelicolor* *van* gene orthologues is also given, and **(E)** metagenomics sequences (please see main text for more details).

(Frasch et al., 2015). Double *vanH_{Ab}A_{Ab}X_{Ab}* and *vanY_{Ab}* knocked-out mutants showed the same GPA resistance phenotype as Δ *vanH_{Ab}A_{Ab}X_{Ab}*. PG precursors ending in D-Ala-D-Lac were still found in the single Δ *vanH_{Ab}A_{Ab}X_{Ab}* and in the double Δ *vanH_{Ab}A_{Ab}X_{Ab}* Δ *vanY_{Ab}* mutants together with D-Ala-D-Ala ending PG precursors and tetrapeptides (Frasch et al., 2015). The residual GPA resistance in these mutants is probably due to an accessory Ddl1_{Ab}, a putative D-Ala-D-Lac ligase encoded in the genome of *Am. balhimycina*, which shares 72% of amino acid sequence identity with VanA_{Ab} (Frasch et al., 2015). Ddl1_{Ab} might add D-Lac to the tetrapeptide PG precursors generated by the D,D-carboxypeptidase VanY_{Ab} (although the presence of some other D-Ala-D-Ala carboxypeptidases encoded in the genome cannot be completely ruled out considering the resistant phenotype of the Δ *vanY_{Ab}* mutant). In the absence of VanH_{Ab}, D-Lac for this reaction is probably obtained from the primary metabolic pool. Expression of *vanH_{Ab}A_{Ab}X_{Ab}* was demonstrated to be independent from the BGC-situated regulator *vlnR_{Ab}* (Kilian et al., 2016). However, *VlnR_{Ab}* is important for the activation of the BGC-situated *vanY_{Ab}* expression (Kilian et al., 2016). Heterologous expression of *vlnR_{Ab}S_{Ab}* in *S. coelicolor* Δ *vanRS* mutants indicated that both *VlnR_{Ab}* and *VlnS_{Ab}* are active and able to replace their counterparts VanR and VanS, which in *S. coelicolor* control the expression of *vanHAX* genes in response to vancomycin (Hong et al., 2004), restoring resistance to both balhimycin and teicoplanin in the complemented strains (Kilian et al., 2016). Overall, it seems that the BGC-situated *vlnR_{Ab}S_{Ab}-vanY_{Ab}* regulatory circuit is functional, but does not play a major role in balhimycin resistance, which is mostly determined by *vanH_{Ab}A_{Ab}X_{Ab}* expression. It would be interesting to test GPA resistance in *ddl1_{Ab}* knocked-out mutant generated in *Am. balhimycina* Δ *vanH_{Ab}A_{Ab}X_{Ab}* Δ *vanY_{Ab}* to better understand the role of this accessory ligase and its connection with the D,D-carboxypeptidase activity of VanY_{Ab} (or of some other still-unknown carboxypeptidases).

Differently from *Am. balhimycina*, in *Act. teichomyceticus* *vanHAX* orthologues – *tei7-6-5* – are located within the *tei* BGC together with *vanRS* orthologues – *tei2-3* (Figure 2B). *tei7-6-5* expression determines the production of PG precursors ending in D-Ala-D-Lac, conferring a GPA-resistant phenotype to *Act. teichomyceticus* (Beltrametti et al., 2007; Binda et al., 2018). Interestingly, the expression of *tei7-6-5* operon is constant during the growth curve and in teicoplanin production conditions (Beltrametti et al., 2007; Yushchuk et al., 2019)

and the VanX D,D-di-peptidase activity was detectable in cellular extracts independently from the addition of teicoplanin (Binda et al., 2018). One probable reason for the constitutive expression of *tei7-6-5* is the non-inducibility of the sensor histidine kinase Tei3, due to its point mutations previously known to confer a constitutive kinase activity to *S. coelicolor* VanS (Beltrametti et al., 2007). Also, the expression of *vanRS* orthologues – *tei2-3* – was also found constitutive under teicoplanin production conditions (Yushchuk et al., 2019) and these genes are co-expressed with *tei4* – coding for a dehydrofolate reductase with no obvious role in teicoplanin-resistance (Yushchuk et al., 2020b). Moreover, *tei2-3-4* expression is independent from *tei* cluster-encoded transcriptional regulators – Tei15* and Tei16* (Yushchuk et al., 2019, 2020b). Constitutive expression of *tei2-3-4* could be granted by *tei2* promoter, which was shown to be highly active in *Act. teichomyceticus*, starting from the very early stage of spore germination (Yushchuk et al., 2020b). More investigations are required for a complete understanding of teicoplanin-resistance in *Act. teichomyceticus*. Study of the Tei3 properties is among the most interesting tasks.

In *N. gerenzanensis* producing the teicoplanin-like A40926, *vanHAX* orthologues were not found neither in the BGC nor in the genome (D'Argenio et al., 2016). The only known mechanism of resistance relies on the action of VanY_n, whose coding gene (*dbv7*) is within the *dbv* BGC (Figure 2C) and whose knockout abolishes the resistance phenotype (Marcone et al., 2010, 2014; Figure 2C). VanY_n is a D,D-carboxypeptidase that cleaves the last D-Ala from pentapeptide PG precursors generating tetrapeptides, drastically reducing GPA affinity for cellular targets (Binda et al., 2012). A L,D-transpeptidase (Ldt) then uses the tetrapeptide acyl donors supplied by VanY_n to synthesize the mature cell wall (Hugonnet et al., 2014). The role of this protein and its features that assimilate/distinguish it from enterococcal VanY and from VanY_{Ab} were investigated in detail (Marcone et al., 2010, 2014; Binda et al., 2012, 2013). Less clear is the regulatory circuit governing *dbv7* expression. Direct VanY_n carboxypeptidase activity measurement in *N. gerenzanensis* growing with the addition of different GPAs, unambiguously showed that VanY_n activity is induced by vancomycin, teicoplanin, and A40926 (Binda et al., 2018). *vanRS* homologues – *dbv6* and *dbv22* – are present in the *dbv* BGC, but the knockout of *dbv6* did not exert any influence on A40926 production and growth of



N. gerezanensis (Lo Grasso et al., 2015). Unfortunately, the GPA resistance phenotype of this mutant was not described. On the other side, transcriptional analysis of *dbv* genes indicated that the expression of *dbv5-6-7* and *dbv23-22* operons is rather constitutive (Alduina et al., 2007). Although the presence of other GPA-sensitive TCS beyond the borders of A40926 BGC cannot be ruled out, role of Dbv6 and Dbv22 in *N. gerezanensis* A40926 self-resistance merits further investigations.

Finally, *S. toyocaensis* possesses, perhaps, the most straightforward resistance mechanism among all the investigated GPA producers (Figure 2D), reminding the situation in *S. coelicolor* (Hong et al., 2004). The BGC-located *vanH_{St}A_{St}X_{St}* operon was shown to be crucial for A47934 resistance and *vanA_{St}* knockout made *S. toyocaensis* completely sensitive

to A47934 (Pootoolal et al., 2002). At the same time, *vanHAX*-genes from the vancomycin producer *Am. orientalis* C329.2 were able to restore A47934 resistance phenotype in the knocked-out mutant (Pootoolal et al., 2002). Functions of VanR_{St} and VanS_{St} (both present in the A47934 BGC, Figures 1, 2D) were also studied in detail, showing that VanS_{St} has a remarkable specificity for A47934 and it is unable to sense teicoplanin or vancomycin (Koteva et al., 2010; Novotna et al., 2016). Moreover, also the interaction between VanR_{St} and VanS_{St} was found to be very specific, since VanR_{St} could not be phosphorylated by a non-cognate sensor-histidine kinase (Novotna et al., 2016). The roles (if there are any) of *staP* and *staO* (orthologues of *S. coelicolor* *vanK* and *vanJ*) in *S. toyocaensis* A47934 self-resistance were not investigated, thus the importance of these auxiliary resistance genes remains to be proved.

OUTLOOK

Soil GPA producers are considered the putative source of GPA resistance determinants, which might have been recruited and differently combined in pathogens. The goal of this mini review is to update the knowledge on the occurrence and role of *van* genes in producing microorganisms. It emerges that more *in silico*, *in vitro*, and *in vivo* investigations on their function and regulation are required to shed light on the intriguing issue of their origin and role. Overall, a detailed phylogenetic analysis would be useful to illuminate the evolution of GPA-resistant determinants in GPA producers and from them to pathogens. A recent pioneering work on the reconstruction of GPA BGC phylogeny (Waglechner et al., 2019) reported on the possible origin and evolution of GPA cluster-situated *van*-genes. According to these authors, *vanA* had likely originated within *Amycolatopsis* genus, whereas *vanH*, *vanX*, and *vanRS* within *Actinoplanes*; and *vanY* probably originated within genus *Nonomuraea* and it was then distributed among GPA BGCs by multiple transfer events. Combination of these genes in

pathogens is today determining the urgent clinical need for new drugs to combat multi-drug resistant Gram-positive pathogens.

AUTHOR CONTRIBUTIONS

EB and OY collected data and papers and co-wrote the review. OY prepared the figures. FM and EB supervised the work.

FUNDING

This work was supported by grant “Fondo di Ateneo per la Ricerca” 2017, 2018 to FM, and Consorzio Italbiotec to EB.

ACKNOWLEDGMENTS

We are grateful to Consorzio Italbiotec for supporting EB.

REFERENCES

- Adamek, M., Alanjary, M., Sales-Ortells, H., Goodfellow, M., Bull, A. T., Winkler, A., et al. (2018). Comparative genomics reveals phylogenetic distribution patterns of secondary metabolites in *Amycolatopsis* species. *BMC Genomics* 19:426. doi: 10.1186/s12864-018-4809-4
- Ahmed, M. O., and Baptiste, K. E. (2018). Vancomycin-resistant enterococci: a review of antimicrobial resistance mechanisms and perspectives of human and animal health. *Microb. Drug Resist.* 24, 590–606. doi: 10.1089/mdr.2017.0147
- Alduina, R., Piccolo, L. L., Dalia, D., Ferraro, C., Gunnarsson, N., Donadio, S., et al. (2007). Phosphate-controlled regulator for the biosynthesis of the dalbavancin precursor A40926. *J. Bacteriol.* 189, 8120–8129. doi: 10.1128/JB.01247-07
- Arthur, M., Depardieu, F., Cabanié, L., Reynolds, P., and Courvalin, P. (1998). Requirement of the VanY and VanX D,D-peptidases for glycopeptide resistance in enterococci. *Mol. Microbiol.* 30, 819–830. doi: 10.1046/j.1365-2958.1998.01114.x
- Arthur, M., Depardieu, F., and Courvalin, P. (1999). Regulated interactions between partner and non-partner sensors and response regulators that control glycopeptide resistance gene expression in enterococci. *Microbiologica* 145, 1849–1858. doi: 10.1099/13500872-145-8-1849
- Arthur, M., Depardieu, F., Gerbaud, G., Galimand, M., Leclercq, R., and Courvalin, P. (1997). The VanS sensor negatively controls VanR-mediated transcriptional activation of glycopeptide resistance genes of *Tn1546* and related elements in the absence of induction. *J. Bacteriol.* 179, 97–106. doi: 10.1128/JB.179.1.97-106.1997
- Arthur, M., Molinas, C., Bugg, T. D., Wright, G. D., Walsh, C. T., and Courvalin, P. (1992). Evidence for *in vivo* incorporation of D-lactate into peptidoglycan precursors of vancomycin-resistant enterococci. *Antimicrob. Agents Chemother.* 36, 867–869. doi: 10.1128/aac.36.4.867
- Arthur, M., and Quintiliani, R. (2001). Regulation of VanA- and VanB-type glycopeptide resistance in enterococci. *Antimicrob. Agents Chemother.* 45, 375–381. doi: 10.1128/aac.45.2.375-381.2001
- Arthur, M., Reynolds, P., and Courvalin, P. (1996). Glycopeptide resistance in enterococci. *Trends Microbiol.* 4, 401–407. doi: 10.1016/0966-842X(96)10063-9
- Banik, J. J., and Brady, S. F. (2008). Cloning and characterization of new glycopeptide gene clusters found in an environmental DNA megalibrary. *Proc. Natl. Acad. Sci. U. S. A.* 105, 17273–17277. doi: 10.1073/pnas.0807564105
- Banik, J. J., Craig, J. W., Calle, P. Y., and Brady, S. F. (2010). Tailoring enzyme-rich environmental DNA clones: a source of enzymes for generating libraries of unnatural natural products. *J. Am. Chem. Soc.* 132, 15661–15670. doi: 10.1021/ja105825a
- Bardone, M. R., Paternoster, M., and Coronelli, C. (1978). Teichomycins, new antibiotics from *Actinoplanes teichomyceticus* nov. sp. II. Extraction and chemical characterization. *J. Antibiot.* 31, 170–177. doi: 10.7164/antibiotics.31.170
- Barka, E. A., Vatsa, P., Sanchez, L., Gavetas-Vaillant, N., Jacquard, C., Meier-Kolthoff, J. P., et al. (2015). Taxonomy, physiology, and natural products of Actinobacteria. *Microbiol. Mol. Biol. Rev.* 80, 1–43. doi: 10.1128/MMBR.00019-15
- Bartley, J. (2002). First case of VRSA identified in Michigan. *Infect. Control Hosp. Epidemiol.* 23:480. doi: 10.1017/s0195941700082333
- Beltrametti, F., Consolandi, A., Carrano, L., Bagatin, F., Rossi, R., Leoni, L., et al. (2007). Resistance to glycopeptide antibiotics in the teicoplanin producer is mediated by *van* gene homologue expression directing the synthesis of a modified cell wall peptidoglycan. *Antimicrob. Agents Chemother.* 51, 1135–1141. doi: 10.1128/AAC.01071-06
- Bérdy, J. (2012). Thoughts and facts about antibiotics: where we are now and where we are heading. *J. Antibiot.* 65, 385–395. doi: 10.1038/ja.2012.27
- Biavasco, F., Giovanetti, E., Miele, A., Vignaroli, C., Facinelli, B., and Varaldo, P. E. (1996). *In vitro* conjugative transfer of VanA vancomycin resistance between Enterococci and *Listeriae* of different species. *Eur. J. Clin. Microbiol. Infect. Dis.* 15, 50–59. doi: 10.1007/BF01586185
- Billot-Klein, D., Blanot, D., Gutmann, L., and van Heijenoort, J. (1994). Association constants for the binding of vancomycin and teicoplanin to N-acetyl-D-alanyl-D-alanine and N-acetyl-D-alanyl-D-serine. *Biochem. J.* 304, 1021–1022. doi: 10.1042/bj3041021
- Binda, E., Cappelletti, P., Marinelli, F., and Marcone, G. L. (2018). Specificity of induction of glycopeptide antibiotic resistance in the producing actinomycetes. *Antibiotics* 7, 36–46. doi: 10.3390/antibiotics7020036
- Binda, E., Marcone, G. L., Berini, F., Pollegioni, L., and Marinelli, F. (2013). *Streptomyces* spp. as efficient expression system for a D,D-peptidase/D,D-carboxypeptidase involved in glycopeptide antibiotic resistance. *BMC Biotechnol.* 13:24. doi: 10.1186/1472-6750-13-24
- Binda, E., Marinelli, F., and Marcone, G. L. (2014). Old and new glycopeptide antibiotics: action and resistance. *Antibiotics* 3, 572–594. doi: 10.3390/antibiotics3040572
- Binda, E., Marcone, G. L., Pollegioni, L., and Marinelli, F. (2012). Characterization of VanYn, a novel 485 D,D-peptidase/D,D-carboxypeptidase involved in glycopeptide antibiotic resistance in *Nonomuraea* sp. ATCC 39727. *FEBS J.* 279, 3203–3213. doi: 10.1111/j.1742-487.4658.2012.08706.x
- Bugg, T. D., Wright, G. D., Dutka-Malen, S., Arthur, M., Courvalin, P., and Walsh, C. T. (1991). Molecular basis for vancomycin resistance in *Enterococcus faecium* BM4147: biosynthesis of a depsipeptide peptidoglycan precursor by

- vancomycin resistance proteins VanH and VanA. *Biochemist* 30, 10408–10415. doi: 10.1021/bi00107a007
- Chiu, H.-T., Hubbard, B. K., Shah, A. N., Eide, J., Fredenburg, R. A., Walsh, C. T., et al. (2001). Molecular cloning and sequence analysis of the complestatin biosynthetic gene cluster. *Proc. Natl. Acad. Sci. U. S. A.* 98, 8548–8553. doi: 10.1073/pnas.151246498
- Cong, Y., Yang, S., and Rao, X. (2020). Vancomycin resistant *Staphylococcus aureus* infections: a review of case updating and clinical features. *J. Adv. Res.* 21, 169–176. doi: 10.1016/j.jare.2019.10.005
- Courvalin, P. (2006). Vancomycin resistance in gram-positive cocci. *Clin. Infect. Dis.* 42, S25–S34. doi: 10.1086/491711
- D'Argenio, V., Pettillo, M., Pasanisi, D., Pagliarulo, C., Colicchio, R., Talà, A., et al. (2016). The complete 12 Mb genome and transcriptome of *Nonomuraea gerenzanensis* with new insights into its duplicated “magic” RNA polymerase. *Sci. Rep.* 6, 1–13. doi: 10.1038/s41598-016-0025-0
- Depardieu, F., Podglajen, I., Leclercq, R., Collatz, E., and Courvalin, P. (2007). Modes and modulations of antibiotic resistance gene expression. *Clin. Microbiol. Rev.* 20, 79–114. doi: 10.1128/CMR.00015-06
- Fontana, R., Ligozzi, M., Pedrotti, C., Padovani, E. M., and Cornaglia, G. C. (1997). Vancomycin-resistant *Bacillus circulans* carrying the vanA gene responsible for vancomycin resistance in enterococci. *Eur. J. Clin. Microbiol. Infect. Dis.* 16, 473–474. doi: 10.1007/BF02471915
- Frasch, H.-J., Kalan, L., Kilian, R., Martin, T., Wright, G. D., and Stegmann, E. (2015). Alternative pathway to a glycopeptide-resistant cell wall in the balhimycin producer *Amycolatopsis balhimycina*. *ACS Infect. Dis.* 1, 243–252. doi: 10.1021/acsinfecdis.5b00011
- Goldstein, B. P., Selva, E., Gastaldo, L., Berti, M., Pallanza, R., Ripamonti, F., et al. (1987). A40926, a new glycopeptide antibiotic with anti-*Neisseria* activity. *Antimicrob. Agents Chemother.* 31, 1961–1966. doi: 10.1128/aac.31.12.1961
- Gonsior, M., Mühlenweg, A., Tietzmann, M., Rausch, S., Poch, A., and Süsmuth, R. D. (2015). Biosynthesis of the peptide antibiotic feglymycin by a linear nonribosomal peptide synthetase mechanism. *Chembiochem* 16, 2610–2614. doi: 10.1002/cbic.201500432
- Healy, V. L., Lessard, I. A., Roper, D. I., Knox, J. R., and Walsh, C. T. (2000). Vancomycin resistance in enterococci: reprogramming of the D-alanyl-D-alanine ligases in bacterial peptidoglycan biosynthesis. *Chem. Biol.* 7, R109–R119. doi: 10.1016/S1074-5521(00)00116-2
- Hong, H. J., Hutchings, M. I., and Buttner, M. J. (2008). Vancomycin resistance VanS/VanR two-component systems. *Adv. Exp. Med. Biol.* 631, 200–213. doi: 10.1007/978-0-387-78885-2_14
- Hong, H. J., Hutchings, M. I., Neu, J. M., Wright, G. D., Paget, M. S. B., and Buttner, M. J. (2004). Characterization of an inducible vancomycin resistance system in *Streptomyces coelicolor* reveals a novel gene (vanK) required for drug resistance. *Mol. Microbiol.* 52, 1107–1121. doi: 10.1111/j.1365-2958.2004.04032.x
- Huang, J., Chen, L., Li, D., Wang, M., Du, F., Gao, Y., et al. (2018). Emergence of a vanG-n carrying and multidrug resistant ICE in zoonotic pathogen *Streptococcus suis*. *Vet. Microbiol.* 222, 109–113. doi: 10.1016/j.vetmic.2018.07.008
- Hugonnet, J.-E., Haddache, N., Veckerl, C., Dubost, L., Marie, A., Shikura, N., et al. (2014). Peptidoglycan cross-linking in glycopeptide-resistant actinomycetales. *Antimicrob. Agents Chemother.* 58, 1749–1756. doi: 10.1128/aac.02329-13
- Jeong, H., Sim, Y. M., Kim, H. J., Lee, D.-W., Lim, S.-K., and Lee, S. J. (2013). Genome sequence of the vancomycin-producing *Amycolatopsis orientalis* subsp. *orientalis* strain KCTC 9412T. *Genome Announc.* 1, e00408–e00413. doi: 10.1128/genome.00408-13
- Kaur, N., Kumar, S., Bala, M., Raghava, G. P. S., and Mayilraj, S. (2013). Draft genome sequence of *Amycolatopsis decaplanina* strain DSM 44594T. *Genome Announc.* 1, e00138–e00113. doi: 10.1128/genome.00138-13
- Kilian, R., Frasn, H.-J., Kulik, A., Wohlleben, W., and Stegmann, E. (2016). The VanRS homologous two-component system VnRSAB of the glycopeptide producer *Amycolatopsis balhimycina* activates transcription of the vanHAXSc genes in *Streptomyces coelicolor*, but not in *A. balhimycina*. *Microb. Drug Resist.* 22, 499–509. doi: 10.1089/mdr.2016.0128
- Koteva, K., Hong, H.-J., Wang, X. D., Nazi, I., Hughes, D., Naldrett, M. J., et al. (2010). A vancomycin photoprobe identifies the histidine kinase VanSc as a vancomycin receptor. *Nat. Chem. Biol.* 6, 327–329. doi: 10.1038/nchembio.350
- Kunstmann, M. P., Mitscher, L. A., Porter, J. N., Shay, A. J., and Darken, M. A. (1968). LL-AV290, a new antibiotic. I. Fermentation, isolation, and characterization. *Antimicrob. Agents Chemother.* 8, 242–245.
- Kwon, Y.-J., Kim, H.-J., and Kim, W.-G. (2015). Complestatin exerts antibacterial activity by the inhibition of fatty acid synthesis. *Biol. Pharm. Bull.* 38, 715–721. doi: 10.1248/bpb.b14-00824
- Labeda, D. P. (1995). *Amycolatopsis coloradensis* sp., nov., the avoparcin (LL-AV290)-producing strain. *Int. J. Syst. Evol. Microbiol.* 45, 124–127. doi: 10.1099/00207713-45-1-124
- Leclercq, R., Derlot, R., Duval, E. J., and Courvalin, P. (1988). Plasmid-mediated resistance to vancomycin and teicoplanin in *Enterococcus faecium*. *N. Engl. J. Med.* 319, 157–161. doi: 10.1056/NEJM198807213190307
- Lei, X., Yuan, F., Shi, Y., Li, X., Wang, L., and Hong, B. (2015). Draft genome sequence of norvancomycin-producing strain *Amycolatopsis orientalis* CPCC200066. *Genome Announc.* 3, e00296–e00215. doi: 10.1128/genome.00296-15
- Li, T., Huang, F., Haydock, S., Mironenko, T., Leadlay, P., and Spencer, J. (2004). Biosynthetic gene cluster of the glycopeptide antibiotic teicoplanin characterization of two glycosyltransferases and the key acyltransferase. *Chem. Biol.* 11, 107–119. doi: 10.1016/j.chembiol.2004.01.001
- Lo Grasso, L., Maffioli, S., Sosio, M., Bibb, M., Puglia, A. M., and Alduina, R. (2015). Two master switch regulators trigger A40926 biosynthesis in *Nonomuraea* sp. strain ATCC 39727. *J. Bacteriol.* 197, 2536–2544. doi: 10.1128/JB.00262-15
- Marcone, G. L., Beltrametti, F., Binda, E., Carrano, L., Foulston, L., Hesketh, A., et al. (2010). Novel mechanism of glycopeptide resistance in the A40926 producer *Nonomuraea* sp. ATCC 39727. *Antimicrob. Agents Chemother.* 54, 2465–2472. doi: 10.1128/AAC.00106-10
- Marcone, G. L., Binda, E., Berini, F., and Marinelli, F. (2018). Old and new glycopeptide antibiotics: from product to gene and back in the post-genomic era. *Biotechnol. Adv.* 36, 534–554. doi: 10.1016/j.biotechadv.2018.02.009
- Marcone, G. L., Binda, E., Carrano, L., Bibb, M., and Marinelli, F. (2014). Relationship between glycopeptide production and resistance in the actinomycete *Nonomuraea* sp. ATCC 39727. *Antimicrob. Agents Chemother.* 58, 5191–5201. doi: 10.1128/aac.02626-14
- Marshall, C. G., Broadhead, G., Leski, B. K., and Wright, G. D. (1997). D-Ala-D-Ala ligases from glycopeptide antibiotic-producing organisms are highly homologous to the enterococcal vancomycin-resistance ligases VanA and VanB. *Proc. Natl. Acad. Sci. U. S. A.* 94, 6480–6483. doi: 10.1073/pnas.94.12.6480
- Marshall, C. G., Lessard, I. A. D., Park, I.-S., and Wright, G. D. (1998). Glycopeptide antibiotic resistance genes in glycopeptide-producing organisms. *Antimicrob. Agents Chemother.* 42, 2215–2220. doi: 10.1128/AAC.42.9.2215
- Miller, W. R., Murray, B. E., Rice, L. B., and Arias, C. A. (2016). Vancomycin-resistant enterococci: therapeutic challenges in the 21st century. *Infect. Dis. Clin. North Am.* 30, 415–439. doi: 10.1016/j.idc.2016.02.006
- Nadkarni, S. R., Patel, M. V., Chatterjee, S., Vijayakumar, E. K. S., Desikan, K. R., Blumbach, J., et al. (1994). Balhimycin, a new glycopeptide antibiotic produced by *Amycolatopsis* sp. Y-86,21022. Taxonomy, production, isolation and biological activity. *J. Antibiot.* 47, 334–341. doi: 10.7164/antibiotics.47.334
- Naruse, N., Oka, M., Konishi, M., and Oki, T. (1993). New antiviral antibiotics, Kistamicins A and B. II. Structure determination. *J. Antibiot.* 46, 1812–1818. doi: 10.7164/antibiotics.46.1812
- Nazari, B., Forneris, C. C., Gibson, M. I., Moon, K., Schramma, K. R., and Seyedsayamdost, M. R. (2017). *Nonomuraea* sp. ATCC 55076 harbours the largest actinomycete chromosome to date and the kistamicin biosynthetic gene cluster. *Med. Chem. Commun.* 8, 780–788. doi: 10.1039/C6MD00637J
- Nicolaou, K. C., Boddy, C. N. C., Bräse, S., and Winssinger, N. (1999). Chemistry, biology, and medicine of the glycopeptide antibiotics. *Angew. Chem. Int. Ed. Engl.* 38, 2096–2152. doi: 10.1002/(sici)1521-3773(19990802)38:15<2096::aid-anie2096>3.0.co;2-f
- Novotna, G. B., Kwun, M. J., and Hong, H.-J. (2016). In vivo characterization of the activation and interaction of the VanR-VanS two-component regulatory system controlling glycopeptide antibiotic resistance in two related *Streptomyces* species. *Antimicrob. Agents Chemother.* 60, 1627–1637. doi: 10.1128/aac.01367-15
- O'Neill, J. (ed.). (2016). *Tackling drug-resistant infections globally: final report and recommendations. The review on antimicrobial resistance.* Available at: http://amr-review.org/sites/default/files/160518_Final%20paper_with%20cover.pdf
- Patel, R., Piper, K., Cockerill, F. R., Steckelberg, J. M., and Yousten, A. A. (2000). The biopesticide *Paenibacillus popilliae* has a vancomycin resistance gene cluster homologous to the enterococcal VanA vancomycin resistance

- gene cluster. *Antimicrob. Agents Chemother.* 44, 705–709. doi: 10.1128/aac.44.3.705-709.2000
- Peltier, J., Courtin, P., Meouche, E. I., Catel-Ferreira, M., Chapot-Chartier, M. P., Lemée, L., et al. (2013). Genomic and expression analysis of the vanG-like gene cluster of *Clostridium difficile*. *Microbiologica* 159, 1510–1520. doi: 10.1099/mic.0.065060-0
- Perkins, H. R., and Nieto, M. (1974). The chemical basis for the action of the vancomycin group of antibiotics. *Ann. N. Y. Acad. Sci.* 235, 348–363. doi: 10.1111/j.1749-6632.1974.tb43276.x
- Pootoolal, J., Thomas, M. G., Marshall, C. G., Neu, J. M., Hubbard, B. K., Walsh, C. T., et al. (2002). Assembling the glycopeptide antibiotic scaffold: the biosynthesis of from *Streptomyces toyocaensis* NRRL15009. *Proc. Natl. Acad. Sci. U. S. A.* 99, 8962–8967. doi: 10.1073/pnas.102285099
- Power, E. G. M., Abdulla, Y. H., Talsania, H. G., Spice, W., Aathithan, S., and French, G. L. (1995). vanA genes in vancomycin-resistant clinical isolates of *Oerskovia turbata* and *Arcanobacterium (Corynebacterium) haemolyticum*. *J. Antimicrob. Chemother.* 36, 595–606. doi: 10.1093/jac/36.4.595
- Poyart, C., Pierre, C., Quesne, G., Pron, B., Berche, P., and Trieu-Cuot, P. (1997). Emergence of vancomycin resistance in the genus *Streptococcus*: characterization of a vanB transferable determinant in *Streptococcus bovis*. *Antimicrob. Agents Chemother.* 41, 24–29.
- Reynolds, P. E., and Courvalin, P. (2005). Vancomycin resistance in enterococci due to synthesis of precursors terminating in D-alanyl-D-serine. *Antimicrob. Agents Chemother.* 49, 21–25. doi: 10.1128/AAC.49.1.21-25.2005
- Reynolds, P. E., Depardieu, F., Dutka-Malen, S., Arthur, M., and Courvalin, P. (1994). Glycopeptide resistance mediated by enterococcal transposon *Th1546* requires production of VanX for hydrolysis of D-alanyl-D-alanine. *Mol. Microbiol.* 13, 1065–1070. doi: 10.1111/j.1365-2958.1994.tb00497.x
- Sanchez, M. L., Wenzel, R. P., and Jones, R. N. (1992). In vitro activity of decaplanin (M86-1410), a new glycopeptide antibiotic. *Antimicrob. Agents Chemother.* 36, 873–875. doi: 10.1128/aac.36.4.873
- Schäberle, T. F., Vollmer, W., Fräsch, H.-J., Hüttel, S., Kulik, A., Röttgen, M., et al. (2011). Self-resistance and cell wall composition in the glycopeptide producer *Amycolatopsis balhimycina*. *Antimicrob. Agents Chemother.* 55, 4283–4289. doi: 10.1128/aac.01372-10
- Shawky, R. M., Puk, O., Wietzorrek, A., Pelzer, S., Takano, E., Wohlleben, W., et al. (2007). The border sequence of the balhimycin biosynthesis gene cluster from *Amycolatopsis balhimycina* contains *bbr*, encoding a StrR-like pathway-specific regulator. *J. Mol. Microbiol. Biotechnol.* 13, 76–88. doi: 10.1159/000103599
- Shearer, M. C., Actor, P., Bowie, B. A., Grappel, S. F., Nash, C. H., Newman, D. J., et al. (1985). Aridicins, novel glycopeptide antibiotics. I. Taxonomy, production and biological activity. *J. Antibiot.* 38, 555–560. doi: 10.7164/antibiotics.38.555
- Shearer, M. C., Giovenella, A. J., Grappel, S. F., Hedde, R. D., Mehta, R. J., Oh, Y. K., et al. (1986). Kibdelins, novel glycopeptide antibiotics. I. Discovery, production, and biological evaluation. *J. Antibiot.* 39, 1386–1394. doi: 10.7164/antibiotics.39.1386
- Skelton, N. J., Williams, D. H., Monday, R. A., and Ruddock, J. C. (1990). Structure elucidation of the novel glycopeptide antibiotic UK-68,597. *J. Org. Chem. Res.* 55, 3718–3723. doi: 10.1021/jo00299a008
- Sosio, M., Stinchi, S., Beltrametti, F., Lazzarini, A., and Donadio, S. (2003). The gene cluster for the biosynthesis of the glycopeptide antibiotic A40926 by *Nonomuraea* species. *Chem. Biol.* 10, 541–549. doi: 10.1016/S1074-5521(03)00120-0
- Spohn, M., Kirchner, N., Kulik, A., Jochim, A., Wolf, F., Muenzer, P., et al. (2014). Overproduction of ristomycin A by activation of a silent gene cluster in *Amycolatopsis japonicum* MG417-CF17. *Antimicrob. Agents Chemother.* 58, 6185–6196. doi: 10.1128/aac.03512-14
- Thaker, M. N., Wang, W., Spanogiannopoulos, P., Waglechner, N., King, A. M., Medina, R., et al. (2013). Identifying producers of antibacterial compounds by screening for antibiotic resistance. *Nat. Biotechnol.* 31, 922–927. doi: 10.1038/nbt.2685
- Truman, A. W., Kwun, M. J., Cheng, J., Yang, S. H., Suh, J.-W., and Hong, H.-J. (2014). Antibiotic resistance mechanisms inform discovery: identification and characterization of a novel *Amycolatopsis* strain producing ristocetin. *Antimicrob. Agents Chemother.* 58, 5687–5695. doi: 10.1128/aac.03349-14
- Vehreschild, M. J. G. T., Haverkamp, M., Biehl, L. M., Lemmen, S., and Fätkenheuer, G. (2019). Vancomycin-resistant enterococci (VRE): a reason to isolate? *Infection* 47, 7–11. doi: 10.1007/s15010-018-1202-9
- van Wageningen, A. V., Kirkpatrick, P. N., Williams, D. H., Harris, B. R., Kershaw, J. K., Lennard, N. J., et al. (1998). Sequencing and analysis of genes involved in the biosynthesis of a vancomycin group antibiotic. *Chem. Biol.* 5, 155–162. doi: 10.1016/S1074-5521(98)90060-6
- Waglechner, N., McArthur, A. G., and Wright, G. D. (2019). Phylogenetic reconciliation reveals the natural history of glycopeptide antibiotic biosynthesis and resistance. *Nat. Microbiol.* 4, 1862–1871. doi: 10.1038/s41564-019-0531-5
- Weigel, L. M., Clewell, D. B., Gill, S. R., Clark, N. C., McDougal, L. K., Flannagan, S. E., et al. (2003). Genetic analysis of a high-level vancomycin-resistant isolate of *Staphylococcus aureus*. *Science* 302, 1569–1571. doi: 10.1126/science.1090956
- WHO (2017). Antibacterial agents in clinical development: an analysis of the antibacterial clinical development pipeline, including tuberculosis. World Health Organization. WHO/EMP/IAU/2017.11
- Wink, J. M., Kroppenstedt, R. M., Ganguli, B. N., Nadkarni, S. R., Schumann, P., Seibert, G., et al. (2003). Three new antibiotic producing species of the genus *Amycolatopsis*, *Amycolatopsis balhimycina* sp. nov., *A. tolypomycina* sp. nov., *A. vancoresmycina* sp. nov., and description of *Amycolatopsis keratiniphila* subsp. *keratiniphila* subsp. nov. and *A. keratiniphila* subsp. *nogabecina* subsp. nov. *Syst. Appl. Microbiol.* 26, 38–46. doi: 10.1078/07320203232237290
- Wright, G. D., Holman, T. R., and Walsh, C. T. (1993). Purification and characterization of VanR and the cytosolic domain of VanS: a two-component regulatory system required for vancomycin resistance in *Enterococcus faecium* BM4147. *Biochemist* 32, 5057–5063. doi: 10.1021/bi00070a013
- Wu, Z., Wright, G. D., and Walsh, C. T. (1995). Overexpression, purification, and characterization of VanX, a D,D-dipeptidase which is essential for vancomycin resistance in *Enterococcus faecium* BM4147. *Biochemist* 34, 2455–2463. doi: 10.1021/bi00008a008
- Xu, L., Huang, H., Wei, W., Zhong, Y., Tang, B., Yuan, H., et al. (2014). Complete genome sequence and comparative genomic analyses of the vancomycin-producing *Amycolatopsis orientalis*. *BMC Genomics* 15:363. doi: 10.1186/1471-2164-15-363
- Yim, G., Kalan, L., Koteva, K., Thaker, M. N., Waglechner, N., Tang, I., et al. (2014). Harnessing the synthetic capabilities of glycopeptide antibiotic tailoring enzymes: characterization of the UK-68,597 biosynthetic cluster. *ChemBiochem* 15, 2613–2623. doi: 10.1002/cbic.201402179
- Yushchuk, O., Homoniuk, V., Ostash, B., Marinelli, F., and Fedorenko, V. (2020b). Genetic insights into the mechanism of teicoplanin self-resistance in *Actinoplanes teichomyceticus*. *J. Antibiot.* 73, 255–259. doi: 10.1038/s41429-019-0274-9
- Yushchuk, O., Horbal, L., Ostash, B., Marinelli, F., Wohlleben, W., Stegmann, E., et al. (2019). Regulation of teicoplanin biosynthesis: refining the roles of *tei* cluster-situated regulatory genes. *Appl. Microbiol. Biotechnol.* 103, 4089–4102. doi: 10.1007/s00253-019-09789-w
- Yushchuk, O., Ostash, B., Truman, A. W., Marinelli, F., and Fedorenko, V. (2020a). Teicoplanin biosynthesis: unraveling the interplay of structural, regulatory, and resistance genes. *Appl. Microbiol. Biotechnol.* 104, 3279–3291. doi: 10.1007/s00253-020-10436-y
- Zeng, D., Debabov, D., Hartsell, T. L., Cano, R. J., Adams, S., Schuyler, J. A., et al. (2016). Approved glycopeptide antibacterial drugs: mechanism of action and resistance. *Cold Spring Harb. Perspect. Med.* 6:a026989. doi: 10.1101/cshperspect.a026989

Conflict of Interest: The authors declare that the research was conducted in the absence of any commercial or financial relationships that could be construed as a potential conflict of interest.

Copyright © 2020 Yushchuk, Binda and Marinelli. This is an open-access article distributed under the terms of the Creative Commons Attribution License (CC BY). The use, distribution or reproduction in other forums is permitted, provided the original author(s) and the copyright owner(s) are credited and that the original publication in this journal is cited, in accordance with accepted academic practice. No use, distribution or reproduction is permitted which does not comply with these terms.



Identification and Characterization of Planktonic Biofilm-Like Aggregates in Infected Synovial Fluids From Joint Infections

Alessandro Bidossi^{1*}, Marta Bottagisio¹, Paolo Savadori² and Elena De Vecchi¹

¹ Laboratory of Clinical Chemistry and Microbiology, IRCCS Istituto Ortopedico Galeazzi, Milan, Italy, ² Department of Endodontics, IRCCS Istituto Ortopedico Galeazzi, Milan, Italy

OPEN ACCESS

Edited by:

Paolo Visca,
Roma Tre University, Italy

Reviewed by:

Maria José Saavedra,
Universidade de Trás os Montes e
Alto Douro, Portugal
Marco Rinaldo Oggioni,
University of Leicester,
United Kingdom
Annalisa Pantosti,
Istituto Superiore di Sanità (ISS), Italy

*Correspondence:

Alessandro Bidossi
alessandro.bidossi@
grupposandonato.it

Specialty section:

This article was submitted to
Antimicrobials, Resistance and
Chemotherapy,
a section of the journal
Frontiers in Microbiology

Received: 13 December 2019

Accepted: 27 May 2020

Published: 30 June 2020

Citation:

Bidossi A, Bottagisio M,
Savadori P and De Vecchi E (2020)
Identification and Characterization
of Planktonic Biofilm-Like Aggregates
in Infected Synovial Fluids From Joint
Infections. *Front. Microbiol.* 11:1368.
doi: 10.3389/fmicb.2020.01368

Recent *in vitro* studies reported the exceptional ability of some bacterial species to form biofilm-like aggregates in human and animal synovial fluids (SF), but evidences from infected clinical samples are still lacking. In this study, we investigated whether this bacterial phenotype was present in infected SFs collected from joint infections and if it was maintained in *in vitro* settings. SFs sent for culture to the Laboratory of Microbiology of our institute were directly analyzed by means of confocal laser scanning microscopy (CLSM), and the infective agents were isolated for further *in vitro* tests. Moreover, sterile SF was collected from patients who did not receive previous antibiotic therapy to investigate the formation of bacterial aggregates, together with biofilm and matrix production on a titanium surface. Finally, antibiotic susceptibility studies were performed by using bovine SF. Four *Staphylococcus aureus*, one *Staphylococcus lugdunensis*, and one *Prevotella bivia* strain were identified in the infected SFs. The CLSM analysis showed that all staphylococci were present as a mixture of single cells and bacterial clumps surrounded by an exopolymeric substance, which comprised SF-derived fibrin, while all *P. bivia* cells appeared separated. Despite that, differences in the ability to aggregate between *S. aureus* and *S. lugdunensis* were observed in clinical SFs. These different phenotypes were further confirmed by *in vitro* growth, even though the application of such *ex vivo* approach lead all staphylococci to form exceptionally large microbial aggregates, which are several folds bigger than those observed in clinical samples. Planktonic aggregates challenged for antibiotic susceptibility revealed a sharp increase of recalcitrance to the treatments. Although this is still at a preliminary stage, the present work confirmed the ability of staphylococci to form free-floating biofilm-like aggregates in infected SF from patients with joint infections. Furthermore, the obtained results pointed out that future *in vitro* research on joint infections will benefit from the use of human- or animal-derived SF. Even though this approach should be carefully validated in further studies comprising a larger microbial population, these findings pose new challenges in the treatment of infected native and prosthetic joints and for the approach to new investigations.

Keywords: joint infections, biofilm, *Staphylococcus*, synovial fluid, aggregates

INTRODUCTION

The analysis of synovial fluid (SF) has long been recommended as a routine procedure in the diagnosis of joint infections. Septic native joints are quite uncommon, with approximately two cases per 100,000 people per year (Ross, 2017), but this event may lead to joint damage and consequent disability. The presence of a prosthetic device drastically increases both the morbidity and the mortality of septic arthritis up to more than 3%, which accounts for almost a third of all the causes for implant revision (Beam and Osmon, 2018). Also, the etiology of native and prosthetic joint infections differs. While in the first case *Staphylococcus aureus* is responsible for more than 50% of the cases, prosthetic joint infections (PJIs) see a very high incidence of low-virulence microorganisms, such as coagulase-negative staphylococci (CoNS) and anaerobes such as *Cutibacterium acnes* (Drago et al., 2017). Indeed the pathogenicity of such opportunistic species mainly relies on their ability to adhere to abiotic surfaces and to form mature biofilm by producing or incorporating polymeric substances (Boyle et al., 2018). As a consequence of this protected mode of growth, the sessile microbes become resilient to antibiotics and the immune system. Furthermore, contrarily to isolated planktonic bacteria, they often fail to grow in standard culture conditions used in diagnostics (Costerton et al., 2011; Dastgheyb et al., 2015a).

Although most of the attention has been paid to biofilms attached to implanted devices, recent direct microscopic analysis of clinical samples from diverse chronic infections revealed that bacterial cells physically aggregated in free-floating clusters (Bjarnsholt et al., 2009; Homøe et al., 2009; Burmølle et al., 2010; Bay et al., 2018). Although such cellular aggregates do not need a surface to form, they exhibit many characteristics of sessile biofilms. Indeed they displayed similar growth rates, resistance to phagocytosis, polymeric matrix components, and a reduced antibiotic susceptibility, which can be restored upon disruption (Alhede et al., 2011).

Evidences of bacterial aggregates in infected joint aspirates from clinical settings are scarce. To our knowledge, only a case report published in 2008 described large *S. aureus* aggregates in the SF of an infected prosthetic elbow, but their presence was briefly discussed as “clumps of bacteria that had shed naturally from the biofilm” (Stoodley et al., 2008). Since then, a few other *in vitro* studies investigated the bacterial behavior and the phenotypes in human and animal SF, focusing their attention mainly on *S. aureus* and CoNS and reporting the exceptional ability of these species to form macroscopic clumps (Dastgheyb et al., 2015a,b,c; Perez and Patel, 2015; Ibberson et al., 2016; Gilbertie et al., 2019). These studies highlighted a multifactorial process of aggregation that involves avid binding of fibrin and fibronectin by means of surface adhesins (Dastgheyb et al., 2015a), incorporation of hyaluronic acid (Ibberson et al., 2016), and uncontrolled accumulation of biomass due to the negative regulation of phenole-soluble modulins, which is responsible for disrupting the interactions between bacterial-derived matrix and cells (Dastgheyb et al., 2015c). As a consequence, the staphylococcal aggregates display a superior antimicrobial tolerance that far exceeds the concentrations that

would normally kill or inhibit their planktonic counterparts (Gilbertie et al., 2019). This phenomenon is partially restored by the dispersal activity of enzymes which are active on the matrix components (Dastgheyb et al., 2015a; Ibberson et al., 2016; Gilbertie et al., 2019).

The aim of the present work was to identify the presence of bacterial clumps in SFs collected from the infected joints of patients referred to our institute and to evaluate the extent of cellular aggregation, the presence of matrix components, and the relative impact on antimicrobial treatment. For this purpose, the SFs from the diagnostic laboratories of our institute were stained and directly analyzed by means of confocal laser scanning microscopy (CLSM), and the infective agents were isolated and employed for further *in vitro* tests.

MATERIALS AND METHODS

Synovial Fluid Collection

Human SFs were collected from patients referred to the Orthopedic Institute Galeazzi, with suspected joint infections, in accordance with a human subject protocol approved by the San Raffaele Hospital Ethical Committee (No. 146/int/2018). A written consent was signed by each patient before the SF aspiration. The SFs, either collected from outpatients or from the operating room, were firstly brought to the Laboratory of Microbiology of the institute to undergo routine diagnostic procedures. After routine processing, an aliquot was directly observed by CLSM. Thereafter, the infective agents were isolated for the subsequent *in vitro* tests. The non-infected SFs from patients who did not receive any previous antibiotic therapy were employed to investigate the *in vitro* formation of planktonic aggregates, biofilm formation on titanium surface, and matrix production. To do that, sterile SFs were decellularized by centrifugation at 3,000 rpm for 10 min and stored at -20°C . All the sterile SFs were pooled before the *in vitro* experiments.

Bacterial Strains

The identification of clinical isolates was carried out on a Vitek2 Compact (BioMérieux) and later confirmed by sequencing of 80 bp of the variable regions V1 and V3 of the 16S rRNA gene by Pyrosequencing (PSQ96RA, Diatech). All strains were stored at -80°C in brain heart infusion (BHI, Merck) broth enriched with 10% glycerol (Sigma Aldrich) until testing. Before the *in vitro* experiments, the bacteria were thawed and reconstituted in tryptic soy agar (Biomérieux) for 24 h at 37°C . *Prevotella bivia* was grown on Schaedler agar (Oxoid) plus 3% defibrinated sheep blood (ThermoFisher) and incubated in anaerobiosis for at least 48 h.

Confocal Microscopy on Clinical SF

All SF samples were immediately analyzed when possible or fixed with 2% paraformaldehyde solution. A 50- μl aliquot was stained for 15 min in the dark by adding the same volume of a solution containing 0.5 μM of SYTO 9 Green Fluorescent Nucleic Acid Stain (Thermo Fisher Diagnostics SpA). After incubation, the samples were spread over the

surface of a glass slide, air-dried, and then observed with an upright TCS SP8 (Leica Microsystems CMS GmbH) CLSM. When needed, the samples were diluted with sterile saline. Only the samples containing bacterial aggregates were further stained to identify self-produced or incorporated extracellular matrix components. In particular, BOBO-3 (Invitrogen), a cell-impermeable DNA stain, was employed at a final concentration of 100 nM to visualize extracellular DNA (eDNA). Wheat-germ agglutinin (WGA) Alexa Fluor 647 conjugate (Invitrogen; final concentration, 5 µg/ml), a lectin that binds to N-acetyl-d-glucosamine and N-acetylneuraminic acid residues, was used to stain staphylococcal poly-N-acetylglucosamine (PNAG) (Frank and Patel, 2007) or SF-derived hyaluronic acid incorporated in bacterial aggregates (Ibberson et al., 2016). FilmTracer SYPRO Ruby Biofilm Matrix Stain (Invitrogen) was added at 1:1 to the sample, allowed to stain for 30 min, and then gently washed three times with sterile saline to examine matrix proteins. Finally, anti-fibrin alpha chain antibody conjugated to Cy5 (Abcore Inc.) was used (50 µg/ml) to visualize the presence of human fibrin in the clumps. The images were then acquired using a $\times 20$ dry objective (HC PL FLUOTAR 20 \times /0.50 DRY) or a $\times 100$ immersion oil objective (HC PL APO 100X/1.40 OIL CS2) and processed with Las X software (Leica Microsystems CMS GmbH).

Biofilm-Like Aggregates and Biofilm Formation on Titanium Discs

The clinical strains were tested *in vitro* for their ability to form aggregates and to attach to the titanium surface. Next, 5-mm-diameter titanium alloy disks (Ti6Al4V, Geass) were placed in a flat-bottom 96-well microplate (VWR) and covered with 180 µl of either sterile SF or BHI (in the case of staphylococci) or thioglycollate broth (for *P. bivia*). The clinical strains reconstituted from an overnight culture were resuspended in sterile saline solution to a turbidity of 0.5 McFarland, from which 20 µl was inoculated in each well to reach a final bacterial concentration of $\sim 10^7$ CFU/ml. The staphylococci were then incubated overnight at 37°C on a shaker at 200 rpm, whereas *P. bivia* was incubated in anaerobiosis for up to 14 days. Thereafter, the supernatant containing aggregated planktonic cells was gently removed with a Pasteur pipette and divided into 50-µl aliquots for CLSM staining (i.e., BOBO-3, WGA, SYPRO Ruby, and anti-fibrin alpha chain antibody conjugated to Cy5), as described in the previous section. The surface of titanium disks was also attentively analyzed by means of CLSM. Briefly, the titanium coupons were washed three times with sterile saline, and 30 µl of staining solution, containing the abovementioned dyes, was applied all over the surface for 30 min in the dark, then washed again, and allowed to dry until the CLSM analysis. The images were acquired as described in the previous paragraph. Each strain was tested in triplicate for each condition, and at least three images were acquired for each replicate. All the acquisitions were performed on the same day using the same stain solutions and applying the same software settings for each sample. Each matrix component was quantified by means of Fiji software (Fiji, ImageJ) and reported as the relative increase in volume with respect to cellular biomass (SYTO 9), indicated as 1 in the scale bar.

Dispersal Treatment of Sessile Biofilms on Titanium Surface and Planktonic Aggregates

The efficacy of chemical or enzymatic treatments to disperse cells within the biofilm matrix was evaluated. To perform this *in vitro* analysis, bovine synovial fluid (BSF) was purchased from Lampire Biological Laboratories since the ability of human pathogens to form aggregates in animal-derived SF was already observed (Perez and Patel, 2015; Gilbertie et al., 2019). Despite the evidence reported in the literature, the ability of the tested clinical isolates to form planktonic biofilm-like aggregates in this BSF was evaluated prior to proceeding with further *in vitro* experiments.

The staphylococcal clinical isolates were grown on titanium disks with either BSF or BHI as described in the paragraph above. After 24 h of incubation, the titanium disks were removed from the wells, gently rinsed three times with sterile saline, and placed in a new 96-well microplate. Afterward, 200 µl of sterile saline containing either proteinase K (100 µg/ml, Sigma Aldrich) or DNase I (200 µg/ml, Thermo Scientific) or sodium metaperiodate (NaIO₄, 10 nM, Sigma Aldrich) or plasmin (150 µg/ml, Sigma Aldrich) was added to each well to test the efficacy of each dispersal treatment. Similarly, planktonic aggregates cultured in BSF for 24 h under agitation were treated by adding the same dispersal agents to reach the concentrations indicated above. The microplates containing both treated titanium disks and planktonic aggregates were then placed at 37°C on a shaker at 200 rpm for 1 h, and the CFU increase was counted by plating appropriate dilutions on agar plates. Four replicates for each treatment were performed for each of the tested strain.

Antibiotic Treatment Exposure

Susceptibility to antibiotics commonly employed in orthopedics was assessed by determining the minimum inhibitory concentration (MIC) and the minimum bactericidal concentration (MBC) by broth microdilution method. In particular, the antibiotic susceptibility of the tested clinical isolates was assessed either in the presence of culture broths [Mueller Hinton for staphylococci (Conda) and thioglycollate (Oxoid) for *P. bivia*] or BSF. In addition, antibiotic susceptibility was investigated on pre-formed bacterial aggregates cultured in BSF, as previously described. To do that, preliminary tests were conducted to standardize the experimental conditions in order to obtain bacterial aggregates with the characteristics previously observed in the clinical scenario. The strains took ~ 6 h to form aggregates and clumps with a size similar to that observed in the clinical specimens. At the end of the 6 h incubation period, the cellular load of each strain was quantified in order to standardize the initial inoculum and make the three modalities of antibiotic susceptibility comparable. With this aim, a bacterial suspension of $\sim 10^5$ CFU/ml was inoculated in BSF and incubated at 37°C on a shaker at 200 rpm. At the end of the 6-h incubation period, two approaches were adopted for the quantification of the final bacterial concentration. First of all, the aliquots of samples were sonicated in a sonication bath (Ultrasonic Bath, VWR) for 5 min at 45 kHz and incubated in agitation for 30 min at 37°C with proteinase K (100 µg/ml). Afterward, the CFUs were counted

by plating appropriate dilutions on agar plates. Furthermore, to assess the efficacy of the dispersal treatment, Gram staining of treated and untreated samples was performed. Simultaneously, a second quantification was performed by means of the resazurin assay, as described by Ravi et al. (2019). Briefly, a standard plate containing 1-fold difference of a known cellular concentration between rows and 10-fold difference between columns was prepared from an overnight culture in a 96-well microplate for the fluorescence-based assays (Invitrogen). Resazurin (Alamar Blue, Invitrogen) was added to each well to reach a concentration of 40 $\mu\text{g/ml}$, and the mixture was incubated in the dark for 2 h. Fluorescence was read at a wavelength of 600 nm with a spectrophotometer (VICTOR X3, Perkin Elmer). Similarly, three aliquots from a 6-h bacterial culture in BSF of each strain were transferred in a microplate. After incubation with resazurin, fluorescence was read and compared to the values obtained by standard plate reading. These results allowed the assessment of MIC and MBC of both planktonic cells and bacterial aggregates following the Clinical and Laboratory Standards Institute guidelines (Clinical and Laboratory Standards Institute guidelines [CLSI], 2015). Briefly, a 0.5 McFarland suspension (about 1.5×10^8 CFU/ml) was prepared in sterile saline, further diluted to reach the appropriate inoculum load, and inoculated in a 96-well microtiter plate containing serial 2-fold dilutions of oxacillin (SigmaAldrich), levofloxacin (Alfa Aesar), and rifampin (Acros Organics) for staphylococci and imipenem (Supelco), ampicillin (Fisher Bioreagents), and metronidazole (Supelco) for *P. bivia*. Vancomycin (PanReac AppliChem ITW Reagents) was tested on all the strains. To investigate the antimicrobial susceptibility of the preformed aggregates, 50 μl of bacterial suspension of $\sim 10^5$ CFU/ml in BSF was added to the wells of a microplate and incubated at 37°C on a shaker at 200 rpm for 6 h. In another plate, a twofold serial dilution of the aforementioned antibiotics was prepared in BSF. At the end of the incubation, 50 μl from each well containing the serially diluted antibiotic was transferred to the wells containing the preformed bacterial aggregates and incubated. The MIC values, corresponding to the lowest antimicrobial concentration able to inhibit any visible bacterial growth, were read after 24 h of incubation at 37°C. The plates containing the aggregates in BSF were centrifuged to let the bacterial clumps deposit on the bottom of the wells so as to clearly establish the growth. MBC was determined by plating 10 μl from each well, showing no turbidity onto the agar plates. Due to the possible presence of residual clumps of cells, before plating, the microplates were sonicated for 5 min at 45 kHz and incubated in agitation for 30 min at 37°C with proteinase K (100 $\mu\text{g/ml}$). After incubation, MBC was read as the lowest concentration able to kill 99.9% of the initial inoculum.

Statistical Analysis

Statistical analyses were performed by means of Graph Pad Prism 5 software (Graph Pad Software, Inc., La Jolla, CA, United States). Shapiro–Wilk test was used to assess the distribution of data. Quantification of matrix composition and evaluation of dispersal treatments were analyzed using one-way non-parametric Kruskal–Wallis test and *post hoc* Dunnett's test. For comparison of volume/surface ratio on titanium in the presence

of BHI medium or SF, a pairwise comparison between the means of the two groups was performed by means of two-tailed, unpaired Student *t*-test for each strain. *P*-values < 0.05, < 0.01, and < 0.001 were considered as significant.

RESULTS

Biofilm-Like Aggregates Are Formed by Staphylococci but Not *P. bivia* in Infected SF

To evaluate the phenotype of bacterial cells in SF, joint aspirates from patients with suspected infection were directly investigated by means of CLSM. Of the 20 synovial fluids with suspected infection, six showed a marked presence of bacterial cells along with massive infiltration of immune cells, which are clearly visible due to the nucleic acid stain SYTO 9 (Figure 1). All specimens exhibited a monomicrobial infection: four were caused by *S. aureus* (one was methicillin resistant and three were methicillin susceptible), one by *S. lugdunensis*, and one by *P. bivia*. *S. aureus* 1 and 4 and *S. lugdunensis* were isolated in the SF of patients with PJIs, while *S. aureus* 2 and 3 and *P. bivia* were from native joint infections. For staphylococci, the CLSM analysis evidenced both single bacterial cells and cellular aggregates with different sizes (Figures 1, 2 and Supplementary Figure S1), ranging from less than 10 cells (*S. lugdunensis*, Figure 1d) to clumps exceeding 20 μm (*S. aureus* 4, Figure 2b). Interestingly, the largest aggregates were observed in the samples associated with prosthetic devices. Only for *S. aureus* 4, all the matrix components were efficiently stained (Figure 2). All matrix stains colocalized with SYTO 9, with a signal intensity proportional to the size of the aggregates. In the right panel of Figure 2a, WGA lectin stain is shown. However, it is not possible to discriminate whether the signal is derived from the PNAG produced by bacteria and/or from incorporated hyaluronic or from other N-acetylglucosamine (GlcNAc) containing polysaccharide. As shown in Figure 3, α -fibrin antibody could efficiently stain *S. aureus* biofilm-like aggregates, thus confirming the importance of binding to human-derived fibrin for the pathogenesis of joint infections. Copious bacterial clumps were observed in the sample infected by the coagulase-negative *S. lugdunensis*. However, those aggregates rarely outnumbered 10 cells (Figure 1d). The highest infiltration of immune cells was detected in the sample infected by *P. bivia*. Therefore, the SF was diluted in sterile saline to appreciate the presence of both prokaryotic and eukaryotic cells (Figures 4a,b). As depicted in Figure 4b, *P. bivia* was present as single cells or couples of cells, probably replicating bacteria, but no aggregate similar to those formed by staphylococci was seen throughout the whole sample.

In vitro Growth in SF Induces the Formation of Macroscopic Aggregates by Staphylococci

As already shown in the recent literature, staphylococci own an incredible capability of forming free-floating aggregates visible to the naked eye in human and animal SFs in laboratory settings

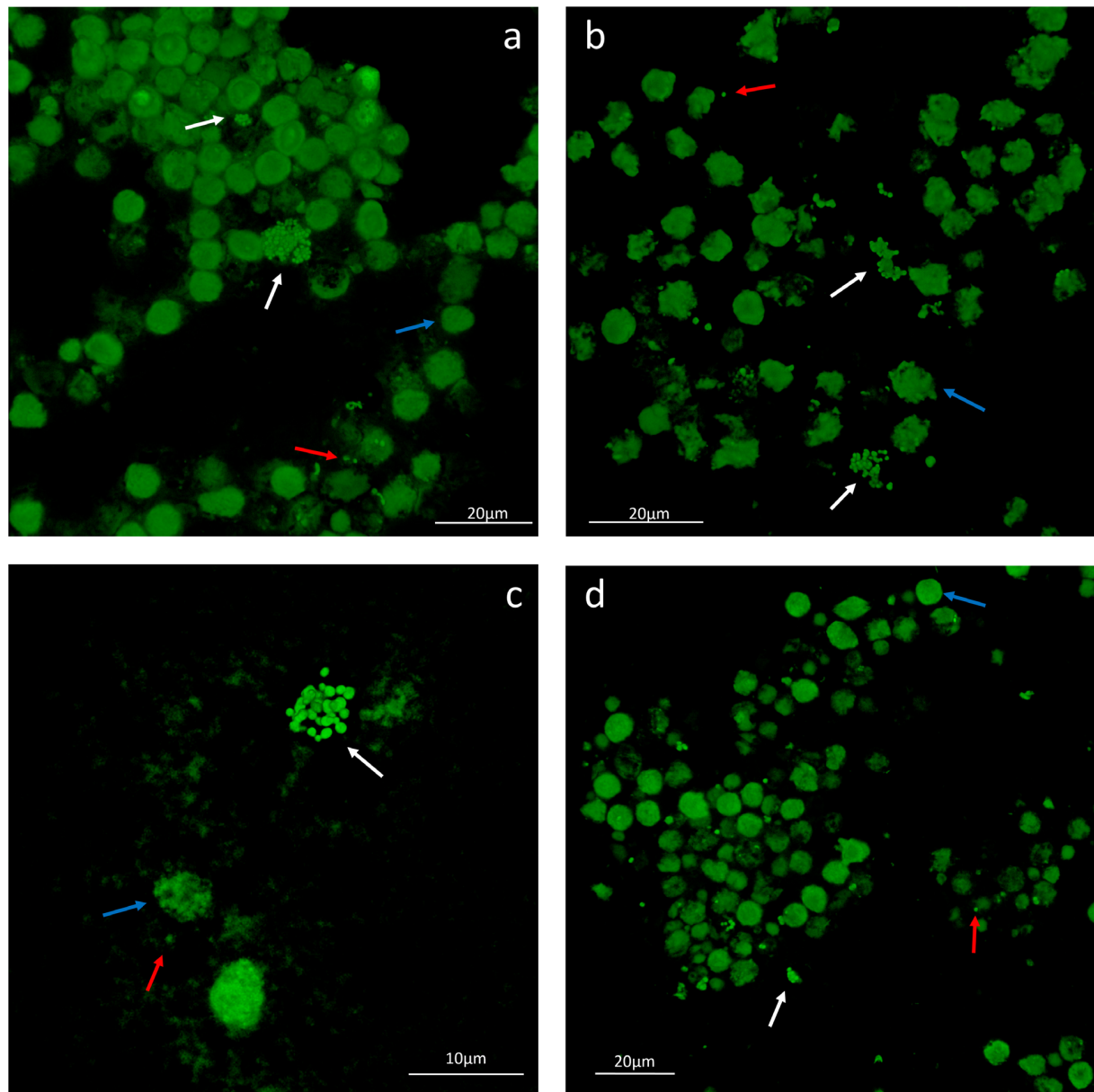


FIGURE 1 | Representative confocal laser scanning microscopy images of infected synovial fluids stained with SYTO 9 nucleic acid stain. **(a)** *Staphylococcus aureus* 1, **(b)** *S. aureus* 2, **(c)** *S. aureus* 3, and **(d)** *Staphylococcus lugdunensis*. The white arrows indicate the biofilm-like aggregates of cells, the red arrow indicates the single bacterial cells, and the blue arrows indicate the immune cells nuclei.

(Dastgheyb et al., 2015a,b,c; Perez and Patel, 2015; Ibberson et al., 2016; Gilbertie et al., 2019). To compare the characteristics of bacterial aggregates *in vitro* to those in clinical samples, the clinical isolates were cultured in sterile SFs from uninfected outpatients. *P. bivia* was grown in anaerobiosis for up to 14 days. Turbidity was visible after 8–10 days in thioglycollate broth and after 10–12 days in SF, however, no bacterial aggregates were detected in accordance with what was observed in the infected sample.

All staphylococci efficiently formed aggregates both in SF and in BSF with similar kinetics. Clumps of cells were

visible to the naked eye after about 9 h of incubation for *S. aureus* strains and 12 h for *S. lugdunensis*. The formation of staphylococcal aggregates was monitored at different time points by CLSM. It was observed that, after 6 h, all staphylococcal aggregates displayed a dimension similar to that observed in the corresponding clinical sample (data not shown).

The matrix production was quantified in each of the acquired images (**Figures 5a,b**) by comparing the biomass of each stained component (WGA-stained PNAG, BOBO-3 stained eDNA, and SYPRO Ruby stained extracellular proteins) to the volume of

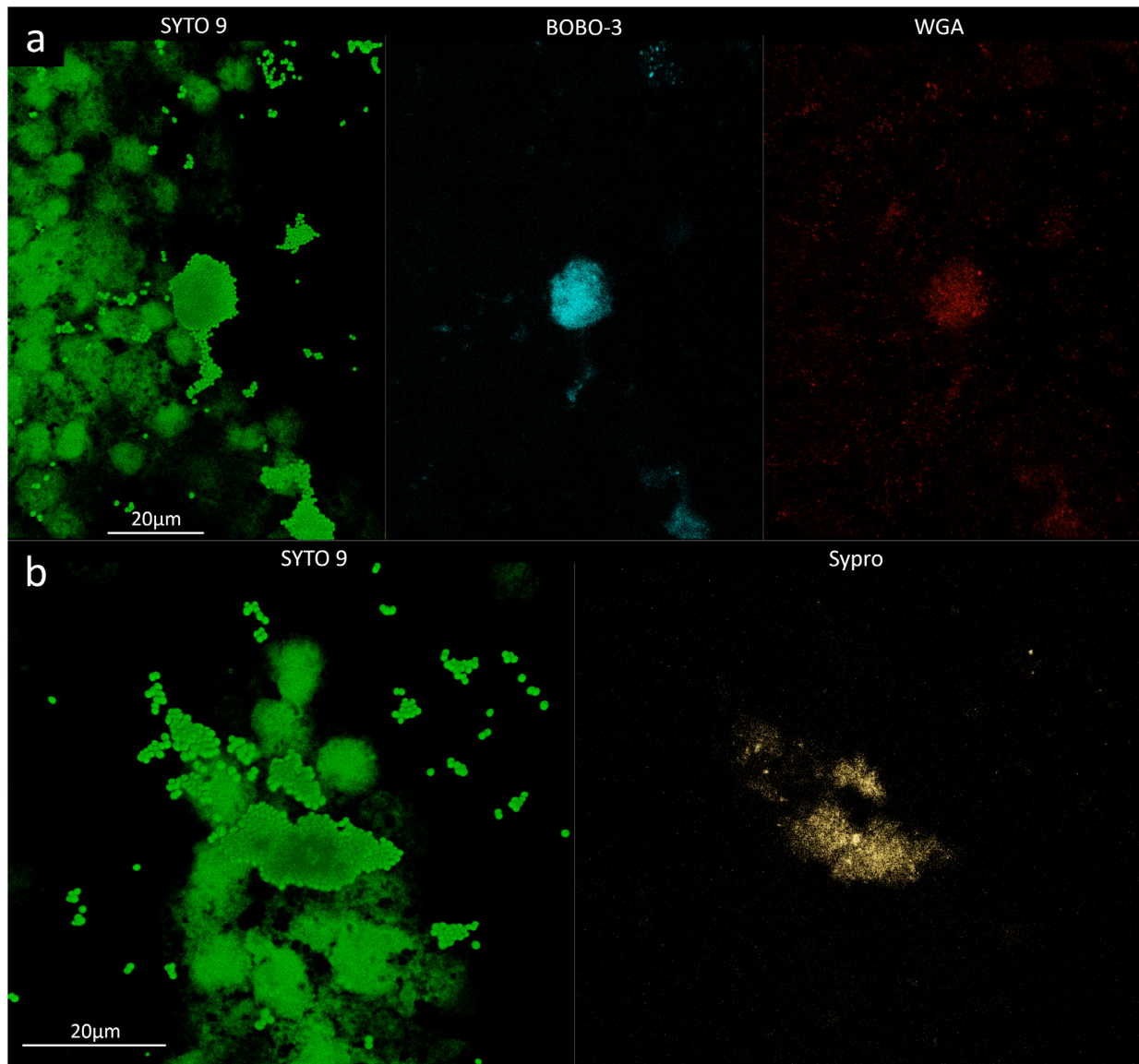


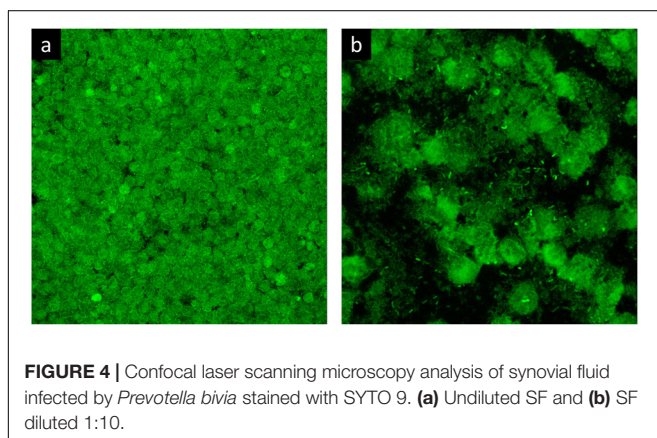
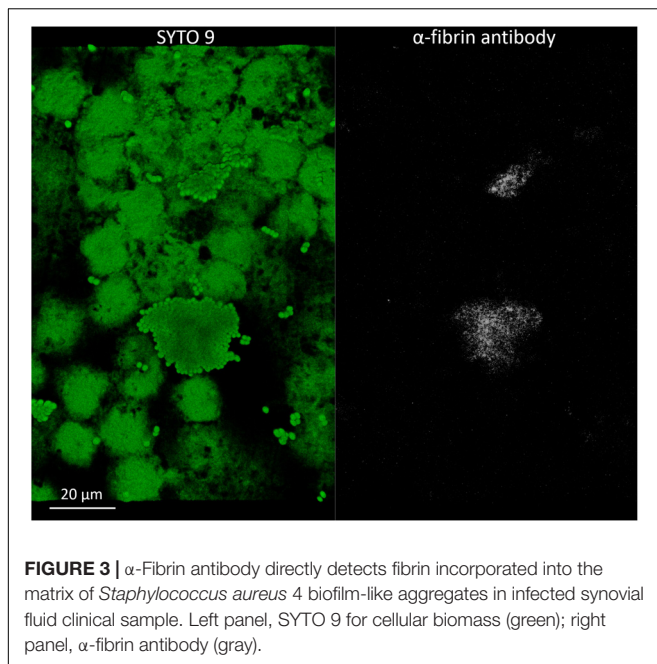
FIGURE 2 | Confocal laser scanning microscopy analysis of synovial fluid infected by *Staphylococcus aureus* 4. **(a)** Sample stained with SYTO 9 for cellular biomass (green, left panel), BOBO-3 for eDNA (light blue, central panel), and WGA stain for GlcNAc containing polysaccharides (red, right panel). **(b)** Sample stained with SYTO 9 for cellular biomass (green, left panel); SYPRO-Ruby staining shows the proteins contained in the biofilm matrix (yellow, right panel).

cells stained with SYTO 9. Due to the weak aggregation of planktonic staphylococci in culture medium (i.e., BHI), the signal emitted from all the dyes was barely detectable by CLSM. Thus, data referring to bacterial aggregates cultured in BHI were not reported. A similar phenotype in terms of matrix composition was observed when comparing biofilm-like clumps and sessile biofilm grown in the presence of BHI or SF (**Figure 6A**). The only significant difference was in the relative content of WGA-stained polysaccharides. Indeed both planktonic aggregates and sessile biofilm displayed an increase of WGA signal ($p < 0.01$) when cultured in SF, possibly due to the incorporation of hyaluronic acid physiologically present in SF. Similarly, fibrin, which is present in SF, was incorporated

in free-floating biofilm-like aggregates of all *S. aureus* and *S. lugdunensis* (**Figure 5c**).

Dispersal Treatment on Sessile Biofilms and Planktonic Aggregates

The contribution of different matrix components to the stability of biofilm and bacterial aggregates was assessed by estimating the cell dispersion (increase of CFU count) after the incubation with both chemical and enzymatic treatments. As shown in **Figure 6B**, proteinase K was always the most efficient treatment ($p < 0.001$) in terms of cell dispersion. Interestingly, treatment with sodium metaperiodate, which hydrolyzes polysaccharides,



exerted the greatest effect on the biofilms grown in BHI broth ($p < 0.001$). Even though also the sessile and planktonic aggregates grown in BSF were affected by sodium metaperiodate ($p < 0.001$), the enzymatic dispersal by plasmin provoked a major increase in CFUs in the supernatant ($p < 0.001$), confirming its important role in staphylococcal clumping. As expected, the plasmin treatment on biofilm grown in BHI was comparable to the untreated control.

Synovial Fluid Induces a Reorganization of Biofilm Architecture on Titanium Surface

To evaluate if SF can influence the organization of the biofilm architecture, staphylococcal isolates were cultured on titanium disks in the presence of either SF or BHI. As shown in **Figure 5c**, the matrix biomass of biofilm grown in BHI is commonly lower than that produced by bacteria grown in SF, except for

eDNA. The lower matrix biomass complied with the observed three-dimensional architecture of the sessile biofilm mainly composed of small aggregates of cells that cover the whole titanium surface when grown in BHI (**Figure 7a**) and in big sparse clumps of cells when grown in SF (**Figure 7b**). Indeed the latter showed a significant increase in the ratio between the volume of biofilms and the covered titanium surface (**Figure 7c**), indicating a thicker biofilm biomass. Such increase varied from 2.57 (*S. lugdunensis*) to 2.8-folds (*S. aureus* 1) with respect to the counterpart grown in BHI.

Antimicrobial Susceptibility

Before assessing the MIC and the MBC of both planktonic cells and bacterial aggregates following the CLSI guidelines, the concentration of bacteria needed to obtain aggregates with a dimension comparable to those observed in clinical SF was evaluated. After 6 h of pre-incubation, no aggregates were visible to the naked eye, but upon microscopic investigation, most of the cells had clumped to form aggregates of 5–30 μm in diameter, with the exception of *S. lugdunensis* aggregates which hardly exceeded diameters larger than 10–15 μm . The initial bacterial inocula assessed by means of resazurin assay and CFU count are reported in **Supplementary Table S2**.

The antibiotic susceptibility profile of the tested strains is reported in **Table 1**. The MIC values in Mueller Hinton (MH) broth were similar for all the strains, except for *S. aureus* 1 that resulted as resistant to oxacillin and levofloxacin. When the same assay was repeated with BSF instead of MH broth, the inhibitory concentrations rose up to four- to 32-folds in all tested strains, particularly those of rifampin and vancomycin. Furthermore, all the tested strains showed vancomycin MIC values beyond the clinical breakpoints.

When *S. aureus* clinical isolates were exposed to antibiotics as pre-formed aggregates, the susceptibility to the treatment further decreased. In fact, all the tested antibiotics inhibited the growth of all *S. aureus* strains with concentrations higher than the clinical breakpoints. Contrarily, only a slight increase of MIC values was observed in the pre-formed aggregate of *S. lugdunensis*.

Also, the MBC values consistently increased, including those that completely eradicate *S. lugdunensis*.

Coherently with the inability of *P. bivia* to clump in SF, changes in its antibiotic susceptibility profile were not detected when cultured in the presence of BSF (**Table 2**).

DISCUSSION

Microbes have evolved to associate together as “communities” to form complex structures encased in a polymeric matrix, known as biofilms (Costerton et al., 1999). Microbial biofilms are ubiquitous in almost every environment. These densely packed cells are able to communicate with each other to adapt to environmental changes, resist to chemical stresses and starving condition, and disperse to colonize new niches. The majority of human infectious diseases involves biofilms of bacterial pathogens, which are less susceptible to antimicrobials and to host immune system, thus providing a plausible explanation

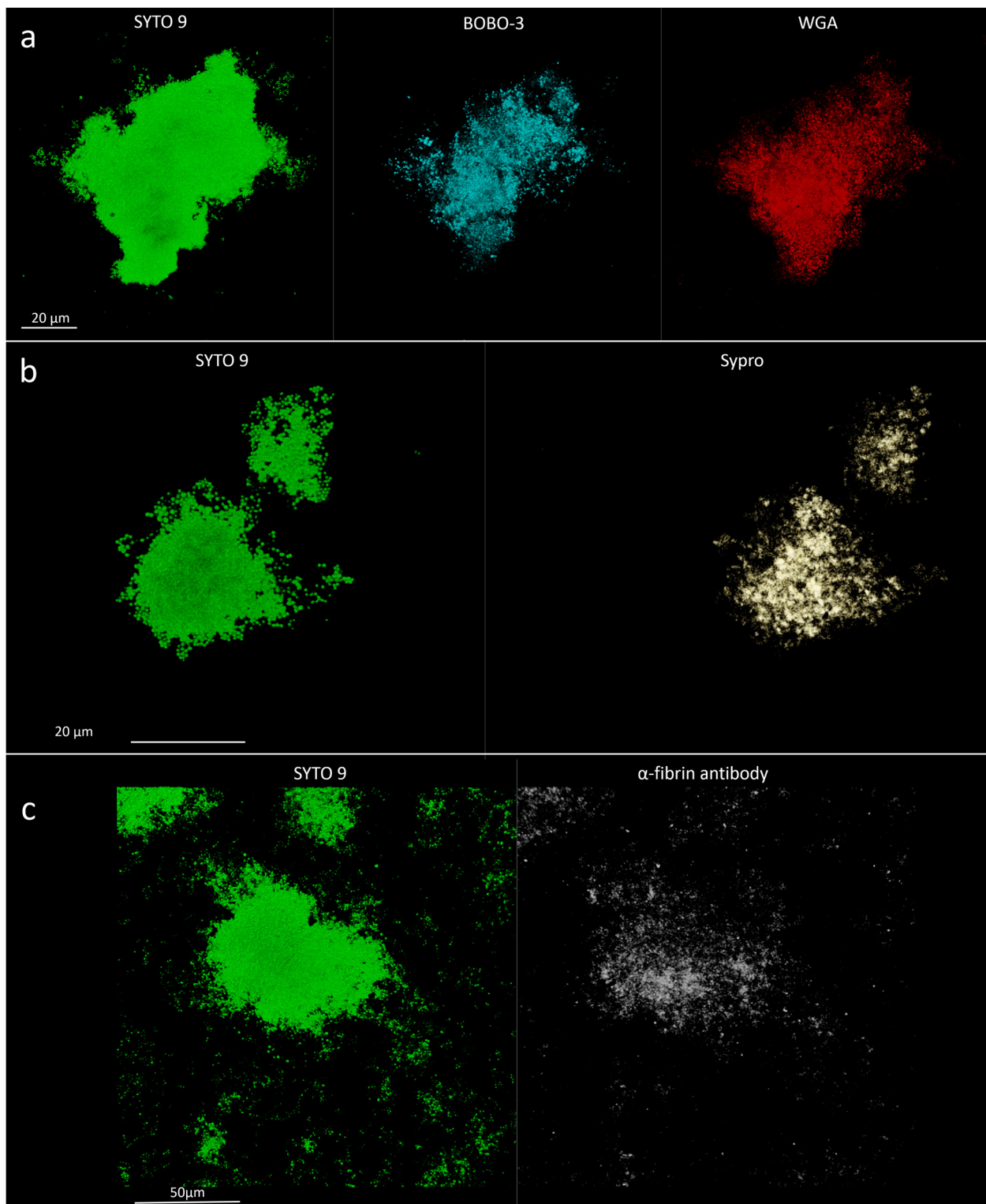
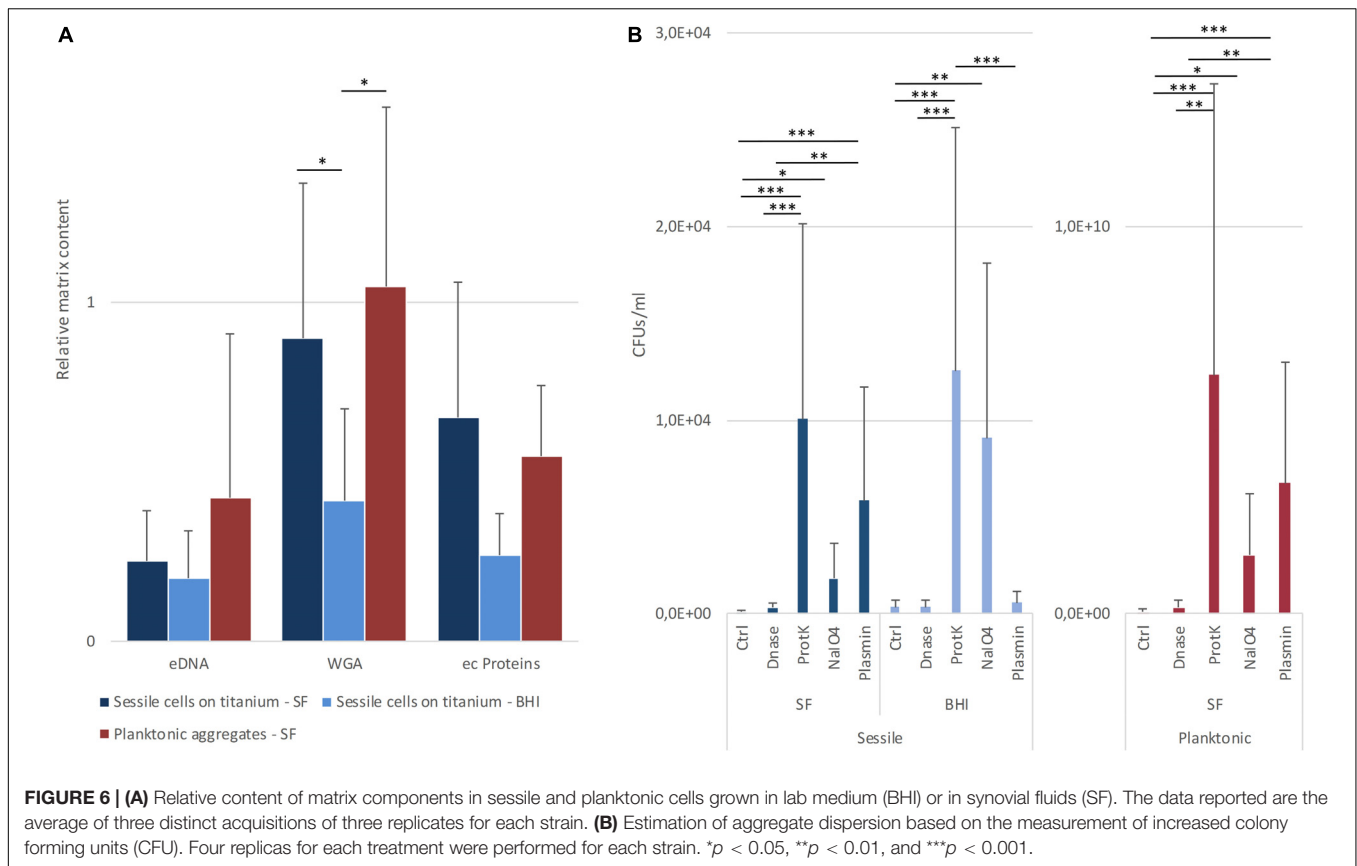


FIGURE 5 | Detection of matrix components in *in vitro* assays. **(a)** *Staphylococcus aureus* 1; left panel, SYTO 9 for cellular biomass; central panel, BOBO-3 for eDNA staining; and right panel, WGA stain for GlcNAc containing polysaccharides. **(b)** *S. aureus* 1; left panel, SYTO 9 for cellular biomass; right panel, SYPRO-Ruby staining. **(c)** Detection of fibrin incorporation in *S. aureus* 2 biofilm-like aggregate; left panel, SYTO 9 for nucleic acids (green); right panel, α-fibrin antibody (gray).



of why therapy failure is common (Hall-Stoodley et al., 2004). The introduction of a foreign body (i.e., implantable devices) is known to trigger bacterial adhesion and biofilm formation as bacteria have a preferred tropism for abiotic surfaces (Zimmerli and Sendi, 2017; Arciola et al., 2018).

Albeit the original definition of biofilm established a mandatory initial attachment to a solid surface (biotic or abiotic), recent microscopic analysis clearly demonstrated the presence of free-floating cellular aggregates in clinical samples from chronic infections (i.e., otitis media, cystic fibrosis, and chronic wounds) (Bjarnsholt et al., 2009; Homøe et al., 2009; Burmølle et al., 2010; Bay et al., 2018). These non-attached clumps of cells share many features with sessile biofilms, such as matrix components (auto-produced or environment-derived) and the ability to resist high concentrations of antimicrobials and immune cell phagocytosis. Hence, it has been proposed to include this microbial lifestyle in the biofilm definition (Alhede et al., 2011). In the last years, thorough *in vitro* researches, the incredible ability of *S. aureus* and *S. epidermidis* to form biofilm-like aggregates in SF has been reported (Dastgheyb et al., 2015a,b,c; Perez and Patel, 2015; Ibberson et al., 2016; Gilbertie et al., 2019). In 2008, in a case report describing an infected prosthetic elbow, direct imaging of periprosthetic tissue, cement spacer, and aspirated joint fluid revealed viable cells of *S. aureus* associated in biofilm aggregates (Stoodley et al., 2008). Since then, no direct evidence of free-floating clumps in SF was reported in the literature. Thus, to ascertain this microbial phenotype, joint aspirates collected

from patients with suspected joint infection were investigated by means of CLSM.

In accordance with the epidemiology of joint infection (Aggarwal et al., 2014; Drago et al., 2017), staphylococci were the overwhelming majority of the infective agents encountered during this study. Compared to *S. lugdunensis*, all four *S. aureus* isolates demonstrated the capability to form larger clumps of cells. Indeed *S. aureus* is known to possess an incredible arsenal of surface clumping factors to bind host fibrinogen and fibrin, which are present in high quantities in SF. Furthermore, *S. aureus* owns at least two coagulases that promote the formation of a fibrin shield around the bacterial cells (Crosby et al., 2016). The pivotal role of fibrin incorporation in the stability of planktonic aggregates was demonstrated in various *in vitro* studies. Indeed treatment with plasmin, tissue plasminogen activator, or proteinase K was among the most efficient enzyme applications in dispersing cells (Dastgheyb et al., 2015a; Gilbertie et al., 2019). The presence of fibrin as a matrix component of biofilm-like aggregates was confirmed here by direct immunostaining, which revealed a dense fibrin clot overlapping the cellular cluster, despite the fact that fibrin and fibrinogen were most likely present throughout the whole sample.

It is interesting to note that the largest clumps of *S. aureus* were observed in SFs aspirated from patients who had undergone a joint arthroplasty. This finding might support the notion that the introduction of foreign, abiotic surfaces might boost biofilm formation. In the case report of Stoodley

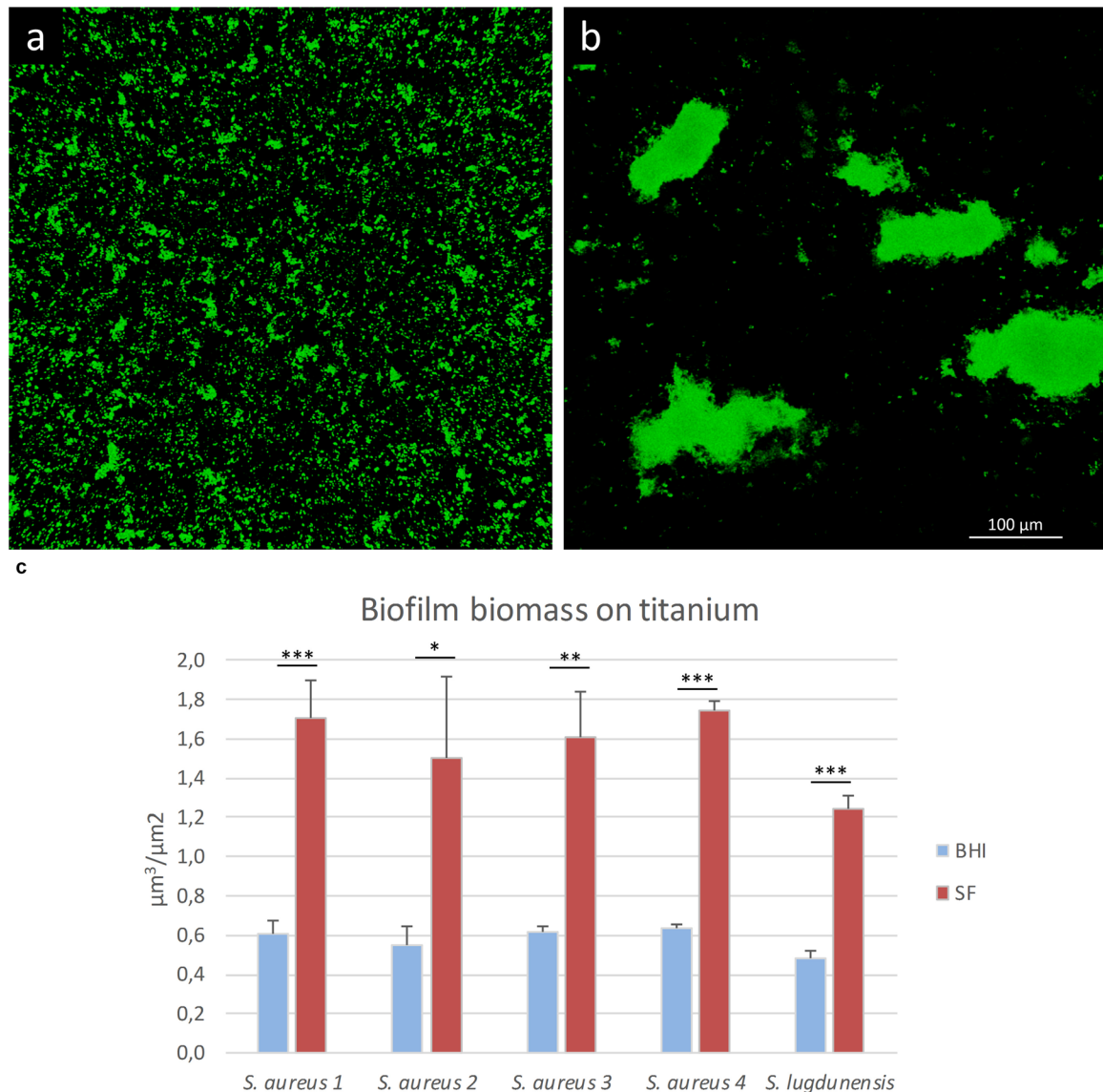


FIGURE 7 | Biofilm formation on titanium alloy in the presence of lab medium or synovial fluid (SF). In this figure, *S. aureus 1* biofilm is grown in the presence of (a) BHI or (b) SF. (c) Biofilm volume/surface ratio of the staphylococcal strains grown in BHI (blue bars) or SF (red bars). The data reported are the average of three distinct acquisitions for each strain. * $p < 0.05$, ** $p < 0.01$, and *** $p < 0.001$.

and colleagues, the aggregates were first identified in the final wound debridement of a total elbow arthroplasty from a patient with a long and complicated clinical history (Stoodley et al., 2008). In that case, clumps of viable cells, with a diameter up to 100 μm , were reported, while in our sample's aggregates did not exceed 30 μm . The dispersal of single cells or clumps of cells from a sessile biofilm is an event that has been widely investigated and represents a complex process that involves the coordination of various signals and molecular effectors (Guilhen et al., 2017). Both dispersal treatment and determination of matrix composition performed in the present study revealed almost overlapping

phenotypes between free-floating aggregates and sessile biofilms grown in SF, possibly sustaining the origin of planktonic clumps from the underlying surface attached to the cells. However, the ability of staphylococci and other species to planktonically coaggregate in SF with kinetics shorter than those needed to attach to a surface matures as a biofilm and dispersal was already demonstrated (Dastgheyb et al., 2015a; Gilbertie et al., 2019). Taken together, evidence might indicate that planktonic coaggregation to form biofilm-like structures and dispersal from sessile biofilms might be two coexisting modalities of infection, in particular for those species able to scavenge host molecules.

TABLE 1 | Minimum inhibitory concentration (MIC) and minimum bactericidal concentration (MBC) of oxacillin (OX), levofloxacin (LVX), rifampin (RI) and vancomycin (VA) against staphylococci in Muller Hinton (MH) broth and in bovine synovial fluid (BSF).

		MIC				MBC			
		OX	LVX	RI	VA	OX	LVX	RI	VA
MH	<i>S. aureus</i> 1	64	16	0.008	1	512	1,024	0.063	16
	<i>S. aureus</i> 2	0.063	0.125	0.008	0.5	1	2	0.031	8
	<i>S. aureus</i> 3	0.125	0.125	0.008	1	1	1	0.063	16
	<i>S. aureus</i> 4	0.125	0.125	0.008	1	4	2	0.125	16
	<i>S. lugdunensis</i>	0.063	0.125	0.008	2	0.25	0.25	0.063	16
BSF	<i>S. aureus</i> 1	256	256	0.25	16	< 1,024	<1,024	1	16
	<i>S. aureus</i> 2	1	1	0.25	4	16	16	1	32
	<i>S. aureus</i> 3	1	4	0.125	16	32	8	0.5	64
	<i>S. aureus</i> 4	1	2	0.25	32	64	8	0.5	64
	<i>S. lugdunensis</i>	1	0.5	0.063	32	4	4	0.125	64
BSF (pre-formed aggregates)	<i>S. aureus</i> 1	< 1,024	<1,024	2	256	< 1,024	<1,024	16	1,024
	<i>S. aureus</i> 2	16	8	1	16	256	256	4	256
	<i>S. aureus</i> 3	8	16	2	64	256	256	8	512
	<i>S. aureus</i> 4	128	128	2	64	1,024	1,024	16	1,024
	<i>S. lugdunensis</i>	1	0.5	0.125	32	32	32	2	256

Data are expressed in mg/L.

TABLE 2 | Minimum inhibitory concentration (MIC) and minimum bactericidal concentration (MBC) of vancomycin (VA), ampicillin (AM), metronidazole (MZ) and imipenem (IP) against *Prevotella bivia* in thyoglycollate (Thy) and in bovine synovial fluid (BSF).

		MIC				MBC			
		VA	AM	MZ	IP	VA	AM	MZ	IP
Thy	4	0.125	0.5	0.063	16	0.125	0.5	0.032	
BSF	4	0.125	0.5	0.032	32	0.25	0.5	0.032	

Data are expressed in mg/L.

Unfortunately, in the present study, the patient's history and clinical data, comprising previous antibiotic treatment, are not available. This shortcoming represents a known limitation, together with the low number of infected SFs encountered in the time span of the study.

Despite the presence of implanted material and a notable bacterial load, *S. lugdunensis* displayed very small clumps of cells. Even though this species is classified as a CoNS, it is characterized by an unusual pathogenicity. Indeed *S. lugdunensis* expresses a coagulase with an activity similar to that of *S. aureus* (Becker et al., 2014) and a fibrinogen-binding protein linked to the bacterial cell wall that acts as a clumping factor (Mitchell et al., 2004). Thus, the *in vivo* phenotype of *S. lugdunensis* might be due to other host-related factors, which can be overcome by *S. aureus* strains with their incredible adaptability and virulence. In fact, *S. lugdunensis* grew *in vitro* to form very large aggregates, although not as large as those of *S. aureus* and with a slower kinetic, also demonstrating its ability to efficiently incorporate SF-derived fibrin. Even if polysaccharide intercellular adhesin locus has been identified in a number of *S. lugdunensis* isolates, biofilm formation relies predominantly on protein factors and eDNA rather than PNAG (Argemi et al., 2017).

Indeed while the *S. lugdunensis* biofilm was negative for WGA staining when grown in a culture medium (Frank and Patel, 2007), in the present study, the aggregates grown *in vitro* in SF were clearly stained by WGA. This could be explained by a possible ability of *S. lugdunensis* to bind and incorporate hyaluronic acid in the matrix joint fluids. Indeed *S. lugdunensis* formed a significantly larger biofilm in the presence of hyaluronic acid than under standard laboratory conditions (Ibberson et al., 2016). In addition, hyaluronic acid was shown to be an important constituent of *S. aureus* planktonic and sessile biofilms. Hyaluronic acid could serve as hindrance to positively charged antibiotics or act as an early signal of aggregation, even if probably not contributing to clump stability as demonstrated by the hyaluronidase treatment (Gilbertie et al., 2019).

Although few other species have been shown to be able to form biofilm-like aggregates in SF (Gilbertie et al., 2019), the herein encountered *P. bivia* neither displayed tightly adhering cells in the clinical sample nor was it able to form a sessile or planktonic biofilm in the presence of both SF and culture medium. While in the past *P. bivia* was shown to bind connective tissue matrix proteins such as fibronectin and laminin (Eiring et al., 1998),

other studies demonstrated a weak or almost absent biofilm-forming ability (Guaglianone et al., 2010; Patterson et al., 2010). The consequences are reflected in the lack of increase of recalcitrance to antimicrobial treatment in the presence of SF, contrarily to those species that are able to aggregate. This finding suggests that such tolerance must rely primarily on the quick grouping of neighboring cells and the presence of particular matrix components, rather than the slow growth of biofilm cells or adaptive events, as antibiotic susceptibility was found to be reversible upon disruption (Alhede et al., 2011).

In this study, two different approaches to evaluate the impact of SF on the susceptibility of antimicrobials commonly used in orthopedic practice were employed. In the first experimental setting, bacteria were inoculated concomitantly with antibiotics to mimic a possible contamination of the surgical site, in which preoperative prophylactic antimicrobial agents are usually present. Differently in the second approach, the cells were inoculated and allowed to aggregate before exposure to antibiotics to resemble the treatment of an infected native joint. Before this experiment, aggregate formation was observed with CLSM, with the obtained clumps of a size resembling those observed in the clinical samples. Here we confirmed that the growth in the presence of SF considerably affects antibiotic susceptibility, showing that bacterial cells are still able to aggregate at concentrations that would be inhibitory in standard culture conditions. In addition, the entity of recalcitrance appears to be species-specific and proportional to the size of clumps that the different species are able to form. Even though *S. lugdunensis* displayed an increase of MIC values similar to that of *S. aureus* strains in the first experimental setting, it showed a minor decrease of susceptibility when pre-aggregated cells were challenged. This is possibly due to the smaller size of aggregates that this strain was able to form in the time span before the treatment. However, the antimicrobial susceptibility of all the tested bacteria drastically decreased when assayed in SF, which represents an important issue considering that infections are likely to start from one single cell (Gerlini et al., 2014) and joint infections might arise from the contamination of sporadic cells. Furthermore, Ghimire et al. recently showed that neutrophils are unable to efficiently phagocytize staphylococcal aggregates exceeding 10 μm in diameter and that they are supposed to be recruited rapidly and in sufficient numbers to scavenge all bacterial cells and prevent them to aggregate and grow to critical dimensions (Ghimire et al., 2019).

CONCLUSION

The obtained results provided evidence that staphylococci are able to form biofilm-like planktonic aggregates in both native and prosthetic infected joints, with the clumps closely resembling their sessile counterparts and able to efficiently scavenge host fibrin. While other species showed the ability to planktonically aggregate in SF, further evidences from clinical samples are needed as only three different species were identified and analyzed in the present work. The use of human- or

animal-derived SF as an *ex vivo* approach for further *in vitro* investigation might improve the value of the results, bringing *in vitro* conditions closer to clinical settings. Here it has been demonstrated that the presence of SF caused a significant reorganization of biofilm architecture on titanium alloy surface, and this knowledge might have an impact on further studies for the improvement of orthopedic biomaterials. On the other hand, *in vitro* bacterial culture in SF rapidly leads to exceptionally large microbial aggregates which are several folds bigger than those observed in clinical samples and might overestimate the phenotypes observed.

DATA AVAILABILITY STATEMENT

The datasets generated for this study are available on request to the corresponding author.

ETHICS STATEMENT

The studies involving human participants were reviewed and approved by the San Raffaele Hospital Ethical Committee (No. 146/int/2018). The patients/participants provided their written informed consent to participate in this study.

AUTHOR CONTRIBUTIONS

AB and ED contributed to the conception and design of the study. AB and MB collected the samples. AB and PS performed all the laboratory assays. AB wrote the first draft of the manuscript. AB, MB, PS, and ED critically revised the manuscript. All authors contributed to manuscript revision, read and approved the submitted version.

FUNDING

This study was supported by the Italian Ministry of Health (RC Project).

SUPPLEMENTARY MATERIAL

The Supplementary Material for this article can be found online at: <https://www.frontiersin.org/articles/10.3389/fmicb.2020.01368/full#supplementary-material>

FIGURE S1 | Scatter plot representation of aggregate dimensions and single cells, identified in clinical samples by means of confocal laser scanning microscopy. The aggregates in each acquired image were measured with LasX software. The size reported in the graph refers to the widest distance between the cells of the same aggregate.

FIGURE S2 | Gram staining of biofilm-like aggregates of *S. aureus* 1 grown in bovine synovial fluid before **(A)** and after **(B)** dispersal by combining sonication and proteinase K enzymatic treatment.

REFERENCES

- Aggarwal, V. K., Bakhshi, H., Ecker, N. U., Parvizi, J., Gehrke, T., and Kendoff, D. (2014). Organism profile in periprosthetic joint infection: pathogens differ at two arthroplasty infection referral centers in Europe and in the United States. *J. Knee Surg.* 27, 399–406. doi: 10.1055/s-0033-1364102
- Alhede, M., Kragh, K. N., Qvortrup, K., Allesen-Holm, M., van Gennip, M., Christensen, L. D., et al. (2011). Phenotypes of non-attached *Pseudomonas aeruginosa* aggregates resemble surface attached biofilm. *PLoS One* 6:e27943. doi: 10.1371/journal.pone.0027943
- Arciola, C. R., Campoccia, D., and Montanaro, L. (2018). Implant infections: adhesion, biofilm formation and immune evasion. *Nat. Rev. Microbiol.* 16, 397–409. doi: 10.1038/s41579-018-0019-y
- Argemi, X., Hansmann, Y., Riegel, P., and Prévost, G. (2017). Is *Staphylococcus lugdunensis* Significant in Clinical Samples? *J. Clin. Microbiol.* 55, 3167–3174. doi: 10.1128/JCM.00846-17
- Bay, L., Kragh, K. N., Eickhardt, S., Poulsen, S. S., Gjerdrum, L. M. R., Ghattian, K., et al. (2018). Bacterial aggregates establish at the edges of acute epidermal wounds. *Adv. Wound Care* 17, 105–113. doi: 10.1089/wound.2017.0770
- Beam, E., and Osmon, D. (2018). Prosthetic joint infection update. *Infect. Dis. Clin. North Am.* 32, 843–859. doi: 10.1016/j.idc.2018.06.005
- Becker, K., Heilmann, C., and Peters, G. (2014). Coagulase-negative staphylococci. *Clin. Microbiol. Rev.* 27, 870–926. doi: 10.1128/CMR.00109-113
- Bjarnsholt, T., Jensen, P. Ø., Fiandaca, M. J., Pedersen, J., Hansen, C. R., Andersen, C. B., et al. (2009). *Pseudomonas aeruginosa* biofilms in the respiratory tract of cystic fibrosis patients. *Pediatr. Pulmonol.* 44, 547–558. doi: 10.1002/ppul.21011
- Boyle, K. K., Wood, S., and Tarity, T. D. (2018). Low-virulence organisms and periprosthetic joint infection-biofilm considerations of these organisms. *Curr. Rev. Musculoskelet. Med.* 11, 409–419. doi: 10.1007/s12178-018-9503-2
- Burmölle, M., Thomsen, T. R., Fazli, M., Dige, I., Christensen, L., Homøe, P., et al. (2010). Biofilms in chronic infections - a matter of opportunity - monospecies biofilms in multispecies infections. *FEMS Immunol. Med. Microbiol.* 59, 324–336. doi: 10.1111/j.1574-695X.2010.00714.x
- Clinical and Laboratory Standards Institute guidelines [CLSI] (2015). *Methods for Dilution Antimicrobial Susceptibility Tests for Bacteria that Grow Aerobically*, 10th Edn. Wayne, PA: CLSI.
- Costerton, J. W., Post, J. C., Ehrlich, G. D., Hu, F. Z., Kreft, R., Nistico, L., et al. (2011). New methods for the detection of orthopedic and other biofilm infections. *FEMS Immunol. Med. Microbiol.* 61, 133–140. doi: 10.1111/j.1574-695X.2010.00766.x
- Costerton, J. W., Stewart, P. S., and Greenberg, E. P. (1999). Bacterial biofilms: a common cause of persistent infections. *Science* 284, 1318–1322. doi: 10.1126/science.284.5418.1318
- Crosby, H. A., Kwiecinski, J., and Horswill, A. R. (2016). *Staphylococcus aureus* aggregation and coagulation mechanisms, and their function in host-pathogen interactions. *Adv. Appl. Microbiol.* 96, 1–41. doi: 10.1016/bs.aambs.2016.07.018
- Dastgheyb, S., Parvizi, J., Shapiro, I. M., Hickok, N. J., and Otto, M. (2015a). Effect of biofilms on recalcitrance of staphylococcal joint infection to antibiotic treatment. *J. Infect. Dis.* 211, 641–650. doi: 10.1093/infdis/jiu514
- Dastgheyb, S. S., Hammoud, S., Ketoni, C., Liu, A. Y., Fitzgerald, K., Parvizi, J., et al. (2015b). Staphylococcal persistence due to biofilm formation in synovial fluid containing prophylactic cefazolin. *Antimicrob. Agents Chemother.* 59, 2122–2128. doi: 10.1128/AAC.04579-4514
- Dastgheyb, S. S., Villaruz, A. E., Le, K. Y., Tan, V. Y., Duong, A. C., Chatterjee, S. S., et al. (2015c). Role of phenol-soluble modulins in formation of *Staphylococcus aureus* biofilms in synovial fluid. *Infect. Immun.* 83, 2966–2975. doi: 10.1128/IAI.00394-315
- Drago, L., De Vecchi, E., Bortolin, M., Zagra, L., Romanò, C. L., and Cappelletti, L. (2017). Epidemiology and antibiotic resistance of late prosthetic knee and hip infections. *J. Arthroplasty* 32, 2496–2500. doi: 10.1016/j.arth.2017.03.005
- Eiring, P., Waller, K., Widmann, A., and Werner, H. (1998). Fibronectin and laminin binding of urogenital and oral prevotella species. *Zentralbl. Bakteriell.* 288, 361–372. doi: 10.1016/s0934-8840(98)80009-1
- Frank, K. L., and Patel, R. (2007). Poly-N-acetylglucosamine is not a major component of the extracellular matrix in biofilms formed by icaADBC-positive *Staphylococcus lugdunensis* isolates. *Infect. Immun.* 75, 4728–4742. doi: 10.1128/IAI.00640-07
- Gerlini, A., Colomba, L., Furi, L., Braccini, T., Manso, A. S., Pammolli, A., et al. (2014). The role of host and microbial factors in the pathogenesis of pneumococcal bacteraemia arising from a single bacterial cell bottleneck. *PLoS Pathog.* 10:e1004026. doi: 10.1371/journal.ppat.1004026
- Ghimire, N., Pettygrove, B. A., Pallister, K. B., Stangeland, J., Stanhope, S., Klapper, I., et al. (2019). Direct microscopic observation of human neutrophil-*Staphylococcus aureus* interaction *In Vitro* suggests a potential mechanism for initiation of biofilm infection on an implanted medical device. *Infect. Immun.* 87:e00745-19. doi: 10.1128/IAI.00745-19
- Gilbertie, J. M., Schnabel, L. V., Hickok, N. J., Jacob, M. E., Conlon, B. P., Shapiro, I. M., et al. (2019). Equine or porcine synovial fluid as a novel ex vivo model for the study of bacterial free-floating biofilms that form in human joint infections. *PLoS One* 14:e0221012. doi: 10.1371/journal.pone.0221012
- Guaglianone, E., Cardines, R., Vuotto, C., Di Rosa, R., Babini, V., Mastrantonio, P., et al. (2010). Microbial biofilms associated with biliary stent clogging. *FEMS Immunol. Med. Microbiol.* 59, 410–420. doi: 10.1111/j.1574-695X.2010.00686.x
- Guilhen, C., Forestier, C., and Balestrino, D. (2017). Biofilm dispersal: multiple elaborate strategies for dissemination of bacteria with unique properties. *Mol. Microbiol.* 105, 188–210. doi: 10.1111/mmi.13698
- Hall-Stoodley, L., Costerton, J. W., and Stoodley, P. (2004). Bacterial biofilms: from the natural environment to infectious diseases. *Nat. Rev. Microbiol.* 2, 95–108. doi: 10.1038/nrmicro821
- Homøe, P., Bjarnsholt, T., Wessman, M., Sørensen, H. C., and Johansen, H. K. (2009). Morphological evidence of biofilm formation in Greenlanders with chronic suppurative otitis media. *Eur. Arch. Otorhinolaryngol.* 266, 1533–1538. doi: 10.1007/s00405-009-0940-949
- Ibberson, C. B., Parlet, C. P., Kwiecinski, J., Crosby, H. A., Meyerholz, D. K., and Horswill, A. R. (2016). Hyaluronan modulation impacts *Staphylococcus aureus* biofilm infection. *Infect. Immun.* 84, 1917–1929. doi: 10.1128/IAI.01418-1415
- Mitchell, J., Tristan, A., and Foster, T. J. (2004). Characterization of the fibrinogen-binding surface protein Fbl of *Staphylococcus lugdunensis*. *Microbiology* 150(Pt 11), 3831–3841.
- Patterson, J. L., Stull-Lane, A., Girerd, P. H., and Jefferson, K. K. (2010). Analysis of adherence, biofilm formation and cytotoxicity suggests a greater virulence potential of *Gardnerella vaginalis* relative to other bacterial-vaginitis-associated anaerobes. *Microbiology* 156(Pt 2), 392–399. doi: 10.1099/mic.0.034280-34280
- Perez, K., and Patel, R. (2015). Biofilm-like aggregation of *Staphylococcus epidermidis* in synovial fluid. *J. Infect. Dis.* 212, 335–336. doi: 10.1093/infdis/jiv096
- Ravi, N. S., Aslam, R. F., and Veeraraghavan, B. (2019). A new method for determination of minimum biofilm eradication concentration for accurate antimicrobial therapy. *Methods Mol. Biol.* 1946, 61–67. doi: 10.1007/978-1-4939-9118-1_6
- Ross, J. J. (2017). Septic arthritis of native joints. *Infect. Dis. Clin. North Am.* 31, 203–218. doi: 10.1016/j.idc.2017.01.001
- Stoodley, P., Nistico, L., Johnson, S., Lasko, L. A., Baratz, M., Gahlot, V., et al. (2008). Direct demonstration of viable *Staphylococcus aureus* biofilms in an infected total joint arthroplasty. A case report. *J. Bone Joint Surg. Am.* 90, 1751–1758. doi: 10.2106/JBJS.G.00838
- Zimmerli, W., and Sendi, P. (2017). Orthopaedic biofilm infections. *APMIS* 125, 353–364. doi: 10.1111/apm.12687

Conflict of Interest: The authors declare that the research was conducted in the absence of any commercial or financial relationships that could be construed as a potential conflict of interest.

Copyright © 2020 Bidossi, Bottagisio, Savadori and De Vecchi. This is an open-access article distributed under the terms of the Creative Commons Attribution License (CC BY). The use, distribution or reproduction in other forums is permitted, provided the original author(s) and the copyright owner(s) are credited and that the original publication in this journal is cited, in accordance with accepted academic practice. No use, distribution or reproduction is permitted which does not comply with these terms.



The Obligate Symbiont “*Candidatus Megaira polyxenophila*” Has Variable Effects on the Growth of Different Host Species

Chiara Pasqualetti^{1,2*}, Franziska Szokoli^{1,3}, Luca Rindi⁴, Giulio Petroni¹ and Martina Schrällhammer²

¹ Dipartimento di Biologia, Università di Pisa, Pisa, Italy, ² Mikrobiologie, Institut für Biologie II, Albert-Ludwigs-Universität Freiburg, Freiburg, Germany, ³ Institut für Hydrobiologie, Technische Universität Dresden, Dresden, Germany, ⁴ Dipartimento di Biologia, CoNISMa, Università di Pisa, Pisa, Italy

OPEN ACCESS

Edited by:

Martin Kaltenpoth,
Johannes Gutenberg University
Mainz, Germany

Reviewed by:

Harald Ronald Gruber-Vodicka,
Max Planck Institute for Marine
Microbiology (MPG), Germany
Simon M. Dittami,
UMR 8227 Laboratoire de Biologie
Intégrative des Modèles Marins,
France

*Correspondence:

Chiara Pasqualetti
chiarapasqualetti@libero.it

Specialty section:

This article was submitted to
Microbial Symbioses,
a section of the journal
Frontiers in Microbiology

Received: 15 January 2020

Accepted: 02 June 2020

Published: 08 July 2020

Citation:

Pasqualetti C, Szokoli F, Rindi L,
Petroni G and Schrällhammer M
(2020) The Obligate Symbiont
“*Candidatus Megaira polyxenophila*”
Has Variable Effects on the Growth
of Different Host Species.
Front. Microbiol. 11:1425.
doi: 10.3389/fmicb.2020.01425

“*Candidatus Megaira polyxenophila*” is a recently described member of *Rickettsiaceae* which comprises exclusively obligate intracellular bacteria. Interestingly, these bacteria can be found in a huge diversity of eukaryotic hosts (protist, green algae, metazoa) living in marine, brackish or freshwater habitats. Screening of amplicon datasets revealed a high frequency of these bacteria especially in freshwater environments, most likely associated to eukaryotic hosts. The relationship of “*Ca. Megaira polyxenophila*” with their hosts and their impact on host fitness have not been studied so far. Even less is known regarding the responses of these intracellular bacteria to potential stressors. In this study, we used two phylogenetically close species of the freshwater ciliate *Paramecium*, *Paramecium primaurelia* and *Paramecium pentaurelia* (Ciliophora, Oligohymenophorea) naturally infected by “*Ca. Megaira polyxenophila*”. In order to analyze the effect of the symbiont on the fitness of these two species, we compared the growth performance of both infected and aposymbiotic paramecia at different salinity levels in the range of freshwater and oligohaline brackish water i.e., at 0, 2, and 4.5 ppt. For the elimination of “*Ca. Megaira polyxenophila*” we established an antibiotic treatment to obtain symbiont-free lines and confirmed its success by fluorescence *in situ* hybridization (FISH). The population and infection dynamics during the growth experiment were observed by cell density counts and FISH. Paramecia fitness was compared applying generalized additive mixed models. Surprisingly, both infected *Paramecium* species showed higher densities under all salinity concentrations. The tested salinity concentrations did not significantly affect the growth of any of the two species directly, but we observed the loss of the endosymbiont after prolonged exposure to higher salinity levels. This experimental data might explain the higher frequency of “*Ca. M. polyxenophila*” in freshwater habitats as observed from amplicon data.

Keywords: brackish, *Paramecium*, stress response, symbiosis, osmolarity, GAMMs

INTRODUCTION

Paramecium (Ciliophora, Oligohymenophorea) is a unicellular protist with a broad, nearly global distribution in fresh and brackish water bodies. This ciliate is studied, among other things (Karunanithi et al., 2019; Kelz and Mashour, 2019; Mayne et al., 2019; Soares et al., 2019; Arnaiz et al., 2020) for the abundance and diversity of its endosymbionts (Floriano et al., 2018; Garushyants et al., 2018; Grosser et al., 2018; Potekhin et al., 2018; Sabaneyeva et al., 2018; Schrallhammer et al., 2018; Castelli et al., 2019a,b; Fokin et al., 2019; Koehler et al., 2019; Lanzoni et al., 2019; Plotnikov et al., 2019). Host-symbiont interactions and their outcome have been studied for example using *Holospira* (Lohse et al., 2006; Hori et al., 2008; Fokin and Görtz, 2009; Nidelet et al., 2009; Duncan et al., 2013, 2018; Banerji et al., 2015; Castelli et al., 2015; Dusi et al., 2015; Garushyants et al., 2018; Grosser et al., 2018) *Caedibacter* (Kusch et al., 2002; Dusi et al., 2014; Grosser et al., 2018; Schu and Schrallhammer, 2018; Koehler et al., 2019) and *Preeria* (Bella et al., 2016; Potekhin et al., 2018). Despite an increasing number of studies, our knowledge about the impact of symbionts on *Paramecium* is limited, especially when considering that this ciliate is among the best studied protists in regard to host-symbiont interactions. Less is known regarding the response of these symbiotic systems exposed to additional environmental stressors. Even in a balanced system, the introduction of a stressor can have severe consequences. The impact of a symbiont could either shift towards virulent behavior (Dusi et al., 2014; Bella et al., 2016; Schu and Schrallhammer, 2018) and hence, represents an additional biotic stressor, or alternatively has a positive effect on the host's stress response and thus on survival, e.g., for salinity stress (Smurov and Fokin, 1998; Duncan et al., 2010) or heat shock (Hori and Fujishima, 2003; Fujishima et al., 2005; Hori et al., 2008; Duncan et al., 2010). Some authors (Fokin and Sabaneyeva, 1990; Smurov and Fokin, 1998) reported a higher bacterial infection frequency in protists, i.e., *Paramecium*, living in brackish environments compared to those living in freshwater environments. This might imply an evolutionary advantage for symbiont-bearing microorganisms in habitats exposed to salinity stress. Members of the genus *Paramecium* are well known to be highly sensitive not only to temperature stress but also to increased salinity concentrations (Duncan et al., 2010). Contrary, it could indicate that stressed protists are more susceptible to infection.

In 2013, a bacterial species of the order *Rickettsiales* has been described as endosymbiont of different ciliates (Schrallhammer et al., 2013). All members of this order are obligate intracellular bacteria hosted by eukaryotic organisms and strictly depend on their hosts for multiplication (Dumler et al., 2001) with the notable exception of the epibiont "*Candidatus* Deianiraea vastatrix" (Castelli et al., 2019a). "*Candidatus* *Megaira* polyxenophila" is remarkable as it has been found associated to potential hosts spanning a huge diversity, e.g., various ciliates (Sun et al., 2009; Vannini et al., 2005; Schrallhammer et al., 2013; Zaila et al., 2017), amoebae (Hess, 2017) chlorophytes and streptophytes (Hollants et al., 2013; Kawafune et al., 2015;

Yang et al., 2016) and even cnidarians (Fraune and Bosch, 2007; Sunagawa et al., 2009). Interestingly, the *Megaira*-infected organisms cover a surprising ecological range from freshwater lakes and ponds to brackish waters and even marine systems. Recently, this bacterium has been found associated with multiple *Paramecium* species, including several members of the *Paramecium aurelia* complex representing a group of phylogenetically very closely related species (Lanzoni et al., 2019). In this work, we found "*Ca. Megaira polyxenophila*" (from here referred as *Ca. M. polyxenophila*) naturally occurring in two species of the *P. aurelia* complex, i.e., *Paramecium pentaurelia* and *Paramecium primaurelia*.

The aim of this study is to analyze the role of *Ca. M. polyxenophila*, determining the symbiont's effect on the growth of two phylogenetically close species of *Paramecium* after establishment of the corresponding symbiont-free cell lines via antibiotic treatment. The obtained infected and aposymbiotic lines were then used to compare their performance under standard laboratory conditions as well as at different salinity levels corresponding to oligohaline brackish water. Difference in growth performance depending on presence or absence of *Ca. M. polyxenophila* will shed light on the function of this endosymbiont and the role of this symbiosis under different environmental conditions such as increasing osmolality.

MATERIALS AND METHODS

Experimental Organisms and Their Cultivation

Two different *Paramecium* species naturally harboring *Ca. M. polyxenophila* were used as endosymbiont-infected lines and to establish symbiont-free cells. The host species, as indicated in Table 1, were *P. pentaurelia* US_YE9 (from here on referred to as YE9) derived from Bloomington, IN, United States, whereas *P. primaurelia* Rio Lg_Jac 2III (from here on referred to as LgJac), was sampled in Rio de Janeiro, Brazil. Both species are freshwater protists. After antibiotic (AB) treatment (see below), we established aposymbiotic cell lines viz. YE9AB and LgJacAB. All cultures were maintained at 19°C in Cerophyll medium (CM) inoculated with *Raoultella planticola* DSM3069 (*Enterobacteriales*, *Enterobacteriaceae*) (Chiellini et al., 2019).

Prior to the experiment, a single cell was isolated from each cell line and was washed several times in spring water from a freshly opened bottle (San Benedetto S. p. A. Italy) in order to minimize the presence of potentially contaminating microorganisms. The cells were then fed daily for 5 days with CM inoculated with *R. planticola* to induce their exponential growth. These monoclonal cultures (both naturally infected and treated) are maintained since more than four years under laboratory conditions.

Identification of *Paramecium* Species

Paramecium species were identified using morphological characteristics (Fokin, 2010) and the cytochrome *c* oxidase 1

TABLE 1 | *Paramecium* species used in this study, their endosymbionts and geographic origin.

<i>Paramecium</i> species	Symbiont	Symbionts' localization	Origin	Sampled by
<i>P. pentaurelia</i> YE9	Ca. <i>M. polyxenophila</i>	Cytoplasm	Bloomington, IN, United States	Yana Eglit
<i>P. pentaurelia</i> YE9AB	None		Established in this study	
<i>P. primaurelia</i> LgJac	Ca. <i>M. polyxenophila</i>	Cytoplasm	Rio de Janeiro, Brazil	Sascha Krennek
<i>P. primaurelia</i> LgJacAB	None		Established in this study	

gene (COX1, Barth et al., 2006). Total DNA was extracted using a modified Chelex-based protocol as follows: approximately 100 *paramecia* cells of each culture were washed three times in sterile spring water and transferred in 100 μ l spring water into 0.5 ml Eppendorf tubes. The tubes were stored for at least 20 min at -20°C to freeze completely. Later, 100 μ l Chelex solution (Bio-Rad Laboratories, Inc., Hercules, CA, United States) was added and the samples were incubated for 20 min at 99°C . Immediately after incubation the tubes were put on ice. PCR products were obtained by using the forward primer M13 (5'-GTA AAA CGA CGG CCA G-3', Strüder-Kypke and Lynn, 2010) for LgJac and degenerated forward primer F199dT-B (5'-TGT AAA ACG ACG GCC AGT TCA GGT GCT GCM TTA GCH ACY ATG-3', Strüder-Kypke and Lynn, 2010) for YE9 as well as the degenerated reverse primer R1143dT (5'-CAG GAA ACA GCT ATG ACT ART ATA GGA TGM CCW CCA TAA GC-3', Strüder-Kypke and Lynn, 2010) for both strains. Purification was performed with the NucleoSpin Gel and PCR Clean-up Kit (Macherey-Nagel GmbH & Co., KG, Düren NRW, Germany), and products were sequenced directly in both directions with the same primers used for amplification at Eurofins Genomics GmbH (Ebersberg, Germany).

In order to confirm their affiliation to the respective *Paramecium* species, the obtained sequences were compared to available *Paramecium* COX1 sequences. A Maximum likelihood (ML) tree was calculated with IQ-TREE (Nguyen et al., 2015) based on 34 sequences from 10 different *Paramecium* species comprising 620 characters. The alignment was trimmed to the length of the shortest sequence. The best-fit evolutionary model (Kalyaanamoorthy et al., 2017) according to Bayesian information criterion (BIC) is TPM2u+F+I+G4. Ultrafast Bootstrap support (BS) with 1000 pseudoreplicates (Hoang et al., 2018) was calculated by IQ-TREE.

Identification of “*Ca. Megaira polyxenophila*”

Prokaryotic SSU rRNA gene sequences were amplified by a touchdown PCR (Don et al., 1991) applying the following annealing temperatures: 58°C (30 s, 5 cycles), 54°C (30 s, 10 cycles), and 50°C (30 s, 25 cycles). For YE9, the bacterial primer combination Bac16SFor (5'-AAG AGT TTG ATC CTG GCT C-3'; modified from Neilan et al., 1997) and Bac16SRev (5'-TAC GGC TAC CTT GTT ACG AC-3'; Neilan et al., 1997) were used for both, PCR and direct sequencing from both sides. PCR on LgJac was performed with the *Alphaproteobacteria* specific forward primer 16S_F19b 5'-CCT GGC TCA GAA CGA ACG-3' (Serra et al., 2016) and the Bacteria specific reverse primer 16S_R1522a 5'-GGA GGT GAT CCA GCC GCA-3'

(Serra et al., 2016) and sequenced using the internal primers 16S F343 ND 5'-TAC GGG AGG CAG CAG-3', 16S R515 ND 5'-ACC GCG GCT GCT GGC AC-3' and 16S F785 ND 5'-GGA TTA GAT ACC CTG GTA-3' (Serra et al., 2016) at GATC Biotech AG (Konstanz, Germany).

A comparison with other 16S rRNA gene sequences of *Ca. M. polyxenophila* and *Ca. Megaira venefica* was performed. Therefore, we run a ML analysis with IQ-TREE based on an alignment (ARB program; Ludwig et al., 2004) of 43 sequences comprising 1343 characters, trimmed at both sides to the length of the shortest sequence. The applied best-fit evolutionary model is TIM3+F+G4 (according to BIC) and 1000 pseudoreplicates were performed for Ultrafast BS.

Fluorescence *in situ* Hybridization

The presence or absence of the endosymbionts was verified by performing fluorescence *in situ* hybridization (FISH) experiments with the universal probe EUB338 (5'-ACT CCT ACG GGA GGC AGC AG-3') (Amann et al., 1990) in combination with the genus-specific probe Megenus_487 (5'-GCCGGGGCTTTTCTGTTGGT-3') detecting “*Ca. Megaira*” (Lanzoni et al., 2019). About 20 ciliate cells were collected, washed three times in water and fixed with 2% paraformaldehyde (PFA, final concentration) on slides as described by Szokoli et al. (2016). Hybridization and washing were carried out as described by Lanzoni et al. (2019). Images were obtained with a Leica DMR microscope, equipped with an HBO 50W/AC-L2 fluorescent lamp, a Leica DFC490 video camera, and Leica IM1000 Software (v.1.0).

Elimination of Endosymbionts via Antibiotic Treatment

The antibiotic treatment was performed in order to obtain genetically identical symbiont-free lines from the infected ones. Symbiont-free cells were obtained from both, *P. pentaurelia* YE9 and *P. primaurelia* LgJac, through antibiotic treatment (YE9AB and LgJacAB, respectively). Therefore, approximately 30 cells of the stock cultures were transferred to 500 μ l of tetracycline (Carl Roth, Karlsruhe, Germany) solution ($130 \mu\text{g ml}^{-1}$) and incubated for 24 h at 20°C . Later, the cells were washed four times. Individual cells were incubated again in tetracycline solution at 20°C for 24–48 h and then transferred to CM inoculated with *R. planticola* as food organism. After some rounds of cell division, single cells were treated again with tetracycline for 24 h and subsequently transferred into bacterized CM. The success of the antibiotic treatment was confirmed by FISH.

Fitness Experiment to Determine the Impact of the Endosymbiont on Host Growth at Different Salinity Conditions

In order to prime the cultures for the fitness experiment at different salinity conditions, *Paramecium* cells were adapted to the different salinity concentrations and fed daily for three days with bacterized CM to induce exponential growth (Supplementary Figure S1).

The cell number for each line was adjusted to approximately the same density (ca. 100 cells ml⁻¹) with sterile CM. To set-up this experiment, a mix containing 8 ml of CM (in case of 0 ppt) or 8 ml of salinity stock solution (8 ppt for a final concentration of 2 ppt; 18 ppt for 4.5 ppt), 12 ml bacterized CM and 20 ml *Paramecium* culture (approximately 100 cells ml⁻¹) were added, the total volume was set to 40 ml per line. The salinities were chosen to represent two different oligohaline brackish water conditions after a preliminary experiment to test the salinity tolerance of the two freshwater paramecia species (data not shown). This mix was then split into three experimental units for each line per salinity combination with 10 ml each (approximately 50 cells ml⁻¹) (Supplementary Figure S1).

Each experimental unit was fed once a week with 3 ml of a 1:4 dilution of the respective salinity stock solution (sterile water, 8 or 18 ppt) and bacterized CM, to sustain the paramecia and to maintain a constant salinity concentration throughout the experiment (either 0, 2, or 4.5 ppt) for a period of 28 days.

Cell density was determined by counting under a stereomicroscope. The counting days were established as reported in Figure 1 in which T0 is the starting day of the salinity experiment. For each sample, three technical replicates each with a volume of 50–100 µl, depending on the cell number, were counted and the mean of cells per ml was calculated. Samples for cell density estimation were counted and then fixed to perform FISH as described above. These samples were collected twice per week for the duration of the experiment (28 days). Salt stock solutions were prepared by dissolving the corresponding amount of Tropic Marine Salts (Red Sea Salt Meersalz, Red Sea, Düsseldorf, Germany) in deionized water and pasteurizing for 5 min at 95°C.

Statistical Analysis

The influence of host species with different infectious status and in different salinity settings on *Paramecium* cell density was assessed by using a generalized additive mixed model (GAMM) with gaussian error (R, package: mgcv, version 1.7-28 (Wood, 2017)). GAMMs allow assessing the influence of covariates on a response variable without specifying *a priori* fixed-function while accounting for non-independence of data due to successive measures in time. For this reason, time has been included both, in the fixed part, as smoothed term, and in the random part to model dependence. In particular, time has been smoothed independently for different combinations of host species, initial infection status and salinity. Fixed effect terms (infection status, salinity and host species) were modeled using a basis dimension of $k = 4$. The significance of the fixed terms and interactions has been obtained by using the anova.gam function of the mgcv

package. The script and dataset are available as Supplementary Table S1 and Supplementary Data Sheet S1. Model accuracy was estimated by the root-mean-square error (RMSE) performing a 10-fold cross-validation on the fixed part of the model using the CVgam function of the gamclass R package. The analysis was performed using R, version 3.6.0.

RESULTS

Elimination of *Ca. M. polyxenophila*

Aposymbiotic cells were obtained from both, YE9 and LgJac, through antibiotic treatment producing respectively YE9AB and LgJacAB. A cell was considered successfully treated when no signal with the genus-specific probe *Megenus_487* (Lanzoni et al., 2019) was observed from food vacuoles, cytoplasm, or nuclei. Successful elimination of *Ca. M. polyxenophila* was verified repeatedly by FISH (Figure 2). In none of the examined cells, *Ca. M. polyxenophila* was detected after the described tetracycline treatment. Other effects of the antibiotic treatment than symbiont elimination, e.g. delayed or abnormal cell division or population growth, were not observed.

Confirmation of Host and Endosymbiont Identities

Morphological analyses of the *Paramecium* strains from Bloomington and Rio de Janeiro revealed the strains belonging to the *Paramecium aurelia*-complex. This observation was confirmed by COX1 sequence analysis (Supplementary Figure S2). More precisely, LgJac affiliated with other *P. primaurelia* sequences whereas YE9 belonged to *P. pentaurelia*. Both affiliations received high BS support (98 and 99%, Supplementary Figure S2).

The endosymbiont's 16S rRNA gene sequences affiliated with other sequences of *Ca. M. polyxenophila* with high BS support (97%, Supplementary Figure S3). The sequence similarity (data not shown) between the type strain of this species (AJ630204) and the here studied intracellular bacteria was 99.93% (LgJac) and 99.55% (YE9).

The obtained sequences are available from NCBI GenBank with following accession numbers: COX1 sequences MT362542 (LgJac) and MT362543 (YE9), 16S rRNA gene sequences MT351038 (LgJac) and MT351039 (YE9).

Fitness Impact of *Ca. M. polyxenophila* and Salinity on *Paramecia*

Time included in the model as the smoothed effect revealed a strongly significant effect on estimated degrees of freedom as expected for a nonlinear density growth (Supplementary Data Sheet S1). Among the three fixed factors, host species and infection status showed a highly significant effect (Table 2). Two interaction terms also showed a significant effect, the interaction between infection status and *Paramecium* species and the interaction between salinity and species (Table 2).

According to the GAMM results which revealed a significant effect for host species, a substantial difference in cell densities

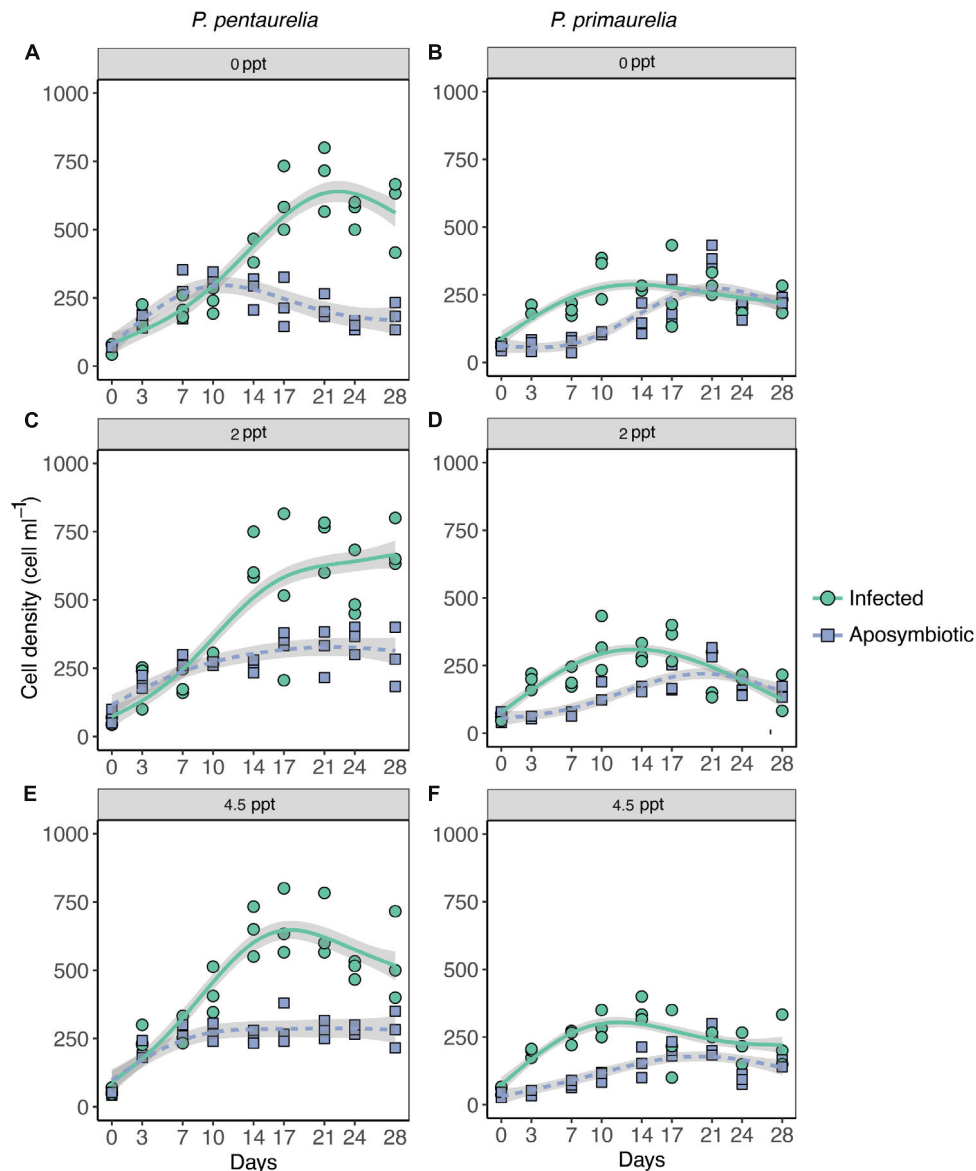


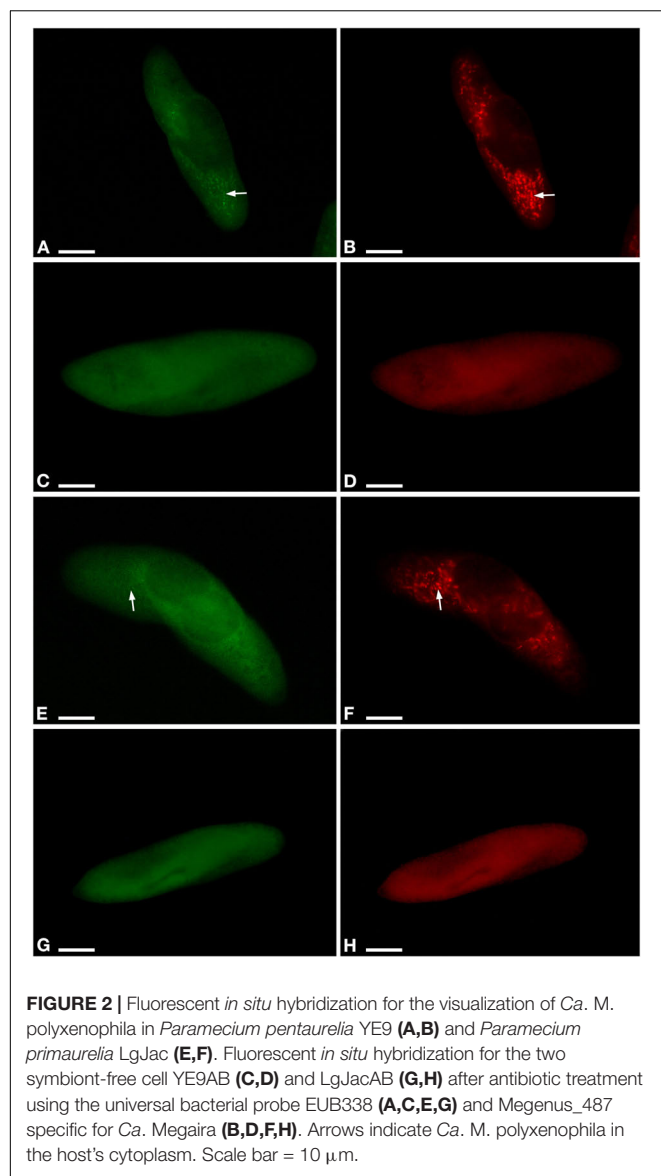
FIGURE 1 | Growth of *Paramecium* lines either infected with *Ca. Megaira polyxenophila* or aposymbiotic at different salinity concentrations over a period of 28 days. *Paramecium pentaurelia* YE9 infected (green line) with *Ca. Megaira polyxenophila* in comparison with the respectively symbiont-free line YE9AB (purple line) at 0 ppt salinity (A), 2 ppt salinity (C), and 4.5 ppt salinity (E). *Paramecium primaurelia* LgJac infected (green line) with *Ca. M. polyxenophila* in comparison with the respectively symbiont-free (purple line) LgJacAB at 0 ppt salinity (B), 2 ppt salinity (D), and 4.5 ppt salinity (F). Data points represent three experimental units and the growth curve is represented by the mean of these three units.

between the two *Paramecium* species were observed as YE9 grew better in comparison with LgJac, reaching 800 and 400 cell ml⁻¹, respectively (Figure 1). At the beginning of the experiment, the starting amount of cells was the same for each line (approximately 50 cells ml⁻¹).

The inspection of growth curves and GAMM results indicated that both infected strains showed a generally higher cell density compared to their aposymbiotic counterparts. A strong significant interaction between *Paramecium* species and infection status was caused by the very strong difference in cell density of YE9 (between 600 and 700 cell ml⁻¹ at the end of the

experiment) compared to YE9AB (200–300 cell ml⁻¹) which was not observed in LgJac (Figure 1). The weak significant interaction between salinity and species was due to the density decrease of LgJac and LgJacAB at the higher salinity levels, revealing its stronger salinity stress susceptibility compared to YE9 (Figure 1).

Both *Paramecium* species experienced growth advantages in presence of *Ca. M. polyxenophila* at every salinity condition (Figure 1). There was no obvious general effect of cultivation at oligohaline brackish conditions, neither on infected nor aposymbiotic lines.



Impact of Salinity on *Ca. M. polyxenophila* Prevalence

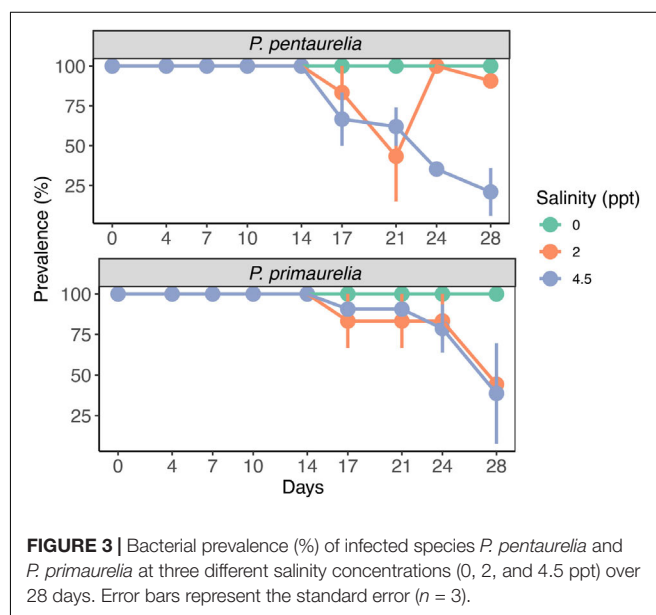
Infected and aposymbiotic paramecia cells of both species were observed by FISH at all sampling time points for all salinity concentrations. The aposymbiotic cells maintained their symbiont-free condition for the complete experiment duration at all tested salinities. FISH results showed that *Ca. M. polyxenophila* was present in YE9 and LgJac at 0 ppt with a prevalence of 100% and in a constant amount at all time points (Figure 3). For the initially *Megaira*-positive cells at 2 and 4.5 ppt, the 100% infection status was maintained until day 17 for both species and declined subsequently. Both species reached the lowest bacterial prevalence at the end of the experiment at 4.5 ppt (Figure 3).

While the percentage of *P. pentastrella* YE9 cells with detected bacterial symbionts continuously declined after day 17 at 4.5 ppt

TABLE 2 | ANOVA style-results of the generalized additive mixed models (GAMM) analysis on the salinity, infection, and species on cell density (cell ml⁻¹).

	df	F	p-Value
Salinity	2	1.076	0.343
Infection status	1	27.792	<0.001
Host species	1	49.660	<0.001
Salinity × infection status	2	0.787	0.456
Salinity × host species	2	3.838	0.023
Infection status × host species	1	22.297	<0.001
Salinity × infection status × host species	2	0.333	0.717

Model accuracy was measured by root-mean-square error (RMSE). R^2 adj. = 0.80; RMSE = 79.13.

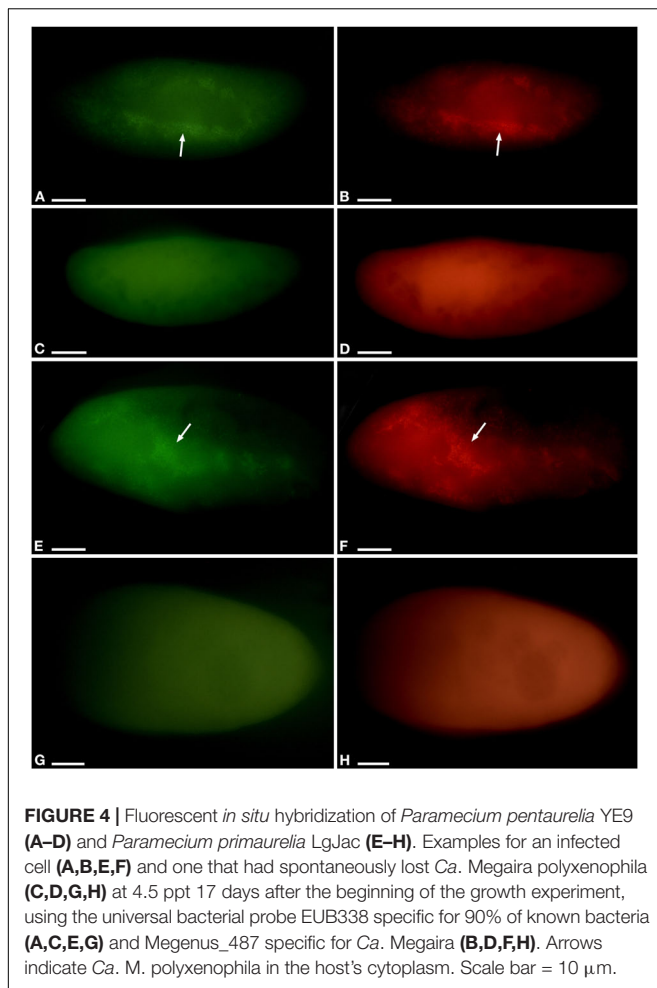


(Figures 3, 4), at 2 ppt the strongest drop in prevalence was observed at day 21. The number of infected cells suddenly recovered and then decreased again. As our approach was to examine approximately 20 cells out of a 1 ml sample at each time point, this strong fluctuation might by chance represent an outlier with such a high number of cells which had spontaneously lost their symbionts.

In case of *P. primaurelia* LgJac, the decrease of *Megaira*-positive cells was very similar at 2 and 4.5 ppt. At the end of the experiment, the infection prevalence dropped to approximately 40% (Figure 3).

DISCUSSION

Our data suggest that the major effect of *Ca. M. polyxenophila* on *Parametium* hosts is not harmful. While *Rickettsiaceae* usually are considered as obligate intracellular parasites (DeLong et al., 2014) at least in the case of *Wolbachia* a wide continuum of symbiotic interactions, ranging from mutualistic and essential for host development, fertility, and survival in filarial nematodes to facultative and parasitic in many arthropod species, has



been observed (Landmann, 2019). Likely, the fitness effects of *Ca. M. polyxenophila* vary similarly between different hosts and different environmental conditions. Nevertheless, these intracellular bacteria are at least conditionally mutualistic in the two examined *Parametium* species without providing essential nutritional benefits.

Both *P. pentaurelia* and *P. primaurelia* exhibit improved growth under all tested conditions in presence of the symbiont. Contrary to our expectations, the tested species showed no obvious fitness reduction by increasing salinity levels. This trend indicates that at least the here applied rather mild salt concentrations corresponding to the lower border of oligohaline brackish conditions might be below the physiological stress level of these paramecia. Like many unicellular organisms, *Parametium* constantly encounter changing environmental conditions e.g., differences in water temperature between seasons, day and night, or even during a day according to the varying solar irradiation. Some fluctuations of environmental conditions remain within the physiological tolerance breadth (Krenek and Berendonk, 2009) whereas others reach stress levels. When paramecia are gradually adapted to stress conditions instead of being suddenly exposed, they can increase their

resistance to this particular stressor (Smurov and Fokin, 1998; Tsukuda, 1989). As the cells examined in the fitness assay underwent an acclimatization phase prior to the experiment the applied salinity conditions remained within the organisms' tolerance range.

Fokin and Sabaneyeva (1990) observed that ciliates living in brackish water apparently harbor more frequently bacterial infections than those in freshwater. We observed a decreasing prevalence of *Ca. M. polyxenophila* starting 2 weeks after the cells were exposed to increased salinity concentrations (2 and 4.5 ppt) while those at freshwater-like conditions remained to 100% infected until the end of the experiment. This is neither a confirmation nor a rejection of the hypothesis that brackish environments favor bacterial infections, but it demonstrates that elevated salt concentrations disrupt the symbiont maintenance in the *Ca. M. polyxenophila-Parametium aurelia* system. Thus, we speculate that long-term exposure to mild environmental stress causes an accumulation of stress signals, for example, an accumulation of misfolded proteins or compatible solutes. While the cellular response of the host will have not necessarily immediate effects on growth, it might either impair bacterial cell division or accidentally cause their expulsion. Alternatively, the increased energy demand in order to adapt to prolonged stress exposure might result in a more directed elimination of the symbionts by lysosomal attack.

As *P. pentaurelia* YE9 and *P. primaurelia* LgJac both benefit from the presence of their symbionts, long-term exposure to brackish salinity conditions will have indirect negative effects on these paramecia.

The loss of *Ca. M. polyxenophila* in brackish conditions might indicate, despite the above mentioned description of this symbiont from marine and brackish host organisms, that they have an adaptation towards freshwater habitats and/or freshwater hosts. This speculation is supported by amplicon sequencing of environmental samples. More than 25% of the amplicon datasets associated with freshwater habitats screened by Lanzoni et al. (2019) revealed positive hits for *Ca. M. polyxenophila*, while the number of marine datasets with signatures of this symbiont was below 5%.

This study provides the first functional analysis of the frequent and promiscuous endosymbiont *Ca. M. polyxenophila*. So far, speculations about a possible opportunistic or parasitic lifestyle of these bacteria (Schrallhammer et al., 2013) are based only on the fact that strains of *Ca. M. polyxenophila* from phylogenetically and geographically distant hosts exhibit very high (99–100%) 16S rRNA gene sequence similarities. This has been considered as strong indication for horizontal transmission capabilities. So far, infection experiments with these bacteria have not been successful under laboratory conditions (Lanzoni et al., 2019). Functional studies regarding the interaction of this symbiont with its host are impaired by (i) its obligate intracellular life style, a trait *Ca. M. polyxenophila* has in common with other members of *Rickettsiales* (Castelli et al., 2016) (ii)

the lack of successful protocols for experimental infection experiments, and so far (iii) for symbiont elimination to obtain genetically identical but aposymbiotic (host) organisms. A successful treatment has been established in this study. Similar approaches for generation of the aposymbiotic lines have been used in case of other endosymbionts of *Paramecium* (Kusch et al., 2002; Dusi et al., 2014; Bella et al., 2016; Grosser et al., 2018). The fact that members of *Rickettsiaceae* are naturally resistant to a variety of antibiotics (Rolain et al., 1998) did complicate the establishment of the present protocol. The aposymbiotic lines LgJAC and YE9AB have been maintained under routine laboratory conditions since at least 5 years. While we cannot completely exclude the small chance that the antibiotic treatment affects *Paramecium* fitness or eliminated free-living bacteria contributing to the observed fitness effects and we would have preferred additional experiments such as infection of naïve cells, those are presently not feasible. Thus, we provide the very first insights into possible effects of *Ca. M. polyxenophila* on its host. As we observed differences in the impact of the endosymbiont in two very closely related host species, it is possible that in more divergent hosts an even broader spectrum of host-symbiont interactions will be observed. As *Ca. M. polyxenophila* infected hosts have been isolated from rather different environments (Lanzoni et al., 2019) the diversity of relevant abiotic factors might further entangle the analysis of the ecological role of this endosymbiont.

DATA AVAILABILITY STATEMENT

All datasets generated for this study are included in the article/**Supplementary Material**.

AUTHOR CONTRIBUTIONS

CP, FS, and MS designed the research. MS performed the molecular analysis. CP and FS performed the experiments. CP and LR performed the statistical analysis. CP, MS, GP, and LR interpreted the results. CP, FS, MS, and LR wrote the manuscript. All authors critically read and approved the manuscript.

REFERENCES

- Amann, R. I., Binder, B. J., Olson, R. J., Chisholm, S. W., Devereux, R., and Stahl, D. A. (1990). Combination of 16S rRNA-targeted oligonucleotide probes with flow cytometry for analyzing mixed microbial populations. *Appl. Environ. Microbiol.* 56, 1919–1925. doi: 10.1111/j.1469-8137.2004.01066.x
- Arnaiz, O., Meyer, E., and Sperling, L. (2020). *ParameciumDB* 2019: integrating genomic data across the genus for functional and evolutionary biology. *Nucleic Acids Res.* 48, D599–D605.
- Banerji, A., Duncan, A. B., Griffin, J. S., Humphries, S., Petchey, O. L., and Kaltz, O. (2015). Density- and trait-mediated effects of a parasite and a predator in a tri-trophic food web. *J. Anim. Ecol.* 84, 723–733. doi: 10.1111/1365-2656.12317
- Barth, D., Krensek, S., Fokin, S. I., and Berendonk, T. U. (2006). Intraspecific genetic variation in *Paramecium* revealed by mitochondrial cytochrome *c* oxidase I

FUNDING

This research was supported by the European Cooperation in Science and Technology BMBS COST Action BM1102, the European Community's H2020 Programme H2020-MSCA-RISE 2019 under grant agreement 872767, and by the ERASMUS placement program. The article processing charge was funded by the German Research Foundation (DFG) and the University of Freiburg in the funding program Open Access Publishing.

ACKNOWLEDGMENTS

The authors gratefully acknowledge Yana Eglit and Sascha Krensek for isolating and providing the strains used in this work, Fabrizio Erra for his assistance with fluorescence microscopy, Simone Gabrielli for help with the preparation of figures, and Gabriele Iannattoni for his support in the lab.

SUPPLEMENTARY MATERIAL

The Supplementary Material for this article can be found online at: <https://www.frontiersin.org/articles/10.3389/fmicb.2020.01425/full#supplementary-material>

FIGURE S1 | Schematic representation of the procedure followed for the fitness experiment.

FIGURE S2 | Species affiliation of LgJAC and YE9 based on COX1 sequence analysis. Maximum likelihood tree of the genus *Paramecium* calculated with IQ-TREE based on an alignment of 34 sequences from 10 different *Paramecium* species comprising 620 characters. Here obtained sequences are reported in bold. Numbers near nodes indicate Ultrafast Bootstrap support values (below 75% not shown), numbers in brackets indicate sequences in collapsed groups. Scale bar corresponds to 0.1 sequence divergence.

FIGURE S3 | Molecular characterization of the endosymbionts of YE9 and LgJAC based on 16S rRNA gene sequences. Maximum likelihood tree calculated with IQ-TREE based on 43 sequences belonging to members of the genera “*Ca. Megaira*” and *Rickettsia* comprising 1343 characters. Here obtained sequences are reported in bold. Numbers near nodes indicate Ultrafast Bootstrap support values (below 70% not shown). Scale bar corresponds to 0.01 sequence divergence. *Ca.* stands for *Candidatus*.

TABLE S1 | Data sheet for fitness analysis.

DATA SHEET S1 | R script.

- sequences. *J. Eukaryot. Microbiol.* 53, 20–25. doi: 10.1111/j.1550-7408.2005.00068.x
- Bella, C., Koehler, L., Grosser, K., Berendonk, T. U., Petroni, G., and Schallhammer, M. (2016). Fitness impact of obligate intranuclear bacterial symbionts depends on host growth phase. *Front. Microbiol.* 7:2084. doi: 10.3389/fmicb.2016.02084
- Castelli, M., Lanzoni, O., Fokin, S. I., Schallhammer, M., and Petroni, G. (2015). Response of the bacterial symbiont *Holospira caryophila* to different growth conditions of its host. *Eur. J. Protistol.* 51, 98–108. doi: 10.1016/j.ejop.2014.11.006
- Castelli, M., Sabaneyeva, E., Lanzoni, O., Lebedeva, N., Floriano, A. M., Gaiarsa, S., et al. (2019a). *Deianiraea*, an extracellular bacterium associated with the ciliate *Paramecium*, suggests an alternative scenario for the evolution of *Rickettsiales*. *ISME J.* 13, 2280–2294. doi: 10.1038/s41396-019-0433-9

- Castelli, M., Serra, V., Senra, M. V., Basuri, C. K., Soares, C. A., Fokin, S. I., et al. (2019b). The hidden world of *Rickettsiales* symbionts: “*Candidatus Spectrickettsia obscura*,” a novel bacterium found in Brazilian and Indian *Paramecium caudatum*. *Microb. Ecol.* 77, 748–758. doi: 10.1007/s00248-018-1243-8
- Castelli, M., Sasser, D., and Petroni, G. (2016). “Biodiversity of “non-model” *Rickettsiales* and their association with aquatic organisms,” in *Rickettsiales*, ed. S. Thomas (Cham: Springer), 59–91. doi: 10.1007/978-3-319-46859-4_3
- Chiellini, C., Pasqualetti, C., Lanzoni, O., Fagorzi, C., Fani, R., Petroni, G., et al. (2019). Harmful effect of *Rheinheimera* sp. EpRS3 (Gammaproteobacteria) against the protist *Euplates aediculatus* (Ciliophora, Spirotrichea): insights into the ecological role of antimicrobial compounds from environmental bacterial strains. *Front. Microbiol.* 10:510. doi: 10.3389/fmicb.2016.0510
- DeLong, E. F., Lory, S., Stackebrandt, E., and Thompson, F. (2014). *The Prokaryotes: Alphaproteobacteria And Betaproteobacteria*. Berlin: Springer.
- Don, R., Cox, P., Wainwright, B., Baker, K., and Mattick, J. (1991). ‘Touchdown’ PCR to circumvent spurious priming during gene amplification. *Nucleic Acids Res.* 19:4008. doi: 10.1093/nar/19.14.4008
- Dumler, J. S., Barbet, A. F., Bekker, C., Dasch, G. A., Palmer, G. H., Ray, S. C., et al. (2001). Reorganization of genera in the families *Rickettsiaceae* and *Anaplasmataceae* in the order *Rickettsiales*: unification of some species of *Ehrlichia* with *Anaplasma*, *Cowdria* with *Ehrlichia* and *Ehrlichia* with *Neorickettsia*, descriptions of six new species combinations and designation of *Ehrlichia equi* and ‘HGE agent’ as subjective synonyms of *Ehrlichia phagocytophila*. *Int. J. Syst. Evol. Microbiol.* 51, 2145–2165. doi: 10.1099/00207713-51-6-2145
- Duncan, A. B., Dusi, E., Schrällhammer, M., Berendonk, T., and Kaltz, O. (2018). Population-level dynamics in experimental mixed infections: evidence for competitive exclusion among bacterial parasites of *Paramecium caudatum*. *Oikos* 127, 1380–1389. doi: 10.1111/oik.05280
- Duncan, A. B., Fellous, S., Accot, R., Alart, M., Sobandi, K. C., Cosiaux, A., et al. (2010). Parasite-mediated protection against osmotic stress for *Paramecium caudatum* infected by *Holospira undulata* is host genotype specific. *FEMS Microbiol. Ecol.* 74, 353–360. doi: 10.1111/j.1574-6941.2010.00952.x
- Duncan, A. B., Gonzalez, A., and Kaltz, O. (2013). Stochastic environmental fluctuations drive epidemiology in experimental host-parasite metapopulations. *Proc. R. Soc. B Biol. Sci.* 280, 20131747. doi: 10.1098/rspb.2013.1747
- Dusi, E., Gougat-Barbera, C., Berendonk, T. U., and Kaltz, O. (2015). Long-term selection experiment produces breakdown of horizontal transmissibility in parasite with mixed transmission mode. *Evolution* 69, 1069–1076. doi: 10.1111/evo.12638
- Dusi, E., Krensek, S., Schrällhammer, M., Sachse, R., Rauch, G., Kaltz, O., et al. (2014). Vertically transmitted symbiont reduces host fitness along temperature gradient. *J. Evol. Biol.* 27, 796–800. doi: 10.1111/jeb.12336
- Floriano, A. M., Castelli, M., Krensek, S., Berendonk, T. U., Bazzocchi, C., Petroni, G., et al. (2018). The genome sequence of “*Candidatus Fokinia solitaria*”: insights on reductive evolution in *Rickettsiales*. *Genome Biol. Evol.* 10, 1120–1126. doi: 10.1093/gbe/evy072
- Fokin, S., and Sabaneyeva, E. (1990). *Paramecium* (Ciliophora, Peniculina) from water with low salinity of the Barents Sea and White Sea coasts and their endobionts. Presented at the *Ecology, Reproduction And Guarding Of The Bioresources Of the North Europe seas. Abstr. of the III Conference*, Murmansk.
- Fokin, S. I. (2010). *Paramecium* genus: biodiversity, some morphological features and the key to the main morphospecies discrimination. *Protistology* 6, 227–235.
- Fokin, S. I., and Görtz, H.-D. (2009). “Diversity of *Holospira* bacteria in *Paramecium* and their characterization,” in *Endosymbionts in Paramecium*, Springer, 161–199.
- Fokin, S. I., Serra, V., Ferrantini, F., Modeo, L., and Petroni, G. (2019). *Candidatus Hafkinia simulans* gen. nov., sp. nov., a novel holospira-like bacterium from the macronucleus of the rare brackish water ciliate *Frontonia salmastra* (Oligohymenophorea, Ciliophora): multidisciplinary characterization of the new endosymbiont and its host. *Microb. Ecol.* 77, 1092–1106. doi: 10.1007/s00248-018-1311-0
- Fraune, S., and Bosch, T. C. (2007). Long-term maintenance of species-specific bacterial microbiota in the basal metazoan *Hydra*. *Proc. Natl. Acad. Sci. U.S.A.* 104, 13146–13151. doi: 10.1073/pnas.0703375104
- Fujishima, M., Kawai, M., and Yamamoto, R. (2005). *Paramecium caudatum* acquires heat-shock resistance in ciliary movement by infection with the endonuclear symbiotic bacterium *Holospira obtusa*. *FEMS Microbiol. Lett.* 243, 101–105. doi: 10.1016/j.femsle.2004.11.053
- Garushyants, S. K., Beliauskaya, A. Y., Malko, D. B., Logacheva, M. D., Rautian, M. S., and Gelfand, M. S. (2018). Comparative genomic analysis of *Holospira* spp., intranuclear symbionts of paramecia. *Front. Microbiol.* 9:738. doi: 10.3389/fmicb.2016.0738
- Grosser, K., Ramasamy, P., Amirabad, A. D., Schulz, M. H., Gasparoni, G., Simon, M., et al. (2018). More than the “killer trait”: infection with the bacterial endosymbiont *Caedibacter taeniospiralis* causes transcriptomic modulation in *Paramecium* host. *Genome Biol. Evol.* 10, 646–656. doi: 10.1093/gbe/evy024
- Hess, S. (2017). Description of *Hyalodiscus flabellus* sp. nov. (Vampyrellida, Rhizaria) and identification of its bacterial endosymbiont, “*Candidatus Megaira polyxenophila*” (*Rickettsiales*, *Alphaproteobacteria*). *Protist* 168, 109–133. doi: 10.1016/j.protis.2016.11.003
- Hoang, D. T., Chernomor, O., Von Haeseler, A., Minh, B. Q., and Vinh, L. S. (2018). UFBoot2: improving the ultrafast bootstrap approximation. *Mol. Biol. Evol.* 35, 518–522. doi: 10.1093/molbev/msx281
- Hollants, J., Leliaert, F., Verbruggen, H., Willems, A., and De Clerck, O. (2013). Permanent residents or temporary lodgers: characterizing intracellular bacterial communities in the siphonous green alga *Bryopsis*. *Proc. R. Soc. B Biol. Sci.* 280:20122659. doi: 10.1098/rspb.2012.2659
- Hori, M., Fujii, K., and Fujishima, M. (2008). Micronucleus-specific bacterium *Holospira elegans* irreversibly enhances stress gene expression of the host *Paramecium caudatum*. *J. Eukaryot. Microbiol.* 55, 515–521. doi: 10.1111/j.1550-7408.2008.00352.x
- Hori, M., and Fujishima, M. (2003). The endosymbiotic bacterium *Holospira obtusa* enhances heat-shock gene expression of the host *Paramecium caudatum*. *J. Eukaryot. Microbiol.* 50, 293–298. doi: 10.1111/j.1550-7408.2003.tb00137.x
- Kalyanamoorthy, S., Minh, B. Q., Wong, T. K., von Haeseler, A., and Jermini, L. S. (2017). ModelFinder: fast model selection for accurate phylogenetic estimates. *Nat. Methods* 14:587. doi: 10.1038/nmeth.4285
- Karunani, S., Oruganti, V., Marker, S., Rodriguez-Viana, A. M., Drews, F., Pirritano, M., et al. (2019). Exogenous RNAi mechanisms contribute to transcriptome adaptation by phased siRNA clusters in *Paramecium*. *Nucleic Acids Res.* 47, 8036–8049. doi: 10.1093/nar/gkz553
- Kawafune, K., Hongoh, Y., Hamaji, T., Sakamoto, T., Kurata, T., Hirooka, S., et al. (2015). Two different rickettsial bacteria invading *Volvox carterii*. *PLoS One* 10:e0116192. doi: 10.1371/journal.pone.0116192
- Kelz, M. B., and Mashour, G. A. (2019). The biology of general anesthesia from *Paramecium* to primate. *Curr. Biol.* 29, R1199–R1210.
- Koehler, L., Flemming, F. E., and Schrällhammer, M. (2019). Towards an ecological understanding of the killer trait-A reproducible protocol for testing its impact on freshwater ciliates. *Eur. J. Protistol.* 68, 108–120. doi: 10.1016/j.ejop.2019.02.002
- Krensek, S., and Berendonk, T. U. (2009). A Long-term conservation tool for cell characteristics: cryopreservation of *Paramecium caudatum*. *Protist* 160, 355–363. doi: 10.1016/j.protis.2009.03.002
- Kusch, J., Czabatinski, L., Nachname, S., Hübner, M., Alter, M., and Albrecht, P. (2002). Competitive advantages of *Caedibacter*-infected paramecia. *Protist* 153, 47–58. doi: 10.1078/1434-4610-00082
- Landmann, F. (2019). The *Wolbachia* endosymbionts. *Bact. Intracell.* 72:139. doi: 10.1128/9781683670261.ch10
- Lanzoni, O., Sabaneyeva, E., Modeo, L., Castelli, M., Lebedeva, N., Verni, F., et al. (2019). Diversity and environmental distribution of the cosmopolitan endosymbiont *Candidatus Megaira*. *Sci. Rep.* 9:1179.
- Lohse, K., Gutierrez, A., and Kaltz, O. (2006). Experimental evolution of resistance in *Paramecium caudatum* against the bacterial parasite *Holospira undulata*. *Evolution* 60, 1177–1186. doi: 10.1111/j.0014-3820.2006.tb01196.x
- Ludwig, W., Strunk, O., Westram, R., Richter, L., Meier, H., Yadhukumar, B., et al. (2004). ARB: a software environment for sequence data. *Nucleic Acids Res.* 32, 1363–1371. doi: 10.1093/nar/gkh293
- Mayne, R., Morgan, J., Whiting, J. G., Phillips, N., and Adamatzky, A. (2019). On measuring nanoparticle toxicity and clearance with *Paramecium caudatum*. *Sci. Rep.* 9, 1–9.
- Neilan, B. A., Jacobs, D., Blackall, L. L., Hawkins, P. R., Cox, P. T., and Goodman, A. E. (1997). rRNA sequences and evolutionary relationships among toxic and

- nontoxic cyanobacteria of the genus *Microcystis*. *Int. J. Syst. Evol. Microbiol.* 47, 693–697. doi: 10.1099/00207713-47-3-693
- Nguyen, L.-T., Schmidt, H. A., Von Haeseler, A., and Minh, B. Q. (2015). IQ-TREE: a fast and effective stochastic algorithm for estimating maximum-likelihood phylogenies. *Mol. Biol. Evol.* 32, 268–274. doi: 10.1093/molbev/msu300
- Nidelet, T., Koella, J. C., and Kaltz, O. (2009). Effects of shortened host life span on the evolution of parasite life history and virulence in a microbial host-parasite system. *BMC Evol. Biol.* 9:65. doi: 10.1186/1471-2148-9-65
- Plotnikov, A. O., Balkin, A. S., Gogoleva, N. E., Lanzoni, O., Khlopko, Y. A., Cherkasov, S. V., et al. (2019). High-throughput sequencing of the 16S rRNA gene as a survey to analyze the microbiomes of free-living ciliates *Paramecium*. *Microb. Ecol.* 78, 286–298. doi: 10.1007/s00248-019-01321-x
- Potekhin, A., Schweikert, M., Nekrasova, I., Vitali, V., Schwarzer, S., Anikina, A., et al. (2018). Complex life cycle, broad host range and adaptation strategy of the intranuclear *Paramecium* symbiont *Preeria caryophila* comb. nov. *FEMS Microbiol. Ecol.* 94:fiy076.
- Rolain, J., Maurin, M., Vestris, G., and Raoult, D. (1998). In vitro susceptibilities of 27 rickettsiae to 13 antimicrobials. *Antimicrob. Agents Chemother.* 42, 1537–1541. doi: 10.1128/aac.42.7.1537
- Sabaneyeva, E., Castelli, M., Szokoli, F., Benken, K., Lebedeva, N., Salvetti, A., et al. (2018). Host and symbiont intraspecific variability: the case of *Paramecium calkinsi* and *Candidatus Trichorickettsia mobilis*. *Eur. J. Protistol.* 62, 79–94. doi: 10.1016/j.ejop.2017.12.002
- Schrallhammer, M., Castelli, M., and Petroni, G. (2018). Phylogenetic relationships among endosymbiotic R-body producer: bacteria providing their host the killer trait. *Syst. Appl. Microbiol.* 41, 213–220. doi: 10.1016/j.syapm.2018.01.005
- Schrallhammer, M., Ferrantini, F., Vannini, C., Galati, S., Schweikert, M., Görtz, H.-D., et al. (2013). ‘*Candidatus Megaira polyxenophila*’ gen. nov., sp. nov.: considerations on evolutionary history, host range and shift of early divergent rickettsiae. *PLoS One* 8:e72581. doi: 10.1371/journal.pone.072581
- Schu, M. G., and Schrallhammer, M. (2018). Cultivation conditions can cause a shift from mutualistic to parasitic behavior in the symbiosis between *Paramecium* and its bacterial symbiont *Caedibacter taeniospiralis*. *Curr. Microbiol.* 75, 1099–1102. doi: 10.1007/s00284-018-1493-1
- Serra, V., Fokin, S. I., Castelli, M., Basuri, C. K., Nitla, V., Verni, F., et al. (2016). ‘*Candidatus Gortzia shahrazadis*’, a novel endosymbiont of *Paramecium multimicronucleatum* and a revision of the biogeographical distribution of *Holospora*-like bacteria. *Front. Microbiol.* 7:1704. doi: 10.3389/fmicb.2016.01704
- Smurov, A., and Fokin, S. (1998). Resistance of *Paramecium caudatum* infected with endonuclear bacteria *Holospora* against salinity impact. *Proc. Zool. RAS* 276, 175–178.
- Soares, H., Carmona, B., Nolasco, S., and Melo, L. V. (2019). Polarity in ciliate models: from cilia to cell architecture. *Front. Cell Dev. Biol.* 7:240. doi: 10.3389/fmicb.2016.240
- Strüder-Kypke, M. C., and Lynn, D. H. (2010). Comparative analysis of the mitochondrial cytochrome c oxidase subunit I (COI) gene in ciliates (Alveolata, Ciliophora) and evaluation of its suitability as a biodiversity marker. *Syst. Biodivers.* 8, 131–148. doi: 10.1080/14772000903507744
- Sun, H., Noe, J., Barber, J., Coyne, R., Cassidy-Hanley, D., Clark, T., et al. (2009). Endosymbiotic bacteria in the parasitic ciliate *Ichthyophthirius multifiliis*. *Appl. Environ. Microbiol.* 75, 7445–7452. doi: 10.1128/aem.00850-09
- Sunagawa, S., DeSantis, T. Z., Piceno, Y. M., Brodie, E. L., DeSalvo, M. K., Voolstra, C. R., et al. (2009). Bacterial diversity and white plague disease-associated community changes in the Caribbean coral *Montastraea faveolata*. *ISME J.* 3:512. doi: 10.1038/ismej.2008.131
- Szokoli, F., Castelli, M., Sabaneyeva, E., Schrallhammer, M., Krensek, S., Doak, T. G., et al. (2016). Disentangling the taxonomy of *Rickettsiales* and description of two novel symbionts (‘*Candidatus Bealeia paramacronuclearis*’ and ‘*Candidatus Fokinia cryptica*’) sharing the cytoplasm of the ciliate protist *Paramecium biaurelia*. *Appl. Environ. Microbiol.* 82, 7236–7247. doi: 10.1128/aem.02284-16
- Tsukuda, H. (1989). Heat and osmotic tolerance in *Paramecium caudatum*, acclimated to different temperatures and salinities. *Compar. Biochem. Physiol. Part A Physiol.* 94, 333–337. doi: 10.1016/0300-9629(89)90555-0
- Vannini, C., Petroni, G., Verni, F., and Rosati, G. (2005). A bacterium belonging to the *Rickettsiaceae* family inhabits the cytoplasm of the marine ciliate *Diophrys appendiculata* (Ciliophora, Hypotrichia). *Microb. Ecol.* 49, 434–442. doi: 10.1007/s00248-004-0055-1
- Wood, S. N. (2017). *Generalized Additive Models: An Introduction With R*. London: Chapman and Hall.
- Yang, A., Narechania, A., and Kim, E. (2016). Rickettsial endosymbiont in the “early-diverging” streptophyte green alga *Mesostigma viride*. *J. Phycol.* 52, 219–229. doi: 10.1111/jpy.12385
- Zaila, K. E., Doak, T. G., Ellerbrock, H., Tung, C.-H., Martins, M. L., Kolbin, D., et al. (2017). Diversity and universality of endosymbiotic rickettsia in the fish parasite *Ichthyophthirius multifiliis*. *Front. Microbiol.* 8:189. doi: 10.3389/fmicb.2016.0189

Conflict of Interest: The authors declare that the research was conducted in the absence of any commercial or financial relationships that could be construed as a potential conflict of interest.

Copyright © 2020 Pasqualetti, Szokoli, Rindi, Petroni and Schrallhammer. This is an open-access article distributed under the terms of the Creative Commons Attribution License (CC BY). The use, distribution or reproduction in other forums is permitted, provided the original author(s) and the copyright owner(s) are credited and that the original publication in this journal is cited, in accordance with accepted academic practice. No use, distribution or reproduction is permitted which does not comply with these terms.



Defining the *Helicobacter pylori* Disease-Specific Antigenic Repertoire

Maria Felicia Soluri^{1,2†}, Simone Puccio^{3†}, Giada Caredda⁴, Paolo Edomi⁵, Mario Milco D'Elia⁶, Fabio Cianchi⁶, Arianna Troilo⁶, Claudio Santoro^{1,2}, Daniele Sblattero^{5*†} and Clelia Peano^{7,8*†}

OPEN ACCESS

Edited by:

Flavia Marinelli,
University of Insubria, Italy

Reviewed by:

Theam Soon Lim,
Universiti Sains Malaysia (USM),
Malaysia

Alberto Danielli,
University of Bologna, Italy

*Correspondence:

Daniele Sblattero
dsblattero@units.it
Clelia Peano
clelia.peano@humanitasresearch.it

[†]These authors have contributed
equally to this work and share first
authorship

[‡]These authors share last authorship

Specialty section:

This article was submitted to
Antimicrobials, Resistance
and Chemotherapy,
a section of the journal
Frontiers in Microbiology

Received: 17 February 2020

Accepted: 16 June 2020

Published: 09 July 2020

Citation:

Soluri MF, Puccio S, Caredda G,
Edomi P, D'Elia MM, Cianchi F,
Troilo A, Santoro C, Sblattero D and
Peano C (2020) Defining the
Helicobacter pylori Disease-Specific
Antigenic Repertoire.
Front. Microbiol. 11:1551.
doi: 10.3389/fmicb.2020.01551

¹ Department of Health Sciences & IRCAD, Università del Piemonte Orientale, Novara, Italy, ² Center for Translational Research on Autoimmune and Allergic Disease, Università del Piemonte Orientale, Novara, Italy, ³ Laboratory of Translational Immunology, IRCCS, Humanitas Clinical and Research Center, Rozzano, Italy, ⁴ Department of Excellence in Pharmacological and Biomolecular Sciences, University of Milan, Milan, Italy, ⁵ Department of Life Sciences, University of Trieste, Trieste, Italy, ⁶ Department of Experimental and Clinical Medicine, School of Human Health Sciences, University of Florence, Florence, Italy, ⁷ Institute of Genetic and Biomedical Research, UoS Milan, National Research Council, Milan, Italy, ⁸ Genomic Unit, IRCCS, Humanitas Clinical and Research Center, Milan, Italy

The analysis of the interaction between *Helicobacter pylori* (HP) and the host *in vivo* is an extremely informative way to enlighten the molecular mechanisms behind the persistency/latency of the bacterium as well as in the progression of the infection. An important source of information is represented by circulating antibodies targeting the bacteria that define a specific “disease signature” with prospective diagnostic implications. The diagnosis of some of the HP induced diseases such as gastric cancer (GC), MALT lymphoma (MALT), and autoimmune gastritis (AIG) is not easy because patients do not show symptoms of illness in early-onset stages, at the same time they progress rapidly. The possibility of identifying markers able to provide an early diagnosis would be extremely beneficial since a late diagnosis results in a delay in undergoing active therapy and reduces the survival rate of patients. With the aim to identify the HP antigens recognized during the host immune-response to the infection and possibly disease progression, we applied a discovery-driven approach, that combines “phage display” and deep sequencing. The procedure is based on the selection of ORF phage libraries, specifically generated from the pathogen's genome, with sera antibodies from patients with different HP-related diseases. To this end two phage display libraries have been constructed starting from genomic DNA from the reference HP 26695 and the pathogenic HP B128 strains; libraries were filtered for ORFs by using an ORF selection vector developed by our group (Di Niro et al., 2005; Soluri et al., 2018), selected with antibodies from patients affected by GC, MALT, and AIG and putative HP antigens/epitopes were identified after Sequencing and ranking. The results show that individual selection significantly reduced the library diversity and comparison of individual ranks for each condition allowed us to highlight a pattern of putative antigens specific for the different pathological outcomes or common for all of them. Within the putative

antigens enriched after selection, we have validated protein CagY/Cag7 by ELISA assay as a marker of HP infection and progression. Overall, we have defined HP antigenic repertoire and identified a panel of putative specific antigens/epitopes for three different HP infection pathological outcomes that could be validated in the next future.

Keywords: *H. pylori* infection, interactome, gastric cancer, MALT lymphoma, autoimmune gastritis, phage display, next generation sequencing

INTRODUCTION

Helicobacter pylori (HP) infects more than 50% of the world's population (Parsonnet, 1995; Goh et al., 2011; Peleteiro et al., 2014; Hooi et al., 2017) thus being the most prevalent human pathogen worldwide. Infection occurs in early childhood and colonization most likely persists for the long-life. The bacterium colonizes the stomach, not only residing on the surface area of the gastric mucosa but also adhering to the gastric epithelium (Stolte and Eidt, 1989; Björkholm et al., 2000). Although in most people the infection remains clinically asymptomatic, most colonized individuals develop coexisting chronic inflammation that significantly increases the risk of site-specific diseases. Many studies have demonstrated that HP infection causes gastric and duodenal ulcer diseases, that can lead to Gastric Cancer (GC) and mucosa-associated lymphoid tissue (MALT) B-cell lymphoma (Wyatt and Rathbone, 1988; Shahar et al., 1994). Several factors act, alone or synergistically, during the infection, and their combination can determine the fate of the infection progression, making the difference between latent infection and the development of a pathological outcome. Dysregulation of the inflammatory/immune host response plays an important role in the progression toward cancer. A genetically determined pro-inflammatory state increases the risk of cancer, and several human polymorphisms occurring within genes of the inflammatory/immune-response have been associated with gastric malignancies development (El-Omar et al., 2000; Yuzhalin, 2011). Among bacterial components, some factors associated with malignancy have been also identified, although the high grade of genomic variability of HP strains has hindered this purpose. The most important virulence factor of HP is the cag pathogenicity island (cagPAI), a genetic locus of about 40 kb that contains 31 genes (Tomb et al., 1997; Alm et al., 1999) and encodes for the so-called type IV secretion system (T4SS). This forms a syringe-like structure that injects bacterial components (mainly peptidoglycan and the oncoprotein cagA) into the host target cell (Rohde et al., 2003). HP strains that harbor the cagPAI (cagPAI+) pathogenicity locus show a significantly increased ability to induce severe pathological outcomes in infected individuals, compared to cagPAI– strains (Blaser et al., 1995; Kuipers et al., 1995; Noto and Peek, 2012; Takahashi-Kanemitsu et al., 2020).

Current treatments of HP infection are based on double-antibiotic therapy combined with proton-pump inhibitors. However, this therapeutic approach is not optimal, not only for its many drawbacks but also for the insurgence of antibiotic resistances and its consequent loss of efficacy (Thung et al., 2016; Hu et al., 2017). Furthermore, this strategy of eradication,

even when successful, does not lead to any protection from subsequent re-infections (Solnick, 1998; Megraud et al., 2013). The development of a vaccine has been a field of research pursued in the last decades. Progress have been made, and different antigens, adjuvants, administration routes, have been explored, leading to promising results, either using prophylactic and therapeutic protocols, in animal models; however, the gaining of protective immunity in humans remains elusive (Aebischer et al., 2008; Müller and Solnick, 2011; Salama et al., 2013; Ikuse et al., 2019). A deeper understanding of host-bacterium interaction is needed. However, this goal is limited by the fact that many molecular aspects of the bacterium are still incompletely characterized, with about 23% of the bacterium proteins that remain without a defined functional annotation (Tomb et al., 1997; Boneca et al., 2003; Resende et al., 2013). Identification and characterization of novel predictive biomarkers could also improve the power of serological tests for detecting and monitoring HP infection and could be beneficial for both therapeutic and diagnostic purposes. HP related GC detection is currently based on the use of markers prone to a high degree of false-negative results, thus making the discovery of novel sensitive biomarkers an urgent issue (Lam and Lo, 2008). Moreover, there is an important need to improve earlier ability to identify patients that are progressing toward cancer development, to target those patients and make them undergo early clinical programs for cancer prevention.

In this study, we aimed to (i) construct a genomic library of *H. pylori* to be representative of all the ORFs of the bacterium, and to (ii) identify novel HP antigens recognized by host immune system response. We applied an unbiased approach based on the production of phage libraries for the displaying of the whole antigenic repertoire of two HP strains. This approach allowed the identification of different antigenic domains of *H. pylori*. Among these we focused our attention on the protein CagY/Cag7. Here we report and characterize, the presence of antibodies against a domain of the CagY protein, in a high percentage of patients affected by different pathological outcomes related to HP infection.

MATERIALS AND METHODS

Bacterial Strains

Two *H. pylori* strains have been used for ORF/filtering libraries preparation: HP 26695 *H. pylori* strain described by Tomb et al. (1997); it was originally isolated from a patient suffering gastritis and shown to be able to elicit immune and inflammatory responses and is considered the reference strain.

HP B128(B8) *H. pylori* strain more recently described and isolated from a patient with a gastric ulcer (Israel et al., 2001; McClain et al., 2009).

Escherichia coli DH5 α F' (Gibco BRL), F'/endA1 hsd17 (rK–mK +) supE44 thi-1recA1 gyrA (Nalr) relA1 (lacZYA-argF) U169 deoR [F80dlacD-(lacZ)M15], were used for both libraries preparation and phage display selection.

Human Sera Samples

Patients' sera have been collected at the Careggi Hospital in Florence in collaboration with the Department of Experimental and Clinical Medicine of the University of Florence; the recruitment of patients has been approved by the Ethical committee protocol number 14936_bio. Autoimmune Gastritis (AIG) patients: all patients with AIG had both autoantibodies against parietal cells (APCA) and intrinsic factor (AIFA) (D'elios et al., 2001; Troilo et al., 2019). Histology is considered the most reliable method for assessing the presence of AIG (Massironi et al., 2019). Histopathological assessment of gastric mucosa was scored according to the Sydney System classification (Dixon et al., 1996) on a visual analog scale (0 = absent, 1 = mild, 2 = moderate, 3 = severe). Six patients were classified at stage II; four patients were classified at stage III. Patients with GC: all patients studied had distal gastric adenocarcinoma. Each patient was carefully clinically evaluated, and the TNM stage recorded. Seven patients were classified with a TNM stage I; 16 patients with TNM stage II; six patients with TNM stage III. Patients with gastric MALT lymphoma: six newly diagnosed MALT lymphoma patients, classified as Ann Arbor stage, were enrolled in this study. Five patients were classified at stage I, only one patient was classified at stage II. Data relative to the classification and stage of the patients have been included in **Supplementary Table 3**. IgG antibodies were purified from all sera samples by affinity chromatography on protein A agarose (Thermo Fisher Scientific). Single sera were diluted in PBS and incubated with protein agarose for 16 h at 4°C with gentle rotations. Bound antibodies were eluted with 0.1 M Glycine pH 2.7 and immediately buffered with 20% vol/vol of 1M Tris–HCl pH 8.5. Following dialysis against PBS, purified antibodies were quantified on SDS-PAGE and Coomassie staining.

Genomic ORF Libraries Preparation

Helicobacter pylori ORFeome-libraries were prepared in the pFILTER3 vector, as previously described (Zacchi et al., 2003; D'Angelo et al., 2011; Soluri et al., 2018). Briefly, the genomic DNA from the three different strains were separately fragmented by ultra-sonication (Covaris) (duty cycle 10%; intensity 5.0; cycles per burst 200; duration 2 × 60 s, total 120 s; mode frequency sweeping; temperature 6°C) to obtain fragments ranging from 200 to 800 bp length. Fragments were treated with the Quick blunting kit (New England Biolabs) to perform end-repairing and phosphorylation and then ligated into the vector previously blunt-cut through *EcoRV* enzyme digestion (New England Biolabs). Transformation of the two libraries obtained into DH5 α F' bacteria cells was performed through electroporation. After electroporation, bacteria were plated on 2×TY agar plates supplemented with 34 μ g/ml

chloramphenicol (pFILTER resistance) and 25 μ g/ml ampicillin (selective marker for ORFs) and grown for 16 h at 37°C. Dilutions of each library were also plated and grown in parallel to determine the library size and efficiency of the filtering. Bacteria were harvested, thoroughly mixed and stored at –80°C in 20% sterile glycerol, in small aliquots. Plasmid DNA was extracted from one aliquot and used to prepare the phagemid libraries. To this aim filtered ORFs were cut from each pFILTER library with *Bss*HII and *Nhe*I restriction enzymes (New England Biolabs), and cloned into a compatible pDAN5 vector (Sblattero and Bradbury, 2000) upstream of the g3p gene. Two different libraries, one for each HP strain, were prepared. Libraries were titrated and analyzed by deep sequencing.

Library Selection Procedure

Four pools of sera were prepared mixing equal amount of purified antibodies derived from three to six donors. Phage particles preparation and selection procedures were done according to established protocols (Di Niro et al., 2009; Dal Ferro et al., 2019). Briefly, phages were diluted in MPBS (2% non-fat milk in PBS), added to 30 μ l of DynaBeads ProteinA (Life Technologies) with 10 μ g of antibodies immobilized on, incubated for 90 min at room temperature in rotation. Beads were washed five times with PBS-0.05% Tween-20 and five times with PBS, and then phages were eluted by the addition of 1 ml DH5 α F' at OD_{600 nm} = 0.5 for 45 min with occasional shaking. Bacteria obtained after the first cycle of selection were amplified and phages prepared for a second cycle where the washing conditions were modified to improve specificity. In the second cycle after incubation with the phages, beads were subjected to 10 times washes with PBS-0.1% Tween-20, then resuspended in PBS and incubated for 10 min on rotation and washed again for 10 times with PBS. Bacteria cells used for the elution were plated on 2×TY agar plates supplemented with 100 μ g/ml of ampicillin and grown for 16 h at 37°C. The outputs of each selection were collected, thoroughly mixed and stored at –80°C with 20% sterile glycerol. Plasmid DNA was extracted and analyzed by deep sequencing.

Illumina Sequencing and Data Analysis

The following protocol has been used to perform recovery, sequencing and analysis of DNA inserts from pFILTER-ORF-library, pDAN5-ORF-library or selected-phage-libraries. DNA inserts were recovered by a first PCR amplification with specific primers annealing on the plasmid backbone. These primers carry at their 5' end specific adaptors sequences for the successive indexing and the direct sequencing of the amplicons (primers sequences and protocol details are explained in Soluri et al., 2018). After the first PCR clean-up, a second Index PCR was performed by using the Nextera XT Index kit (Illumina) to produce double indexed amplicon pool. Libraries have been qualitatively evaluated on the 2200 TapeStation (Agilent) to verify their size and in parallel quantified by Real Time PCR by using the KAPA Biosystem library quantification kit (Roche) following manufacturer's protocol. Libraries were sequenced by generating long reads, at least 250 bp Paired End by using the MiSeq Illumina instrument. Bioinformatic analysis was

performed by using the InteractomeSeq webtool (Puccio et al., 2020) with a pipeline specifically developed by our group for the analysis of this kind of data. In brief the data analysis workflow allows generating a list of putative domains with genomic annotations just starting from raw sequencing reads. The pipeline is composed of four sequential steps: (1) input files are checked (raw reads, reference genome sequence, annotation list) to verify their proper format; (2) low-quality sequencing data or reads with a length lower than 100 base are trimmed using Cutadapt (Martin, 2011); (3) reads are aligned with blastn (Madden, 2013) to the genome sequence allowing up to 5% of mismatches, and a SAM file is generated. Only reads with quality score greater than 30 ($Q > 30$) are further subjected to SAMtools (Li et al., 2009) processing and converted into a BAM file; reads falling into a CDSs for at least 80% of their length are identified by invoking BEDTOOLS (Quinlan and Hall, 2010); then, for each CDS portion covered by mapping reads, the analysis pipeline calculate and take into account gene coverage (the total number of reads assigned to a gene), max depth (the maximum number of reads covering a specific genic portion) and the focus index (obtained from the ratio between max depth and coverage). CDS portions showing a focus index higher than 0.8 and a coverage higher than the average coverage observed for all mapping regions in the BAM file are classified as putative domain/epitope. (4) Finally, a list of putative domains is generated in tabular separated format and their relative tracks that can be viewed in the genome browser. Comparison between common and specific domains enriched in different selection experiments can be performed and Venn diagrams are generated. Raw sequencing Data available at Sequence Read Archive under Bioproject Accession number PRJNA506709.

Cloning and Expression of Recombinant Protein

Helicobacter pylori HP0527 ORF corresponding to aa 566–655 was chosen for validation. The phage expressing the selected fragment was recovered from the phagemid library thanks to two back-to-back oligonucleotides mapping to the center of the enriched domain identified by the overlapping reads. ORF coding fragment was then excised from the phagemid vector and cloned into a compatible pGEX-4T1 (GE-Healthcare) vector for the expression of the selected ORF as GST-fusion product. The successful cloning of the specific gene fragment was assessed by sequencing analysis. Positive colonies were grown until $OD_{600\text{ nm}} = 0.5$ and induced by IPTG with a final concentration of 0.2 mM for 16 h at 28°C. The recombinant protein was purified with GST affinity resin (Sigma-Aldrich). Purity and integrity of purified GST-ORF protein domain were checked by SDS-PAGE followed by Coomassie gel staining. Concentration was assessed by densitometry using ImageJ analysis software (Wayne Rasband, NIH, United States¹) and calculated based on a standard BSA curve. This analysis was paralleled by measure the OD at 280 nm of the protein preparation. The purified protein was also checked by western blotting with α -GST and α -FLAG antibody.

¹<https://imagej.nih.gov/ij/>

ELISA Assay

An ELISA assay was set up to validate the antigenicity of the selected HP0527 protein portion. Briefly, 96 plate ELISA wells (Greiner) were coated by an overnight incubation at 4°C with 200 ng/well of recombinant GST-protein diluted in PBS. After washing with PBS, wells were blocked with 200 μ l of blocking solution (PBS-0.05% Tween-20-2% milk) through incubation at 37°C for 1 h. Wells were again washed for three times with PBS-0.05% Tween-20 and incubated with sera samples diluted 1:500 in blocking solution, for 2 h at 37°C. After five washes with PBS-0.05% Tween-20 and five washes with PBS, wells were incubated for 1 h at 37°C with a goat α -human IgG HRP conjugated (Sigma-Aldrich) diluted 1:5000 in blocking solution. Wells were washed again, immune-complexes revealed with TMB and the plate read at 450 nm. Samples with absorbance \geq of the mean OD450 value obtained with healthy control sera plus 2 standard deviations (SD) were considered positive.

Statistical Analysis

ELISA results were analyzed by using GraphPad Prism 8 software and differences between groups evaluated by the Mann–Whitney test; a p -values < 0.05 was considered statistically significant.

RESULTS

Construction of *Helicobacter pylori* Phage Display ORFs Library

We have developed a pipeline for the identification and validation of novel antigenic proteins in different pathological conditions (D'Angelo et al., 2013; Antony et al., 2019). The approach combines the use of ORF filtering to select folded protein domains, phage display system to select the domain of interest and the power of deep sequencing technology for the identification of enriched clones. This procedure has been shown to be feasible for making and selecting libraries from bacteria whole genomes (D'Angelo et al., 2011; Gourlay et al., 2015) therefore we applied it to identify novel HP antigenic proteins.

Two HP strains were initially selected: the HP 26695, considered the reference strain, and originally isolated in the United Kingdom from a patient suffering from gastritis, and HP B128, isolated in the United States from a patient with a gastric ulcer. By using genomic DNA from both strains, ORF filtered libraries were individually produced. The genomic DNA was extracted and randomly fragmented in the range of 200–800 bp; this length range should provide a broad representation of the whole “domainome” of the bacterium (Kuznetsov et al., 2006). gDNA fragments were end-repaired and cloned into the filtering vector in which only folded ORF fragments can allow transformant *E. coli* cells to survive under selective pressure. After the filtering procedure the size of the libraries was reduced to 1/50 respect to the non-filtered ones, with a final size being 1.4×10^6 and 1×10^6 colonies for HP 26695 and HP B128, respectively. This selection rate was in keeping with theoretical calculation as well as our previous observations (Zacchi et al., 2003; D'Angelo et al., 2011) suggesting successful ORF filtration.

Fragment size variability was assessed by PCR on random clones showing an average length of 150–200 bp. Considering the size of the starting *H. pylori* genome the libraries provide coverage of around 100-fold. After the filtering step, the ORF DNA fragments were subcloned into a phage display vector to allow their expression as a fusion protein with the g3p protein. The final library size was 1×10^6 clones per each strain.

ORF-Filtered Genomic Libraries Characterization by Deep Sequencing

The phage display libraries were analyzed by deep sequencing. Plasmid DNA was extracted from each library and ORFs were amplified, sequenced and analyzed to determine whether they were representative of the whole ORFeome of the two HP strains. More than 1.4 million and 1 million reads were produced for HP 26695 and HP B128 phage libraries respectively, thus reaching a total genome sequencing depth higher than 76X and 77X for HP 26695 and HP B128. Considering the coverage of the known CDSs of both strains we found that more than 93% of the total CDSs for both HP 26695 and of HP B128 were represented in their respective ORF libraries. When looking at the percentage of nucleotide covered by the reads inside CDSs, this was respectively, 73.5 and 76.8% (**Table 1**) for HP 26695 and of HP B128. In total we identified 1372 CDS domains represented into the HP 26695 phage library and 1597 CDS domains in the HP B128 phage library. It should be noted that the number of domains detected can be higher than the number of total CDSs in the genome because more than one domain can be found inside a single CDS.

Comparison of the Two ORF-Filtered Libraries

After the initial characterization, we tried to understand if the libraries obtained from the two HP strains, had a high level of similarity, thus we performed a mapping comparison by aligning the reads obtained from the sequencing of the two genomic ORF-filtered libraries of HP 26695 and of HP B128 against the reference genomic sequence of HP 26695 (accession number NC_000915). After mapping 91.61% of the trimmed reads of HP 26695 library aligned with its own reference genome, at the same time we observed that 89.10% of trimmed reads of HP B128 library aligned with the genome sequence of HP 26695 (**Table 1**). After this analysis, we concluded that the genetic diversity that separates these two strains does not significantly affect the nature of ORFs/domains sequences filtered out. In the light of these results, we decided to use the HP 26695 as the reference genome and to use its CDSs annotation to functionally read out the results deriving after the selection step performed with sera from patients. At this point to understand if the common ORFs/domains, represented inside the two genomic phage libraries could have the same features, in terms of the portions of the CDS filtered out, we compared their amino acidic sequences by blasting all the HP 26695 protein domains against all the HP B128 protein domains using BLASTX (search protein databases using a translated nucleotide query). The blasting step was performed

by imposing the following parameters: amino acidic sequence identity >30% and length overlapping >50%. Among the 1268 common domains 98.82% have an amino acid sequence identity higher than 30%. Thus, the overlapping between the two genomic ORF filtering libraries was confirmed also from a functional point of view.

Selection of Phage ORFs Library With HP Patient's Sera

Based on the previous results we decided to pool the two ORFs library and use them as a single reagent in order to maximize the diversity of functional domains displayed on phage.

We focused on three different HP related diseases: GC, AIG, and MALT lymphoma. For each of these diseases we prepared a pool of sera, using affinity-purified Igs, to be used for the selection of the library: pool A, was made by six patients who developed GC (Selection A); Pool B, from four patients who developed AIG (Selection B) and Pool C from three patients who developed MALT lymphoma (Selection C). Finally, as control we also prepared a pool from healthy donors that were HP positive (Control Selection). The pooling of sera was applied as it was previously shown (D'Angelo et al., 2013) to be successful in reducing the inter-individual variability of antibody titer.

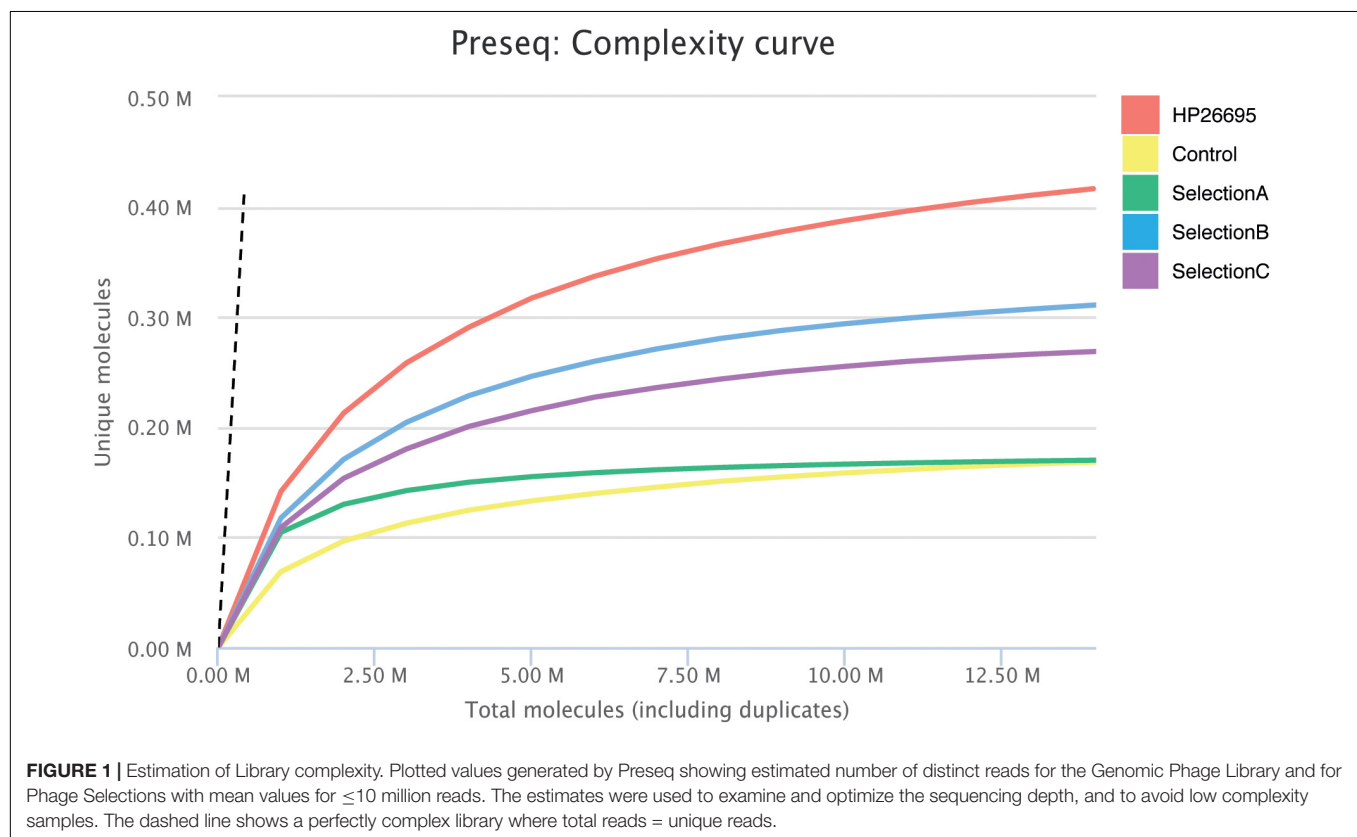
Each of the four pools of sera was independently used as a bait to select the pooled ORF phage display library. Before each round of selection, to reduce unspecific binding, a clearing selection step was introduced by incubating phages with magnetic beads pre-coated with a recombinant construct carrying the Fc portion of human IgG. Two consecutive cycles of selection and amplification were performed, increasing stringency of washing and binding conditions in the second cycle.

Selected Libraries Characterization by Deep Sequencing

After the second cycle of selection DNA coding for ORF fragments was amplified and sequenced. In total, more than nine million paired-end reads were produced by sequencing the four different selections. We generated 2,169,178 reads for the Control-Selection library (healthy controls), 815,891 reads for the Selection A (GC-sera), 3,737,010 reads for Selection B (AIG-sera) and 1,633,626 reads for Selection C (MALT-sera). After the alignment step it resulted that from 72 up to 81% of the reads were mapped against the reference genome (**Table 1**). When analyzing the CDSs present in the selected libraries we counted only the ones being represented by a minimum of ten reads, the total number of HP CDSs represented in the four selection libraries was 1225, 1130, 1331, 1263, respectively (**Table 1**). Interestingly the number of CDS detected after the selection was comparable with that presented in the starting library nevertheless the portion of CDSs covered by the selected sequences decreased to 48.44% (Control Selection), 61.86% (Selection A), 52.01% (Selection B) and 44.97% (Selection C) (**Table 1**). The reduction of the ORF library coverage after selection with sera is clearly represented by the Preseq plot in **Figure 1** that shows a progressive reduction of the complexity curve from the genomic phage library that shows the maximum

TABLE 1 | Sequencing and mapping metrics.

	HP 26695	HP B128	Control	SelA	SelB	SelC
Raw reads	1,425,554	1,031,956	2,169,178	815,891	3,737,010	1,633,626
Reads after trimming	1,216,124	954,895	1,798,722	680,764	3,149,939	1,278,335
Mapping Reads	1,114,184	746,325	1,294,576	503,401	2,563,391	961,686
% of Mapping reads	91.61%	89.10%	71.97%	73.94%	81.37%	75.22%
Unmapping reads	11,158	158,301	166,831	113,397	257,481	128,346
Mean coverage	76.81X	76.81X	96.13X	31.19X	155.82X	56.97X
CDS covered	1372	1597	1225	1130	1331	1263
% CDS covered	93.46%	93.80%	83.44%	76.97%	90.66%	86.03%
Nucleotides covered inside CDS	1,068,020	1,164,096	703,739	898,694	755,447	653,331
% of Nucleotide covered inside CDS	73.51%	76.80%	48.44%	61.86%	52.01%	44.97%

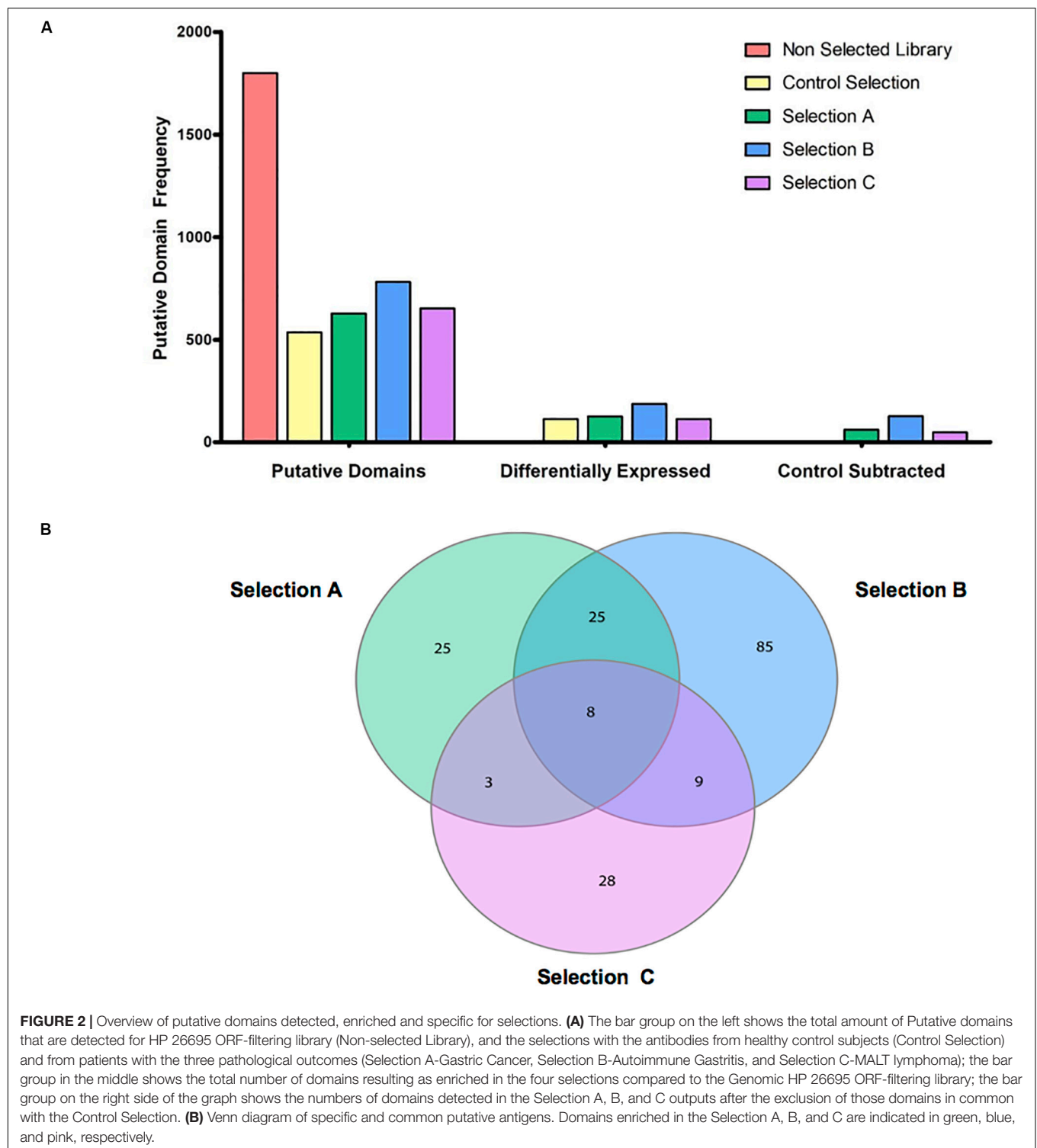


variability up to the Healthy Control phage library that has the lowest complexity. This result suggests that enrichment of specific portions of CDSs/Domains likely occurred after selection with the patient's sera.

Ranking of Enriched Domains/Epitopes

The identified domains in the four libraries were ranked according to three consecutive steps of analysis. Initially, we counted the putative epitopes that were enriched and identified in the Control Selection (Healthy Control-sera) and in the Selection A (GC-sera), Selection B (AIG-sera), and Selection C (MALT-sera) these being 535, 627, 780, and 652, respectively (**Figure 2A**) (the list of all the annotated domains is reported in **Supplementary Table 1** and the complete nucleotide and amino

acids sequences is reported in the **Supplementary File**). Among the top proteins the more recurrent in all the three selections with sera from patients (Sel A, Sel B, Sel C) and in the selection with the sera from healthy controls, worth of note are: HP0527 cag pathogenicity island protein Cag7 (CagY), HP0459 protein VirB4 and HP1341 siderophore-mediated iron transport protein TonB. Among these top represented and positively recognized proteins the only one that is specifically listed only in the patients' sera selections (Sel A, Sel B, Sel C) is HP0527 cag pathogenicity island protein Cag7 (CagY), as a matter of fact, both HP0459 protein VirB4 and HP1341 siderophore-mediated iron transport protein TonB are recognized and listed also among the top recurrent dominant proteins in the selection with the sera from HP positive Healthy Controls.



As a second step, we looked at the domains/epitopes resulting as differentially enriched (Q -value (<0.05 and Focus (>0.8) in the selected phage libraries respect to the ORF-filtering genomic phage library; these were 115, 125, 183, and 117, respectively for the Healthy Control, Selection A, Selection B, and Selection C. As a third step among these domains we filtered out a sub-list of

domains/epitopes specifically enriched only in the pathological outcomes and absent in the Healthy Control Selection. This step was aimed to reduce poly-reactive domains and consists of a subtractive comparison between the domains lists of the three pathological selections and the list of the Healthy Control Selection (**Figure 2A**).

Finally, we analyzed the overlap within the lists of domains/epitopes specifically enriched only in the Selection A, Selection B, and Selection C; as shown in **Figure 2B** in the Venn diagram most of the enriched domains, found after selections against sera (in total 138), are specific for the three pathological outcomes: Selection A ($n = 25$), Selection B ($n = 85$), and Selection C ($n = 28$), while only 45 enriched domains are common to two or to all the selections. In **Supplementary Table 2** the complete list of the domains/epitopes specifically enriched in the selections is reported.

Identification, Expression and Purification of a CagY/Cag7 Domain as Putative Antigenic Clone

As previously elucidated, it is very important to find novel biomarkers that can provide a “disease signature” for different pathological outcomes, or biomarkers associated to HP infection progression. Among the sub-lists of domains/epitopes specific for GC, AIG, MALT lymphoma, and absent in the HP + healthy controls we selected the top list ones, having the highest Fold Change values (see **Supplementary Table 2**) as putative candidate targets for production as recombinant protein and validation with ELISA assay. One of the most interesting domain enriched after sera selections was belonging to the gene HP0527, also named CagY/Cag7. The genomic library contains a large number of fragments mapping at the C terminal that were not specifically enriched after selection with sera. Interestingly after selection with sera of MALT lymphoma patients a domain mapping in their middle repeat region (MRR) was specifically enriched, mapping of the reads on the reference gene is shown in **Figure 3A**. HP0527 encodes for a large protein of 1927 amino acids described as one of the main components of *H. pylori* cag T4SS-associated pilum and proposed to be able to act as a sort of molecular switch that modifies the host pro-inflammatory responses by modulating the T4SS function and tuning CagA injection (Barrozo et al., 2013, 2016). To validate the antigenicity of this specific CagY domain, we recovered from the selected library the corresponding ORFs, thanks to two back-to-back oligonucleotides mapping to the center of the enriched domain. Several fragments of CagY protein were initially recovered from the library and finally the ORF portion corresponding to aa 566–655 of the CagY protein was chosen for subsequent validation. The selected ORF fragment was cloned in a vector allowing the production of a GST-ORF-FLAG recombinant protein. After purification by affinity chromatography the protein was checked by SDS-PAGE followed by Coomassie staining and showed more than 95% of purity (**Figure 3B**), Western blotting with both α -GST and α -FLAG antibodies (**Figure 3C**) confirmed the presence of full-length protein with very little degradation.

Validation of CagY/Cag7 Protein Immunoreactivity by ELISA

The recombinant purified protein was used as a capture antigen in an indirect ELISA. After preliminary set-up experiments at different antigen coating concentrations and sera dilutions, we established appropriate assay conditions. Finally, we performed

a large-scale assay using all the recruited sera; the antigen was tested against a set of 96 serum samples obtained from different patients. Sera were collected from patients with GC ($n = 29$ sera), AIG ($n = 10$ sera), and MALT lymphoma ($n = 6$ sera). Fifty-one sera from healthy subjects both HP positive and negative were collected and used as controls. It should be noted that the number of patients affected by AIG and MALT lymphoma, that was possible to recruit, is much less than the number of patients affected by GC because these two pathologies are rare diseases. ELISA reactivity toward the purified CagY antigen was different among the tested groups (**Supplementary Table 3**). Cut off values for positivity was calculated using sera from healthy subjects that were showing globally a very low signal toward the antigen (mean OD = 0.142) and this reactivity was independent of the seropositivity for *H. pylori* infection (**Supplementary Table 3**). On the contrary, the specificity of the test was higher than 96% indicating that the protein domain tested is specific for infection progression toward pathological outcomes and not simply related to HP infection. Patients' sera showed anti-CagY positive reaction, sensitivity was 31% of GC patients (9 over 29 sera), 30% of AIG patients (3 over 10 sera) and 83.3% for MALT Lymphoma patients (5 over 6 sera) (**Figure 4**). Comparison between sample groups showed a statistically significant difference in immunoreactivity of MALT lymphoma patients' sera compared with control donors ($p < 0.001$, Mann–Whitney U test).

DISCUSSION

The mechanisms of GC induced by *H. pylori* are not fully understood. It is accepted that during the infection a complex and dynamic interaction between the bacterium and the host is established, in which the development of the disease is a result of both infecting *H. pylori* strain virulence and host immune set up. Accordingly, the identification and characterization of *H. pylori* proteins or protein domains able to evoke an immune response could be of great help to enhance understanding of how bacterium and host interact one with each other. The pathogen-specific humoral immune response is an important and informative host element that can potentially help to perform early and/or differential diagnosis allowing discrimination among disease severity.

In the last years many attempts to identify novel biomarkers for GC early diagnosis have been made and several studies have been published reporting the evaluation of antibody titer against different *H. pylori* antigens in different outcomes of infection. In the majority of cases these antigens have been chosen based on previous evidence of their pathological role in *H. pylori* infection. Only a few studies reported an approach based on the use of the entire protein repertoire of the bacterium. In the most convincing study authors used immunoproteomic approaches and some *H. pylori* antigens were identified (Haas et al., 2002; Mini et al., 2006). Although this approach is unbiased it presents some drawbacks linked to the relatively high abundance of the antigen required by the assay and by the use of antigens in non-native conformations. Meinke et al. (2009) reported the use of

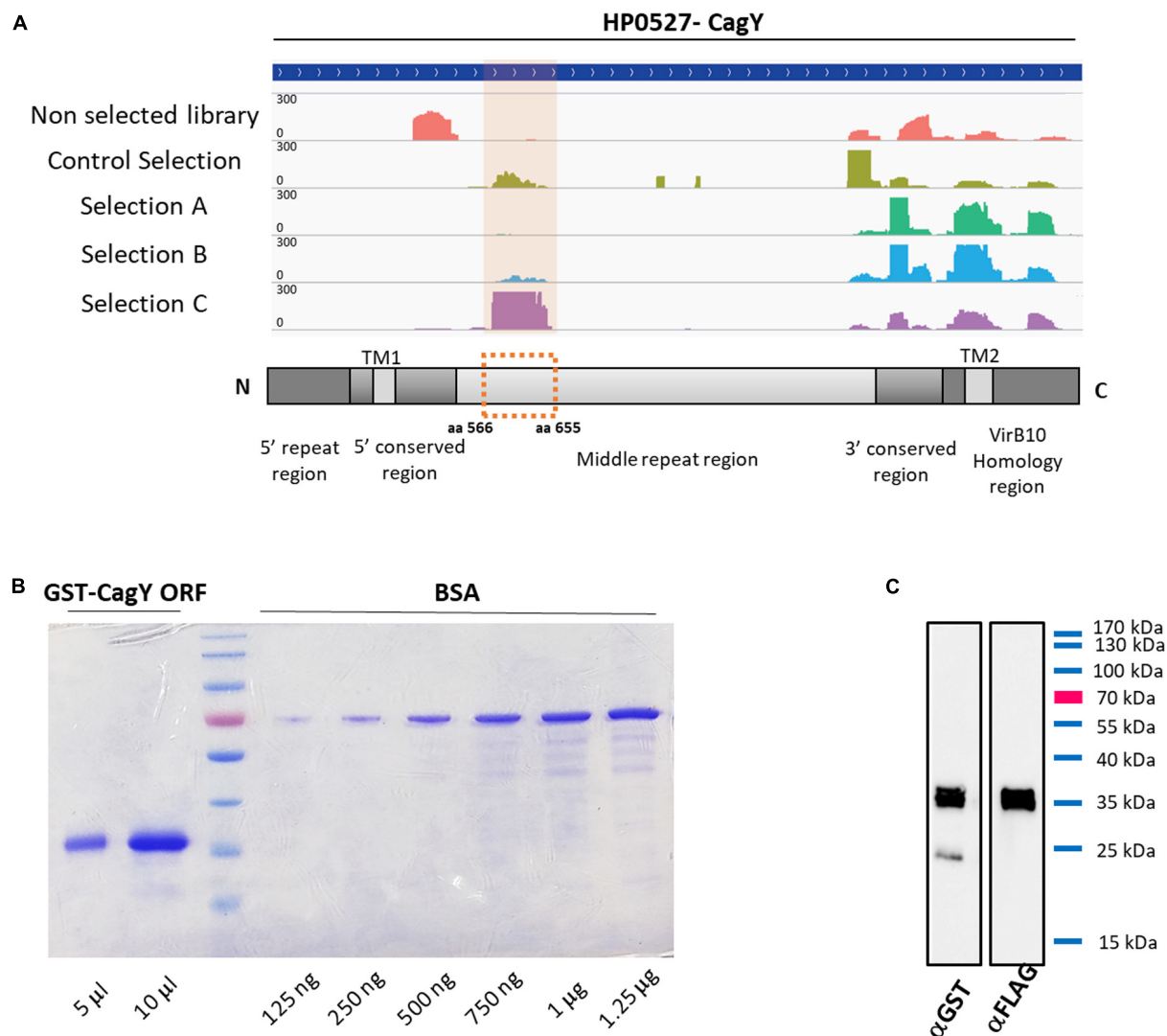


FIGURE 3 | Characterization of selected CagY ORF. **(A)** Mapping of the reads for CagY on the reference gene sequence HP0527, before and after selection with patients' sera and schematic representation of the CagY gene structure showing the alignment of the validated ORF on the CagY MRR domain. **(B)** Representative Coomassie gel staining of recombinant GST-CagY ORF-FLAG protein after purification on glutathione-coupled agarose resin, showing the absence of contaminants or degradation. BSA was used as a standard for protein quantification and a curve from 125 ng to 1.25 μ g was run. **(C)** Representative western blotting of the purified GST-CagY ORF-FLAG protein with α -GST and α -FLAG antibodies, showing the integrity of the protein preparation.

a more comprehensive approach based on the bacterial display expression of *H. pylori* protein repertoire, and tried to define the antigenome profile of two *H. pylori* strains, recognized by patients with GC and duodenal ulcer. Although unbiased this approach has an important limit in the number of selected clones that can be analyzed by Sanger sequencing. Over the last years we have developed a high-throughput platform for the identification of novel biomarkers that takes advantage of next generation sequencing technology, which enormously increases the potentiality of the analysis. Our approach is based on the use of an innovative phage display system that using the β -lactamase gene as an ORF and folding reporter allows to improve the functionality and the representativity of the proteins library fragments displayed on the surface of the phage.

The platform has been validated in different contexts showing to be functional and useful for the identification of novel antigens in different pathological conditions and for the study of bacterial genomic DNA for advanced annotation (D'Angelo et al., 2011, 2013; Gourlay et al., 2015; Antony et al., 2019). Furthermore, in the context of bacterial-host interaction, further to be representative of the whole bacterial genomic DNA, our method allows also a representation of the complete ORFeome of a bacterium at the protein level, thus being a useful tool for the identification of novel biomarkers of the infection and/or of specific clinical outcomes. DNA typing has demonstrated that *H. pylori* strains are extremely different due to a high rate of mutation or recombination of their genome. This variability reflects strain virulence and may be paralleled by differences

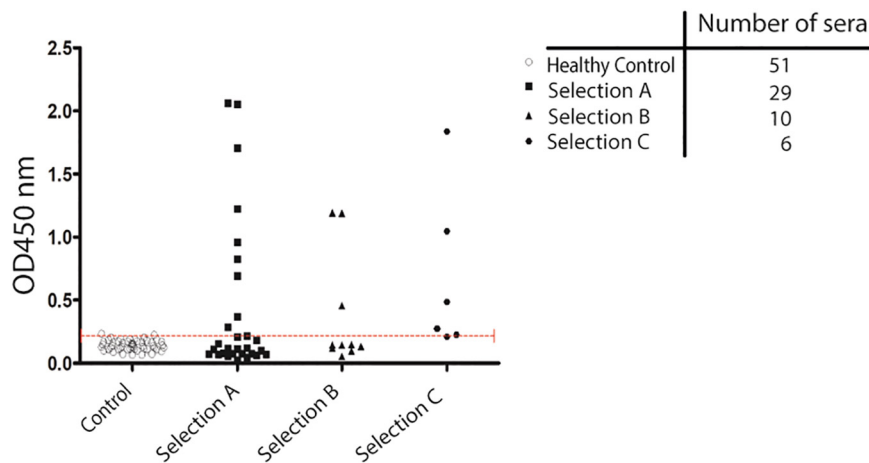


FIGURE 4 | Validation of antigenicity of protein CagY by ELISA. Scatter plot showing the distribution of ELISA signal on CagY protein fragment. Antigen was challenged with a 1:500 dilution of sera from different groups of patients: HP positive and negative Healthy patients (51), from patients with Gastric Cancer (29 sera), Autoimmune Gastritis (10 sera), and MALT lymphoma (6 sera). Dotted line indicates cut-off level. Mann-Whitney U test was used to calculate differences between groups and a p -value < 0.05 was considered significant.

in protein expression or function (Owen, 1995). In order to obtain an antigenic repertoire of the bacterium as wider as possible, we used two *H. pylori* strains that were clinically isolated and whose genome sequences are completely available and fully annotated. Sequencing analysis of the phage libraries obtained showed that they were representative of the entire ORFeome of the bacterium, covering about 90% of the genome, thus the two phage libraries obtained were considered representative of the whole antigenic repertoire of *H. pylori*. Moreover, comparison of the two libraries both at the DNA and protein level showed that the nature of ORFs/domains present into both of them was extremely similar (Table 1) confirming the possibility of using them as a single reagent with no risk of introducing bias. After selection with patients' sera antibodies the diversity of the libraries was significantly reduced, thus indicating that non-antigenic ORFs were lost during panning procedure and only potentially antigenic domains were selected. No bias toward one of the two HP strains was observed in the reads present in the selected libraries, indicating that the ORF repertoire of the two strains was equally represented on the phage particles.

Among the most enriched antigens recovered after selection we focused our attention on a domain of HP0527/CagY gene. This is an important component of the T4SS of the bacterium, and different reports have demonstrated that its presence is essential for *H. pylori* to induce cellular motility, adherence to target cell via $\alpha 5 \beta 1$ integrin binding, as well as CagA translocation and IL-8 induction (Rohde et al., 2003; Al-Ghoul et al., 2004; Koelblen et al., 2017). CagY is a surface-exposed protein of approximately 220 kDa protruding from the inner to the outer bacterial membrane (Kutter et al., 2008; Backert et al., 2015, 2016). The protein contains an unusual sequence structure with a high degree of variability given by the presence of two regions characterized by tandem repeats: a small 5' repeat region (FRR) and a large MRR (Aras et al., 2003). Interestingly after selection, several clones, not perfectly identically mapping on the

same region were recovered. The portion of the CagY selected corresponded to the N terminal part of the MRR region of the protein. These results indicate that the selection was done by virtue of a real antigenicity of the identified domain. The finding of antibodies against the MRR region of CagY is of particular interest since it has been demonstrated that this region controls the conformation of the full-length protein and, by modifying its integrin binding ability, is able to modulate T4SS function (Skoog et al., 2018); this mechanism is involved in the persistence of *H. pylori* infection. In-frame recombination events within the MRR repeats yield different CagY variants present in different bacterial strains. Moreover, recombination can also occur during infection, both *in vitro* and *in vivo* conferring to the bacteria both gain and loss of function. This finding led to the suggestion that this phenomenon is functional to immune evasion of the bacterium (Aras et al., 2003). However, the observation that CagY recombination occurs *in vivo* leading to the production of proteins with different size, both functional and non-functional, suggests that the bacterium could take advantage of inflammation at least in some situations. Recently Barrozo et al. (2013, 2016) demonstrated that CagY antigenic variation is not linked to the function of escaping the host immune response but rather to modulate it. Using both mouse and non-primate models they confirmed that CagY recombination is dependent to the host immune system pressure and showed that during infection it can both abrogate or restore the T4SS function. The authors propose that CagY works as a molecular switchable to "tune" the host immune response establishing the optimal inflammatory conditions to maximize the bacterium fitness. These findings highlight the hypothesis that CagY protein might be visible by the immune system at least in some phases of the infection and an immune response to it might be present in the host. Coherently the antigenicity of CagY has been demonstrated in rat and in mice where a *Lactococcus lactis* expressing the carboxy-terminal 383 amino acids has shown to induce immunity against CagY both

at the mucosal and systemic levels (Kim et al., 2009). However so far a serum immune response to CagY has not been found in humans. Here, thanks to the use of an innovative approach we demonstrated that antibodies against CagY are present in the sera of individuals infected by *H. pylori* who have developed GC, AIG, and MALT lymphoma, thus relating immune response to CagY to HP infection progression toward pathological outcomes and in particular toward MALT lymphoma, as shown in **Figure 4**. Further investigations are needed, and larger sample size should be assayed in a more perspective way, to evaluate the feasibility of screening CagY antibodies as a potential biomarker in the diagnosis of *H. pylori* associated malignancies development.

To further investigate if the proteins' domains significantly enriched with a log2 fold change higher than 1.5 and listed in **Supplementary Table 2** have been already outlined as reactive antigens in previous literature we have overlapped these lists with the HP antigens list published by Meinke et al. (2009). The authors in this work have described the ANTIGENome of two clinical isolates of *H. pylori* derived from patients with GC and duodenal ulcer. By using 72 sera from patients with gastric adenocarcinoma and 324 HP positive controls, they identified 124 annotated HP genes and 54 non-annotated peptides as antigens. The 19 proteins that overlap between our list and the list published by Meinke et al. (2009) have been evidenced in yellow in **Supplementary Table 2**, worth of note is again CagY (Cag7) that in the list published by Meinke is the protein having the highest number of hits, even higher than the number of hits associated to CagA and VacA.

Among the proteins listed in **Supplementary Table 2** we have focused our attention also on some other relevant hits that, in the light of previous literature, we have further discussed (these proteins are evidenced in bold in **Supplementary Table 2**). Among the proteins listed as uniquely recognized by sera from patients with GC (Selection A) and AIG (Selection B) we found the flagellar hook-associated protein FlgL (HP0295) and the flagellar basal body protein FliL (HP0809). It is known that *H. pylori* flagella may influence the colonization, inflammation, and immune evasion (Gu, 2017), in particular the hook junction protein FlgK and FlgL prevent the protein proteolysis when the flagellum is not assembled, while the gene coding for FliL is needed for swimming in pathogenic species of *H. pylori*. Finding antibodies selectively recognizing these proteins in the sera from infected patients can be considered relevant and promising for future validations. Another structural protein of the *H. pylori* flagellum that we find specifically enriched using sera of patients with AIG (Selection B) is the flagellar sheath adhesin HpaA (HP0797). This antigen is of particular interest since it has been demonstrated that is among the flagellar components expressed by *H. pylori* strains isolated from patients with stomach disease (Gu, 2017) and that it is a target of humoral immunity (Tang et al., 2008). In particular Tang and collaborators tested the positive rate of IgG antibodies against HpaA in the sera from 151 *H. pylori*-infected patients with chronic gastritis, peptic ulcer or gastric adenocarcinoma and found a target antigen positive/negative rate of 100% and a target antibody positive/negative rate of 87.4%. Thus, our finding of specific recognition of an HpaA protein domain by sera of patients with AIG can be considered relevant

and promising for future validation of this antigen as a putative new biomarker also for this pathological outcome. We then found both in the list of proteins recognized by sera from patients with AIG (Selection B) and with MALT lymphoma (Selection C) some relevant outer membrane proteins (Voss et al., 2014) the iron-regulated outer membrane protein FrpB (HP0916–HP1512) and the iron(III) dicitrate transport protein FecA (HP1400). *H. pylori* needs iron in order to survive and in the human host there are several iron sources such as Transferrin (Tf), Lactoferrin (Lf), Hemoglobin (Hb), or haem. To obtain iron this pathogen has developed a mechanism consisting on expressing outer membrane proteins that bind Hb or haem (Braun and Hantke, 2011). Those proteins bind the iron source directly and several proteins have been investigated, for instance, FrpB is a protein family composed of three proteins: FrpB1, FrpB2, and FrpB3 (Dhaenens et al., 1997; Alm et al., 2000). *H. pylori* in particular is a human pathogen that requires a high concentration of iron because it has been reported that it can cause anemia when it is infecting humans (Beckett et al., 2016; Flores et al., 2017). This can explain why *H. pylori* has several genes, which express many proteins involved in iron acquisition such as FrpB1, FrpB2 or FrpB3, and FecA.

Both AIG and MALT lymphoma are known to be associated with anemia (Kulnigg-Dabsch, 2016; Pabona et al., 2016). AIG is also called pernicious anemia because one of the earliest symptoms of the disease is iron-deficiency anemia (IDA) which develops as a consequence of achlorhydria from oxyntic atrophy. During AIG the chronic inflammatory process causes, in the corpus and fundus of the stomach, a massive destruction of parietal cells, and this in turn determines a reduction of secretion of gastric acid required for the absorption of inorganic iron (Kulnigg-Dabsch, 2016) thus causing iron deficiency. *H. pylori* expresses FrpB1, FrpB2, and FrpB3 proteins to scavenge iron and they are regulated according to availability of iron source, in patients with AIG the iron is available in the stomach but it is not absorbed by the host, so it can be scavenged by *H. pylori*. Thus in the light of this work we think that our finding related to an antibody response against FrpB proteins in patients with AIG can be considered an important starting point for future validation of this protein also with sera from patients with AIG. At the same time we found enriched FrpB protein also in selection made with sera from patients with MALT lymphoma that is known to be associated with anemia as well. The mechanism in MALT lymphoma can be the same described for AIG, linking FrpB proteins expression to iron availability in the stomach of these patients.

A relevant increase was also found for the virulence-associated protein VapD (HP0967) by sera of patients with AIG (selection B). In a recent paper by Morales-Espinosa et al. (2020) high level of expression of virulence-associated protein D (VapD) of *H. pylori* were outlined inside adenocarcinoma gastric (AGS) cells and in gastric biopsies from patients suffering from different HP-related diseases. They observed that VapD is only expressed in the bacterium as a consequence of its interaction with the host cells, suggesting that it might contribute to *H. pylori* persistence inside the gastric epithelial cells, being involved in the protection of the bacterium from the intracellular environment and in its

growth rate reduction, as well as enabling long-term infection and treatment resistance. However in their work Morales-Espinosa et al. (2020) Did not test the reactivity of patients sera against VapD protein, they analyzed VapD expression in AGS cells in *in vitro* time course experiments and they tested the expression level of VapD by RT qPCR in 82 gastric biopsies from patients outlying high expression levels of this gene/protein *in vivo* in particular in association with follicular gastritis. Thus, in the light of this work we think that our finding related to an antibody response against VapD in patients can be considered promising for future validations. Finally we found both in the list of proteins recognized by sera from patients with AIG (Selection B) and with MALT lymphoma (Selection C) the two homologs of the virulence factor CagE (Cag23), also annotated as protein VirB4 (HP0459–HP0544) (Shariq et al., 2015). This virulence factor has been previously found associated with HP-induced duodenal ulceration in children and enhanced production of IL8 that can impact the pathological outcome (Day et al., 2000), thus we think our finding of a specific antibody response against CagE in AIG and MALT can be considered again relevant an worth of future validations.

DATA AVAILABILITY STATEMENT

The datasets generated for this study can be found in the Sequence Read Archive Bioproject, Accession Number PRJNA506709.

ETHICS STATEMENT

The studies involving human participants were reviewed and approved by the Careggi Hospital in Florence in collaboration with the Department of Experimental and Clinical Medicine of

the University of Florence; Ethical committee protocol number 14936_bio. The patients/participants provided their written informed consent to participate in this study.

AUTHOR CONTRIBUTIONS

MS and GC performed the experiments and wrote the manuscript. SP performed the data analysis and wrote the manuscript. PE, MD'E, and CS participated to the experimental design and revised the manuscript. FC and AT collected samples and data from patients and contributed to the revision of the manuscript. DS and CP designed the experiments, wrote the manuscript, and supervised the research. All authors contributed to the article and approved the submitted version.

FUNDING

This work was supported by Grants from the Italian Ministry of University and Research (2010P3S8BR_002 to CP).

SUPPLEMENTARY MATERIAL

The Supplementary Material for this article can be found online at: <https://www.frontiersin.org/articles/10.3389/fmicb.2020.01551/full#supplementary-material>

TABLE S1 | List of all the domains/epitopes represented in the phage libraries obtained after selection against sera.

TABLE S2 | List of the Differentially enriched domains/epitopes after selections with sera.

TABLE S3 | List of the sera samples used for CagY domain validation and ELISA reactivity values toward the purified CagY antigen.

REFERENCES

- Aebischer, T., Bumann, D., Eppe, H. J., Metzger, W., Schneider, T., Cherepnev, G., et al. (2008). Correlation of T cell response and bacterial clearance in human volunteers challenged with *Helicobacter pylori* revealed by randomised controlled vaccination with Ty21a-based *Salmonella* vaccines. *Gut* 57, 1065–1072. doi: 10.1136/gut.2007.145839
- Al-Ghoul, L., Wessler, S., Hundertmark, T., Krüger, S., Fischer, W., Wunder, C., et al. (2004). Analysis of the type IV secretion system-dependent cell motility of *Helicobacter pylori*-infected epithelial cells. *Biochem. Biophys. Res. Commun.* 322, 860–866. doi: 10.1016/j.bbrc.2004.07.199
- Alm, R. A., Bina, J., Andrews, B. M., Doig, P., Hancock, R. E. W., and Trust, T. J. (2000). Comparative genomics of *Helicobacter pylori*: analysis of the outer membrane protein families. *Infect. Immun.* 68, 4155–4168. doi: 10.1128/IAI.68.7.4155-4168.2000
- Alm, R. A., Ling, L. S. L., Moir, D. T., King, B. L., Brown, E. D., Doig, P. C., et al. (1999). Genomic-sequence comparison of two unrelated isolates of the human gastric pathogen *Helicobacter pylori*. *Nature* 397, 176–180. doi: 10.1038/16495
- Antony, F., Deantonio, C., Cotella, D., Soluri, M. F., Tarasiuk, O., Raspagliesi, F., et al. (2019). High-throughput assessment of the antibody profile in ovarian cancer ascitic fluids. *Oncoimmunology* 8:e1614856. doi: 10.1080/2162402X.2019.1614856
- Aras, R. A., Fischer, W., Perez-Perez, G. I., Crosatti, M. L., Ando, T., Haas, R., et al. (2003). Plasticity of Repetitive DNA sequences within a bacterial (Type IV) secretion system component. *J. Exp. Med.* 198, 1349–1360. doi: 10.1084/jem.20030381
- Backert, S., Neddermann, M., Maubach, G., and Naumann, M. (2016). Pathogenesis of *Helicobacter pylori* infection. *Helicobacter* 21, 19–25. doi: 10.1111/hel.12335
- Backert, S., Tegtmeyer, N., and Fischer, W. (2015). Composition, structure and function of the *Helicobacter pylori* cag pathogenicity island encoded type IV secretion system. *Future Microbiol.* 10, 955–965. doi: 10.2217/fmb.15.32
- Barrozo, R. M., Cooke, C. L., Hansen, L. M., Lam, A. M., Gaddy, J. A., Johnson, E. M., et al. (2013). Functional plasticity in the Type IV secretion system of *Helicobacter pylori*. *PLoS Pathog.* 9:e1003189. doi: 10.1371/journal.ppat.1003189
- Barrozo, R. M., Hansen, L. M., Lam, A. M., Skoog, E. C., Martin, M. E., Cai, L. P., et al. (2016). CagY Is an immune-sensitive regulator of the *Helicobacter pylori* Type IV secretion system. *Gastroenterology* 151, 1164–1175.e3. doi: 10.1053/j.gastro.2016.08.014
- Beckett, A. C., Piazzuelo, M. B., Noto, J. M., Peek, R. M., Washington, M. K., Algood, H. M. S., et al. (2016). Dietary composition influences incidence of *Helicobacter pylori*-induced iron deficiency anemia and gastric ulceration. *Infect. Immun.* 84, 3338–3349. doi: 10.1128/IAI.00479-16
- Björkholm, B., Zhukhovitsky, V., Löfman, C., Hultén, K., Enroth, H., Block, M., et al. (2000). *Helicobacter pylori* entry into human gastric epithelial cells: a potential determinant of virulence, persistence, and treatment failures. *Helicobacter* 5, 148–154. doi: 10.1046/j.1523-5378.2000.00023.x

- Blaser, M. J., Perez-Perez, G. I., Kleanthous, H., Cover, T. L., Peek, R. M., Chyou, P. H., et al. (1995). Infection with *Helicobacter pylori* strains possessing cagA is associated with an increased risk of developing adenocarcinoma of the stomach. *Cancer Res.* 55, 2111–2115.
- Boneca, I. G., de Reuse, H., Epinat, J. C., Pupin, M., Labigne, A., and Moszer, I. (2003). A revised annotation and comparative analysis of *Helicobacter pylori* genomes. *Nucleic Acids Res.* 31, 1704–1714. doi: 10.1093/nar/gkg250
- Braun, V., and Hantke, K. (2011). Recent insights into iron import by bacteria. *Curr. Opin. Chem. Biol.* 15, 328–334. doi: 10.1016/j.cbpa.2011.01.005
- Dal Ferro, M., Rizzo, S., Rizzo, E., Marano, F., Luisi, I., Tarasiuk, O., et al. (2019). Phage display technology for human monoclonal antibodies. *Methods Mol. Biol.* 1904, 319–338. doi: 10.1007/978-1-4939-8958-4_15
- D'Angelo, S., Mignone, F., Deantonio, C., Di Niro, R., Bordoni, R., Marzari, R., et al. (2013). Profiling celiac disease antibody repertoire. *Clin. Immunol.* 148, 99–109. doi: 10.1016/j.clim.2013.04.009
- D'Angelo, S., Velappan, N., Mignone, F., Santoro, C., Sblattero, D., Kiss, C., et al. (2011). Filtering “genic” open reading frames from genomic DNA samples for advanced annotation. *BMC Genomics* 12(Suppl. 1):S5. doi: 10.1186/1471-2164-12-S5
- Day, A. S., Jones, N. L., Lynett, J. T., Jennings, H. A., Fallone, C. A., Beech, R., et al. (2000). cagE is a virulence factor associated with *Helicobacter pylori* – induced duodenal ulceration in children. *J. Infect. Dis.* 181, 1370–1375. doi: 10.1086/315394
- D'elios, M. M., Bergman, M. P., Azzurri, A., Amedei, A., Benagiano, M., De Pont, J. J., et al. (2001). H⁺, K⁺-ATPase (proton pump) is the target autoantigen of Th1-type cytotoxic T cells in autoimmune gastritis. *Gastroenterology* 120, 377–386. doi: 10.1053/gast.2001.21187
- Dhaenens, L., Szczepara, F., and Husson, M. O. (1997). Identification, characterization, and immunogenicity of the lactoferrin-binding protein from *Helicobacter pylori*. *Infect. Immun.* 65, 514–518. doi: 10.1128/iai.65.2.514-518.1997
- Di Niro, R., D'Angelo, S., Secco, P., Marzari, R., Santoro, C., and Sblattero, D. (2009). Profiling the autoantibody repertoire by screening phage-displayed human cDNA libraries. *Methods Mol. Biol.* 570, 353–369. doi: 10.1007/978-1-60327-394-7_20
- Di Niro, R., Ferrara, F., Not, T., Bradbury, A. R. M., Chirido, F., Marzari, R., et al. (2005). Characterizing monoclonal antibody epitopes by filtered gene fragment phage display. *Biochem. J.* 388(Pt 3), 889–894. doi: 10.1042/BJ20041983
- Dixon, M. F., Genta, R. M., Yardley, J. H., and Correa, P. (1996). Classification and grading of gastritis. The updated Sydney system. International workshop on the histopathology of Gastritis, Houston 1994. *Am. J. Surg. Pathol.* 20, 1161–1181. doi: 10.1097/00000478-199610000-00001
- El-Omar, E. M., Carrington, M., Chow, W. H., McColl, K. E. L., Bream, J. H., Young, H. A., et al. (2000). Interleukin-1 polymorphisms associated with increased risk of gastric cancer. *Nature* 404, 398–402. doi: 10.1038/35006081
- Flores, S. E., Aitchison, A., Day, A. S., and Keenan, J. I. (2017). *Helicobacter pylori* infection perturbs iron homeostasis in gastric epithelial cells. *PLoS One* 12:e0184026. doi: 10.1371/journal.pone.0184026
- Goh, K. L., Chan, W. K., Shiota, S., and Yamaoka, Y. (2011). Epidemiology of *Helicobacter pylori* infection and public health implications. *Helicobacter* 16 Suppl. 1(??):1–9. doi: 10.1111/j.1523-5378.2011.00874.x
- Gourlay, L. J., Peano, C., Deantonio, C., Perletti, L., Pietrelli, A., Villa, R., et al. (2015). Selecting soluble/foldable protein domains through single-gene or genomic ORF filtering: structure of the head domain of *Burkholderia pseudomallei* antigen BPSL2063. *Acta Crystallogr. Sect. D Biol. Crystallogr.* 71(Pt 11), 2227–2235. doi: 10.1107/S1399004715015680
- Gu, H. (2017). Role of flagella in the pathogenesis of *Helicobacter pylori*. *Curr. Microbiol.* 74, 863–869. doi: 10.1007/s00284-017-1256-4
- Haas, G., Karaali, G., Ebermayer, K., Metzger, W. G., Lamer, S., Zimny-Arndt, U., et al. (2002). Immunoproteomics of *Helicobacter pylori* infection and relation to gastric disease. *Proteomics* 2, 313–324. doi: 10.1002/1615-9861(200203)2:3<313::AID-ROT313<3.0.CO;2-7
- Hooi, J. K. Y., Lai, W. Y., Ng, W. K., Suen, M. M. Y., Underwood, F. E., Tanyingoh, D., et al. (2017). Global prevalence of *Helicobacter pylori* Infection: systematic review and meta-analysis. *Gastroenterology* 153, 420–429. doi: 10.1053/j.gastro.2017.04.022
- Hu, Y., Zhu, Y., and Lu, N. H. (2017). Novel and effective therapeutic regimens for *Helicobacter pylori* in an era of increasing antibiotic resistance. *Front. Cell. Infect. Microbiol.* 7:168. doi: 10.3389/fcimb.2017.00168
- Ikuse, T., Blanchard, T. G., and Czinn, S. J. (2019). Inflammation, immunity, and vaccine development for the gastric pathogen *Helicobacter pylori*. *Curr. Top. Microbiol. Immunol.* 421, 1–19. doi: 10.1007/978-3-030-15138-6_1
- Israel, D. A., Salama, N., Arnold, C. N., Moss, S. F., Ando, T., Wirth, H. P., et al. (2001). *Helicobacter pylori* strain-specific differences in genetic content, identified by microarray influence host inflammatory responses. *J. Clin. Invest.* 107, 611–620. doi: 10.1172/JCI11450
- Kim, S. J., Lee, J. Y., Jun, D. Y., Song, J. Y., Lee, W. K., Cho, M. J., et al. (2009). Oral administration of *Lactococcus lactis* expressing *Helicobacter pylori* Cag7-ct383 protein induces systemic anti-Cag7 immune response in mice. *FEMS Immunol. Med. Microbiol.* 57, 257–268. doi: 10.1111/j.1574-695X.2009.00605.x
- Koelblen, T., Bergé, C., Cherrier, M. V., Brillet, K., Jimenez-Soto, L., Ballut, L., et al. (2017). Molecular dissection of protein–protein interactions between integrin $\alpha 5 \beta 1$ and the *Helicobacter pylori* Cag type IV secretion system. *FEBS J.* 284, 4143–4157. doi: 10.1111/febs.14299
- Kuipers, E. J., Pérez-pérez, G. I., Meuwissen, S. G. M., and Blaser, M. J. (1995). *Helicobacter pylori* and atrophic gastritis: importance of the cagA status. *J. Natl. Cancer Inst.* 87, 1777–1780. doi: 10.1093/jnci/87.23.1777
- Kulnigg-Dabsch, S. (2016). Autoimmune gastritis. *Wien. Med. Wochenschr.* 166, 424–430. doi: 10.1007/s10354-016-0515-5
- Kutter, S., Buhrdorf, R., Haas, J., Schneider-Brachert, W., Haas, R., and Fischer, W. (2008). Protein subassemblies of the *Helicobacter pylori* cag type IV secretion system revealed by localization and interaction studies. *J. Bacteriol.* 190, 2161–2171. doi: 10.1128/JB.01341-07
- Kuznetsov, V. A., Pickalov, V. V., and Kanapin, A. A. (2006). “Proteome complexity measures based on counting of domain-to-protein links for replicative and non-replicative domains,” in *Bioinformatics of Genome Regulation and Structure II*, eds N. Kolchanov, R. Hofstaedt, and L. Milanesi (Boston, MA: Springer). doi: 10.1007/0-387-29455-4_32
- Lam, K. W. K., and Lo, S. C. L. (2008). Discovery of diagnostic serum biomarkers of gastric cancer using proteomics. *Proteomics Clin. Appl.* 2, 219–228. doi: 10.1002/prca.200780015
- Li, H., Handsaker, B., Wysoker, A., Fennell, T., Ruan, J., Homer, N., et al. (2009). The sequence alignment/Map format and SAMtools. *Bioinformatics* 25, 2078–2079. doi: 10.1093/bioinformatics/btp352
- Madden, T. (2013). *The BLAST Sequence Analysis Tool*. Available online at: <http://www.ncbi.nlm.nih.gov/books/NBK153387/> (accessed April 18, 2016).
- Martin, M. (2011). Cutadapt removes adapter sequences from high-throughput sequencing reads. *EMBnet.J.* 17, 10–12. doi: 10.14806/ebj.17.1.200
- Massironi, S., Zilli, A., Elvevi, A., and Invernizzi, P. (2019). The changing face of chronic autoimmune atrophic gastritis: an updated comprehensive perspective. *Autoimmun. Rev.* 18, 215–222. doi: 10.1016/j.autrev.2018.08.011
- McClain, M. S., Shaffer, C. L., Israel, D. A., Peek, R. M., and Cover, T. L. (2009). Genome sequence analysis of *Helicobacter pylori* strains associated with gastric ulceration and gastric cancer. *BMC Genomics* 10:3. doi: 10.1186/1471-2164-10-3
- Megraud, F., Coenen, S., Versporten, A., Kist, M., Lopez-Brea, M., Hirschl, A. M., et al. (2013). *Helicobacter pylori* resistance to antibiotics in Europe and its relationship to antibiotic consumption. *Gut* 62, 34–42. doi: 10.1136/gutjnl-2012-302254
- Meinke, A., Storm, M., Henics, T., Gelbmarm, D., Prustomersky, S., Kovács, Z., et al. (2009). Composition of the ANTIGENome of *Helicobacter pylori* defined by human serum antibodies. *Vaccine* 27, 3251–3259. doi: 10.1016/j.vaccine.2009.01.066
- Mini, R., Bernardini, G., Salzano, A. M., Renzone, G., Scaloni, A., Figura, N., et al. (2006). Comparative proteomics and immunoproteomics of *Helicobacter pylori* related to different gastric pathologies. *J. Chromatogr. B* 833, 63–79. doi: 10.1016/j.jchromb.2005.12.052
- Morales-Espinosa, R., Delgado, G., Serrano, L. R., Castillo, E., Santiago, C. A., Hernández-Castro, R., et al. (2020). High expression of *Helicobacter pylori* VapD in both the intracellular environment and biopsies from gastric patients with severity. *PLoS One* 15:e0230220. doi: 10.1371/journal.pone.0230220

- Müller, A., and Solnick, J. V. (2011). Inflammation, immunity, and vaccine development for *Helicobacter pylori*. *Helicobacter* 16(Suppl. 1), 26–32. doi: 10.1111/j.1523-5378.2011.00877.x
- Noto, J. M., and Peek, R. M. (2012). The *helicobacter pylori* cag pathogenicity island. *Methods Mol. Biol.* 921, 41–50. doi: 10.1007/978-1-62703-5-2_7
- Owen, R. J. (1995). 1 Bacteriology of *Helicobacter pylori*. *Baillieres. Clin. Gastroenterol.* 9, 415–446. doi: 10.1016/0950-3528(95)90041-1
- Pabona, J. M., Bath, K., Siba, Y., Edwards, C., Goldstein, A., Ahluwalia, M., et al. (2016). Mucosa-associated lymphoid tissue (MALT) lymphoma presenting with both gastric and small bowel involvement: a case report. *Am. J. Gastroenterol.* 111:S1131. doi: 10.14309/00000434-201610001-02326
- Parsonnet, J. (1995). The incidence of *Helicobacter pylori* infection. *Aliment. Pharmacol. Ther.* 9(Suppl. 2), 45–51.
- Peleteiro, B., Bastos, A., Ferro, A., and Lunet, N. (2014). Prevalence of *Helicobacter pylori* infection worldwide: a systematic review of studies with national coverage. *Dig. Dis. Sci.* 59, 1698–1709. doi: 10.1007/s10620-014-3063-0
- Puccio, S., Grillo, G., Consiglio, A., Soluri, M. F., Sblattero, D., Cotella, D., et al. (2020). InteractomeSeq: a web server for the identification and profiling of domains and epitopes from phage display and next generation sequencing data. *Nucleic. Acids Res.* 48, W200–W207. doi: 10.1093/nar/gkaa363
- Quinlan, A. R., and Hall, I. M. (2010). BEDTools: a flexible suite of utilities for comparing genomic features. *Bioinformatics* 26, 841–842. doi: 10.1093/bioinformatics/btq033
- Resende, T., Correia, D. M., Rocha, M., and Rocha, I. (2013). Re-annotation of the genome sequence of *Helicobacter pylori* 26695. *J. Integr. Bioinform.* 10:233. doi: 10.1515/jib-2013-233
- Rohde, M., Püls, J., Buhrdorf, R., Fischer, W., and Haas, R. (2003). A novel sheathed surface organelle of the *Helicobacter pylori* cag type IV secretion system. *Mol. Microbiol.* 49, 219–234. doi: 10.1046/j.1365-2958.2003.03549.x
- Salama, N. R., Hartung, M. L., and Müller, A. (2013). Life in the human stomach: persistence strategies of the bacterial pathogen *Helicobacter pylori*. *Nat. Rev. Microbiol.* 11, 385–390. doi: 10.1038/nrmicro3016
- Sblattero, D., and Bradbury, A. (2000). Exploiting recombination in single bacteria to make large phage antibody libraries. *Nat. Biotechnol.* 18, 75–80. doi: 10.1038/71958
- Shahar, E., Folsom, A. R., Melnick, S. L., Tockman, M. S., Comstock, G. W., Gennaro, V., et al. (1994). The role of diagnostic roentgenology in medicine. *N. Engl. J. Med.* 262, 1201–1209. doi: 10.1056/nejm196006162622401
- Shariq, M., Kumar, N., Kumari, R., Kumar, A., Subbarao, N., and Mukhopadhyay, G. (2015). Biochemical analysis of CagE: A VirB4 homologue of *helicobacter pylori* cag-T4SS. *PLoS One* 10:e0142606. doi: 10.1371/journal.pone.0142606
- Skoog, E. C., Morikis, V. A., Martin, M. E., Foster, G. A., Cai, L. P., Hansen, L. M., et al. (2018). CagY-dependent regulation of type IV secretion in *helicobacter pylori* is associated with alterations in integrin binding. *mBio* 9:e00717-18. doi: 10.1128/mBio.00717-18
- Solnick, J. V. (1998). Antibiotic resistance in *Helicobacter pylori*. *Clin. Infect. Dis.* 27, 90–92. doi: 10.1086/514641
- Soluri, M. F., Puccio, S., Caredda, G., Grillo, G., Licciulli, V. F., Consiglio, A., et al. (2018). Interactome-seq: a protocol for domainome library construction, validation and selection by phage display and next generation sequencing. *J. Vis. Exp.* e56981. doi: 10.3791/56981
- Stolte, M., and Eidt, S. (1989). Lymphoid follicles in antral mucosa: immune response to *Campylobacter pylori*? *J. Clin. Pathol.* 42, 1269–1271. doi: 10.1136/jcp.42.12.1269
- Takahashi-Kanemitsu, A., Knight, C. T., and Hatakeyama, M. (2020). Molecular anatomy and pathogenic actions of *Helicobacter pylori* CagA that underpin gastric carcinogenesis. *Cell. Mol. Immunol.* 17, 50–63. doi: 10.1038/s41423-019-0339-5
- Tang, R. X., Luo, D. J., Sun, A. H., and Yan, J. (2008). Diversity of *Helicobacter pylori* isolates in expression of antigens and induction of antibodies. *World J. Gastroenterol.* 14, 4816–4822. doi: 10.3748/wjg.14.4816
- Thung, I., Aramin, H., Vavinskaya, V., Gupta, S., Park, J. Y., Crowe, S. E., et al. (2016). Review article: the global emergence of *Helicobacter pylori* antibiotic resistance. *Aliment. Pharmacol. Ther.* 43, 514–533. doi: 10.1111/apt.13497
- Tomb, J. F., White, O., Kerlavage, A. R., Clayton, R. A., Sutton, G. G., Fleischmann, R. D., et al. (1997). The complete genome sequence of the gastric pathogen *Helicobacter pylori*. *Nature* 388, 539–547. doi: 10.1038/41483
- Troilo, A., Grassi, A., Petrone, L., Cianchi, F., Benagiano, M., Bella, C., et al. (2019). Intrinsic factor recognition promotes T helper 17/T helper 1 autoimmune gastric inflammation in patients with pernicious anemia. *Oncotarget* 10, 2921–2929. doi: 10.18632/oncotarget.26874
- Voss, B. J., Gaddy, J. A., McDonald, W. H., and Cover, T. L. (2014). Analysis of surface-exposed outer membrane proteins in *Helicobacter pylori*. *J. Bacteriol.* 196, 2455–2471. doi: 10.1128/JB.01768-14
- Wyatt, J. I., and Rathbone, B. J. (1988). Immune response of the gastric mucosa to campylobacter pylori. *Scand. J. Gastroenterol.* 142, 44–49. doi: 10.3109/00365528809091712
- Yuzhalin, A. (2011). The role of interleukin DNA polymorphisms in gastric cancer. *Hum. Immunol.* 72, 1128–1136. doi: 10.1016/j.humimm.2011.08.003
- Zacchi, P., Sblattero, D., Florian, F., Marzari, R., and Bradbury, A. R. M. (2003). Selecting open reading frames from DNA. *Genome Res.* 13, 980–990. doi: 10.1101/gr.861503

Conflict of Interest: The authors declare that the research was conducted in the absence of any commercial or financial relationships that could be construed as a potential conflict of interest.

The reviewer AD declared a past co-authorship with the author CP to the handling editor.

Copyright © 2020 Soluri, Puccio, Caredda, Edomi, D'Elios, Cianchi, Troilo, Santoro, Sblattero and Peano. This is an open-access article distributed under the terms of the Creative Commons Attribution License (CC BY). The use, distribution or reproduction in other forums is permitted, provided the original author(s) and the copyright owner(s) are credited and that the original publication in this journal is cited, in accordance with accepted academic practice. No use, distribution or reproduction is permitted which does not comply with these terms.



Genomic and Long-Term Transcriptomic Imprints Related to the Daptomycin Mechanism of Action Occurring in Daptomycin- and Methicillin-Resistant *Staphylococcus aureus* Under Daptomycin Exposure

OPEN ACCESS

Edited by:

Flavia Marinelli,
University of Insubria, Italy

Reviewed by:

Pedro Matos Pereira,
New University of Lisbon, Portugal
Iñigo Lasa,
Universidad Pública de Navarra,
Spain

*Correspondence:

Viviana Cafiso
v.cafiso@unict.it

Specialty section:

This article was submitted to
Antimicrobials, Resistance
and Chemotherapy,
a section of the journal
Frontiers in Microbiology

Received: 09 December 2019

Accepted: 20 July 2020

Published: 14 August 2020

Citation:

Cafiso V, Stracquadanio S, Lo Verde F, De Guidi I, Zega A, Pigola G and Stefani S (2020) Genomic and Long-Term Transcriptomic Imprints Related to the Daptomycin Mechanism of Action Occurring in Daptomycin- and Methicillin-Resistant *Staphylococcus aureus* Under Daptomycin Exposure. *Front. Microbiol.* 11:1893. doi: 10.3389/fmicb.2020.01893

Viviana Cafiso^{1*}, Stefano Stracquadanio¹, Flavia Lo Verde¹, Irene De Guidi¹, Alessandra Zega¹, Giuseppe Pigola² and Stefania Stefani¹

¹ Department of Biomedical and Biotechnological Sciences, University of Catania, Catania, Italy, ² Department of Clinical and Experimental Medicine, University of Catania, Catania, Italy

Daptomycin (DAP) is one of the last-resort treatments for heterogeneous vancomycin-intermediate *Staphylococcus aureus* (hVISA) and vancomycin-intermediate *S. aureus* (VISA) infections. DAP resistance (DAP-R) is multifactorial and mainly related to cell-envelope modifications caused by single-nucleotide polymorphisms and/or modulation mechanisms of transcription emerging as result of a self-defense process in response to DAP exposure. Nevertheless, the role of these adaptations remains unclear. We aim to investigate the comparative genomics and late post-exponential growth-phase transcriptomics of two DAP-resistant/DAP-susceptible (DAP^{R/S}) methicillin-resistant *S. aureus* (MRSA) clinical strain pairs to focalize the genomic and long-term transcriptomic fingerprinting and adaptations related to the DAP mechanism of action acquired *in vivo* under DAP pressure using Illumina whole-genome sequencing (WGS), RNA-seq, bioinformatics, and real-time qPCR validation. Comparative genomics revealed that membrane protein and transcriptional regulator coding genes emerged as shared functional coding-gene clusters harboring mutational events related to the DAP-R onset in a strain-dependent manner. Pairwise transcriptomic enrichment analysis highlighted common and strain pair-dependent Kyoto Encyclopedia of Genes and Genomes (KEGG) pathways, whereas DAP^{R/S} double-pair cross-filtering returned 53 differentially expressed genes (DEGs). A multifactorial long-term transcriptomic-network characterized DAP^R MRSA includes alterations in (i) peptidoglycan biosynthesis, cell division, and cell-membrane (CM) organization genes, as well as a *cidB/lytS* autolysin genes; (ii) *ldh2* involved in fermentative metabolism; (iii) CM-potential perturbation genes; and (iv) oxidative and heat/cold stress response-related genes. Moreover, a D-alanyl-D-alanine decrease in cell-wall mucopeptide characterized DAP/glycopeptide

cross-reduced susceptibility mechanisms in DAP^R MRSA. Our data provide a snapshot of DAP^R MRSA genomic and long-term transcriptome signatures related to the DAP mechanism of action (MOA) evidencing that a complex network of genomic changes and transcriptomic adaptations is required to acquire DAP-R.

Keywords: daptomycin-resistant methicillin-resistant *Staphylococcus aureus*, genomics, SNPome, virulome, resistome, RNA-seq, transcriptomics

INTRODUCTION

Methicillin-resistant *Staphylococcus aureus* (MRSA) remains one of the major multidrug-resistant pathogens responsible for severe infections with high mortality rates (Stefani et al., 2015; Yoon et al., 2016; Britt et al., 2017). The subset of daptomycin-resistant (DAP^R) *S. aureus* is of particular concern for the cumulative non-reversible metabolic changes demonstrated in resistant strains and for the difficulty in the treatment of severe infections (Bayer et al., 2013; Reed et al., 2019).

The DAP mechanism of action (DAP-MOA) has not been fully elucidated yet. The model of DAP-MOA proposes that DAP binds the cytoplasmic membrane leading to its permeabilization and depolarization caused by a loss of cytoplasm potassium ions (Allen et al., 1987). This mechanism, which can account for DAP's bactericidal effect, would correlate with several changes in the membrane components, for example, with the level of phosphatidylglycerol. The complex mechanism of DAP resistance (DAP-R) was reviewed by Miller et al. (2016). Briefly, *S. aureus* can adopt different strategies to resist DAP. The first is to alter the net cell-surface charge, preventing the positively charged DAP-calcium binding to the cell envelope by electrostatic repulsion, mainly due to *dlt* over-expression—increasing the alanylation rate of the wall teichoic acids (Yang et al., 2009; Cafiso et al., 2014)—and to *mprF* mutations increasing the amount of the positively charged lysyl-phosphatidylglycerol on the outer membrane, conferring a “gain-of-function” and positively increasing the cell-envelope charge (Rubio et al., 2011; Bayer et al., 2015; Ernst et al., 2018; Sabat et al., 2018; Ernst and Peschel, 2019). The second is the alteration of membrane phospholipid composition, with decreased phosphatidylglycerol amount, or changes in membrane fluidity interfering with DAP binding and oligomerization (Jones et al., 2008; Kilelee et al., 2010; Mishra et al., 2011; Zhang et al., 2014). A third mechanism is the involvement of global regulatory genes modulating cell-envelope stress and maintenance, affecting the expression of the cell-wall (CW) “stimulon” (Utaida et al., 2003; Cafiso et al., 2012). Specifically, *VraSR* operon (Muthaiyan et al., 2008; Mehta et al., 2012; Sabat et al., 2018; Taglialegna et al., 2019), orthologous to the *Bacillus subtilis* *LiaSR* (Jordan et al., 2006), was involved and up-regulated by vancomycin and DAP exposure, and associated with CW biosynthesis via transcription of PBP2 (penicillin-binding protein 2), *tagA* (wall teichoic acids-synthesis), *prsA* (a-chaperone), and *murZ* (UDP-N-acetylglucosamine-enolpyruvyl transferase) (Kuroda et al., 2003; Mwangi et al., 2007). YycFG (also named WalKR), among the two-component regulatory systems (TCRSs), was

implicated in the control of the peptidoglycan biosynthesis through the regulation of LytM and AtlA (Dubrac and Msadek, 2004; Fukushima et al., 2011). A YycFG down-regulation was associated with a decreased peptidoglycan turnover, augmented cross-linking, increased glycan chain length, and resistance to lysis by Triton X-100 (Dubrac et al., 2007). YycG senses changes in membrane fluidity and responds by adjusting CW cross-linking, compensating the stresses caused by osmotic pressure (Türk and Bierbaum, 2012). In DAP^R strains, *yycFG* can accumulate mutations (Friedman et al., 2006; Howden et al., 2011), impairing the YycFG function and altering CW homeostasis to survive the DAP action, that is, lowering peptidoglycan turnover and increasing cross-linking. Mutations in the RNA polymerase *rpoB* and *rpoC* subunits were associated with DAP-R (Friedman et al., 2006). A621E mutation in RpoB was associated with an increased expression of the *dlt*-operon and correlated with an increase in positive cell-surface charge, whereas A621E and A477D substitutions were linked to an increased CW biosynthesis and thickness (Cui et al., 2010; Bæk et al., 2015).

Different cellular metabolic shifts, including a decreased activity of the tricarboxylic acid cycle (TCA), were described in DAP^R strains (Fischer et al., 2011; Gaupp et al., 2015).

This investigation aimed to face the analysis of DAP-R mechanisms in MRSA strains on the basis of the acquired knowledge and considering new aspects. First, the “already known” DAP-R mechanisms (*dlt* over-expression, *mprF* mutations, and increased net positive cell-surface charge) do not always correlate with changes in DAP minimum inhibitory concentrations (MICs) (Mishra et al., 2014); second, during an infection, the bacteria elapse long periods in limited/arrested growth as in the late growth phases (Kolter et al., 1993); third, DAP is also active on non-dividing and not metabolically active bacteria (Mascio et al., 2007; McCall et al., 2019).

On this rationale, our study investigated genomics and, for the first time, the comparative late growth-phase transcriptomics of clinical DAP^R versus DAP^S isogenic MRSA by using whole-genome sequencing (WGS), RNA-seq, and bioinformatics to reveal their genomic traits as well as the long-term fingerprinting and adaptations related to DAP-MOA occurring in the acquisition of DAP-R by DAP^S isolates.

These new findings could advance the knowledge in the field, revealing the genomic and long-term transcriptomic key features acquired *in vivo* by the DAP^R versus their parental isogenic DAP^S ancestor under DAP exposure and maintained after DAP removal, becoming stable traits characterizing DAP^R MRSA.

Our data showed that DAP-MOA-related strain-dependent non-synonymous single-nucleotide polymorphisms (nsSNPs)

in cell membrane (CM), structural/functional protein, and transcriptional regulator coding genes, combined with a complex transcriptional network, appeared as key factors characterizing DAP^R MRSA versus DAP^S parents.

MATERIALS AND METHODS

Bacterial Strains

Two *S. aureus* epidemiologically unrelated isogenic strain pairs of DAP^S (1A, 3A) and DAP^R MRSA (1C, 3B) isolated under DAP therapy, previously collected from patients hospitalized in two Italian hospitals, were investigated. The two isogenic strain pairs were provided by two different Italian hospitals (Cafiso et al., 2014); consequently, an ethical approval was not necessary as per institutional and national guidelines and regulations. Specifically, the 1A and 1C strains were isolated in Palermo by a skin infection, whereas the 3A and 3B strains were isolated by a soft tissue infection in a patient in Bergamo. Each pair included an initial pre-DAP therapy strain (1A and 3A) and its isogenic isolate after development of DAP-R during DAP administration. Each strain pair was previously assigned to the same pulsotype, multilocus sequence typing (MLST) type, SCCmec type, and *agr* group (Cafiso et al., 2014). The D-alanylated wall teichoic acid content, the lysinylated-phosphatidylglycerol amount, the CM fluidity, and the susceptibility to prototypic cationic host defense peptides of platelet and leukocyte origins were previously determined (Mishra et al., 2014). Finally, exponential or stationary growth-phase expression and SNPs in the “already DAP-R associated genes,” *mprF* and *dltA*, were previously reported (Table 1) (Cafiso et al., 2014; Mishra et al., 2014).

Whole-Genome Sequencing

Whole-genome sequencing was performed using the Illumina MiSeq sequencing system.

DNA Extraction and Illumina Shotgun Paired-End Library Preparation

Genomic DNA was extracted using PureLink Genomic DNA Mini Kit (Invitrogen) according to the manufacturer's protocol. The quality of the DNA was assessed using Qubit and its concentration ascertained by Picogreen (Life Technologies). Paired-end (PE) reads libraries were prepared by Nextera XT DNA Library Prep Kit (Illumina, San Diego, CA, United States) following the manufacturer's protocol, and their quality evaluation was performed as previously published (Cafiso et al., 2019). The indexed libraries were quantified as previously published (Cafiso et al., 2019) pooled at a final concentration of 2 nM and used for Illumina MiSeq sequencing with a PE 300 (2 × 300 bp). Raw reads were processed using FastQC (v.0.11.7) to assess data quality. Cutadapter tool (v.1.16), implemented in Python (v.3.5.2), was used to remove residual PCR primer and to filter low-quality bases ($Q_{\text{score}} < 30$) and short reads (<150 bp). The filtered trimmed reads were included in the downstream analysis. The total number of PE reads was reported with the estimated coverage in **Supplementary Figure S1**.

De novo Genome Assembly

De novo genome assembly was performed using SPAdes software (v.3.12.0), producing a contig file for each sample. Post-assembly controls and metrics were generated using Quast (v.4.6.3). **Supplementary Figure S2** shows *de novo* Genome Assembly Report.

Genome Alignments

Genome alignments were performed by Mauve (Multiple Genome Alignments) (v.2.4.0).

Gene Annotation

The assembled scaffolds were processed using Prokka (v.1.12) software.

DNA-Sequencing Data Accession Number

The genomic reads were deposited in the National Center for Biotechnology Information (NCBI) Genome database in the Sequence Read Archive (SRA) under study accession no. SRP166981 (BioProject: PRJNA498510).

Single-Nucleotide Polymorphisms

Single-nucleotide polymorphisms calls were carried out from the PE library raw reads as previously published (Cafiso et al., 2019). Briefly, Illumina raw reads were trimmed using Trimmomatic (v.0.38), requiring a minimum base quality of 20 (Phred scale) and a minimum read length of 36 nucleotides, and aligned by “Bwa mem” (v.0.7.17). For detection of SNPs, and insertions and deletions (indels), each bam file was sorted using Samtools (v.1.9), and duplicated reads were marked using the Picard Mark Duplicates utility. Complex variants, SNPs, and indels were detected using “Freebayes” (v.1.2.0), which required a minimum mapping quality of 30 (Phred scale) and a minimum base quality of 20. CSI phylogeny, a Center for Genomic Epidemiology service¹, was used to identify the closest relationships between the strain pairs and four different reference genomes (RefGen) deposited in GenBank, that is, *S. aureus* NCTC8325 (CP000253.1), *S. aureus* USA 300 (CP000255.1), *S. aureus* MU50 (BA000017.4), and *S. aureus* ST398 (NC_017333.1).

Staphylococcus aureus NCTC8325 (CP000253.1) was selected as common RefGen for SNP mapping in agreement to the data obtained. The graphical output was a Phylogenetic tree shown in **Supplementary Figure S3**.

The majority of the sequenced reads was properly aligned with the corresponding reference genome, in detail, 90.98% for 1A, 91.08% for 1C, 96.45% for 3A, and 95.81% for 3B.

To select SNPs present in the DAP^R strains, all SNPs were computationally filtered in both pairwise mode and double-cross filtering to find out if only nsSNPs present simultaneously in both two DAP^R strains and the DAP^S parents.

¹<http://genomicepidemiology.org/>

TABLE 1 | Phenotypic and molecular characterization of the MRSA strain pairs.

Strains	DAP pheno-type	MICs (mg/L)				Glyco-peptide hetero-resis-tance	Molecular characterization						DAP-R versus DAP-S expression		Virulome	Resistome	Resistance gene SNPs			
		OXA	DAP	VAN	TEC		PFGE	MLST	SCC <i>mec</i>	spa-type	agr-type	Plas-mids	<i>dltA</i>	<i>mprF</i>			Gene	Nucleotide change	AA change	Resistance
1A	DAP ^S	32	<0.25	1	<0.25	VSSA	A1/ <i>Apal</i>	398	IVa	t1939	I	pDLK1 (<i>ermC</i>)	–	–	<i>spa</i> , <i>aur</i> , <i>cap8</i> , <i>adsA</i> , <i>cna</i> , <i>clpB</i> , <i>coa</i> , <i>ebp</i> , <i>esxA</i> , <i>fnbA</i> , <i>geh</i> , <i>hysA</i> , <i>lip</i> , <i>map</i> , <i>sbi</i> , <i>srtB</i> , <i>vWbp</i> , <i>clfA/B</i> , <i>esaA/B</i> , <i>essA/B/C</i> , <i>hla</i> , <i>hnb</i> , <i>hld</i> , <i>hlgA</i> , <i>hlgB</i> , <i>hlgC</i> , <i>icaRABCD</i> , <i>isdA-G</i> , <i>sdrC/D/E</i> , <i>sspA/B/C</i>	Aminoglycoside- <i>R</i> (<i>aac6'</i> - <i>aph2''</i>) β-Lactam- <i>R</i> (<i>mecA</i>) Fosfomycin- <i>R</i> (<i>fosD</i>) Macrolide- <i>R</i> (<i>ermC</i>) Macrolide- <i>R</i> (<i>vgaA</i>) <i>V</i> Phenicol- <i>R</i> (<i>fexB</i>) Tetracycline- <i>R</i> (<i>tet38</i>) Tetracycline- <i>R</i> (<i>tetM</i>) Trimethoprim- <i>R</i> (<i>dfrC</i>)	<i>rpoB</i> <i>griA</i>	GCT → GAT TCC → TTC	A477D S80F	Rifampicin Ciprofloxacin
1C	DAP ^R	64	4	2	2	hGISA	A1/ <i>Apal</i>	398	IVa	t1939	I	pS194 (<i>str</i>) pDLK1 (<i>ermC</i>)	↑	↑ ¹	<i>spa</i> , <i>aur</i> , <i>cap8</i> , <i>adsA</i> , <i>cna</i> , <i>coa</i> , <i>ebp</i> , <i>esxA</i> , <i>clpB</i> , <i>geh</i> , <i>hysA</i> , <i>lip</i> , <i>map</i> , <i>sbi</i> , <i>srtB</i> , <i>vWbp</i> , <i>clfA/B</i> , <i>esaA/B</i> , <i>essA/B/C</i> , <i>fnbA/B</i> , <i>hla</i> , <i>hnb</i> , <i>hld</i> , <i>hlgA</i> , <i>hlgB</i> , <i>hlgC</i> , <i>icaRABCD</i> , <i>isdA-G</i> , <i>sdrC/D/E</i> , <i>sspA/B/C</i>	Aminoglycoside- <i>R</i> (<i>aac6'</i> - <i>aph2''</i>) Aminoglycoside- <i>R</i> (<i>str</i>) β-Lactam- <i>R</i> (<i>mecA</i>) Fosfomycin- <i>R</i> (<i>fosD</i>) Macrolide- <i>R</i> (<i>ermC</i>) Macrolide- <i>R</i> (<i>vgaA</i>) <i>V</i> Phenicol- <i>R</i> (<i>fexB</i>) Tetracycline- <i>R</i> (<i>tet38</i>) Tetracycline- <i>R</i> (<i>tetM</i>) Trimethoprim- <i>R</i> (<i>dfrC</i>)	<i>rpoB</i> <i>griA</i>	GCT → GAT TCC → TTC	A477D S80F	Rifampicin Ciprofloxacin
3A	DAP ^S	2	0.5	1	16	hGISA	G1/ <i>Smal</i>	8	IVc	t008	I	SAP063A (<i>blaZ</i>)	–	–	<i>spa</i> , <i>aur</i> , <i>cap8</i> , <i>adsA</i> , <i>cna</i> , <i>coa</i> , <i>ebp</i> , <i>esxA</i> , <i>clpB</i> , <i>geh</i> , <i>hysA</i> , <i>lip</i> , <i>map</i> , <i>sbi</i> , <i>srtB</i> , <i>vWbp</i> , <i>clfA/B</i> , <i>esaA/B</i> , <i>essA/B/C</i> , <i>fnbA/B</i> , <i>hla</i> , <i>hnb</i> , <i>hld</i> , <i>hlgA</i> , <i>hlgB</i> , <i>hlgC</i> , <i>lukF-PV</i> , <i>lukD</i> , <i>lukE</i> , <i>icaRABCD</i> , <i>isdA-G</i> , <i>sdrC/D/E</i> , <i>sspA/B/C</i> , <i>splA</i> , <i>splB</i> , <i>splE</i> , <i>sed</i> , <i>sej</i> , <i>ser</i>	β-Lactam- <i>R</i> (<i>blaZ</i>) β-Lactam- <i>R</i> (<i>mecA</i>) Tetracycline- <i>R</i> (<i>tet38</i>) Fosfomycin- <i>R</i> (<i>fosD</i>)	<i>griA</i> <i>griB</i> <i>gyrA</i>	TCC → TAC CCT → TCT TCA → TTA	S80Y P585S S84L	Ciprofloxacin Ciprofloxacin Ciprofloxacin

(Continued)

TABLE 1 | Continued

Strains	DAP pheno-type	MICs (mg/L)	Glyco-peptide hetero-resis-tance	Molecular characterization						DAP-R versus DAP-S expression	Virulome	Resistome	Resistance gene SNPs							
				PFGE	MLST	SCC <i>mec</i>	spa-type	agr-type	Plas-mids				<i>dltA</i>	<i>mpvF</i>	Gene	Nucleotide change	AA change	Resistance		
3B	DAP ^R	16	4	2	2	qVISA	G2/SmaI	8	I/c	1008	I	SAP063A (blaZ)	↑	↓ ²	spa, aur, cap8, adxA, cna, coa, ebp esxA, clpB, geh, hysA, lfp, map, sbi, srlB, wlbp dltA/B esaA/B esaB/C frbA/B hla, hlb, hld hlgA, hlgB, hlgC lukF-PV, lukD, lukE icaRABCD lsdA-G sdrC/D/E sspA/B/C spa, srlB, srlE sed, sel, ser	β-Lactam-R (blaZ) β-Lactam-R (mecA) Tetracycline-R (tet38) Fosfomycin-R (fosD) Aminoglycoside-R (aac6' aph2'') Macrolide-R (ermC)	rpoB griA griB griA	CAT → TAT TCC → TAC CCT → TCT TCA → TTA	S84L S80Y P68SS S84L	Rifampicin Ciprofloxacin Ciprofloxacin Ciprofloxacin

¹S295L AA changes in MpfF; ²no mutation in mpfF; ↑, over-expression; ↓, under-expression; MRSA, methicillin-resistant *Staphylococcus aureus*; DAP, daptomycin; MICs, minimum inhibitory concentrations; DAP-R, daptomycin resistant; DAP-S, daptomycin susceptible; SNP, single-nucleotide polymorphism; PFGE, pulsed-field gel electrophoresis; MLST, multilocus sequence typing.

Genomic Epidemiology

Whole-genome sequencing raw data were analyzed to investigate the genomic epidemiology with ResFinder (v.3.2) and Point Finder (v.3.1.0) services for the detection of the acquired antimicrobial resistance (AMR) genes and to detect the known nsSNPs related to AMR using a 98% threshold for nucleotide sequence identity and 60% for the minimum length coverage (Zankari et al., 2012). MLST was genomically checked using the MLST (v2.0) (Larsen et al., 2012), spa-typing was confirmed by spaTyper (v.1.0) (Bartels et al., 2014), the identification of acquired virulence genes was performed by VirulenceFinder (v.2.0) (Joensen et al., 2014), and the plasmid strain profile was investigated by PlasmidFinder server (v.2.1) (Carattoli et al., 2014). All tools are available on the Center for Genomic Epidemiology website¹. The genomic epidemiology of strain pairs was also analyzed by Nullarbor pipeline².

Core Genome Single-Nucleotide Polymorphisms

The core genome SNP (cgSNP) detection shared among all strains was computationally carried out by Nullarbor².

Enrichment Analysis

Enrichment analysis was performed by DAVID (v.6.8) using the default high stringency parameter set³ (Huang et al., 2009a,b).

Genomic Single-Nucleotide Polymorphism Effect Prediction

The prediction of the whole-genome SNPs (SNPome) effects was performed by SnpEff (v.4.3T), a genomic variant annotation and functional effect prediction toolbox. High (HI), low (LI), moderate (MI), and modifier impacting (MFI) effects were assigned according to the criteria previously published and in use in the tool⁴ (Cingolani et al., 2012). High impact: the variant is assumed to have disruptive impact in the protein, probably causing protein truncation and loss of function or triggering nonsense mediated decay. Low impact: the variant is assumed to be mostly harmless or unlikely to change protein behavior. Moderate impact: the variant is a non-disruptive variant that might change protein effectiveness. Modifier impact: the variant is a usually non-coding variant or variants affecting non-coding genes where predictions are difficult or there is no evidence of impact.

RNA-Seq

RNA-Seq Bacterial Cultures

For the construction of all RNA-seq libraries, an aliquot of an overnight culture was diluted 1:50 in 30 ml of brain heart infusion (BHI) in a sterile 50-ml flask (OD_{600 nm} 0.05) to obtain an approximately 5×10^5 CFU/ml inoculum for each strain. Cells were grown under shaking at 250 rpm with normal atmospheric conditions at 37°C and harvested in the late post-exponential

²<http://github.com/tseemann/nullarbor>

³<http://david.abcc.ncicrf.gov/>

⁴<http://snpeff.sourceforge.net>

growth phase ($1.5\text{--}4 \times 10^{10}$ CFU/ml, ~ 18 h). RNA extraction started immediately after cell harvesting to maintain RNA integrity. The cell density was determined by colony counting after plating onto Mueller–Hinton (MH) agar and incubation. Growth curves of the four DAP-free MRSA strains were shown in the **Supplementary Figure S4**.

RNA-Seq Libraries

RNA-seq was performed using the Illumina MiSeq sequencing system, and biological replicates were performed using two different libraries, a single-end library with 50-bp reads [Short-Insert Library (SI)] and a PE read library with 150-bp reads [Tru-Seq Library (TS)] starting from two different RNA extractions according to the following protocols as a strategy to optimize the collected RNA-seq data (Pereira et al., 2017; Cafiso et al., 2019).

Tru-Seq Library RNA Extraction

RNA was extracted using the NucleoSpin RNA (Macherey-Nagel, Dueren, Germany) kit following the manufacturer's protocol with minor modifications. Pellets were lysed by the bead-beating procedure with 50 μ l of RA1 buffer. Then 3.5 μ l of β -mercaptoethanol was added, and the lysates were filtered through NucleoSpin Filters. The RNA-binding condition was adjusted by adding 70% ET-OH to the lysates, and the RNA was extracted with TRIzol reagent (Invitrogen) according to the manufacturer's protocol. The total RNA quality was verified using a 2200 TapeStation RNA Screen Tape device (Agilent, Santa Clara, CA, United States), and its concentration was ascertained using an ND-1000 spectrophotometer (NanoDrop, Wilmington, DE, United States). The Agilent TapeStation 2200 system, an automated instrument for nucleic acid gel electrophoresis, assigned RNA integrity number (RIN) values ranging from 1 to 10, with 10 being the highest quality. Only samples with preserved 16S and 23S peaks and RIN values > 8 were used for the library's construction. The RIN values > 8 indicate intact and high-quality RNA samples for downstream applications as previously published (Fleige and Pfaffl, 2006). Ribosomal RNA was removed using the Bacteria Ribo-Zero rRNA Removal Kit from 2 μ g of RNA. The depleted RNA was used for the Illumina TruSeq RNA stranded kit without PolyA enrichment. The obtained libraries were evaluated with high-sensitivity D1000 screen Tape (Agilent Tape Station 2200), and the indexed libraries quantified with the ABI9700 qPCR instrument using the KAPA Library Quantification Kit in triplicates was according to the manufacturer's protocol (Kapa Biosystems, Woburn, MA, United States). From the pooled library, 2-nM final concentrations were used for sequencing with a 150 PE read sequencing module (Cafiso et al., 2019).

Short-Insert Library RNA Extraction

RNA was extracted with TRIzol reagent (Invitrogen) according to the manufacturer's protocol. After ribosomal depletion, sequencing libraries were prepared using the Illumina mRNA-seq sample preparation kit following the supplier's instructions except that total RNA was not fragmented and double-stranded cDNA was size-selected (100–400 bp) to maximize the recovery of small size RNA.

The prepared libraries were evaluated with high-sensitivity D1000 screen Tape (Agilent Tape Station 2200) as described for the TS Library. The indexed libraries were quantified in triplicate with the ABI9700 qPCR instrument using the KAPA Library Quantification Kit, according to the manufacturer's protocol (Kapa Biosystems, Woburn, MA, United States). From the pooled library, 5 μ l at a final concentration of 4 nM was used for MiSeq sequencing with an A single-end stranded library with reads of 50-bp sequencing module (Cafiso et al., 2019).

Tru-Seq Library Preparation and Sequencing

The samples were processed using the Illumina MiSeq, using an A PE library with reads of 150 bp and average insert size of 350/400 bp. After sequence data generation, raw reads were processed using FastQC (v.0.11.2) to assess data quality. The sequenced reads were then trimmed using Trimmomatic (v.0.33.2) to remove only sequencing adapters for PE reads. A minimum base quality of 15 (Phred scale) over a four-base sliding window was required. Only sequences with a length above 36 nucleotides were included in the downstream analysis. Similarly, only trimmed reads were included in the downstream analysis (Cafiso et al., 2019).

Short-Insert Library Preparation and Sequencing

The samples were processed using the Illumina MiSeq technology with an A single-end stranded library with reads of 50 bp. After sequence data generation, raw reads were processed using FastQC (v.0.11.2) to assess data quality. Reads were then trimmed using Trimmomatic (v.0.33.2) to remove sequencing adapters for single-end reads, requiring a minimum base quality of 15 (Phred scale) and a minimum read length of 15 nucleotides. Only trimmed reads were included in the downstream analysis (Cafiso et al., 2019).

Tru-Seq and Short-Insert Library Analysis

TS and SI RNA-seq reads were annotated on *S. aureus* NCTC 8325 RefGen (CP000253.1), as well as transcripts assembled and quantified using Rockhopper (v.2.03) (McClure et al., 2013; Tjaden, 2015), specifically designed for bacterial gene structures and transcriptomes. Analyses were run using default parameter settings with verbose output to obtain expression data. Rockhopper normalizes read counts for each sample using the upper quartile gene expression level. Starting from the *p*-values calculated according to the Anders and Huber approach, differentially expressed genes (DEGs) were assigned by computing *q*-values ≤ 0.01 on the basis of the Benjamini–Hochberg correction with a false discovery rate of $< 1\%$. In addition, Rockhopper is a versatile tool using biological replicates when available, and surrogate replicates when biological replicates for two different conditions are unavailable, considering the two conditions under investigation as surrogate replicates for each other (McClure et al., 2013).

Finally, filtering analyses were computationally carried out for sorting, first, the DEGs in the DAP^R strains versus their DAP^S parental strain and, then, a selection of only those present contemporarily in both DAP^R isolates showing the same expression (under-expression or over-expression) (Cafiso et al., 2019).

Determination of the Affected Pathways

The online tool DAVID (v.6.8) was selected to identify the affected pathways among the DEGs. The gene lists were uploaded as Official Gene Symbols of the *S. aureus* NCTC 8325 RefGen and automatically selecting the list type (Gene list) of *S. aureus*. The Functional Annotation Chart was visualized using the *p*-value threshold of 0.01 and a minimum count number of four genes. The information on the affected pathways was obtained from Kyoto Encyclopedia of Genes and Genomes (KEGG) within the analysis in DAVID, using the mentioned thresholds. The affected biological processes were obtained from the Gene Ontology (GO) Consortium within the analysis in DAVID (Cafiso et al., 2019).

RNA Functional Categories

Functional categories of DEGs were investigated by BLAST, PANTHER Classification System, GO Consortium, ExPASy (STRING), and KEGG pathway (Cafiso et al., 2019).

RNA-Sequencing Data Accession Number

RNA-seq raw reads were deposited at the Gene Expression Omnibus (GEO) database under study accession no. GSE121797 (BioProject: PRJNA498510).

Downstream Statistical Analysis

An heatmap of the entire set of DEGs and principal component analysis (PCA) on the five discovered DEG functional categories, in DAP^R MRSA versus their DAP^S parents, were performed by XLSTAT 2020 Excel data analysis add-on (v.2020.1.3) using default setting.

Real-Time qPCR

To validate RNA-seq data, real-time qPCRs were performed on the most DAP^R-relevant transcripts (SAOUHSC_02317, SAOUHSC_00022, SAOUHSC_00486, SAOUHSC_02922, SAOUHSC_01806, SAOUHSC_01334, and SAOUHSC_00545) using RNAs of three experiments performed under the RNA-seq growth conditions. Real-time qPCRs were carried out following published protocols (Cafiso et al., 2012, 2014); the primer sequences are shown in **Supplementary Table S1** and used with the following thermal profile: 95°C for 3 min; 35 cycles at 95°C for 10 s, 60°C for 30 s, and 72°C for 45 s; and a final cycle at 95°C for 1 min, 60°C for 30 s, and 95°C for 30 s. *gyrB* was the normalizer. Statistical analyses were conducted as previously described (Pfaffl et al., 2002).

L-Lactic Acid Concentration Assay

Single strains were grown under shaking at 250 rpm in standard atmospheric conditions at 37°C and harvested in the late post-exponential growth phase. The lactate conversion was measured by enzymatic lactate oxidation into pyruvate using a D-lactic acid/L-lactic acid commercial test (R-Biopharm, Germany). L-Lactic acid concentrations were calculated using the D-lactic acid/L-lactic acid ultraviolet method according to the manufacturer's instructions (R-Biopharm), which is based on the conversion of D-lactate or L-lactate by D-lactate dehydrogenase and L-lactate dehydrogenase, respectively, to pyruvate and

NADH. The L-lactic acid concentrations were expressed in g/L. Three biological and technical replicates were performed for each strain. A statistical significance was attributed in Student's *t*-test with *p*-values < 0.05.

RESULTS

Genomics

Core Genome Single-Nucleotide Polymorphism Phylogeny

Pairwise cgSNP distance analysis showed a very close phylogeny of the DAP^R strains respect to the DAP^S parents. Thirty-six cgSNP differences were found between the 1A and 1C, whereas 41 cgSNPs were found between the 3A versus 3B isolated during a period of both 4 and 6 months under DAP therapy, respectively.

Genomic Epidemiology

The genomic epidemiology showed the membership of the 1A/C strain pair to the ST398-SCCmecIVa-t1939-*agrI* both harboring the plasmid pDLK1 carrying *ermC*, together with the pS194 harboring the *str* gene (**Table 1**) only in 1C, both conferring aminoglycoside resistance. The 3A/B strain pair was confirmed to be ST8-SCCmec-IVc-t008-*agrI* having the SAP063A plasmid carrying *blaZ* determining β-lactam resistance, and with the 3B having in addition the pDLK1 carrying *ermC* (**Table 1**).

Integrating the Center for Genomic Epidemiology and Nullarbor outputs, the strain pair resistomes (acquired AMR genes and known chromosomal SNPs conferring antimicrobial resistance) and virulomes (chromosomal and acquired virulence genes) are outlined as shown in **Table 1**.

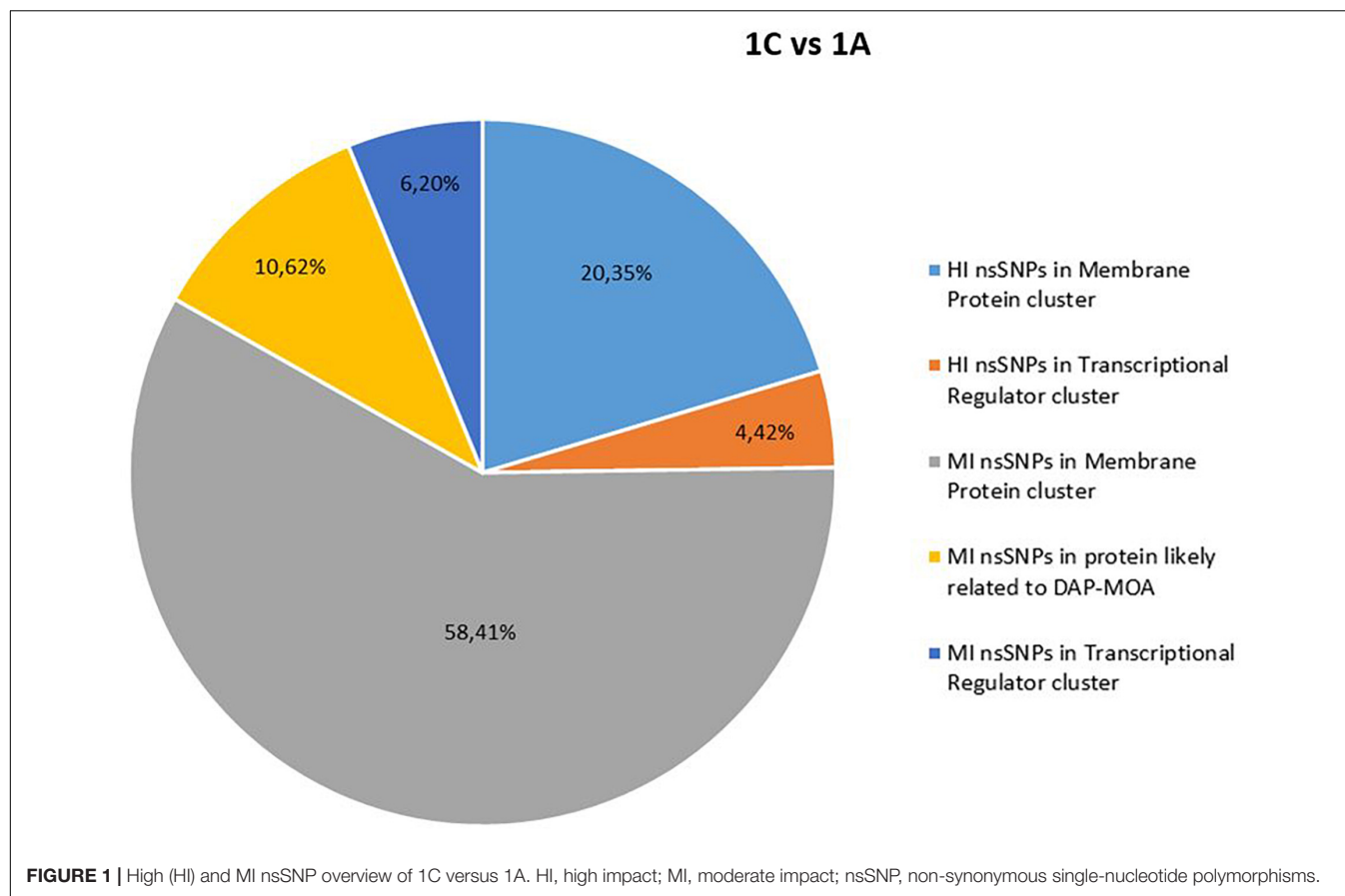
Genome Comparison

Mauve Genome alignments of the single DAP^R MRSA genome versus its DAP^S parent showed the lack of new genetic elements associable to DAP-R. The unique additional genetic traits present in DAP^R MRSA strains were the two plasmids, that is, pS194 in 1C and pDLK1 in 3B.

SNPome and Possibly Related to Daptomycin Resistance Acquisition Non-synonymous Single-Nucleotide Polymorphisms

DAP^{R/S} strain-pair SNPome carried out versus *S. aureus* NCTC8325 RefGen recorded a variant rate of 64 in the DAP^{R/S} 1A/C strain pair with the presence of 43,720 variants in 1C and 43,947 in 1A; otherwise, a variant rate of 893 was found in 3B and 592 in 3A, with the presence of 3,157 variants and 4,762 variants, respectively.

In the DAP^{R/S} 1 A/C strain pair, according to the criteria of SnpEff tool, 0.924% mutations were putatively predicted with HI on their products; 57.118% with LI; 23.665% with MI; and 18.293% with MFI, in 1C. Among these, 23.376% were missense (M), 0.25% were nonsense (NS), and 76.374% were silent (S). In 1A, similarly, 0.978% had HI, 56.833% had LI, 23.759% had MI, and 18.431% had MFI, with



23.701% of M mutations, 0.314% of NS mutations, and 75.984% of S mutations.

No shared HI and MI acquired nsSNPs in DAP-MOA-related targets were found in both DAP^R and DAP^S MRSA strain pairs (**Figures 1, 2**); however, high stringent DAVID enrichment analysis evidenced HI and/or MI DAP-MOA-related nsSNPs in the same functional protein clusters, with recovered coding genes and nsSNPs predominantly different between the two DAP^{R/S} MRSA strain pairs.

In details, HI and/or MI DAP-MOA-related nsSNPs were detected in two UP_SEQ_FEATURE clusters of targets putatively related to DAP-MOA, that is, membrane proteins (including transmembrane proteins, lipoproteins, and two-component histidine kinase systems and transporters) and transcriptional regulators. In addition, only in DAP^R 3B versus DAP^S 3A MRSA were HI DAP-MOA-related nsSNPs also recovered in the UP_SEQ_FEATURE Signal Peptide Protein cluster including gene coding proteins involved in CW turnover and teichoic acid metabolism. Furthermore, in both DAP^R and DAP^S MRSA strain pairs, MI DAP-MOA-related nsSNPs were also detected in a miscellaneous of gene coding proteins putatively related to DAP-MOA including proteins related to autolysis, cell division, peptidoglycan transport and cell shape, diacylglycerol metabolism, phosphatidylglycerol modifications (MprF), proteins involved the cardiolipin biosynthetic process (Cls1), and lipoteichoic acid biosynthesis (DltB) (**Supplementary Table S2**).

RNAome Structures

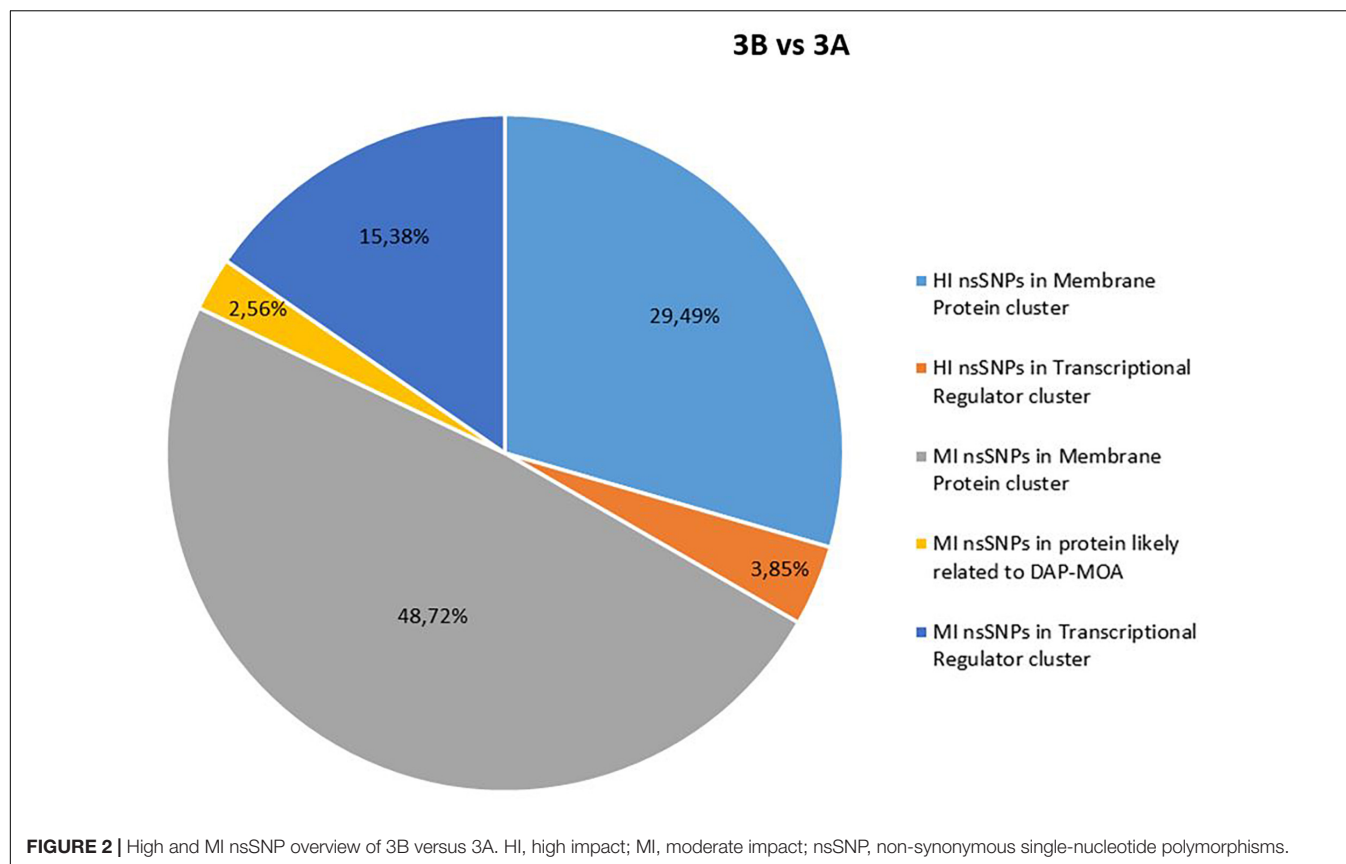
The RNAome structures, shown in TS and SI libraries, of the single DAP^R versus DAP^S strain pairs are reported in **Tables 2, 3**.

DAVID Pairwise Enrichment Analysis

Integrating data obtained from the two libraries, DAVID enrichment pairwise analysis ($p\text{-value} \leq 0.05$) (Huang et al., 2009a,b) of the over-expressed DEGs evidenced the enrichment of only the ABC transporter KEGG pathway in both DAP^{R/S} strain pairs (**Supplementary Tables S3, S4**). In addition, among the under-expressed DEGs, we found several enriched KEGG pathways responsible for ABC transporter, glycolysis and pyruvate metabolism, purine and propanoate metabolism, phosphotransferase system (PTS), and two-component regulatory systems. Among the TCRs, SaeR/S (SAOUHSC_00714/SAOUHSC_00715) was found in both pairs and WalK (SAOUHSC_00021) only in the 3A/B pair (**Supplementary Table S3**). Diverse strain-dependent enriched over-expressed/under-expressed KEGG pathways were observed in the single 1A/C and 3A/B pair as shown in **Supplementary Tables S3, S4**.

Cross-Filtered Double-Pair Differentially Expressed Genes

Stringently double-pair cross-refiltering of the RNA-seq data—to define the signatures exclusively present in either DAP^R

**TABLE 2 |** RNAomes—Tru-Seq library Rockhopper summary.

	1A	1C	3A	3B
Total reads	853,091	873,327	1,010,514	1,011,410
Aligned reads	826,706 (97%)	847,504 (97%)	986,353 (98%)	979,230 (97%)
Sense	50%	50%	49%	49%
Antisense	48%	48%	46%	47%
Unannotated	1%	1%	1%	1%
1A and 1C		3A and 3B		
5'-UTR	13	99		
3'-UTR	3	70		
Not antisense	8	11		
Antisense	19	22		
Differentially expressed genes	341	210		
Likely operons	1,057	1,122		
Multigene operons	538	547		

MRSA strains or their DAP^S parents, and with the same expression profiling in the same library (SI or TS)—highlighted the co-occurrence of 53 statistically significant DEGs: nine over-expressed and 44 under-expressed protein-coding genes were found (Figures 3, 4 and Supplementary Table S5).

TABLE 3 | RNAomes—short-insert library Rockhopper summary.

	1A	1C	3A	3B
Total reads	306,666	197,745	431,264	365,885
Aligned reads	58,942 (19%)	35,115 (18%)	155,706 (36%)	51,346 (14%)
Sense	80%	86%	53%	80%
Antisense	1%	0%	1%	0%
Unannotated	5%	7%	7%	5%
	1A and 1C		3A and 3B	
5'-UTR	10		37	
3'-UTR	5		11	
Not antisense	451		813	
Antisense	861		1,656	
Differentially expressed genes	222		413	
Likely operons	1,040		1,069	
Multigene operons	533		544	

According to the GO numbers and Clusters of Orthologous Group (COG) groups, we categorized the characterizing DAP^R DEGs in different clusters, as follows.

Cell division, cell wall, and cell membrane

Three DEGs implicated in peptidoglycan biosynthesis, two DEGs for the CW autolysis, and five DEGs involved in cell division and CM structure were found.

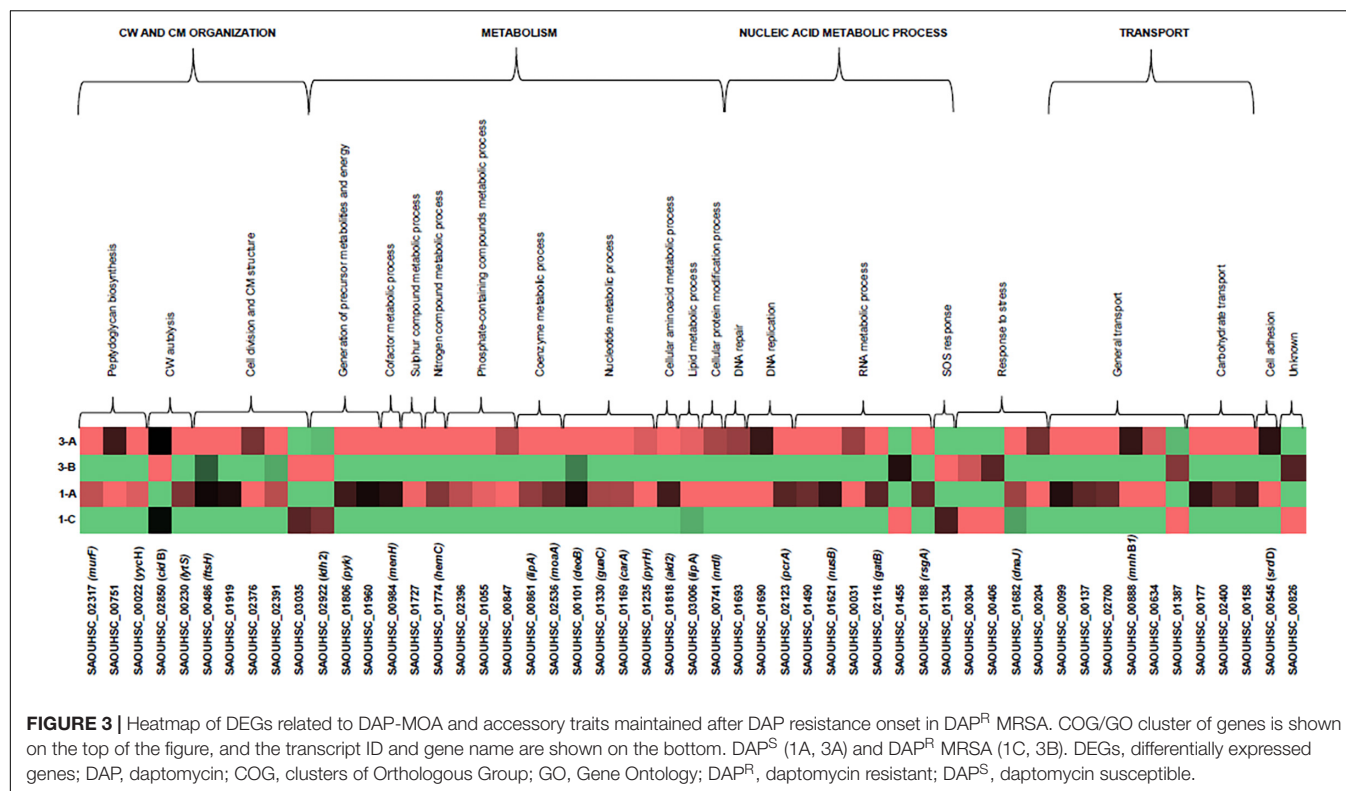


FIGURE 3 | Heatmap of DEGs related to DAP-MOA and accessory traits maintained after DAP resistance onset in DAP^R MRSA. COG/GO cluster of genes is shown on the top of the figure, and the transcript ID and gene name are shown on the bottom. DAP^S (1A, 3A) and DAP^R MRSA (1C, 3B). DEGs, differentially expressed genes; DAP, daptomycin; COG, clusters of Orthologous Group; GO, Gene Ontology; DAP^R, daptomycin resistant; DAP^S, daptomycin susceptible.

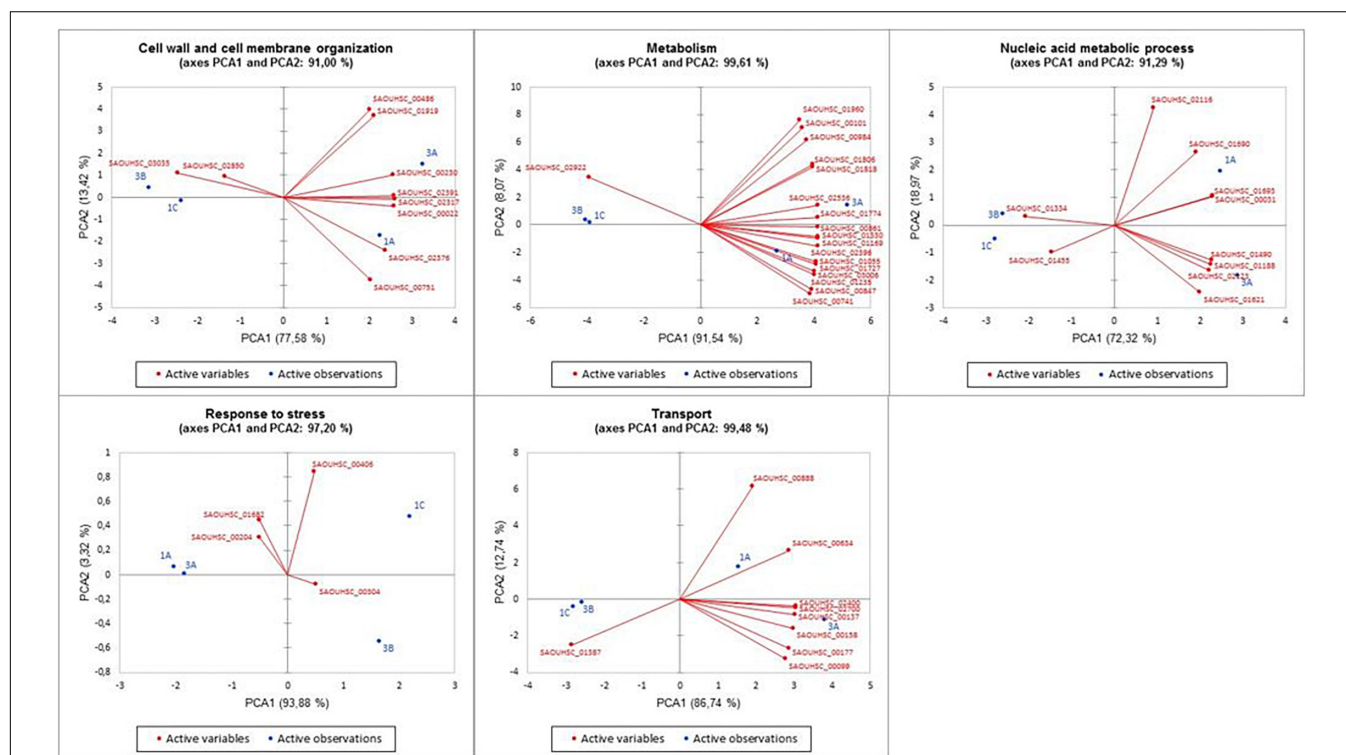


FIGURE 4 | Principal component analysis of the five discovered DEG functional categories versus the DAP^R/DAP^S MRSA. PCA plots show the relations between strains and genes in the different clusters. PCA, principal component analysis; DEG, differentially expressed gene; DAP^R, daptomycin resistant; DAP^S, daptomycin susceptible; MRSA, methicillin-resistant *Staphylococcus aureus*.

For peptidoglycan biosynthesis, we found under-expression in the UDP-*N*-acetylmuramoyl-tripeptide-*D*-alanyl-*D*-alanine ligase *murF*, in SAOUHSC_00751 hypothetical protein encoding gene (neighboring and consequently predicted as functionally related to the UDP-*N*-acetylenolpyruvoylglucosamine reductase MurB for the CW formation STRING_{score}: 0.808), and in YycFG (WalKR) negative regulator, *yycH*. In CW autolysis, over-expression was shown in *cidB* autolysin and under-expression in the sensor histidine kinase *lytS*.

As concerns cell division and CM structure, under-expression was displayed in *ftsH*, incorporating the PBPs into the CM, in SAOUHSC_01919, SAOUHSC_02376, and SAOUHSC_02391 uncharacterized proteins located—according to the GO Cellular Component term (GO-CC): 0016021—in the CM, whereas over-expression was recorded only in SAOUHSC_03035 integral membrane protein.

Metabolism

A complex network involving differential expression was shown in metabolic genes. As regards the generation of precursor metabolites and energy, L-lactate dehydrogenase-2 encoding gene *ldh2* involved in lactic fermentation was over-expressed, whereas the pyruvate kinase gene *pyk* involved in glycolysis and the protoporphyrinogen-oxidase SAOUHSC_01960 (porphyrin biosynthesis) were under-expressed. In the cofactor metabolism, under-expression was recorded in 2-succinyl-6-hydroxy-2,4-cyclohexadiene-1-carboxylate synthase *menH*.

Regarding the compound metabolism, under-expression was found in cysteine-desulfurase SAOUHSC_01727 for sulfur-compound metabolism; in the porphobilinogen-deaminase *hemC* related to the nitrogen-compound metabolism; in SAOUHSC_02396 Cof-like hydrolase, SAOUHSC_01055 inositol-monophosphatase, and SAOUHSC_00847 ABC transporter involved in the metabolism of phosphate-containing compounds; in SAOUHSC_00861 lipoyl-synthase *lipA* for the coenzyme and cofactor metabolism; and in the molybdenum cofactor biosynthesis *moaA*.

With regard to nucleotide metabolism, phosphopentomutase *deoB*, GMP reductase *guaC*, carbamoyl-phosphate synthase small chain *carA*, and uridylate kinase *pyrH* were under-expressed. With regard to the amino acid and lipid catabolism, our data evidenced under-expression in alanine dehydrogenase *ald2* and lipase-1 *lipA*. In the cellular protein modification process, under-expression was observed in *nrdI* coding the Class Ib ribonucleotide reductase stimulatory protein.

Nucleic acid metabolism

Under-expression was found in the SAOUHSC_01693 DNA-binding protein for DNA repair, and in the SAOUHSC_01690 of the DNA polymerase III complex and the ATP-dependent DNA-elicase, *pcrA*. In the RNA transcription and regulation, our data showed under-expression in DNA-binding protein HU coding gene functionally related to ClpC (STRING_{score}: 0.555), in transcription anti-termination *nusB*, in SAOUHSC_00031 tRNA-dihydrouridine synthase, and in the aspartyl/glutamyl-tRNA amidotransferase subunit B *gatB* (tRNA metabolism).

Examining ribosome biogenesis and maturation, we found over-expression in ATPase, whereas under-expression was found in *rsgA* (ribosome biogenesis). In SOS response, we observed over-expression in SAOUHSC_01334 hypothetical protein functionally related to LexA repressor (STRING_{score}: 0.614) (DNA-damage response).

Stress response

Referring to the stress response, SAOUHSC_00304 luciferase-like monooxygenase (oxidative stress response) and SAOUHSC_00406 uncharacterized protein [previously annotated as poly(3-hydroxybutyrate) (PHB) depolymerase family protein] determining the use of PHB as a carbon source and energy storage in starvation conditions, were over-expressed. *dnaJ* (prevention of stress-denatured protein aggregation in response to hyperosmotic condition and heat shock) and the SAOUHSC_00204 globin domain protein, nitric oxide dioxygenase (nitrosative stress response), were under-expressed.

Transport

Under-expression was observed in SAOUHSC_00099, SAOUHSC_00137, and SAOUHSC_02700 transporters; in the SAOUHSC_00888 Na⁺/H⁺ antiporter *mnhB1*; and in SAOUHSC_00634 ABC metal ion transporter involved in cell adhesion. Over-expression was only found in SAOUHSC_01387 inorganic phosphate transmembrane transporter.

Results from carbohydrate transporters showed under-expression in SAOUHSC_00177 maltose ABC permease, in the SAOUHSC_02400 putative mannitol-specific PTS component, and in the SAOUHSC_00158 *N*-acetylmuramic acid transporter belonging to the phosphotransferase system.

Cell adhesion

Under-expression was shown in the serine-aspartate repeat-containing *sdrD*, a staphylococcal virulence factor.

Unknown function

Over-expression was observed in SAOUHSC_00826 encoding a conserved uncharacterized protein.

RNA-Seq Data Validation

RNA-seq data validation performed by real-time qPCR on the most DAP^R-relevant genes confirmed the *murF* (SAOUHSC_02317), *yycH* (SAOUHSC_00022), *ftsH* (SAOUHSC_00486), *ldh2* (SAOUHSC_02922), *pyk* (SAOUHSC_01806), SOS response protein related to LexA (SAOUHSC_01334), and *sdrD* (SAOUHSC_00545) expression profiles detected in RNA-seq data in both DAP^R *S. aureus* and DAP^S parents (Supplementary Figure S5).

Lactic Acid Quantification Assay

To biologically validate the bioinformatic prediction of the over-expression in L-lactate dehydrogenase-2, quantification assays of the amount of lactic acid were performed, showing a statistically significant increased concentration of L-Lactate in both DAP^R MRSA and their DAP^S parental strains (Figure 5).

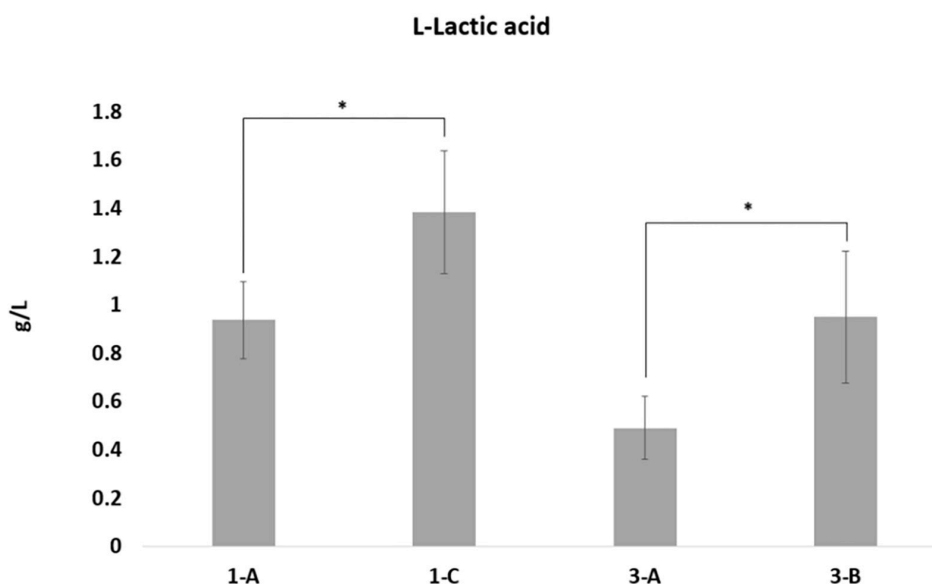


FIGURE 5 | L-Lactic acid quantification. L-Lactic acid production by the four strains was calculated using the L-lactic acid ultraviolet method according to the manufacturer's instructions (D-lactic acid/L-lactic acid kit, R-Biopharm), based on conversion of L-lactate by L-lactate dehydrogenase to pyruvate and NADH. L-Lactate production differences with p -values < 0.05 , obtained by Student's t -test, were considered statistically significant. * is for the statistical significance.

DISCUSSION

In *S. aureus*, DAP-R is a complex and multifactorial mechanism shaped by the co-occurrence of intrinsic, acquired, and adaptive determinants that, harmonizing in concert, confer resistance. We investigated two clinical epidemiologically unrelated DAP^{R/S} MRSA strain pairs isolated from different patients in two different Italian hospitals. The two patients failed glycopeptide therapy and were then treated with DAP (Cafiso et al., 2014).

Previous investigations on the same DAP^{R/S} MRSA strain pairs characterized some traits related to DAP-R, including a dysregulation in the two key determinants of net positive surface charge, *dltA* and *mprF*, both during exponential and stationary growth phases; a significant increase in the D-alanylated wall teichoic acids amount correlating with *DltA* gain-in-function; a heightened elaboration of lysyl-phosphatidylglycerol reflecting *MprF* gain-in-function; an increased CM fluidity; a strain-dependent CM fatty acid perturbation due to an increase in the anteiso-branch chain species corresponding to a reduction in the major iso-branched chain and saturated fatty acids (SFAs); and a reduced susceptibility to prototypic cationic host defense peptides of platelet and leukocyte origins (Cafiso et al., 2014; Mishra et al., 2014; Boudjemaa et al., 2018).

In the present study, genome-wide CSI phylogeny and the cgSNP analysis of the same strain pairs revealed the close relation of the DAP^{R/S} MRSA isolated from the same patient under DAP therapy administered in hospital during a period of several months. Concomitantly, genomic epidemiology confirmed their previously published molecular typing (Cafiso et al., 2014) as well as plasmids and intrinsic resistance trait content; whereas acquired AMR genes and SNP profiling highlighted the acquisition of genetic traits related to the onset of additional

antimicrobial resistances. In addition, virulome analysis showed a high virulence gene toxin content of the ST8 DAP^{R/S} 3A/B strain pair with respect to the ST398 DAP^{R/S} 1A/C.

Comparative genomics did not reveal newly acquired mobile genetic elements in both DAP^R MRSA and their DAP^S parents putatively related to DAP-R onset. On the contrary, *in depth*, SNPomics showed HI and MI DAP-MOA-related nsSNPs in shared functional coding-gene clusters, despite the diversity of the ST398 and ST8 genomic backgrounds with respect to the *S. aureus* NCTC8325 RefGen (proved to be the genome most closely related to both strain pairs in study).

Comparing DAP^R versus their DAP^S parents on *S. aureus* NCTC8325 RefGen, functional protein coding-gene clusters were found to be a hot spot of nsSNPs in a pairwise shared way. However, within these clusters, the detected putative HI and MI DAP-MOA-related nsSNPs in the target genes varied between the two strain pairs, indicating a strain-dependent behavior, defining two different DAP^R genomic backgrounds.

Our data, supported by previous findings on laboratory induced DAP^R MRSA of specific clones HG003, USA300-TCH1516, MSSA476, MW2, and MRSA252 mutants (Coe et al., 2019), first described and defined in two clinical DAP^{R/S} MRSA of genomic backgrounds (ST8 and ST398) strain-dependent shared and functional protein clusters as hot spots of genomic variations. In particular, membrane protein (transmembrane proteins, lipoproteins, and transporters), transcriptional regulator (Sigma-70, RpoB, RpoC, RsbU, GraX, SarR, SarU, SarX, ArlS, WalK, AgrC/A, MsrR, Msa, KdpD, SAOUHSC_02390, and SAOUHSC_00673), and cell-envelope modification (Sle1, UgtP, DltB, FmtA, LspA, Cls1, MprF, and SAOUHSC_01063) protein coding-gene clusters emerged as accumulation sites of mutational events related to the DAP-R onset, randomly

occurring in the same gene. Therefore, the CM structural and the functional proteins (cell envelope, cell division, and stress response system proteins) together with several transcriptional regulators represented the cellular targets undergoing genomic gain-in changes under DAP pressure.

The late growth phase transcriptional analysis, mimicking the *in vivo* infection-site growth, outline for the first time the long-term transcriptomic fingerprinting and networks involved in the adaptation to become DAP^R MRSA. DAVID analysis highlighted common enriched pairwise over-expressed/under-expressed KEGG pathways in transport and TCRs, SaeS/R, and WalK, even though not in both strain pairs for WalK. Some differences in the enriched KEGG pathways can be attributable to strain-dependent features and different genomic background. The SaeR/S regulatory system (SAOUHSC_00714/SAOUHSC_00715) controls the production of exoproteins involved in adhesion and invasion of host cells, that is, hemolysins (*hla* and *hly*), *coa*, Dnase, and *spa*- and CW-associated proteins (*emp*, *eap*, and *fmbA*), whereas WalK was previously related to glycopeptide resistance (Kolter et al., 1993; Shoji et al., 2011).

Transcriptomes revealed long-term imprints closely or indirectly related to the DAP-MOA and several accessory traits corroborating the multiple transcriptomic adaptations acquired with DAP-R onset, following DAP exposure and maintained by DAP^R MRSA.

In particular, we considered as closely related features the CW and CM structure and organization traits as well as the primary metabolism ones owing to their link to the DAP-MOA and indirectly related features whether involved in biological pathways not directly related to DAP-MOA as the survival mechanisms of bacteria, that is, oxidative stress response, reactive oxygen species (ROS) detoxification, and ABC transporters.

The cell-envelope organization and structure are a key trait closely related to the DAP-MOA showing a multilevel feedback. Changes in the cell-envelope organization and structure appear, in fact, related to the modulation of four different pathways—that is, the peptidoglycan biosynthesis, cytolysis, cell division, and CM structure—considered related to DAP-MOA targets.

In details, adaptations in CW and CM organization and changes in the profile and content of the membrane proteins—affecting the availability of these DAP targets (Pogliano et al., 2012)—can be speculated *via* a modulation of the YycFG expression by *yycH* and membrane-protein gene under-expression. In *Bacillus subtilis*, *yycH* is accessory system to YycFG repressing the YycG histidine kinase function (Fukushima et al., 2008). Changes in genes modulating cell-envelope stress and maintenance, including YycFG, had been previously associated with the development of DAP^R in clinical and laboratory-derived DAP^R *S. aureus* mutants, as well as with resistance to vancomycin (Utaida et al., 2003; Gaupp et al., 2015). The YycFG was reported as a key regulator of different processes affecting CW metabolism, CM lipid homeostasis and biofilm formation, changes in membrane fluidity, and CW cross-linking compensating osmotic pressure stresses (Dubrac and Msadek, 2004; Fukushima et al., 2011; Delauné et al., 2012).

Alterations in peptidoglycan synthesis were supposed *via* *murF* and SAOUHSC_00751 (functionally related to MurB) under-expression, indicating a putative decreased addition of the C-terminal D-alanyl-D-alanine dipeptide to the CW precursor muropeptide, a critical control point of peptidoglycan synthesis in *S. aureus*. The biosynthesis and attachment of the D-alanyl-D-alanine dipeptide are catalyzed by the different proteins encoded by *ddlA* and *murF*, with the MurF attaching the dipeptide to the UDP-N-acetylmuramic acid (MurNAc)-tripeptide, thus completing the biosynthesis of the peptidoglycan block, the UDP-linked MurNAc-pentapeptide. The D-alanyl-D-alanine C-terminal residues are essential for reactions taking place at the CW (Sobral et al., 2006). Even though DAP is structurally related to amphomycin, and similar lipopeptides as well as peptidoglycan biosynthesis inhibitors, no experimental studies share evidence on a similar MOA (Taylor and Palmer, 2016; Gómez Casanova et al., 2017). In our opinion, this signature could represent a new putative intrinsic daptomycin/glycopeptide cross-resistance mechanism because the D-alanyl-D-alanine dipeptide also represents glycopeptide targets. This transcriptomic trait experimentally supports the association of DAP-R and glycopeptide reduced susceptibility in MRSA, as well as, for the first time, providing experimental evidence on a relationship between DAP^R onset and dysfunctionality in peptidoglycan biosynthesis, likely linked to a concomitance DAP inhibitor activity as reported for similar lipopeptide antimicrobials.

In addition, PBP incorporation into the CM and the quality control of cytoplasmic and integral membrane proteins could be affected through damaged-protein degradation and the protein-folding by *ftsH* under-expression (Lithgow et al., 2004). Autolysis is a crucial signature of the DAP^R transcriptomic pathway and is closely related to the DAP-MOA, as demonstrated by *cidB* over-expression and *lytS* under-expression. Our data showed that DAP-R could lead to an increased activity of extracellular murein hydrolases *via* *cidB* over-expression. CidAB and LytS/R represent the key of the bacterial lysis regulatory pathway (Groicher et al., 2000; Patton et al., 2006). Furthermore, the LytSR system has been hypothesized to function as a staphylococcal “voltmeter,” rapidly sensing $\Delta\psi$ changes and leading to adaptations for resistance to host defense cationic antimicrobial peptides (HDPs) (Yang et al., 2013). Because the bactericidal mechanisms of action of the HDPs, as well as DAP, involve disruption of $\Delta\psi$ associated with the CM (either primarily or secondarily), DAP—owing to its similarity to HDPs—could perturb the staphylococcal CM and alter transmembrane potential ($\Delta\Psi$) impacting on programmed cell death and autolysis. Under stress conditions, for example, the presence of antimicrobials, CidAB can collapse the proton motive force and allow access of autolysins to their substrate resulting in cellular lysis modulating programmed cell death (Patton et al., 2006).

Different metabolic adaptations are directly linked to the DAP-MOA characterize DAP^R MRSA. A fermentative metabolism appears to be the main metabolic pathway as expected in late growth phase, as demonstrated by the L-lactate dehydrogenase *ldh2* over-expression associated with the increase in the lactic acid concentration reflecting the L-lactate

dehydrogenase activity and the concomitant pyruvate kinase *pyk* under-expression. Shifting toward a fermentative metabolism leads to ATP deficiency and an alteration of membrane potential ($\Delta\Psi$) as a consequence of a decrease in the loss of oxidative phosphorylation, in agreement with previous findings showing that the succinate dehydrogenase levels, TCA enzyme, were lower in a DAP^R strain with respect to DAP^S strains (Fischer et al., 2011). *menH* under-expression (also functionally related to MurF) involved in menaquinone and phyloquinone epoxide biosynthesis was observed in DAP^R strains. Menaquinone is a component of the staphylococcal membrane required for correct electron transport chain (ETC) functionality; thus, the *menH* under-expression may also be related to DAP-R acquisition.

Carbohydrate and inorganic phosphate transmembrane transport represents another key point indirectly related to the DAP-MOA in DAP^R MRSA. In detail, our data showed a predominant under-expression of various transporter coding genes, including three genes responsible for carbohydrate transport. On the contrary, over-expression of the inorganic phosphate transmembrane transporter was observed. In particular, the over-expression of the inorganic phosphate transmembrane transporters could be implicated for its STRING predicted functionality related to the *walR*, *arlR*, and *ssrA* master regulators involved in autolysis, biofilm formation, CW metabolism, adhesion, multidrug resistance, virulence, and the global regulation of staphylococcal virulence factors in response to environmental oxygen levels as well as repression of *agr*, *spa*, and *tst* transcription.

Accessory DAP-R fingerprints were also discovered in DAP^R MRSA. DAP-R alters the metabolism of amino-acid, lipid, cofactors, pyrimidine, and purine as demonstrated by the under-expression of various metabolic genes. Alterations in the pyrimidine and purine metabolic pathways have been indeed previously reported in DAP^R *S. aureus* (Cui et al., 2010). Looking at the nucleic acid metabolism, different genes required for DNA replication, transcription, and translation appeared differentially expressed comparing DAP^R versus DAP^S strains. The over-expression of SAOUHSC_01334—annotated as *sosA*—could indicate an SOS-response block. *sosA* appears to be LexA regulated, exhibiting an over-expression similar to that of the SOS genes (Cirz et al., 2007; Mesak et al., 2008). An SOS-response block related to hypermutator behavior is considered a key mechanism of mutational antibiotic resistance. As regards the oxidative stress response, SAOUHSC_00304 mono-oxygenase over-expression could reflect the generation of ROS (Gaupp et al., 2012). In addition, the globin domain containing protein with nitric oxide dioxygenase activity (SAOUHSC_00204) under-expression—catalyzing nitric oxide (NO) to nitrate (NO³⁻) conversion—could cause an accumulation of reactive oxidant species such as NO. All these data could indicate the involvement of oxidative stress response enzymes in DAP-R responsible for cell survival because of an increased activity of ROS detoxification. Other different heat and cold shock stress response genes were found differentially expressed in DAP^R *S. aureus*. In particular, *dnaJ* under-expression could be related to a decreased production of the chaperone protein DnaJ, involved in the response to hyper-osmotic and heat shock stress, preventing or

restoring aggregation of denatured proteins. The use of different carbon sources in stress and nutrient limitation conditions were found, which could facilitate the survival of DAP^R strains in starvation and stress conditions via PHB-depolymerase family protein over-expression. As regards cell adhesion, our data showed a putative decreased adhesion ability of DAP^R versus DAP^S *S. aureus* via *sdrD* under-expression, although this was in contrast with previous findings (Song et al., 2013). SdrD, cell surface-associated calcium-binding protein, interacts with the extracellular matrix of higher eukaryotes.

In addition, different PCAs supported the correlation of the five distinctive functional DEG clusters with a daptomycin resistance or susceptible phenotype.

New consideration should be given for *mprF* and *dltA* expression. In the late post-exponential growth phase RNA-seq data, *mprF* expression trend showed increased transcripts in 1C versus 1A and decreased in 3B versus 3A, even though not statistically significant. Even *dltA* expression did not display statistically significant differential expression in any strain pairs; however, the expression trend displayed a decreased amount of transcripts in DAP^R strains in both strain pairs (data shown in files submitted to GEO). Based on these data, we hypothesize a growth-phase/strain-dependent *mprF* expression in the late growth phase transcriptomes correlating with the increased lysyl-phosphatidylglycerol synthesis in 1C versus 1A strain pair and a decrease in 3B versus 3A strain pair described in our previously published data on stationary cultures (Mishra et al., 2014). On the contrary, a growth phase-dependent *dltA* expression was observed in the late post-exponential growth phase in both strain pairs in agreement with other findings (Yang et al., 2009). Ultimately, although the bioinformatic cutoffs used to analyze these transcriptomic data are the standard ones, they could be too stringent both to simultaneously identify all RNAomic features characterizing DAP^R *S. aureus* and to fully reflect the complexity of this biological system.

CONCLUSION

Our data define the complex genomic and long-term transcriptomic fingerprinting and adaptations of DAP^R MRSA, providing new insights into their distinctive traits focusing on targets related to DAP-MOA. Briefly, we can summarize that DAP^R MRSA acquired diverse genomic and transcriptomic changes to cope with and preserve bacterial cell from DAP action. CM structural/functional proteins and transcriptional regulators emerged as the cell targets related to genomic changes gained under DAP pressure. Furthermore, DAP-MOA-related transcriptomic adaptations were found in CW and CM organization, that is, peptidoglycan biosynthesis, cell division, and CM structure, as well as in the autolytic system, in primary metabolism via a shift toward fermentation, and in CM-potential perturbation. Finally, accessory traits can also impact on DAP^R such as multilevel amplified stress responses mainly including oxidative stress response determining cell survival due to an increased ROS detoxification and the ABC transporters.

DATA AVAILABILITY STATEMENT

The datasets generated for this study can be found in this article/**Supplementary Material**. WGS raw reads were deposited at Sequence Read Archive (SRA) under study accession no. SRP166981 (BioProject: PRJNA498510). RNA-seq raw reads were deposited at the Gene Expression Omnibus database (GEO) under study accession no. GSE121797 (BioProject: PRJNA498510).

AUTHOR CONTRIBUTIONS

VC and SSte conceived and designed the study. VC, SStr, FL, ID, and AZ performed the transcriptomics, real-time qPCR, and bioinformatics. GP contributed to the bioinformatics analysis. All authors analyzed the data and contributed to the manuscript.

REFERENCES

- Allen, N. E., Hobbs, J. N., and Alborn, W. E. Jr. (1987). Inhibition of peptidoglycan biosynthesis in gram-positive bacteria by LY146032. *Antimicrob. Agents Chemother.* 31, 1093–1099. doi: 10.1128/AAC.31.7.1093
- Bartels, D. M., Petersen, A., Worning, P., Boye Nielsen, J., Larner-Svensson, H., and Krogh Johansen, H. (2014). Comparing whole-genome sequencing with Sanger sequencing for spa typing of methicillin-resistant *Staphylococcus aureus*. *J. Clin. Microbiol.* 52, 4305–4308. doi: 10.1128/JCM.01979-1914
- Bayer, A. S., Mishra, N. N., Chen, L., Kreiswirth, B. N., Rubio, A., and Yang, S. J. (2015). Frequency and distribution of single-nucleotide polymorphisms within mprF in methicillin-resistant *Staphylococcus aureus* clinical isolates and their role in cross-resistance to daptomycin and host defense antimicrobial peptides. *Antimicrob. Agents Chemother.* 59, 4930–4937. doi: 10.1128/AAC.00970-15
- Bayer, A. S., Schneider, T., and Sahl, H. G. (2013). Mechanisms of daptomycin resistance in *Staphylococcus aureus*: role of the cell membrane and cell wall. *Ann. N.Y. Acad. Sci.* 1277, 139–158. doi: 10.1111/j.1749-6632.2012.06819.x
- Boudjemaa, R., Cabriel, C., Dubois-Brissonnet, F., Bourg, N., Dupuis, G., Gruss, A., et al. (2018). Impact of bacterial membrane fatty acid composition on the failure of daptomycin to kill *Staphylococcus aureus*. *Antimicrob. Agents Chemother.* 62:e00023-18. doi: 10.1128/AAC.00023-18
- Britt, N. S., Patel, N., Shireman, T. I., El Atrouni, W. I., Horvat, R. T., and Steed, M. E. (2017). Relationship between vancomycin tolerance and clinical outcomes in *Staphylococcus aureus* bacteraemia. *J. Antimicrob. Chemother.* 72, 535–542. doi: 10.1093/jac/dkw453
- Bæk, K. T., Thøgersen, L., Mogensen, R. G., Møllergaard, M., Thomsen, L. E., Petersen, A., et al. (2015). Stepwise decrease in daptomycin susceptibility in clinical *Staphylococcus aureus* isolates associated with an initial mutation in rpoB and a compensatory inactivation of the clpX gene. *Antimicrob. Agents Chemother.* 59, 6983–6991. doi: 10.1128/AAC.01303-15
- Cafiso, V., Bertuccio, T., Purrello, S., Campanile, F., Mammìna, C., Sartor, A., et al. (2014). dltA over-expression: a strain-independent keystone of daptomycin resistance in methicillin-resistant *Staphylococcus aureus*. *Int. J. Antimicrob. Agents* 43, 26–31. doi: 10.1016/j.ijantimicag.2013.10.001
- Cafiso, V., Bertuccio, T., Spina, D., Purrello, S., Campanile, F., Di Pietro, C., et al. (2012). Modulating activity of vancomycin and daptomycin on the expression of autolysis cell-wall turnover and membrane charge genes in hVISA and VISA strains. *PLoS One* 7:e29573. doi: 10.1371/journal.pone.0029573
- Cafiso, V., Stracquadanio, S., Lo Verde, F., Gabriele, G., Mezzatesta, M. L., Caio, C., et al. (2019). Colistin resistant *A. baumannii*: genomic and transcriptomic traits acquired under colistin therapy. *Front. Microbiol.* 7:3195. doi: 10.3389/fmicb.2018.03195
- Carattoli, A., Zankari, E., Garcia-Fernandez, A., Voldby Larsen, M., Lund, O., and Villa, L. (2014). In silico detection and typing of plasmids using plasmidfinder

FUNDING

This study was supported by a research grant PRIN 2017SFBFER from MIUR Italy.

ACKNOWLEDGMENTS

We wish to thank the Scientific Bureau of the University of Catania (Italy) for language support services.

SUPPLEMENTARY MATERIAL

The Supplementary Material for this article can be found online at: <https://www.frontiersin.org/articles/10.3389/fmicb.2020.01893/full#supplementary-material>

- and plasmid multilocus sequence typing. *Antimicrob. Agents Chemother.* 58, 3895–3903. doi: 10.1128/AAC.02412-14
- Cingolani, P., Platts, A., Wang le, L., Coon, M., Nguyen, T., Wang, L., et al. (2012). A program for annotating and predicting the effects of single nucleotide polymorphisms, SnpEff: SNPs in the genome of *Drosophila melanogaster* strain w1118; iso-2; iso-3. *Fly* 6, 80–92. doi: 10.4161/fly.19695
- Cirz, R. T., Jones, M. B., Gingles, N. A., Minogue, T. D., Jarrahi, B., Peterson, S. N., et al. (2007). Complete and SOS-mediated response of *Staphylococcus aureus* to the antibiotic ciprofloxacin. *J. Bacteriol.* 189, 531–539. doi: 10.1128/JB.01464-06
- Coe, K. A., Lee, W., Stone, M. C., Komazin-Meredith, G., Meredith, T. C., Grad, Y. H., et al. (2019). Multi-strain Tn-Seq reveals common daptomycin resistance determinants in *Staphylococcus aureus*. *PLoS Pathog.* 15:e1007862. doi: 10.1371/journal.ppat.1007862
- Cui, L., Isii, T., Fukuda, M., Ochiai, T., Neoh, H. M., Camargo, I. L., et al. (2010). An RpoB mutation confers dual heteroresistance to daptomycin and vancomycin in *Staphylococcus aureus*. *Antimicrob. Agents Chemother.* 54, 5222–5233. doi: 10.1128/AAC.00437-10
- Delauné, A., Dubrac, S., Blanchet, C., Poupel, O., Mäder, U., Hiron, A., et al. (2012). The WalKR system controls major staphylococcal virulence genes and is involved in triggering the host inflammatory response. *Infect. Immun.* 80, 3438–3453. doi: 10.1128/IAI.00195-12
- Dubrac, S., Boneca, I. G., Poupel, O., and Msadek, T. (2007). New insights into the WalK/WalR (YycG/YycF) essential signal transduction pathway reveal a major role in controlling cell wall metabolism and biofilm formation in *Staphylococcus aureus*. *J. Bacteriol.* 189, 8257–8269. doi: 10.1128/JB.00645-07
- Dubrac, S., and Msadek, T. (2004). Identification of genes controlled by the essential YycG/YycF two-component system of *Staphylococcus aureus*. *J. Bacteriol.* 186, 1175–1181. doi: 10.1128/JB.186.4.1175-1181.2004
- Ernst, C. M., and Peschel, A. (2019). MprF-mediated daptomycin resistance. *Int. J. Med. Microbiol.* 309, 359–363. doi: 10.1016/j.ijmm.2019.05.010
- Ernst, C. M., Slavetinsky, C. J., Kuhn, S., Hauser, J. N., Nega, M., Mishra, N. N., et al. (2018). Gain-of-function mutations in the phospholipid flippase MprF confer specific daptomycin resistance. *mBio* 9:e01659-18. doi: 10.1128/mBio.01659-18
- Fischer, A., Yang, S. J., Bayer, A. S., Vaezzadeh, A. R., Herzig, S., Stenz, L., et al. (2011). Daptomycin resistance mechanisms in clinically derived *Staphylococcus aureus* strains assessed by a combined transcriptomics and proteomics approach. *J. Antimicrob. Chemother.* 66, 1696–1711. doi: 10.1093/jac/dkr195
- Fleige, S., and Pfaffl, M. W. (2006). RNA integrity and the effect on the real-time qRT-PCR performance. *Mol. Aspects Med.* 27, 126–139. doi: 10.1016/j.mam.2005.12.003
- Friedman, L., Alder, J. D., and Silverman, J. A. (2006). Genetic changes that correlate with reduced susceptibility to daptomycin in *Staphylococcus aureus*. *Antimicrob. Agents Chemother.* 50, 2137–2145. doi: 10.1128/AAC.00039-06

- Fukushima, T., Furihata, I., Emmins, R., Daniel, R. A., Hoch, J. A., and Szurmant, H. (2011). A role for the essential YycG sensor histidine kinase in sensing cell division. *Mol. Microbiol.* 79, 503–522. doi: 10.1111/j.1365-2958.2010.07464.x
- Fukushima, T., Szurmant, H., Kim, E. J., Perego, M., and Hoch, J. A. (2008). A sensor histidine kinase co-ordinates cell wall architecture with cell division in *Bacillus subtilis*. *Mol. Microbiol.* 69, 621–632. doi: 10.1111/j.1365-2958.2008.06308.x
- Gaupp, R., Ledala, N., and Somerville, G. A. (2012). Staphylococcal response to oxidative stress. *Front. Cell. Infect. Microbiol.* 2:33. doi: 10.1371/journal.pone.0058469
- Gaupp, R., Lei, S., Reed, J. M., Peisker, H., Boyle-Vavra, S., Bayer, A. S., et al. (2015). *Staphylococcus aureus* metabolic adaptations during the transition from a daptomycin susceptibility phenotype to a daptomycin non susceptibility phenotype. *Antimicrob. Agents Chemother.* 59, 4226–4238. doi: 10.1128/AAC.00160-15
- Gómez Casanova, N., Siller Ruiz, M., and Muñoz Bellido, J. L. (2017). Mechanisms of resistance to daptomycin in *Staphylococcus aureus*. *Rev. Esp. Quimioter.* 30, 391–396.
- Groicher, K. H., Firek, B. A., Fujimoto, D. F., and Bayles, K. W. (2000). The *Staphylococcus aureus* lrgAB operon modulates murein hydrolase activity and penicillin tolerance. *J. Bacteriol.* 182, 1794–1801. doi: 10.1128/JB.182.7.1794-1801.2000
- Howden, B. P., McEvoy, C. R., Allen, D. L., Chua, K., Gao, W., Harrison, P. F., et al. (2011). Evolution of multidrug resistance during *Staphylococcus aureus* infection involves mutation of the essential two component regulator WalKR. *PLoS Pathog.* 7:e1002359. doi: 10.1371/journal.ppat.1002359
- Huang, D. W., Sherman, B. T., and Lempicki, R. A. (2009a). Bioinformatics enrichment tools: paths toward the comprehensive functional analysis of large gene lists. *Nucleic Acids Res.* 37, 1–13. doi: 10.1093/nar/gkn923
- Huang, D. W., Sherman, B. T., and Lempicki, R. A. (2009b). Systematic and integrative analysis of large gene lists using DAVID bioinformatics resources. *Nat. Protoc.* 4, 44–57. doi: 10.1038/nprot.2008.211
- Joensen, K. G., Scheutz, F., Lund, O., Hasman, H., Kaas, R. S., Nielsen, E. M., et al. (2014). Real-time whole-genome sequencing for routine typing, surveillance, and outbreak detection of verotoxigenic *Escherichia Coli*. *J. Clin. Microbiol.* 52, 1501–1510. doi: 10.1128/JCM.03617-3613
- Jones, T., Yeaman, M. R., Sakoulas, G., Yang, S., Proctor, R. A., Sahl, H. G., et al. (2008). Failures in clinical treatment of *Staphylococcus aureus* infection with daptomycin are associated with alterations in surface charge, membrane phospholipid asymmetry, and drug binding. *Antimicrob. Agents Chemother.* 52, 269–278. doi: 10.1128/AAC.00719-07
- Jordan, S., Junker, A., Helmann, J. D., and Mascher, T. (2006). Regulation of LiaRS-dependent gene expression in *Bacillus subtilis*: identification of inhibitor proteins, regulator binding sites, and target genes of a conserved cell envelope stress-sensing two-component system. *J. Bacteriol.* 188, 5153–5166. doi: 10.1128/JB.00310-06
- Kilele, E., Pokorny, A., Yeaman, M. R., and Bayer, A. S. (2010). Lysyl-phosphatidylglycerol attenuates membrane perturbation rather than surface association of the cationic antimicrobial peptide 6W-RP-1 in a model membrane system: implications for daptomycin resistance. *Antimicrob. Agents Chemother.* 54, 4476–4479. doi: 10.1128/AAC.00191-10
- Kolter, R., Siegle, D. A., and Tormo, A. (1993). The stationary phase of the bacterial life cycle. *Annu. Rev. Microbiol.* 47, 855–874. doi: 10.1146/annurev.mi.47.100193.004231
- Kuroda, M., Kuroda, H., Oshima, T., Takeuchi, F., Mori, H., and Hiramatsu, K. (2003). Two-component system VraSR positively modulates the regulation of cell-wall biosynthesis pathway in *Staphylococcus aureus*. *Mol. Microbiol.* 49, 807–821. doi: 10.1046/j.1365-2958.2003.03599.x
- Larsen, M. V., Cosentino, S., Rasmussen, S., Friis, C., Hasman, H., and Lykke Marvig, R. (2012). Multilocus sequence typing of total-genome-sequenced bacteria. *J. Clin. Microbiol.* 50, 1355–1361. doi: 10.1128/JCM.06094-6011
- Lithgow, J. K., Ingham, E. I., and Foster, S. (2004). Role of the hprT-ftsH locus in *Staphylococcus aureus*. *Microbiology* 150, 373–381. doi: 10.1099/mic.0.26674-0
- Mascio, C. T., Alder, J. D., and Silverman, J. A. (2007). Bactericidal action of daptomycin against stationary-phase and nondividing *Staphylococcus aureus* cells. *Antimicrob. Agents Chemother.* 51, 4255–4260. doi: 10.1128/AAC.00824-07
- McCall, I. C., Shah, N., Govindan, A., Baquero, F., and Levin, B. R. (2019). Antibiotic killing of diversely generated populations of nonreplicating bacteria. *Antimicrob. Agents Chemother.* 63:e02360-18. doi: 10.1128/AAC.02360-18
- McClure, R., Balasubramanian, D., Sun, Y., Bobrovskyy, M., Sumby, P., Genco, C. A., et al. (2013). Computational analysis of bacterial RNA-seq data. *Nucleic Acids Res.* 41:e140. doi: 10.1093/nar/gkt444
- Mehta, S., Cuirolo, A. X., Plata, K. B., Riosa, S., Silverman, J. A., Rubio, A., et al. (2012). VraSR two-component regulatory system contributes to mprF-mediated decreased susceptibility to daptomycin in vivo-selected clinical strains of methicillin-resistant *Staphylococcus aureus*. *Antimicrob. Agents Chemother.* 56, 92–102. doi: 10.1128/AAC.00432-10
- Mesak, L. R., Miao, V., and Davies, J. (2008). Effects of subinhibitory concentrations of antibiotics on SOS and DNA repair gene expression in *Staphylococcus aureus*. *Antimicrob. Agents Chemother.* 9, 3394–3397. doi: 10.1128/AAC.01599-07
- Miller, W. R., Munita, J. M., and Arias, C. A. (2016). Mechanism of action and resistance to daptomycin in *Staphylococcus aureus* and Enterococci. *Cold Spring Harb. Perspect. Med.* 6:a026997. doi: 10.1101/cshperspect.a026997
- Mishra, N. N., Bayer, A. S., Weidenmaier, C., Grau, T., Wanner, S., Stefani, S., et al. (2014). Phenotypic and genotypic characterization of daptomycin-resistant methicillin-resistant *Staphylococcus aureus* strains: relative roles of *mprF* and *dlt* operons. *PLoS One* 9:e107426. doi: 10.1371/journal.pone.0107426
- Mishra, N. N., McKinnell, J., Yeaman, M. R., Rubio, A., Nast, C. C., Chen, L., et al. (2011). In vitro cross-resistance to daptomycin and host defense cationic antimicrobial peptides in clinical methicillin-resistant *Staphylococcus aureus* isolates. *Antimicrob. Agents Chemother.* 55, 4012–4018. doi: 10.1128/AAC.00223-11
- Muthaiyan, A., Silverman, J. A., Jayaswal, R. K., and Wilkinson, B. J. (2008). Transcriptional profiling reveals that daptomycin induces the *Staphylococcus aureus* cell wall stress stimulon and genes responsive to membrane depolarization. *Antimicrob. Agents Chemother.* 52, 980–990. doi: 10.1128/AAC.01121-07
- Mwangi, M. M., Wu, S. W., Zhou, Y., Sieradzki, K., de Lencastre, H., Richardson, P., et al. (2007). Tracking the in vivo evolution of multidrug resistance in *Staphylococcus aureus* by whole-genome sequencing. *Proc. Natl. Acad. Sci. U.S.A.* 104, 9451–9456. doi: 10.1073/pnas.0609839104
- Patton, T. G., Yang, S. J., and Bayles, K. W. (2006). The role of proton motive force in expression of the *Staphylococcus aureus* cid and lrg operons. *Mol. Microbiol.* 59, 1395–1404. doi: 10.1111/j.1365-2958.2006.05034.x
- Pereira, M. A., Imada, E. L., and Muniz Guedes, R. L. (2017). RNA-seq: applications and best practices,” in *Applications of RNA-Seq and Omics Strategies: From Microorganisms to Human Health*, eds F. Marchi, P. Cirillo, and E. C. Mateo (Norderstedt: BoD). doi: 10.5772/intechopen.69250
- Pfaffl, M. W., Horgan, G. W., and Dempfle, L. (2002). Relative expression software tool (REST) for group wise comparison and statistical analysis of relative expression results in real-time PCR. *Nucleic Acids Res.* 30:e36. doi: 10.1093/nar/30.9.e36
- Pogliano, J., Pogliano, N., and Silverman, J. A. (2012). Daptomycin-mediated reorganization of membrane architecture causes mislocalization of essential cell division proteins. *J. Bacteriol.* 194, 4494–4504. doi: 10.1128/JB.00011-12
- Reed, J. M., Gardner, S. G., Mishra, N. N., Bayer, A. S., and Somerville, G. A. (2019). Metabolic interventions for the prevention and treatment of daptomycin non-susceptibility in *Staphylococcus aureus*. *J. Antimicrob. Chemother.* 74, 2274–2283. doi: 10.1093/jac/dkz194
- Rubio, A., Conrad, M., Haselbeck, R. J., Kedar, G. C., Brown-Driver, V., Finn, J., et al. (2011). Regulation of mprF by antisense RNA restores daptomycin susceptibility to daptomycin-resistant isolates of *Staphylococcus aureus*. *Antimicrob. Agents Chemother.* 55, 364–367. doi: 10.1128/AAC.00429-10
- Sabat, A. J., Tinelli, M., Grundmann, H., Akkerboom, V., Monaco, M., Del Grosso, M., et al. (2018). Daptomycin resistant *Staphylococcus aureus* clinical strain with novel non-synonymous mutations in the mprF and vraS genes: a new insight into daptomycin resistance. *Front. Microbiol.* 9:2705. doi: 10.3389/fmicb.2018.02705
- Shoji, M., Cui, L., Iizuka, R., Komoto, A., Neoh, H. M., Watanabe, Y., et al. (2011). walK and clpP mutations confer reduced vancomycin susceptibility in *Staphylococcus aureus*. *Antimicrob. Agents Chemother.* 55, 3870–3881. doi: 10.1128/AAC.01563-10

- Sobral, R. G., Ludovice, A. M., de Lencastre, H., and Tomasz, A. (2006). Role of *murF* in cell wall biosynthesis: isolation and characterization of a *murF* conditional mutant of *Staphylococcus aureus*. *J. Bacteriol.* 188, 2543–2553. doi: 10.1128/JB.188.7.2543-2553.2006
- Song, Y., Rubio, A., Jayaswal, R. K., Silverman, J. A., and Wilkinson, B. J. (2013). Additional routes to *Staphylococcus aureus* daptomycin resistance as revealed by comparative genome sequencing, transcriptional profiling, and phenotypic studies. *PLoS One* 8:e58469. doi: 10.1371/journal.pone.0058469
- Stefani, S., Campanile, F., Santagati, M., Mezzatesta, M. L., Cafiso, V., and Pacini, G. (2015). Insights and clinical perspectives of daptomycin resistance in *Staphylococcus aureus*: a review of the available evidence. *Int. J. Antimicrob. Agents* 46, 278–289. doi: 10.1016/j.ijantimicag.2015.05.008
- Taglialegna, A., Varela, M. C., Rosato, R. R., and Rosato, A. E. (2019). VraSR and virulence trait modulation during daptomycin resistance in methicillin-resistant *Staphylococcus aureus* infection. *mSphere* 4:e00557-18. doi: 10.1128/mSphere.00557-18
- Taylor, S. D., and Palmer, M. (2016). The action mechanism of daptomycin. *Bioorg. Med. Chem.* 24, 6253–6268. doi: 10.1016/j.bmc.2016.05.052
- Tjaden, B. (2015). De novo assembly of bacterial transcriptomes from RNA-seq data. *Genome Biol.* 16:1. doi: 10.1186/s13059-014-0572-2
- Türk, M., and Bierbaum, G. (2012). Purification and Activity Testing of the Full-Length YycFGHI Proteins of *Staphylococcus aureus*. *PLoS One* 7:e30403. doi: 10.1371/journal.pone.0030403
- Utaida, S., Dunman, P. M., Macapagal, D., Murphy, E., Projan, S. J., Singh, V. K., et al. (2003). Genome-wide transcriptional profiling of the response of *Staphylococcus aureus* to cell-wall-active antibiotics reveals a cell-wall-stress stimulon. *Microbiology* 149, 2719–2732. doi: 10.1099/mic.0.26426-0
- Yang, S. J., Kreiswirth, B. N., Sakoulas, G., Yeaman, M. R., Xiong, Y. Q., Sawa, A., et al. (2009). Enhanced expression of *dltABCD* is associated with the development of daptomycin non susceptibility in a clinical endocarditis isolate of *Staphylococcus aureus*. *J. Infect. Dis.* 200, 1916–1920. doi: 10.1086/648473
- Yang, S. J., Xiong, Y. Q., Yeaman, M. R., Bayles, K. W., Abdelhady, W., and Bayer, A. S. (2013). Role of the *LytSR* two-component regulatory system in adaptation to cationic antimicrobial peptides in *Staphylococcus aureus*. *Antimicrob. Agents Chemother.* 57, 3875–3882. doi: 10.1128/AAC.00412-13
- Yoon, Y. K., Park, D. W., Sohn, J. W., Kim, H. Y., Kim, Y. S., Lee, C. S., et al. (2016). Effects of inappropriate empirical antibiotic therapy on mortality in patients with healthcare-associated methicillin-resistant *Staphylococcus aureus* bacteremia: a propensity-matched analysis. *BMC Infect. Dis.* 15:331. doi: 10.1186/s12879-016-1650-8
- Zankari, E., Hasman, H., Cosentino, S., Vestergaard, M., Rasmussen, S., Lund, O., et al. (2012). Identification of acquired antimicrobial resistance genes. *J. Antimicrob. Chemother.* 67, 2640–2644. doi: 10.1093/jac/dks261
- Zhang, T., Muraih, J. K., Tishbi, N., Herskowitz, J., Victor, R. L., Silverman, J., et al. (2014). Cardiolipin prevents membrane translocation and permeabilization by daptomycin. *J. Biol. Chem.* 289, 11584–11599. doi: 10.1074/jbc.M114.554444

Conflict of Interest: The authors declare that the research was conducted in the absence of any commercial or financial relationships that could be construed as a potential conflict of interest.

Copyright © 2020 Cafiso, Stracquadanio, Lo Verde, De Guidi, Zega, Pigola and Stefani. This is an open-access article distributed under the terms of the Creative Commons Attribution License (CC BY). The use, distribution or reproduction in other forums is permitted, provided the original author(s) and the copyright owner(s) are credited and that the original publication in this journal is cited, in accordance with accepted academic practice. No use, distribution or reproduction is permitted which does not comply with these terms.



Expression Profile of Multidrug Resistance Efflux Pumps During Intracellular Life of Adherent-Invasive *Escherichia coli* Strain LF82

Giulia Fanelli, Martina Pasqua, Bianca Colonna, Gianni Prosseda* and Milena Grossi*

Istituto Pasteur Italia, Dipartimento di Biologia e Biotecnologie "Charles Darwin", Sapienza-Università di Roma, Rome, Italy

OPEN ACCESS

Edited by:

Pietro Alifano,
University of Salento, Italy

Reviewed by:

Jakob Møller-Jensen,
University of Southern Denmark,
Denmark

Sébastien Coyne,
Evotec, France

*Correspondence:

Gianni Prosseda
gianni.prosseda@uniroma1.it
Milena Grossi
milena.grossi@uniroma1.it

Specialty section:

This article was submitted to
Antimicrobials, Resistance and
Chemotherapy,
a section of the journal
Frontiers in Microbiology

Received: 31 March 2020

Accepted: 22 July 2020

Published: 17 August 2020

Citation:

Fanelli G, Pasqua M, Colonna B,
Prosseda G and Grossi M (2020)
Expression Profile of Multidrug
Resistance Efflux Pumps During
Intracellular Life of Adherent-Invasive
Escherichia coli Strain LF82.
Front. Microbiol. 11:1935.
doi: 10.3389/fmicb.2020.01935

Efflux pumps (EPs) are present in all living cells and represent a large and important group of transmembrane proteins involved in transport processes. In bacteria, multidrug resistance efflux pumps (MDR EPs) confer resistance to antibiotics at different levels and are deeply implicated in the fast and dramatic emergence of antibiotic resistance. Recently, several reports have outlined the great versatility of MDR EPs in exporting a large variety of compounds other than antibiotics, thus promoting bacterial adaptation to a wide range of habitats. In several bacterial pathogens, MDR EPs contribute to increase the virulence potential and are directly involved in the crosstalk with host cells. In this work, we have investigated the possible role of MDR EPs in the infectious process of the adherent-invasive *Escherichia coli* (AIEC), a group of pathogenic *E. coli* that colonize the ileal mucosa of Crohn disease (CD) patients causing a strong intestinal inflammation. The results we have obtained indicate that, with the exception of *mdtM*, all MDR-EPs encoding genes present in *E. coli* K12 are conserved in the AIEC prototype strain LF82. The analysis of MDR EP expression during LF82 infection of macrophages and epithelial cells reveals that their transcription is highly modulated during the bacterial intracellular life. Notably, some EP genes are regulated in a cell-type specific manner, strongly suggesting that their function is required for LF82 successful infection. AIEC are able to adhere to and invade intestinal epithelial cells and, importantly, to survive and multiply within macrophages. Thus, we further investigated the role of EPs specifically induced by macrophage environment. We present evidence indicating that deletion of *mdtEF* genes, encoding an MDR EP belonging to the resistance nodulation division (RND) family, significantly impairs survival of LF82 in macrophages and that the wild type phenotype can be restored by trans-complementation with functional MdtEF pump. Altogether, our results indicate a strong involvement of MDR EPs in host pathogen interaction also in AIEC and highlight the contribution of MdtEF to the fitness of LF82 in the macrophage environment.

Keywords: efflux pumps, adherent invasive *Escherichia coli*, *Escherichia coli* pathogens, bacteria-host interactions, bacterial transmembrane complexes

INTRODUCTION

Efflux pumps (EPs) are membrane protein complexes found in all living organisms. In many bacteria, including pathogens, EPs mediate the efflux of one or more antibiotics, thus strongly contributing to the development of multidrug resistance (MDR; Li et al., 2015; Du et al., 2018). EPs are usually present in the inner membrane as single-component transporters. In Gram-negative bacteria, they can form a tripartite structure spanning both membranes and consisting of an inner membrane protein, a periplasmic adaptor protein and an outer membrane protein (Hinchliffe et al., 2013). On the basis of sequence similarity, transport function and energy source bacterial MDR EPs have been grouped into six families: ATP binding cassette (ABC), resistance nodulation division (RND), major facilitator superfamily (MFS), multidrug and toxic compound extrusion (MATE), small multidrug resistance (SMR), and proteobacterial antimicrobial compound efflux (PACE; Du et al., 2018). Recently, an additional family has been identified: the p-Aminobenzoyl-glutamate transporter (AbgT) family (Delmar and Yu, 2016). EPs use the proton motive force of the inner membrane as energy source. ABC EPs are an exception as they rely on ATP hydrolysis (Li et al., 2015; Du et al., 2018).

Multidrug resistance efflux pumps (MDR EPs) have been thoroughly studied because of their clinical relevance in bacterial infections (Li et al., 2015; Du et al., 2018). In recent years, it has become clear that the importance of MDR EPs goes beyond the efflux of antibiotics (Piddock, 2006; Alvarez-Ortega et al., 2013; Alcalde-Rico et al., 2016; Pasqua et al., 2019b) and involves several cellular functions. In particular, due to their ability to extrude a variety of different compounds, MDR EPs play a relevant role in the interactions of bacteria with plant and animal cells, in the maintenance of cellular homeostasis, in the detoxification of metabolic intermediates, and in cell-to-cell communication. Moreover, MDR EPs actively contribute to virulence of bacterial pathogens in plant and animals, including humans (Piddock, 2006; Alcalde-Rico et al., 2016). In opportunistic pathogens associated with cystic fibrosis, e.g., *Pseudomonas aeruginosa*, *Acinetobacter baumannii*, and *Stenotrophomonas maltophilia*, MDR EPs contribute to the export of quorum sensing molecules and favor the formation of biofilms (Alav et al., 2018; Pasqua et al., 2019b).

In some enteropathogens, MDR EPs, besides contributing to resistance to bile salts (Alvarez-Ortega et al., 2013; Leuzzi et al., 2015; Urdaneta and Casadesús, 2018), play a relevant role in the intracellular life of the bacterium. For example, in *Salmonella* Typhimurium MDR EPs are required for an efficient invasion and survival within macrophages and intestinal cells (Buckley et al., 2006; Bogomolnaya et al., 2013) while in *Listeria monocytogenes* they favor bacterial intracellular spread and

tissue invasion through their capability to activate IFN- β production in infected mouse macrophages (Crimmins et al., 2008). Furthermore, it has been shown that, in *Staphylococcus aureus*, EPs contribute to the invasion of human epithelia and facilitate the persistence within staphylococcal-induced abscesses (Truong-Bolduc et al., 2015) and that, in *Mycobacterium tuberculosis*, an increased expression of MDR EP genes promotes bacterial replication in macrophages and survival in mouse models (Bianco et al., 2011).

In a recent study (Pasqua et al., 2019a), we were able to demonstrate that the MDR EmrKY EP significantly contributes to the survival of *Shigella flexneri* in macrophages. *S. flexneri* belongs to the *Escherichia coli* species and its invasive process is characterized by the capability to invade macrophages, where it multiplies and induces cell death (Schroeder and Hilbi, 2008; Pasqua et al., 2017). The bacteria released from dying macrophages invade neighboring enterocytes, where they rapidly lyse the vacuole and actively replicate. Invasion of macrophages and epithelial cells is a pathogenicity step also found in another group of enteropathogenic *E. coli*, the adherent and invasive *E. coli* (AIEC; Darfeuille-Michaud, 2002; Croxen et al., 2013). AIEC represent a pathotype associated with Crohn disease (CD), an inflammatory syndrome affecting the intestinal tract (Darfeuille-Michaud, 2002; Palmela et al., 2018; Shaler et al., 2019). AIEC strains do not express virulence factors typically found in other pathogenic *E. coli* and cluster within the *E. coli* B2 phylogenetic group whose members are mostly extraintestinal *E. coli* (Miquel et al., 2010). Despite the capability to invade the same host cells, AIEC and *Shigella* exhibit different intracellular survival strategies. AIEC replicate extensively in large vacuoles within macrophages without inducing host cell death (Glasser et al., 2001) and stimulate the production of large amount of TNF- α , leading to chronic inflammation. Moreover, in AIEC strains, the invasion of human intestinal epithelia occurs *via* a macropinocytosis-like process and involves the interaction of bacterial Type 1 pili with the CEACAM6 glycoprotein receptor, which is abnormally expressed in CD patients (Barnich et al., 2007). As opposed to *Shigella*, in epithelial cells, AIEC strains do not lyse the vacuole soon after invasion and replicate within late endosomes to escape cell autophagy (Lapaquette et al., 2010).

The different behavior of AIEC and *Shigella* within host cells has prompted us to investigate the expression of the MDR EPs of clinical strain LF82, considered as an AIEC prototype (Boudeau et al., 1999), during the invasion of epithelial cells and macrophages. The results we have obtained indicate that within these environments bacteria display a strong induction of several EPs, some of which are host-cell specific. As the extensive replication of LF82 in macrophage phagolysosomes is a critical step for the intracellular survival of the pathogen (Glasser et al., 2001; Demarre et al., 2019), we have focused on EPs highly expressed only within macrophages and have found that MdtEF, a MDR EP belonging to the RND family, significantly contributes to bacterial fitness in this environment.

Abbreviations: ABC, ATP binding cassette; AbgT, p-aminobenzoyl-glutamate transporter; AIEC, Adherent invasive *E. coli*; CD, Crohn disease; DAPI, 4',6-diamidino-2-phenylindole; EP, Efflux pump; MDR, Multidrug resistance; MFS, Major facilitator superfamily; MATE, Multidrug and toxic compound efflux; PACE, Proteobacterial antimicrobial compound efflux; p.i., Post infection; PI, Propidium iodide; RND, Resistance nodulation division; TNF, Tumor necrosis factor.

MATERIALS AND METHODS

Bacterial Strains, Plasmids, and Growth Conditions

Bacterial strains and plasmids used in this study are listed in **Supplementary Table S1**. *E. coli* LF82 is an AIEC strain isolated from a chronic ileal lesion of a CD patient (Boudeau et al., 1999). The LF82 $\Delta mdtEF$ strain, containing a deletion of the *mdtEF* genes, and MG1655 $\Delta acrAB$, deleted of entire *acrAB* operon, have been constructed using the one-step method of gene inactivation (Datsenko and Wanner, 2000) by transforming LF82 pKD46 or MG1655 pKD46 with amplicon obtained using pKD13 as template and the oligo pairs EFF/EFR for *mdtEF* deletion and ABF-ABR for *acrAB* deletion (**Supplementary Tables S1, S2**).

Plasmid pGEF3 was obtained by cloning the *mdtEF* genes into pGIP7, a pACYC184 expression vector carrying the *lacI^q* gene and *ptac* promoter (Falconi et al., 2001; **Supplementary Table S1**). The *mdtEF* amplicon obtained using MG1655 as template and oligo pairs pACmdtEFF/pACmdtEFR (**Supplementary Table S2**) was digested with *Bam*HI and cloned into pGIP7 downstream the *ptac* promoter. Plasmid pGEF3 and deletion of *mdtEF* and *acrAB* genes have been verified by DNA sequencing (Biofab, Rome). Bacterial cells were grown aerobically in Luria-Bertani (LB) medium at 37°C. Congo Red at 0.01% was added to Trypticase soy agar to monitor the LF82 Congo Red phenotype. Antibiotics, and chemicals were used at the following concentrations: ampicillin 30 µg/ml, chloramphenicol 25 µg/ml, erythromycin 12.5 µg/ml or 25 µg/ml, kanamycin 30 µg/ml, and gentamicin 10 µg/ml or 100 µg/ml for infection procedures.

General Procedures

DNA purification, restriction, cloning, plasmid transformation, and gel electrophoresis were carried out as previously described (De Carolis et al., 2011; Leuzzi et al., 2017). The oligonucleotide sequences, designed on the basis of the LF82 genome (Miquel et al., 2010) or MG1655 genome, are reported in **Supplementary Table S2**. PCR reactions were routinely performed using the DreamTaq DNA polymerase (Thermo Fisher Scientific) or, when required a higher fidelity of PCR product, the Ex taq DNA polymerase (Takara). DNA sequence data were compared to known nucleotide and protein sequences using the BLAST server (National Center for Biotechnology Information). Analysis of distribution of MDR EPs in the genome of other AIEC strains was performed using the EcoCyc database (Keseler et al., 2017).

Cell Cultures and Infections

Both the human promonocytic U937 and the human monocytic THP-1 cell lines were grown in Roswell Park Memorial Institute (RPMI) 1640 (Gibco) medium containing 10% heat-inactivated fetal bovine serum (FBS; Euroclone), 0.05 IU/ml penicillin, and 0.05 IU/ml streptomycin (PS), referred to as RF10, at 37°C in a humidified 5% CO₂ atmosphere. Before bacterial

infection, both U937 and THP-1 cells were differentiated into macrophages. U937 cells were seeded in 6-well tissue culture plates (Falcon), at a density of 1.5×10^6 cells/well, in RF10 supplemented with 80 nM phorbol myristate acetate (PMA; Sigma). After 2 days, PMA containing medium was removed and cells were left for further 4 days in RF10. Two hours before bacterial infection, RF10 was replaced with fresh RPMI. THP-1 monocytes were seeded in 6-well tissue culture plates (Falcon) at a density of 1.0×10^6 cells/well in growth medium supplemented with 50 nM PMA. After 48 h, PMA containing medium was removed and cells left for further 24 h in RF10. Two hours before bacterial addition, RF10 was replaced with fresh RPMI. The human epithelial colorectal adenocarcinoma Caco-2 cell line was grown in Dulbecco minimal essential medium (DMEM; Gibco) containing 10% FBS and PS, referred to as DF10, at 37°C in a humidified 5% CO₂ atmosphere. For bacterial infection, cells were seeded in 6-well tissue culture plates (Falcon) at a density of 4.0×10^5 cells/well in growth medium. After 48 h, cells were serum-starved over-night in DMEM supplemented with 0.5% FBS and PS (DF0.5). Two hours before bacterial infection, DF0.5 was replaced with fresh DMEM without serum and antibiotics. Bacteria were added to the cell cultures at a multiplicity of infection of 100. After addition of bacteria, plates were centrifuged for 15 min at $750 \times g$ and incubated 30 (U937 and THP1) or 45 min (Caco-2) at 37°C under 5% CO₂ atmosphere to allow bacterial entry. Then extracellular bacteria were removed by three extensive washing with phosphate-buffered saline (PBS). This point was taken as time zero (T0). Fresh medium (RPMI or DMEM) containing gentamicin (100 µg/ml) was added to the other plates to kill extracellular bacteria, and infected cells were incubated at 37°C up to 4 or 5 h.

RNA Isolation and Quantitative Real Time PCR

To monitor gene expression during host cell infection, one 6-well tissue culture plate was considered for each time point to maximize the yield of intracellular bacteria. Intracellular LF82 bacteria were recovered by lysing infected cells with 1% Triton X-100 (Sigma) for 5 min. Bacteria were diluted 1:2 with PBS to decrease Triton concentration before proceeding with RNA extraction (Di Martino et al., 2016). Two micrograms of total RNA were treated with DNase I and retro-transcribed using the High Capacity cDNA Reverse Transcription Kit (Thermo Fischer Scientific). qRT-PCR was performed in a 30 µl reaction mix containing 3 µl cDNA using Power SYBR Green PCR Master Mix (Thermo Fischer Scientific) on a 7300 Real-Time PCR System (Thermo Fischer Scientific). At least three wells were run for each sample. Relative quantification was performed using the comparative cycle threshold ($2^{-\Delta\Delta C_t}$) method (Livak and Schmittgen, 2001). Primers for the *nusA* transcript (endogenous control) and target transcripts were designed with the aid of the Primer Express software v2.0 (Thermo Fischer Scientific) and experimentally validated for suitability for the $2^{-\Delta\Delta C_t}$ method. All primers used are listed in **Supplementary Table S2**. In the case of EP systems

consisting of more than one protein (AcrAB, EmrAB, EmrKY, MacAB, MdtJI, AcrEF, and MdtABC) encoded by genes clustered in a single operon, we monitored the transcription of the promoter-proximal gene.

Live and Dead Assay

Intracellular dead bacteria were evaluated by staining the entire population with 4',6-diamidino-2-phenylindole (DAPI; Sigma) and labeling dead cells with Propidium iodide (PI; Sigma). At the indicated time points, infected macrophages were lysed by adding 1% Triton X-100 in 1× PBS. The cell lysate was pelleted at 13,000 rpm for 5 min. The pellet containing intracellular bacteria was washed once in 1× PBS and suspended in 1x PBS containing 10 µg/ml DAPI and 15 µM PI. Samples were incubated 20 min at room temperature in the dark. Bacteria were centrifuged at 13,000 rpm for 5 min and washed once with 1× PBS. Pellet was resuspended in 20 µl 1X PBS containing 50% glycerol; 5 µl of the stained bacteria were added to the glass slide and overlaid with the coverslip for immediate observation and counting.

Statistical Analyses

The statistical differences of the EP gene expression level between intracellular bacteria and bacteria grown in RPMI or DMEM were determined using Microsoft Excel by calculating the values of *p* derived from a one-way ANOVA. The statistical difference between the percentage of dead intracellular LF82 wt strain and the percentage of dead intracellular LF82 derivatives at each time point was determined by a two-tailed *t*-test.

RESULTS

In silico Identification of the MDR EP Encoding Genes in AIEC LF82 Strain and Their Expression Profile During Infection of Host Cells

LF82 is a prototype strain of AIEC, isolated from CD patients (Boudeau et al., 1999). As previously reported (Miquel et al., 2010), the genome of LF82 contains 130 LF82 specific CDSs. Most of them (88.5%) are not found in any *E. coli* genome while the remaining percentage has no homology with genes identified in any pathogenic bacteria. Since among these LF82 specific CDSs there were no genes coding for MDR EPs, we searched in the genome of LF82 homologs for each of the 20 functional MDR EPs encoding operons described in *E. coli* K12 (Nishino and Yamaguchi, 2001; Kobayashi et al., 2006).

As shown in **Table 1**, 19 out of the 20 genetic systems encoding MDR EPs described in *E. coli* K12 MG1655 are present in LF82 genome. The *mdtM* gene is completely absent due to a severe rearrangement in the *mdtM-rpnD* locus as compared to MG1655 with the insertion of LF82 specific genes (Miquel et al., 2010). The remaining MDR EPs and their encoding genes show high homology with those of commensal *E. coli* K12 strain (**Table 1**). The pattern of functional MDR

TABLE 1 | Analysis of the multidrug efflux pump encoding genes present in the adherent-invasive *Escherichia coli* (AIEC) LF82 genome.

Family	MG1655	LF82	DNA Sequence homology (%)*	Protein homology (%)*
ABC	<i>macAB</i>	+	98.17	98.65; 99.38
	<i>bcr</i>	+	96.81	99.49
	<i>emrAB</i>	+	98.06	99.74; 99.80
	<i>emrD</i>	+	97.81	99.49
	<i>emrKY</i>	+	97.41	98.19; 100
MFS	<i>fsr</i>	+	97.87	99.75
	<i>mdtA</i>	+	98.05	100
	<i>mdtG</i>	+	98.45	99.51
	<i>mdtH</i>	+	98.35	100
	<i>mdtL</i>	+	96.51	98.47
	<i>mdtM</i>	–	–	–
	<i>acrAB</i>	+	98.81	99.75; 100
	<i>acrD</i>	+	98.5	99.81
RND	<i>acrEF</i>	+	97.26	98.96; 99.52
	<i>cusB</i>	+	97.3	98.77
	<i>mdtABC</i>	+	95.35	98.80; 99.71; 98.83
	<i>mdtEF</i>	+	97.72	99.74; 99.42
SMR	<i>emrE</i>	+	98.8	99.09
	<i>mdtJI</i>	+	98.53	100; 100
MATE	<i>mdtK</i>	+	97.82	99.78

The 20 genetic systems encoding functional efflux pumps in *Escherichia coli* have been selected according to Nishino and Yamaguchi (2001). The comparative analysis between the genome of *E. coli* K-12 and AIEC LF82 strain was carried out using NCBI BLAST (<http://blast.ncbi.nlm.nih.gov/Blast.cgi>). The nucleotide sequences of each efflux pump encoding gene were obtained from EcoCyc (<https://ecocyc.org>).

+ Efflux pump encoding genes present in the LF82 genome.

– Not present in the LF82 genome.

*Sequence and amino acid homology expressed as a percentage.

EPs of LF82 is the most common among those observed in highly invasive AIEC strains, isolated from CD patients, belonging to the B2 phylogroup (data not shown).

LF82 is a pathogenic AIEC strain that is able to invade epithelial cells and survive and replicate widely in macrophages without inducing cell death (Boudeau et al., 1999; Glasser et al., 2001), suggesting that the bacterium is able to adapt and establish an equilibrium with the host cell. The expression of LF82 MDR EPs was therefore analyzed at early stage of the invasive process during the first 4 h of infection of human U937 monoblasts differentiated into macrophage-like cells and of Caco-2 epithelial cells. The global analysis by qRT-PCR shows that the expression of some of the conserved MDR EP encoding genes, such as *mdtG*, *mdtH*, *emrD*, *emrA* (MSF family), *mdtA*, *acrD* (RND family), and *macA* (ABC family), is weakly modified by host cell environment with few differences between the two cell types, or downregulated in both cell types, as for *emrE* (SMR family), which is heavily repressed particularly in macrophages, and *bcr* (MFS family; **Figure 1**). Concerning the other MDR EP genes conserved in LF82, results obtained by qRT-PCR analysis demonstrated that some of them are constantly upregulated during the infection of both cell types (**Figure 2**), while the expression of four genes, namely *fsr*, *mdtL*, *mdtEF*, and *acrA*, is regulated in a cell specific manner (**Figure 3A**).

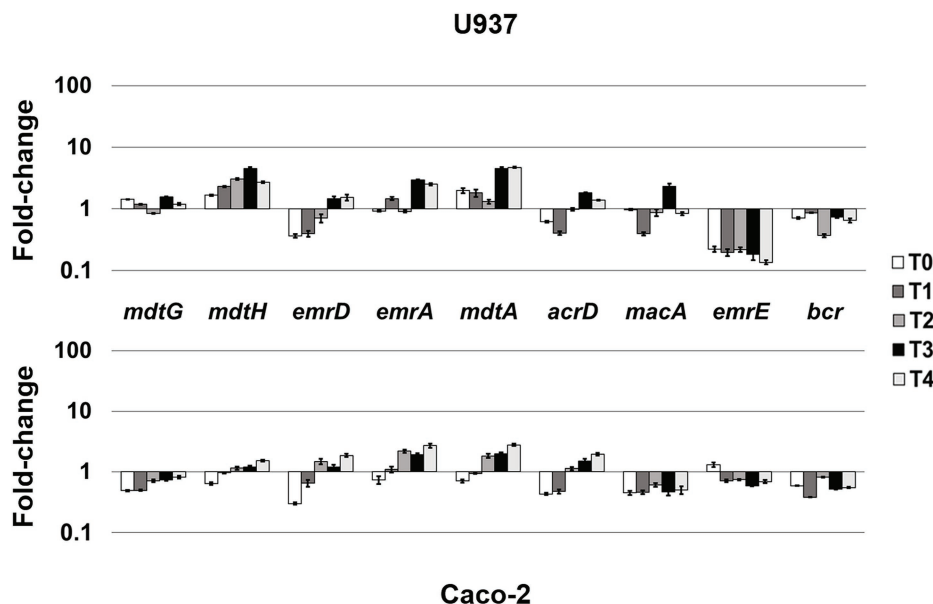


FIGURE 1 | Mild-responsive MDR EPs to different cellular environments. Relative transcription of the EP encoding genes *mdtG*, *mdtH*, *emrD*, *emrA*, *mdtA*, *acrD*, *macA*, *emrE*, and *bcr* during LF82 infection of U937 and Caco-2 cells. Quantitative analysis of the transcripts was performed by qRT-PCR. Total RNA was extracted from LF82 bacteria at various time points p.i., from 0 h (corresponding to bacterial adhesion to and entry into target cells, T0) up to 4 h (T4) p.i. and from control bacteria grown in RPMI (U937) or DMEM (Caco-2). Each experiment was repeated three times and at least three wells were run for each sample. The results are shown as fold-change relative to the expression of each gene in control bacteria set to 1.0. A one-way ANOVA performed between intracellular bacteria and control bacteria yielded $p < 0.01$ for all the EP genes shown. Error bars represent SD.

Some MDR EP Genes Are Induced Regardless of the Cell Type LF82 Is Infecting

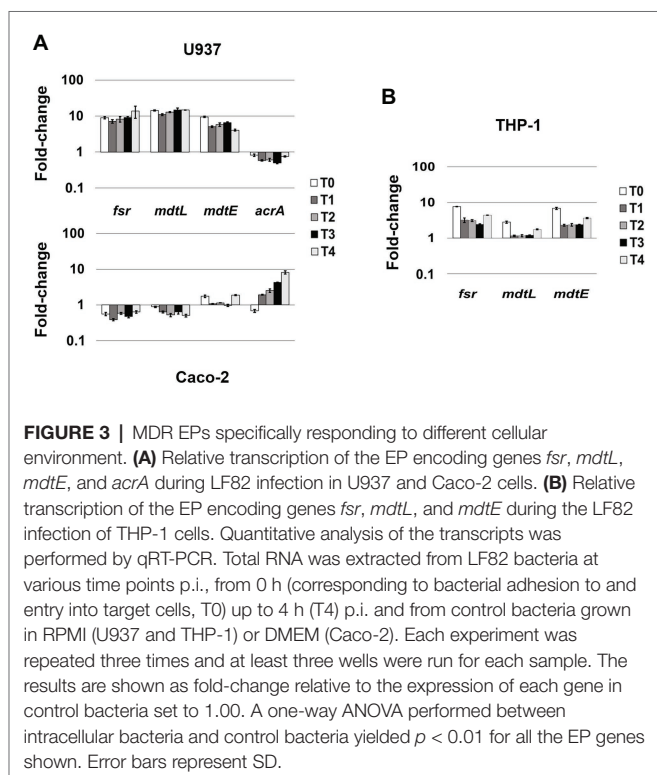
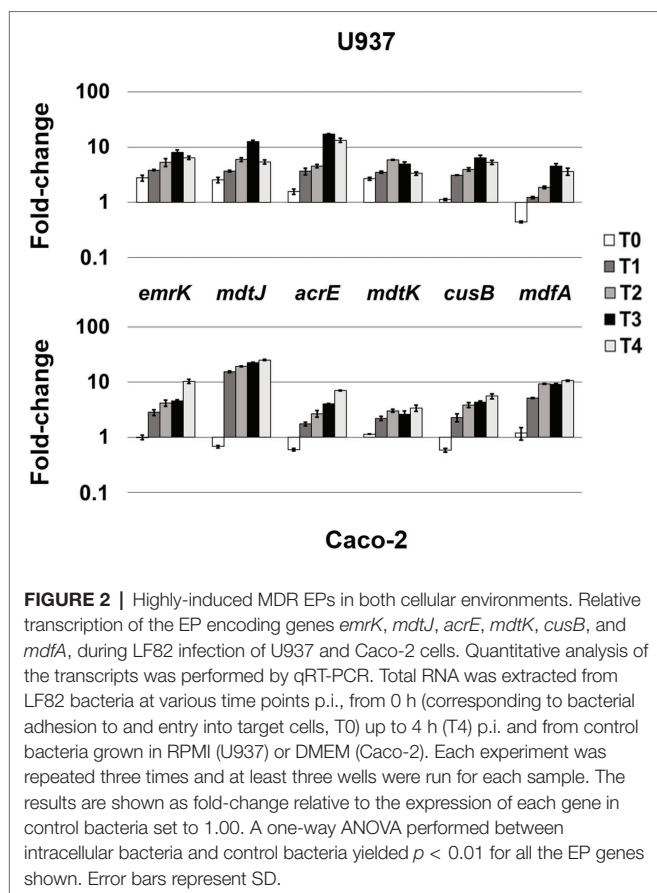
The analysis of the transcriptional profile of all the genes encoding MDR EPs revealed that the genes *emrK* and *mdfA* (MFS family), *mdtJ* (SMR family), *acrE* and *cusB* (RND family), and *mdtK* (MATE family) are invariably induced during the infection of both U937 and Caco-2 cells, although at different extent (**Figure 2**). In particular, when LF82 strain infects macrophages, the *emrK*, *mdtJ*, *acrE*, and *mdtK* transcripts accumulate promptly after bacterium entry into the cell (T0), increasing throughout the infection period analyzed (**Figure 2**, upper panel). During the infection of epithelial cells, induction of the same genes is observed later, at 1 h post infection (p.i.), afterwards their expression follows a behavior similar to that observed in U937-derived macrophages, since the genes are strongly upregulated (**Figure 2**, lower panel). Particularly, the *mdtJ* transcript accumulates up to 25-fold at 4 h p.i., as compared to LF82 grown in DMEM medium (**Figure 2**, lower panel). The expression profile of the *cusB* gene is also quite comparable in the two cell types, with some differences at the very early stage of infection (T0) where the transcript levels keep unaltered in U937 cells, compared to control bacteria grown in RPMI medium, while decrease in LF82 infecting Caco-2 cells. Finally, among these group of EP genes, *mdfA* appears to be an exception, as its behavior at T0 is specular to that observed for the other EPs in the two cells types, being unchanged in epithelial cells, as compared to the control LF82, while

downregulated in macrophages. The delay of induction observed in epithelial cells for virtually all these EP genes may be explained by the different mode of bacterium entry into the two cell types, direct phagocytosis by macrophages (Glasser et al., 2001) versus pilum-CEACAM6 interaction-dependent macropinocytosis (Glasser et al., 2001; Barnich et al., 2007), which might imply that bacteria face cellular response much earlier in macrophages than in epithelial cells.

Collectively, these data suggest that these MDR EP genes respond to stimuli common to both infected macrophages and epithelial cells and that their enhancement might be important for the overall invasive process of the bacterium.

fsr, *mdtL*, *mdtEF*, and *acrA* MDR EP Genes Are Differentially Expressed During the Infection of Macrophages and Epithelial Cells

Unlike the genes described above, whose induction is independent from the cell type LF82 is infecting either macrophages or epithelial cells, the modulation of *fsr*, *mdtL*, *mdtEF*, and *acrA* EP genes appears to be driven by specific cell environment. Indeed, the transcript levels of the *fsr* and *mdtL*, encoding MDR EPs of the MFS family and *mdtE* encoding an MDR EP of the RND family, are strongly increased when LF82 invades U937-derived macrophages, as compared to LF82 grown in RPMI (**Figure 3A**). In particular, induction of the *fsr*, *mdtL*, and *mdtE* genes occurs immediately as bacteria adhere and enter the host cell (T0; **Figure 3A**, upper panel). Conversely, the expression of these same genes is either downregulated, as



in the case of *fsr* and *mdtL*, or virtually unchanged, as for *mdtE*, throughout the infection of epithelial cells (Figure 3A, lower panel). On the other way around, the *acrA* gene encoding the AcrAB EP (RND family) is specifically expressed when the LF82 invades epithelial cells. The transcription level of *acrA* gene increases over the time during Caco-2 cell infection (up to 8-fold), as compared to LF82 grown in DMEM (Figure 3A, lower panel). In contrast, the *acrA* gene is constantly downregulated during the infection of macrophages (Figure 3A, upper panel).

Overall, these findings suggest that the expression of some MDR EP genes in the LF82 AIEC strain represents a kind of signature mirroring the bacterial response to specific host-cell environment, either macrophagic or epithelial.

Resident macrophages in the intestinal tract are among the sentinels devoted at limiting systemic microbial dissemination and defending the organism from pathogen attacks. On the other hand, it is largely acknowledged that macrophages fail to restrict intracellular AIECs, which, in turn, survive and replicate inside them (Glasser et al., 2001; Vazeille et al., 2015; Palmela et al., 2018; Demarre et al., 2019). Hence, the specific induction of *fsr*, *mdtL*, and *mdtE* genes observed in LF82 infecting U937 cells might be part of the bacterial strategies to counter the host-cell defenses. To strengthen this observation, the expression profile of these EP genes was also verified in THP-1 monocyte-derived into macrophages, widely used as model system to study the infection process of LF82 and other AIEC clinical strains (O'Brien et al., 2017; Demarre et al., 2019). Figure 3B shows that, although induced at lesser extent, the overall behavior of the three genes is quite similar to that observed in U937 cells. Noteworthy, the induction of these EP genes in LF82 is particularly significant as soon after the addition of bacteria to THP-1 cells, with *mdtL* being the least upregulated at T0 and almost unmodified at the other time points analyzed.

MdtEF Contributes to the Survival of LF82 Inside Macrophages

More and more studies are addressing the emergent role of EPs in bacterial pathogenesis and virulence beyond that of conferring MDR (Piddock, 2006; Alcalde-Rico et al., 2016; Pasqua et al., 2019b). Recently, we have described how several EP genes are modulated in *S. flexneri* upon infection of macrophages and epithelial cells and how they can be functional for the macrophage invasive process (Pasqua et al., 2019a). *Shigella* and AIECs are two invasive *E. coli* pathotypes using very different virulence tools and strategies (Croxen et al., 2013). One of all is the outcome of macrophage infection, where *Shigella* rapidly exits the entry vacuole and eventually kills the cell (Ogawa and Sasakawa, 2006) while AIECs replicate inside the phagosome without inducing cell death (Glasser et al., 2001). Interestingly, during the evolution process toward intracellular lifestyle AIECs have conserved some genetic systems encoding MDR EPs, which are, instead, lost by *Shigella* (Pasqua et al., 2019a). Of note, *mdtEF* is among the MDR EP genes disrupted in *Shigella*, thus the specific induction seen in LF82 infecting macrophages may reflect, at least in part, the profound differences of the pathogenic mechanisms between the two pathogens. To get more insights on the value of the very early response of the LF82 inside macrophages, a LF82

mdtEF deletion mutant was generated by site specific mutagenesis (LF82 Δ *mdtEF*) and used to infect THP-1-derived macrophages. Parallel infections were performed with the wild type LF82 strain. Although AIECs persist and replicate inside macrophages, they are continuously under macrophage attack and a fraction of intracellular dead bacteria is always present (Demarre et al., 2019). Hence, we asked whether lack of functional MdtEF could affect intramacrophagic LF82 survival. At the indicated time points, intracellular bacteria were recovered from infected macrophages and stained with PI and DAPI; the amount of PI positive dead LF82 and LF82 Δ *mdtEF* cells were evaluated under fluorescence microscopy. Data shown in **Figure 4** confirm that a constant proportion, ranging from 10 to 17% of dead LF82 bacteria is detectable throughout the infection period analyzed. Interestingly, lack of MdtEF leads to a significant increase of bacteria that succumb to macrophage attack. Indeed, the percentage of PI positive LF82 Δ *mdtEF* shifts up 2–2.5-fold, depending on the time point considered, ranging from 24 to 38%. In order to assess the direct contribution of MdtEF in conferring intramacrophagic LF82 viability, we made attempts to restore the wild type phenotype in a LF82 Δ *mdtEF* by expressing a functional MdtEF protein complex. To this end, we constructed pGEF3 by cloning the *mdtEF* genes into the pGIP7 vector (**Supplementary Table S1**). Functionality of MdtEF pump encoded by pGEF3 was verified by testing the capability of pGEF3 to confer resistance to erythromycin in a *E. coli* K12 strain depleted of AcrAB, the major MDR EP (MG1655 Δ *acrAB*; **Supplementary Table S3**). Parallel infections of THP-1 macrophages were carried out with LF82, LF82 Δ *mdtEF*, LF82 Δ *mdtEF* pGIP7, or LF82 Δ *mdtEF* pGEF3. As expected, LF82 Δ *mdtEF* pGIP7 strain behaves as the deleted mutant (data not shown). On the other way around, trans-complementation with pGEF3, encoding a functional MdtEF pump, completely restores the phenotype of LF82 Δ *mdtEF* strain.

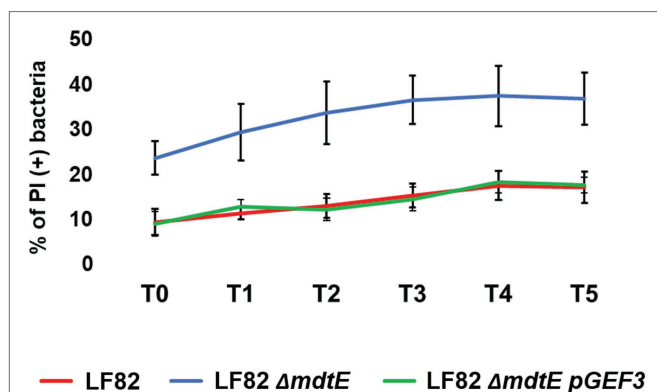


FIGURE 4 | MdtEF pump favors survival of LF82 within macrophages. Intracellular bacteria were recovered from THP-1 differentiated macrophages at 0, 1, 2, 3, 4, and 5 h p.i. (referred to as T0, T1, T2, T3, T4, and T5, respectively) and soon after stained with DAPI/PI. The values are expressed as percentage of PI (+) dead bacteria relative to DAPI (+) bacteria. The results shown are the average of at least three independent experiments. A two-tailed *t* test performed between LF82 and LF82 Δ *mdtEF* or between LF82 Δ *mdtEF* pGEF3 and LF82 Δ *mdtEF* yielded a $p < 0.01$ at each time point while comparison between LF82 and LF82 Δ *mdtEF* pGEF3 yielded $p > 0.1$. Error bars represent SD.

Indeed, **Figure 4** shows that the proportion of dead LF82 Δ *mdtEF* pGEF3 bacteria is fully superimposable to that of dead wild type LF82 bacteria. The reduced viability of the LF82 Δ *mdtEF* indicates that the MdtEF EP participates in the bacterial response to the macrophage attack promoting LF82 survival.

Attempts to translate the viability phenotypes into a different number of colony forming bacteria failed due to the extremely high variability of growth curves obtained from different infection experiments both with the wild type and the mutant strains. This is in agreement with a recent study that well documents how intramacrophagic challenges induces a high LF82 phenotypic heterogeneity (Demarre et al., 2019), influencing the growth properties of intracellular bacteria. Altogether, these data indicate that increasing expression of the MdtEF encoding genes might be functional to activate a strategy for persisting in the harsh environment of the macrophage phagolysosome.

DISCUSSION

In the present study, we analyzed the differential expression of genes encoding the MDR EPs of the AIEC LF82 strain during the first steps of its intracellular life. We found that some of these genes are highly and specifically activated during infection of macrophages while others are specifically induced when bacteria infect epithelial cells. Among MDR EPs significantly activated in the macrophage environment, we have focused on MdtEF, an EP belonging to the RND family, and we were able to show that its expression is linked to reduced mortality of LF82 within macrophages.

AIEC are a peculiar group of enteropathogenic *E. coli*, very frequently found in CD patients, able to colonize the intestinal epithelial cells and to actively replicate in macrophages (Darfeuille-Michaud, 2002; Palmela et al., 2018; Shaler et al., 2019). Adhesion of AIEC on ileal enterocytes is mediated by the interaction of bacterial type1 pili with the host cell receptor CEACAM6. The high expression of this receptor at the apical surface of enterocytes in CD patients accounts for the massive presence of AIEC in their intestinal epithelia (Barnich et al., 2007). In addition to invasion of intestinal epithelial cells, AIEC are able to translocate through the epithelium and gain access to the macrophages. AIEC replicate extensively within macrophage phagolysosomes without triggering cell death. Continuous replication of AIEC in infected macrophages results in secretion of high levels of TNF- α , causing strong intestinal inflammation in CD patients (Glasser et al., 2001). The intravacuolar microenvironment of macrophage phagolysosomes not only protects bacteria from autophagy (Lapaquette et al., 2010) but also favors full expression of the virulence phenotype and active replication (Bringer et al., 2006). Recently, it has been shown that persistence within macrophages exposes AIEC LF82 to several stresses, resulting in a complex bacterial response that promotes the formation of non-growing and antibiotic tolerant variants (Demarre et al., 2019).

A growing body of studies suggests that the functional significance of MDR EPs goes beyond their capability to extrude a wide range of antibiotics as these pumps are also involved in relevant aspects of bacterial cell physiology, including

interactions with host cells (Alcalde-Rico et al., 2016; Du et al., 2018; Pasqua et al., 2019b). While in other enteroinvasive bacteria, such as *Salmonella* and *Shigella*, it was shown that MDR EPs contribute to the bacterial survival within the host cells (Buckley et al., 2006; Pasqua et al., 2019a), no data are available for AIEC strains. LF82 is a reference AIEC strain isolated from CD patients (Boudeau et al., 1999) that has been widely used to investigate bacteria-host interactions. As compared to the commensal *E. coli* K12, we observed that the LF82 genome contains all functional MDR EPs previously described with the exception of MtdM, whose operon has been disrupted by the insertion of AIEC specific genes. We found that the expression of many of the MDR EP genes conserved in LF82 is strongly modified by intracellular environment, suggesting a potential involvement of these systems in the infection process also in AIEC. Notably, some MDR EPs are invariably induced regardless of the cell type LF82 is infecting, indicating that the bacterium is subjected to common stimuli in both U937-derived macrophages and Caco-2 epithelial cells (Figure 2). Among these MDR EPs, EmrKY is of particular interest. Indeed, as we have previously reported, in *Shigella*, EmrKY is selectively expressed in macrophages and inhibited in epithelial cells (Pasqua et al., 2019a), while here we found that in AIEC this EP is actively transcribed in both cell types throughout the analyzed infection period. As demonstrated before the acidic cytoplasmic pH determined by *Shigella* infection of macrophages is responsible for EmrKY induction (Pasqua et al., 2019a). AIEC and *Shigella* both belong to the *E. coli* species and share the capacity to invade macrophages and epithelial cells (Croxen et al., 2013). However, their infection strategy greatly differs, as *Shigella* rapidly escapes from phagolysosome upon infection of both macrophagic and epithelial cells and multiplies in the cytoplasm (Schroeder and Hilbi, 2008), while AIEC remain and multiply inside the phagolysosome or the late endosome in macrophages and epithelial cells, respectively (Glasser et al., 2001; Lapaquette et al., 2010). Hence, the induction of *emrK* gene in LF82 during the infection of both macrophages and epithelial cells is likely because AIEC are continuously exposed to an acidic environment, such as that of phagolysosome or late endosome, in both cell types.

In addition to the LF82 EPs being highly induced by both cell environments, we observed that the expression of few EP genes is specifically induced when the bacterium infects U937-derived macrophages or Caco-2 epithelial cells. Particularly, the gene *acrA*, encoding the periplasmic component of the AcrAB efflux pump, is upregulated when LF82 strain invades epithelial cells, while is downregulated in macrophages. The AcrAB efflux pump belongs to the RND family and it is known as the major *E. coli* MDR efflux system (Nishino and Yamaguchi, 2001); therefore, its downregulation in the macrophage environment might be complemented by overexpression of other pumps that could fulfill, at least in part, the same function. Accordingly, the expression levels of the *fsr* and *mdtL*, encoding MDR EPs of the MFS family and *mdtE* encoding an EP of the RND family, are strongly increased when LF82 invades U937-derived macrophages, while lowered when Caco-2 cells are infected. Whether the activity associated to these MDR

EPs can complement the downregulation of AcrAB has still to be determined. However, the specular expression profile of this group of EPs in LF82 infecting either macrophages or epithelial cells appears intriguing. In this context, it is worth mentioning that in *Salmonella* Typhimurium the silencing of *acrA* or *acrF*, which encode the transporter component of two RND EPs, increases the expression of *acrD*, a gene encoding another RND EP (Eaves et al., 2004).

The induction of Fsr and MdtE appears to be a common response of LF82 to macrophagic environment as we find them upregulated during the infection of a different monocytic cell line, the widely used THP-1-derived macrophages (Figure 3B). This observation strongly supports the hypothesis that these EPs might be part of the pathogenic strategy of LF82, favoring survival and multiplication inside macrophages.

From an evolutionary point of view, MdtEF is of particular interest, as it is among the MDR EPs lost by *Shigella* (Pasqua et al., 2019a), likely because unnecessary during the intracellular life.

MdtEF forms a tripartite EP with the common outer membrane channel TolC. In *E. coli* K12, the overexpression of MdtEF confers resistance to a large panel of antibiotics and toxic compounds, including fatty acids and sodium deoxycholate (Nishino and Yamaguchi, 2001). The *mdtEF* genes are located downstream the *gadE* gene, which encodes the key regulator of a major acid resistance system. Transcriptional regulation from the *gadE* promoter has been extensively studied and involves, among others, the response regulators ArcA, EvgA, and PhoP, the nucleoid associated protein H-NS, the sigma factor RpoS and the regulatory sRNA DsrA (Nishino et al., 2011; Zhang et al., 2011). The expression of *mdtEF* genes is induced by various physiological and environmental stimuli, e.g., stationary growth phase or presence of indole and acetylglucosamine, as well as by oxygen and acid stress (Deng et al., 2013). While it has been shown that MdtEF protects the *E. coli* cells from nitrosative damage during anaerobic conditions (Zhang et al., 2011), its potential role in pathogenicity has not yet been fully explored. The data we have obtained on the viability phenotype of intracellular LF82 bacteria expressing or not the MdtEF pump indicate that this EP, probably because of its capacity to extrude a large panel of compounds, might favor the intravacuolar survival of LF82, likely pumping out toxic metabolites. The capability of the *mdtEF* genes expressed by the pGEF3 plasmid to fully restore the intracellular viability in LF82 Δ *mdtEF* strain further confirms the contribution of this EP to the LF82 fitness in the harsh macrophage niche. It has been recently reported (Demarre et al., 2019) that, inside the macrophages, LF82 strain rapidly activates the response to acid and oxidative stress, to envelope alterations and to the lack of important nutrients. The inclusion of *mdtEF* operon in a complex regulatory network able to perceive and respond to the severe stresses from macrophage phagolysosome allows the rapid induction of its transcription soon after the bacterial entry into the cell. The prompt activation of MdtEF encoding genes would provide a high abundance of this pump, promoting a quick defensive response to the hostile phagolysosome environment.

Further studies will be necessary to clearly define the contribution of other EPs in the interactions of LF82 with the host cells. Up to now, the role we disclosed for MdtEF in improving survival inside the stressing environment of the macrophagic phagosome represents the first evidence of the involvement of an MDR EP in the infection strategy of an AIEC invasive strain. This further highlights the critical role of the RND systems in both MDR and virulence.

DATA AVAILABILITY STATEMENT

The raw data supporting the conclusions of this article will be made available by the authors, without undue reservation.

AUTHOR CONTRIBUTIONS

GF, MG, MP, GP, and BC conceived and designed the experiments. GF, MP, and MG performed the experiments. GF, MP, GP, and MG analyzed the data. BC, MG, and GP contributed reagents, materials, and analysis tools. GF, BC, MG, and GP

wrote the paper. All authors contributed to the article and approved the submitted version.

FUNDING

This research was supported by grants from Italian Ministry of University and Research (PRIN 2017-20177J5Y3P) and from Sapienza University of Rome.

ACKNOWLEDGMENTS

We gratefully acknowledge the late Arlette Darfeuille Michaud and her lab for providing strain LF82.

SUPPLEMENTARY MATERIAL

The Supplementary Material for this article can be found online at: <https://www.frontiersin.org/articles/10.3389/fmicb.2020.01935/full#supplementary-material>

REFERENCES

- Alav, I., Sutton, J. M., and Rahman, K. M. (2018). Role of bacterial efflux pumps in biofilm formation. *J. Antimicrob. Chemother.* 73, 2003–2020. doi: 10.1093/jac/dky042
- Alcalde-Rico, M., Hernando-Amado, S., Blanco, P., and Martínez, J. L. (2016). Multidrug efflux pumps at the crossroad between antibiotic resistance and bacterial virulence. *Front. Microbiol.* 7:1483. doi: 10.3389/fmicb.2016.01483
- Alvarez-Ortega, C., Olivares, J., and Martínez, J. L. (2013). RND multidrug efflux pumps: what are they good for? *Front. Microbiol.* 4:7. doi: 10.3389/fmicb.2013.00007
- Barnich, N., Carvalho, F. A., Glasser, A. L., Darcha, C., Jantschke, P., Allez, M., et al. (2007). CEACAM6 acts as a receptor for adherent-invasive *E. coli*, supporting ileal mucosa colonization in Crohn disease. *J. Clin. Invest.* 117, 1566–1574. doi: 10.1172/JCI30504
- Bianco, M. V., Blanco, F. C., Forrellad, M. A., Aguilar, D., Eleonora, C., Klepp, L. I., et al. (2011). Knockout mutation of p27-p55 operon severely reduces replication of *Mycobacterium bovis* in a macrophagic cell line and survival in a mouse model of infection. *Virulence* 2, 233–237. doi: 10.4161/viru.2.3.15888
- Bogomolnaya, L. M., Andrews, K. D., Talamantes, M., Maple, A., Ragoza, Y., Vazquez-Torres, A., et al. (2013). The ABC-type efflux pump MacAB protects *Salmonella enterica* serovar typhimurium from oxidative stress. *mBio* 4, e00630–e00713. doi: 10.1128/mBio.00630-13
- Boudeau, J., Glasser, A. L., Masseret, E., Joly, B., and Darfeuille-Michaud, A. (1999). Invasive ability of an *Escherichia coli* strain isolated from the ileal mucosa of a patient with Crohn's disease. *Infect. Immun.* 67, 4499–4509. doi: 10.1128/IAI.67.9.4499-4509.1999
- Bringer, M. A., Glasser, A. L., Tung, C. H., Méresse, S., and Darfeuille-Michaud, A. (2006). The Crohn's disease-associated adherent-invasive *Escherichia coli* strain LF82 replicates in mature phagolysosomes within J774 macrophages. *Cell. Microbiol.* 8, 471–484. doi: 10.1111/j.1462-5822.2005.00639.x
- Buckley, A. M., Webber, M. A., Cooles, S., Randall, L. P., La Ragione, R. M., Woodward, M. J., et al. (2006). The AcrAB-TolC efflux system of *Salmonella enterica* serovar typhimurium plays a role in pathogenesis. *Cell. Microbiol.* 8, 847–856. doi: 10.1111/j.1462-5822.2005.00671.x
- Crimmins, G. T., Herskovits, A. A., Rehder, K., Sivick, K. E., Lauer, P., Dubensky, T. W., et al. (2008). *Listeria monocytogenes* multidrug resistance transporters activate a cytosolic surveillance pathway of innate immunity. *Proc. Natl. Acad. Sci. U. S. A.* 105, 10191–10196. doi: 10.1073/pnas.0804170105
- Croxen, M. A., Law, R. J., Scholz, R., Keeney, K. M., Wlodarska, M., and Finlay, B. B. (2013). Recent advances in understanding enteric pathogenic *Escherichia coli*. *Clin. Microbiol. Rev.* 26, 822–880. doi: 10.1128/CMR.00022-13
- Darfeuille-Michaud, A. (2002). Adherent-invasive *Escherichia coli*: a putative new *E. coli* pathotype associated with Crohn's disease. *Int. J. Med. Microbiol.* 25, 322–337. doi: 10.1078/1438-4221-00201
- Datsenko, K. A., and Wanner, B. L. (2000). One-step inactivation of chromosomal genes in *Escherichia coli* K-12 using PCR products. *Proc. Natl. Acad. Sci. U. S. A.* 97, 6640–6645. doi: 10.1073/pnas.120163297
- De Carolis, E., Posteraro, B., Florio, A. R., Colonna, B., Prosseda, G., Bugli, F., et al. (2011). Analysis of heat-induced changes in protein expression of *Stenotrophomonas maltophilia* K279a reveals a role for GroEL in the host-temperature adaptation. *Int. J. Med. Microbiol.* 301, 273–281. doi: 10.1016/j.ijmm.2010.10.001
- Delmar, J. A., and Yu, E. W. (2016). The AbgT family: a novel class of antimetabolite transporters. *Protein Sci.* 25, 322–337. doi: 10.1002/pro.2820
- Demarre, G., Prudent, V., Schenk, H., Rousseau, E., Bringer, M. A., Barnich, N., et al. (2019). The Crohn's disease-associated *Escherichia coli* strain LF82 relies on SOS and stringent responses to survive, multiply and tolerate antibiotics within macrophages. *PLoS Pathog.* 15:e1008123. doi: 10.1371/journal.ppat.1008123
- Deng, Z., Shan, Y., Pan, Q., Gao, X., and Yan, A. (2013). Anaerobic expression of the gadE-mdtEF multidrug efflux operon is primarily regulated by the two-component system ArcBA through antagonizing the H-NS mediated repression. *Front. Microbiol.* 4:194. doi: 10.3389/fmicb.2013.00194
- Di Martino, M. L., Romilly, C., Wagner, E. G. H., Colonna, B., and Prosseda, G. (2016). One gene and two proteins: a leaderless mRNA supports the translation of a shorter form of the *Shigella* VirF regulator. *mBio* 7, e01860–e01916. doi: 10.1128/mBio.01860-16
- Du, D., Wang-Kan, X., Neuberger, A., van Veen, H. W., Pos, K. M., Piddock, L. J. V., et al. (2018). Multidrug efflux pumps: structure, function and regulation. *Nat. Rev. Microbiol.* 16, 523–539. doi: 10.1038/s41579-018-0048-6
- Eaves, D. J., Ricci, V., and Piddock, L. J. V. (2004). Expression of *acrB*, *acrF*, *acrD*, *marA*, and *soxS* in *Salmonella enterica* serovar typhimurium: role in multiple antibiotic resistance. *Antimicrob. Agents Chemother.* 48, 1145–1150. doi: 10.1128/AAC.48.4.1145-1150.2004
- Falconi, M., Prosseda, G., Giangrossi, M., Beghetto, E., and Colonna, B. (2001). Involvement of FIS in the H-NS-mediated regulation of virF gene of *Shigella* and enteroinvasive *Escherichia coli*. *Mol. Microbiol.* 42, 439–452. doi: 10.1046/j.1365-2958.2001.02646.x
- Glasser, A. L., Boudeau, J., Barnich, N., Perruchot, M. H., Colombel, J. F., and Darfeuille-Michaud, A. (2001). Adherent invasive *Escherichia coli* strains from patients with Crohn's disease survive and replicate within macrophages

- without inducing host cell death. *Infect. Immun.* 69, 5529–5537. doi: 10.1128/IAI.69.9.5529-5537.2001
- Hinchliffe, P., Symmons, M. F., Hughes, C., and Koronakis, V. (2013). Structure and operation of bacterial tripartite pumps. *Annu. Rev. Microbiol.* 67, 221–242. doi: 10.1146/annurev-micro-092412-155718
- Keseler, I. M., Mackie, A., Santos-Zavaleta, A., Billington, R., Bonavides-Martinez, C., Caspi, R., et al. (2017). The EcoCyc database: reflecting new knowledge about *Escherichia coli* K-12. *Nucleic Acids Res.* 45, D543–D550. doi: 10.1093/nar/gkw1003
- Kobayashi, A., Hirakawa, H., Hirata, T., Nishino, K., and Yamaguchi, A. (2006). Growth phase-dependent expression of drug exporters in *Escherichia coli* and its contribution to drug tolerance. *J. Bacteriol.* 188, 5693–5703. doi: 10.1128/JB.00217-06
- Lapaquette, P., Glasser, A. L., Huett, A., Xavier, R. J., and Darfeuille-Michaud, A. (2010). Crohn's disease-associated adherent-invasive *E. coli* are selectively favoured by impaired autophagy to replicate intracellularly. *Cell. Microbiol.* 12, 99–113. doi: 10.1111/j.1462-5822.2009.01381.x
- Leuzzi, A., Di Martino, M. L., Campilongo, R., Falconi, M., Barbagallo, M., Marcocci, L., et al. (2015). Multifactor regulation of the MdtJl polyamine transporter in *Shigella*. *PLoS One* 10:e0136744. doi: 10.1371/journal.pone.0136744
- Leuzzi, A., Grossi, M., Di Martino, M. L., Pasqua, M., Micheli, G., Colonna, B., et al. (2017). Role of the SRRz/Rz1 lambdoid lysis cassette in the pathoadaptive evolution of *Shigella*. *Int. J. Med. Microbiol.* 307, 268–275. doi: 10.1016/j.ijmm.2017.03.002
- Li, X. Z., Plésiat, P., and Nikaido, H. (2015). The challenge of efflux-mediated antibiotic resistance in gram-negative bacteria. *Clin. Microbiol. Rev.* 28, 337–418. doi: 10.1128/CMR.00117-14
- Livak, K. J., and Schmittgen, T. D. (2001). Analysis of relative gene expression data using real-time quantitative PCR and the 2- $\Delta\Delta$ CT method. *Methods* 25, 402–408. doi: 10.1006/meth.2001.1262
- Miquel, S., Peyretaillade, E., Claret, L., de Vallée, A., Dossat, C., Vacherie, B., et al. (2010). Complete genome sequence of Crohn's disease-associated adherent-invasive *E. coli* strain LF82. *PLoS One* 5:e12714. doi: 10.1371/journal.pone.0012714
- Nishino, K., and Yamaguchi, A. (2001). Analysis of a complete library of putative drug transporter genes in *Escherichia coli*. *J. Bacteriol.* 183, 5803–5812. doi: 10.1128/JB.183.20.5803-5812.2001
- Nishino, K., Yamasaki, S., Hayashi-Nishino, M., and Yamaguchi, A. (2011). Effect of overexpression of small non-coding DsrA RNA on multidrug efflux in *Escherichia coli*. *J. Antimicrob. Chemother.* 66, 291–296. doi: 10.1093/jac/dkq420
- O'Brien, C. L., Bringer, M. A., Holt, K. E., Gordon, D. M., Dubois, A. L., Barnich, N., et al. (2017). Comparative genomics of Crohn's disease-associated adherent-invasive *Escherichia coli*. *Gut* 66, 1382–1389. doi: 10.1136/gutjnl-2015-311059
- Ogawa, M., and Sasakawa, C. (2006). Intracellular survival of *Shigella*. *Cell. Microbiol.* 8, 177–184. doi: 10.1111/j.1462-5822.2005.00652.x
- Palmela, C., Chevarin, C., Xu, Z., Torres, J., Sevrin, G., Hirtten, R., et al. (2018). Adherent-invasive *Escherichia coli* in inflammatory bowel disease. *Gut* 67, 574–587. doi: 10.1136/gutjnl-2017-314903
- Pasqua, M., Grossi, M., Scinicariello, S., Aussel, L., Barras, F., Colonna, B., et al. (2019a). The MFS efflux pump EmrKY contributes to the survival of *Shigella* within macrophages. *Sci. Rep.* 9:2906. doi: 10.1038/s41598-019-39749-3
- Pasqua, M., Grossi, M., Zennaro, A., Fanelli, G., Micheli, G., Barras, F., et al. (2019b). The varied role of efflux pumps of the MFS family in the interplay of bacteria with animal and plant cells. *Microorganisms* 7:285. doi: 10.3390/microorganisms7090285
- Pasqua, M., Michelacci, V., Di Martino, M. L., Tozzoli, R., Grossi, M., Colonna, B., et al. (2017). The intriguing evolutionary journey of enteroinvasive *E. coli* (EIEC) toward pathogenicity. *Front. Microbiol.* 8:2390. doi: 10.3389/fmicb.2017.02390
- Piddock, L. J. V. (2006). Multidrug-resistance efflux pumps - not just for resistance. *Nat. Rev. Microbiol.* 4, 629–636. doi: 10.1038/nrmicro1464
- Schroeder, G. N., and Hilbi, H. (2008). Molecular pathogenesis of *Shigella* spp.: controlling host cell signaling, invasion, and death by type III secretion. *Clin. Microbiol. Rev.* 21, 134–156. doi: 10.1128/CMR.00032-07
- Shaler, C. R., Elhenawy, W., and Coombes, B. K. (2019). The unique lifestyle of Crohn's disease-associated adherent-invasive *Escherichia coli*. *J. Mol. Biol.* 431, 2970–2981. doi: 10.1016/j.jmb.2019.04.023
- Truong-Bolduc, Q. C., Bolduc, G. R., Medeiros, H., Vyas, J. M., Wang, Y., and Hooper, D. C. (2015). Role of the Tet38 efflux pump in *Staphylococcus aureus* internalization and survival in epithelial cells. *Infect. Immun.* 83, 4362–4372. doi: 10.1128/IAI.00723-15
- Urdaneta, V., and Casadesús, J. (2018). Adaptation of *Salmonella enterica* to bile: essential role of AcrAB-mediated efflux. *Environ. Microbiol.* 20, 1405–1418. doi: 10.1111/1462-2920.14047
- Vazeille, E., Buisson, A., Bringer, M. A., Goutte, M., Ouchchane, L., Hugot, J. P., et al. (2015). Monocyte-derived macrophages from Crohn's disease patients are impaired in the ability to control intracellular adherent-invasive *Escherichia coli* and exhibit disordered cytokine secretion profile. *J. Crohns Colitis* 9, 410–420. doi: 10.1093/ecco-jcc/jjv053
- Zhang, Y., Xiao, M., Horiyama, T., Zhang, Y., Li, X., Nishino, K., et al. (2011). The multidrug efflux pump MdtEF protects against nitrosative damage during the anaerobic respiration in *Escherichia coli*. *J. Biol. Chem.* 286, 26576–26584. doi: 10.1074/jbc.M111.243261

Conflict of Interest: The authors declare that the research was conducted in the absence of any commercial or financial relationships that could be construed as a potential conflict of interest.

Copyright © 2020 Fanelli, Pasqua, Colonna, Prosseda and Grossi. This is an open-access article distributed under the terms of the Creative Commons Attribution License (CC BY). The use, distribution or reproduction in other forums is permitted, provided the original author(s) and the copyright owner(s) are credited and that the original publication in this journal is cited, in accordance with accepted academic practice. No use, distribution or reproduction is permitted which does not comply with these terms.



Antibiotic Resistance: Moving From Individual Health Norms to Social Norms in One Health and Global Health

Sara Hernando-Amado¹, Teresa M. Coque², Fernando Baquero² and José L. Martínez^{1*}

¹ Centro Nacional de Biotecnología, Consejo Superior de Investigaciones Científicas (CSIC), Madrid, Spain, ² Hospital Universitario Ramón y Cajal, Instituto Ramón y Cajal de Investigación Sanitaria (IRYCIS) and Centro de Investigación Biomédica en Red Epidemiología y Salud Pública (CIBERESP), Madrid, Spain

OPEN ACCESS

Edited by:

Paolo Visca,
Roma Tre University, Italy

Reviewed by:

Tim Johnson,
Purdue University, United States
Raffaele Zarrilli,
University of Naples Federico II, Italy
Amy Pruden,
Virginia Tech, United States

*Correspondence:

José L. Martínez
jlmtnez@cnb.csic.es

Specialty section:

This article was submitted to
Antimicrobials, Resistance
and Chemotherapy,
a section of the journal
Frontiers in Microbiology

Received: 30 March 2020

Accepted: 21 July 2020

Published: 28 August 2020

Citation:

Hernando-Amado S, Coque TM,
Baquero F and Martínez JL (2020)
Antibiotic Resistance: Moving From
Individual Health Norms to Social
Norms in One Health and Global
Health. *Front. Microbiol.* 11:1914.
doi: 10.3389/fmicb.2020.01914

Antibiotic resistance is a problem for human health, and consequently, its study had been traditionally focused toward its impact for the success of treating human infections in individual patients (individual health). Nevertheless, antibiotic-resistant bacteria and antibiotic resistance genes are not confined only to the infected patients. It is now generally accepted that the problem goes beyond humans, hospitals, or long-term facility settings and that it should be considered simultaneously in human-connected animals, farms, food, water, and natural ecosystems. In this regard, the health of humans, animals, and local antibiotic-resistance-polluted environments should influence the health of the whole interconnected local ecosystem (One Health). In addition, antibiotic resistance is also a global problem; any resistant microorganism (and its antibiotic resistance genes) could be distributed worldwide. Consequently, antibiotic resistance is a pandemic that requires Global Health solutions. Social norms, imposing individual and group behavior that favor global human health and in accordance with the increasingly collective awareness of the lack of human alienation from nature, will positively influence these solutions. In this regard, the problem of antibiotic resistance should be understood within the framework of socioeconomic and ecological efforts to ensure the sustainability of human development and the associated human–natural ecosystem interactions.

Keywords: One Health, Global Health, antibiotic resistance, waste water, farming

INTRODUCTION

The problem of antibiotic resistance (AR) has been traditionally addressed by focusing on human-linked environments, typically health care facilities. Nevertheless, it is now generally accepted that most ecosystems may contribute to the selection and spread of AR (Aminov, 2009; Martínez et al., 2009; Davies and Davies, 2010; Martínez, 2014; Berendonk et al., 2015; Larsson et al., 2018). A key conceptual point is that, based on cultural, humanitarian, and economic reasons, we have historically preserved the health of individual humans and farming animals. To that purpose, the same families of antimicrobial agents have been used. As a consequence, their positive (healing) and negative (selection of AR, therapeutic failure) effects have influenced the common health of humans and animals in particular locations (One Health). The concept *One Health*, first used

in early twentieth century, expands the integrative thinking about human and animal medicine, including for the first time ecology, public health, and societal aspects (Zinsstag et al., 2011). In the case of AR, the One Health perspective focuses on the risk assessment of emergence, transmission, and maintenance of AR at the interface between humans, animals, and any other linked (local) environment (Robinson et al., 2016; Jean, 2017). Consequently, the application of One Health approaches demands integrative surveillance tools and interventions based on multidisciplinary approaches that include ecological and sociodemographic factors, besides more classic epidemiological models.

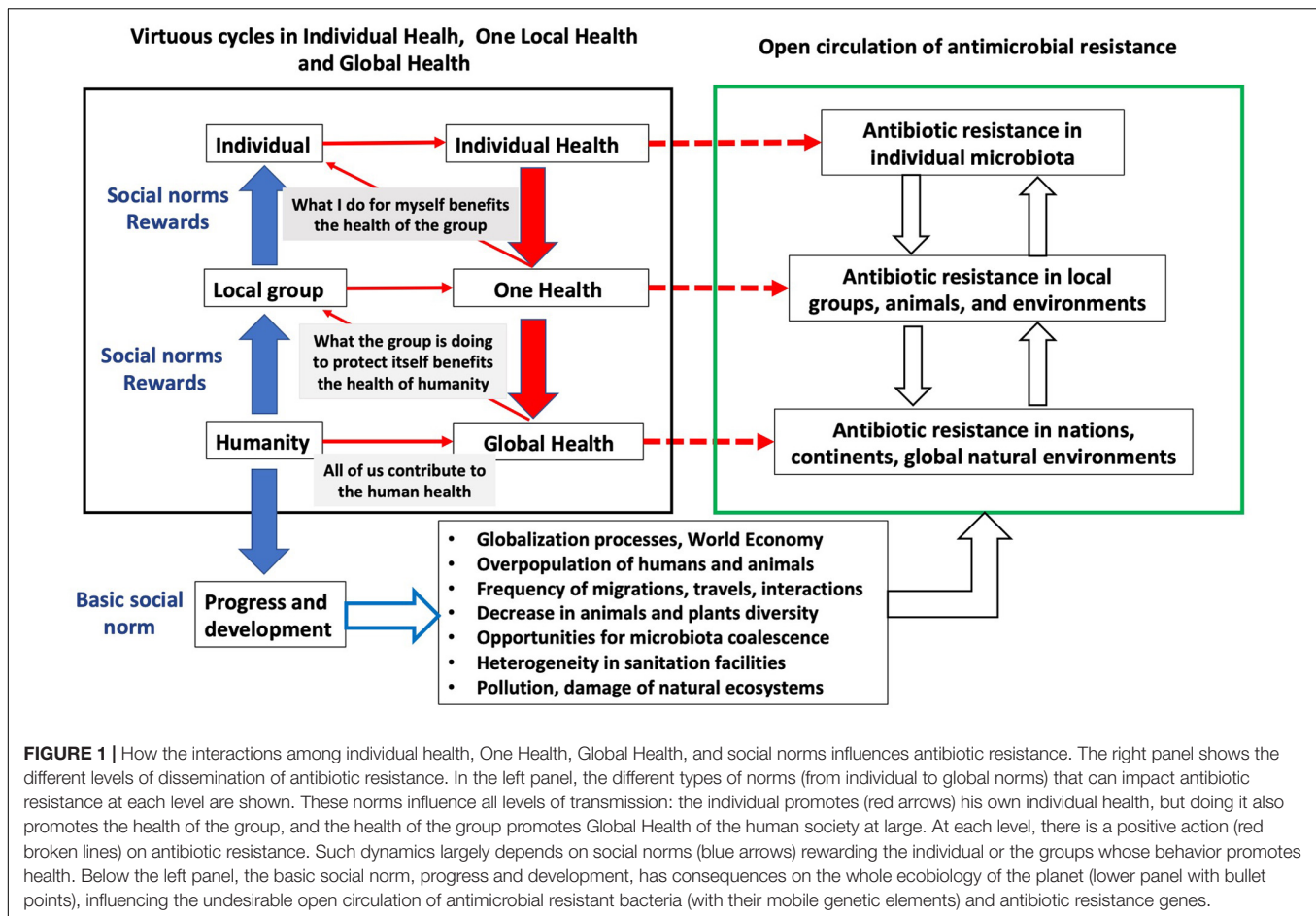
Global Health is based on a broad collaborative and transnational approach to establish “health for all humans.” In this case, it focuses AR at a general (global) scale, considering that the selection and global spread of antibiotic-resistant bacteria (ARBs) and antibiotic resistance genes (ARGs) are a problem that influences the health of human societies with disparate social and economic structures and is linked to many societal and ecological factors (Chokshi et al., 2019). Interventions to reduce AR burden in a global world certainly require common and integrated policy responses of countries, international organizations, and other actors (stakeholders included). Its goal is the equitable access to health and minimizing health risks all over the globe. Besides its objective aspects (i.e., how travelers, migrating birds, or international commerce may contribute to AR spread), it has important international political aspects. It focuses in how countries and international organizations address the elements connecting and potentially spreading AR among humans, animals, and natural ecosystems at the Earth scale (Wernli et al., 2017). In summary, the problems and the potential solutions concerning AR are not confined to particular regions, but have a global dimension: a problem for all humans, animals, and natural ecosystems, which should be solved with interventions aiming to improve health for all of them (Brown et al., 2006; Koplan et al., 2009; Laxminarayan et al., 2013). In the context of AR, a healthy environment would be an environment where AR is low or can be controlled by human interventions (Hernando-Amado et al., 2019; Andersson et al., 2020).

Of course, the Global Health concept of “health of an environment” (Iavarone and Pasetto, 2018; Pérez and Pierce Wise, 2018; Bind, 2019; van Bruggen et al., 2019) or, in general, Planetary Health (Lerner and Berg, 2017), has an unavoidable anthropogenic flavor. In practice, we consider “healthy environments” or “healthy ecosystems” those that minimize their current or their potential harm for the human individual or the society, in our case for AR. In other words, we adopt a selfish strategy, which should be necessarily implemented by the international (global) institutions. Selfishness (Kangas, 1997) applies mainly to individuals, but also to societal groups. However, these groups have not enough possibilities to act alone in the case of infectious diseases in general and AR in particular, which may expand worldwide. Therefore, individual selfishness for health should be integrated in local One Health and also in Global Health actions. The goal of controlling AR is a highly complex one, and its dimension has been compared to climate change or biodiversity loss, problems where individual actions

are not enough for providing a solution, and consequently, individual freedom is confronted with collective responsibility (Looker and Hallett, 2006).

The construction of human societies reflects the tension between individual freedom and social rules/laws. The implementation of different social rules/laws for regulating human activities within a society is mainly based on moral (as Kant’s categorical imperative (Kant, 1785) or religious-based brotherhood (Matthew 22:35–40) statements), social stability (as anticrime laws; Schiavone, 2012), organizative (type of government and how it is formed, group identity), and efficacy (as antitrust laws; Ricardo, 1821) arguments. However, these arguments mainly apply for establishing the socioeconomic organization as well as the individual welfare within a society. The situation concerning human health is somehow different. There are individual diseases, such as cancer or stroke, and social diseases, such as transmissible infections. For the firsts, social norms (as consciousness of the importance of the control of cholesterol, excess sugar uptake, or hypertension levels) are well established, and even laws (non-smoking regulations) had been implemented in occasions. However, the main impact of these regulations is at the individual health level (Wikler, 2002), because the associated diseases are not physically transmissible. A different situation happens in the case of infectious diseases in general and of AR in particular. For these diseases, everything that happens in a single person affects any one around. Further, the fact that an ARG emerging in a given geographic area can spread worldwide implies that neither individual norms nor country-based norms have been sufficient until now to counteract the worldwide spread of AR.

One important aspect of laws in democratic societies is that they must be well accepted by the community, so that the acceptance of social norms usually comes first than their implementations as rules/laws. Actually, the efficiency of democracy for responding to social crisis (as current AR or COVID-19 crises), in opposition to other more autocratic regimens where decisions are implemented top-down, had been the subject of debate from the early beginning of democratic revolutions (Tocqueville, 1838; Hobbes, 1968; Rousseau, 1974; Spinoza, 2007). In this regard, it is important to remark that One Health aspects of AR can be tackled in the basis of country-level regulations that are linked to the socioeconomic and cultural aspects of each country (Chandler, 2019; Chokshi et al., 2019). However, because global Earth governance does not exist, Global Health control of AR is based on recommendations, rather than in rules/laws. Consequently, the acceptance of social norms, starting within individuals or small organizations and expanding throughout the whole society (Figure 1), is fundamental to provide global solutions to the AR problem (Nyborg et al., 2016; Chandler, 2019). The acceptance by the community of these social norms, considering that the way of promoting these norms might differ in different parts of the world (Cislaghi and Heise, 2018; Cislaghi and Heise, 2019), largely depends on the transfer to the society of the knowledge required to understand the mechanisms and the impact for human health of the emergence and transmission of AR, an information that is discussed below.



DEFINING THE BRICKS BUILDING UP ANTIBIOTIC RESISTANCE IN A GLOBALIZED WORLD

The classic definition of AR is based only on the clinical outcome of the infected patient. An organism is considered resistant when the chances for the successful treatment of the infection it produces are low (Martinez et al., 2015). This definition, which is the most relevant in clinical settings, presents some limitations for studies based on One Health approaches that include the analysis of non-infective organisms, which lack a clinical definition of resistance, as well as analysis of the distribution of ARGs, in several occasions, using non-culture-based methods (Martinez et al., 2015). Even in the case of animal medicine, antibiotic concentration breakpoints defining resistance are still absent for some veterinary-specific antimicrobials and poorly defined for different types of animals with disparate weights, which would influence the availability of the drug inside animal body (Toutain et al., 2017; Sweeney et al., 2018). To analyze AR beyond clinical settings, the term *resistome*, understood as the set of genetic elements that can confer AR, irrespectively of the level of resistance achieved, in a given organism/microbiome was coined (D'Costa et al., 2006; Wright, 2007; Perry et al., 2014).

AR acquisition is the consequence of either mutation (or recombination) or recruitment of ARGs through horizontal gene transfer (HGT), transformation included. AR mutations are generally confined to their original genomes, propagating vertically and not spreading among bacterial populations, although some few exceptions of horizontal transfer of chromosomal regions containing AR mutations have been described (Coffey et al., 1991; Ferrandiz et al., 2000; Novais et al., 2016; Nichol et al., 2019). The set of mutations that confer AR can be dubbed as the mutational resistome. Current whole-genome-sequencing methods of analysis can allow defining the mutational resistome in an isolated microorganism (Cabot et al., 2016; Lopez-Causape et al., 2017). However, they are not robust enough yet for determining the mutational resistome in metagenomes. Consequently, the impact of these analyses in One Health studies is still limited and will not be further discussed in the present review.

Concerning their relevance for acquiring AR, ARGs can be divided in two categories. The first one comprises the genes forming the intrinsic resistome (Fajardo et al., 2008), which includes those that are naturally present in the chromosomes of all (or most) members of a given bacterial species and have not been acquired recently as the consequence of antibiotic selective pressure. Despite that these genes contribute to AR of bacterial

pathogens, they are responsible just for the basal level of AR, which is taken into consideration when antibiotics are developed. In this regard, unless these genes, or the elements regulating their expression mutate, they are not a risk for acquiring resistance and have been considered as phylogenetic markers (Martinez et al., 2015). Further, it has been discussed that these genes may contribute to the resilience of microbiomes to antibiotic injury (Ruppe et al., 2017b), hence constituting stabilizing element of microbial populations when confronted with antibiotics more than a risk for AR acquisition by pathogens.

The second category, dubbed as the *mobilome*, is formed by ARGs located in mobile genetic elements (MGEs) that can be transferred both vertically and horizontally, hence allowing AR dissemination among different bacteria (Frost et al., 2005; Siefert, 2009; Jorgensen et al., 2014; Lange et al., 2016; Martinez et al., 2017).

While the analysis of the resistome of microbiota from different ecosystems has shown that ARGs are ubiquitously present in any studied habitat (D'Costa et al., 2006; Walsh, 2013; Jana et al., 2017; Lanza et al., 2018; Chen et al., 2019b), the impact of each one of these ARGs for human health is different. Indeed, it has been stated that the general resistome of a microbiome is linked to phylogeny and to biogeography, indicating that most ARGs are intrinsic and do not move among bacteria (Pehrsson et al., 2016). However, some ARGs escape to this rule and are shared by different ecosystems and organisms (Forsberg et al., 2012; Fondi et al., 2016). These mobile ARGs, frequently present in plasmids (Tamminen et al., 2012; Pehrsson et al., 2016), are the ones that are of special concern for human health.

Although not belonging to the antibiotic resistome, genes frequently associated with resistance to other antimicrobials, such as heavy metals or biocides, as well as the genes of the MGEs backbones, eventually involved in the transmission and selection of ARGs among microbial populations, the mobilome at large, are also relevant to track the emergence and dissemination of AR among different habitats (Lanza et al., 2015; Martinez et al., 2017; Baquero et al., 2019).

HGT processes are recognized as the main mechanisms for transmission of genetic information (Baquero, 2017). From the ecological point of view, HGT should be understood as a cooperative mechanism that allows the exploitation of common goods as ARGs (Baquero et al., 2019) by different members within bacterial communities. In fact, some studies suggest that the ecological consequences of HGT events in AR evolution are contingent on the cooperation of complex bacterial communities, besides the acquisition of individual adaptive traits (Smillie et al., 2011). However, the understanding of the ecological causes and consequences of ARGs transmission among organisms and microbiomes is still limited from the One Health and Global Health perspectives.

HGT-mediated AR is a hierarchical process (**Figure 2**) in which ARGs are recruited by gene-capture systems as integrons and afterward integrated in MGEs as plasmids, insertion conjugative elements, or bacteriophages (Frost et al., 2005; Garcia-Aljaro et al., 2017; Gillings et al., 2017; Botelho and Schulenburg, 2020), which afterward are acquired by specific bacterial clones. Selection at each of these levels will also select

for all the elements involved in AR spread. For instance, the acquisition of an ARG by a clone may promote the expansion of the latter (and of all the genetic elements it contains, other ARGs included) in antibiotic-rich environments, such as hospitals or farms (Martinez and Baquero, 2002; Schaufler et al., 2016), and *vice versa*, the introduction of an ARG in an already successful clone may increase the chances of this resistance gene for its dissemination even in environments without antibiotics, unless the associated fitness costs are high. In this sense, if ARG acquisition reduces the fitness, and this implies a decreased capability for infecting humans (see below), the burden for human health might eventually be lower. Nevertheless, it is relevant to highlight that AR transmission cannot be understood just by analyzing the genetic mechanisms involved and the consequences of such acquisition for the bacterial physiology. Indeed, as discussed below, there are ecological and socioeconomic elements that strongly influence AR dissemination.

HIGHWAY TO ANTIBIOTIC RESISTANCE

The evolution of AR comprises the emergence, the transmission, and the persistence of ARBs (Martinez et al., 2007; Baquero et al., 2011). Concerning human health, selection of ARBs/ARGs is particularly relevant at the individual health level, whereas transmission is a main element to be taken into consideration at the One Health and Global Health levels (**Figure 2**). Indeed, unless AR is transmitted, it will be just an individual problem that would not affect the community at large.

It is generally accepted that non-clinical ecosystems are often primary sources of ARGs (Davies, 1994). As above stated, after their capture and integration in MGEs (**Figure 2**), ARGs and their bacterial hosts can contaminate different ecosystems, which might then be involved in their global spread (Martinez, 2012; Fondi et al., 2016; Gillings, 2017; Gillings et al., 2017). This means that nearly any ecosystem on Earth, along with the human-driven changes produced in it, may modulate evolution of AR. Importantly, the huge escalation and worldwide expansion of a limited set of animals, plants, and their derived products, including foods, due to the anthropogenic selection of a few breeds and cultivars for mass production in livestock and agricultural industries (Okeke and Edelman, 2001; Zhu et al., 2017) of economic interest have collapsed the variability and biodiversity of animals and plants (Seddon et al., 2016). Because these organisms harbor particular host-adapted bacteria, which are frequently under antibiotic challenge, this situation, together with the ecological similarities of human habitats, might favor AR spread (Martiny et al., 2006; Manyi-Loh et al., 2018). Indeed, while in underdeveloped areas of the world food animals are very diverse, intensive farming, common in developed countries, ensures a “shared-stable” environment where only the most productive types prevail (Kim et al., 2017). The common genetic origin of these types and the process of microbiota acquisition from nearby animals in intensive farming should homogenize also their microbiomes with consequences for AR dissemination. Actually, it has been shown that the loss of microbial diversity

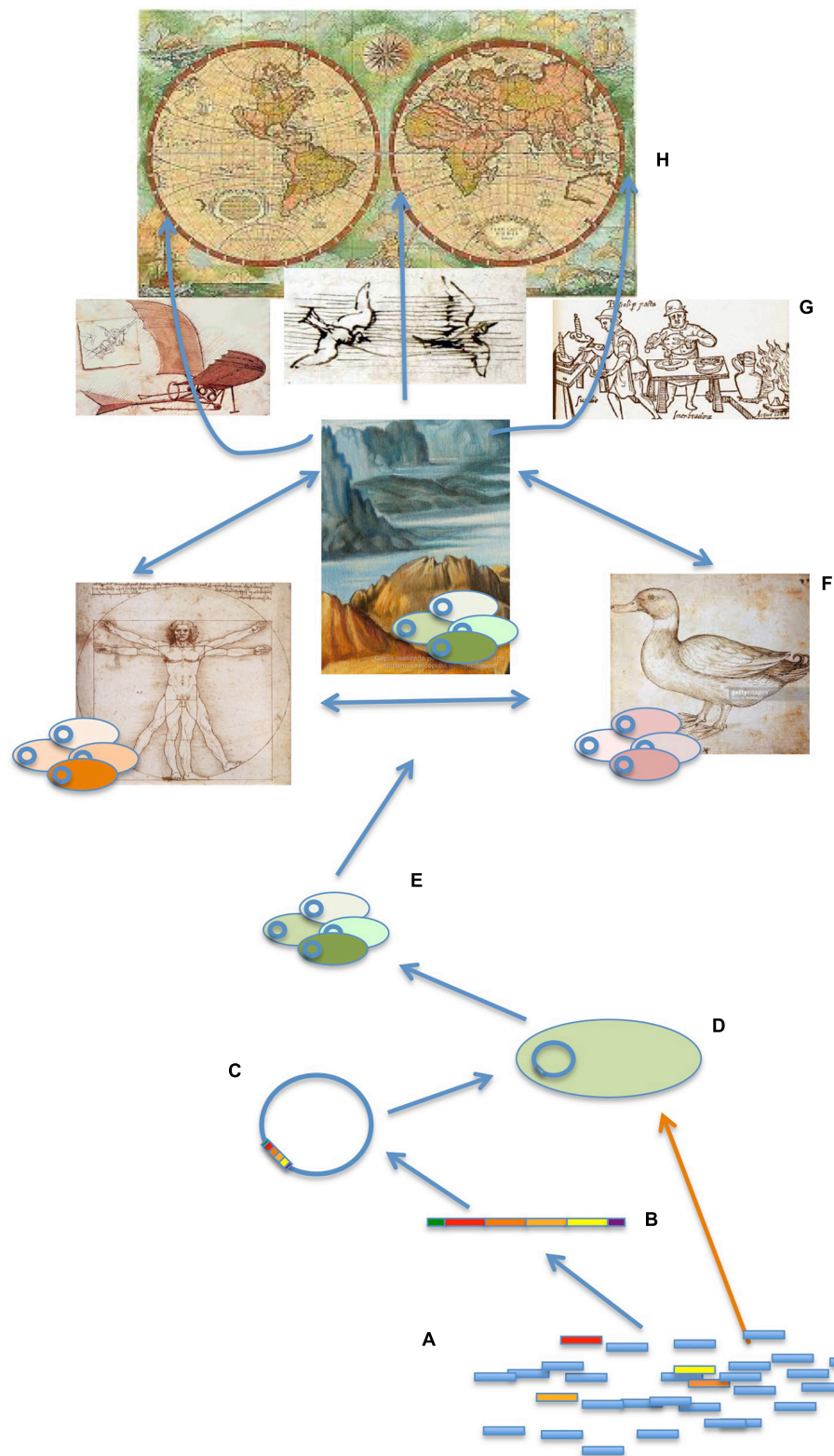


FIGURE 2 | Genetic, ecological, and socioeconomic elements mediating the transmission of antibiotic resistance. ARGs are ubiquitously present in any studied microbiome (A). However, only a few of them are transferred to human/animal pathogens, hence constituting a health problem. The genetics events implied include the acquisition of ARGs by gene-recruiting genetic elements such as integrons (B); the integration of these elements in MGEs as plasmids, bacteriophages, or (Continued)

FIGURE 2 | Continued

insertion conjugative elements **(C)**; and the acquisition of these elements by specific bacterial clones **(D)**. These ARBs can share these elements among the members of gene-sharing communities **(E)** and also move among different ecosystems, including humans, animals (particularly relevant farm animals), and natural ecosystems (with a particular relevance for water bodies). The connection of these ecosystems, as well as the reduced diversity of animals, plants, and in general habitats as the consequence of human activities, allows the different microbiomes to be in contact, favoring ARGs transmission among the microorganism they encompass **(F)**. This transmission is facilitated at the global scale by travel, animal migration, trade of goods, and eventually by meteorological phenomena, climate change included **(G)**, hence producing a Global Health problem **(H)**. While most studies on the dissemination of ARGs focus on MGEs (Davies, 1997; Muniesa et al., 2013; Lanza et al., 2015; Garcia-Aljaro et al., 2017), recent works suggest that the contribution of natural transformation (orange arrow), allowing the direct uptake of ARGs by natural competent microorganisms, may have been underestimated (Domingues et al., 2012; Blokesch, 2017). Further, competence can occur due to interbacterial predation (Veening and Blokesch, 2017), a biological interaction that may facilitate the acquisition of beneficial adaptive traits by predator bacterial species (Cooper et al., 2017; Veening and Blokesch, 2017). Other HGT mechanisms, such as DNA packing in extracellular vesicles (ECV) or transference of DNA through intercellular nanotubes, also seem to be relevant in nature (Dubey and Ben-Yehuda, 2011; Fulsundar et al., 2014). While the biotic conditions that may enhance HGT have been studied in detail, less is known concerning abiotic modulation of ARGs transfer. Under contemporary conditions, at least 10^{24} microorganisms are affected by a freeze-and-thaw cycle, at least 10^{19} are agitated by sand, and at least 10^{17} are subjected to conditions suitable for electrotransformation every year (Kotnik and Weaver, 2016).

may favor AR spread (Chen et al., 2019a). Note that, beyond the transmission of particular AR spreading clones, AR is expected to spread in farms by the modification (eventually homogenization) of animals' microbiota. Notwithstanding, even farm workers are subject to microbiome acquisition from animals, leading to microbiome coalescence (Baquero et al., 2019; Sun et al., 2020). It is to be noticed, and the recent COVID-19 crisis exemplifies it, that besides economic development, cultural habits are relevant in the use of animals for food, a feature that has not been analyzed in detail, particularly with respect to their role as vectors potentially involved in AR dissemination.

Despite that the homogenization of hosts may help in AR transmission, the spread of ARBs has some constraints, because the differential capability of each bacterial clone for colonizing different hosts may modulate their dissemination. Indeed, while some species and clones are able to colonize/infect different animal species, humankind included, several others present some degree of host specificity (Price et al., 2017; Sheppard et al., 2018). Further, it has been shown that the capacity to colonize a new host is frequently associated with a reduction in the capacity for colonizing the former one. The same happens for mobile ARGs; they are encoded in MGEs that present different degrees of host specificity, which defines the formation of gene-exchange communities, where the interchange of genetic material among members is facilitated (Skippington and Ragan, 2011). Conversely, the incorporation of different replicons and modules within plasmid backbones, a feature increasingly reported (Douarre et al., 2020), would enable ARG replication in different clonal/species background and thus modify the community network of ARGs. Actually, the risk for humans of animal-based AR seems to be linked in most cases to shuttle, generalist clones able to colonize humans and particular animals (Price et al., 2017; Sheppard et al., 2018). The understanding of the elements driving the transfer of AR among animals, humans included (**Figure 3**), requires the comprehensive survey of the clones and ARGs that are moving among them (European Food Safety Authority et al., 2020). Tools to track the global epidemiology of antimicrobial-resistant microorganisms such as Bigsdb (Jolley et al., 2018) or comprehensive databases of ARGs, ideally providing information of their mobility (Zankari et al., 2012; Alcock et al., 2020), are fundamental for studying AR transmission at a global level.

It is worth mentioning that, because humans constitute a single biological species, the human-associated organisms spread easily among all individuals. In fact, more prominent differences in humans' microbiome composition can be observed between individuals than among ethnic groups, even though, as expected, the resemblance in microbiotas is higher among those groups that are geographically clustered (Deschasaux et al., 2018; Gaulke and Sharpton, 2018). Some groups of human population are, however, more prone to acquire ARBs, due either to socioeconomic or to cultural factors. In LMICs (low- to medium-income countries) and BRICS (Brazil, Russia, India, China, and South Africa) countries, the combination of wide access to antibiotics, weak health care structures, and poor sanitation defines certainly a dangerous landscape. Moreover, the progressive aging of the Western population might favor the establishment and further expansion of an elderly reservoir of ARBs and ARGs, an issue that deserves further studies. The hypothesis that the microbiome of elder people might be a reservoir of AR is based not only on their cumulative history of antibiotic exposure and contacts with health care centers, but also on the rampant use of antibiotics of this population more prone to suffer from acute, chronic, or recurrent infections. Significant worldwide advances in the organization of medical care of the elderly people lead to frequent hospitalizations, but health care centers may also facilitate the selection and further amplification of AR in the community. In addition, this may subsequently favor the entry of high-risk clones and of ARGs in the hospital setting (Hujer et al., 2004).

As stated above, there is a global increasing permeability of the natural biological barriers that have historically prevented bacterial dissemination through different ecosystems. Besides local spread of AR in environments shared by animals and humans, which has to be addressed under a One Health approach, AR can disseminate worldwide (**Figure 2**) by economic corridors that promote the global interchange of goods and trade or human travelers or by natural bridges, such as animal migration paths or natural phenomena such as air and water movements (Okeke and Edelman, 2001; Baquero et al., 2008; Allen et al., 2010; Overdevest et al., 2011; Kluytmans et al., 2013; Fondi et al., 2016). The result is the appearance of similar ARBs and ARGs in different geographic areas. As the consequence, AR is a Global Health problem in the sense that an ARB that emerges in a

given place can rapidly spread worldwide. Indeed, multidrug-resistant bacteria, similar to those encountered in clinical settings, have been detected in human isolated populations that were not previously in contact with antibiotic, as well as in wildlife (Clemente et al., 2015). This indicates that pollution with ARGs is present even in places where antibiotic concentrations are low (Kümmerer, 2004) and might involve mechanisms of transmission that do not require selection. For instance, migrating birds can carry enteropathogenic bacteria resistant to different antibiotics (Middleton and Ambrose, 2005; Poeta et al., 2008), and international travelers, even those not receiving antibiotic treatments, also contribute to AR transfer among different geographic regions (Murray et al., 1990; Reuland et al., 2016). In the group of long travelers are refugee people, in which dissemination of multidrug-resistant strains is favored by the poor sanitary conditions and overcrowding camps that refugees confront (Maltezou, 2016).

A final issue concerning AR is its stability in the absence of selection. It has been proposed that the acquisition of AR reduces bacterial competitiveness in the absence of antibiotics (fitness costs) (Andersson and Hughes, 2010; Martinez et al., 2011); certainly, a wishful proposition such as, if true, the reduction in the use of drugs or eventually antibiotic-cycling strategies should decrease AR (Beardmore et al., 2017). Nevertheless, eliminating the use of an antibiotic does not produce a full decline of AR (Sundqvist et al., 2010). In fact, different studies have shown that AR not always reduces fitness but also can even increase bacterial competitiveness (Andersson and Hughes, 2010; Schaufli et al., 2016). In addition, compensatory mutations or physiological changes that restore fitness can be selected in resistant bacteria (Andersson, 2006; Schulz zur Wiesch et al., 2010; Olivares et al., 2014). It is a fact, however, that although ARBs are found nearly everywhere, including wild animals, natural ecosystems, or people from isolated populations without contact with antibiotics, among others (Durso et al., 2012; Clemente et al., 2015; Alonso et al., 2016; Fitzpatrick and Walsh, 2016; Power et al., 2016), AR prevalence is consistently lower when antibiotics are absent, which suggests that pollution may impact AR, a feature that is discussed below.

ANTIBIOTIC RESISTANCE IN AN ANTHROPOGENICALLY IMPACTED WORLD

Pollution of natural ecosystems is associated with activities that have driven relevant economic transition, in principle favoring human welfare, such as mining, industry, intensive land use, or intensive farming, among others. Notwithstanding, globalization of health services, as well as the shift toward intensive farming, besides their positive contribution to human well-being, has rendered an increasing pollution by compounds with pharmacological properties of natural ecosystems, particularly water bodies, which may disrupt the stability of these ecosystems (Oldenkamp et al., 2019). Among them, antibiotics are considered the most relevant cause of AR selection. Despite regulations for reducing their use (Van Boeckel et al., 2017),

a substantial increase in global antibiotic consumption has occurred in the last years, and an even greater increase is forecasted in the next years (Klein et al., 2018).

However, antibiotics are not the unique pollutants that can prime the selection and spread of AR. In this regard, it is important to highlight that heavy metals are one of the most abundant pollutants worldwide (Panagos et al., 2013). Their abundance results from anthropogenic-related activities, such as mining, industry, agriculture, farming, or aquaculture and even for therapeutic use in ancient times. Importantly, they may persist in nature for long periods of time. Further, likely because metal pollution occurred before the use of antibiotics, heavy metal resistance genes were incorporated to MGE backbones before ARGs (Mindlin et al., 2005; Staehlin et al., 2016). This means that heavy metals may coselect for MGEs and the ARGs they harbor (Partridge and Hall, 2004; Staehlin et al., 2016; Zhao et al., 2019a). Even more, the presence of heavy metals, as well as of biocides or sublethal antibiotic concentrations (Jutkina et al., 2018; Zhang et al., 2018), may stimulate HGT, as well as modify the dynamics of antibiotics, such as tetracyclines, in natural ecosystems (Hsu et al., 2018). Coselection may also occur when a single resistance mechanism, such as an efflux pump, confers resistance to both heavy metals and antibiotics (cross-resistance) (Pal et al., 2017).

Although most published works analyze the effect of different pollutants on their capacity to select ARBs or ARGs, it is important to highlight that ARGs should also be considered pollutants themselves. Actually, a recent work indicates a close relationship between the abundance of ARGs and fecal pollution (Karkman et al., 2019). In this respect, it is worth mentioning that, differing to classic pollutants, ARGs/ARBs are not expected to disappear along time and space, but rather, their abundance may even increase as the consequence of selection and transmission (Martinez, 2012). While the direct selection of AR by antibiotics or the coselection mediated by other pollutants, as the aforementioned heavy metals, has been discussed (Wales and Davies, 2015), the effect of other types of human interventions on the dissemination of ARGs and ARBs through natural ecosystems has been analyzed in less detail. As an example, it has been proposed that wastewater treatment plants, where commensals, ARBs, ARGs, and antibiotics coexist, could act as bioreactors favoring the selection and transmission of ARGs between different organisms (Rizzo et al., 2013; Su et al., 2017; Manaia et al., 2018), although evidences supporting this statement are scarce (Munck et al., 2015; Azuma et al., 2019).

In addition to the aforementioned pollutants with a direct effect in AR selection, it is worth noting that there are other abundant contaminants, such as sepiolite (present in cat litters or used as a dietary coadjuvant in animal feed) or microplastics, present in almost all aquatic ecosystems, which can favor the transmission of ARGs or MGEs between bacterial species (Rodriguez-Beltran et al., 2013; Kotnik and Weaver, 2016; Arias-Andres et al., 2018), hence amplifying the AR problem at a global scale.

Finally, the possible effect of climate change on the spread of AR is worth mentioning. Indeed, it modifies the biogeography

of vectors (such as flies, fleas or birds) involved in the spread of infectious diseases (Fuller et al., 2012; Beugnet and Chalvet-Monfray, 2013). In addition, the increase of local temperatures seems to correlate with an increased AR abundance in common pathogens (MacFadden et al., 2018). Besides, climate change is affecting ocean currents (Martinez-Urtaza et al., 2016), which may allow the intercontinental distribution of ARBs and ARGs (Martinez, 2009a,b). Although this phenomenon might contribute to the globalization of AR, further research is needed to clearly demonstrate a cause–effect relationship.

It is relevant to mention that increased pollution and climate change are the unwanted consequences of human development. It would then be worth discussing how human development in general may impact (positively and negatively) AR, a feature that is analyzed below.

ANTIBIOTIC RESISTANCE AS A GLOBAL DEVELOPMENT PROBLEM

Human development is a necessity of our human behavior, although different models of development have been and are proposed, each one producing different impacts in the structure of human societies and on the preservation and stability of natural ecosystems (Fenech et al., 2003; Farley and Voinov, 2016; Seddon et al., 2016). Nevertheless, even for different socioeconomic models, there are some social norms that tend to be widely accepted, in particular those aiming to improve individual well-being. This implies the establishment of a society of welfare, understood as a right of any human on Earth, a feature that depends on the economic development, and can be particularly relevant in the case of transmissible infectious diseases in general and of AR in particular.

A continuously repeated mantra in worldwide AR policies is that the abusive consumption of antibiotics for the treatment or prevention of infections in humans and animals constitutes the major driver of AR. However, we should keep in mind that antibiotics constitute an important example of human progress supporting individual and global human health. In fact, the origin of the massive production of antimicrobials was a consequence of the needs resulting from World War II in the 1940s. This was followed by many decades of human progress, most importantly by the common understanding of equal human rights, which was followed by the economic and social development (including medicine and food industry) of densely populated regions in the planet, including India and China. These countries are currently among the leaders in the production and consumption of antimicrobial agents. Notwithstanding, as in any area of economy, progress bears a cost that, in this case, is antibiotic pollution of the environment, globally accelerating the process of the emergence, the transmission, and the persistence of ARBs (Martinez et al., 2007; Baquero et al., 2011).

The non-controlled use of antibiotics is facilitated in LMICs with disparate economic growth by different factors. Heterogeneous regulation of antibiotic sales and prescriptions (often weak or missing) and the increase of online on-bulk sales

in recent years contribute to their overuse (Mainous et al., 2009). Most of live-saving medicines represent out-of-pocket costs in most LMICs, which led to an exacerbated use of cheap (usually old and less effective) antibiotics, phasing out their efficacy and increasing the demands and prices for the most expensive ones, eventually resulting in treatment unavailability (Newton et al., 2011). Further, the cost of treating AR infections is much higher than that of treating susceptible ones, which is increasing the cost of health services (Wozniak et al., 2019). Conversely, the growing economic capability of LMICs in the BRICS category triggers the access of the population to health services and last-resort antibiotics. These countries also face a sudden high demand for meat and thus a prompt industrialization of animal production that has favored the misuse of antibiotics for growth promotion facilitated by their online availability (Mainous et al., 2009). In addition, counterfeit or substandard antibiotics recently become a serious global problem (Gostin et al., 2013), which is exacerbated in LMICs, where they represent up to a third of the available drugs. Noteworthy, 42% of all reports received by the WHO Global Surveillance and Monitoring System on substandard and falsified medicines worldwide come from Africa, and most of them correspond to antimalarials and antibiotics (Newton et al., 2011; Gostin et al., 2013; Hamilton et al., 2016; Petersen et al., 2017).

Despite this situation, it is important to highlight that human consumption of antibiotics is an unavoidable need to preserve human health. In fact, most health problems dealing with infections in LMICs are still caused by a poor access to antibiotics, not by an excessive use of them. Proof of this is the fact that the distribution of antibiotics has reduced endemic illnesses and children mortality in Sub-Saharan Africa (Keenan et al., 2018). This means that, while a global decline in the use of antibiotics would be desirable to diminish the problem of AR, there are still several parts in the globe where antibiotic use should still increase to correctly fight infections. In fact, our primary goal should not be to reduce the use of antibiotics, but to ensure the effective therapy of infectious diseases for the long term. This does not mean that AR is not a relevant problem in LMICs; it means that reducing antibiotic use is not enough to solve the problem. Indeed, the current high morbidity and mortality due to infectious diseases (malaria, tuberculosis, low respiratory infections, sepsis, and diarrhea) in LMICs will be worsened in the absence or low efficiency of therapeutic treatments. Further, AR has economic consequences. According to World Bank, 24.1 million people could fall into extreme poverty by 2050 because of AR, most of them from LMICs (Jonas and World Bank Group Team, 2017).

Consequently, besides a Global Health problem, AR has an important economic impact (Rudholm, 2002), hence constituting a Global Development Problem, endangering not only the achievements toward the Millennium Development Goals but also the Sustainable Development Goals (van der Heijden et al., 2019). World Bank estimates that AR could impact the gross domestic product from 1 to 3.8%, which is even higher than what is estimated for the climate change (Jonas and World Bank Group Team, 2017). These economic foresights are linked to the threads of increased poverty, food sustainability, Global Health

deterioration (associated with both food safety and affordability to health care), and environment protection. All these issues are also impacted by the overuse and misuse of antibiotics, its lack of effectiveness, and the affordability to medicines and health care (van der Heijden et al., 2019).

When talking about reducing antibiotic consumption, it is important to remind that up to two-thirds of overall antibiotic usage is for animal husbandry (Done et al., 2015). Further, recent work states that the use of antibiotics in crops, particularly in LMICs, might have been largely underestimated (Taylor and Reeder, 2020). Despite that evidences on the presence of common ARGs distributed among animals and humans were published decades ago (Bager et al., 1997; Wegener et al., 1997; Aarestrup, 1998; Aarestrup et al., 1998), and although the use of antibiotics as growth promoters has been banned in different countries (Cox and Ricci, 2008), they are still allowed in many others (Mathew et al., 2007). Of relevance is the fast increase of antibiotic consumption for animal food production in China (23% in 2010) and other BRICS countries (Van Boeckel et al., 2015). As stated previously, in these countries, increased income has produced a fast increase in meat products demand, due to changes in diet of their population. In addition, the increasing international competitiveness in meat production of these countries has fostered the rampant development of their industrial farming. Together with the fact that legislation on antibiotics use remains weak, this situation increases the risk of emergence of AR linked to animal production. Nevertheless, the problem is not restricted only to LMICs, because antibiotics consumption rose as well in the high-income countries as the United States (13%) (Van Boeckel et al., 2015), where approximately 80% of the antimicrobials purchased in 2011 were applied in livestock production as non-therapeutic administration (Done et al., 2015). The development of intensive methods of fish production has also contributed to the rise in the use of antimicrobials and the selection of resistance determinants that can be shared among fish and human bacterial pathogens (Cabello et al., 2013).

Economic development has facilitated as well more global transport, waste disposal, and tourism, favoring AR spread within and between different geographical areas (Ruppe et al., 2017a; Ruppe and Chappuis, 2017). However, economic growth can also reduce the AR burden, especially when it enables the development of regulations and infrastructures that might reduce the risks of infection and AR spread. This is particularly relevant in the case of public health interventions on food, water, and sewage. Because AR pathogens are mainly introduced in natural ecosystems through the release of human/animal stools (Karkman et al., 2019), the best way of reducing this impact is through the use of wastewater treatment plants, which are still absent in several places worldwide. Indeed, it has been described that drinking water is a relevant vehicle for the spread of ARBs in different countries (Walsh et al., 2011; Fernando et al., 2016) and that raw wastewater irrigation used for urban agriculture may increase the abundance of mobile ARGs in the irrigated soil (Bougnom et al., 2020). Notably, the analysis of ARGs in wastewaters has shown that the prevalence of ARGs in the

environment in each country might be linked to socioeconomic aspects mainly related to economic development, as general sanitation, particularly the availability of drinking and wastewater treatments, malnutrition, number of physicians and health workers, human overcrowding, or external debt grace period (Hendriksen et al., 2019). The field of AR has mainly focused in the mechanisms of selection; the main driver for the increased burden of AR would be then the use of antibiotics itself. However, these results indicate that transmission, even in the absence of direct human-to-human contact, might be, at least, equally relevant. In this situation, an important element to reduce the AR burden will be to break the transmission bridges among different ecosystems that could be reservoirs of ARGs.

Even when wastewater-treatment plants are available, the presence of ARBs in drinking, fresh, and coastal waters, as well as in sediments nearby industrial and urban discharges, has been described in several countries (Ma et al., 2017; Leonard et al., 2018). As in the case of fecal contamination markers, a reduction in the amount of ARGs to non-detectable levels would be extremely difficult even when advanced water treatment procedures are applied. A standard definition of polluting ARB/ARG markers, as well as their acceptable levels, is then needed. This would be required not only for potable water, but also for water reutilization, as well as for land application and release of sewage effluents, because in all cases the reused water/sewage may carry ARBs and ARGs, together with pollutants, such as antibiotics, metals, biocides, or microplastics, which, as above stated, may select for AR (Baquero et al., 2008; Moura et al., 2010; Yang et al., 2017; Zhu et al., 2017; Larsson et al., 2018; Imran et al., 2019; Wang et al., 2020) and may even induce HGT.

The examples discussed above justify that human health in general and AR in particular are closely interlinked with economic development (Sharma, 2018). Economic differences are also found at individual level, because there is a positive relationship between economic status and health (Tipper, 2010). In addition, social behavior might also impact AR, a feature discussed in the following section.

SOCIAL NORMS AND TIPPING POINTS IN ANTIBIOTIC RESISTANCE: A SOCIOECOLOGICAL APPROACH

Different socioeconomic factors can modulate the spread of infective bacteria in general and of AR in particular. Among them, the increasing crowding of humans and foodborne animal populations favors transmission at the local level (One Health), whereas trade of goods and human travel (Figure 2) favor worldwide transmission (Global Health) (Laxminarayan et al., 2013; Hernando-Amado et al., 2019).

Besides these global changes in social behavior, linked to economic development, more specific socioeconomic factors (income, education, life expectancy at birth, health care structure, governance quality), sociocultural aspects (inequalities, uncertainty avoidance, integration of individuals into primary

groups, gender biases, cultural long-term orientation), and personality dimension highly influence antibiotic use and AR transmission (Gaygisiz et al., 2017). For instance, although the governance quality seems to be the most important factor associated with a proper antibiotic use, Western countries with distinct national culture patterns show different levels of antibiotics consumption (Kenyon and Manoharan-Basil, 2020). A better understanding of human social responses facing ailments, especially epidemics and antibiotic use, requires then a more detailed analysis of the differences between collectivistic (individuals living integrated into primary groups) and individually long-term oriented societies (oriented to future individual rewards) (Hofstede, 2001; Gaygisiz et al., 2017; Kenyon and Manoharan-Basil, 2020).

Consistent with the sociological elements of AR, many of the aspects influencing AR reviewed above depend on social norms (**Figure 1**). In the classic view of the psychoanalyst Erich Fromm presented in his book “Escape From Freedom” (Fromm, 1941), human individual behavior is oriented to avoid being excluded from a higher social group. Indeed, not following social common rules can be eventually considered as a mental disorder; a sociopathology. A social norm is defined as a predominant behavioral pattern within a group, supported by a shared understanding of acceptable actions and sustained through social interactions within that group (Nyborg et al., 2016). In democratic societies, laws usually derive from already accepted social norms; otherwise, they would be changed, and in that sense, the establishment of accepted social norms for fighting AR is a prerequisite to implement the global approaches, based on worldwide rules, which are required for tackling this relevant problem.

Interestingly, the AR problem is a bottom-up process, where small emergent changes (in some type of individual patients, in some groups, in some locations) cumulatively escalate to gain a global dimension. Frequently, that occurs by crossing tipping points, that is, points where the local AR incidence becomes significant enough to cause a larger, eventually Global, Health problem. Because of that, the implementation of solutions should be adapted to the control of critical tipping points in the small groups of individuals to disrupt the bottom-up processes. However, as AR spread can occur everywhere and at any time, global surveillance and mechanisms of control should be implemented to prevent a top-down process of global AR expansion.

Individual selfishness for AR is the cornerstone of social norms. This concept was coined and developed by one of us over a decade ago (Baquero, 2007). Let us imagine that each individual is aware that each consumption of an antibiotic increases the personal risk of himself/herself or for his/her closer relatives (frequently exchanging microorganisms) of dying because of an antibiotic-resistant infection. The situation is analogous to the consumption of cholesterol-rich or highly salted food, or drinks with excess of sugar, concerning individual health. However, in the case of AR, it requires the understanding of the impact of individual actions at the global level. In this respect, anti-AR social actions should resemble more antitobacco and even general pollution/ecological campaigns.

At the individual level, there is inertia that precludes changing habits, until a tipping point is crossed and health is compromised. The conclusions of studies mainly based on long-term cohort analysis, such as the Framingham program for the influence of diet or smoking on personal cardiovascular disease (Mahmood et al., 2014), have become social norms that are naturally imposed by the ensemble of individuals. This creates a kind of societal culture, leading to appropriate individual behaviors, in occasions without the need of specific laws (diet), in occasion favoring the implementation of such laws (antismoking). However, we lack similar studies on issues such as these dealing with personal-familiar risks that have successfully shifted social norms, driven by groups of individuals and based on the promotion of individual behaviors in the case of AR.

Despite that quantitative models on how individual antibiotic use may impact AR at the population level are still absent, it is worth mentioning that a reduced antibiotic consumption has also begun to occur in a number of countries just as a result of a change in individual behavior (Edgar et al., 2009), and some tools and indicators to address these changes have been suggested (Ploy et al., 2020). The “tragedy of the commons” metaphor, first proposed in the XIX century (Lloyd, 1833) and later on discussed in 1968 (Hardin, 1968), has been used for addressing the sociology of AR, by showing how individual selfishness promotes antibiotic use, increases resistance, and influences the health of the community by impairing antibiotic efficacy (Baquero and Campos, 2003; Foster and Grundmann, 2006). Ensuring the prestige of individuals that follow the social rules is needed to counteract the tragedy of the commons. Nevertheless, it is important noticing that the tension between individual freedom and social rules that is inherent to the construction of democratic societies (Tocqueville, 1838; Hobbes, 1968; Rousseau, 1974; Spinoza, 2007) also applies here. One example of this situation is vaccination, considered in the last century as one of the most important advances to fight infectious diseases and now being the focus of antivaccination campaigns (Megget, 2020), a movement that has been considered by the WHO as one of the top 10 Global Health threats of 2019¹. It is commonly accepted that social norms are mainly created by learning and education, a rational path that promotes health (Chen and Fu, 2018). Also, the increasing activities of “personalized medicine,” including antibiotic stewardship, follow the same trend (Gould and Lawes, 2016). However, the antivaccination movement is an example of how the narrative, as well as the use of decentralized, social information channels such as the Internet search, blogs, and applications to facilitate communication such as Twitter, Facebook or WhatsApp, is of particular relevance in the construction of social norms, not necessarily based on scientific and rational grounds (Jacobson et al., 2020; Scott and Mars, 2020).

The impact of social norms goes beyond human societies as human activities alter natural ecosystems; consequently, humans cannot be aliens of nature. We should then shape a socioecological system, linking the individuals, the groups, and

¹<https://www.who.int/news-room/feature-stories/ten-threats-to-global-health-in-2019>

the entire society, as well as natural ecosystems, also potentially damaged by AR, in a common multilevel adaptive system based on social norms and policies at the individual, local (One Health), and global (Global Health) scale (Levin et al., 2013). The recent crisis of COVID-19 illustrates the influence of social norms in the individual behavior. Each one of the individuals, protecting himself/herself, also protects the others. A person not wearing on face mask is frowned upon, and on the contrary, somebody attaching to the rules increases reputation. The individual adopts the right behavior being influenced by the judgment of others. In addition, different political regimes (democracy or autocracy), as well as their organization (centralized, federal), together with the capacity of the health services to support the norms and their efficacy to communicate the chosen policy to the citizenry, may shape the individual responses to social norms (Greer et al., 2020; Häyry, 2020; Kavanagh and Singh, 2020).

Notwithstanding, two reasons that have been proposed to explain the low prevalence of COVID-19 in Japan were related with social norms more than with biological issues. These reasons, which are not common to other countries, were the socially accepted use of face masks and the mandatory vaccination of all the population against tuberculosis, which might protect from SARS-CoV-2 infection (Iwasaki and Grubaugh, 2020), a feature that is still to be confirmed.

The loss of social prestige of individuals taking antibiotics without prescription, as well as the pharmacies delivering these drugs or do not respect environmental protection, or the overconsumption of antibiotics in hospitals or in farms, or even in certain countries, is progressively constituting a “social norm,” converted in rules able to reduce AR emergence and spread. Of course, family and school education, as well as governmental campaigns, including the use of social media (Grajales et al., 2014) reinforces such social norms, which could allow the support of the society for the implementation of different interventions, some of them described below.

CONTROLLING RESISTANCE: LOCAL AND GLOBAL INTERVENTIONS

Controlling resistance not only requires establishing local interventions, which could be relatively easily implemented, but would also require global interventions that every country should follow, despite their disparate regulatory systems. Local and global interventions are necessarily intertwined; for example, the use of a new drug to treat a single individual depends on regulations at the county level (One Health approach), but the worldwide prevalence and transmission of resistance to this drug, as well as the regulations of its use, should be established internationally (Global Health approach).

Three main interventions to tackle AR have been historically considered: first, reduction of the antibiotic selective pressure by decreasing antimicrobials use; second, reduction of transmission of ARBs using improved hygienic procedures that prevent spread; third, development of novel antimicrobials with limited capacity

to select ARBs or the design of new treatment strategies based on use of non-antibiotic-based approaches or, more recently, on the exploitation of trade-offs associated with AR evolution (Imamovic and Sommer, 2013; Gonzales et al., 2015; Barbosa et al., 2018; Imamovic et al., 2018). These interventions have been basically limited to local initiatives, applied mainly to hospitals and, more recently, to farms. However, AR has emerged and spread globally, in bacteria from different environments, so the health and dynamics of the global microbiosphere could be affected by antibiotics. In a sense, AR is affecting the Planetary Health (Lerner and Berg, 2017), and the needed interventions for tackling this problem cannot be restricted to hospital settings (Figure 3).

The proposed reduction in the use of antibiotics (Blaskovich, 2018) must be compensated with alternative approaches for fighting infectious diseases. In this regard, strategies based on improving the capability of the immune system for counteracting infections (Levin et al., 2017; Traven and Naderer, 2019) or the use of non-antibiotic approaches to prevent them, such as vaccines (Jansen and Anderson, 2018), may help to reduce the burden of AR infections. Indeed, vaccination against *Haemophilus influenzae* and *Streptococcus pneumoniae* has been demonstrated to be an effective intervention for reducing AR (Jansen and Anderson, 2018). However, while vaccination has been extremely useful to prevent viral infections, it has been less promising in the case of bacterial ones. Recent approaches, including reverse vaccinology, may help in filling this gap (Delany et al., 2013; Ni et al., 2017). Moreover, vaccination should not be restricted to humans, because veterinary vaccination can also contribute to animal wealth and farm productivity (Francis, 2018). Besides, the use of vaccines in animal production reduces the use of antibiotics at farms/fisheries, hence reducing the selection pressure toward AR.

Other strategies to reduce antibiotic selective pressure include the use of bacteriophages (a revitalized strategy in recent years) (Viertel et al., 2014; Forti et al., 2018), not only in clinical settings, but also in natural ecosystems (Zhao et al., 2019b), as well as the use of biodegradable antibiotics (Chin et al., 2018) or adsorbents, able to reduce selective pressure on commensal microbiome (De Gunzburg et al., 2015, 2017). Besides reducing the chances of selecting ARBs, the use of antibiotics adsorbents may preserve the microbiomes, reducing the risks of infections (Chapman et al., 2016). Importantly, the procedures for removing antibiotics should not be limited to clinical settings, but their implementation in wastewater treatment plants would reduce selection of AR in non-clinical ecosystems (Tian et al., 2020).

Concerning the development of new antimicrobials (Hunter, 2020), while there is a basic economic issue related to the incentives to pharmaceutical companies (Sciarretta et al., 2016; Theuretzbacher et al., 2017), the focus is on the possibility of developing novel compounds with low capacity for selecting AR (Ling et al., 2015; Chin et al., 2018). For this purpose, multitarget (Li et al., 2014) or antiresistance drugs, such as membrane microdomain disassemblers (Garcia-Fernandez et al., 2017), are also promising. Furthermore, antimicrobial peptides, with a dual role as immunomodulators and antimicrobials, may also help fight infections (Hancock et al., 2016). In fact, some works

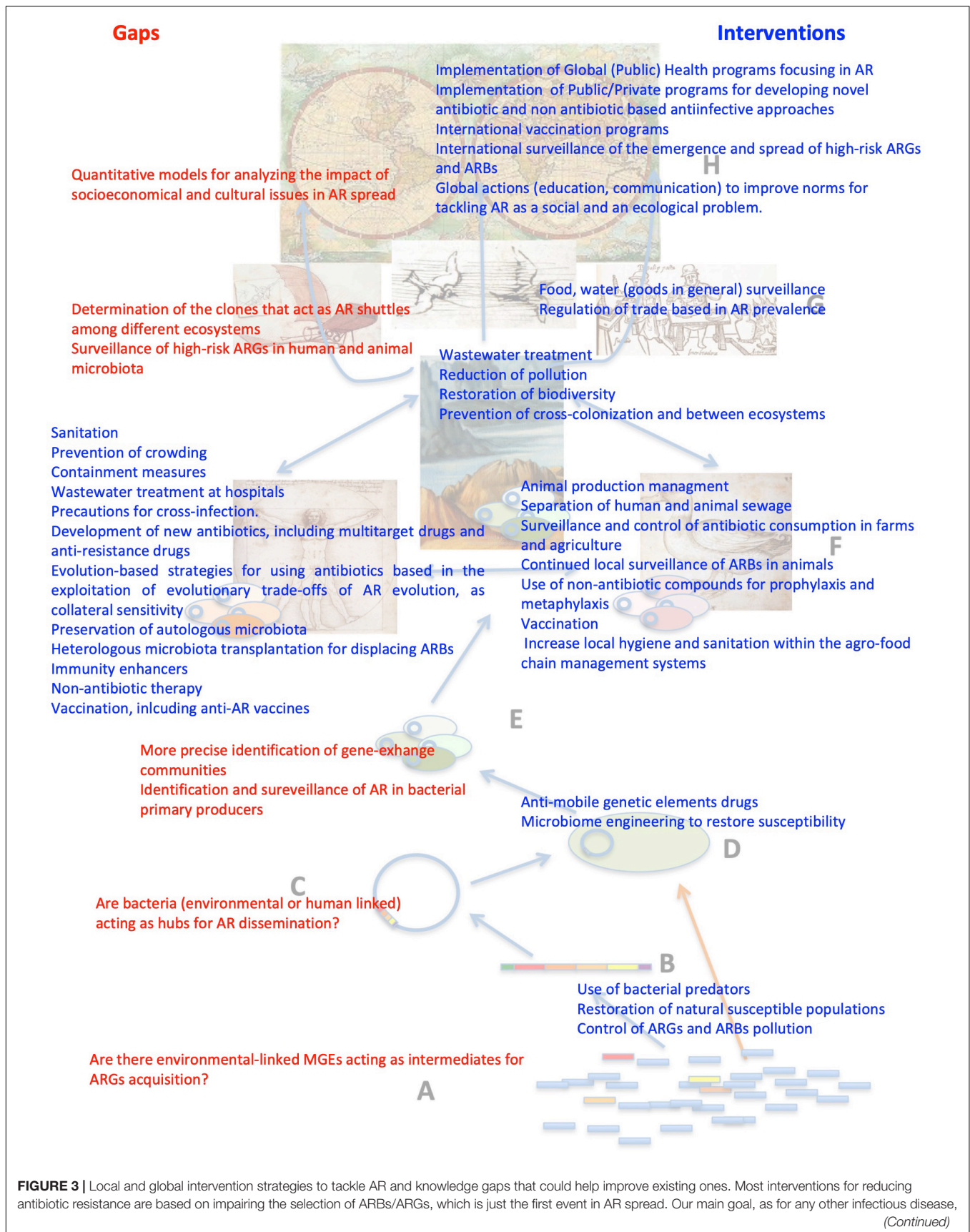


FIGURE 3 | Continued

would be reducing transmission. This does not mean that selective pressure is not relevant for transmission. Indeed, without positive selection, HGT events are not fixed, allowing the enrichment of some ARGs that are consequently more prone to diversification, both because they are more abundant and more frequently subjected to selection (Davies, 1997; Martinez, 2009a,b; Salverda et al., 2010) and because they can explore different landscapes when present as merodiploids in multicopy plasmids (Rodríguez-Beltrán et al., 2018). Therefore, reducing the selective pressure, either due to antibiotics or by other coselecting agents as heavy metals, still stands as a major intervention against AR emergence and transmission. To address this issue, we need to know more on the amount of pollutants, their selective concentrations, and their mechanisms of coselection and cross-selection in different ecosystems. This is a general example illustrating the gaps in knowledge in the AR field that need to be filled as well as strategies that may help in tackling this problem. The figure includes several other examples of the gaps in knowledge (red) that require further studies and the interventions (blue) that may help to tackle AR.

have shown that ARB frequently present collateral sensitivity to antimicrobial peptides (Lázár et al., 2018) and that, importantly, some antimicrobial peptides present limited resistance or cross-resistance (Kintses et al., 2019; Spohn et al., 2019).

From a conservative point of view, based on the use of the drugs we already have, it would be desirable to fight AR using evolution-based strategies for developing new drugs or treatment strategies. Regarding this, the exploitation of the evolutionary trade-offs associated with the acquisition of AR, as collateral sensitivity, could allow the rational design of treatments based on the alternation or the combination of pairs of drugs (Imamovic and Sommer, 2013; Gonzales et al., 2015; Barbosa et al., 2018; Imamovic et al., 2018).

In addition to interventions that reduce the selective pressure of antibiotics or that implement new therapeutic approaches, reducing transmission is also relevant to fight infections. The development of drugs or conditions (as certain wastewater treatments) able to reduce mutagenesis or to inhibit plasmid conjugation may also help in reducing the spread of resistance (Thi et al., 2011; Alam et al., 2016; Lin et al., 2016; Lopatkin et al., 2017; Valencia et al., 2017; Kudo et al., 2019). Besides specific drugs to reduce the dissemination of the genetic elements involved in AR, socioeconomic interventions to break the bridges that allow transmission (Baquero et al., 2019) between individuals and, most importantly (and less addressed), between resistance entities (Hernando-Amado et al., 2019) are needed (Figure 3). More efficient animal management, not only allowing less antibiotics use but also reducing animal crowding (and hence AR transmission), as well as improved sanitation procedures, including the universalization of water treatment, will certainly help in this task (Berendonk et al., 2015; Manaia, 2017; Hernando-Amado et al., 2019). Notably, wastewater treatment plants are usually communal facilities where the residues of the total population of a city are treated. Hospitals are the hotspots of AR in a city; hence, on-site hospital (and eventually on-farm) wastewater treatment may help to reduce the pollution of communal wastewater by antibiotics and ARBs (Cahill et al., 2019; Paulus et al., 2019), hence reducing AR transmission.

Concerning trade of goods, it is relevant to remark that, although there are strict regulations to control the entrance of animals or plants from sites with zoonotic or plant epidemic diseases (Brown and Bevins, 2018), there are no regulations on the exchange of goods from geographic regions with a high AR prevalence, a feature that might be taken into consideration for reducing the worldwide spread of AR.

Once ARBs are selected and disseminated, interventions based on the ecological and evolutionary (eco-evo) aspects of AR

(Bengtsson-Palme et al., 2018; Lehtinen et al., 2019) should be applied to restore (and select for) susceptibility of bacterial populations, as well as to preserve drug-susceptible microbiomes in humans and in animals (Baquero et al., 2011, 2015). Eco-evo strategies include the development of drugs specifically targeting ARBs. For that, drugs activated by mechanisms of resistance, vaccines targeting high-risk disseminating resistance clones or the resistance mechanisms themselves (Kim et al., 2016; Ni et al., 2017), or drugs targeting metabolic paths that can be specifically modified in ARBs (Baquero and Martinez, 2017) might be useful. The use of bacteriophages such as *Bdellovibrio* to eliminate pathogens without the need for antibiotics has been proposed; although its utility for treating infections is debatable, it might be useful in natural ecosystems (Shatzkes et al., 2016). More recent work suggests that some earthworms may favor the degradation of antibiotics and the elimination of ARBs (Wikler, 2002), a feature that might be in agreement with the finding that ARBs are less virulent (and hence might be specifically eliminated when the worm is present) in a *Caenorhabditis elegans* virulence model (Sanchez et al., 2002; Ruiz-Diez et al., 2003; Paulander et al., 2007; Olivares et al., 2012). However, the information on the potential use of worms for reducing AR in the field is still preliminary and requires further confirmation. Noteworthy, AR is less prone to be acquired by complex microbiomes (Mahnert et al., 2019; Wood, 2019), a feature that supports the possibility of interventions on the microbiota to reduce AR. Among them, fecal transplantation (Chapman et al., 2016; Pamer, 2016) or the use of probiotics able to outcompete ARBs (Keith and Pamer, 2019) has been proposed as strategies for recovering susceptible microbiomes.

CODA: ANTIBIOTIC RESISTANCE, A PANDEMIC TO WHICH A GLOBAL WORLD SEEMS TO BE ACCUSTOMED

The recent crisis of COVID-19 (Garrett, 2020) resembles the pandemic expansion of ARGs and clearly shows that pandemic outbreaks cannot be solved by just applying local solutions. Further, unless all population is controlled, and comprehensive public-health protocols are applied to the bulk of the population, such global pandemics will be hardly controlled. The case of COVID-19 is rather peculiar, because we are dealing with a novel virus. Very strict interventions have been applied, mainly trying to control something that is a novel, unknown, disease; we have been learning along the pandemic and still ignore what will come further. AR is already a very well-known pandemic affecting humans, animals, and natural ecosystems

(Anderson, 1999; Verhoef, 2003). In this case, we have tools that might predict the outcome, and likely because the degree of uncertainty is lower than in the case of COVID-19, we have not applied clear, common, and comprehensive procedures to reduce the spread of AR. It is true that we know the evolution of antibiotics consumption and AR prevalence in several countries, and also interventions, mostly based on social norms, have been applied. Social norms have reduced the unnecessary prescription of antibiotics, or pharmacy sales without prescription, and the use of antibiotics for fattening animals has been banned in several countries, being still allowed in several others. Nevertheless, these actions are not general, and more aggressive, global actions are still needed. Coming back to the COVID-19 example, while the aim of health services worldwide is to detect any possible source of SARS-CoV-2, surveillance of infections (eventually by ARBs) is not universal. In other words, it does not apply to all citizens in all countries. The reasons can be just political such as the inclusion of immigrants in public health services (Scotto et al., 2017) or the consequence of limited financial resources and technical capacity that countries such as those belonging to the LMIC category can face (Gandra et al., 2020). The problem is not only on citizens, because different non-human reservoirs, such as wastewater, drinking water, or freshwater, may jointly contribute to AR dissemination (Hendriksen et al., 2019). In this regard, it is important to highlight that low quality of water is regularly associated to poverty. Universalization of health services, sanitization, access to clean water, and in general reduction of poverty are relevant step-forward elements for reduction of the burden of infectious diseases in general and of AR in particular. The time has come to tackle AR, and this cannot be done just by taking actions at the individual or even country level, but by taking convergent actions across the globe. As stated by John Donne (1923) in his poem, “No Man Is an Island,” written after his recovery from an infectious disease (likely typhus): “No man is an Iland, intire of itselfe; every man is a peece of the Continent, a part of

the maine; if a Clod bee washed away by the Sea, Europe is the lesse, as well as if a Promontorie were, as well as if a Manor of thy friends or of thine owne were; any mans death diminishes me, because I am involved in Mankinde; And therefore never send to know for whom the bell tolls; It tolls for thee.”

This reflection on how infectious diseases in general should be faced by the society was published at 1624, but the idea behind still applies nowadays, especially for AR.

AUTHOR CONTRIBUTIONS

All authors have contributed to the concept of the review and in its writing.

FUNDING

JM was supported by grants from the Instituto de Salud Carlos III [Spanish Network for Research on Infectious Diseases (RD16/0016/0011)], from the Spanish Ministry of Economy and Competitiveness (BIO2017-83128-R) and from the Autonomous Community of Madrid (B2017/BMD-3691). Work in TC and FB laboratory was supported by grants funded by the Joint Programming Initiative in Antimicrobial Resistance (JPIAMR Third call, STARCS, JPIAMR2016-AC16/00039), the Instituto de Salud Carlos III of Spain/Ministry of Economy and Competitiveness and the European Development Regional Fund “A way to achieve Europe” (ERDF) for co-funding the Spanish R&D National Plan Estatal de I + D + i 2013-2016 (PI18/1942), CIBERESP (CIBER in Epidemiology and Public Health; CB06/02/0053), the Regional Government of Madrid (InGeMICS-B2017/BMD-3691) and the Fundación Ramón Areces. The funders did not have any role neither in the design, nor in the writing of the current review.

REFERENCES

- Aarestrup, F. M. (1998). Association between decreased susceptibility to a new antibiotic for treatment of human diseases, everninomicin (Sch 27899), and resistance to an antibiotic used for growth promotion in animals, avilamycin. *Microb. Drug Resist.* 4, 137–141. doi: 10.1089/mdr.1998.4.137
- Aarestrup, F. M., Bager, F., Jensen, N. E., Madsen, M., Meyling, A., and Wegener, H. C. (1998). Surveillance of antimicrobial resistance in bacteria isolated from food animals to antimicrobial growth promoters and related therapeutic agents in Denmark. *Apmis* 106, 606–622. doi: 10.1111/j.1699-0463.1998.tb01391.x
- Alam, M. K., Alhazmi, A., Decoteau, J. F., Luo, Y., and Geyer, C. R. (2016). RecA inhibitors potentiate antibiotic activity and block evolution of antibiotic resistance. *Cell Chem. Biol.* 23, 381–391. doi: 10.1016/j.chembiol.2016.02.010
- Alcock, B. P., Raphenya, A. R., Lau, T. T. Y., Tsang, K. K., Bouchard, M., Edalatmand, A., et al. (2020). Card 2020: antibiotic resistance surveillance with the comprehensive antibiotic resistance database. *Nucleic Acids Res.* 48, D517–D525.
- Allen, H. K., Donato, J., Wang, H. H., Cloud-Hansen, K. A., Davies, J., and Handelsman, J. (2010). Call of the wild: antibiotic resistance genes in natural environments. *Nat. Rev. Microbiol.* 8, 251–259. doi: 10.1038/nrmicro2312
- Alonso, C. A., Gonzalez-Barrio, D., Tenorio, C., Ruiz-Fons, F., and Torres, C. (2016). Antimicrobial resistance in faecal *Escherichia coli* isolates from farmed red deer and wild small mammals. Detection of a multiresistant *E. coli* producing extended-spectrum beta-lactamase. *Comp. Immunol. Microbiol. Infect. Dis.* 45, 34–39. doi: 10.1016/j.cimid.2016.02.003
- Aminov, R. I. (2009). The role of antibiotics and antibiotic resistance in nature. *Environ. Microbiol.* 11, 2970–2988. doi: 10.1111/j.1462-2920.2009.01972.x
- Anderson, R. M. (1999). The pandemic of antibiotic resistance. *Nat. Med.* 5, 147–149. doi: 10.1038/5507
- Andersson, D. I. (2006). The biological cost of mutational antibiotic resistance: any practical conclusions? *Curr. Opin. Microbiol.* 9, 461–465. doi: 10.1016/j.mib.2006.07.002
- Andersson, D. I., Balaban, N. Q., Baquero, F., Courvalin, P., Glaser, P., Gophna, U., et al. (2020). Antibiotic resistance: turning evolutionary principles into clinical reality. *FEMS Microbiol. Rev.* 44, 171–188. doi: 10.1093/femsre/fuaa001
- Andersson, D. I., and Hughes, D. (2010). Antibiotic resistance and its cost: is it possible to reverse resistance? *Nat. Rev. Microbiol.* 8, 260–271. doi: 10.1038/nrmicro2319
- Arias-Andres, M., Klumper, U., Rojas-Jimenez, K., and Grossart, H. P. (2018). Microplastic pollution increases gene exchange in aquatic ecosystems. *Environ. Pollut.* 237, 253–261. doi: 10.1016/j.envpol.2018.02.058
- Azuma, T., Otomo, K., Kunitou, M., Shimizu, M., Hosomaru, K., Mikata, S., et al. (2019). Environmental fate of pharmaceutical compounds and antimicrobial-resistant bacteria in hospital effluents, and contributions to pollutant loads in the surface waters in Japan. *Sci. Total Environ.* 657, 476–484. doi: 10.1016/j.scitotenv.2018.11.433

- Bager, F., Madsen, M., Christensen, J., and Aarestrup, F. M. (1997). Avoparcin used as a growth promoter is associated with the occurrence of vancomycin-resistant *Enterococcus faecium* on Danish poultry and pig farms. *Prev. Vet. Med.* 31, 95–112. doi: 10.1016/s0167-5877(96)01119-1
- Baquero, F. (2007). *Evaluation of Risks and Benefits of Consumption of Antibiotics: From Individual to Public Health*. Hoboken, NY: John Wiley & Sons, Inc.
- Baquero, F. (2017). Transmission as a basic process in microbial biology. Lwoff Award Prize Lecture. *FEMS Microbiol. Rev.* 41, 816–827. doi: 10.1093/femsre/fux042
- Baquero, F., and Campos, J. (2003). The tragedy of the commons in antimicrobial chemotherapy. *Rev. Esp. Quimioter.* 16, 11–13.
- Baquero, F., Coque, T. M., and De La Cruz, F. (2011). Ecology and evolution as targets: the need for novel eco-evo drugs and strategies to fight antibiotic resistance. *Antimicrob. Agents Chemother.* 55, 3649–3660. doi: 10.1128/aac.00013-11
- Baquero, F., Coque, T. M., Martinez, J. L., Aracil-Gisbert, S., and Lanza, V. F. (2019). Gene transmission in the one health microbiosphere and the channels of antimicrobial resistance. *Front. Microbiol.* 10:2892. doi: 10.3389/fmicb.2019.02892
- Baquero, F., Lanza, V. F., Canton, R., and Coque, T. M. (2015). Public health evolutionary biology of antimicrobial resistance: priorities for intervention. *Evol. Appl.* 8, 223–239. doi: 10.1111/eva.12235
- Baquero, F., Martinez, J. L., and Canton, R. (2008). Antibiotics and antibiotic resistance in water environments. *Curr. Opin. Biotechnol.* 19, 260–265. doi: 10.1016/j.copbio.2008.05.006
- Baquero, F., and Martinez, J. L. (2017). Interventions on metabolism: making antibiotic-susceptible bacteria. *mBio* 8:e01950-17. doi: 10.1128/mBio.01950-17
- Barbosa, C., Beardmore, R., Schulenburg, H., and Jansen, G. (2018). Antibiotic combination efficacy (Ace) networks for a *Pseudomonas aeruginosa* model. *PLoS Biol.* 16:e2004356. doi: 10.1371/journal.pbio.2004356
- Beardmore, R. E., Peña-Miller, R., Gori, F., and Iredell, J. (2017). Antibiotic cycling and antibiotic mixing: which one best mitigates antibiotic resistance? *Mol. Biol. Evol.* 34, 802–817.
- Bengtsson-Palme, J., Kristiansson, E., and Larsson, D. G. J. (2018). Environmental factors influencing the development and spread of antibiotic resistance. *FEMS Microbiol. Rev.* 42:fux053.
- Berendonk, T. U., Manaia, C. M., Merlin, C., Fatta-Kassinos, D., Cytryn, E., Walsh, F., et al. (2015). Tackling antibiotic resistance: the environmental framework. *Nat. Rev. Microbiol.* 13, 310–317.
- Beugnet, F., and Chalvet-Monfray, K. (2013). Impact of climate change in the epidemiology of vector-borne diseases in domestic carnivores. *Comp. Immunol. Microbiol. Infect. Dis.* 36, 559–566. doi: 10.1016/j.cimid.2013.07.003
- Bind, M. A. (2019). Causal modeling in environmental health. *Annu. Rev. Public Health* 40, 23–43. doi: 10.1146/annurev-publhealth-040218-044048
- Blaskovich, M. A. T. (2018). The fight against antimicrobial resistance is confounded by a global increase in antibiotic usage. *Acs Infect. Dis.* 4, 868–870. doi: 10.1021/acsinfectdis.8b00109
- Blokesch, M. (2017). In and out-contribution of natural transformation to the shuffling of large genomic regions. *Curr. Opin. Microbiol.* 38, 22–29. doi: 10.1016/j.mib.2017.04.001
- Botelho, J., and Schulenburg, H. (2020). The role of integrative and conjugative elements in antibiotic resistance evolution. *Trends Microbiol.* doi: 10.1016/j.tim.2020.05.011 [Epub ahead of print].
- Bougnom, B. P., Thiele-Bruhn, S., Ricci, V., Zongo, C., and Piddock, L. J. V. (2020). Raw wastewater irrigation for urban agriculture in three African cities increases the abundance of transferable antibiotic resistance genes in soil, including those encoding extended spectrum beta-lactamases (Esbls). *Sci. Total Environ.* 698:134201. doi: 10.1016/j.scitotenv.2019.134201
- Brown, T. M., Cueto, M., and Fee, E. (2006). The World Health Organization and the transition from “international” to “global” public health. *Am. J. Public Health* 96, 62–72. doi: 10.2105/ajph.2004.050831
- Brown, V. R., and Bevins, S. N. (2018). A review of african swine fever and the potential for introduction into the United States and the Possibility of subsequent establishment in feral swine and native ticks. *Front. Vet. Sci.* 5:11. doi: 10.3389/fvets.2018.00011
- Cabello, F. C., Godfrey, H. P., Tomova, A., Ivanova, L., Dolz, H., Millanao, A., et al. (2013). Antimicrobial use in aquaculture re-examined: its relevance to antimicrobial resistance and to animal and human health. *Environ. Microbiol.* 15, 1917–1942. doi: 10.1111/1462-2920.12134
- Cabot, G., Lopez-Causape, C., Ocampo-Sosa, A. A., Sommer, L. M., Dominguez, M. A., Zamorano, L., et al. (2016). Deciphering the resistome of the widespread *Pseudomonas aeruginosa* Sequence Type 175 international high-risk clone through whole-genome sequencing. *Antimicrob. Agents Chemother.* 60, 7415–7423.
- Cahill, N., O'Connor, L., Mahon, B., Varley, Á, McGrath, E., Ryan, P., et al. (2019). Hospital effluent: a reservoir for carbapenemase-producing Enterobacterales? *Sci. Total Environ.* 672, 618–624. doi: 10.1016/j.scitotenv.2019.03.428
- Chandler, C. I. R. (2019). Current accounts of antimicrobial resistance: stabilisation, individualisation and antibiotics as infrastructure. *Palgrave Commun.* 5:2344.
- Chapman, B. C., Moore, H. B., Overbey, D. M., Morton, A. P., Harnke, B., Gerich, M. E., et al. (2016). Fecal microbiota transplant in patients with *Clostridium difficile* infection: a systematic review. *J. Trauma Acute Care Surg.* 81, 756–764.
- Chen, Q.-L., An, X.-L., Zheng, B.-X., Gillings, M., Peñuelas, J., Cui, L., et al. (2019a). Loss of soil microbial diversity exacerbates spread of antibiotic resistance. *Soil Ecol. Lett.* 1, 3–13. doi: 10.1007/s42832-019-0011-0
- Chen, Q. L., Cui, H. L., Su, J. Q., Penuelas, J., and Zhu, Y. G. (2019b). Antibiotic resistomes in plant microbiomes. *Trends Plant Sci.* 24, 530–541. doi: 10.1016/j.tplants.2019.02.010
- Chen, X., and Fu, F. (2018). Social learning of prescribing behavior can promote population optimum of antibiotic Use. *Front. Phys.* 6:139. doi: 10.3389/fphy.2018.00139
- Chin, W., Zhong, G., Pu, Q., Yang, C., Lou, W., De Sessions, P. F., et al. (2018). A macromolecular approach to eradicate multidrug resistant bacterial infections while mitigating drug resistance onset. *Nat. Commun.* 9:917.
- Chokshi, A., Sifri, Z., Cennimo, D., and Horg, H. (2019). global contributors to antibiotic resistance. *J. Glob Infect. Dis.* 11, 36–42.
- Cislaghi, B., and Heise, L. (2018). Theory and practice of social norms interventions: eight common pitfalls. *Global Health* 14:83.
- Cislaghi, B., and Heise, L. (2019). Using social norms theory for health promotion in low-income countries. *Health Promot. Int.* 34, 616–623. doi: 10.1093/heapro/day017
- Clemente, J., Pehrsson, E., Blaser, M., Sandhu, K., Gao, Z., Wang, B., et al. (2015). The microbiome of uncontacted Amerindians. *Sci. Adv.* 1:e1500183. doi: 10.1126/sciadv.1500183
- Coffey, T. J., Dowson, C. G., Daniels, M., Zhou, J., Martin, C., Spratt, B. G., et al. (1991). Horizontal transfer of multiple penicillin-binding protein genes, and capsular biosynthetic genes, in natural populations of *Streptococcus pneumoniae*. *Mol. Microbiol.* 5, 2255–2260. doi: 10.1111/j.1365-2958.1991.tb02155.x
- Cooper, R. M., Tsimring, L., and Hasty, J. (2017). Inter-species population dynamics enhance microbial horizontal gene transfer and spread of antibiotic resistance. *Elife* 6:e25950. doi: 10.7554/eLife.25950
- Cox, L. A. Jr., and Ricci, P. F. (2008). Causal regulations vs. political will: why human zoonotic infections increase despite precautionary bans on animal antibiotics. *Environ. Int.* 34, 459–475. doi: 10.1016/j.envint.2007.10.010
- Davies, J. (1994). Inactivation of antibiotics and the dissemination of resistance genes. *Science* 264, 375–382. doi: 10.1126/science.8153624
- Davies, J., and Davies, D. (2010). Origins and evolution of antibiotic resistance. *Microbiol. Mol. Biol. Rev.* 74, 417–433.
- Davies, J. E. (1997). Origins, acquisition and dissemination of antibiotic resistance determinants. *Ciba Found. Symp.* 207, 15–27.
- D'Costa, V. M., McGrann, K. M., Hughes, D. W., and Wright, G. D. (2006). Sampling the antibiotic resistome. *Science* 311, 374–377. doi: 10.1126/science.1120800
- De Gunzburg, J., Ducher, A., Modess, C., Wegner, D., Oswald, S., Dressman, J., et al. (2015). Targeted adsorption of molecules in the colon with the novel adsorbent-based medicinal product, Dav132: a proof of concept study in healthy subjects. *J. Clin. Pharmacol.* 55, 10–16. doi: 10.1002/jcph.359
- De Gunzburg, J., Ghazlane, A., Ducher, A., Le Chatelier, E., Duval, X., and Ruppe, E. (2017). Protection of the human gut microbiome from antibiotics. *J. Infect. Dis.* 217, 628–636.
- Delany, I., Rappuoli, R., and Seib, K. L. (2013). Vaccines, reverse vaccinology, and bacterial pathogenesis. *Cold Spring Harb. Perspect. Med.* 3:a012476. doi: 10.1101/cshperspect.a012476

- Deschasaux, M., Bouter, K. E., Prodan, A., Levin, E., Groen, A. K., Herrema, H., et al. (2018). Depicting the composition of gut microbiota in a population with varied ethnic origins but shared geography. *Nat. Med.* 24, 1526–1531. doi: 10.1038/s41591-018-0160-1
- Domingues, S., Harms, K., Fricke, W. F., Johnsen, P. J., Da Silva, G. J., Nielsen, K. M., et al. (2012). Natural transformation facilitates transfer of transposons, integrons and gene cassettes between bacterial species. *PLoS Pathog.* 8:e1002837. doi: 10.1371/journal.ppat.1002837
- Done, H. Y., Venkatesan, A. K., and Halden, R. U. (2015). Does the recent growth of aquaculture create antibiotic resistance threats different from those associated with land animal production in agriculture? *Aaps J.* 17, 513–524. doi: 10.1208/s12248-015-9722-z
- Donne, J. (1923). *Devotions Upon Emergent Occasions*. Cambridge: The University press, 1923.
- Douarre, P. E., Mallet, L., Radomski, N., Felten, A., and Mistou, M. Y. (2020). Analysis of compass, a new comprehensive plasmid database revealed prevalence of multireplicon and extensive diversity of IncF plasmids. *Front. Microbiol.* 11:483. doi: 10.3389/fmicb.2020.00483
- Dubey, G. P., and Ben-Yehuda, S. (2011). Intercellular nanotubes mediate bacterial communication. *Cell* 144, 590–600. doi: 10.1016/j.cell.2011.01.015
- Durso, L. M., Miller, D. N., and Wienhold, B. J. (2012). Distribution and quantification of antibiotic resistant genes and bacteria across agricultural and non-agricultural metagenomes. *PLoS One* 7:e48325. doi: 10.1371/journal.pone.0048325
- Edgar, T., Boyd, S. D., and Palame, M. J. (2009). Sustainability for behaviour change in the fight against antibiotic resistance: a social marketing framework. *J. Antimicrob. Chemother.* 63, 230–237. doi: 10.1093/jac/dkn508
- European Food Safety Authority, and European Centre for Disease Prevention and Control (2020). The European union summary report on antimicrobial resistance in zoonotic and indicator bacteria from humans, animals and food in 2017/2018. *Efsa J.* 18:e06007.
- Fajardo, A., Martinez-Martin, N., Mercadillo, M., Galan, J. C., Ghysels, B., Matthijs, S., et al. (2008). The neglected intrinsic resistome of bacterial pathogens. *PLoS One* 3:e1619. doi: 10.1371/journal.pone.0001619
- Farley, J., and Voinov, A. (2016). Economics, socio-ecological resilience and ecosystem services. *J. Environ. Manag.* 183, 389–398. doi: 10.1016/j.jenvman.2016.07.065
- Fenech, A., Foster, J., Hamilton, K., and Hansell, R. (2003). Natural capital in ecology and economics: an overview. *Environ. Monit. Assess.* 86, 3–17.
- Fernando, D. M., Tun, H. M., Poole, J., Patidar, R., Li, R., Mi, R., et al. (2016). Detection of antibiotic resistance genes in source and drinking water samples from a first nations community in Canada. *Appl. Environ. Microbiol.* 82, 4767–4775. doi: 10.1128/aem.00798-16
- Ferrandiz, M. J., Fenoll, A., Linares, J., and De La Campa, A. G. (2000). Horizontal transfer of *parC* and *gyrA* in fluoroquinolone-resistant clinical isolates of *Streptococcus pneumoniae*. *Antimicrob. Agents Chemother.* 44, 840–847.
- Fitzpatrick, D., and Walsh, F. (2016). Antibiotic resistance genes across a wide variety of metagenomes. *FEMS Microbiol. Ecol.* 92:fiv168. doi: 10.1093/femsec/fiv168
- Fondi, M., Karkman, A., Tamminen, M. V., Bosi, E., Virta, M., Fani, R., et al. (2016). “Every Gene Is Everywhere but the Environment Selects”: global geolocalization of gene sharing in environmental samples through network analysis. *Genome Biol. Evol.* 8, 1388–1400. doi: 10.1093/gbe/evw077
- Forsberg, K. J., Reyes, A., Wang, B., Selleck, E. M., Sommer, M. O., and Dantas, G. (2012). The shared antibiotic resistome of soil bacteria and human pathogens. *Science* 337, 1107–1111. doi: 10.1126/science.1220761
- Forti, F., Roach, D. R., Cafora, M., Pasini, M. E., Horner, D. S., Fiscarelli, E. V., et al. (2018). Design of a broad-range bacteriophage cocktail that reduces *Pseudomonas aeruginosa* Biofilms and treats acute infections in two animal models. *Antimicrob. Agents Chemother.* 62:e02573-17.
- Foster, K. R., and Grundmann, H. (2006). Do we need to put society first? The potential for tragedy in antimicrobial resistance. *PLoS Med.* 3:e29. doi: 10.1371/journal.pmed.0030029
- Francis, M. J. (2018). Recent advances in vaccine technologies. *Vet. Clin. North Am. Small Anim. Pract.* 48, 231–241.
- Fromm, E. (1941). *Escape From Freedom*. New York, NY: Farrar & Rinehart.
- Frost, L. S., Leplae, R., Summers, A. O., and Toussaint, A. (2005). Mobile genetic elements: the agents of open source evolution. *Nat. Rev. Microbiol.* 3, 722–732. doi: 10.1038/nrmicro1235
- Fuller, T., Bensch, S., Muller, I., Novembre, J., Perez-Tris, J., Ricklefs, R. E., et al. (2012). The ecology of emerging infectious diseases in migratory birds: an assessment of the role of climate change and priorities for future research. *Ecohealth* 9, 80–88. doi: 10.1007/s10393-012-0750-1
- Fulsundar, S., Harms, K., Flaten, G. E., Johnsen, P. J., Chopade, B. A., Nielsen, K. M., et al. (2014). Gene transfer potential of outer membrane vesicles of *Acinetobacter baylyi* and effects of stress on vesiculation. *Appl. Environ. Microbiol.* 80, 3469–3483. doi: 10.1128/AEM.04248-13
- Gandra, S., Alvarez-Uria, G., Turner, P., Joshi, J., Limmathurotsakul, D., and Van Doorn, H. R. (2020). Antimicrobial resistance surveillance in low- and middle-income countries: progress and challenges in eight South Asian and Southeast Asian Countries. *Clin. Microbiol. Rev.* 33:e00048-19.
- Garcia-Aljaro, C., Balleste, E., and Muniesa, M. (2017). Beyond the canonical strategies of horizontal gene transfer in prokaryotes. *Curr. Opin. Microbiol.* 38, 95–105. doi: 10.1016/j.mib.2017.04.011
- Garcia-Fernandez, E., Koch, G., Wagner, R. M., Fekete, A., Stengel, S. T., Schneider, J., et al. (2017). Membrane microdomain disassembly inhibits mrsa antibiotic resistance. *Cell* 171, 1354.e20–1367.e20.
- Garrett, L. (2020). Covid-19: the medium is the message. *Lancet* 395, 942–943. doi: 10.1016/s0140-6736(20)30600-0
- Gaulke, C. A., and Sharpton, T. J. (2018). The influence of ethnicity and geography on human gut microbiome composition. *Nat. Med.* 24, 1495–1496. doi: 10.1038/s41591-018-0210-8
- Gaygisiz, Ü., Lajunen, T., and Gaygisiz, E. (2017). Socio-economic factors, cultural values, national personality and antibiotics use: a cross-cultural study among European countries. *J. Infect. Public Health* 10, 755–760. doi: 10.1016/j.jiph.2016.11.011
- Gillings, M. R. (2017). Lateral gene transfer, bacterial genome evolution, and the Anthropocene. *Ann. N. Y. Acad. Sci.* 1389, 20–36. doi: 10.1111/nyas.13213
- Gillings, M. R., Paulsen, I. T., and Tetu, S. G. (2017). Genomics and the evolution of antibiotic resistance. *Ann. N. Y. Acad. Sci.* 1388, 92–107. doi: 10.1111/nyas.13268
- Gonzales, P. R., Pesesky, M. W., Bouley, R., Ballard, A., Biddy, B. A., Suckow, M. A., et al. (2015). Synergistic, collaterally sensitive beta-lactam combinations suppress resistance in *Mrsa*. *Nat. Chem. Biol.* 11, 855–861. doi: 10.1038/nchembio.1911
- Gostin, L. O., Buckley, G. J., and Kelley, P. W. (2013). Stemming the global trade in falsified and substandard medicines. *Jama* 309, 1693–1694.
- Gould, I. M., and Lawes, T. (2016). Antibiotic stewardship: prescribing social norms. *Lancet* 387, 1699–1701. doi: 10.1016/s0140-6736(16)00007-6
- Grajales, F. J., Sheps, S., Ho, K., Novak-Lauscher, H., and Eysenbach, G. (2014). Social media: a review and tutorial of applications in medicine and health care. *J. Med. Internet Res.* 16:e13. doi: 10.2196/jmir.2912
- Greer, S. L., King, E. J., Da Fonseca, E. M., and Peralta-Santos, A. (2020). The comparative politics of Covid-19: the need to understand government responses. *Glob. Public Health* 1–4. doi: 10.1080/17441692.2020.1783340 [Epub ahead of print].
- Hamilton, W. L., Doyle, C., Halliwell-Ewen, M., and Lambert, G. (2016). Public health interventions to protect against falsified medicines: a systematic review of international, national and local policies. *Health Policy Plan* 31, 1448–1466. doi: 10.1093/heapol/czw062
- Hancock, R. E., Haney, E. F., and Gill, E. E. (2016). The immunology of host defence peptides: beyond antimicrobial activity. *Nat. Rev. Immunol.* 16, 321–334. doi: 10.1038/nri.2016.29
- Hardin, G. (1968). The tragedy of the commons. *Science* 162:1243.
- Häyry, M. (2020). The Covid-19 pandemic: healthcare crisis leadership as ethics communication. *Camb Q. Health Ethics* 22, 1–9. doi: 10.1017/s0963180120000444
- Hendriksen, R. S., Munk, P., Njage, P., Van Bunnik, B., McNally, L., Lukjancenko, O., et al. (2019). Global monitoring of antimicrobial resistance based on metagenomics analyses of urban sewage. *Nat. Commun.* 10:1124.
- Hernando-Amado, S., Coque, T. M., Baquero, F., and Martinez, J. L. (2019). Defining and combating antibiotic resistance from one health and global health perspectives. *Nat. Microbiol.* 4, 1432–1442. doi: 10.1038/s41564-019-0503-9
- Hobbes, T. (1968). *Leviathan*. Baltimore: Penguin Books.
- Hofstede, G. (2001). *Culture's Consequences: Comparing Values, Behaviors, Institutions, and Organizations Across Nations*. Thousand Oaks, CA: Sage.

- Hsu, L. C., Liu, Y. T., Syu, C. H., Huang, M. H., Tzou, Y. M., and Teah, H. Y. (2018). Adsorption of tetracycline on Fe (hydr)oxides: effects of pH and metal cation (Cu(2+), Zn(2+) and Al(3+)) addition in various molar ratios. *R. Soc. Open Sci.* 5:171941. doi: 10.1098/rsos.171941
- Hujer, A. M., Bethel, C. R., Hujer, K. M., and Bonomo, R. A. (2004). Antibiotic resistance in the institutionalized elderly. *Clin. Lab Med.* 24, 343–361. doi: 10.1016/j.cll.2004.03.005
- Hunter, P. (2020). A war of attrition against antibiotic resistance: current strategies try to keep antibiotic resistance at bay and further encourage research to produce genuinely novel antibacterials. *Embo Rep.* 21:e50807.
- Iavarone, I., and Pasetto, R. (2018). Icshnet. environmental health challenges from industrial contamination. *Epidemiol. Prev.* 42, 5–7.
- Imamovic, L., Ellabaan, M. M. H., Dantas Machado, A. M., Citterio, L., Wulff, T., Molin, S., et al. (2018). Drug-driven phenotypic convergence supports rational treatment strategies of chronic infections. *Cell* 172, 121.e14–134.e14.
- Imamovic, L., and Sommer, M. O. (2013). Use of collateral sensitivity networks to design drug cycling protocols that avoid resistance development. *Sci. Transl. Med.* 5:204ra132. doi: 10.1126/scitranslmed.3006609
- Imran, M., Das, K. R., and Naik, M. M. (2019). Co-selection of multi-antibiotic resistance in bacterial pathogens in metal and microplastic contaminated environments: an emerging health threat. *Chemosphere* 215, 846–857. doi: 10.1016/j.chemosphere.2018.10.114
- Iwasaki, A., and Grubaugh, N. D. (2020). Why does Japan have so few cases of Covid-19? *Embo Mol. Med.* 12:e12481.
- Jacobson, R. M., St Sauver, J. L., Griffin, J. M., Maclaughlin, K. L., and Finney Rutten, L. J. (2020). How health care providers should address vaccine hesitancy in the clinical setting: evidence for presumptive language in making a strong recommendation. *Hum. Vaccin Immunother.* 3, 1–5. doi: 10.1080/21645515.2020.1735226
- Jana, B., Cain, A. K., Doerrler, W. T., Boinett, C. J., Fookes, M. C., Parkhill, J., et al. (2017). The secondary resistome of multidrug-resistant *Klebsiella pneumoniae*. *Sci. Rep.* 7:42483.
- Jansen, K. U., and Anderson, A. S. (2018). The role of vaccines in fighting antimicrobial resistance (Amr). *Hum. Vaccin Immunother.* 14, 2142–2149. doi: 10.1080/21645515.2018.1476814
- Jean, B. P. (2017). One health and the politics of antimicrobial resistance. *Emerg. Infect. Dis. J.* 23:724. doi: 10.3201/eid2304.161871
- Jolley, K. A., Bray, J. E., and Maiden, M. C. J. (2018). Open-access bacterial population genomics: bigsdb software, the Pubmlst.org website and their applications. *Wellcome open Res.* 3, 124–124.
- Jonas, O., World Bank Group Team (2017). *Drug-Resistant Infections: A Threat to Our Economic Future*. Washington, DC: The World Bank Group.
- Jorgensen, T. S., Kiiil, A. S., Hansen, M. A., Sorensen, S. J., and Hansen, L. H. (2014). Current strategies for mobilome research. *Front. Microbiol.* 5:750. doi: 10.3389/fmicb.2014.00750
- Jutkina, J., Marathe, N. P., Flach, C. F., and Larsson, D. G. J. (2018). Antibiotics and common antibacterial biocides stimulate horizontal transfer of resistance at low concentrations. *Sci. Total Environ.* 616–617, 172–178. doi: 10.1016/j.scitotenv.2017.10.312
- Kangas, O. E. (1997). Self-interest and the common good: the impact of norms, selfishness and context in social policy opinions. *J. Soc. Econ.* 26, 475–494. doi: 10.1016/s1053-5357(97)90010-x
- Kant, I. (1785). *Grundlegung zur Metaphysik der Sitten*. Riga, J.F: Hartknoch.
- Karkman, A., Parnanen, K., and Larsson, D. G. J. (2019). Fecal pollution can explain antibiotic resistance gene abundances in anthropogenically impacted environments. *Nat. Commun.* 10:80.
- Kavanagh, M. M., and Singh, R. (2020). Democracy, capacity, and coercion in pandemic response-covid 19 in comparative political perspective. *J. Health Polit. Policy Law* 28:8641530.
- Keenan, J. D., Bailey, R. L., West, S. K., Arzika, A. M., Hart, J., Weaver, J., et al. (2018). Azithromycin to reduce childhood mortality in sub-saharan Africa. *N. Engl. J. Med.* 378, 1583–1592.
- Keith, J. W., and Pamer, E. G. (2019). Enlisting commensal microbes to resist antibiotic-resistant pathogens. *J. Exp. Med.* 216, 10–19. doi: 10.1084/jem.20180399
- Kenyon, C., and Manoharan-Basil, S. S. (2020). Cultural drivers of antibiotic consumption in high-income countries: a global ecological analysis. *Microb. Drug Resist.* doi: 10.1089/mdr.2019.0497 [Epub ahead of print].
- Kim, J., Hanotte, O., Mwai, O. A., Dessie, T., Bashir, S., Diallo, B., et al. (2017). The genome landscape of indigenous African cattle. *Genome Biol.* 18:34.
- Kim, L., Mcgee, L., Tomczyk, S., and Beall, B. (2016). Biological and epidemiological features of antibiotic-resistant streptococcus pneumoniae in pre- and post-conjugate vaccine eras: a united states perspective. *Clin. Microbiol. Rev.* 29, 525–552. doi: 10.1128/cmr.00058-15
- Kintses, B., Jangir, P. K., Fekete, G., Számel, M., Méhi, O., Spohn, R., et al. (2019). Chemical-genetic profiling reveals limited cross-resistance between antimicrobial peptides with different modes of action. *Nat. Commun.* 10:5731.
- Klein, E. Y., Van Boeckel, T. P., Martinez, E. M., Pant, S., Gandra, S., Levin, S. A., et al. (2018). Global increase and geographic convergence in antibiotic consumption between 2000 and 2015. *Proc. Natl. Acad. Sci. U.S.A.* 115, E3463–E3470.
- Kluytmans, J. A., Overvest, I. T., Willemsen, I., Kluytmans-Van Den Bergh, M. F., Van Der Zwaluw, K., Heck, M., et al. (2013). Extended-spectrum beta-lactamase-producing *Escherichia coli* from retail chicken meat and humans: comparison of strains, plasmids, resistance genes, and virulence factors. *Clin. Infect. Dis.* 56, 478–487. doi: 10.1093/cid/cis929
- Koplan, J. P., Bond, T. C., Merson, M. H., Reddy, K. S., Rodriguez, M. H., Sewankambo, N. K., et al. (2009). Towards a common definition of global health. *Lancet* 373, 1993–1995. doi: 10.1016/s0140-6736(09)60332-9
- Kotnik, T., and Weaver, J. C. (2016). Abiotic gene transfer: rare or rampant? *J. Membr. Biol.* 249, 623–631. doi: 10.1007/s00232-016-9897-y
- Kudo, H., Usui, M., Nagafuji, W., Oka, K., Takahashi, M., Yamaguchi, H., et al. (2019). Inhibition effect of flavophospholipol on conjugative transfer of the extended-spectrum β -lactamase and vanA genes. *J. Antibiot.* 72, 79–85. doi: 10.1038/s41429-018-0113-4
- Kümmerer, K. (2004). Resistance in the environment. *J. Antimicrob. Chemother.* 54, 311–320.
- Lange, A., Beier, S., Steimle, A., Autenrieth, I. B., Huson, D. H., and Frick, J. S. (2016). Extensive mobilome-driven genome diversification in mouse gut-associated *Bacteroides vulgatus* mpk. *Genome Biol. Evol.* 8, 1197–1207. doi: 10.1093/gbe/evw070
- Lanza, V. F., Baquero, F., Martinez, J. L., Ramos-Ruiz, R., Gonzalez-Zorn, B., Andremon, A., et al. (2018). In-depth resistome analysis by targeted metagenomics. *Microbiome* 6:11.
- Lanza, V. F. N., Tedim, A. P., Martínez, J. L., Baquero, F., and Coque, T. M. (2015). The plasmidome of firmicutes: impact on the emergence and the spread of resistance to antimicrobials. *Microbiol. Spectr.* 3:LAS-0039–2014. doi: 10.1128/microbiolspec.PLAS-0039-2014
- Larsson, D. G. J., Andremon, A., Bengtsson-Palme, J., Brandt, K. K., De Roda Husman, A. M., Fagerstedt, P., et al. (2018). Critical knowledge gaps and research needs related to the environmental dimensions of antibiotic resistance. *Environ. Int.* 117, 132–138. doi: 10.1016/j.envint.2018.04.041
- Laxminarayan, R., Duse, A., Wattal, C., Zaidi, A. K., Wertheim, H. F., Sumpradit, N., et al. (2013). Antibiotic resistance-the need for global solutions. *Lancet Infect. Dis.* 13, 1057–1098.
- Lázár, V., Martins, A., Spohn, R., Daruka, L., Grézel, G., Fekete, G., et al. (2018). Antibiotic-resistant bacteria show widespread collateral sensitivity to antimicrobial peptides. *Nat. Microbiol.* 3, 718–731. doi: 10.1038/s41564-018-0164-0
- Lehtinen, S., Blanquart, F., Lipsitch, M., and Fraser, C. (2019). On the evolutionary ecology of multidrug resistance in bacteria. *PLoS Pathog.* 15:e1007763. doi: 10.1371/journal.ppat.1007763
- Leonard, A. F. C., Zhang, L., Balfour, A. J., Garside, R., Hawkey, P. M., Murray, A. K., et al. (2018). Exposure to and colonisation by antibiotic-resistant *E. coli* in UK coastal water users: environmental surveillance, exposure assessment, and epidemiological study (Beach Bum Survey). *Environ. Int.* 114, 326–333. doi: 10.1016/j.envint.2017.11.003
- Lerner, H., and Berg, C. (2017). A comparison of three holistic approaches to health: one health, ecohealth, and planetary health. *Front. Vet. Sci.* 4:163. doi: 10.3389/fvets.2017.00163
- Levin, B. R., Baquero, F., Ankomah, P. P., and McCall, I. C. (2017). Phagocytes, Antibiotics, and Self-Limiting Bacterial Infections. *Trends Microbiol.* 25, 878–892. doi: 10.1016/j.tim.2017.07.005
- Levin, S., Xepapadeas, A., Anne-Sophie, C. P., Norberg, J., De Zeeuw, A., Folke, C., et al. (2013). Social-ecological systems as complex adaptive systems: modeling and policy implications. *Environ. Dev. Econ.* 18, 111–132.

- Li, K., Schurig-Briccio, L. A., Feng, X., Upadhyay, A., Pujari, V., Lechartier, B., et al. (2014). Multitarget drug discovery for tuberculosis and other infectious diseases. *J. Med. Chem.* 57, 3126–3139.
- Lin, W., Li, S., Zhang, S., and Yu, X. (2016). Reduction in horizontal transfer of conjugative plasmid by Uv irradiation and low-level chlorination. *Water Res.* 91, 331–338. doi: 10.1016/j.watres.2016.01.020
- Ling, L. L., Schneider, T., Peoples, A. J., Spoering, A. L., Engels, I., Conlon, B. P., et al. (2015). A new antibiotic kills pathogens without detectable resistance. *Nature* 517, 455–459.
- Lloyd, W. F. (1833). *Two lectures on the Checks to Population [microform]*. Oxford: University of Oxford in Michaelmas term 1832 / by W.F. Lloyd, Printed for the author.
- Looker, K. J., and Hallett, T. B. (2006). Individual freedom versus collective responsibility: too many rights make a wrong? *Emerg. Themes Epidemiol.* 3:14.
- Lopatkin, A. J., Meredith, H. R., Srimani, J. K., Pfeiffer, C., Durrett, R., and You, L. (2017). Persistence and reversal of plasmid-mediated antibiotic resistance. *Nat. Commun.* 8:1689.
- Lopez-Causape, C., Sommer, L. M., Cabot, G., Rubio, R., Ocampo-Sosa, A. A., Johansen, H. K., et al. (2017). Evolution of the *Pseudomonas aeruginosa* mutational resistome in an international Cystic Fibrosis clone. *Sci. Rep.* 7:5555.
- Ma, L., Li, B., Jiang, X. T., Wang, Y. L., Xia, Y., Li, A. D., et al. (2017). Catalogue of antibiotic resistome and host-tracking in drinking water deciphered by a large scale survey. *Microbiome* 5:154.
- MacFadden, D. R., Mcgough, S. F., Fisman, D., Santillana, M., and Brownstein, J. S. (2018). Antibiotic resistance increases with local temperature. *Na. Clim. Change* 8, 510–514. doi: 10.1038/s41558-018-0161-6
- Mahmood, S. S., Levy, D., Vasan, R. S., and Wang, T. J. (2014). The framingham heart study and the epidemiology of cardiovascular disease: a historical perspective. *Lancet* 383, 999–1008. doi: 10.1016/s0140-6736(13)61752-3
- Mahnert, A., Moissl-Eichinger, C., Zojer, M., Bogumil, D., Mizrahi, I., Rattei, T., et al. (2019). Man-made microbial resistances in built environments. *Nat. Commun.* 10:968.
- Mainous, A. G., Everett, C. J., Post, R. E., Diaz, V. A., and Hueston, W. J. (2009). Availability of antibiotics for purchase without a prescription on the internet. *Ann. Fam. Med.* 7, 431–435. doi: 10.1370/afm.999
- Maltezou, H. C. (2016). Antibiotic resistance and the refugee crisis in Europe - Preemptive action is indicated. *Travel Med. Infect. Dis.* 14, 69–70. doi: 10.1016/j.tmaid.2016.03.009
- Manaia, C. M. (2017). Assessing the risk of antibiotic resistance transmission from the environment to humans: non-direct proportionality between abundance and risk. *Trends Microbiol.* 25, 173–181. doi: 10.1016/j.tim.2016.11.014
- Manaia, C. M., Rocha, J., Scaccia, N., Marano, R., Radu, E., Biancullo, F., et al. (2018). Antibiotic resistance in wastewater treatment plants: tackling the black box. *Environ. Int.* 115, 312–324. doi: 10.1016/j.envint.2018.03.044
- Manyi-Loh, C., Mamphweli, S., Meyer, E., and Okoh, A. (2018). Antibiotic use in agriculture and its consequential resistance in environmental sources: potential public health implications. *Molecules* 23:795. doi: 10.3390/molecules23040795
- Martinez, J. L. (2009a). Environmental pollution by antibiotics and by antibiotic resistance determinants. *Environ. Pollut.* 157, 2893–2902. doi: 10.1016/j.envpol.2009.05.051
- Martinez, J. L. (2009b). The role of natural environments in the evolution of resistance traits in pathogenic bacteria. *Proc. Biol. Sci.* 276, 2521–2530. doi: 10.1098/rspb.2009.0320
- Martinez, J. L. (2012). Natural antibiotic resistance and contamination by antibiotic resistance determinants: the two ages in the evolution of resistance to antimicrobials. *Front. Microbiol.* 3:1. doi: 10.3389/fmicb.2012.00001
- Martinez, J. L. (2014). General principles of antibiotic resistance in bacteria. *Drug Discov. Today Technol.* 11, 33–39. doi: 10.1016/j.ddtec.2014.02.001
- Martinez, J. L., and Baquero, F. (2002). Interactions among strategies associated with bacterial infection: pathogenicity, epidemicity, and antibiotic resistance. *Clin. Microbiol. Rev.* 15, 647–679. doi: 10.1128/cmr.15.4.647-679.2002
- Martinez, J. L., Baquero, F., and Andersson, D. I. (2007). Predicting antibiotic resistance. *Nat. Rev. Microbiol.* 5, 958–965. doi: 10.1038/nrmicro1796
- Martinez, J. L., Baquero, F., and Andersson, D. I. (2011). Beyond serial passages: new methods for predicting the emergence of resistance to novel antibiotics. *Curr. Opin. Pharmacol.* 11, 439–445. doi: 10.1016/j.coph.2011.07.005
- Martinez, J. L., Coque, T. M., and Baquero, F. (2015). What is a resistance gene? Ranking risk in resistomes. *Nat. Rev. Microbiol.* 13, 116–123. doi: 10.1038/nrmicro3399
- Martinez, J. L., Coque, T. M., Lanza, V. F., De La Cruz, F., and Baquero, F. (2017). Genomic and metagenomic technologies to explore the antibiotic resistance mobilome. *Ann. N. Y. Acad. Sci.* 1388, 26–41. doi: 10.1111/nyas.13282
- Martinez, J. L., Fajardo, A., Garmendia, L., Hernandez, A., Linares, J. F., Martinez-Solano, L., et al. (2009). A global view of antibiotic resistance. *FEMS Microbiol. Rev.* 33, 44–65.
- Martinez-Urtaza, J., Trinanes, J., Gonzalez-Escalona, N., and Baker-Austin, C. (2016). Is El Nino a long-distance corridor for waterborne disease? *Nat. Microbiol.* 1:16018.
- Martiny, J. B., Bohannan, B. J., Brown, J. H., Colwell, R. K., Fuhrman, J. A., Green, J. L., et al. (2006). Microbial biogeography: putting microorganisms on the map. *Nat. Rev. Microbiol.* 4, 102–112. doi: 10.1038/nrmicro1341
- Mathew, A. G., Cissell, R., and Liamthong, S. (2007). Antibiotic resistance in bacteria associated with food animals: a United States perspective of livestock production. *Foodborne Pathog. Dis.* 4, 115–133. doi: 10.1089/fpd.2006.0066
- Megget, K. (2020). Even covid-19 can't kill the anti-vaccination movement. *BMJ* 369:m2184. doi: 10.1136/bmj.m2184
- Middleton, J. H., and Ambrose, A. (2005). Enumeration and antibiotic resistance patterns of fecal indicator organisms isolated from migratory Canada geese (*Branta canadensis*). *J. Wildl. Dis.* 41, 334–341. doi: 10.7589/0090-3558-41.2.334
- Mindlin, S., Minakhin, L., Petrova, M., Kholodii, G., Minakhina, S., Gorlenko, Z., et al. (2005). Present-day mercury resistance transposons are common in bacteria preserved in permafrost grounds since the Upper Pleistocene. *Res. Microbiol.* 156, 994–1004. doi: 10.1016/j.resmic.2005.05.011
- Moura, A., Henriques, I., Smalla, K., and Correia, A. (2010). Wastewater bacterial communities bring together broad-host range plasmids, integrons and a wide diversity of uncharacterized gene cassettes. *Res. Microbiol.* 161, 58–66. doi: 10.1016/j.resmic.2009.11.004
- Munck, C., Albertsen, M., Telke, A., Ellabaan, M., Nielsen, P. H., and Sommer, M. O. (2015). Limited dissemination of the wastewater treatment plant core resistome. *Nat. Commun.* 6:8452.
- Muniesa, M., Colomer-Lluch, M., and Jofre, J. (2013). Could bacteriophages transfer antibiotic resistance genes from environmental bacteria to human-body associated bacterial populations? *Mob. Genet. Elements* 3:e25847. doi: 10.4161/mge.25847
- Murray, B. E., Mathewson, J. J., Dupont, H. L., Ericsson, C. D., and Reves, R. R. (1990). Emergence of resistant fecal *Escherichia coli* in travelers not taking prophylactic antimicrobial agents. *Antimicrob. Agents Chemother.* 34, 515–518. doi: 10.1128/aac.34.4.515
- Newton, P. N., Amin, A. A., Bird, C., Passmore, P., Dukes, G., Tomson, G., et al. (2011). The primacy of public health considerations in defining poor quality medicines. *PLoS Med.* 8:e1001139. doi: 10.1371/journal.pmed.1001139
- Ni, Z., Chen, Y., Ong, E., and He, Y. (2017). Antibiotic resistance determinant-focused *Acinetobacter baumannii* vaccine designed using reverse vaccinology. *Int. J. Mol. Sci.* 18:458. doi: 10.3390/ijms18020458
- Nichol, D., Rutter, J., Bryant, C., Hujer, A. M., Lek, S., Adams, M. D., et al. (2019). Antibiotic collateral sensitivity is contingent on the repeatability of evolution. *Nat. Commun.* 10:334.
- Novais, C., Tedim, A. P., Lanza, V. F., Freitas, A. R., Silveira, E., Escada, R., et al. (2016). Co-diversification of *Enterococcus faecium* core genomes and Pbp5: evidences of pbp5 horizontal transfer. *Front. Microbiol.* 7:1581. doi: 10.3389/fmicb.2016.01581
- Nyborg, K., Anderies, J. M., Dannenberg, A., Lindahl, T., Schill, C., Schluter, M., et al. (2016). Social norms as solutions. *Science* 354, 42–43.
- Okeke, I. N., and Edelman, R. (2001). Dissemination of antibiotic-resistant bacteria across geographic borders. *Clin. Infect. Dis.* 33, 364–369. doi: 10.1086/321877
- Oldenkamp, R., Beusen, A. H. W., and Huijbregts, M. A. J. (2019). Aquatic risks from human pharmaceuticals—modelling temporal trends of carbamazepine and ciprofloxacin at the global scale. *Environ. Res. Lett.* 14:034003. doi: 10.1088/1748-9326/ab0071
- Olivares, J., Alvarez-Ortega, C., Linares, J. F., Rojo, F., Köhler, T., and Martínez, J. L. (2012). Overproduction of the multidrug efflux pump Mexef-OprN does not impair *Pseudomonas aeruginosa* fitness in competition tests, but produces specific changes in bacterial regulatory networks. *Environ. Microbiol.* 14, 1968–1981. doi: 10.1111/j.1462-2920.2012.02727.x

- Olivares, J., Alvarez-Ortega, C., and Martinez, J. L. (2014). Metabolic compensation of fitness costs associated with overexpression of the multidrug efflux pump Mexef-OprN in *Pseudomonas aeruginosa*. *Antimicrob. Agents Chemother.* 58, 3904–3913. doi: 10.1128/aac.00121-14
- Overdevest, I., Willemsen, L., Rijnsburger, M., Eustace, A., Xu, L., Hawkey, P., et al. (2011). Extended-spectrum beta-lactamase genes of *Escherichia coli* in chicken meat and humans. The Netherlands. *Emerg. Infect. Dis.* 17, 1216–1222. doi: 10.3201/eid1707.110209
- Pal, C., Asiani, K., Arya, S., Rensing, C., Stekel, D. J., Larsson, D. G. J., et al. (2017). Metal resistance and its association with antibiotic resistance. *Adv. Microb. Physiol.* 70, 261–313. doi: 10.1016/bs.ampbs.2017.02.001
- Pamer, E. G. (2016). Resurrecting the intestinal microbiota to combat antibiotic-resistant pathogens. *Science* 352, 535–538. doi: 10.1126/science.aad9382
- Panagos, P., Van Liedekerke, M., Yigini, Y., and Montanarella, L. (2013). Contaminated sites in Europe: review of the current situation based on data collected through a European network. *J. Environ. Public Health* 2013:158764.
- Partridge, S. R., and Hall, R. M. (2004). Complex multiple antibiotic and mercury resistance region derived from the r-det of Nr1 (R100). *Antimicrob. Agents Chemother.* 48, 4250–4255. doi: 10.1128/aac.48.11.4250-4255.2004
- Paulander, W., Pennhag, A., Andersson, D. I., and Maisnier-Patin, S. (2007). *Caenorhabditis elegans* as a model to determine fitness of antibiotic-resistant *Salmonella enterica* serovar Typhimurium. *Antimicrob. Agents Chemother.* 51, 766–769. doi: 10.1128/aac.00615-06
- Paulus, G. K., Hornstra, L. M., Alygizakis, N., Slobodnik, J., Thomaidis, N., and Medema, G. (2019). The impact of on-site hospital wastewater treatment on the downstream communal wastewater system in terms of antibiotics and antibiotic resistance genes. *Int. J. Hyg. Environ. Health* 222, 635–644. doi: 10.1016/j.ijheh.2019.01.004
- Pehrsson, E. C., Tsukayama, P., Patel, S., Mejia-Bautista, M., Sosa-Soto, G., Navarrete, K. M., et al. (2016). Interconnected microbiomes and resistomes in low-income human habitats. *Nature* 533, 212–216. doi: 10.1038/nature17672
- Pérez, A., and Pierce Wise Sr, J. (2018). One environmental health: an emerging perspective in toxicology. *F1000Res.* 7:918. doi: 10.12688/f1000research.14233.1
- Perry, J. A., Westman, E. L., and Wright, G. D. (2014). The antibiotic resistome: what's new? *Curr. Opin. Microbiol.* 21, 45–50.
- Petersen, A., Held, N., and Heide, L. (2017). Surveillance for falsified and substandard medicines in Africa and Asia by local organizations using the low-cost Gphf Minilab. *PLoS One* 12:e0184165. doi: 10.1371/journal.pone.0184165
- Ploy, M. C., Andreumont, A., Valtier, B., and Le Jeune, C. (2020). Antibiotic resistance: tools for effective translational research. *Therapie* 75, 7–12. doi: 10.1016/j.therap.2019.12.003
- Poeta, P., Radhouani, H., Igrejas, G., Goncalves, A., Carvalho, C., Rodrigues, J., et al. (2008). Seagulls of the berlingas natural reserve of portugal as carriers of fecal *Escherichia coli* harboring Ctx-M and Tem extended-spectrum beta-lactamases. *Appl. Environ. Microbiol.* 74, 7439–7441. doi: 10.1128/aem.00949-08
- Power, M. L., Samuel, A., Smith, J. J., Stark, J. S., Gillings, M. R., and Gordon, D. M. (2016). *Escherichia coli* out in the cold: dissemination of human-derived bacteria into the Antarctic microbiome. *Environ. Pollut.* 215, 58–65. doi: 10.1016/j.envpol.2016.04.013
- Price, L. B., Hungate, B. A., Koch, B. J., Davis, G. S., and Liu, C. M. (2017). Colonizing opportunistic pathogens (Cops): the beasts in all of us. *PLoS Pathog.* 13:e1006369. doi: 10.1371/journal.ppat.1006369
- Reuland, E. A., Sonder, G. J., Stolte, I., Al Naiemi, N., Koek, A., Linde, G. B., et al. (2016). Travel to Asia and traveller's diarrhoea with antibiotic treatment are independent risk factors for acquiring ciprofloxacin-resistant and extended spectrum beta-lactamase-producing *Enterobacteriaceae*-a prospective cohort study. *Clin. Microbiol. Infect.* 22, e1–e7.
- Ricardo, D. (1821). *On the Principles of Political Economy and Taxation*. Hamilton, ON: McMaster University.
- Rizzo, L., Manaia, C., Merlin, C., Schwartz, T., Dagot, C., Ploy, M. C., et al. (2013). Urban wastewater treatment plants as hotspots for antibiotic resistant bacteria and genes spread into the environment: a review. *Sci. Total Environ.* 447, 345–360. doi: 10.1016/j.scitotenv.2013.01.032
- Robinson, T. P., Bu, D. P., Carrique-Mas, J., Fevre, E. M., Gilbert, M., Grace, D., et al. (2016). Antibiotic resistance is the quintessential One Health issue. *Trans. R. Soc. Trop. Med. Hyg.* 110, 377–380. doi: 10.1093/trstmh/trw048
- Rodriguez-Beltran, J., Hernandez-Beltran, J. C. R., Delafuente, J., Escudero, J. A., Fuentes-Hernandez, A., Maclean, R. C., et al. (2018). Multicopy plasmids allow bacteria to escape from fitness trade-offs during evolutionary innovation. *Nat. Ecol. Evol.* 2, 873–881. doi: 10.1038/s41559-018-0529-z
- Rodriguez-Beltran, J., Rodriguez-Rojas, A., Yubero, E., and Blazquez, J. (2013). The animal food supplement sepiolite promotes a direct horizontal transfer of antibiotic resistance plasmids between bacterial species. *Antimicrob. Agents Chemother.* 57, 2651–2653. doi: 10.1128/aac.02363-12
- Rousseau, J.-J. (1974). *The Essential Rousseau: The Social Contract, Discourse on the Origin of Inequality, Discourse on the Arts and Sciences, The Creed of a Savoyard Priest*. New York, NY: New American Library.
- Rudholm, N. (2002). Economic implications of antibiotic resistance in a global economy. *J. Health Econ.* 21, 1071–1083. doi: 10.1016/s0167-6296(02)00053-x
- Ruiz-Diez, B., Sanchez, P., Baquero, F., Martinez, J. L., and Navas, A. (2003). Differential interactions within the *Caenorhabditis elegans*-*Pseudomonas aeruginosa* pathogenesis model. *J. Theor. Biol.* 225, 469–476. doi: 10.1016/s0022-5193(03)00288-1
- Ruppe, E., Andreumont, A., and Armand-Lefevre, L. (2017a). Digestive tract colonization by multidrug-resistant *Enterobacteriaceae* in travellers: an update. *Travel. Med. Infect. Dis.* 21, 28–35. doi: 10.1016/j.tmaid.2017.11.007
- Ruppe, E., Ghazlane, A., Tap, J., Pons, N., Alvarez, A.-S., Maziers, N., et al. (2017b). Prediction of the intestinal resistome by a novel 3D-based method. *bioRxiv* [Preprint]. doi: 10.1101/196014
- Ruppe, E., and Chappuis, F. (2017). What and how should we tell travellers about antimicrobial resistance? *J. Travel. Med.* 24:taw089.
- Salverda, M. L., De Visser, J. A., and Barlow, M. (2010). Natural evolution of Tem-1 β -lactamase: experimental reconstruction and clinical relevance. *FEMS Microbiol. Rev.* 34, 1015–1036. doi: 10.1111/j.1574-6976.2010.00222.x
- Sanchez, P., Linares, J. F., Ruiz-Diez, B., Campanario, E., Navas, A., Baquero, F., et al. (2002). Fitness of in vitro selected *Pseudomonas aeruginosa* nalB and nfxB multidrug resistant mutants. *J. Antimicrob. Chemother.* 50, 657–664. doi: 10.1093/jac/dkf185
- Schauler, K., Semmler, T., Pickard, D. J., De Toro, M., De La Cruz, F., Wieler, L. H., et al. (2016). Carriage of extended-spectrum beta-lactamase-plasmids does not reduce fitness but enhances virulence in some strains of pandemic *E. coli* Lineages. *Front. Microbiol.* 7:336. doi: 10.3389/fmicb.2016.00336
- Schiavone, A. (2012). *The Invention of Law in the West*. Cambridge, MA: Belknap Press of Harvard Univ. Press.
- Schulz zur Wiesch, P., Engelstadter, J., and Bonhoeffer, S. (2010). Compensation of fitness costs and reversibility of antibiotic resistance mutations. *Antimicrob. Agents Chemother.* 54, 2085–2095. doi: 10.1128/aac.01460-09
- Sciarretta, K., Rottingen, J. A., Opalska, A., Van Hengel, A. J., and Larsen, J. (2016). Economic incentives for antibacterial drug development: literature review and considerations from the transatlantic task force on antimicrobial resistance. *Clin. Infect. Dis.* 63, 1470–1474. doi: 10.1093/cid/ciw593
- Scott, R. E., and Mars, M. (2020). Behaviour change and e-Health - looking broadly: a scoping narrative review. *Stud. Health Technol. Inform.* 268, 123–138.
- Scott, G., Fazio, V., and Lo Muzio, L. (2017). Tuberculosis in the immigrant population in Italy: state-of-the-art review. *Infez Med.* 25, 199–209.
- Seddon, N., Mace, G. M., Naeem, S., Tobias, J. A., Pigot, A. L., Cavanagh, R., et al. (2016). Biodiversity in the anthropocene: prospects and policy. *Proc. Biol. Sci.* 283:20162094.
- Sharma, R. (2018). Health and economic growth: evidence from dynamic panel data of 143 years. *PLoS One* 13:e0204940. doi: 10.1371/journal.pone.0204940
- Shatzkes, K., Singleton, E., Tang, C., Zuenka, M., Shukla, S., Gupta, S., et al. (2016). Predatory bacteria attenuate *Klebsiella pneumoniae* burden in rat lungs. *mBio* 7:e01847-16. doi: 10.1128/mBio.01847-16
- Sheppard, S. K., Guttman, D. S., and Fitzgerald, J. R. (2018). Population genomics of bacterial host adaptation. *Nat. Rev. Genet.* 19, 549–565. doi: 10.1038/s41576-018-0032-z
- Siefert, J. L. (2009). Defining the mobilome. *Methods Mol. Biol.* 532, 13–27. doi: 10.1007/978-1-60327-853-9_2
- Skippington, E., and Ragan, M. A. (2011). Lateral genetic transfer and the construction of genetic exchange communities. *FEMS Microbiol. Rev.* 35, 707–735. doi: 10.1111/j.1574-6976.2010.00261.x
- Smillie, C. S., Smith, M. B., Friedman, J., Cordero, O. X., David, L. A., and Alm, E. J. (2011). Ecology drives a global network of gene exchange connecting the human microbiome. *Nature* 480, 241–244. doi: 10.1038/nature10571

- Spinoza, B. (2007). *Published 1670 Theological-Political Treatise*. Cambridge: Cambridge University Press.
- Spohn, R., Daruka, L., Lázár, V., Martins, A., Vidovics, F., Grézal, G., et al. (2019). Integrated evolutionary analysis reveals antimicrobial peptides with limited resistance. *Nat. Commun.* 10:4538.
- Staehlin, B. M., Gibbons, J. G., Rokas, A., O'halloran, T. V., and Slot, J. C. (2016). Evolution of a heavy metal homeostasis/resistance island reflects increasing copper stress in enterobacteria. *Genome Biol. Evol.* 8, 811–826.
- Su, J.-Q., An, X.-L., Li, B., Chen, Q.-L., Gillings, M. R., Chen, H., et al. (2017). Metagenomics of urban sewage identifies an extensively shared antibiotic resistome in China. *Microbiome* 5:84.
- Sun, J., Liao, X. P., D'souza, A. W., Boolchandani, M., Li, S. H., Cheng, K., et al. (2020). Environmental remodeling of human gut microbiota and antibiotic resistome in livestock farms. *Nat. Commun.* 11:1427.
- Sundqvist, M., Geli, P., Andersson, D. I., Sjolund-Karlsson, M., Runeheggen, A., Cars, H., et al. (2010). Little evidence for reversibility of trimethoprim resistance after a drastic reduction in trimethoprim use. *J. Antimicrob. Chemother.* 65, 350–360. doi: 10.1093/jac/dkp387
- Sweeney, M. T., Lubbers, B. V., Schwarz, S., and Watts, J. L. (2018). Applying definitions for multidrug resistance, extensive drug resistance and pandrug resistance to clinically significant livestock and companion animal bacterial pathogens. *J. Antimicrob. Chemother.* 73, 1460–1463. doi: 10.1093/jac/dky043
- Tamminen, M., Virta, M., Fani, R., and Fondi, M. (2012). Large-scale analysis of plasmid relationships through gene-sharing networks. *Mol. Biol. Evol.* 29, 1225–1240. doi: 10.1093/molbev/msr292
- Taylor, P., and Reeder, R. (2020). Antibiotic use on crops in low and middle-income countries based on recommendations made by agricultural advisors. *Cabi Agric. Biosci.* 1:1.
- Theuretzbacher, U., Ardal, C., and Harbarth, S. (2017). Linking sustainable use policies to novel economic incentives to stimulate antibiotic research and development. *Infect. Dis. Rep.* 9:6836.
- Thi, T. D., López, E., Rodríguez-Rojas, A., Rodríguez-Beltrán, J., Couce, A., Guelfo, J. R., et al. (2011). Effect of recA inactivation on mutagenesis of *Escherichia coli* exposed to sublethal concentrations of antimicrobials. *J. Antimicrob. Chemother.* 66, 531–538. doi: 10.1093/jac/dkq496
- Tian, X., Palomo, A., Zhang, H., Luan, X., Liu, R., Awad, M., et al. (2020). Minimum influent concentrations of oxytetracycline, streptomycin and spiramycin in selecting antibiotic resistance in biofilm type wastewater treatment systems. *Sci. Total Environ.* 720:137531. doi: 10.1016/j.scitotenv.2020.137531
- Tipper, A. (2010). Economic models of the family and the relationship between economic status and health. *Soc. Sci. Med.* 70, 1567–1573. doi: 10.1016/j.socscimed.2010.01.028
- Tocqueville, A. D. (1838). *Democracy in America*. New York, NY: G. Dearborn & Co.
- Toutain, P. L., Bousquet-Mélou, A., Damborg, P., Ferran, A. A., Mevius, D., Pelligand, L., et al. (2017). En Route towards European clinical breakpoints for veterinary antimicrobial susceptibility testing: a position paper explaining the vetcast approach. *Front. Microbiol.* 8:2344. doi: 10.3389/fmicb.2017.02344
- Traven, A., and Naderer, T. (2019). Central metabolic interactions of immune cells and microbes: prospects for defeating infections. *Embo Rep.* 20:e47995.
- Valencia, E. Y., Esposito, F., Spira, B., Blázquez, J., and Galhardo, R. S. (2017). Ciprofloxacin-mediated mutagenesis is suppressed by subinhibitory concentrations of amikacin in *Pseudomonas aeruginosa*. *Antimicrob. Agents Chemother.* 61:e02107-16. doi: 10.1128/AAC.02107-16
- Van Boeckel, T. P., Brower, C., Gilbert, M., Grenfell, B. T., Levin, S. A., Robinson, T. P., et al. (2015). Global trends in antimicrobial use in food animals. *Proc. Natl. Acad. Sci. U.S.A.* 112, 5649–5654.
- Van Boeckel, T. P., Glennon, E. E., Chen, D., Gilbert, M., Robinson, T. P., Grenfell, B. T., et al. (2017). Reducing antimicrobial use in food animals. *Science* 357, 1350–1352.
- van Bruggen, A. H. C., Goss, E. M., Havelaar, A., Van Diepeningen, A. D., Finckh, M. R., and Morris, J. G. Jr. (2019). One Health - Cycling of diverse microbial communities as a connecting force for soil, plant, animal, human and ecosystem health. *Sci. Total Environ.* 664, 927–937. doi: 10.1016/j.scitotenv.2019.02.091
- van der Heijden, M., Sandgren, A., pränting, M., Karvanen, M., Aagaard, H., Zorzet, A., et al. (2019). *When the Drugs Don't Work. Antibiotic Resistance as a Global Development Problem*. Uppsala: The Dag Hammarskjöld Foundation.
- Veening, J. W., and Blokesch, M. (2017). Interbacterial predation as a strategy for Dna acquisition in naturally competent bacteria. *Nat. Rev. Microbiol.* 15, 621–629. doi: 10.1038/nrmicro.2017.66
- Verhoef, J. (2003). Antibiotic resistance: the pandemic. *Adv. Exp. Med. Biol.* 531, 301–313. doi: 10.1007/978-1-4615-0059-9_26
- Viertel, T. M., Ritter, K., and Horz, H. P. (2014). Viruses versus bacteria-novel approaches to phage therapy as a tool against multidrug-resistant pathogens. *J. Antimicrob. Chemother.* 69, 2326–2336. doi: 10.1093/jac/dku173
- Wales, A. D., and Davies, R. H. (2015). Co-Selection of resistance to antibiotics, biocides and heavy metals, and its relevance to foodborne pathogens. *Antibiotics* 4, 567–604. doi: 10.3390/antibiotics4040567
- Walsh, F. (2013). Investigating antibiotic resistance in non-clinical environments. *Front. Microbiol.* 4:19. doi: 10.3389/fmicb.2013.00019
- Walsh, T. R., Weeks, J., Livermore, D. M., and Toleman, M. A. (2011). Dissemination of Ndm-1 positive bacteria in the New Delhi environment and its implications for human health: an environmental point prevalence study. *Lancet Infect. Dis.* 11, 355–362. doi: 10.1016/s1473-3099(11)70059-7
- Wang, S., Xue, N., Li, W., Zhang, D., Pan, X., and Luo, Y. (2020). Selectively enrichment of antibiotics and Args by microplastics in river, estuary and marine waters. *Sci. Total Environ.* 708, 134594. doi: 10.1016/j.scitotenv.2019.134594
- Wegener, H. C., Bager, F., and Aarestrup, F. M. (1997). Surveillance of antimicrobial resistance in humans, food stuffs and livestock in Denmark. *Eur. Surveill.* 2, 17–19. doi: 10.2807/esm.02.03.00180-en
- Wernli, D., Jorgensen, P. S., Morel, C. M., Carroll, S., Harbarth, S., Levrat, N., et al. (2017). Mapping global policy discourse on antimicrobial resistance. *BMJ Glob. Health* 2:e000378. doi: 10.1136/bmjgh-2017-000378
- Wikler, D. (2002). Personal and social responsibility for health. *Ethics Int. Affairs* 16, 47–55. doi: 10.1111/j.1747-7093.2002.tb00396.x
- Wood, K. (2019). Microbial ecology: complex bacterial communities reduce selection for antibiotic resistance. *Curr. Biol.* 29, R1143–R1145.
- Wozniak, T. M., Barnsbee, L., Lee, X. J., and Pacella, R. E. (2019). Using the best available data to estimate the cost of antimicrobial resistance: a systematic review. *Antimicrob. Resist. Infect. Control* 8:26.
- Wright, G. D. (2007). The antibiotic resistome: the nexus of chemical and genetic diversity. *Na. Rev. Microbiol.* 5, 175–186. doi: 10.1038/nrmicro1614
- Yang, Y., Xu, C., Cao, X., Lin, H., and Wang, J. (2017). Antibiotic resistance genes in surface water of eutrophic urban lakes are related to heavy metals, antibiotics, lake morphology and anthropic impact. *Ecotoxicology* 26, 831–840. doi: 10.1007/s10646-017-1814-3
- Zankari, E., Hasman, H., Cosentino, S., Vestergaard, M., Rasmussen, S., Lund, O., et al. (2012). Identification of acquired antimicrobial resistance genes. *J. Antimicrob. Chemother.* 67, 2640–2644. doi: 10.1093/jac/dks261
- Zhang, Y., Gu, A. Z., Cen, T., Li, X., He, M., Li, D., et al. (2018). Sub-inhibitory concentrations of heavy metals facilitate the horizontal transfer of plasmid-mediated antibiotic resistance genes in water environment. *Environ. Pollut.* 237, 74–82. doi: 10.1016/j.envpol.2018.01.032
- Zhao, Y., Cocerva, T., Cox, S., Tardif, S., Su, J. Q., Zhu, Y. G., et al. (2019a). Evidence for co-selection of antibiotic resistance genes and mobile genetic elements in metal polluted urban soils. *Sci. Total Environ.* 656, 512–520. doi: 10.1016/j.scitotenv.2018.11.372
- Zhao, Y., Ye, M., Zhang, X., Sun, M., Zhang, Z., Chao, H., et al. (2019b). Comparing polyvalent bacteriophage and bacteriophage cocktails for controlling antibiotic-resistant bacteria in soil-plant system. *Sci. Total Environ.* 657, 918–925. doi: 10.1016/j.scitotenv.2018.11.457
- Zhu, Y. G., Gillings, M., Simonet, P., Stekel, D., Banwart, S., and Penueles, J. (2017). Microbial mass movements. *Science* 357, 1099–1100. doi: 10.1126/science.aao3007
- Zinsstag, J., Schelling, E., Waltner-Toews, D., and Tanner, M. (2011). From “one medicine” to “one health” and systemic approaches to health and well-being. *Prev. Vet. Med.* 101, 148–156. doi: 10.1016/j.prevetmed.2010.07.003

Conflict of Interest: The authors declare that the research was conducted in the absence of any commercial or financial relationships that could be construed as a potential conflict of interest.

Copyright © 2020 Hernando-Amado, Coque, Baquero and Martínez. This is an open-access article distributed under the terms of the Creative Commons Attribution License (CC BY). The use, distribution or reproduction in other forums is permitted, provided the original author(s) and the copyright owner(s) are credited and that the original publication in this journal is cited, in accordance with accepted academic practice. No use, distribution or reproduction is permitted which does not comply with these terms.



Inhibitory Effects of Lipopeptides and Glycolipids on *C. albicans*–*Staphylococcus* spp. Dual-Species Biofilms

Chiara Ceresa¹, Maurizio Rinaldi¹, Francesco Tessarolo^{2,3†}, Devid Maniglio^{2†}, Emanuele Fedeli¹, Erica Tambone², Patrizio Caciagli⁴, Ibrahim M. Banat⁵, Mayri Alessandra Diaz De Rienzo⁶ and Letizia Fracchia^{1*}

¹ Department of Pharmaceutical Sciences, Università del Piemonte Orientale “A. Avogadro”, Novara, Italy, ² BIOTech Center for Biomedical Technologies, Department of Industrial Engineering, Università di Trento, Trento, Italy, ³ Healthcare Research and Innovation Program (IRCS-FBK-PAT), Bruno Kessler Foundation, Trento, Italy, ⁴ Section of Electron Microscopy, Department of Medicine Laboratory, Azienda Provinciale per i Servizi Sanitari di Trento, Trento, Italy, ⁵ School of Biomedical Sciences, Faculty of Life and Health Sciences, Ulster University, Coleraine, United Kingdom, ⁶ School of Pharmacy and Biomolecular Sciences, Faculty of Science, Liverpool John Moores University, Liverpool, United Kingdom

OPEN ACCESS

Edited by:

Flavia Marinelli,
University of Insubria, Italy

Reviewed by:

Jasna Novak (maiden Beganovic),
University of Zagreb, Croatia
Ermenegilda Parrilli,
University of Naples Federico II, Italy

*Correspondence:

Letizia Fracchia
letizia.fracchia@uniupo.it

[†] These authors have contributed
equally to this work

Specialty section:

This article was submitted to
Antimicrobials, Resistance
and Chemotherapy,
a section of the journal
Frontiers in Microbiology

Received: 25 March 2020

Accepted: 17 December 2020

Published: 13 January 2021

Citation:

Ceresa C, Rinaldi M, Tessarolo F,
Maniglio D, Fedeli E, Tambone E,
Caciagli P, Banat IM,
Diaz De Rienzo MA and Fracchia L
(2021) Inhibitory Effects
of Lipopeptides and Glycolipids on
C. albicans–*Staphylococcus* spp.
Dual-Species Biofilms.
Front. Microbiol. 11:545654.
doi: 10.3389/fmicb.2020.545654

Microbial biofilms strongly resist host immune responses and antimicrobial treatments and are frequently responsible for chronic infections in peri-implant tissues. Biosurfactants (BSs) have recently gained prominence as a new generation of anti-adhesive and antimicrobial agents with great biocompatibility and were recently suggested for coating implantable materials in order to improve their anti-biofilm properties. In this study, the anti-biofilm activity of lipopeptide AC7BS, rhamnolipid R89BS, and sophorolipid SL18 was evaluated against clinically relevant fungal/bacterial dual-species biofilms (*Candida albicans*, *Staphylococcus aureus*, *Staphylococcus epidermidis*) through quantitative and qualitative *in vitro* tests. *C. albicans*–*S. aureus* and *C. albicans*–*S. epidermidis* cultures were able to produce a dense biofilm on the surface of the polystyrene plates and on medical-grade silicone discs. All tested BSs demonstrated an effective inhibitory activity against dual-species biofilms formation in terms of total biomass, cell metabolic activity, microstructural architecture, and cell viability, up to 72 h on both these surfaces. In co-incubation conditions, in which BSs were tested in soluble form, rhamnolipid R89BS (0.05 mg/ml) was the most effective among the tested BSs against the formation of both dual-species biofilms, reducing on average 94 and 95% of biofilm biomass and metabolic activity at 72 h of incubation, respectively. Similarly, rhamnolipid R89BS silicone surface coating proved to be the most effective in inhibiting the formation of both dual-species biofilms, with average reductions of 93 and 90%, respectively. Scanning electron microscopy observations showed areas of treated surfaces that were free of microbial cells or in which thinner and less structured biofilms were present, compared to controls. The obtained results endorse the idea that coating of implant surfaces with BSs may be a promising strategy for the prevention of *C. albicans*–*Staphylococcus* spp. colonization on medical devices, and can potentially contribute to the reduction of the high economic efforts undertaken by healthcare systems for the treatment of these complex fungal–bacterial infections.

Keywords: biosurfactants, multi-species biofilm, anti-adhesion, anti-biofilm, biomaterials, medical devices

INTRODUCTION

Biofilms are complex biological structures, composed of sessile multicellular communities encapsulated in a hydrated matrix of polysaccharides and proteins, in which microorganisms become more resistant to drug therapy and host immune response (Chen and Wen, 2011; Pompilio and Di Bonaventura, 2018). Microbial cells forming biofilms also communicate through the quorum sensing (QS) system, which is responsible of regulating genes expression, production of proteases and other signals that enable high-density bacterial cluster to flourish (Buch et al., 2019; Irerere et al., 2019).

Biofilms give rise to chronic infections both in tissues (e.g., lung infection in cystic fibrosis, chronic wound infections) and on the surface of implantable medical devices (e.g., orthopedic prostheses, endotracheal tubes, intravenous and urinary catheters, heart valves), which are characterized by the development of persistent and progressive diseases mainly due to the inflammatory response surrounding these biofilms (Clinton and Carter, 2015; Percival et al., 2015; Teo et al., 2016; Omar et al., 2017; Song et al., 2018). This makes many biofilm infections difficult to diagnose or to adequately treat.

Although most tissue and medical device-associated infections are caused by a single pathogen, an increasing number of polymicrobial infections have been reported in the clinical practice (Mihai et al., 2015; Rodrigues et al., 2019). The involved microorganisms are believed to coexist and realize synergistic interactions within the biofilm environment resulting in enhanced pathogenicity, virulence, and resistance to antimicrobials, thus leading to more aggressive forms of infections (Marculescu and Cantey, 2008; Burmølle et al., 2014). An emerging finding in polymicrobial biofilm research is the presence of both eukaryotic and prokaryotic pathogens (Brogden et al., 2005). The coexistence of *Candida albicans* and *Staphylococcus* species, in particular, has been frequently associated with extremely complicated infections and high mortality rates (Tsui et al., 2016). Biofilm-associated diseases related to *C. albicans* and *Staphylococcus* species, including wound infections, periodontitis, denture stomatitis, and medical devices related infections involving catheters and orthopedic implants have all been described before (Adam et al., 2002; Gupta et al., 2005; Valenza et al., 2008; Cuesta et al., 2010; Harriott and Noverr, 2011). These polymicrobial infections are difficult to diagnose and are mostly untreatable with the conventional antibiotic treatment strategies and commonly requires complex multi-drug therapy and in the vast majority of cases, the removal of infected medical devices (Harriott and Noverr, 2009; Pammi et al., 2013; Carolus et al., 2019).

This worldwide public health problem requires the development of innovative approaches able to efficiently tackle infections associated with these bacteria, fungi, and their biofilms. For this reason, several surface-coating strategies have been proposed to safeguard medical devices from microbial adhesion and colonization (John et al., 2007; Zilberman and Elsner, 2008; Ramasamy and Lee, 2016; Francolini et al., 2017; Khatoon et al., 2018; Wang and Tang, 2018; Ghensi et al., 2019). Unfortunately, surface-treated biomaterials showed, in some

cases, limited efficacy over time as well as an inherent risk of cytotoxicity toward cell tissues (Francolini and Donelli, 2010). Therefore, the application of natural molecules for the creation of new safe and effective biocompatible antibacterial and/or anti-adhesive biomaterial coatings or pharmaceutical products to prevent and treat both single-species and polymicrobial biofilm infections are urgently required (Vasilev et al., 2011).

Focusing on this goal, biosurfactants (BSs) have been suggested as a new group of antimicrobial/anti-biofilm biocompatible compounds useful in a wide range of pharmaceutical and biomedical applications (Diaz De Rienzo et al., 2014; Elshikh et al., 2017; Lydon et al., 2017; Juma et al., 2020). BSs are amphiphilic molecules, produced by a wide group of microorganisms, which partition at and alter the physical-chemical conditions of the interfaces and are characterized by interesting biological activities like antimicrobial, anti-adhesive, and anti-biofilm properties (Banat et al., 2014; Simms et al., 2020). BSs ability to destabilize the integrity and permeability of cell membranes and to modify surface properties of biomaterials, affecting microbial vitality and adhesion, limiting biofilm formation, or reducing the structural integrity of existing biofilms have been reported (Fracchia et al., 2015, 2019; Satpute et al., 2016).

Toward this goal, during the past few years, we have demonstrated the ability of lipopeptides, rhamnolipids, and sophorolipids BSs, alone or in combination with antimicrobials and quorum-sensing molecules to inhibit microbial adhesion and biofilm formation of mono-species biofilms of fungal or bacterial pathogens on biomedical materials such as silicone (Ceresa et al., 2016, 2017, 2018, 2019b, 2020). The activity of BSs against biofilm formation on model surfaces such as polystyrene, glass, silicone, and polydimethylsiloxane has also been described in other works (Sharma and Saharan, 2016; Aleksic et al., 2017; Janek et al., 2018; Satpute et al., 2018). Conversely, to our knowledge, no studies have been conducted yet concerning the use of BSs against these clinically relevant fungal-bacterial polymicrobial biofilms.

In this perspective, the present study aimed at testing the efficacy of three different BSs (lipopeptide AC7BS, rhamnolipid R89BS, and sophorolipid SL18) as anti-adhesive and anti-biofilm agents against the formation of clinically relevant multi-species biofilms composed by fungal and bacterial species (*C. albicans*–*Staphylococcus aureus*, *C. albicans*–*Staphylococcus epidermidis*) employing a multidisciplinary and multifaceted approach.

MATERIALS AND METHODS

Study Design

The study was organized in seven experimental phases: (1) definition of the dual-species biofilm model with quantification of biomass production and metabolic activity on polystyrene and silicone elastomer and comparison with the corresponding single species counterpart; (2) identification of the non-cytotoxic BSs concentrations with a significant inhibitory activity against single species biofilm formation; (3) evaluation of the anti-biofilm and antimicrobial activity of BSs at the non-cytotoxic concentrations against polymicrobial cultures, in co-incubation; (4) evaluation

of the anti-biofilm and antimicrobial activity of silicone discs coated with BSs against polymicrobial cultures; (5) assessment of cells surface hydrophobicity and membrane permeability changes induced by BSs in soluble form; (6) observation of the dual-species biofilm micro-structure on BSs-coated silicone discs; and (7) preliminary assessment of BSs-coated silicone discs biocompatibility.

Strains

The rhamnolipid-producer strain *Pseudomonas aeruginosa* 89, a clinical isolate from a patient with cystic fibrosis, was cultured from frozen stocks onto Tryptic Soy Agar (TSA, Scharlab, Barcelona, ES) at 37°C for 18–20 h. The lipopeptide-producer strain *Bacillus subtilis* AC7, from the inside of stems of *Robinia pseudoacacia*, was cultured from frozen stocks onto Luria Bertani agar (LBA, Sigma–Aldrich, St. Louis, MO, United States) at 28°C for 18–20 h. The sophorolipid-producer strain *Candida bombicola* ATCC 22214, obtained from the American Type Culture Collection (ATCC, Manassas, VA, United States), was cultured from frozen stocks onto Sabouraud dextrose agar (SDA, Scharlab, Barcelona, ES) at 25°C for 18–20 h. All the biofilm-producer strains used in this study were obtained from the ATCC (Manassas, VA, United States). *C. albicans* ATCC 10231, *S. aureus* ATCC 25923, *S. aureus* ATCC 6538, and *S. epidermidis* ATCC 35984 were cultured from frozen stocks onto SDA and TSA plates, respectively, and incubated overnight at 37°C.

Biosurfactants Production and Extraction

Lipopeptide AC7BS and rhamnolipid R89BS were produced and extracted as described by Ceresa et al. (2018, 2019b). Briefly, a loop of *B. subtilis* AC7 from a LBA overnight culture was grown in 20 ml of LB broth at 28°C for 4 h at 140 r/min. Afterward, 2 ml of this culture was used to inoculate 500 ml of LB broth and was incubated at 28°C for 24 h at 140 r/min. A loop of *P. aeruginosa* 89 from a TSA overnight culture was grown in 40 ml of Nutrient Broth II (Sifin Diagnostics GmbH, Berlin, DE) for 4 h at 37°C at 140 r/min. Afterward, 8 ml of this culture was added to 400 ml of Siegmund–Wagner medium and incubated at 37°C for 5 days at 120 r/min. Cell-free supernatants were acidified to pH 2.2 with 6 M HCl (AC7BS) or 6 M H₂SO₄ (R89BS) and stored overnight at 4°C. Lipopeptide AC7BS and rhamnolipid R89BS were extracted three times with 167 ml ethyl acetate:methanol (4:1) or 134 ml ethyl acetate (Sigma–Aldrich, St. Louis, MO, United States), respectively. Organic phases were anhydri-fied, filtrated, and vacuum-dried. BSs were recovered by dissolution in acetone (Sigma–Aldrich, St. Louis, MO, United States) and collected in glass tubes. Acetone was, then, evaporated and BSs were weighted.

Sophorolipid SL18 was obtained from a fed batch cultivation of *C. bombicola* ATCC 22214, according to Ceresa et al. (2020). Briefly, the cells (10% v/v) were grown in 2 l of Glucose Yeast Urea (GYU) medium [100 g/l glucose (Sigma–Aldrich, St. Louis, MO, United States), 10 g/l yeast extract (Sigma–Aldrich, St. Louis, MO, United States), and 1 g/l urea (Sigma–Aldrich, St. Louis, MO, United States)]. Oleic acid (99%, Sigma–Aldrich,

St. Louis, MO, United States) was supplemented as a feeding source at a concentration of 20% to generate lactonic congeners. Fermentation was performed for 8 days at 200 r/min and 30°C. Sophorolipid SL18 were, then, extracted twice with ethyl acetate (1:1 extract ratio) (Sigma–Aldrich, St. Louis, MO, United States) and partially purified by three washings with hexane (Sigma–Aldrich, St. Louis, MO, United States) to remove residual fatty acids.

At the end of the extraction process, the presence, the purity, and the composition of the three BSs were confirmed by ESI/MS analysis as previously described (Ceresa et al., 2016, 2019b, 2020). All the following biological tests and microscopy analyses were performed using the same batch of production for each BS. BSs were dissolved in Phosphate Buffer Solution pH 7.4 (PBS) at the different concentrations of use. The solutions were filtered through a 0.2 µm filter and stored at room temperature.

Silicone Cleaning and Sterilization

Silicone-elastomeric discs (SEDs—0.8 cm in diameter and 1.5 mm in thickness) were cut from medical-grade silicone sheets (TECNOEXTR s.r.l, Palazzolo sull'Oglio, IT) and prepared as described in Ceresa et al. (2015). Briefly, discs were cleaned with a 1.4% (v/v) RBS™ 50 solution (Sigma–Aldrich, St. Louis, MO, United States), sonicated for 5 min at 60 kHz, and rinsed twice in Milli-Q water. Silicone was, then, dipped in MeOH (99%, Sigma–Aldrich, St. Louis, MO, United States), sonicated, and rinsed as previously described. Afterward, SEDs were autoclaved, dried, and moved aseptically into 48-well plates.

Anti-biofilm Assays

Mono- and dual-species biofilm formation: fungal and bacterial cells were suspended in Roswell Park Memorial Institute (RPMI) 1640 (Sigma–Aldrich, St. Louis, MO, United States) buffered with MOPS (Sigma–Aldrich, St. Louis, MO, United States) and supplemented with 2% Glucose (Biolife, Monza, IT), pH 7.0 (RPMI +2%G). Cell density was adjusted up to 10⁶ and 10⁷ colony forming unit (CFU)/ml for *C. albicans* and *Staphylococcus* spp. respectively. Polystyrene was used as a substrate for the growth of biofilms in co-incubation assays and silicone was used for the growth of biofilms in the coating assays. Surfaces were inoculated with 0.5 ml of the suspension and incubated at 37°C in static conditions up to 72 h; growth medium was removed and replaced with fresh RPMI +2%G every 24 h. Blank polystyrene and silicone control surfaces (without biofilm) were also included in the experimental setting. The ability of microbial strains to form polymicrobial biofilms, compared to the mono-species ones, was evaluated by the determination of biofilm biomass and metabolic activity of sessile cells as described below. All experiments were carried out in quadruplicate and repeated two times.

Co-incubation conditions (BSs in soluble form in polystyrene plates): in order to determine the minimum non-cytotoxic concentration of BSs (Ceresa et al., 2018, 2019b) able to inhibit single-species biofilm formation on polystyrene by at least 80%, increasing concentrations of lipopeptide AC7BS (0.125–0.5 mg/ml) and rhamnolipid R89BS (0.0125–0.05 mg/ml) were tested. The wells were filled with 50 µl of 10× BSs

solutions (treated samples) or with an equal volume of PBS (control samples) and 0.5 ml of single-species suspensions of *C. albicans* (10^6 CFU/ml) and *Staphylococcus* spp. (10^7 CFU/ml) in RPMI +2%G. The 48-well plates were incubated for 24 h at 37°C. The effect was evaluated in terms of biofilm biomass reduction as described below. All experiments were carried out in quadruplicate and repeated twice.

Subsequently, the selected concentrations of BSs were tested against dual-species biofilm formation. The bottom of the wells was covered with 50 µl of the selected $10\times$ BSs solutions (treated samples) or with an equal volume of PBS (control samples). Then, 0.5 ml of the dual-species suspensions of *C. albicans* (10^6 CFU/ml) and *Staphylococcus* spp. (10^7 CFU/ml) in RPMI +2%G were added to each well. The plates were incubated up to 72 h at 37°C. Growth medium was removed and replaced with fresh RPMI +2%G supplemented with $10\times$ BSs solutions (treated samples) or with an equal volume of PBS (control samples) every 24 h. Blank surfaces (without biofilm) were also included in the experimental setting. The ability of microbial surfactants to inhibit dual-species biofilm formation in co-incubation conditions was evaluated by the determination of biofilm biomass and metabolic activity of sessile and planktonic cells as described below. Experiments were performed in quadruplicate and repeated twice.

Coating conditions: the treatment of silicone surfaces was carried out in 48-well plates by immersing SEDs in BS solutions (rhamnolipid R89BS: 2 mg/ml; lipopeptide AC7BS: 2 mg/ml; sophorolipid SL18: 8 mg/ml) at 37°C for 24 h at 180 r/min. These solutions were chosen as previously optimized in Ceresa et al. (2016; 2019b; 2020). Afterward, discs were moved into new plates and dried before use. Five hundred microliters of the dual-species suspensions (*C. albicans* at the concentration of 10^6 CFU/ml and *Staphylococcus* spp. at the concentration of 10^7 CFU/ml) in RPMI +2%G were added to each well. SEDs were incubated up to 72 h at 37°C. Every 24 h, discs were moved into fresh media. Blank surfaces (without biofilm) were also included. The anti-biofilm activity of BSs was evaluated at 24, 48, and 72 h by the determination of biofilm biomass, metabolic activity of sessile and planktonic cells, and viable cell counting as described below. Experiments were performed in quadruplicate and repeated twice.

Biofilm Biomass

The determination of the total biomass was carried out by crystal violet staining according to Ceresa et al. (2019b), with minor changes. Briefly, biofilms were washed twice and stained with 0.5 ml of the CV solution (0.1%) for 10 min. After the removal of the excess of dye, CV was dissolved with 0.5 ml of acetic acid (33% in water). Absorbance of the solutions was measured at 570 nm (A_{570}) (Victor3VTM, Perkin Elmer, Italy), data were normalized to blank surfaces (background), and percentages of inhibition were calculated using the following formula:

$$\left(1 - \frac{A_{\text{treat}}}{A_{\text{CTRL}}}\right) \times 100 \quad (1)$$

where

A_{treat} : absorbance of treated samples

A_{CTRL} : absorbance of controls.

Biofilm Metabolic Activity

The determination of biofilm metabolic activity was carried out by means of the colorimetric MTT assay according to Ceresa et al. (2019b), with minor changes. Briefly, biofilms were washed twice and, then, dipped in 0.5 ml of MTT working solution [0.075% MTT (Scharlab, Barcelona, ES) solution supplemented with 0.1% glucose (Biolife, Monza, IT) and 10 µM menadione (Sigma-Aldrich, St. Louis, MO, United States)]. After 30 min of incubation at 37°C in static conditions, MTT solution was removed and formazan crystals formed by metabolic active cells within biofilms were dissolved with 0.5 ml of the lysis solution [dimethyl sulfoxide (DMSO)/0.1 M glycine buffer (pH 10.2) solution (7:1)]. The A_{570} of the solutions was measured, data were normalized to background, and percentages of inhibition were calculated according to formula (1).

Planktonic Cells Metabolic Activity

The metabolic activity of planktonic cells in supernatants was evaluated by the MTT assay according to Ceresa et al. (2019b), with minor changes. Briefly, growth media and washing solutions, from each treated and untreated surface, were collected after 24, 48, and 72 h. Microbial cells were harvested by centrifugation at 17,000 r/min for 15 min and incubated in 0.5 ml of the MTT working solution for 30 min. Afterward, cells were collected by centrifugation at 17,000 r/min for 15 min, MTT solution was removed, and formazan crystals were dissolved with 0.5 ml of the lysis solution. The A_{570} of the solutions was measured and data were normalized to background.

Quantification of Viable Sessile Cells

The number of microbial cells forming the multi-species biofilms was determined by the spread plate method as described in Ceresa et al. (2015). Briefly, after two washings, biofilms were detached from silicone surfaces and broke up by four cycles of sonication (30 s) and stirring (30 s). The obtained suspensions were serially diluted in PBS and seeded both on Mannitol Salt Agar (MSA, Scharlab, Barcelona, ES) plates, selective for staphylococcal species, and on Sabouraud Chloramphenicol Agar (SCA, Scharlab, Barcelona, ES) plates, selective for fungal species. After 24 h at 37°C, the colonies were counted and the number of *C. albicans*, *S. aureus*, or *S. epidermidis* cells within the polymicrobial biofilm was quantified.

Anti-adhesive Assay

Silicone-elastomeric discs surface coating with the BSs was carried out as described by Papa et al. (2015), with minor changes. Briefly, a volume of 20 µl of BS solutions (rhamnolipid R89BS: 2 mg/ml; lipopeptide AC7BS: 2 mg/ml; sophorolipid SL18: 8 mg/ml) or 20 µl of PBS as control, were deposited on the silicone surfaces. SEDs were then placed under laminar flow to allow complete drying and, subsequently, moved into 48-well plates. The discs were filled with 0.5 ml of the dual-species suspensions (*C. albicans* at the concentration of 10^6 CFU/ml and *Staphylococcus* spp. at the concentration of 10^7 CFU/ml in RPMI +2%G) and incubated at 37°C for 4 h.

The quantification of cells attached on SEDs was carried out using crystal violet staining as reported in Section “Biofilm Biomass.” All experiments were carried out in quadruplicate and repeated twice.

Cell Surface Hydrophobicity and Membrane Permeability Changes by BSs in Soluble Form

Cell Surface Hydrophobicity

Bacterial and fungal suspensions were prepared in PBS to obtain an optical density (OD) at 600 nm, respectively, of 0.5 and 0.4 and treated with BSs (final concentration R89BS—0.05 mg/ml, AC7BS—0.5 mg/ml) at 37°C for 1 h at 150 r/min. Untreated suspensions were taken as control. Cell hydrophobicity was measured by microbial adherence to hexadecane (Scharlab, Barcelona, ES) according to Rosenberg et al. (1980). Microbial cells were collected by centrifugation at 4000 r/min for 15 min and resuspended in PUM Buffer, pH 7.1 (22.2 g K₂HPO₄·3H₂O, 7.26 g KH₂PO₄, 1.8 g urea, 0.2 g MgSO₄·7H₂O and distilled water to 1 l). One milliliter of hexadecane was mixed to 4 ml of cell suspensions in a glass tube at high speed for 2 min and equilibrated for 10 min. Afterward, the ODs of the initial cell suspensions and aqueous phases were measured at 550 nm (Genova Plus, Jenway, United Kingdom) and cell hydrophobicity was calculated using the following formula:

$$\left(1 - \frac{\text{OD}_{\text{aqueous phase}}}{\text{OD}_{\text{initial cell suspension}}}\right) \times 100 \quad (2)$$

Cell Membrane Permeability

Bacterial and fungal suspensions were prepared in PBS to obtain an OD at 600 nm, respectively, of 0.5 and 0.4 and treated with BSs (final concentration: R89BS—0.05 mg/ml, AC7BS—0.5 mg/ml) at 37°C for 1 h at 150 r/min. Untreated suspensions were taken as control. Cell membrane permeability was evaluated by checking crystal violet enhanced penetration. Cells were collected by centrifugation at 4000 r/min for 15 min and resuspended in PBS containing crystal violet (10 µg/ml) and incubated at 37°C at 150 r/min for 20 min. Afterward, cells were collected by centrifugation at 4000 r/min for 15 min and the absorbance (A) of the solutions was measured at 590 nm (Genova Plus, Jenway, United Kingdom). The percentage of crystal violet uptake was estimated using the following formula:

$$\left(\frac{A_{\text{sample}}}{A_{\text{initial crystal violet solution}}}\right) \times 100 \quad (3)$$

Experiments were performed in triplicate and repeated three times.

Biofilm Architecture

The micromorphology and architecture of multi-species biofilm on SEDs was visualized using the scanning electron microscope (SEM) Quanta 200F FEG (Fei, Eindhoven, Netherlands) in high-vacuum mode. Samples were prepared for SEM imaging according to Ceresa et al. (2019b), with minor changes. Briefly, after two washings, biofilms were fixed

in 2.5% glutaraldehyde, washed twice in distilled water, dehydrated in a graded ethanol series, and coated with a 10 nm layer of gold with a sputter coater (Emitech K500X, Quorum Technologies, Laughton, United Kingdom). A set of representative images at a magnification of 500×, 1000×, 2000×, and 4000× were obtained from untreated (controls) and pre-coated SEDs with rhamnolipid R89BS or sophorolipid SL18 and incubated with either *C. albicans*–*S. epidermidis* or *C. albicans*–*S. aureus* at 24, 48, and 72 h. Secondary electron signal was collected to investigate structural details of microbial cells and extracellular matrix on the biofilm. The primary beam energy was set to 5 keV to minimize damage to the organic structures. Possible artifacts due to the sample preparation process were considered according to indications provided by Hrubanova et al. (2018) and previous experience performed in imaging microbial biofilm formed *in vitro* on medical devices (Tessarolo et al., 2007; Signoretto et al., 2013).

Biocompatibility of BS-Coated Silicone Discs

The *in vitro* biocompatibility of BSs-coated discs was evaluated in 48-well plates by the MTT assay (Ceresa et al., 2019a). Spontaneously immortalized human skin keratinocyte—HaCaT cells (10⁴ cells/well) were seeded in Dulbecco's Modified Eagle's Medium (DMEM) high glucose (EuroClone, Milan, IT) supplemented with 4% FBS (EuroClone, Milan, IT), L-glutamine 200 nM (EuroClone, Italy) and 1% Pen/Strep (EuroClone, Milan, IT), and incubated at 37°C in 5% CO₂. After 24 h, growth medium was removed and replaced with the eluates obtained from BSs-coated SEDs after static release at 37°C for 24 h. Negative control consisted in cells treated with 0.5% Triton X, whereas positive control was represented by cells w/o any treatment. Fifty microliters of the MTT solution (5 mg/ml) was added into each well. Plates were then incubated for 24 and 72 h at 37°C. Formazan crystals were dissolved with 200 µl of 0.05 M HCl/isopropanol (50:1) and A570 was measured at the two time points. The percentage of cell viability was estimated using the following formula:

$$\left(\frac{A_{\text{sample}}}{A_{\text{CTRL+}}}\right) \times 100 \quad (4)$$

where

A_{sample} : absorbance of BSs or CTRL—samples

$A_{\text{CTRL+}}$: absorbance of positive controls.

Experiments were performed in triplicate and repeated twice.

Data Analysis and Statistics

All analyses and graphics were performed using the statistical program R, 3.6.2 (R Core Team, 2019). One-way ANOVA was applied to compare mono- and dual-species biofilms. Two-way ANOVA followed by Tukey *post hoc* test was used to investigate the anti-biofilm activity of BSs on dual-species biofilms and the metabolic activity of planktonic cells. To estimate log₁₀ CFU/disk from colony counts, the R package dupiR was used (Comoglio et al., 2013). Differences

in the percentage composition of dual-species biofilms were investigated by two-sample *t*-test for equality of proportions with continuity correction. Two-sample *t*-test was performed to evaluate the significance of data in hydrophobicity and membrane permeability assays. One-way ANOVA followed by Tukey *post hoc* test was performed to evaluate the significance of data in the biocompatibility assay in comparison to positive and negative controls. Differences were considered statistically significant at $p < 0.05$.

RESULTS

Biosurfactants Anti-biofilm and Anti-adhesive Activity

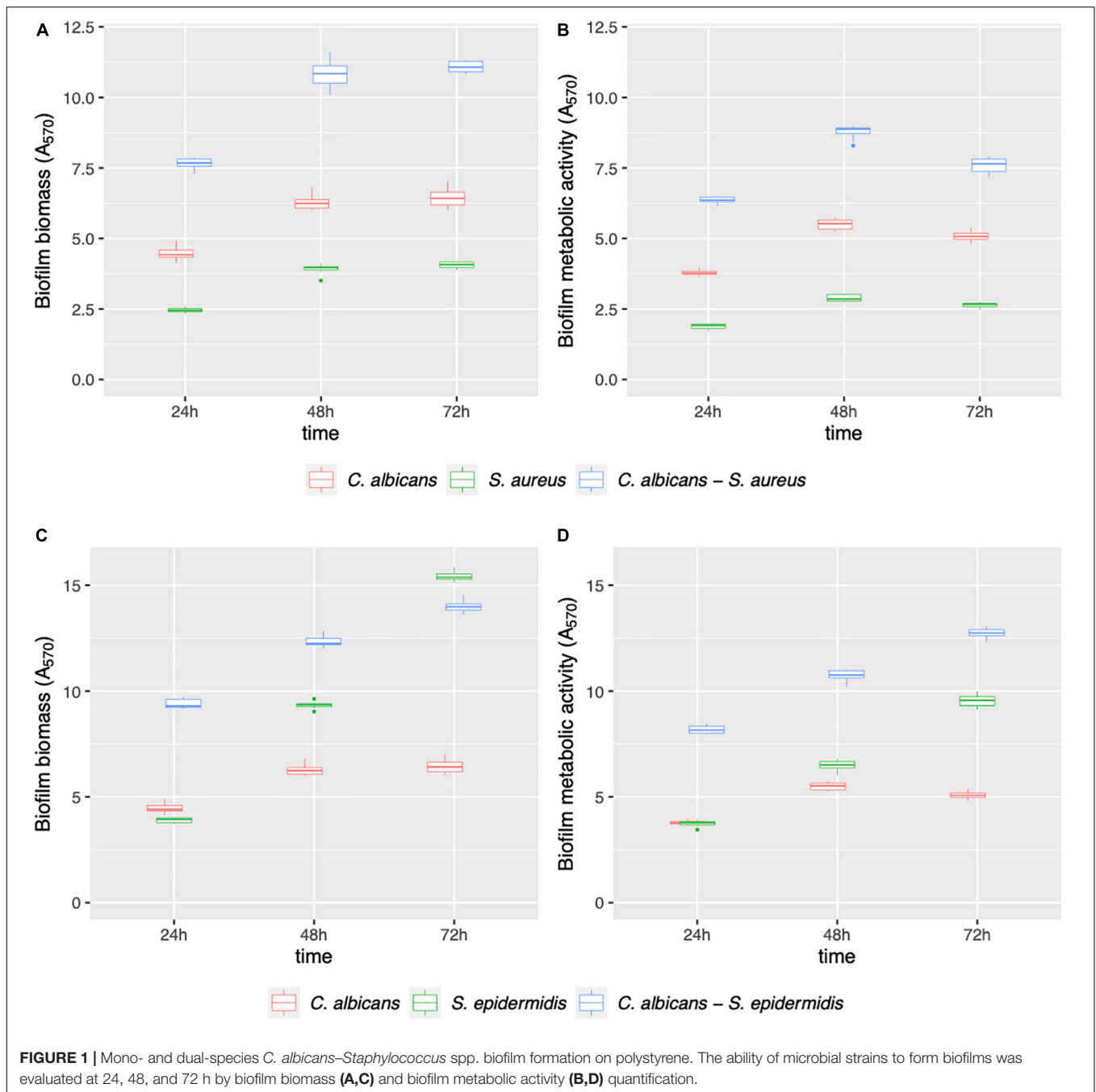
Mono- and dual-species biofilms of *C. albicans*–*Staphylococcus* spp. were grown on polystyrene (Figure 1) and on silicone surfaces (Figure 2) up to 72 h. Biofilm biomass and biofilm metabolic activity were quantified at 24, 48, and 72 h. *C. albicans*–*S. aureus* biomass and metabolic activity were higher than those of the two individual species both on polystyrene and on silicone at all incubation times ($p < 0.001$). Concerning *C. albicans*–*S. epidermidis*, biomass and metabolic activity were always higher than those observed for the individual species, on both surfaces, up to 48 h ($p < 0.001$). On the contrary, at 72 h, biomass and metabolic activity of dual-species biofilms were lower than those observed for *S. epidermidis* biofilms, with the exception of metabolic activity on polystyrene ($p < 0.001$).

AC7BS and R89BS were selected to perform the co-incubation assays as they were previously reported as not cytotoxic versus MRC5 cells monolayers at the concentrations active against biofilm (Ceresa et al., 2018, 2019b). On the contrary, SL-18 was not included in this assay since it was previously detected as cytotoxic when used in soluble form at concentrations active against *C. albicans* and *S. aureus* single species biofilms (Ceresa et al., 2020). Increasing concentrations of lipopeptide AC7BS (0.125–0.5 mg/ml) and rhamnolipid R89BS (0.0125–0.05 mg/ml) were tested and the minimum concentration of BSs that counteracted single-species biofilms formation on polystyrene by at least 80% (inhibition level threshold) was identified (Figure 3). In general, the formation of *C. albicans* and *S. aureus* biofilms was reduced in a concentration-dependent manner by the two BSs while the formation of *S. epidermidis* biofilm was effectively inhibited ($\geq 80\%$) only by rhamnolipid R89BS (Figure 3A). In particular, the three mono-species biofilms were inhibited by about 87% by rhamnolipid R89BS at a concentration of 0.05 mg/ml. Concerning lipopeptide AC7BS (Figure 3B), the threshold inhibition level was reached at a concentration of 0.5 mg/ml only for *C. albicans* and *S. aureus* biofilms (82%) but not for *S. epidermidis*, which had a maximum inhibition of only 27%. For this reason, this BS was excluded from the subsequent anti-biofilm assays against *C. albicans*–*S. epidermidis* dual-species biofilms.

The boxplot in Figure 4 shows the effect of rhamnolipid R89BS and lipopeptide AC7BS against *C. albicans*–*S. aureus* and

of R89BS against *C. albicans*–*S. epidermidis* biofilm formation up to 72 h. In general, as confirmed by two-way ANOVA and Tukey *post hoc* test, for each co-culture, biofilm formation on polystyrene was significantly dependent on BSs treatment ($p < 0.001$) and incubation time ($p < 0.001$). Regardless of the two strain combinations involved in the dual-species biofilm development, biofilm biomass (Figures 4A,D) and metabolic activity (Figures 4B,E) were equally inhibited by the BSs. The anti-biofilm activity of rhamnolipid R89BS was stable up to 72 h, while, for lipopeptide AC7BS, a slight reduction was detected between 24 and 72 h. In particular, as observed in Table 1, rhamnolipid R89BS proved to be the most effective BS for the inhibition of *C. albicans*–*S. aureus* biofilm growth and an excellent agent for the prevention of *C. albicans*–*S. epidermidis* biofilm formation, with mean percentages of reduction of 94% (*C. albicans*–*S. aureus*) and 95% (*C. albicans*–*S. epidermidis*), after 72 h co-incubation. In addition, to define whether part of the observed effect was the result of an antimicrobial activity of the BSs, the metabolic activity of planktonic cells in the supernatants was assessed (Figures 4C,F). The absorbance values of the cell supernatants co-incubated with BSs were significantly higher in comparison to the controls ($p < 0.001$) suggesting that, in the treated wells, cells existed in a planktonic state rather than by forming a biofilm. However, in the case of *C. albicans*–*S. aureus* co-cultures, the lower absorbance values observed in the rhamnolipid R89BS-treated wells compared to those of the lipopeptide AC7BS-treated wells ($p < 0.001$), suggested an antimicrobial activity of the rhamnolipid (Figure 4C).

The results of BSs pre-coating on SEDs further confirmed the inhibitory activity of these natural microbial molecules against the formation of *C. albicans*–*S. aureus* (rhamnolipid R89BS, lipopeptide AC7BS, sophorolipid SL18) and *C. albicans*–*S. epidermidis* (rhamnolipid R89BS, sophorolipid SL18) mixed biofilms (Figure 5). As previously observed in co-incubation conditions, for each co-culture, the development of biofilms on silicone surfaces was significantly dependent on BSs treatment ($p < 0.001$) and incubation time ($p < 0.001$). Biofilm biomass (Figures 5A,D) and metabolic activity (Figures 5B,E) were equally inhibited on all BSs-coated discs (SEDs). Concerning the dual-species biofilms of *C. albicans*–*S. aureus*, the anti-biofilm activity of rhamnolipid R89BS- and sophorolipid SL18-coated SEDs was stable up to 72 h, while a slight reduction of the efficacy of lipopeptide AC7BS-coated SEDs was observed during this time. The anti-biofilm activity of rhamnolipid R89BS coating was stable also for *C. albicans*–*S. epidermidis* mixed biofilms, while that of sophorolipid SL18-coated SEDs slightly decreased over time. In general, starting from 48 h of incubation, the surface treatment of silicone with rhamnolipid R89BS proved to be the most effective in counteracting the growth of both polymicrobial biofilms. In particular, after 72 h, average inhibitions of 93 and 90% against *C. albicans*–*S. aureus* and *C. albicans*–*S. epidermidis* biofilms were found, respectively. Table 2 shows the percentages of biomass and metabolic activity inhibition at the different time-points. To exclude that the observed activity was due to an antimicrobial action of the BSs, the metabolic activity of the planktonic cells in the wells was evaluated (Figures 5C,F). As observed in co-incubation conditions, the absorbance values



of the supernatants of the BSs-coated silicone discs were significantly higher than those obtained for the corresponding controls ($p < 0.001$). Conversely, no significant variations were found between the absorbance values of planktonic cells recorded for the different BSs treatments ($p > 0.05$).

In addition, to evaluate whether the tested BSs exhibited their anti-biofilm action in equal proportions on the single species forming the polymicrobial biofilms on the silicone surfaces, the number of cells of *C. albicans*, *S. aureus*, and *S. epidermidis* was determined on selective media for both control and coated discs (Supplementary Tables 1, 2) and the percentage compositions

were calculated (Tables 3, 4). In general, at all incubation times, biofilms on the control discs mainly consisted of bacterial cells (98.6–99.8%) and only for a small percentage of the yeast cells (0.2–1.4%). In particular, the yeast cells were present in a major proportion in *C. albicans*–*S. aureus* biofilms (Table 3) than in *C. albicans*–*S. epidermidis* (Table 4). Interestingly, at 24 h, the presence of BSs on the silicone surface was associated with a significant increase in the yeast species percentage compared to that observed on the controls ($p < 0.001$). However, this value decreased over time and returned to levels similar to those observed for the controls.

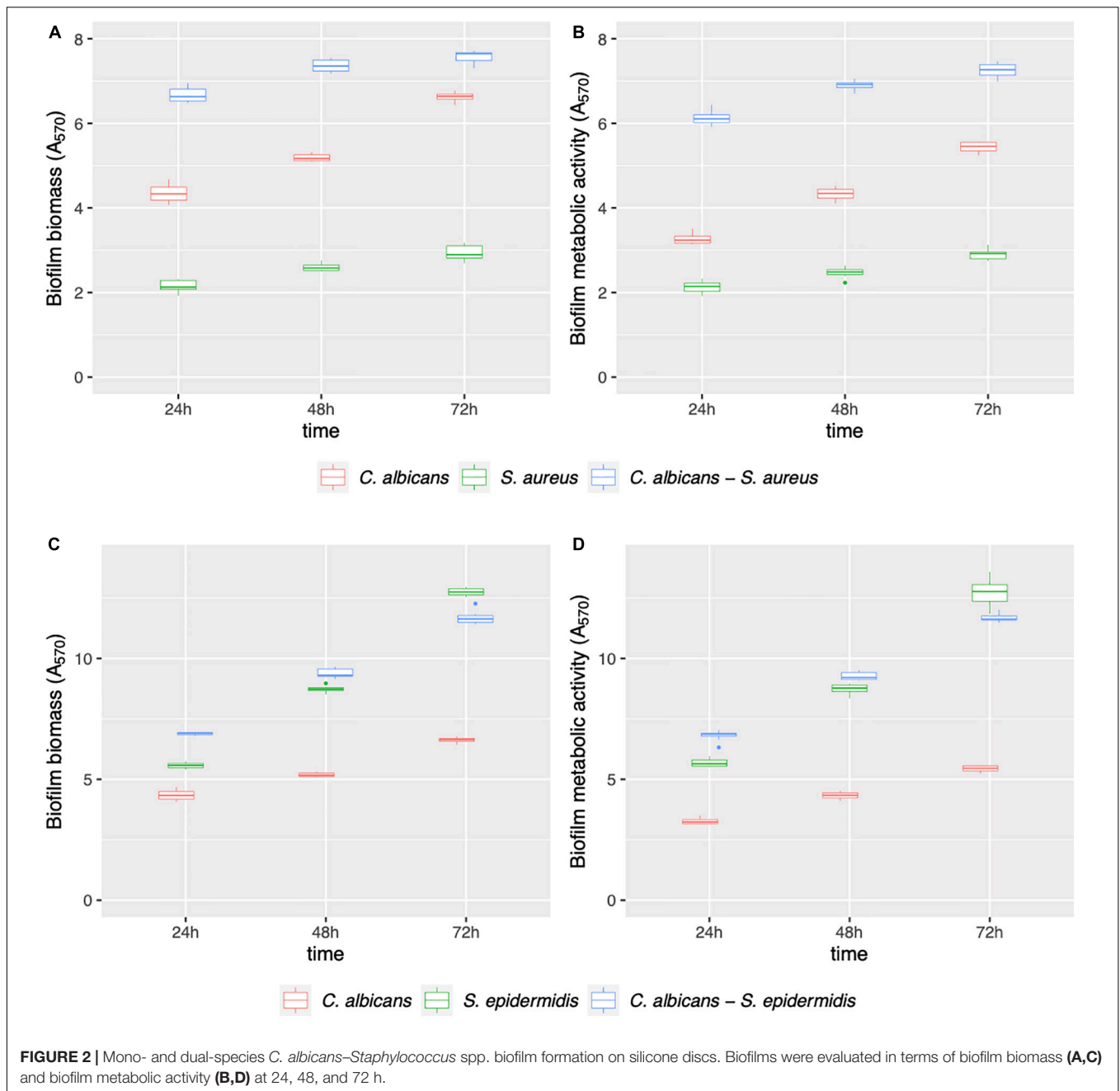


FIGURE 2 | Mono- and dual-species *C. albicans*–*Staphylococcus* spp. biofilm formation on silicone discs. Biofilms were evaluated in terms of biofilm biomass (A,C) and biofilm metabolic activity (B,D) at 24, 48, and 72 h.

Finally, to assess the activity of BSs coating on SEDs on the early phases of biofilm formation (adhesion phase), the amount of *C. albicans*–*S. aureus* and *C. albicans*–*S. epidermidis* adherent cells was evaluated after 4 h incubation by means of the CV method (Figure 6). Similarly, to biofilm formation, microbial cells adhesion to silicone surfaces was also significantly dependent on BSs treatment ($p < 0.001$). Concerning *C. albicans*–*S. aureus*, the highest anti-adhesive activity was observed for rhamnolipid R89BS (71%), followed by sophorolipid SL18 (64%) and lipopeptide AC7BS (51%). As to *C. albicans*–*S. epidermidis*, rhamnolipid R89BS coating proved to be the most effective with an inhibition of

adhesion of 62% while for sophorolipid SL18 showed a 54% inhibition.

Cell Surface Hydrophobicity and Membrane Permeability Changes by BSs in Soluble Form

In order to evaluate the possible effect of BSs on the tested opportunistic pathogens in co-incubation conditions, cell surface hydrophobicity (CSH) and membrane permeability were assessed. As shown in Figure 7A, after 1 h incubation with R89BS and AC7BS, CSH and membrane permeability of *C. albicans*,

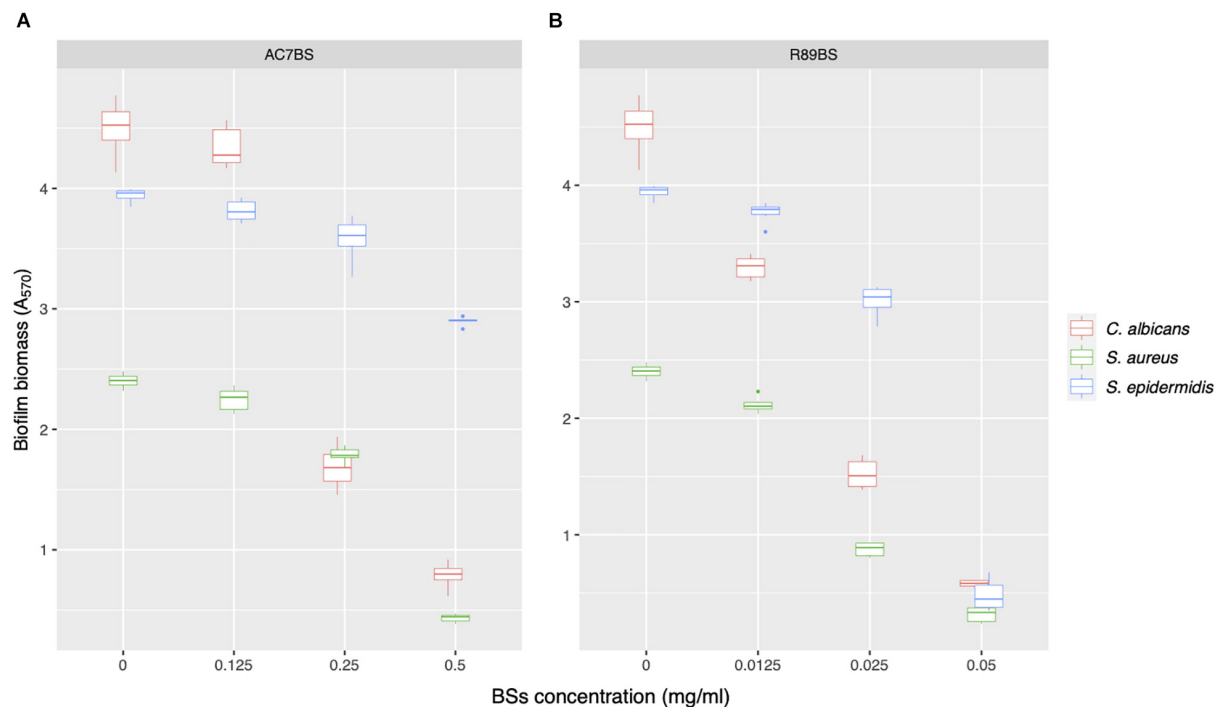


FIGURE 3 | Activity of BSs in soluble form on *C. albicans*, *S. aureus*, and *S. epidermidis* biofilm formation. The anti-biofilm activity of AC7BS (A) and R89BS (B) was evaluated in co-incubation conditions by the determination of biofilm biomass.

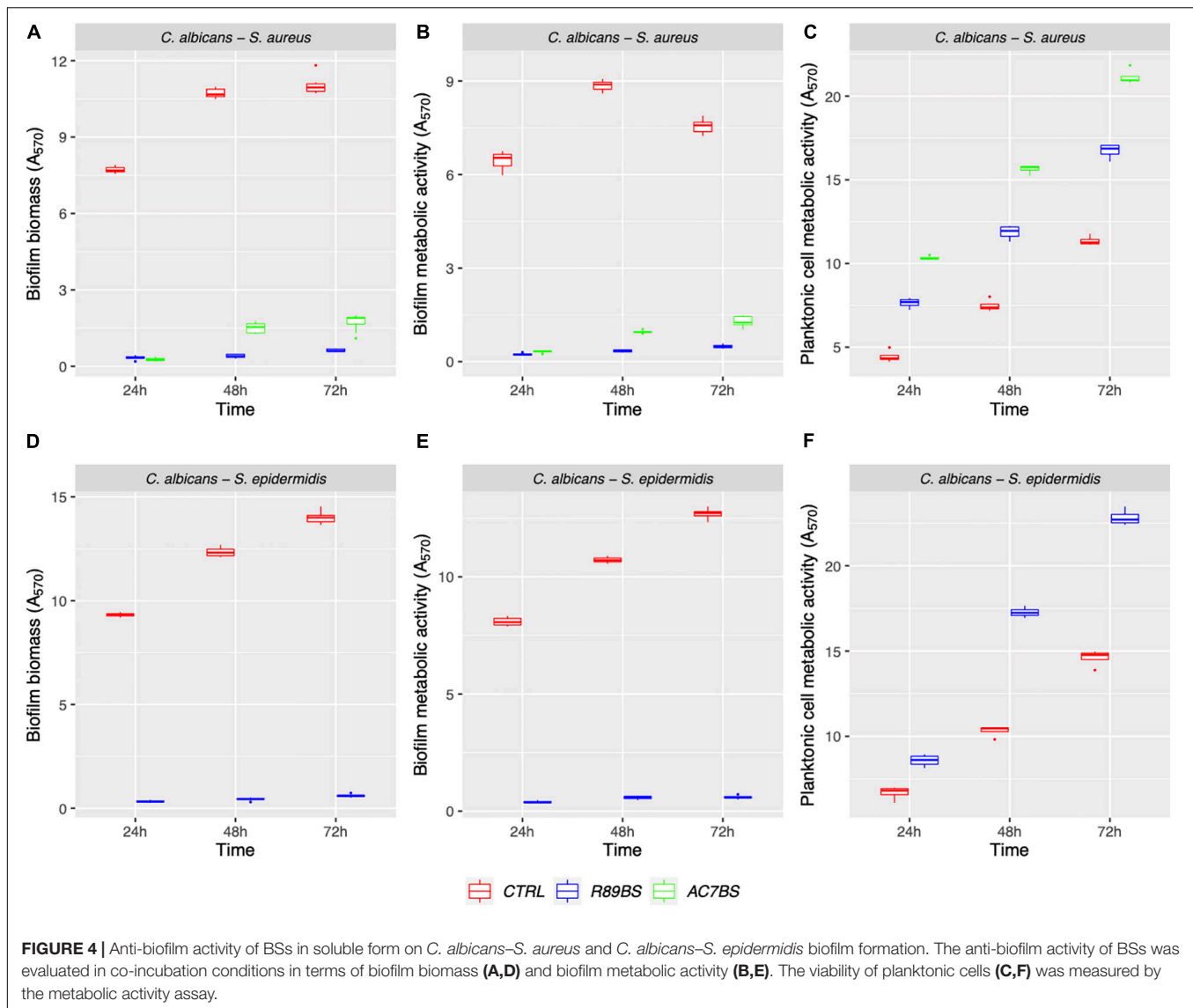
S. aureus, and *S. epidermidis* were different from the untreated controls. BSs treatment induced a significant modification of CSH for all the tested strains ($p < 0.05$). In particular, it resulted in a decrease of CSH both for bacterial and fungal cells. Bacterial CSH decreased from 99% (mean percentage for untreated control samples) to values ranging from 38 to 71% for BSs treated samples. Fungal CSH in comparison was reduced from 44% (mean percentage for control samples) to values ranging from 31 to 37% for BSs treated samples. The changes of CSH induced by BSs were related to the microbial strain: in particular, *S. aureus* was the most susceptible to cell hydrophobicity changes, followed by *S. epidermidis* and *C. albicans*. The treatment with BSs also altered cell membrane permeability for all the tested strains ($p < 0.05$) (Figure 7B). In particular, BSs induced an increase in crystal violet uptake by bacterial cells from 46% (mean percentage for untreated control samples) to values ranging from 54 to 74% and a slight increase in the case of fungal cells from 53% (mean percentage for untreated control samples) to values ranging from 56 to 59%. Again, the changes of membrane permeability induced by BSs were related to the microbial strain: in particular, *S. aureus* and *S. epidermidis* were more susceptible to BSs than *C. albicans*.

Scanning Electron Microscopy of Multi-species Biofilms on SEDs

Scanning electron microscopic images presenting the features of the biofilm formed on untreated (controls) and pre-coated SEDs with rhamnolipid R89BS and sophorolipid SL18 at the longest incubation time are presented in Figure 8. The SEM investigation

showed the presence of both fungal hyphae and coccoid bacteria adhering to the surface of all samples. In general, there was a more pronounced spatial correlation between *S. aureus* and *C. albicans* (Figures 8A,C,E) than between *S. epidermidis* and *C. albicans* (Figures 8B,D,F), irrespective of the surface treatment. More specifically, *S. aureus* was prevalently found in close contact with fungal hyphae, almost completely covering the *Candida* mycelium at 72 h in control SEDs (Figure 8A), while *S. epidermidis* never realized a full coating of the *C. albicans* structures (Figure 8B) and was more prone to adhere directly to the SEDs surface (Figure 8D).

In agreement with the results obtained from quantitative tests of biofilm biomass performed on corresponding samples, untreated controls showed a well-structured dual-species biofilm at each time-points, having a more three-dimensional arrangement and a thicker appearance at longer incubation times (Figures 8A,B). A similar increasing trend in the number of cells at the surface was also observed for rhamnolipid R89BS and sophorolipid SL18 pre-coated SEDs. However, the number of microbial cells at the treated surface was drastically reduced in respect of controls and the large majority of the sample surface was free of cells or presented small clusters with few three-dimensional microbial aggregates at 24 and 48 h (Supplementary Figures S1, S2). This was also the case for *S. aureus* and *C. albicans* dual-species biofilm at 72 h (Figures 8C,E), but not for *S. epidermidis* and *C. albicans* dual-species biofilm where only a minor portion of the treated surface was free of cells (Figure 8D) or mainly fully covered (Figure 8F). At 72 h, some differences in *C. albicans*–*S. epidermidis* biofilms were



also noted between rhamnolipid R89BS and sophorolipid SL18 pre-coated discs, with the latter presenting areas showing a mature biofilm (Figure 8F), although less structured and thick than the controls (Figure 8B). Rhamnolipid R89BS pre-coated SEDs showed only minor portions of the disc surface still free of microorganisms (Figure 8D).

Cytotoxicity of BSs-Coated Silicone Discs

No cytotoxic effect was detected on spontaneously immortalized human skin keratinocyte when exposed for 24 h to the BSs-coated SEDs eluates obtained from static release conditions. In fact, at this time-point, the viability of HaCat cells was comparable to positive controls ($p > 0.05$), independently to the type of BS involved in the coating procedure (Supplementary Figure S3A). After 72 h of cells exposure to the eluates, cell viability slightly decreased to values ranging from 92% for SL18 to 78% for

R89BS (Supplementary Figure S3B) but was always above the limit (70%) according to the ISO 10993-5 standard (Xian, 2009; Rodríguez-López et al., 2020).

DISCUSSION

Microbial colonization and biofilm formation on medical devices represent one of the major challenges in infection control (Percival et al., 2015; Wang et al., 2017; Khatoon et al., 2018). Biofilms protect microbial cells from antimicrobials and the immune system of hosts and, in most cases, this may lead to the dysfunction of the devices and eventual removal (Percival et al., 2015; Khatoon et al., 2018; Sharma et al., 2019).

Nowadays, *C. albicans* is considered as the prevailing fungal pathogen responsible for severe hospital-acquired infections and has also been reported to form polymicrobial biofilms in coexistence with bacterial species such as *S. aureus*, *S. epidermidis*,

TABLE 1 | Inhibition percentages of dual-species *C. albicans*–*S. aureus* and *C. albicans*–*S. epidermidis* biofilm formation on polystyrene in co-incubation assays. The anti-biofilm activity of BSs in soluble form was detected by CV (biofilm biomass) and MTT assays (biofilm metabolic activity).

Strains	Assessment	Time (h)	Treatment	
			AC7BS (%)	R89BS (%)
C–Sa	Biofilm biomass	24	96.4	95.6
		48	85.8	96.2
		72	84.3	94.3
	Biofilm metabolic activity	24	95.0	96.4
		48	89.2	96.1
		72	83.0	93.5
C–Se	Biofilm biomass	24	–	96.5
		48	–	96.5
		72	–	95.7
	Biofilm metabolic activity	24	–	95.1
		48	–	94.6
		72	–	95.3

C–Sa, *C. albicans*–*S. aureus*;

C–Se, *C. albicans*–*S. epidermidis*;

–, not evaluated.

P. aeruginosa, and *Streptococcus* spp. (Liu et al., 2019). These microbial pathogens are well known for their ability to form persistent biofilms on biotic and abiotic surfaces such as tissues, organs, and medical-devices, including dentures, voice prostheses, implants, endotracheal tubes, feeding tubes, and most frequently, catheters (Carolus et al., 2019; Liu et al., 2019).

The existence of these multi-species communities makes the challenge against biofilms even more complex because it does not only require effective antimicrobials against all pathogenic microorganisms present in the microbial community, but limits the effectiveness of to date-developed species-specific biofilm targeting strategies (Koo et al., 2017). Based on these considerations, numerous researchers have aimed their studies at identifying new and effective approaches to counteract polymicrobial biofilms, both in terms of inhibition of microbial adhesion and disruption of mature biofilms (Villa and Cappitelli, 2013). Among these, the use of new antimicrobial peptides has been suggested as a promising treatment against fungal/bacterial polymicrobial biofilms (Qu et al., 2016; de Alteriis et al., 2018; Gupta et al., 2019). Through a different mechanism of action, these molecules can cause microbial death, inhibit bacterial growth, and compromise biofilm formation and architecture. Weiland-Bräuer et al. (2019) identified, in the metagenome-derived bacterial quorum quenching (QQ), proteins QQ-5 and QQ-7 as an effective strategy to prevent *C. albicans* and *S. epidermidis* biofilm formation, by inhibiting *C. albicans* yeast-to-hyphae transition and inducing the expression of the *icaR* gene, thus repressing the synthesis of polysaccharide intercellular adhesion (PIA).

A further strategy currently proposed to treat *C. albicans*–*S. aureus* infections is based on combined therapies of existing antimicrobials or treatments with natural molecules, such as plant extracts or essential oils, alone or in combination with

antibiotics or antifungals (Budzynska et al., 2017; Scaffaro et al., 2018; Tan et al., 2019).

In this scenario, BSs effectively appear to be promising new candidates for biofilm inhibition in the biomedical field due to their interesting antimicrobial, anti-adhesive properties (Banat et al., 2010; Rodrigues and Teixeira, 2010; Fracchia et al., 2019; Naughton et al., 2019). These molecules, in fact, are able to counteract effectively biofilms by decreasing microbial cells viability and by reducing microbial adhesion (Satpute et al., 2016; Fracchia et al., 2019; Paraszkiewicz et al., 2019; Naughton et al., 2019). When BSs bind to cell wall surface, they may form a film that changes the wettability and the surface energy of the cell leading to severe changes in its hydrophobicity and increasing its permeability by the release of LPS and the formation of transmembrane pores. When applied as coating agents, BSs interfere with microbial adhesion and limit biofilm formation altering the chemical and physical properties of the surfaces (e.g., reduction of roughness and hydrophobicity or increase of wettability) on which biofilms develop (Rodrigues et al., 2006; Quinn et al., 2013; Satpute et al., 2019).

In this study, we demonstrated the ability of different BSs to inhibit the formation of fungal and bacterial dual-species biofilms for up to three days in both co-incubation and pre-coating assays. One lipopeptide (AC7BS) and two glycolipids (R89BS and SL18) were tested. As observed by the positive ESI–MS analysis, AC7BS is composed of surfactin (98%) and fengycin (2%) homologs (Ceresa et al., 2016). Surfactin family members are represented by C13, C14, and C15 homologs whereas fengycin family members are represented by two main fengycin isoforms corresponding to C17 fengycin A and C17 fengycin B. The negative electrospray ionization (ESI) MS analysis of R89BS extract showed the presence of mono- (75%) and di- (25%) rhamnolipid homologs. Mono-rhamnolipid family members are represented by C10–C10, C8–C10, and C10–C12 homologs whereas di-rhamnolipid family members by C10–C8, C10–C10, and C10–C12 homologs (Ceresa et al., 2019b). Sophorolipid SL18 is a mixture of lactonic congeners (Ceresa et al., 2020). The fungal strain *C. albicans* and the bacterial strains *S. aureus* and *S. epidermidis* were selected as they represent a major cause of medical device associated infections due to their ability to adhere to biomaterials and form antimicrobial-resistant multispecies biofilms (Arciola et al., 2005; von Eiff et al., 2006; Sardi et al., 2013; Carolus et al., 2019).

The experiments reported in this study were carried out using culture media and growth conditions that support the reproducible development of well-structured dual-species biofilms, as demonstrated by the high values of biofilm biomass and cell metabolic activity detected for the controls and by SEM images of control biofilms. BSs were tested in solution or coated on silicone surfaces by physical absorption. Dual-species cultures were evaluated by the quantification of different parameters: biomass, metabolic activity, and number of viable cells. The microstructure of dual-species biofilms on treated and untreated silicone was also characterized by SEM analysis.

The lipopeptide AC7BS and the rhamnolipid R89B, tested in soluble form in co-incubation conditions, showed a significant inhibitory activity against the formation of dual-species biofilms of *C. albicans* and *Staphylococcus* spp. determining high levels

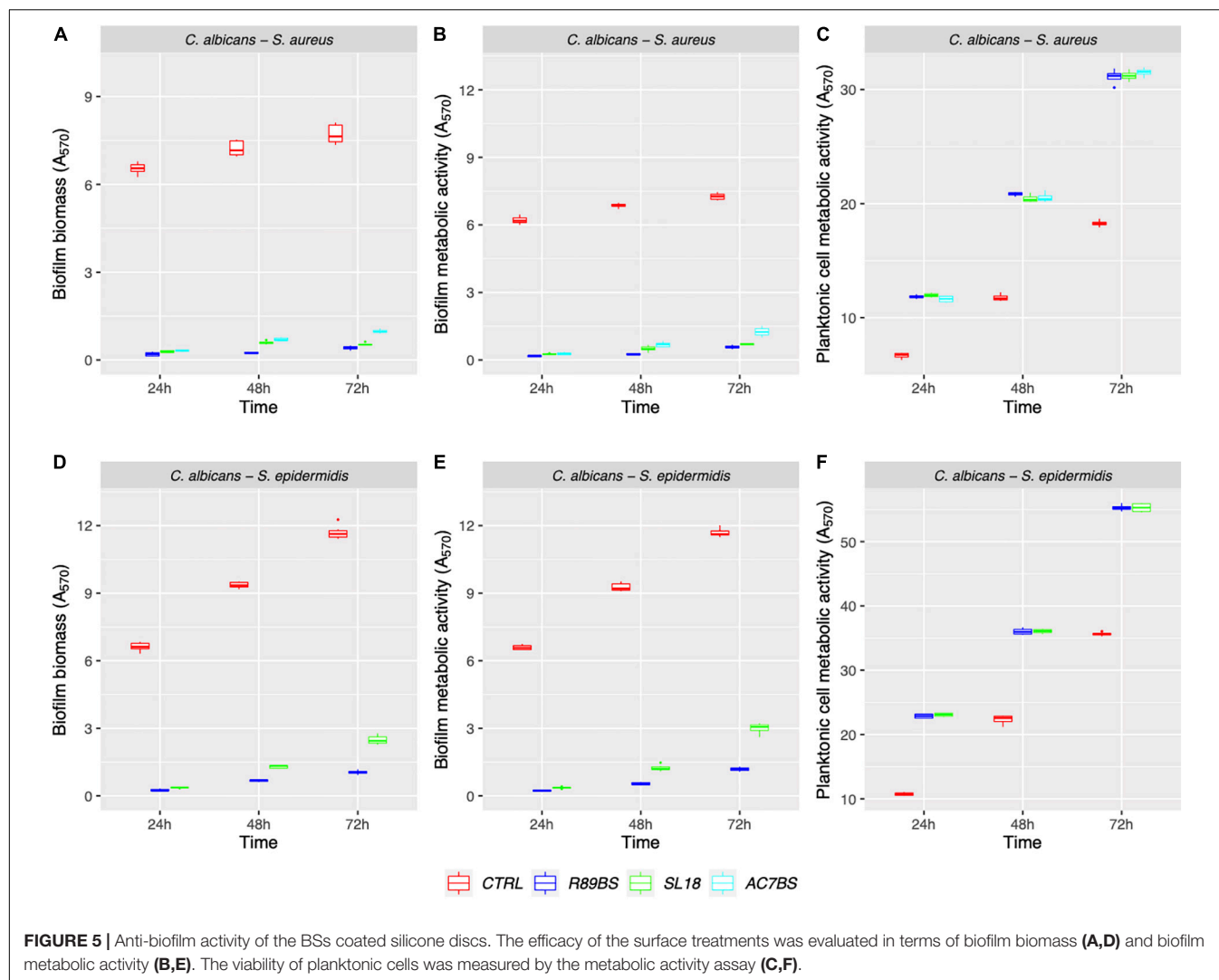


FIGURE 5 | Anti-biofilm activity of the BSs coated silicone discs. The efficacy of the surface treatments was evaluated in terms of biofilm biomass (A,D) and biofilm metabolic activity (B,E). The viability of planktonic cells was measured by the metabolic activity assay (C,F).

of reduction, both in terms of total biomass and metabolic activity with inhibitions ranging from 84 to 96% at 72 h. These findings suggest a potential applicability of these BSs as components of pharmaceutical formulations, such as injectable scaffolds or hydrogels enriched with antimicrobial or anti-biofilm agents useful in wound healing. Similar conclusions were also reached by for better wound healing when microbial glycolipid BS-containing ointment was used as a transdermal substitute treatment process (Gupta et al., 2017).

Coating of silicone surfaces with lipopeptide AC7BS, rhamnolipid R89BS, and sophorolipid SL18 was as much beneficial, further confirming the inhibitory activity of these natural molecules against the formation of both dual-species biofilms, with percentages of inhibition at 72 h ranging from 77 to 93%. R89BS in particular was found to be the most effective BS in inhibiting both dual-species biofilms on both surfaces.

Both rhamnolipids and sophorolipids have also shown to be active against other multi-species cultures (Diaz De Rienzo et al., 2016). They observed using the BioFlux flow through conditions, that a combination of caprylic acid (0.01% v/v) and rhamnolipids

(0.04% v/v) caused the disruption of single and mixed biofilms for *P. aeruginosa* and *S. aureus*. Biofilms were also efficiently dislodged by the combination of rhamnolipids (0.04% v/v) with sophorolipids (0.01% v/v). Interestingly, these authors observed that biofilm disruption of *S. aureus* and mixed cultures was caused by the anti-biofilm properties of BSs without affecting cell viability whereas for the *P. aeruginosa* biofilms, a high rate of killed cells was observed.

According to the studies conducted so far, in co-incubation conditions, the anti-biofilm activity of the tested BSs seemed to be related to a reduction of CSH and thus to a change in cells ability to adhere to the silicone surface (Elshikh et al., 2016). For rhamnolipid R89BS, the effect was also partly associated to its antibacterial activity on staphylococcal cells, as demonstrated in a previous work (Ceresa et al., 2019b) and confirmed in this study by the observed decrease of the planktonic cells metabolic activity and the increase in membrane permeability. On the contrary, an antifungal effect on *C. albicans* was not observed at the tested concentrations, indicating that the antimicrobial activity of the rhamnolipid is also microorganism dependent as

TABLE 2 | Inhibition percentages of dual-species *C. albicans*–*S. aureus* and *C. albicans*–*S. epidermidis* biofilm formation on BSs treated silicone discs by CV (biofilm biomass) and MTT assays (biofilm metabolic activity).

Strains	Assessment	Time (h)	Treatment		
			AC7BS (%)	R89BS (%)	SL18 (%)
C–Sa	Biofilm biomass	24	95.1	96.9	95.6
		48	90.2	96.7	91.8
		72	87.3	94.6	93.1
	Biofilm metabolic activity	24	95.6	97.2	95.8
		48	90.0	96.3	92.6
		72	82.8	92.0	90.3
C–Se	Biofilm biomass	24	–	96.1	94.4
		48	–	97.7	86.1
		72	–	91.0	78.8
	Biofilm metabolic activity	24	–	96.5	94.5
		48	–	94.1	86.7
		72	–	89.8	74.4

C–Sa, *C. albicans*–*S. aureus*;C–Se, *C. albicans*–*S. epidermidis*;

–, not evaluated.

observed by Diaz De Rienzo et al. (2016). Lipopeptide AC7BS was in general less effective in counteracting *S. epidermidis* biofilm formation as suggested by the fact that the inhibition level threshold of 80% was not reached when tested in co-incubation conditions against single species biofilm. In addition, CSH assays indicated that *S. epidermidis* was less susceptible to cell hydrophobicity changes induced by AC7BS compared to *S. aureus*. Moreover, *S. epidermidis* cell permeability was less affected in the presence of AC7BS in comparison to rhamnolipid R89BS. It may be hypothesized that the ability of this strain to produce a high amount of slime (Arciola et al., 2001; Williams and Bloebaum, 2010) might have interfered with the activity of AC7BS in the co-incubation conditions. Furthermore, AC7BS did not show any antimicrobial activity against *S. epidermidis* [Ceresa et al. Biosurfactant-based coatings inhibit fungal and bacterial biofilm on medical-grade silicone. TERMIS 2017. Davos, Switzerland, eCM Meeting Abstracts 2017, Collection 2; TERMIS EU (P821)] whereas, as far as R89BS is concerned, a MIC₉₉ was detected at 120 µg/mL (Ceresa et al., 2019a) indicating a higher efficacy of the rhamnolipid against this strain compared to the lipopeptide.

TABLE 3 | Percentage (%) composition of *C. albicans*–*S. aureus* dual-species biofilms on the surface of silicone discs.

Time (h)	Strains	Treatment			
		CTRL (%)	AC7BS (%)	R89BS (%)	SL18 (%)
24	<i>C. albicans</i>	1.4	4.5	4.9	4.0
	<i>S. aureus</i>	98.6	95.5	95.1	96.0
48	<i>C. albicans</i>	1.4	1.6	1.7	0.9
	<i>S. aureus</i>	98.6	98.4	98.3	99.1
72	<i>C. albicans</i>	1.3	1.4	0.3	0.5
	<i>S. aureus</i>	98.7	98.6	99.7	99.5

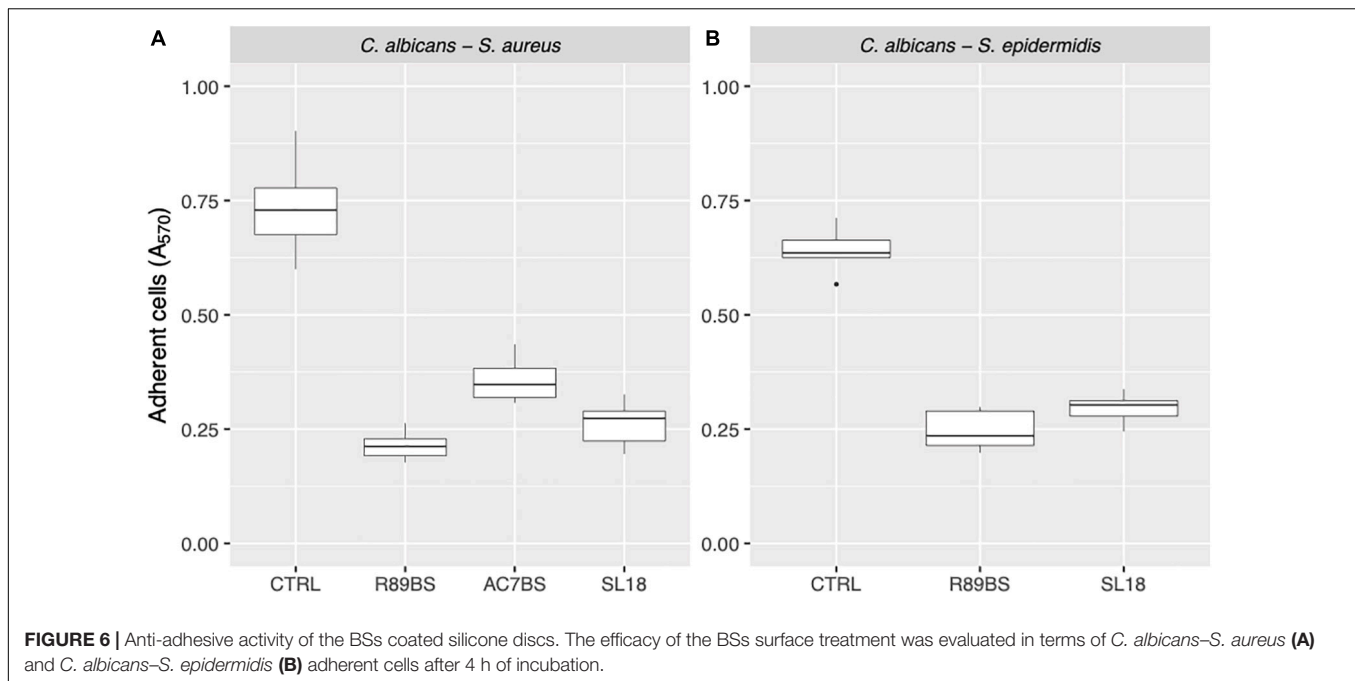
TABLE 4 | Percentage (%) composition of *C. albicans*–*S. epidermidis* dual-species biofilms on the surface of silicone discs.

Time (h)	Strains	Treatment		
		CTRL (%)	R89BS (%)	SL18 (%)
24	<i>C. albicans</i>	0.2	1.0	0.6
	<i>S. epidermidis</i>	99.8	99.0	99.4
48	<i>C. albicans</i>	0.2	0.2	0.1
	<i>S. epidermidis</i>	99.8	99.8	99.9
72	<i>C. albicans</i>	0.2	0.2	0.2
	<i>S. epidermidis</i>	99.8	99.8	99.8

When applied on silicone surfaces as coating agents, BSs effects were mostly related to their anti-adhesive properties. Surface physicochemical characterization of BSs-coated discs showed an increased level of wettability, i.e., a reduction of hydrophobicity (static contact angle for AC7BS-coated SEDs: $94.4^\circ \pm 10.0^\circ$; dynamic contact angle for R89BS-coated SEDs: $84.4^\circ \pm 2.2^\circ$ (advancing) and $72.2^\circ \pm 2.5^\circ$ (receding)), in comparison to control discs ($112^\circ \pm 5^\circ$) (Ceresa et al., 2016, 2019b). In addition, concerning R89BS, the anti-biofilm effect in the pre-coating conditions was not due to an antimicrobial activity, as indicated by the fact that planktonic cells metabolic activity was similar to that observed in the presence of the other BSs, thus suggesting that the amount of R89 deposited on the silicone surface was largely below the biocidal concentration for staphylococci.

The impact of the BSs pre-coating in the formation of dual-species biofilm on the surface of medical grade silicon was also observed by SEM inspection. R89BS and SL18 almost completely prevented the attachment of the dual-species biofilms up to 48 h, and a clear reduction in the amount of biofilm with respect to controls was still evident at 72 h of incubation.

Differences in the cell arrangements and, more specifically, in the relative spatial distribution of cocci and yeasts were noted between *C. albicans*–*S. aureus* and *C. albicans*–*S. epidermidis*, whereas no influence on the inter-species spatial association was observed by comparing BS-coated and untreated silicone surfaces. A stronger association between the fungal and bacterial cells was observed in the *C. albicans*–*S. aureus* biofilm. As previously reported by Harriott and Noverr (2009), *S. aureus* mainly formed microcolonies on the surface of the biofilm, with *C. albicans* serving as the underlying scaffolding. Compared to *S. epidermidis*, *S. aureus* was not as effective in forming biofilms on abiotic surfaces, requiring pre-coating and supplementation of nutrients (Cassat et al., 2007). *C. albicans* was shown to play an essential role in producing extracellular matrix that facilitates *S. aureus* adhesion and sessile microcolonies formation (Harriott and Noverr, 2009). The *C. albicans*–*S. epidermidis* biofilm was characterized by a more open hyphal network and the association of *S. epidermidis* cells with the fungal structures was less marked. *S. epidermidis* cells were found beneath and above the yeast cells and hyphal layers and the Staphylococci cells were clearly adherent to both morphological forms of the fungus as previously reported by



other authors (Adam et al., 2002). Anyway, the adhesion and microcolonies formations of *S. epidermidis* on the surface of the silicone samples were frequently noted also in absence of fungal cells, possibly due to their higher ability to produce extracellular matrix.

Apparent discrepancies between results from the biofilm biomass evaluation (Table 2) and the corresponding SEM images (e.g., Figures 8C,D differ significantly despite similar reduction rates) are due to differences in the corresponding controls. Despite SEM present a similar surface coverage of the controls, absorbance data indicate different biofilm biomass of the controls (Figure 2), most probably due to different biofilm thickness, not properly appreciable at SEM. Confocal laser scanning microscopy analysis carried out in a previous work demonstrated that the silicone coating with AC7BS expressed a detectable capacity in controlling *Candida* biofilm thickness after 48 h incubation (Ceresa et al., 2018).

No clear effect on the production of extracellular matrix by *Candida* was noted following the silicone precoating with R89BS or SL18. Indeed, the comparative analysis of *Candida* biofilm on the pre-coated discs with the controls did not show major differences in the amount of extracellular matrix. However, it has to be considered that SEM imaging in high vacuum brought to significant collapse of the matrix volume, limiting the sensitivity of this technique in revealing small changes in the matrix.

The strong association of *S. aureus* and *C. albicans* was indeed found in both untreated controls and pre-coated surfaces demonstrating the ability of *Candida* to provide an anchoring support for *S. aureus*. The anti-biofilm effect of the tested BSs could be therefore mainly related to the anti-adhesive properties rather than to a change in the microbial phenotypes including a reduction of the extracellular matrix

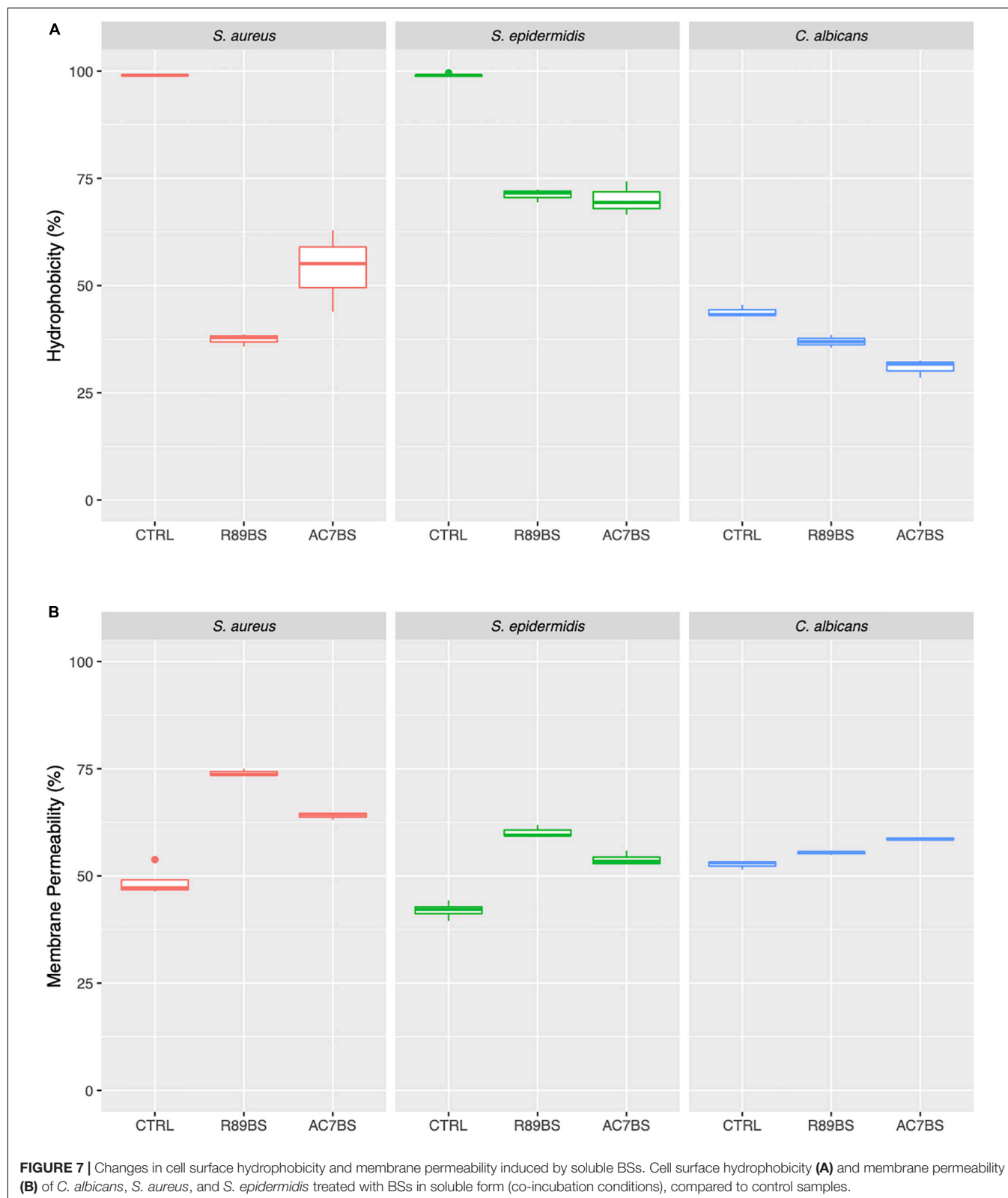
production as reported by Gupta et al. (2019) using cholic acid-peptide conjugates.

Furthermore, the use of R89BS and SL18 as coating agents did not result in a clear modification of the *C. albicans* hyphal morphology. However, it would be interesting to evaluate in future whether these BSs, both in their soluble and coated form, are able to cause a delay on *Candida* yeast-to hyphal transition at the initial phases of biofilm formation, thus as reported for sophorolipids from *Starmerella bombicola* MTCC1910 (Haque et al., 2016) and a *Lactobacillus rhamnosus* (Tan et al., 2017).

Another important aspect is the biocompatibility of the AC7BS-, R89BS-, and SL18-coated silicone discs. It has been previously demonstrated that at concentrations lower than or equal to 0.2 mg/ml for R89BS and 0.5 mg/ml for AC7BS were not cytotoxic for MRC5 cells monolayers (Ceresa et al., 2018, 2019b). In this work, additional evaluations revealed no or negligible cytotoxicity on HaCaT cells when exposed to the BSs-coated discs eluates for up to 72 h, paving the way for further investigation toward future *in vivo* applications.

CONCLUSION

In the present work, the activities of different BSs against yeast and bacterial biofilms were demonstrated through using a polymicrobial biofilm model able to support the growth of bacterial–fungal biofilms. The tests were conducted both under co-incubation and pre-coating conditions to evaluate, on the one hand, the inhibitory effect of BSs in solution against the polymicrobial biofilms and, on the other hand, the effectiveness of BSs as coating agents of medical devices



to limit microbial infection. BSs successfully limited the formation of polymicrobial biofilms up to 3 days under both experimental conditions.

The obtained results, together with the non-toxic nature of BSs at the tested concentrations and the biocompatibility of BSs-coated discs, further support the idea of a possible

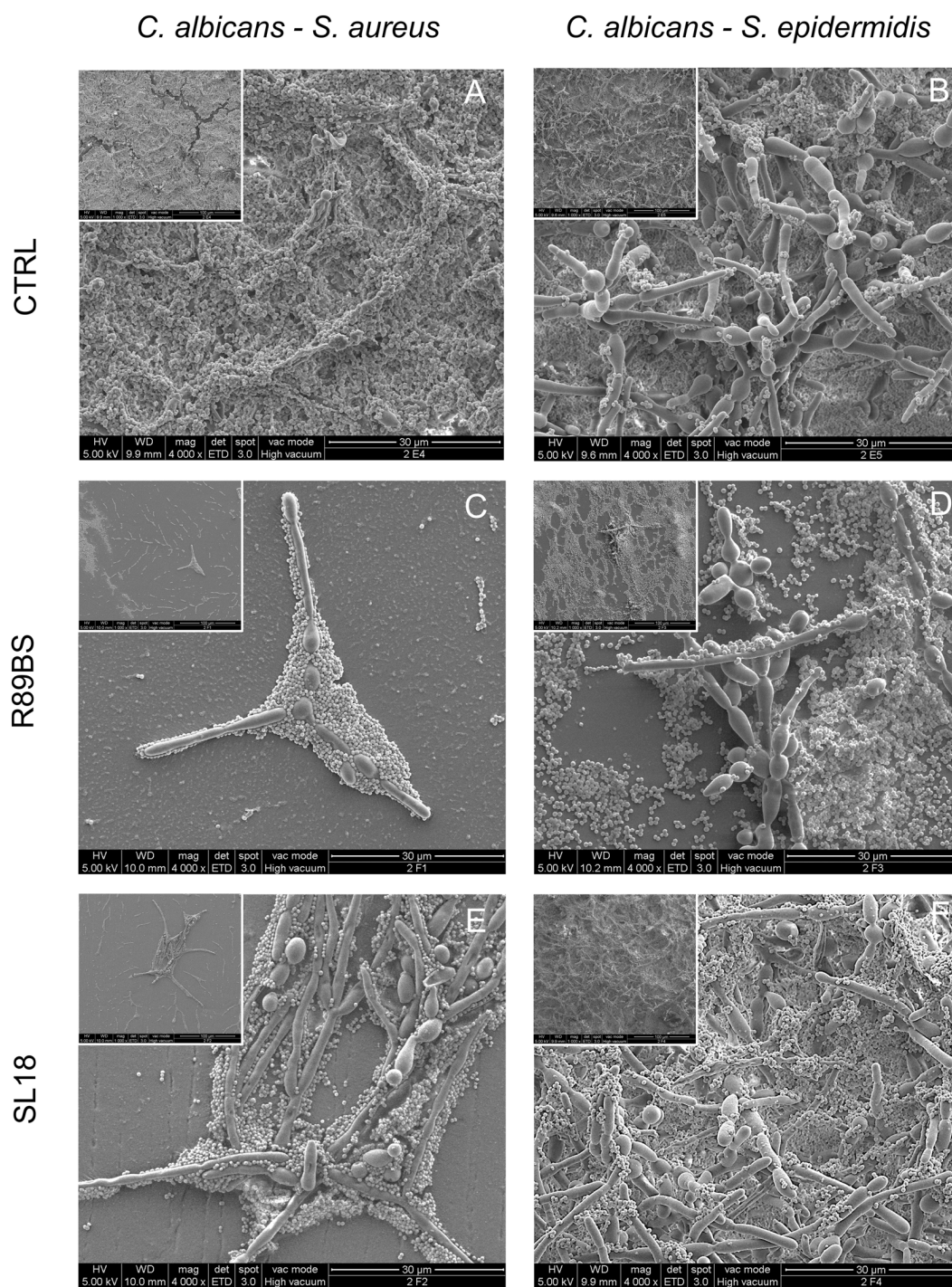


FIGURE 8 | Scanning electron microscopy images of the dual-species biofilms formed on the silicone discs surface at 72 h. *C. albicans*-*S. aureus* on the left column and *C. albicans*-*S. epidermidis* on the right column. Different surface pre-coating treatments are presented: untreated controls (top row), rhamnolipid R89BS (middle row), and sophorolipid SL18 (bottom row) treated discs. Insets present a lower magnification of the corresponding image to appreciate both macrostructural arrangement of the biofilm on the surface and micro-structural architecture of the two species in each biofilm sample. Original magnification: 4000x (1000x for the insets).

applicability of these natural molecules in the biomedical field. In particular, BSs coating might be a promising strategy, supporting preventative infection measures and

antimicrobial therapy, to reduce implant colonization and mitigate infections, thus prolonging the lifetime of implantable medical devices.

DATA AVAILABILITY STATEMENT

The raw data supporting the conclusions of this article will be made available by the authors, without undue reservation, to any qualified researcher.

AUTHOR CONTRIBUTIONS

CC and LF conceptualized the study. CC, FT, DM, and LF designed the experiments. PC, IB, and MD supervised the study. CC, FT, DM, EF, and ET performed the experiments. CC and MR collected data. MR carried out data analysis and statistics. PC, IB, MD, and LF contributed materials and analysis tools. CC, FT, MR, and LF wrote the original draft. CC, MR, FT, DM, IB, MD, and LF wrote, revised, and edited the manuscript. All authors read and approved the final manuscript.

FUNDING

This research has a financial support of the “Università del Piemonte Orientale”. CC holds a research fellowship (Bando

Fondazione CRT, Id. 393) supported by Università degli Studi del Piemonte Orientale and ET holds a research fellowship funded by Fondazione Cassa di Risparmio di Trento e Rovereto (Grant for young researchers involved in excellence research projects, ref. n 2017.0340), which are deeply acknowledged.

ACKNOWLEDGMENTS

The authors are grateful to Dr. Federico Piccoli of the Section for Electron Microscopy at the Department of Laboratory Medicine, Azienda Provinciale per i Servizi Sanitari di Trento for technical support in the acquisition and interpretation of SEM images. Dr. Alice Marchetti is also kindly acknowledged for technical assistance.

SUPPLEMENTARY MATERIAL

The Supplementary Material for this article can be found online at: <https://www.frontiersin.org/articles/10.3389/fmicb.2020.545654/full#supplementary-material>

REFERENCES

- Adam, B., Baillie, G. S., and Douglas, L. J. (2002). Mixed species biofilms of *Candida albicans* and *Staphylococcus epidermidis*. *J. Med. Microbiol.* 51, 344–349. doi: 10.1099/0022-1317-51-4-344
- Aleksic, I., Petkovic, M., Jovanovic, M., Milivojevic, D., Vasiljevic, B., Nikodinovic-Runic, J., et al. (2017). Anti-biofilm properties of bacterial di-rhamnolipids and their semi-synthetic amide derivatives. *Front. Microbiol.* 8:2454. doi: 10.3389/fmicb.2017.02454
- Arciola, C. R., An, Y. H., Campoccia, D., Donati, M. E., and Montanaro, L. (2005). Etiology of implant orthopedic infections: a survey on 1027 clinical isolates. *Int. J. Artif. Organs* 28, 1091–1100. doi: 10.1177/039139880502801106
- Arciola, C. R., Baldassarri, L., and Montanaro, L. (2001). Presence of *icaA* and *icaD* genes and slime production in a collection of staphylococcal strains from catheter-associated infections. *J. Clin. Microbiol.* 39, 2151–2156. doi: 10.1128/JCM.39.6.2151-2156.2001
- Banat, I. M., Díaz De Rienzo, M. A., and Quinn, G. A. (2014). Microbial biofilms: biosurfactants as antibiofilm agents. *Appl. Microbiol. Biotechnol.* 98, 9915–9929. doi: 10.1007/s00253-014-6169-6
- Banat, I. M., Franzetti, A., Gandolfi, I., Bestetti, G., Martinotti, M. G., Fracchia, L., et al. (2010). Microbial biosurfactants production, applications and future potential. *Appl. Microbiol. Biotechnol.* 87, 427–444. doi: 10.1007/s00253-010-2589-0
- Brogden, K. A., Guthmiller, J. M., and Taylor, C. E. (2005). Human polymicrobial infections. *Lancet* 365, 253–255. doi: 10.1016/S0140-6736(05)70155-0
- Buch, P. J., Chai, Y., and Goluch, E. D. (2019). Treating polymicrobial infections in chronic diabetic wounds. *Clin. Microbiol. Rev.* 32:e00091-18. doi: 10.1128/CMR.00091-18
- Budzynska, A., Rozalska, S., Sadowska, B., and Rozalska, B. (2017). *Candida albicans*/*Staphylococcus aureus* dual-species biofilm as a target for the combination of essential oils and fluconazole or mupirocin. *Mycopathologia* 182, 989–995. doi: 10.1007/s11046-017-0192-y
- Burmølle, M., Ren, D., Bjarnsholt, T., and Sørensen, S. J. (2014). Interactions in multispecies biofilms: do they actually matter? *Trends Microbiol.* 22, 84–91. doi: 10.1016/j.tim.2013.12.004
- Carolus, H., Van Dyck, K., and Van Dijck, P. (2019). *Candida albicans* and *Staphylococcus* species: a threatening twosome. *Front. Microbiol.* 10:2162. doi: 10.3389/fmicb.2019.02162
- Fondazione CRT, Id. 393) supported by Università degli Studi del Piemonte Orientale and ET holds a research fellowship funded by Fondazione Cassa di Risparmio di Trento e Rovereto (Grant for young researchers involved in excellence research projects, ref. n 2017.0340), which are deeply acknowledged.
- Cassat, J. E., Lee, C. Y., and Smeltzer, M. S. (2007). Investigation of biofilm formation in clinical isolates of *Staphylococcus aureus*. *Methods Mol. Biol.* 391, 127–144. doi: 10.1007/978-1-59745-468-1_10
- Ceresa, C., Fracchia, L., Marchetti, A., Rinaldi, M., and Bosetti, M. (2019a). Injectable scaffolds enriched with silver to inhibit bacterial invasion in tissue regeneration. *Materials* (Basel) 12:E1931. doi: 10.3390/ma12121931
- Ceresa, C., Fracchia, L., Williams, M., Banat, I. M., and Díaz De Rienzo, M. A. (2020). The effect of sophorolipids against microbial biofilms on medical-grade silicone. *J. Biotechnol.* 309, 34–43. doi: 10.1016/j.jbiotec.2019.12.019
- Ceresa, C., Rinaldi, M., Chiono, V., Carmagnola, I., Allegrone, G., and Fracchia, L. (2016). Lipopeptides from *Bacillus subtilis* AC7 inhibit adhesion and biofilm formation of *Candida albicans* on silicone. *Antonie Van Leeuwenhoek* 109, 1375–1388. doi: 10.1007/s10482-016-0736-z
- Ceresa, C., Rinaldi, M., and Fracchia, L. (2017). Synergistic activity of antifungal drugs and lipopeptide AC7 against *Candida albicans* biofilm on silicone. *AIMS Bioeng.* 4, 318–334. doi: 10.3934/bioeng.2017.2.318
- Ceresa, C., Tessarolo, F., Caola, I., Nollo, G., Cavallo, M., Rinaldi, M., et al. (2015). Inhibition of *Candida albicans* adhesion on medical-grade silicone by a *Lactobacillus*-derived biosurfactant. *J. Appl. Microbiol.* 118, 1116–1125. doi: 10.1111/jam.12760
- Ceresa, C., Tessarolo, F., Maniglio, D., Caola, I., Nollo, G., Rinaldi, M., et al. (2018). Inhibition of *Candida albicans* biofilm by lipopeptide AC7 coated medical-grade silicone in combination with farnesol. *AIMS Bioeng.* 5, 192–208. doi: 10.3934/bioeng.2018.3.192
- Ceresa, C., Tessarolo, F., Maniglio, D., Tambone, E., Carmagnola, I., Fedeli, E., et al. (2019b). Medical-grade silicone coated with rhamnolipid R89 is effective against *Staphylococcus* spp. *Biofilms Mol.* 24:E3843. doi: 10.3390/molecules24213843
- Chen, L., and Wen, Y. M. (2011). The role of bacterial biofilm in persistent infections and control strategies. *Int. J. Oral. Sci.* 3, 66–73. doi: 10.4248/IJOS11022
- Clinton, A., and Carter, T. (2015). Chronic wound biofilms: pathogenesis and potential therapies. *Lab Med.* 46, 277–284. doi: 10.1309/LMBNSWKU14JPN7SO
- Comoglio, F., Fracchia, L., and Rinaldi, M. (2013). Bayesian inference from count data using discrete uniform priors. *PLoS One* 8:e74388. doi: 10.1371/journal.pone.0074388
- Cuesta, A. I., Jewtuchowicz, V., Brusca, M. I., Nastri, M. L., and Rosa, A. C. (2010). Prevalence of *Staphylococcus* spp and *Candida* spp in the oral cavity and periodontal pockets of periodontal disease patients. *Acta Odontol. Latinoam.* 23, 20–26.

- de Alteriis, E., Lombardi, L., Falanga, A., Napolano, M., Galdiero, S., Siciliano, A., et al. (2018). Polymicrobial antibiofilm activity of the membranotropic peptide gH625 and its analogue. *Microb. Pathog.* 125, 189–195. doi: 10.1016/j.micpath.2018.09.027
- Diaz De Rienzo, M. A., Dolman, B., Guzman, F., Kaisermann, C., Winterburn, J., Banat, I. M., et al. (2014). Antimicrobial properties of sophorolipids produced by *Candida bombicola* ATCC 22214 against gram positive and Gram-negative bacteria. *New Biotechnol.* 31, S66–S67. doi: 10.1016/j.nbt.2014.05.1764
- Diaz De Rienzo, M. A., Stevenson, P. S., Marchant, R., and Banat, I. M. (2016). Effect of biosurfactants on *Pseudomonas aeruginosa* and *Staphylococcus aureus* biofilms in a BioFlux channel. *Appl. Microbiol. Biotechnol.* 100, 5773–5779. doi: 10.1007/s00253-016-7310-5
- Elshikh, M., Marchant, R., and Banat, I. M. (2016). Biosurfactants: promising bioactive molecules for oral-related health applications. *FEMS Microbiol. Lett.* 363:fnw213. doi: 10.1093/femsle/fnw213
- Elshikh, M., Moya-Ramírez, I., Moens, H., Roelants, S., Soetaert, W., Marchant, R., et al. (2017). Rhamnolipids and lactonic sophorolipids: natural antimicrobial surfactants for oral hygiene. *J. Appl. Microbiol.* 123, 1111–1123. doi: 10.1111/jam.13550
- Fracchia, L., Banat, J. J., Cavallo, M., Ceresa, C., and Banat, I. M. (2015). Potential therapeutic applications of microbial surface-active compounds. *AIMS Bioeng.* 2, 144–162. doi: 10.3934/bioeng.2015.3.144
- Fracchia, L., Ceresa, C., and Banat, I. M. (2019). “Biosurfactants in cosmetic, biomedical and pharmaceutical industry,” in *Microbial Biosurfactants and their Environmental and Industrial Applications*, eds I. M. Banat and R. Thavasi (Boca Raton, FL: CRS Press), 258–288. doi: 10.1201/b21950-11
- Francolini, I., and Donelli, G. (2010). Prevention and control of biofilm-based medical-device-related infections. *FEMS Immunol. Med. Microbiol.* 59, 227–238. doi: 10.1111/j.1574-695X.2010.00665.x
- Francolini, I., Vuotto, C., Piozzi, A., and Donelli, G. (2017). Antifouling and antimicrobial biomaterials: an overview. *APMIS* 125, 392–417. doi: 10.1111/apm.12675
- Ghensi, P., Bettio, E., Maniglio, D., Bonomi, E., Piccoli, F., Gross, S., et al. (2019). Dental implants with anti-biofilm properties: a pilot study for developing a new sericin-based coating. *Materials* (Basel). 12:E2429. doi: 10.3390/ma12152429
- Gupta, N., Haque, A., Mukhopadhyay, G., Narayan, R. P., and Prasad, R. (2005). Interactions between bacteria and *Candida* in the burn wound. *Burns* 31, 375–378. doi: 10.1016/j.burns.2004.11.012
- Gupta, S., Raghuvanshi, N., Varshney, R., Banat, I. M., Srivastava, A. K., Pruthi, P. A., et al. (2017). Accelerated in vivo wound healing evaluation of microbial glycolipid containing ointment as a transdermal substitute. *Biomed. Pharmacother.* 94, 1186–1196. doi: 10.1016/j.biopha.2017.08.010
- Gupta, S., Thakur, J., Pal, S., Gupta, R., Mishra, D., Kumar, S., et al. (2019). Cholic acid-peptide conjugates as potent antimicrobials against interkingdom polymicrobial biofilms. *Antimicrob. Agents Chemother.* 63:e00520-19. doi: 10.1128/AAC.00520-19
- Haque, F., Alfatah, M., Ganesan, K., and Bhattacharyya, M. S. (2016). Inhibitory effect of sophorolipid on *Candida albicans* biofilm formation and hyphal growth. *Sci. Rep.* 6:23575. doi: 10.1038/srep23575
- Harriott, M. M., and Noverr, M. C. (2009). *Candida albicans* and *Staphylococcus aureus* form polymicrobial biofilms: effects on antimicrobial resistance. *Antimicrob. Agents Chemother.* 53, 3914–3922. doi: 10.1128/AAC.00657-09
- Harriott, M. M., and Noverr, M. C. (2011). Importance of *Candida*-bacterial polymicrobial biofilms in disease. *Trends Microbiol.* 19, 557–563. doi: 10.1016/j.tim.2011.07.004
- Hrubanova, K., Krzyzanek, V., Nebesarova, J., Ruzicka, F., Pilat, Z., and Samek, O. (2018). Monitoring *Candida parapsilosis* and *Staphylococcus epidermidis* biofilms by a combination of scanning electron microscopy and raman spectroscopy. *Sensors* (Basel) 18:E4089. doi: 10.3390/s18124089
- Irorere, U. V., Kwienien, M., Tripathi, L., Cobice, D., McClean, S., Marchant, R., et al. (2019). Quorum sensing as a potential target for increased production of rhamnolipid biosurfactant in *Burkholderia thailandensis* E264. *Appl. Microbiol. Biotechnol.* 103, 6505–6517. doi: 10.1007/s00253-019-09942-5
- Janek, T., Krasowska, A., Czyżnikowska, Ż., and Łukaszewicz, M. (2018). Trehalose lipid biosurfactant reduces adhesion of microbial pathogens to polystyrene and silicone surfaces: an experimental and computational approach. *Front. Microbiol.* 9:2441. doi: 10.3389/fmicb.2018.02441
- John, T., Rajpurkar, A., Smith, G., Fairfax, M., and Triest, J. (2007). Antibiotic pretreatment of hydrogel ureteral stent. *J. Endourol.* 21, 1211–1216. doi: 10.1089/end.2007.9904
- Juma, A., Lemoine, P., Simpson, A. B. J., Murray, J., O'Hagan, B. M. G., Naughton, P. J., et al. (2020). Microscopic investigation of the combined use of antibiotics and biosurfactants on methicillin resistant *Staphylococcus aureus*. *Front. Microbiol.* 11:1477. doi: 10.3389/fmicb.2020.01477
- Khatoun, Z., McTiernan, C. D., Suuronen, E. J., Mah, T. F., and Alarcon, E. I. (2018). Bacterial biofilm formation on implantable devices and approaches to its treatment and prevention. *Heliyon* 4:e01067. doi: 10.1016/j.heliyon.2018.e01067
- Koo, H., Allan, R. N., Howlin, R. P., Stoodley, P., and Hall-Stoodley, L. (2017). Targeting microbial biofilms: current and prospective therapeutic strategies. *Nat. Rev. Microbiol.* 15, 740–755. doi: 10.1038/nrmicro.2017.99
- Liu, H., Chen, H., Sun, Y., Zhang, X., Lu, H., Li, J., et al. (2019). Characterization of the mechanism and impact of staphylokinase on the formation of *Candida albicans* and *Staphylococcus aureus* polymicrobial biofilms. *J. Med. Microbiol.* 68, 355–367. doi: 10.1099/jmm.0.000914
- Lydon, H. L., Baccile, N., Callaghan, B., Marchant, R., Mitchell, C. A., and Banat, I. M. (2017). Adjuvant antibiotic activity of acidic sophorolipids with potential for facilitating wound healing. *Antimicrob. Agents Chemother.* 61:e02547-16. doi: 10.1128/AAC.02547-16
- Marculescu, C. E., and Cantey, J. R. (2008). Polymicrobial prosthetic joint infections: risk factors and outcome. *Clin. Orthop. Relat. Res.* 466, 1397–1404. doi: 10.1007/s11999-008-0230-7
- Mihai, M. M., Holban, A. M., Giurcaneanu, C., Popa, L. G., Oanea, R. M., and Lazar, V. (2015). Microbial biofilms: impact on the pathogenesis of periodontitis, cystic fibrosis, chronic wounds and medical device-related infections. *Curr. Top. Med. Chem.* 15, 1552–1576. doi: 10.2174/1568026615666150414123800
- Naughton, P., Marchant, R., Naughton, V., and Banat, I. (2019). Microbial biosurfactants: current trends and applications in agricultural and biomedical industries. *J. Appl. Microbiol.* 127, 12–28. doi: 10.1111/jam.14243
- Omar, A., Wright, J. B., Schultz, G., Burrell, R., and Nadworny, P. (2017). Microbial biofilms and chronic wounds. *Microorganisms* 5:E9. doi: 10.3390/microorganisms5010009
- Pammi, M., Liang, R., Hicks, J., Mistretta, T. A., and Versalovic, J. (2013). Biofilm extracellular DNA enhances mixed species biofilms of *Staphylococcus epidermidis* and *Candida albicans*. *BMC Microbiol.* 13:257. doi: 10.1186/1471-2180-13-257
- Papa, R., Selan, L., Parrilli, E., Tilotta, M., Sannino, F., Feller, G., et al. (2015). Activities from marine cold adapted bacteria against *Staphylococci* and *Pseudomonas aeruginosa*. *Front. Microbiol.* 6:1333. doi: 10.3389/fmicb.2015.01333
- Paraszkiewicz, K., Moryl, M., Płaza, G., Bhagat, D., Satpute, S. K., and Bernat, P. (2019). Surfactants of microbial origin as antibiofilm agents. *Int. J. Environ. Health Res.* 11, 1–20. doi: 10.1080/09603123.2019.1664729
- Percival, S. L., Suleman, L., Vuotto, C., and Donelli, G. (2015). Healthcare-associated infections, medical devices and biofilms: risk, tolerance and control. *J. Med. Microbiol.* 64, 323–334. doi: 10.1099/jmm.0.000032
- Pompilio, A., and Di Bonaventura, G. (2018). Microbial biofilm: a “sticky” problem. *Microbiol. Med.* 33:7851. doi: 10.4081/mm.2018.7851
- Qu, Y., Locock, K., Verma-Gaur, J., Hay, I. D., Meagher, L., and Traven, A. (2016). Searching for new strategies against polymicrobial biofilm infections: guanlylated polymethacrylates kill mixed fungal/bacterial biofilms. *J. Antimicrob. Chemother.* 71, 413–421. doi: 10.1093/jac/dkv334
- Quinn, G. A., Maloy, A. P., Banat, M. M., and Banat, I. M. (2013). A comparison of effects of broad-spectrum antibiotics and biosurfactants on established bacterial biofilms. *Curr. Microbiol.* 67, 614–623. doi: 10.1007/s00284-013-0412-8
- Ramasamy, M., and Lee, J. (2016). Recent nanotechnology approaches for prevention and treatment of biofilm-associated infections on medical devices. *Biomed. Res. Int.* 2016:1851242. doi: 10.1155/2016/1851242
- R Core Team (2019). *R: A Language and Environment for Statistical Computing*. Vienna: R Foundation for Statistical Computing. Available online at: <https://www.Rproject.org/>
- Rodrigues, L. R., Banat, I. M., van der Mei, H. C., Teixeira, J. A., and Oliveira, R. (2006). Interference in adhesion of bacteria and yeasts isolated from explanted voice prostheses to silicone rubber by rhamnolipid biosurfactants. *J. Appl. Microbiol.* 100, 470–480. doi: 10.1111/j.1365-2672.2005.02826.x

- Rodrigues, L. R., and Teixeira, J. A. (2010). Biomedical and therapeutic applications of biosurfactants. *Adv. Exp. Med. Biol.* 672, 75–87. doi: 10.1007/978-1-4419-5979-9_6
- Rodrigues, M. E., Gomes, F., and Rodrigues, C. F. (2019). *Candida* spp./bacteria mixed biofilms. *J. Fungi* (Basel). 6:5. doi: 10.3390/jof6010005
- Rodríguez-López, L., López-Prieto, A., López-Álvarez, M., Pérez-Davila, S., Serra, J., and González, P. (2020). Characterization and cytotoxic effect of biosurfactants obtained from different sources. *ACS Omega* 48, 31381–31390. doi: 10.1021/acsomega.0c04933
- Rosenberg, M., Gutnick, D., and Rosenberg, E. (1980). Adherence of bacteria to hydrocarbons: a simple method for measuring cell-surface hydrophobicity. *FEMS Microbiol. Lett.* 9, 29–33. doi: 10.1111/j.1574-6968.1980.tb05599.x
- Sardi, J. C., Scorzoni, L., Bernardi, T., Fusco-Almeida, A. M., and Mendes Giannini, M. J. (2013). *Candida* species: current epidemiology, pathogenicity, biofilm formation, natural antifungal products and new therapeutic options. *J. Med. Microbiol.* 62, 10–24. doi: 10.1099/jmm.0.045054-0
- Satpute, S. K., Banpurkar, A. G., Banat, I. M., Sangshetti, J. N., Patil, R. H., and Gade, W. N. (2016). Multiple roles of biosurfactants in biofilms. *Curr. Pharm. Des.* 22, 1429–1448. doi: 10.2174/1381612822666160120152704
- Satpute, S. K., Mone, N. S., Das, P., Banat, I. M., and Banpurkar, A. G. (2019). Inhibition of pathogenic bacterial biofilms on PDMS based implants by *L. acidophilus* derived biosurfactant. *BMC Microbiol.* 19:39. doi: 10.1186/s12866-019-1412-z
- Satpute, S. K., Mone, N. S., Das, P., Banpurkar, A. G., and Banat, I. M. (2018). *Lactobacillus acidophilus* derived biosurfactant as a biofilm inhibitor: a promising investigation using microfluidic approach. *Appl. Sci.* 8:1555. doi: 10.3390/app8091555
- Scaffaro, R., Lopresti, F., D'Arrigo, M., Marino, A., and Nostro, A. (2018). Efficacy of poly(lactic acid)/carvacrol electrospun membranes against *Staphylococcus aureus* and *Candida albicans* in single and mixed cultures. *Appl. Microbiol. Biotechnol.* 102, 4171–4181. doi: 10.1007/s00253-018-8879-7
- Sharma, D., Misba, L., and Khan, A. U. (2019). Antibiotics versus biofilm: an emerging battleground in microbial communities. *Antimicrob. Resist. Infect. Control* 8:76. doi: 10.1186/s13756-019-0533-3
- Sharma, D., and Saharan, B. S. (2016). Functional characterization of biomedical potential of biosurfactant produced by *Lactobacillus helveticus*. *Biotechnol. Rep. (Amst.)* 11, 27–35. doi: 10.1016/j.btre.2016.05.001
- Signoretto, C., Marchi, A., Bertoncelli, A., Burlacchini, G., Milli, A., Tassarolo, F., et al. (2013). Effects of mushroom and chicory extracts on the shape, physiology and proteome of the cariogenic bacterium *Streptococcus mutans*. *BMC Complement. Altern. Med.* 13:117. doi: 10.1186/1472-6882-13-117
- Simms, A. A., Naughton, P. J., Marchant, R., and Banat, I. M. (2020). Microbial biosurfactants in cosmetic and personal skincare pharmaceutical formulations. *Pharmaceutics* 12:1099. doi: 10.3390/pharmaceutics12111099
- Song, R., Murphy, M., Li, C., Ting, K., Soo, C., and Zheng, Z. (2018). Current development of biodegradable polymeric materials for biomedical applications. *Drug Des. Devel. Ther.* 12, 3117–3145. doi: 10.2147/DDDT.S165440
- Tan, Y., Leonhard, M., Moser, D., Ma, S., and Schneider-Stickler, B. (2019). Antibiofilm efficacy of curcumin in combination with 2-aminobenzimidazole against single- and mixed-species biofilms of *Candida albicans* and *Staphylococcus aureus*. *Colloids Surf. B Biointerfaces* 174, 28–34. doi: 10.1016/j.colsurfb.2018.10.079
- Tan, Y., Leonhard, M., Moser, D., and Schneider-Stickler, B. (2017). Inhibition activity of *Lactobacilli* supernatant against fungal-bacterial multispecies biofilms on silicone. *Microb. Pathog.* 113, 197–201. doi: 10.1016/j.micpath.2017.10.051
- Teo, A. J. T., Mishra, A., Park, I., Kim, Y.-J., Park, W.-T., and Yoon, Y.-J. (2016). Polymeric biomaterials for medical implants and devices. *ACS Biomater. Sci. Eng.* 2, 454–472. doi: 10.1021/acsbomaterials.5b00429
- Tassarolo, F., Caola, I., Fedel, M., Stacchiotti, A., Caciagli, P., Guarrera, G. M., et al. (2007). Different experimental protocols for decontamination affect the cleaning of medical devices. A preliminary electron microscopy analysis. *J. Hosp. Infect.* 65, 326–333. doi: 10.1016/j.jhin.2006.10.015
- Tsui, C., Kong, E. F., and Jabra-Rizk, M. A. (2016). Pathogenesis of *Candida albicans* biofilm. *Pathog. Dis.* 74:ftw018. doi: 10.1093/femspd/ftw018
- Valenza, G., Tappe, D., Turnwald, D., Frosch, M., König, C., Hebestreit, H., et al. (2008). Prevalence and antimicrobial susceptibility of microorganisms isolated from sputa of patients with cystic fibrosis. *J. Cyst. Fibros.* 7, 123–127. doi: 10.1016/j.jcf.2007.06.006
- Vasilev, K., Griesser, S. S., and Griesser, H. J. (2011). Antibacterial surfaces and coatings produced by plasma techniques. *Plasma Process. Polym.* 8, 1010–1023. doi: 10.1002/ppap.201100097
- Villa, F., and Cappitelli, F. (2013). Plant-derived bioactive compounds at sub-lethal concentrations: towards smart biocide-free antibiofilm strategies. *Phytochem. Rev.* 12, 245–254. doi: 10.1007/s11101-013-9286-4
- von Eiff, C., Arciola, C. R., Montanaro, L., Becker, K., and Campoccia, D. (2006). Emerging *Staphylococcus* species as new pathogens in implant infections. *Int. J. Artif. Organs* 29, 360–367. doi: 10.1177/039139880602900405
- Wang, M., and Tang, T. (2018). Surface treatment strategies to combat implant-related infection from the beginning. *J. Orthop. Translat.* 17, 42–54. doi: 10.1016/j.jot.2018.09.001
- Wang, Y., Jayan, G., Patwardhan, D., and Phillips, K. S. (2017). “Antimicrobial and anti-biofilm medical devices: public health and regulatory science challenges,” in *Antimicrobial Coatings and Modifications on Medical Devices*, eds Z. Zhang and V. Wagner (Cham: Springer), 37–75. doi: 10.1007/978-3-319-57494-3_2
- Weiland-Bräuer, N., Malek, I., and Schmitz, R. A. (2019). Metagenomic quorum quenching enzymes affect biofilm formation of *Candida albicans* and *Staphylococcus epidermidis*. *PLoS One* 14:e0211366. doi: 10.1371/journal.pone.0211366
- Williams, D. L., and Bloebaum, R. D. (2010). Observing the biofilm matrix of *Staphylococcus epidermidis* ATCC 35984 grown using the CDC biofilm reactor. *Microsc. Microanal.* 16, 143–152. doi: 10.1017/S143192760999136X
- Xian, W. (2009). “Module III: biocompatibility testing: cytotoxicity and adhesion,” in *A Laboratory Course in Biomaterials*, ed. Taylor & Francis Group (Boca Raton, FL: CRC Press), 99–128. doi: 10.1201/b15832
- Zilberman, M., and Elsner, J. J. (2008). Antibiotic-eluting medical devices for various applications. *J. Control Release* 130, 202–215. doi: 10.1016/j.jconrel.2008.05.020

Conflict of Interest: The authors declare that the research was conducted in the absence of any commercial or financial relationships that could be construed as a potential conflict of interest.

Copyright © 2021 Ceresa, Rinaldi, Tassarolo, Maniglio, Fedeli, Tambone, Caciagli, Banat, Diaz De Rienzo and Fracchia. This is an open-access article distributed under the terms of the Creative Commons Attribution License (CC BY). The use, distribution or reproduction in other forums is permitted, provided the original author(s) and the copyright owner(s) are credited and that the original publication in this journal is cited, in accordance with accepted academic practice. No use, distribution or reproduction is permitted which does not comply with these terms.

Advantages of publishing in Frontiers



OPEN ACCESS

Articles are free to read
for greatest visibility
and readership



FAST PUBLICATION

Around 90 days
from submission
to decision



HIGH QUALITY PEER-REVIEW

Rigorous, collaborative,
and constructive
peer-review



TRANSPARENT PEER-REVIEW

Editors and reviewers
acknowledged by name
on published articles

Frontiers

Avenue du Tribunal-Fédéral 34
1005 Lausanne | Switzerland

Visit us: www.frontiersin.org

Contact us: frontiersin.org/about/contact



REPRODUCIBILITY OF RESEARCH

Support open data
and methods to enhance
research reproducibility



DIGITAL PUBLISHING

Articles designed
for optimal readership
across devices



FOLLOW US

@frontiersin



IMPACT METRICS

Advanced article metrics
track visibility across
digital media



EXTENSIVE PROMOTION

Marketing
and promotion
of impactful research



LOOP RESEARCH NETWORK

Our network
increases your
article's readership